

25 Copies

MPR-SAT-FE-68-2

APRIL 5, 1968

GEORGE C. MARSHALL SPACE
FLIGHT CENTER

SATURN

(NASA-TM-X-61111) RESULTS OF THE FOURTH
SATURN IB LAUNCH VEHICLE TEST FLIGHT AS-204
(NASA) 359 p

N90-70429

Unclass
00/15 0257072

RESULTS OF THE FOURTH SATURN IB LAUNCH VEHICLE TEST FLIGHT

AS-204



PREPARED BY
SATURN IB FLIGHT EVALUATION
WORKING GROUP



NATIONAL AERONAUTICS AND SPACE ADMINISTRATION

[REDACTED]

GEORGE C. MARSHALL SPACE FLIGHT CENTER
HUNTSVILLE, ALABAMA

Memorandum

TO : See Addressees

DATE: July 9, 1968

FROM : Chief, Trajectory Section,
R-AERO-FFT

In Reply Refer To:
R-AERO-FF-74-68

SUBJECT : Revision of AS-204 acceleration model during propellant dump

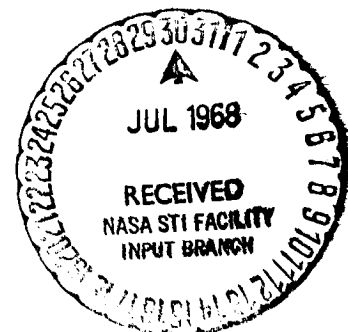
REFERENCES : (1) Saturn IB Flight Evaluation Working Group, "Results of the Fourth Saturn IB Launch Vehicle Test Flight AS-204," MPR-SAT-FE-682, dated April 5, 1968

(2) Aerospace Physics Branch, Chrysler Corporation Space Division, "Saturn AS-204/LM-1 Postflight Trajectory," TN-AP-68-311, dated April 1968

1. Apparent discrepancies between information in paragraph 9.6.3 and Figure 9.18 of Reference 1 and paragraph 4.4 and Figure 19 of Reference 2 have necessitated a re-evaluation of the effect of the AS-204 propellant dump (passivation) on the orbital trajectory. The following discrepancies are noted:

- a. Reference 1 indicates a thrust level drop off beginning at 8830 seconds (Range Time) while Reference 2 shows an acceleration drop off at 8855 seconds.
- b. The slopes of the two curves from 8800 seconds to 8860 seconds are strikingly dissimilar.
- c. Reference 1 indicates a peak thrust of 3415 N (768 lbf) and if the acceleration shown in Reference 2 be converted to a thrust (using mass data from Table 6-IIe in Reference 1) a maximum of 2310 N (520 lbf) results.

2. Examination of data used in Reference 2 revealed a data gap from 8800 seconds to 8856 seconds, which spans the area of interest. Additional data in the form of an oscillogram of the encoder (velocity) pick offs from the three guidance accelerometers, were obtained and analyzed. This analysis consisted of applying a polynomial curve fit to the velocity data; differentiating the polynomials with respect to time; and then evaluating the resulting (acceleration) polynomials at common times. The component accelerations thus obtained were root sum squared to give the total acceleration shown in Figure 1.



3. The new analysis reveals the following information:

- a. Acceleration level reaches a peak at 8827 seconds.
- b. The slopes of the curves in Figure 1 and 9.18 of Reference 1 are much more similar.
- c. Peak thrust (at 8827 seconds) is 3449 N (776 lbf) if the acceleration shown in Figure 1 be converted to thrust using mass data from Table 6-IIe in Reference 1.

4. In light of this additional analysis, Figure 1 should be considered the actual acceleration profile in Reference 2 for the period from 8800 seconds to 8860 seconds. Any further questions should be directed to Mr. C. L. Varnado, 205-876-2937.

J. B. Haussler
J. B. Haussler

APPROVAL:

CONCURRENCE:

J. P. Lindberg
J. P. Lindberg, Chief,
Flight Test Analysis Division

R. J. Jackson
R. J. Jackson, R-AERO-P

E. D. Geissler
E. D. Geissler, Director,
Aero-Astroynamics Laboratory

Enc:

1. Figure 1, "AS-204 Acceleration During Passivation"

Addressees:

DEP-T, Dr. Rees
R-AERO-DIR, Dr. Geissler
R-AERO-DIR, Mr. Jean
R-AERO-A, Mr. Dahm (3)
R-AERO-Y, Mr. Vaughan (2)
R-AERO-DD, Mr. Ryan
R-AERO-D, Mr. Horn
R-AERO-G, Mr. Baker
R-AERO-F, Mr. Lindberg (2)
R-AERO-FT, Mr. Benson (2)
R-AERO-FM, Mr. Hardage (2)
R-AERO-FF, Mr. Hagood (4)
R-AERO-F, Mr. Fulmer
R-AERO-P, Mr. Jackson
R-ASTR-DIR, Dr. Haeussermann
R-ASTR-DIR, Mr. Hoberg
R-ASTR-F, Mr. Hosenthien

Addressees: (Cont'd)

R-ASTR-N, Mr. Moore
R-ASTR-NGI, Mr. Nicaise
R-ASTR-I, Mr. Powell
R-ASTR-IRD, Mr. Kerr (2)
R-COMP-DIR, Dr. Hoelzer
R-COMP-RR, Mr. Cochran
R-COMP-RRT, Mr. Craft
R-COMP-RRT, Mr. Fletcher
R-EO-DIR, Dr. Johnson
R-ME-DIR, Mr. Kuers
R-P&VE-DIR, Dr. Lucas
R-P&VE-DIR, Mr. Palaoro
R-P&VE-P, Mr. Paul
R-P&VE-PP, Mr. Swalley (3)
R-P&VE-S, Mr. Kroll
R-P&VE-S, Mr. Hunt
R-P&VE-V, Mr. Aberg
R-P&VE-V, Mr. Schulze (3)
R-P&VE-PTD, Mr. McAnelly
R-TEST-DIR, Mr. Heimburg
R-TEST-S, Mr. Driscoll
R-QUAL-DIR, Dr. Stuhlinger
R-SE-DIR, Mr. Richard (2)
R-AS-DIR, Mr. Williams
I-DIR, Dr. Mrazek
I-I/IB-MGR, Col. Teir
I-I/IB-T, Mr. Fikes
I-I/IB-SI/IB, Mr. Thompson
I-I/IB-S-IVB, Mr. McCulloch
I-I/IB-U, Mr. Simmons
I-MO-MGR, Dr. Speer
MS-T, (5)
MS-IL (8)
MS-IP
I-RM-M
CCP
MS-H

Addressees (cont'd)

External

Headquarters, National Aeronautics & Space Administration
Washington 25, D.C. 20546

Scientific & Technical Information Division (5)
Attn: General Phillips, Code MA (2)
Office of Tracking and Data Acquisition, Code T
Office of Advanced Research and Technology, Code R

Goddard Space Flight Center
National Aeronautics & Space Administration
Greenbelt, Maryland 20771

Attn: Mr. LaGow, Code 300
Mr. Womick, Code 552
Mr. Cape, Code 552
Mr. Covington, Code 501
Mr. Donegan, Code 501
Dr. Siry, Code 547
Dr. Von Bun, Code 507

Manned Spacecraft Center
Houston, Texas 77058

Attn: Mr. R. E. McKann, Code PT-121 (6)
Mr. F. McCreary, FM-12 (2)

DAC/MSFC
Bldg. 4481, Room 58
Attn: Mr. Thelander (7)

Scientific & Technical Information Facility (25)
P.O. Box 5700
Bethesda, Maryland 20014
Attn: NASA Representative (S-AK/RKT)

John F. Kennedy Space Center
National Aeronautics & Space Administration
Kennedy Space Center, Florida 32899

Attn: Technical Library (2)
Mrs. L. B. Russell
Dr. Debus, DIR
Dr. Knothe, TEC
Mr. Sandler, INS
Dr. Bruns, INS-I
Dr. Gruene, JA
Col. Bagnula, EDV (2)

Addressees: (cont'd)

RCA Performance Analysis
Cocoa Beach Office
Mail Unit 645
P.O.Box 4036
Patrick Air Force Base, Florida 32925
Attn: Mr. E. A. Hoffmann-Heyden (3)

Director, Ames Research Center
National Aeronautics & Space Administration
Moffett Field, California 94035
Attn: Dr. Julian Allen

Director Lewis Research Center
National Aeronautics & Space Administration
21000 Brookpark Road
Cleveland, Ohio 44135
Attn: Dr. Silverstein

Director, Langley Research Center
National Aeronautics & Space Administration
Langley Station
Hampton, Virginia 23365
Attn: Mr. Floyd L. Thompson

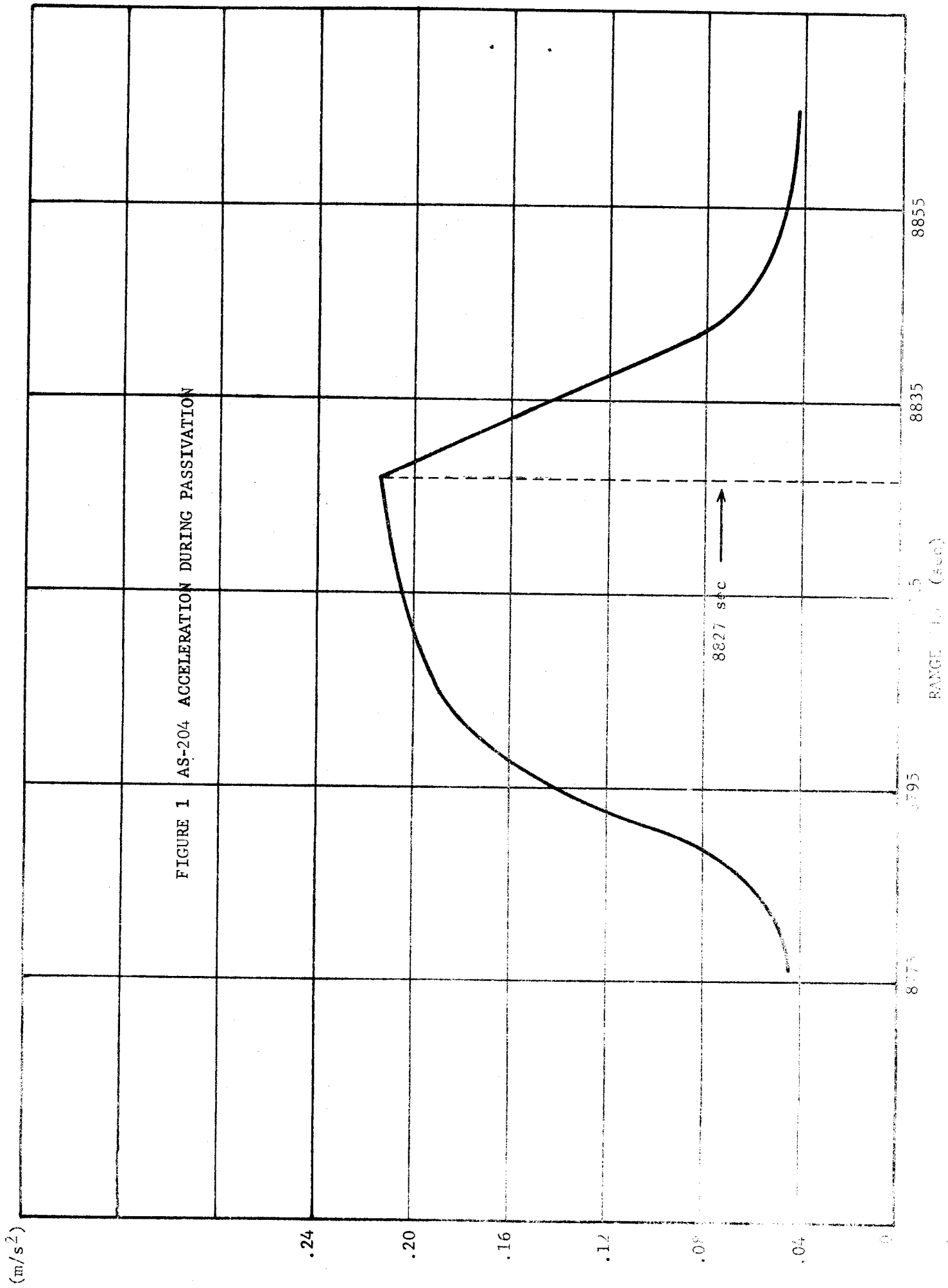
Director, Flight Research Center
National Aeronautics & Space Administration
P.O.Box 273
Edwards, California 93423
Attn: Mr. Paul F. Bikle

Director, Wallops Station
National Aeronautics & Space Administration
Wallops Island, Virginia 23337
Attn: Mr. R.L. Krieger

Jet Propulsion Laboratory
4800 Oak Grove Drive
Pasadena, California 91103
Attn: Mr. Irl Newlan, Reports Group (Mail 111-122)
Mr. H. Levy, CCMTA (Mail 179-203)

North American Aviation
Space & Information Division System
12214 Lakewood Blvd. South
Downey, California 90241
Attn: Mr. W. T. Schleich, BC-05 (2)

Nortronics
6025 Technology Drive
Huntsville, Alabama 35805
Attn: Mr. W. Klabunde, Section 7960



MPR-SAT-FE-68-2

RESULTS OF THE FOURTH SATURN IB LAUNCH VEHICLE TEST FLIGHT
AS-204

By

Saturn Flight Evaluation Working Group

George C. Marshall Space Flight Center

ABSTRACT

Saturn IB AS-204 was launched at 1748:08 EST on January 22, 1968 from KSC Launch Complex 37B, under favorable weather conditions. The vehicle lifted off after a total delay of 3 hrs and 48 min due to holds, on a launch azimuth of 90 deg east of north and rolled to a flight azimuth of 72 deg east of north. The actual trajectory was near nominal.

All major systems performed within design limits and close to predicted values throughout flight. Although no malfunctions or deviations occurred that adversely affected flight or mission accomplishment, a few refinements based on flight test results are being incorporated. These are discussed in detail in the body of the report.

The AS-204 test flight demonstrated successfully the performance of the orbital safing experiment including propellant venting, propellant dump, cold helium dump, and stage/engine pneumatic supply dump. This flight also demonstrated the adequacy of the attitude control and vehicle electrical systems to perform for extended duration in orbit.

Any questions or comments pertaining to the information contained in this report are invited, and should be directed to:

Director, George C. Marshall Space Flight Center
Marshall Space Flight Center, Alabama 35812
Attention: Chairman, Saturn Flight Evaluation Working Group
R-AERO-F (Phone 876-4575)

GEORGE C. MARSHALL SPACE FLIGHT CENTER

MPR-SAT-FE-68-2

RESULTS OF THE FOURTH SATURN IB LAUNCH VEHICLE TEST FLIGHT
AS-204

SATURN FLIGHT EVALUATION
WORKING GROUP

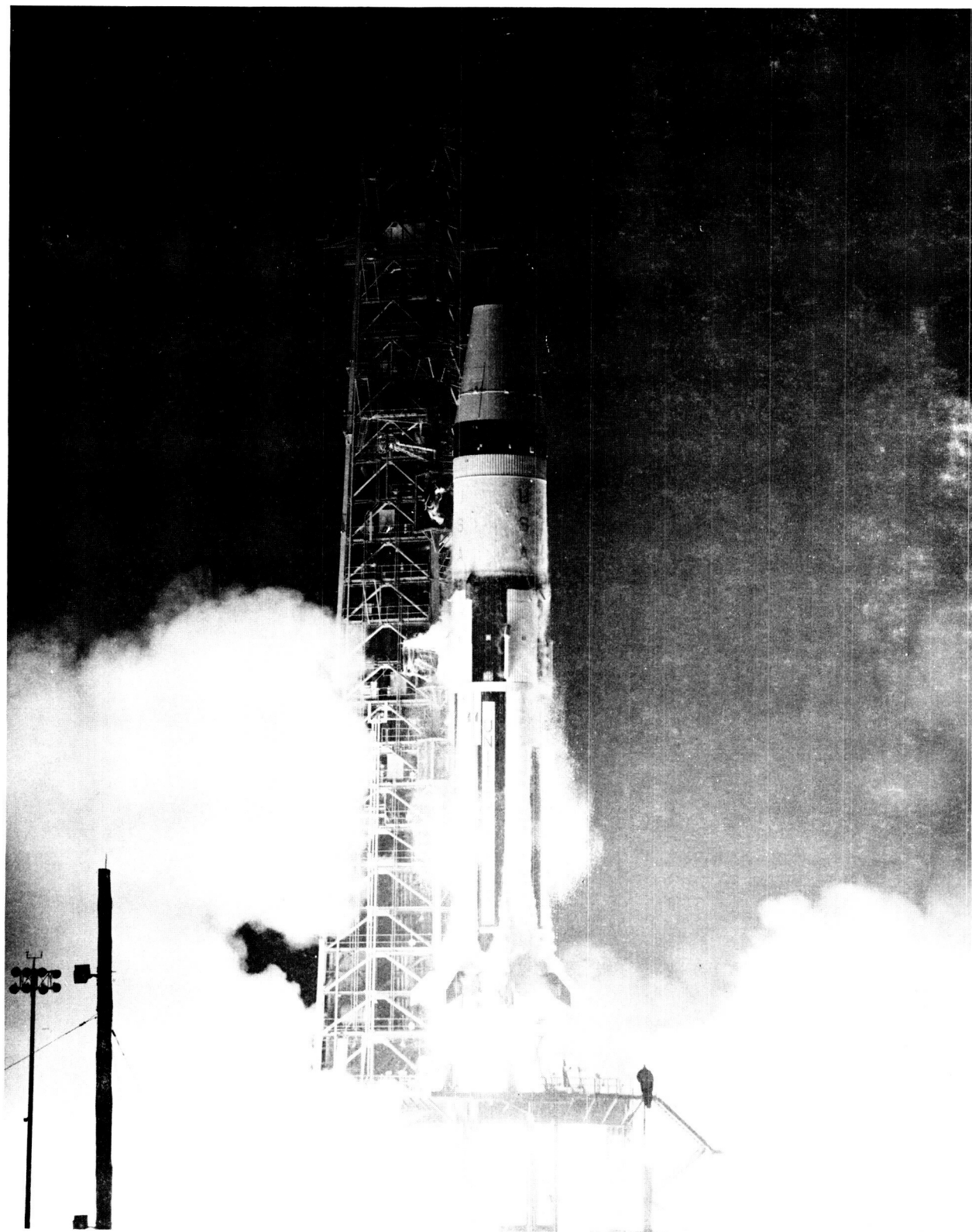


TABLE OF CONTENTS

	Page
1.0 Flight Test Summary	1
2.0 Introduction	4
3.0 Test Objectives	5
3.1 Primary Test Objectives	5
3.2 Secondary Test Objectives	5
4.0 Times of Events	6
4.1 Summary	6
4.2 Sequence of Events	6
5.0 Launch Operations	16
5.1 Summary	16
5.2 Prelaunch Milestones	16
5.3 Countdown	16
5.4 Propellant and Cold Helium Loading	19
5.4.1 RP-1 Loading	19
5.4.2 LOX Loading	20
5.4.3 LH ₂ Loading	20
5.4.4 Cold Helium Loading	20
5.4.5 Auxiliary Propulsion System Loading	20
5.4.6 S-IB Stage Propellant Load	21
5.4.7 S-IVB Stage Propellant Load	21
5.5 Holddown	21
5.6 Ground Support Equipment	25
5.7 Launch Facility Measurement	25
6.0 Mass Characteristics	26
6.1 Summary	26
6.2 Mass Analysis	26
6.3 Center-of-Gravity and Moment-of-Inertia Analysis	27
7.0 Trajectory	39
7.1 Summary	39
7.2 Tracking Data Utilization	39
7.3 Trajectory Analysis, Powered Flight	41
7.4 Parking Orbit Trajectory	48
7.5 S-IVB Orbit Safing Experiment	48
8.0 S-IB Propulsion	52
8.1 Summary	52
8.2 S-IB Propulsion Performance	52
8.2.1 Stage Performance	53
8.2.2 Individual Engine Characteristics	65

TABLE OF CONTENTS (CONT)

	Page
8.3 S-IB Propellant Usage	68
8.4 S-IB Pressurization Systems	71
8.4.1 Fuel Pressurization System	71
8.4.2 LOX Pressurization System	74
8.4.3 Control Pressure System	76
9.0 S-IVB Propulsion and Associated Systems	78
9.1 Summary	78
9.2 S-IVB Propulsion Performance	78
9.2.1 Engine Chillydown	78
9.2.2 Start Characteristics	80
9.2.3 Mainstage Engine Performance	80
9.2.4 Cutoff Characteristics	82
9.3 S-IVB Stage Propellant Utilization	87
9.3.1 Propellant Mass Analysis	87
9.3.2 PU Valve Response and Thrust Fluctuations	87
9.4 S-IVB Propellant Pressurization Systems	93
9.4.1 Fuel Pressurization System	93
9.4.2 LOX Pressurization System	97
9.5 S-IVB Pneumatic Systems	102
9.6 S-IVB Orbital Safing Experiment	107
9.6.1 Experiment Purpose and Events	107
9.6.2 LH ₂ and LOX Tank Venting	109
9.6.3 Propellant Dump	112
9.6.4 Cold Helium Dump	112
9.6.5 Pneumatic Spheres	114
9.6.6 Crossover Duct and LOX Turbine Temperatures	116
10.0 Auxiliary Propulsion System	118
10.1 Summary	118
10.2 APS Performance	118
10.2.1 Propellant and Pressurization System	118
10.2.2 APS Motor Performance	122
11.0 Hydraulic System	125
11.1 Summary	125
11.2 S-IB Stage Hydraulic System	125
11.3 S-IVB Stage Hydraulic System	125
12.0 Guidance and Control	132
12.1 Summary	132
12.2 System Description	132
12.2.1 Changes for Saturn IB AS-204	132
12.2.2 Function and Hardware Description	133
12.2.3 Navigation Scheme Description	133

TABLE OF CONTENTS (CONT)

	Page
12.3 Launch Vehicle Flight Control	136
12.3.1 S-IB Stage Control Analysis	136
12.3.2 S-IVB Stage Control Analysis	147
12.3.3 Control During Orbit	157
12.3.4 Control Component Analysis	173
12.3.4.1 Control Accelerometers	173
12.3.4.2 Rate Gyros	173
12.3.4.3 Actuator Performance	176
12.4 Launch Vehicle Navigation and Guidance	176
12.4.1 Navigation and Guidance Scheme	
Performance Analysis	178
12.4.2 Navigation and Guidance Comparison	181
12.4.2.1 Powered Flight Comparison	181
12.4.2.2 Measured Velocity Changes During Orbit	185
12.4.3 Guidance System Component Analysis	189
12.4.3.1 LVDC/LVDA Analysis	189
12.4.3.2 ST-124M3 Stabilized Platform Analysis	189
13.0 Separation	190
13.1 Summary	190
13.2 S-IB/S-IVB Separation	190
13.2.1 Ullage Motor Performance	190
13.2.2 Retrorocket Performance	190
13.2.3 Separation Dynamics	195
13.3 LV/LM-1 Separation	195
14.0 Vehicle Electrical Systems	200
14.1 Summary	200
14.2 S-IB Stage Electrical System	200
14.3 S-IVB Stage Electrical System	202
14.4 Instrument Unit Electrical System	205
15.0 Range Safety and Command Systems	208
15.1 Summary	208
15.2 Command Destruct Systems	208
15.3 Digital Guidance Command System	208
16.0 Emergency Detection System	210
16.1 Summary	210
16.2 System Description	210
16.3 EDS Buses	210
16.4 EDS Event Times	210
16.5 Thrust OK Indications	210
16.6 EDS Rate Gyros	213
16.7 Launch Vehicle Attitude Reference Monitoring	213

TABLE OF CONTENTS (CONT)

	Page
16.8 EDS Distributor	213
17.0 Structures	214
17.1 Summary	214
17.2 Total Vehicle Loads and Moments	214
17.2.1 Longitudinal Loads	214
17.2.2 Bending Moments	216
17.2.3 Body Bending Oscillations	216
17.2.4 Longitudinal Dynamic Analysis (POGO)	216
17.3 S-IB Stage Analysis	222
17.3.1 S-IB Fin Bending and Torsion	222
17.3.2 S-IB Stage Vibrations	222
17.3.3 H-1 Engine Vibrations	222
17.4 S-IVB Stage Analysis	230
17.4.1 S-IVB Vibrations	230
17.4.2 J-2 Engine Vibrations	230
17.4.3 S-IVB Forward Skirt In-Flight Flutter Experiment	230
17.4.4 S-IVB Internal Acoustics	237
17.5 Instrument Unit Vibration	237
18.0 Pressure and Thermal Environment	240
18.1 Summary	240
18.2 Vehicle Pressure and Acoustic Environment	240
18.2.1 External Surface Pressures	240
18.2.2 External Acoustics	243
18.2.3 S-IB Stage Internal Pressures	247
18.2.4 S-IB Stage Base Pressure	247
18.2.5 S-IB/S-IVB Interstage Environment	247
18.2.6 S-IVB Stage Pressure Differential	247
18.3 Vehicle Thermal Environment	253
18.3.1 S-IB Stage Aerodynamic Heating	253
18.3.2 S-IVB Stage Aerodynamic Heating	253
18.3.3 APS and Forward and Aft Skirt Temperatures	256
18.3.4 S-IB Stage Base Thermal Environment	256
18.4 Instrument Unit Environmental Control Systems	265
18.4.1 Thermal Conditioning System	265
18.4.2 Gas Bearing Supply System	273
19.0 Aerodynamics	280
19.1 Summary	280
19.2 Fin Surface	280
19.3 Drag	280

TABLE OF CONTENTS (CONT)

	Page
20.0 Instrumentation	283
20.1 Summary	283
20.2 Vehicle Measuring Analysis	283
20.2.1 S-IB Stage Measuring Analysis	283
20.2.2 S-IVB Stage Measuring Analysis	285
20.2.3 IU Measuring Analysis	285
20.3 Airborne Telemetry Systems	285
20.3.1 S-IB Stage	285
20.3.2 S-IVB Stage	287
20.3.3 Instrument Unit	387
20.4 Airborne Tape Recorder	287
20.5 RF Systems Analysis	288
20.5.1 Telemetry	288
20.5.2 Tracking	290
20.6 Optical Instrumentation	293
20.6.1 Photographic Coverage	293
20.6.2 Film Analysis	293
21.0 Spacecraft	294
21.1 Summary	294
21.2 Spacecraft Performance	294
22.0 Summary of Malfunctions and Deviations	296
22.1 Summary	296
22.2 Systems Malfunctions and Deviations	296
A.0 Vehicle Description	298
A.1 Summary	298
A.2 S-IB Stage	298
A.2.1 S-IB Configuration	298
A.2.2 S-IB-4 Configuration Differences	301
A.3 S-IVB Stage	303
A.3.1 S-IVB Configuration	303
A.3.2 S-IVB-204 Configuration Differences	306
A.4 Instrument Unit	311
A.4.1 IU Configuration	311
A.4.2 S-IU-204 Configuration Differences	312
A.5 Payload	317
A.5.1 Lunar Module (LM)	317
A.5.2 Spacecraft Lunar Module Adapter (SLA)	320
A.5.3 Nose Cone	320
B.0 Atmospheric Summary	321
B.1 Introduction	321
B.2 General Atmospheric Conditions at Launch Time	321

TABLE OF CONTENTS (CONC)

	Page
B.3 Surface Observations at Launch Time	321
B.4 Upper Air Measurements	321
B.5 Thermodynamic Data	325
References	336
Approval	337
Distribution	338

LIST OF FIGURES

Figure		Page
5-1	Fuel Temperature/Density Relationship	22
6-1	Vehicle Mass, Center-of-Gravity, and Mass Moment of Inertia During S-IB Stage Powered Flight	35
6-2	Vehicle Mass, Center-of-Gravity, and Mass Moment of Inertia During S-IVB Powered Flight	36
7-1	S-IB and S-IVB Trajectory	42
7-2	Earth-Fixed Velocity	43
7-3	Total Inertial Acceleration	45
7-4	Mach Number and Dynamic Pressure	47
7-5	AS-204 Ground Track	50
8-1	S-IB Individual Engine and Stage Thrust Buildup	55
8-2	S-IB Stage Longitudinal Thrust and Specific Impulse	56
8-3	S-IB Stage Propellant Mixture Ratio and Flowrate	58
8-4	S-IB Stage LOX and Fuel Flowrates	60
8-5	Longitudinal Engine Thrust and LOX Density	62
8-6	S-IB Inboard and Outboard Engine Thrust Decay	66
8-7	Individual Engine Performance Parameters	67
8-8	Average Propellant Levels Above Theoretical Tank Bottom	72
8-9	Fuel Tank Ullage and Helium Sphere Pressure	73
8-10	LOX Pressurization System Characteristics	75
8-11	Control Supply Pressure	77
9-1	J-2 Fuel Turbine System and Thrust Chamber Jacket Temperatures	79
9-2	S-IVB Stage Start Transient	81
9-3	S-IVB Steady-State Operation (Engine Analysis)	84
9-4	S-IVB Propellant Flowrates	85
9-5	S-IVB Cutoff Transient	86
9-6	Second Flight Stage Best Estimate Masses	89
9-7	S-IVB-204 PU Valve Position History	91
9-8	S-IVB PU System LH ₂ and LOX Nonlinearities	94
9-9	LH ₂ Tank Pressurization Performance	96
9-10	LH ₂ Pump Conditions	98
9-11	LH ₂ and LOX Pump Inlet Start Requirements	99
9-12	LOX Tank Ullage Pressure	101
9-13	LOX Pump Conditions	103
9-14	Stage Pneumatic Control and Purge System Performance	105
9-15	J-2 Start Bottle Performance	106
9-16	LH ₂ and LOX Tank Ullage Performance in Orbit	110
9-17	Cold Helium Dump Performance	111
9-18	LOX Dump Performance	113
9-19	S-IVB Stage Pneumatic Supply Pressure and LOX Turbine/Crossover Duct Temperatures	115
9-20	Engine Control Sphere Pressure During Dump Experiment	117

LIST OF FIGURES (CONT)

Figure		Page
10-1	APS Propellant Remaining and Temperatures	119
10-2	APS Propellant Use	121
10-3	APS Total Impulse	124
11-1	S-IB Hydraulic Oil Level, Pressure, and Temperature	126
11-2	S-IVB Hydraulic System Temperatures During Liftoff and Powered Flight	129
11-3	S-IVB Hydraulic System Temperatures During Orbital Coast	130
11-4	S-IVB Hydraulic Reservoir Oil Levels During Liftoff, Powered Flight, and Orbital Coast	131
12-1	Navigation, Guidance, and Control System Block Diagram	134
12-2	S-IB Stage Command Angles	139
12-3	Free Stream Angle-of-Attack	140
12-4	Attitude Error S-IB Powered Flight	141
12-5	Angular Rates S-IB Powered Flight	142
12-6	Control Acceleration S-IB Powered Flight	143
12-7	S-IB Average Actuator Position	145
12-8	Slosh During S-IB Powered Flight	146
12-9	S-IVB Stage Command Angles - Pitch	148
12-10	S-IVB Stage Command Angles - Yaw	149
12-11	Attitude Errors and APS Firings During S-IVB Powered Flight	150
12-12	Angular Rate Gyros During S-IVB Powered Flight	151
12-13	S-IVB Pitch and Yaw Actuator Position	152
12-14	LH ₂ Slosh During S-IVB Powered Flight	156
12-15	LOX Slosh During S-IVB Powered Flight	158
12-16	S-IVB Stage Command Angles Following S-IVB Cutoff	159
12-17	S-IVB Stage Command Angles During LM Separation	160
12-18	S-IVB Attitude Errors During LM Separation	161
12-19	S-IVB Angular Rate Gyros During LM Separation	162
12-20	S-IVB Attitude Errors During Maneuver to Retrograde Attitude	164
12-21	S-IVB Angular Rate Gyros During Maneuver to Retorgrade Attitude	165
12-22	S-IVB Stage Command Angles During Propellant Removal Test	166
12-23	S-IVB Attitude Errors and APS Firings During Propellant Removal Test	167
12-24	S-IVB Attitude Errors and APS Firings During Propellant Removal Test	168
12-25	S-IVB Angular Rate Gyros During Propellant Removal Test	169
12-26	S-IVB Actuator Position During Propellant Removal Test	170

LIST OF FIGURES (CONT)

Figure		Page
12-27	S-IVB Pitch, Yaw, Roll Gimbal Angles (Hawaii, Rev. 7)	171
12-28	S-IVB Composite Gimbal Angles (Hawaii, Rev. 7)	172
12-29	Roll Attitude Error and Roll Rate Gyro Output	175
12-30	Crossrange (Y) Component of Inertial Velocity	179
12-31	Yaw Offset and S-IVB Stage Cutoff Conditions	180
12-32	Guidance Velocity Differences (Trajectory Minus Measured)	183
12-33	Measured Velocity Change Orbital Events	187
13-1	S-IVB Ullage Motor Performance	192
13-2	Retrorocket Thrust	194
13-3	S-IB/S-IVB Relative Velocity and Longitudinal Acceleration	197
13-4	Lateral Accelerations During S-IB/S-IVB Separation	198
13-5	S-IB/S-IVB Separation Distance	199
14-1	S-IB Stage Current and Voltage	201
14-2	S-IVB Battery Current and Voltage	203
14-3	S-IVB Battery Temperatures	204
14-4	Instrument Unit Voltage, Current, and Temperature	207
17-1	Vehicle Longitudinal Force Distribution	215
17-2	Longitudinal Load (From Strain Data at Sta 23.9 m)	217
17-3	Vehicle Bending Moment	218
17-4	Vehicle Bending Modes	219
17-5	Vehicle Bending Amplitudes	220
17-6	Maximum Dynamic Response	223
17-7	Fin Bending and Torsion Modes	224
17-8	S-IB Structure Vibration Envelopes	226
17-9	S-IB Component Vibrations	227
17-10	S-IB Fin Vibration Envelopes	228
17-11	H-1 Engine Vibration Envelopes	229
17-12	S-IVB Vibration Envelopes	231
17-13	S-IVB Forward Skirt Dynamic Strain Measurements	233
17-14	Differential Pressure Across Panels	235
17-15	Time Slices of Dynamic Strain Output for Measurement S-92	236
17-16	S-IVB Forward Skirt Dynamic Strain and Sound Pressure Level	238
17-17	IU Vibration Envelopes	239
18-1	S-IB Stage Tank Surface Pressure Environment	241
18-2	Surface Pressure Environment on 60° Fairing	242
18-3	Vehicle Noise Environment at Liftoff	244
18-4	Overall Sound Pressure Level at Various Locations	245
18-5	Fluctuating Pressure Coefficient and Mach 1 Acoustic Spectra	246
18-6	S-IB Stage Internal and Base Pressures	248
18-7	S-IB Stage Base Pressures	249

LIST OF FIGURES (CONC)

Figure		Page
18-8	Flame Shield Pressure Environment	250
18-9	S-IB/S-IVB Interstage Pressure Environment	251
18-10	Forward and Aft Compartment Differential Pressures	252
18-11	Upper and Lower Tail Shroud Temperatures	254
18-12	S-IVB Stage Aerodynamic Heating Environment	255
18-13	Heat Shield Outer Region Thermal Environment	260
18-14	Heat Shield Inner Region Thermal Environment	261
18-15	Heat Shield Skin and Differential Temperatures	262
18-16	Flame Shield Thermal Environment	263
18-17	Flame Shield Access Chute Structural Temperatures	264
18-18	Outboard Engine Aspirator Environment	266
18-19	Inboard Engine Nozzle and Exhaust Duct Heating Rates	267
18-20	Environmental Control System Mechanical Diagram	268
18-21	Primary Mission Temperature Control Parameters	270
18-22	Sublimator Start-Up Parameters	271
18-23	TCS Verification Temperature Control Parameters	272
18-24	Water System Flowrate Operation During Start-Up	274
18-25	Predicted and Actual TCS GN ₂ Pressures	275
18-26	Gas Bearing Supply System Pressures	277
18-27	Gas Bearing Supply Pressures During Ascent	278
18-28	GBS Sphere Pressure and Predicted Usage Rates	279
19-1	Fin Differential Pressure Coefficients	281
19-2	Base Drag and Axial Force Coefficients	282
20-1	AS-204 RF System Coverage	289
20-2	Orbital Telemetry Coverage	291
20-3	Orbital Radar Coverage	292
A-1	AS-204 Configuration	299
A-2	S-IB Stage	300
A-3	S-IVB Stage	304
A-4	Instrument Unit Layout and Antenna Orientation	313
A-5	Instrument Unit Components Layout	314
A-6	AS-204 Payload	318
B-1	AS-204 Launch Time Scalar Wind Speed	326
B-2	AS-204 Launch Time Wind Direction	327
B-3	AS-204 Launch Time Pitch Wind Speed Component (W_x)	328
B-4	AS-204 Launch Time Yaw Wind Speed Component (W_z)	329
B-5	AS-204 Launch Time Pitch (S_x) and Yaw (S_z) Component Wind Shears	331
B-6	Relative Deviation of AS-204 Temperature and Density From PAFB (63) Reference Atmosphere	333
B-7	Relative Deviation of Pressure and Absolute Deviation of the Index of Refraction From the PAFB (63) Reference Atmosphere, AS-204	334

LIST OF TABLES

Table		Page
4-I	AS-204 Event Times Summary	7
4-II	AS-204 Sequence of Events	8
5-I	AS-204 Prelaunch Milestones	17
5-II	Countdown Summary	18
5-III	AS-204 S-IB Stage Propellant Weights at Ignition Command	23
5-IV	AS-204 S-IVB Stage Propellant Weights at S-IB Ignition Command	24
6-I	AS-204 Flight Sequence Mass Summary	28
6-II	Vehicle Masses	29
6-III	Mass Characteristics Comparison	37
7-I	Summary of C-Band Tracking	40
7-II	Insertion Conditions Data Utilization	40
7-III	Cutoff Conditions	44
7-IV	Significant Events	46
7-V	Thrust Decay Velocity Gain	41
7-VI	S-IVB Insertion Parameters	49
7-VII	S-IVB/LM Separation Parameters	49
7-VIII	Effects of S-IVB Orbital Safing Experiments	51
8-I	S-IB Stage Propulsion System Event Times	54
8-II	Engine Start Characteristics	53
8-III	S-IB Stage Inflight Performance Parameters	57
8-IV	Average S-IB Stage Sea Level Propulsion Parameters	61
8-V	Inflight Performance Deviations Analysis	63
8-VI	Velocity Deviation Analysis	64
8-VII	Time Deviation Analysis	65
8-VIII	AS-204 Average Individual Engine Performance at 30 Seconds	69
8-IX	Propellant Utilization	70
8-X	Cutoff Probe Activation Characteristics	71
9-I	Start Transient Performance	80
9-II	S-IVB Propulsion System Performance	83
9-III	S-IVB Cutoff Transient Performance	88
9-IV	S-IVB Propellant Mass History	90
9-V	PU System Deviations	92
9-VI	Stage Pneumatic Helium Usage	104
9-VII	Orbital Events Summary	108
10-I	AS-204 APS Propellant Use	120
11-I	S-IVB Hydraulic System Pressures	128
12-I	Maximum Control Parameters	138
12-II	S-IB Stage Separation Parameters	147
12-III	Maximum Values of Critical Flight Control Parameters	153
12-IV	APS Impulse Summary	155
12-V	LM Separation Parameters	157
12-VI	S-IB Actuator Maximum Performance Data	177

LIST OF TABLES (CONC)

Table		Page
12-VII	S-IB Actuator Maximum Parameters	177
12-VIII	Vehicle Attitudes During Orbital Guidance Maneuvers	182
12-IX	Guidance Inertial Platform Velocity Comparison	184
12-X	Navigation Comparison	186
13-I	Ullage Motor Performance	191
13-II	Retrorocket Performance	193
13-III	Separation Events	196
15-I	DCS Events	209
16-I	EDS/Switch Selector Events	211
16-II	EDS/Discrete Events	211
16-III	Thrust OK Switch Operating Times	212
17-I	Response Frequencies	221
17-II	S-IB Vibration Summary	225
17-III	S-IVB Vibration Summary	232
18-I	S-IVB 204 APS Component Temperatures (Module II)	257
18-II	S-IVB 204 Component Temperatures	258
20-I	Measurement Malfunctions	284
20-II	AS-204 Launch Vehicle Telemetry System Description	286
22-I	Summary of Malfunctions and Deviations	297
B-I	Surface Observations at AS-204 Launch Time	322
B-II	Solar Radiation (0.35 to 4.0 microns) At AS-204 Launch Time	323
B-III	Systems Used to Measure Upper Air Wind Data, AS-204	324
B-IV	Maximum Wind Speed in High Dynamic Pressure Region	330
B-V	Extreme Wind Shear in High Dynamic Pressure Region	332

ABBREVIATIONS

Abbreviation

APD	Adapter Positioning Device
ABS	Air Bearing Supply System
AS	Apollo-Saturn
AGC	Automatic Gain Control
AGCS	Automatic Ground Control Station
APS	Auxiliary Propulsion System
CG	Center-of-Gravity
CIF	Central Information Facility
CW	Clockwise
CM	Command Module
CSM	Command Service Module
CSP	Control Signal Processor
CCF	Converter Compressor Facility
CCW	Counterclockwise
CO	Cutoff
DOM	Data Output Multiplexer
DDAS	Digital Data Acquisition System
ELS	Earth Landing System
EST	Eastern Standard Time
ETR	Eastern Test Range
EPS	Electrical Power System
ESE	Electrical Support Equipment
EDS	Emergency Detection System
EMR	Engine Mixture Ratio
EMRC	Engine Mixture Ratio Change
ESC	Engine Start Command
ECS	Environmental Control System
ETW	Error Time Words
EBW	Exploding Bridge Wire
FRR	Flight Readiness Review
GFCV	GOX Flow Control Valve
GBI	Grand Bahama Island
GTI	Grand Turk Island
GSE	Ground Support Equipment
GRR	Guidance Reference Release
IECO	Inboard Engine Cutoff
IGM	Iterative Guidance Mode
LC	Launch Complex
LCC	Launch Control Center
LES	Launch Escape System
LET	Launch Escape Tower
LV	Launch Vehicle

ABBREVIATIONS (CONC)

Abbreviation

LVDA	Launch Vehicle Data Adapter
LVDA	Launch Vehicle Digital Computer
MOV	Main Oxidizer Valve
MILA	Merritt Island Launch Area
MI	Mineral Insulation
NPSP	Net Positive Suction Pressure
NC	Normally Closed
NO	Normally Open
OECO	Outboard Engine Cutoff
OASPL	Overall Sound Pressure Level
PACPS	Platform AC Power Supply
PSD	Power Spectral Density
PCD	Pressure Control Device
PTCS	Propellant Tanking Computer System
PU	Propellant Utilization
PCM	Pulse Code Modulation
PDM	Pulse Duration Modulation
RCS	Reaction Control System
RMR	Reference Mixture Ratio
RMRC	Reference Mixture Ratio Change
RDSM	Remote Digital Submultiplexer
RMS	Root Mean Square
SA	Saturn
SM	Service Module
SPS	Service Propulsion System
SSB	Single Side Band
SV	Space Vehicle
S/C or SC	Spacecraft
SCS	Spacecraft Control System
SLA	Spacecraft LEM Adapter
SMC	Steering Misalignment Correction Term
SCO	Sub Carrier Oscillators
SS	Switch Selector
TM	Telemetry
T/C	Thrust Chamber
F/M	Thrust/Mass
TOPS	Thrust OK Pressure Switches
UT	Universal Time
VCO	Voltage Controlled Oscillators
VSWR	Visual Standing Wave Ratio

CONVERSION FACTORS TO
INTERNATIONAL SYSTEM OF UNITS OF 1960

Parameter		Multiply	By	To Obtain
acceleration		ft/s ²	3.048×10^{-1} (exact)	m/s ²
area		in ²	6.4516×10^{-4} (exact)	m ²
barometer pressure		mbs	1.00×10^{-2} (exact)	N/cm ²
density		lbm/ft ³	1.6018463×10^1	kg/m ³
energy		Btu	1.0543503×10^3 (thermal chem.)	watt-s
flow rate	mass	lbm/s	4.5359237×10^{-1} (exact)	kg/s
	volume	gpm	$6.30901964 \times 10^{-5}$	m ³ /s
force		lbf	4.448221615	N (Newton)
heating rate		Btu/ft ² -s	1.1348931 (therm chem.)	watt/cm ²
impulse		lbf-s	4.448221615	N-s
length		ft	3.048×10^{-1} (exact)	m
		in	2.54×10^{-2} (exact)	m
mass		lbm	4.5359237×10^{-1} (exact)	kg
moment		lbf-ft	1.35581794	N-m
		lbf-in	$1.12984829 \times 10^{-1}$	N-m
moment of inertia		lbf-ft-s ²	1.35581794	kg-m ²
power		Btu/hr	2.9287508×10^{-4}	kw
pressure		lbf/in ²	$6.894757293 \times 10^{-1}$	N/cm ²
		lbf/ft ²	$4.788025898 \times 10^{-3}$	N/cm ²
specific weight		lbf/ft ³	1.570874638×10^2	N/m ³
temperature		°F+459.67	$5.555555556 \times 10^{-1}$	°K
		°C+273.15	1.00	°K
velocity		ft/s	3.048×10^{-1} (exact)	m/s
		knot*	$5.144444444 \times 10^{-1}$	m/s
volume		ft ³	$2.8316846592 \times 10^{-2}$ (exact)	m ³
		gallon**	$3.785411784 \times 10^{-3}$ (exact)	m ³

Note: $g_0 = 9.80665 \text{ m/s}^2$ (exact)

*knot (International)

**gallon (U.S. Liquid)

MPR-SAT-FE-68-2

RESULTS OF THE FOURTH LAUNCH VEHICLE TEST FLIGHT AS-204

1.0 FLIGHT TEST SUMMARY

Saturn IB Space Vehicle AS-204, fourth of the Saturn IB series vehicles, was launched at 1748:08 EST on January 22, 1968, and placed Apollo 5 (Lunar Module-1) in orbit. The flight test was the fourth in a series of Saturn IB R&D test flights. The primary objectives were: to verify operation and integrity of Lunar Module subsystems, to evaluate Lunar Module staging, and to evaluate S-IVB/IU orbital performance. Other important objectives were to evaluate: the S-IVB forward skirt inflight panel flutter, the J-2 engine crossover duct temperature, the S-IVB LH₂ and LOX propellant dumps, and the launch vehicle orbital coast lifetime capability.

AS-204 was launched from Launch Complex 37B at Cape Kennedy, Florida, after a total unexpected hold time of 3 hours and 48 minutes. The initial countdown plan scheduled one six hour hold, 3 hours and 30 minutes prior to scheduled liftoff. The unscheduled hold resulted from a freon flow problem in the spacecraft and occurred at 2 hours and 30 minutes prior to liftoff. During this hold an AGCS DDAS power supply problem was encountered. The spacecraft problem and the DDAS problem were corrected and the count was continuous until liftoff. AS-204 was launched from a launch azimuth of 90 degrees east of north. After launch the vehicle rolled into a flight azimuth of 72 degrees east of north.

The actual trajectory of AS-204 was very close to nominal. The total space-fixed velocity was 3.3 m/s lower than nominal at outboard engine cutoff and 0.7 m/s lower than nominal at S-IVB cutoff. At S-IVB cutoff the altitude was 0.23 km higher than nominal and the surface range was 30.99 km shorter than nominal. At S-IVB/IU/LM-1 separation the total space-fixed velocity was 0.9 m/s higher than nominal.

The S-IB stage propulsion system performed satisfactorily throughout flight. The stage thrust, mass loss rates, and specific impulse were 1.24%, 0.14%, and 1.10% higher than predicted, respectively, based upon flight simulation results. Inboard engine cutoff occurred 0.37 sec earlier than predicted, and outboard engine cutoff occurred 0.09 sec earlier than predicted, or 3.28 sec following inboard engine cutoff. Outboard engine cutoff resulted from LOX starvation of engines 1 and 2. All S-IB stage mechanical systems functioned satisfactorily.

The S-IVB stage propulsion system performance was satisfactory throughout flight. On the basis of flight simulation, the overall average S-IVB thrust, mass loss rate, and specific impulse were 1.38% higher, 1.66% higher, and 0.30% lower than predicted, respectively. The propellant utilization (PU)

system operated in the closed loop configuration on AS-204 and provided an average propellant mixture ratio of 5.5 to 1 during the high thrust period and 4.70 to 1 during the low thrust period. PU valve cutback occurred at 469.9 sec (325.0 sec after J-2 Start Command), 20.0 sec later than predicted. Propellant loading and utilization control by the PU system was satisfactory. The propellant load was within +0.41% LOX and -0.39% LH₂ of the desired load. Operation of the propellant pressurization systems and pneumatic systems was satisfactory. The LOX turbine inlet and painted crossover duct temperatures in orbit were very close to expected.

All portions of the orbital safing experiment were performed successfully, including propellant venting, propellant dump, cold helium dump, and stage and engine pneumatic supply dump. The stage pneumatic sphere pressure did not decrease to the expected level due to a higher than expected initial pressure. However, the rate and manner in which the sphere was vented were satisfactory.

The Auxiliary Propulsion System (APS) engines responded properly to commands given by the Instrument Unit. A 17 to 18 Hz oscillation on the roll rate signal for the first 80 sec following S-IB/S-IVB separation adversely affected the APS roll control, permitting a 2.3 deg maximum roll attitude error during that period. Nominal attitude error is 1 degree. By 6 hr: 16 min: 4 sec (22,600 sec), 55% of the available oxidizer and 57.5% of the available fuel were used.

In general, the performance of the guidance system was satisfactory. The cross range accelerometer exceeded a reasonableness test value prior to liftoff, resulting in a velocity bias error of 0.45 m/s throughout flight. A yaw offset of -1.5 deg developed at S-IVB ullage rocket ignition and remained throughout powered flight. Neither of these events significantly affected end conditions at S-IVB cutoff. Orbital maneuvers were executed as planned.

The control system functioned properly. The maximum values observed for the control parameters, near the maximum dynamic pressure region, were attitude errors of 1.8 deg in pitch, -1.1 deg in yaw, and -1.0 deg in roll; and angles-of-attack (calculated from FPS-16 radar data) of -2.5 deg in pitch and 1.5 deg in yaw. Control system transients at S-IB/S-IVB separation and during S-IVB flight were well within the capability of the system. After the first 60 sec of S-IVB flight, the APS system corrected for a constant roll torque which created an attitude error of approximately +0.5 degrees. During orbit, all transients were well within the capabilities of the control system.

S-IB/S-IVB separation was accomplished as planned and the sequence executed in the desired time period. The S-IVB engine cleared the interstage approximately 0.97 sec following the separation command. Separation transients were small and within the design requirement.

LV/LM-1 separation occurred at 3,235.24 seconds. Small transients were imparted to the S-IVB during separation, but were within design requirements.

The vehicle electrical systems performed satisfactorily throughout flight. The batteries on both the S-IVB stage and the Instrument Unit fulfilled all mission requirements.

The Digital Guidance Command System was active on AS-204; however, no guidance update commands were issued. Seven mode commands were issued during the third pass. The DCS and LVDC responded properly to the first mode word, but the data words were never sent.

Only the launch vehicle portion of the Emergency Detection System (EDS) was flown on AS-204. The EDS sensors and logic functioned properly, and all abort parameters remained below the abort limits.

Structural analysis of AS-204 indicates that all structural components performed satisfactorily. There were no structural loads of sufficiently high magnitude to threaten the structural integrity of the launch vehicle. The maximum bending moment, 25% of design bending moment, was experienced at 72.5 seconds. Overall vibration and acoustic levels were as expected. The S-IVB forward skirt panel dynamic strain measurements gave no indication of flutter on 12 of the 16 measurements. On the remaining measurements a complex periodic wave shape was observed between 80 and 87 sec that was characteristic of limited amplitude flutter, as expected. The measured composite strain signal was insignificant for AS-204 in both amplitude and duration.

The pressure and thermal environment of the AS-204 flight was in general agreement with predicted. Analysis of the Thermal Conditioning System indicated deviations in three performance parameters. These were low water flowrates during sublimator startup, low sublimator water inlet pressures, and excessive GN_2 consumption. The low water pressure and flowrates did not affect the performance of the Thermal Conditioning System as measured by system temperatures. The excessive GN_2 consumption has been attributed to leakage.

The Gas Bearing Supply System maintained temperature within specification. The differential pressure across the gas bearings was slightly higher than the specified value, but did not adversely affect the mission.

The measurement evaluation on AS-204 revealed that 99.08% of the 1196 measurements, active at liftoff, performed satisfactorily. A total of 12 measurements failed during flight. Performance of the RF system was generally satisfactory. However, the S-IVB stage PCM/FM transmitter output power indicated a sudden drop in output power at 18 min: 20 sec (1100 sec), dropping from 26.8 watts to 13.6 watts. The minimum requirement was 25 watts. FM/FM transmitter 3 output power was also below the required 25 watts minimum, but this transmitter output power was known to be low (24.9 watts) prior to launch.

Camera coverage was excellent. The reliability based on 96 engineering sequential cameras was 92.7%, with 7 malfunctions.

2.0 INTRODUCTION

This report presents the results of the early engineering evaluation of AS-204, the fourth Saturn IB vehicle flight-tested. The evaluation is centered on the performance of the major vehicle systems, with special emphasis on malfunctions and deviations.

This report is published by the Saturn Flight Evaluation Working Group--composed of representatives of Marshall Space Flight Center, John F. Kennedy Space Center, and MSFC's prime contractors--and in cooperation with the Manned Spacecraft Center. Significant contributions to the evaluation have been made by:

George C. Marshall Space Flight Center

Research and Development Operations

Aero-Astrodynamics Laboratory

Astrionics Laboratory

Computation Laboratory

Propulsion and Vehicle Engineering Laboratory

Industrial Operations

John F. Kennedy Space Center

Manned Spacecraft Center

Chrysler Corporation Space Division

Douglas Aircraft Company

International Business Machines Corporation

Rocketdyne Division of North American Rockwell

The official MSFC position at this time is represented by this report. It will not be followed by a similar report unless continued analysis or new evidence should prove the conclusions presented herein to be significantly incorrect. Final stage evaluation reports will, however, be published by the stage contractors. Reports covering major subjects and special subjects will be published as required.

3.0 TEST OBJECTIVES

3.1 PRIMARY TEST OBJECTIVES

All primary test objectives were achieved and were as follows:

1. Verify operation or integrity of the following Lunar Module (LM) subsystems:

- (a) Ascent Propulsion System (APS) - Including Restart
- (b) Descent Propulsion System (DPS) - Including Restart
- (c) Structure

2. Evaluate LM Staging.

3. Evaluate S-IVB/IU orbital performance. Specifically:

(a) Evaluate the launch vehicle attitude control system operation and maneuvering capability.

(b) Verify the S-IVB LH₂ and LOX tank pressure rise rates.

(c) Demonstrate nose cone separation from the S-IVB/IU/SLA.

(d) Evaluate the operational adequacy of the launch vehicle systems; including guidance and control, electrical, mechanical, and instrumentation.

3.2 SECONDARY TEST OBJECTIVES

All secondary test objectives were achieved and were as follows:

- 1. Evaluate S-IVB forward skirt in-flight panel flutter.
- 2. Evaluate J-2 engine crossover duct temperature experiment.
- 3. Evaluate S-IVB LH₂ and LOX propellant dump experiment.
- 4. Evaluate launch vehicle orbital coast life time capability.

4.0 TIMES OF EVENTS

4.1 SUMMARY

Table 4-I presents a summary of event times, obtained from the performance analysis of launch vehicle AS-204. Event times generally were quite close to predicted. The most significant deviations from predicted shown in the table are engine mixture ratio shift and cutoff of the S-IVB stage. Causes of these time deviations are discussed in detail in Section 9.0 of this report.

4.2 SEQUENCE OF EVENTS

Range zero was 22:48:08 UT and liftoff occurred 0.36 sec later or at 22:48:08.36 UT. Guidance Reference Release (GRR) would be expected at -4.84 sec range time (time from range zero). Guidance Reference Release actually occurred at -4.96 seconds. First motion of the vehicle occurred at 0.20 sec range time.

Switch selectors in the S-IB stage, S-IVB stage, and Instrument Unit provided programmed event sequencing for the vehicle. The Launch Vehicle Digital Computer (LVDC) provided programmed input to the appropriate switch selector. If a switch selector malfunction had occurred, a complement address would have been sent to the switch selector, thereby providing redundancy. The analysis indicated that no output resulted from complement addresses to the switch selector; hence, the operation was normal.

Table 4-II lists the switch selector event times. The nominal time bases in range time were established as follows:

Liftoff (Time Base 1) = 0.36 sec

Start of Time Base 2 = 135.91 sec

Outboard Engine Cutoff (Time Base 3) = 142.25 sec

S-IVB Engine Cutoff (Guidance) +0.2 sec (Time Base 4) = 593.56 sec

TABLE 4-I
AS-204 EVENT TIMES SUMMARY

Event	Range Time (sec)	
	Actual	Act-Pred
First Motion	0.20	-
Liftoff	0.36	-
Start Pitch	9.70	-0.66
Start Roll	10.67	0.31
End Roll	28.67	0.31
Enable Engines EDS Cutoff	60.31	-0.05
Stop Pitch	133.50	0.14
Low Level Sense (LLS)	135.91	-0.33
IECO	138.97	-0.37
OECO	142.25	-0.09
S-IB/S-IVB Separation	143.50	-0.14
S-IVB Start Command	144.90	-0.14
Start IGM	159.48	0.14
Engine Mixture Ratio Change Detected (Guidance Computer)	502.83	26.88
S-IVB Cutoff (Guidance Signal)	593.35	-5.00
LM Separation	3235.24	0.04

TABLE 4-11
AS-204 SEQUENCE OF EVENTS

Function	Stage	Time From Base (sec)		Range Time (sec)		
		Actual	Predicted	Actual	Predicted	Act-Pred
Guidance Reference Release (GRR)	*	-5.32	-5.20	-4.96	-	-
Initiate S-IB Mainstage Ignition Sequence	*	-3.33	-3.30	-2.97	-	-
First Motion	*	-0.16	-0.20	0.20	-	-
<u>Liftoff - Start of Time Base 1 (T₁)</u>		0.0	0.0	0.36	-	-
Multiple Engine Cutoff Enable	S-IB	9.95	10.0	10.31	10.36	-0.05
Initiate Pitch Maneuver	*	9.34	10.0	9.70	10.36	-0.66
Initiate Roll Maneuver	*	10.31	10.0	10.67	10.36	0.31
Telemeter Calibration On	S-IB	19.95	20.0	20.31	20.36	-0.05
Telemeter Calibration Off	S-IB	24.97	25.0	25.33	25.36	-0.03
Telemetry Calibrator In-Flight Calibrate On	IU	26.95	27.0	27.31	27.36	-0.05
End Roll	IU	-	-	28.67	28.36	0.31
LOX Tank Relief Control Valve Enable	S-IB	29.76	29.8	30.12	30.16	-0.04
Telemetry Calibrator In-Flight Calibrate Off	IU	31.95	32.0	32.31	32.36	-0.05
Tape Recorder Record On	S-IB	38.95	39.0	39.31	39.36	-0.05
Flight Control Computer Switch Point 1	IU	39.95	40.0	40.31	40.36	-0.05
Launch Vehicle Engines EDS Cutoff Enable	IU	59.95	60.0	60.31	60.36	-0.05
Maximum Dynamic Pressure (Max Q)	*	-	-	71.50	74.16	-2.66
Telemetry Calibrator In-Flight Calibrate On	IU	90.15	90.2	90.51	90.56	-0.05
Telemetry Calibrator In-Flight Calibrate Off	IU	95.15	95.2	95.51	95.56	-0.05
Flight Control Computer Switch Point 2	IU	99.97	100.0	100.33	100.36	-0.03
Telemeter Calibration On	S-IB	119.75	119.8	120.11	120.16	-0.05
Flight Control Computer Switch Point 3	IU	119.96	120.0	120.32	120.36	-0.04
Control Accelerometer Power Off	IU	120.17	120.2	120.53	120.56	-0.03
Telemeter Calibration Off	S-IB	124.85	124.9	125.21	125.26	-0.05
Special TM Calibration On	S-IVB	125.05	125.1	125.41	125.46	-0.05
Regular TM Calibration On	S-IVB	125.26	125.3	125.62	125.66	-0.04
Regular TM Calibration Off	S-IVB	130.26	130.3	130.62	130.66	-0.04
Special TM Calibration Off	S-IVB	130.47	130.5	130.83	130.86	-0.03
Excessive Rate (P,Y,R) Auto-Abort Inhibit Enable	IU	131.46	131.5	131.82	131.86	-0.04
Excessive Rate (P,Y,R) Auto-Abort Inhibit	IU	131.67	131.7	132.03	132.06	-0.03
S-IB Two Engines Out Auto-Abort Inhibit Enable	IU	131.85	131.9	132.21	132.26	-0.05
S-IB Two Engines Out Auto-Abort Inhibit	IU	132.06	132.1	132.42	132.46	-0.04
Propellant Level Sensors Enable	S-IB	132.27	132.3	132.63	132.66	-0.03
Tilt Arrest	*	-	-	133.50	133.36	0.14
<u>Start Of Time Base 2 (T₂)</u>	S-IB	0.0	0.0	135.91	136.24	-0.33
Tape Recorder Record On	IU	0.16	0.2	136.07	136.44	-0.37

*Not Switch Selector Event

TABLE 4-II (CONT)

Function	Stage	Time From Base (sec)		Range Time (sec)		
		Actual	Predicted	Actual	Predicted	Act-Pred
Fast Record On	S-IVB	0.35	0.4	136.26	136.64	-0.38
Inboard Engines Cutoff	S-IB	3.06	3.1	138.97	139.34	-0.37
Auto-Abort Enable Relays Reset	IU	3.27	3.3	139.18	139.54	-0.36
Charge Ullage Ignition EBW Firing Units	S-IVB	3.97	4.0	139.88	140.24	-0.36
Prevalves Open	S-IVB	4.35	4.4	140.26	140.64	-0.38
LOX Depletion Cutoff Enable	S-IB	4.56	4.6	140.47	140.84	-0.37
Fuel Depletion Cutoff Enable	S-IB	5.55	5.6	141.46	141.84	-0.38
<u>Outboard Engines Cutoff Signal - Time Base 3 (T3)</u>	S-IB	0.0	0.0	142.25	142.34	-0.09
Engine Cutoff Signal Off	S-IVB	0.37	0.4	142.62	142.74	-0.12
Ullage Rockets Ignition	S-IVB	1.05	1.1	143.30	143.44	-0.14
S-IB/S-IVB Separation	S-IB	1.25	1.3	143.50	143.64	-0.14
Flight Control Computer S-IVB Burn Mode on "B"	IU	1.35	1.4	143.60	143.74	-0.14
Flight Control Computer S-IVB Burn Mode On "A"; S-IVB Engine Out Indication "B" Enable	IU	1.45	1.5	**143.70	143.84	-0.14
Engine Ready Bypass On	S-IVB	1.65	1.7	**143.90	144.04	-0.14
LH ₂ Chilldown Pump Off	S-IVB	2.06	2.1	144.31	144.44	-0.13
LOX Chilldown Pump Off	S-IVB	2.27	2.3	144.52	144.64	-0.12
Engine Ignition Sequence Start	S-IVB	2.65	2.7	144.90	145.04	-0.14
Engine Ignition Sequence Start Relay Reset	S-IVB	3.15	3.2	**145.40	145.54	-0.14
LOX Tank Flight Pressurization Switch Enable	S-IVB	3.45	3.5	**145.70	145.84	-0.14
Fuel Injection Temperature OK Bypass	S-IVB	3.65	3.7	**145.90	146.04	-0.14
S-IVB Engine Out Indication "A" Enable	IU	3.86	3.9	146.11	146.24	-0.13
LH ₂ Tank Pressurization Control Switch Enable	S-IVB	5.26	5.3	147.51	147.64	-0.13
90% J-2 Thrust Level	*	-	-	148.39	148.34	0.05
PU System Activate	S-IVB	8.66	8.7	150.91	151.04	-0.13
Emergency Playback Enable	S-IVB	9.65	9.7	151.90	152.04	-0.14
Fast Record Off	S-IVB	9.75	9.8	152.00	152.14	-0.14
Charge Ullage Jettison EBW Firing Units	S-IVB	10.16	10.2	152.41	152.54	-0.13
Ullage Rockets Jettison	S-IVB	13.27	13.3	155.52	155.64	-0.12
Fuel Injection Temperature OK Bypass Reset	S-IVB	13.65	13.7	155.90	156.04	-0.14
Command Active Guidance Initiation	*	-	-	159.48	159.34	0.14
Tape Recorder Record Off	IU	18.95	19.0	161.20	161.34	-0.14
Ullage EBW Firing Units Charge Relays Reset	S-IVB	19.25	19.3	161.50	161.64	-0.14
Ullage Rockets Ignition and Jettison Relays Reset	S-IVB	19.45	19.5	161.70	161.84	-0.14
Telemetry Calibrator In-Flight Calibrate On	IU	28.75	28.8	171.00	171.14	-0.14

*Not Switch Selector Event

**Data Dropout, Computed Values Used

TABLE 4-II (CONT)

Function	Stage	Time From Base (sec)		Range Time (sec)		
		Actual	Predicted	Actual	Predicted	Act-Pred
Telemetry Calibrator In-Flight Calibrate Off	IU	33.77	33.8	176.02	176.14	-0.12
Water Coolant Valve Open	IU	37.65	37.7	179.90	180.04	-0.14
Flight Control Computer Switch Point 4	IU	143.66	143.7	285.91	286.04	-0.13
Telemetry Calibrator In-Flight Calibrate On	IU	207.65	207.7	349.90	350.04	-0.14
Regular TM Calibration On	S-IVB	208.67	208.7	350.92	351.04	-0.12
Telemetry Calibrator In-Flight Calibrate Off	IU	212.67	212.7	354.92	355.04	-0.12
Regular TM Calibration Off	S-IVB	213.65	213.7	355.90	356.04	-0.14
LH ₂ Tank Pressurization Control Switch Disable	S-IVB	302.85	302.9	445.10	445.24	-0.14
EMR Shift Sensed By IGM	*	-	-	502.83	475.95	26.88
Telemetry Calibrator In-Flight Calibrate On	IU	358.77	358.8	501.02	501.14	-0.12
Telemetry Calibrator In-Flight Calibrate Off	IU	363.75	363.8	506.00	506.14	-0.14
Childdown Shutoff Valves Close	S-IVB	425.35	425.4	567.60	567.74	-0.14
Emergency Playback Inhibit	S-IVB	440.35	440.4	582.60	582.74	-0.14
Propellant Depletion Cutoff Arm	S-IVB	***	457.1	***	599.44	***
Guidance Cutoff Signal	*	-	-	593.35	598.35	-5.00
<u>Start Time Base 4 (T₄)</u>	S-IVB	0.0	0.0	593.56	598.55	-4.99
LOX Tank Vent Valve Open	S-IVB	0.20	0.2	593.76	598.75	-4.99
LH ₂ Tank Vent Valve Open	S-IVB	0.37	0.4	593.93	598.95	-5.02
LOX Tank Pressurization Shutoff Valves Close	S-IVB	0.75	0.8	594.31	599.35	-5.04
Prevalves Close	S-IVB	0.96	1.0	594.52	599.55	-5.03
LOX Tank Flight Pressurization Switch Disable	S-IVB	1.17	1.2	594.73	599.75	-5.02
LOX Childdown Pump Purge Off	S-IVB	1.55	1.6	595.11	600.15	-5.04
Propellant Depletion Cutoff Disarm	S-IVB	1.76	1.8	595.32	600.35	-5.03
PU System Deactivate	S-IVB	3.06	3.1	596.62	601.65	-5.03
PU Inverter & DC Power Off	S-IVB	3.25	3.3	596.81	601.85	-5.04
Flight Control Computer S-IVB Burn Mode Off "B"	IU	3.37	3.4	596.93	601.95	-5.02
Flight Control Computer S-IVB Burn Mode Off "A"	IU	3.46	3.5	597.02	602.05	-5.03
Auxiliary Hydraulic Pump Flight Mode Off	S-IVB	3.67	3.7	597.23	602.25	-5.02
Tape Recorder Playback Reverse On	IU	3.85	3.9	597.41	602.45	-5.04
Emergency Playback Enable	S-IVB	4.06	4.1	597.62	602.65	-5.03
Orbital Insertion (S-IVB Cutoff Sig. + 10 sec)	*	-	-	603.35	608.35	-5.00
Emergency Playback Inhibit	S-IVB	29.85	29.9	623.41	628.45	-5.04
Tape Recorder Playback Reverse Off	IU	31.95	32.0	625.51	630.55	-5.04
LOX Tank Vent Valve Close	S-IVB	40.15	40.2	633.71	638.75	-5.04
LOX Tank Vent Valve Boost Close On	S-IVB	43.15	43.2	636.71	641.75	-5.04

*Not Switch Selector Event

***Not Issued Because Of Early S-IVB Cutoff

TABLE 4-II (CONT)

Function	Stage	Time From Base (sec)		Range Time (sec)		
		Actual	Predicted	Actual	Predicted	Act-Pred
Nose Cone/SLA Separation Sequence Start "A"	IU	44.95	45.0	638.51	643.55	-5.04
Nose Cone/SLA Separation Sequence Start "B"	IU	45.15	45.2	638.71	643.75	-5.04
LOX Tank Vent Valve Boost Close Off	S-IVB	45.35	45.4	638.91	643.95	-5.04
Telemetry Calibrator In-Flight Calibrate On	IU	50.25	50.3	643.81	648.85	-5.04
Telemetry Calibrator In-Flight Calibrate Off	IU	55.25	55.3	648.81	653.85	-5.04
Nose Cone/SLA Separation Sequence Start Reset	IU	55.45	55.5	**649.01	654.05	-5.04
Chiltdown Shutoff Valves Open	S-IVB	60.25	60.3	653.81	658.85	-5.04
Prevalves Open	S-IVB	60.45	60.5	654.01	659.05	-5.04
Slow Record On	S-IVB	99.66	99.7	693.22	698.25	-5.03
Slow Record On	S-IVB	109.65	109.7	703.21	708.25	-5.04
AZUSA Transponder Power Off	IU	299.95	300.0	**893.51	898.55	-5.04
SLA Panel Deployment A	IU	599.95	600.0	1193.51	1198.55	-5.04
SLA Panel Deployment B	IU	600.15	600.2	1193.71	1198.75	-5.04
SLA Panel Deployment A****	IU	679.56	-	1273.12	-	-
SLA Panel Deployment B****	IU	680.43	-	1273.99	-	-
LH ₂ Tank Vent Valve Close	S-IVB	1260.37	1260.4	**1853.93	1858.95	-5.02
LH ₂ Tank Vent Valve Boost Close On	S-IVB	1263.37	1263.4	**1856.93	1861.95	-5.02
LH ₂ Tank Vent Valve Boost Close Off	S-IVB	1265.37	1265.4	**1858.93	1863.95	-5.02
Slow Record On	S-IVB	1699.65	1699.7	2293.21	2298.25	-5.04
Slow Record Off	S-IVB	1731.65	1731.7	2325.21	2330.25	-5.04
Recorder Playback On	S-IVB	1731.85	1731.9	2325.41	2330.45	-5.04
Recorder Playback Off	S-IVB	1943.85	1943.9	2537.41	2542.45	-5.04
Slow Record On	S-IVB	1944.05	1944.1	2537.61	2542.65	-5.04
Slow Record On	S-IVB	1954.05	1954.1	2547.61	2552.64	-5.04
Telemetry Calibrator In-Flight Calibrate On	IU	2624.64	2624.7	3218.20	3223.25	-5.05
Special TM Calibration On	S-IVB	2624.84	2624.9	3218.40	3223.45	-5.05
Regular TM Calibration On	S-IVB	2625.05	2625.1	3218.61	3223.65	-5.04
Telemetry Calibrator In-Flight Calibrate Off	IU	2629.65	2629.7	3223.21	3228.25	-5.04
Regular TM Calibration Off	S-IVB	2630.05	2630.1	3223.61	3228.65	-5.04
Special TM Calibration Off	S-IVB	2630.25	2630.3	3223.81	3228.85	-5.04
LM Separation	*	-	-	3235.24	3235.20	0.04
Slow Record On	S-IVB	2719.66	2719.7	3313.22	3318.25	-5.03
LH ₂ Tank Vent Valve Open	S-IVB	2804.95	2805.0	3398.51	3403.55	-5.04
Temperature Control Sensor Bias On	IU	3722.15	3722.2	**4315.71	4320.75	-5.04
Cooling System Electronic Assembly Power Off	IU	3822.15	3822.2	**4415.71	4420.75	-5.04

*Not Switch Selector Event

**Computed Values Used

****This Command Was In The Generalized Switch Selector Program For Ground Control Use Through The Digital Command System

TABLE 4-II (CONT)

Function	Stage	Time From Base (sec)		Range Time (sec)		
		Actual	Predicted	Actual	Predicted	Act-Pred
LH ₂ Tank Vent Valve Close	S-IVB	4004.95	4005.0	**4598.51	4603.55	-5.04
LH ₂ Tank Vent Valve Boost Close On	S-IVB	4007.95	4008.0	**4601.51	4606.55	-5.04
LH ₂ Tank Vent Valve Boost Close Off	S-IVB	4009.95	4010.0	**4603.51	4608.55	-5.04
Telemetry Calibrator In-Flight Calibrate On	IU	4754.65	4754.7	**5348.21	5353.25	-5.04
Special TM Calibration On	S-IVB	4754.85	4754.9	**5348.41	5353.45	-5.04
Regular TM Calibration On	S-IVB	4755.05	4755.1	**5348.61	5353.65	-5.04
Telemetry Calibrator In-Flight Calibrate Off	IU	4759.65	4759.7	**5353.21	5358.25	-5.04
Regular TM Calibration Off	S-IVB	4760.05	4760.1	**5353.61	5358.65	-5.04
Special TM Calibration Off	S-IVB	4760.25	4760.3	**5353.81	5358.85	-5.04
Slow Record On	S-IVB	4760.65	4760.7	**5354.21	5359.25	-5.04
Slow Record Off	S-IVB	4790.65	4790.7	**5384.21	5389.25	-5.04
Recorder Playback On	S-IVB	4790.85	4790.9	**5384.41	5389.45	-5.04
Recorder Playback Off	S-IVB	5146.65	5146.7	5740.21	5745.25	-5.04
Slow Record On	S-IVB	5146.85	5146.9	5740.41	5745.45	-5.04
Slow Record On	S-IVB	5156.85	5156.9	5750.41	5755.45	-5.04
Passivation Enable	S-IVB	5221.15	5221.2	5814.71	5819.75	-5.04
LH ₂ Tank Vent Valve Open	S-IVB	5549.95	5550.0	6143.51	6148.55	-5.04
Telemetry Calibrator In-Flight Calibrate On	IU	5695.65	5695.7	**6289.21	6294.25	-5.04
Special TM Calibration On	S-IVB	5695.85	5695.9	6289.41	6294.45	-5.04
Regular TM Calibration On	S-IVB	5696.05	5696.1	6289.61	6294.65	-5.04
Telemetry Calibrator In-Flight Calibrate Off	IU	5700.65	5700.7	6294.21	6299.25	-5.04
Regular TM Calibration Off	S-IVB	5701.05	5701.1	6294.61	6299.65	-5.04
Special TM Calibration Off	S-IVB	5701.25	5701.3	6294.81	6299.85	-5.04
Auxiliary Hydraulic Pump Coast Mode On	S-IVB	5779.95	5780.0	**6373.51	6378.55	-5.04
LH ₂ Tank Vent Valve Close	S-IVB	6149.95	6150.0	6743.51	6748.55	-5.04
LH ₂ Tank Vent Valve Boost Close On	S-IVB	6152.95	6153.0	6746.51	6751.55	-5.04
LH ₂ Tank Vent Valve Boost Close Off	S-IVB	6154.95	6155.0	6748.51	6753.55	-5.04
Slow Record On	S-IVB	7241.66	7241.7	7835.22	7840.25	-5.03
Slow Record Off	S-IVB	7273.66	7273.7	7867.22	7872.25	-5.03
Recorder Playback On	S-IVB	7273.86	7273.9	7867.42	7872.45	-5.03
Recorder Playback Off	S-IVB	7541.85	7541.9	8135.41	8140.45	-5.04
Slow Record On	S-IVB	7542.05	7542.1	8135.61	8140.65	-5.04
Slow Record On	S-IVB	7552.05	7552.1	8145.61	8150.65	-5.04
Auxiliary Hydraulic Pump Flight Mode On	S-IVB	8174.75	8174.8	8768.31	8773.35	-5.04
Flight Control Computer S-IVB Burn Mode On "A"	IU	8180.05	8180.1	8773.61	8778.65	-5.04

**Computed Values Used

TABLE 4-II (CONT)

Function	Stage	Time From Base (sec)		Range Time (sec)		
		Actual	Predicted	Actual	Predicted	Act-Pred
Flight Control Computer S-IVB Burn Mode On "B"	IU	8180.25	8180.3	8773.81	8778.85	-5.04
Engine Mainstage Control Valve Open On	S-IVB	8180.75	8180.8	8774.31	8779.35	-5.04
Engine Helium Control Valve Open On	S-IVB	8180.95	8181.0	8774.51	8779.55	-5.04
Telemetry Calibrator In-Flight Calibrate On	IU	8209.65	8209.7	8803.21	8808.25	-5.04
Special TM Calibration On	S-IVB	8209.85	8209.9	8803.41	8808.45	-5.04
Regular TM Calibration On	S-IVB	8210.05	8210.1	8803.61	8808.65	-5.04
Telemetry Calibrator In-Flight Calibrator Off	IU	8214.65	8214.7	8808.21	8813.25	-5.04
Regular TM Calibration Off	S-IVB	8215.05	8215.1	8808.61	8813.65	-5.04
Special TM Calibration Off	S-IVB	8215.25	8215.3	8808.81	8813.85	-5.04
Slow Record On	S-IVB	8217.65	8217.7	8811.21	8816.25	-5.04
Flight Control Computer S-IVB Burn Mode Off "A"	IU	8261.95	8262.0	8855.51	8860.55	-5.04
Flight Control Computer S-IVB Burn Mode Off "B"	IU	8262.15	8262.2	8855.71	8860.75	-5.04
Engine Mainstage Control Valve Open Off	S-IVB	8300.95	8301.0	8894.51	8899.55	-5.04
Engine Helium Control Valve Open Off	S-IVB	8301.95	8302.0	8895.51	8900.55	-5.04
Engine Ignition Phase Control Valve Open	S-IVB	8310.75	8310.8	8904.31	8909.35	-5.04
Engine Helium Control Valve Open On	S-IVB	8310.95	8311.0	8904.51	8909.55	-5.04
Engine Ignition Phase Control Valve Closed	S-IVB	8490.95	8491.0	9084.51	9089.55	-5.04
Engine Helium Control Valve Open Off	S-IVB	8491.95	8492.0	9085.51	9090.55	-5.04
Auxiliary Hydraulic Pump Coast Mode On	S-IVB	8494.45	8494.5	9088.01	9093.05	-5.04
Auxiliary Hydraulic Pump Flight Mode Off	S-IVB	8494.65	8494.7	9088.21	9093.25	-5.04
LH ₂ Tank Vent Valve Open	S-IVB	8500.75	8500.8	9094.31	9099.35	-5.04
LOX Tank Vent Valve Open	S-IVB	8500.95	8501.0	9094.51	9099.55	-5.04
Water Coolant Valve Open	IU	8836.94	Variable	9430.50	Variable	-
Water Coolant Valve Close	IU	9137.44	Variable	9731.00	Variable	-
LOX Tank Pressurization Shutoff Valves Open	S-IVB	9755.95	9756.0	10349.51	10354.55	-5.04
Slow Record On	S-IVB	9758.66	9758.7	10352.22	10357.25	-5.03
Slow Record Off	S-IVB	9790.65	9790.7	10384.21	10389.25	-5.04
Recorder Playback On	S-IVB	9790.85	9790.9	10384.41	10389.45	-5.04
Recorder Playback Off	S-IVB	10072.85	10072.9	**10666.41	10671.45	-5.04
Slow Record On	S-IVB	10073.05	10073.1	**10666.61	10671.65	-5.04
Slow Record On	S-IVB	10083.05	10083.1	**10676.61	10681.65	-5.04
Telemetry Calibrator In-Flight Calibrate On	IU	10407.65	10407.7	**11001.21	11006.25	-5.04
Special TM Calibration On	S-IVB	10407.85	10407.9	**11001.41	11006.45	-5.04
Regular TM Calibration On	S-IVB	10408.05	10408.1	11001.61	11006.65	-5.04
Telemetry Calibrator In-Flight Calibrate Off	IU	10412.65	10412.7	11006.21	11011.25	-5.04

**Computed Values Used

TABLE 4-II (CONT)

Function	Stage	Time From Base (sec)		Range Time (sec)		
		Actual	Predicted	Actual	Predicted	Act-Pred
Regular TM Calibration Off	S-IVB	10413.05	10413.1	11006.61	11011.65	-5.04
Special TM Calibration Off	S-IVB	10413.25	10413.3	11006.81	11011.85	-5.04
Water Coolant Valve Close	IU	10634.10	Variable	11227.66	Variable	-
LOX Tank Pressurization Shutoff Valves Close	S-IVB	11057.55	11057.6	11651.11	11656.15	-5.04
LOX Tank Vent Valve Close	S-IVB	11057.75	11057.8	11651.31	11656.35	-5.04
LH ₂ Tank Vent Valve Close	S-IVB	11057.95	11058.0	11651.51	11656.55	-5.04
LOX Tank Vent Valve Boost Close On	S-IVB	11060.75	11060.8	11654.31	11659.35	-5.04
LH ₂ Tank Vent Valve Boost Close On	S-IVB	11060.95	11061.0	11654.51	11659.55	-5.04
LOX Tank Vent Valve Boost Close Off	S-IVB	11062.75	11062.8	11656.31	11661.35	-5.04
LH ₂ Tank Vent Valve Boost Close Off	S-IVB	11062.95	11063.0	11656.51	11661.55	-5.04
Telemetry Calibrator In-Flight Calibrate On	IU	11179.65	11179.7	11773.21	11778.25	-5.04
Special TM Calibration On	S-IVB	11179.85	11179.9	11773.41	11778.45	-5.04
Regular TM Calibration On	S-IVB	11180.05	11180.1	11773.61	11778.65	-5.04
Telemetry Calibrator In-Flight Calibrate Off	IU	11184.65	11184.7	11778.21	11783.25	-5.04
Regular TM Calibration Off	S-IVB	11185.05	11185.1	11778.61	11783.65	-5.04
Special TM Calibration Off	S-IVB	11185.25	11185.3	11778.81	11783.85	-5.04
Slow Record On	S-IVB	11921.65	11921.7	**12515.21	12520.25	-5.04
Slow Record Off	S-IVB	11953.65	11953.7	**12547.21	12552.25	-5.04
Recorder Playback On	S-IVB	11953.85	11953.9	**12547.41	12552.45	-5.04
Recorder Playback Off	S-IVB	12190.85	12190.9	12784.41	12789.45	-5.04
Slow Record On	S-IVB	12228.65	12228.7	12822.21	12827.25	-5.04
Slow Record On	S-IVB	12238.66	12238.7	12832.22	12837.25	-5.03
Water Coolant Valve Open	IU	13038.79	Variable	13632.35	Variable	-
Water Coolant Valve Close	IU	13343.44	Variable	13937.00	Variable	-
LH ₂ Tank Vent Valve Open	S-IVB	13662.95	13623.0	**14216.51	14221.55	-5.04
LOX Tank Vent Valve Open	S-IVB	13623.15	13623.2	**14216.71	14221.75	-5.04
Telemetry Calibrator In-Flight Calibrate On	IU	13785.65	13785.7	14379.21	14384.25	-5.04
Special TM Calibration On	S-IVB	13785.85	13785.9	14379.41	14384.45	-5.04
Regular TM Calibration On	S-IVB	13786.15	13786.2	14379.71	14384.75	-5.04
Telemetry Calibrator In-Flight Calibrate Off	IU	13790.65	13790.7	14384.21	14389.25	-5.04
Regular TM Calibration Off	S-IVB	13791.15	13791.2	14384.71	14389.75	-5.04
Special TM Calibration Off	S-IVB	13791.35	13791.4	14384.91	14389.95	-5.04
Slow Record On	S-IVB	13797.65	13797.7	14391.21	14396.25	-5.04
Water Coolant Valve Open	IU	15146.94	Variable	15740.50	Variable	-
Slow Record On	S-IVB	15306.65	15306.7	15900.21	15905.25	-5.04

**Computed Values Used

TABLE 4-II (CONC)

Function	Stage	Time From Base (sec)		Range Time (sec)		
		Actual	Predicted	Actual	Predicted	Act-Pred
Slow Record Off	S-IVB	15338.65	15338.7	15932.21	15937.25	-5.04
Recorder Playback On	S-IVB	15338.85	15338.9	15932.41	15937.45	-5.04
Loss of S-IVB/IU Attitude Control	*	-	-	37235.00	16200.20	21034.80
Water Coolant Valve Close	IU	15743.98	Variable	16337.54	Variable	-
Recorder Playback Off	S-IVB	15750.85	15750.9	16344.41	16349.45	-5.04
Slow Record On	S-IVB	15751.05	15751.1	16344.61	16349.65	-5.04
LH ₂ Tank Vent Valve Close	S-IVB	16386.95	16387.0	16980.51	16985.55	-5.04
LOX Tank Vent Valve Close	S-IVB	16387.15	16387.2	16980.71	16985.75	-5.04
LH ₂ Tank Vent Valve Boost Close On	S-IVB	16389.95	16390.0	16983.51	16988.55	-5.04
LOX Tank Vent Valve Boost Close On	S-IVB	16390.15	16390.2	16983.71	16988.75	-5.04
LH ₂ Tank Vent Valve Boost Close Off	S-IVB	16391.95	16392.0	16985.51	16990.55	-5.04
LOX Tank Vent Valve Boost Close Off	S-IVB	16392.15	16392.2	16985.71	16990.75	-5.04
Open Helium Control Vent	S-IVB	16392.35	16392.4	16985.91	16990.95	-5.04
Water Coolant Valve Open	IU	16645.45	Variable	17239.01	Variable	-
Close Helium Control Vent	S-IVB	16692.35	16692.4	**17285.91	17290.95	-5.04
Water Coolant Valve Close	IU	21755.03	Variable	22348.59	Variable	-
Passivation Disable (This Command Was In The Generalized Switch Selector Program For Ground Control Use Through The DCS Command.)	S-IVB		N/A			

*Not Switch Selector Event

**Computed Values Used

5.0 LAUNCH OPERATIONS

5.1 SUMMARY

Apollo/Saturn vehicle AS-204, the fourth vehicle to be flown in the Saturn IB series, was launched from Launch Complex 37, Pad B, at Cape Kennedy. Launch weather conditions were favorable at the launch site; the winds were light from the north, and visibility was greater than 16 km (10 mi), although there were high scattered clouds.

The final countdown was picked up at T-22 hours at 1000 EST on January 21, 1968. The countdown proceeded without significant problems until a hold was called at T-2 hours and 30 minutes (1130 EST) due to a freon flow problem affecting the spacecraft. During this hold a power supply problem was encountered in the Digital Data Acquisition System (DDAS) of the Automatic Ground Control Station (AGCS). Total hold time was 3 hours and 48 minutes. The countdown was resumed at 1518 EST, and launch occurred at 1748:08 EST.

In general, the ground systems performance was satisfactory with the exception of the two items mentioned above. The launch control measurements indicated nominal operation of the vehicle and support systems. Following the launch, an assessment indicated that damage to the facility was less than anticipated.

5.2 PRELAUNCH MILESTONES

After January 27, 1967 the launch vehicle was redesignated to launch an unmanned Lunar Module, reconfigured to accomplish that mission, and moved from Launch Complex 34 to Launch Complex 37, Pad B. A chronological summary of events and preparations leading to the launch of the AS-204/LM-1 is shown in Table 5-I.

5.3 COUNTDOWN

The AS-204 final count was picked up at T-22 hours at 1000 EST on January 21, 1968. A planned six (6) hour hold occurred at T-3 hours and 30 minutes (0430 EST) on January 22, 1968. The hold was to allow for crew rest and for unscheduled work. The test configuration and the procedural setup required most of the crew to remain at their stations or perform work throughout the hold. During the hold, one of the Eastern Test Range (ETR) Impact Predictor computer systems failed and could not be restored. The alternate range computer system performed as intended through launch. The countdown picked up on time at 1030 EST and proceeded without incident until T-2 hours and 30 minutes (1130 EST), at which time a hold was called due to a Freon system problem affecting the spacecraft water boiler temperature. The problem required access to the launch pad and safety regulations required the stopping of cryogenic flow for pad access. LOX loading was manually reverted (pumps stopped and valves safed) at 35% aboard S-IB because of the Freon flow problem. The Freon system problem was worked, the pad area cleared, and LOX loading was

TABLE 5-I
AS-204 PRELAUNCH MILESTONES

Date	
August 7, 1966	S-IVB stage arrived at KSC.
August 14, 1966	S-IB stage arrived at KSC, and was transported to hangar AF for receiving inspection.
August 16, 1966	Instrument Unit (IU) arrived at KSC.
April 6, 1967	S-IB stage de-erected at Launch Complex 34 and transported to Launch Complex 37.
April 7, 1967	S-IB stage erected on Launch Complex 37B.
April 10, 1967	S-IVB stage erected and mechanically mated.
April 11, 1967	IU erected and mechanically mated.
June 13, 1967	Launch Vehicle (L/V) electrical mate test.
June 14, 1967	L/V switch selector functional test.
July 17, 1967	L/V pull test.
July 18, 1967	L/V dynamic pull test.
August 1, 1967	L/V combined Guidance and Control (G&C) Test.
August 7, 1967	L/V plugs in Overall Test (OAT).
September 8, 1967	L/V full pressure test.
November 2, 1967	L/V combined G&C test.
November 6, 1967	L/V malfunction OAT.
November 19, 1967	Spacecraft Lunar Module Adapter (SLA) and Lunar Module (LM) erected and mechanically mated.
November 30, 1967	MCC-H interface test.
December 5, 1967	IU and Space Vehicle (S/V) electrical mate test.
December 12, 1967	S/V plugs in OAT.
December 15, 1967	S/V plugs out OAT.
December 23, 1967	S/V Flight Readiness Test (FRT) completed.
December 29, 1967	S-IB ordnance installation.
January 14, 1968	S-IB stage RP-1 loaded.
January 16, 1968	Commenced preparations for Countdown Demonstration Test (CDDT).
January 18, 1968	Picked up count at T-23 hours 30 minutes. Start of final phase of the CDDT.
January 19, 1968	CDDT was terminated at 2036 EST.
January 20, 1968	CDDT was declared successful.
January 21, 1968	S/V launch countdown was picked up at 1000 EST at T-22 hours.
January 22, 1968	LAUNCH occurred at 1748:08 EST.

reinitiated at 1308 EST. Prior to reaching a LOX level which would match the T-2 hours and 30 minutes count time, a power supply in the AGCS DDAS output register failed. The decision was made to continue LOX loading until both S-IB and S-IVB stages were in a replenish mode; then pad clearance was given to work the power supply problem. The problem was cleared through replacement from another unit. The countdown was resumed at 1518 EST and launch occurred at 1748:08 EST.

Table 5-II is a summary of the terminal countdown problems and the resulting lost time.

TABLE 5-II

COUNTDOWN SUMMARY

A six hour built-in hold at T-3 hr 30 min was scheduled in the countdown.		
Lost time due to unscheduled holds was as follows:		
Countdown Time	Lost Time (min)	
T-2 hr 30 min	88	GSE Freon Cooling System flow problem to spacecraft.
	60	LOX tank fill during hold.
	80	AGCS DDAS power supply problem.
Total Lost Time	228	

The following significant problems occurred during countdown but caused no delay:

1. The Ground Support Cooling Unit coolant temperature oscillated throughout the countdown and numerous set point adjustments of the unit were made.

2. The repeater in the command module of the azimuth laying and alignment equipment failed 2 hours into the 6-hour built-in hold at 0630 EST. Platform positioning was accomplished by manual torquing for drift checks.

3. The tank fill and drain line vibration measurement started failing with vehicle LOX chilldown. At 2% S-IB LOX, the measurement failed completely. The measurement was not critical and was considered scrubbed for the launch.

4. At the beginning of LH₂ loading a hydrogen leak was detected via TV on the S-IVB debris valve. The leakage increased significantly during fast fill and the hydrogen gas monitor system actuated. The monitor system saturated at 8% on the sensor (zero percent is no leakage and the warning light is triggered at approximately 2%). However, the leak location, the sensor location, and the wind direction caused the indication to be worse than the actual case. Loading was continued and the leak subsided when replenish was reached.

5. During RP-1 replenish, fuel tank 3 temperature measurement failed. This caused considerable worry since fuel tank 4 temperature measurement had operated erratically for initial RP-1 loading. However, fuel tanks 1, 2, and 4 temperature measurements operated correctly throughout the countdown.

6. At T-25 minutes, during power transfer, the flight control computer inverter detector in the IU switched from the primary to secondary (spare) inverter. It was determined that this was caused by a voltage transient during the transfer. The unit was restored to the primary inverter and the transfer mode was rerun. The problem did not repeat and the countdown proceeded.

5.4 PROPELLANT AND COLD HELIUM LOADING

In loading the S-IB stage, the Propellant Tanking Computer System (PTCS) measures the pressure difference between sensing lines in the stage propellant systems. The differential pressure required to tank the LOX and fuel, together with PTCS reference values, are obtained from a propellant loading table.

5.4.1 RP-1 LOADING

RP-1 was loaded for launch prior to CDDT on January 14, 1968. Technical Bulletin, dated December 5, 1967, Revision D was used for loading data. This loading was the first attempt to demonstrate the RCA 110A Propellant Tanking System Monitor (PTSM) test program. This program was originally planned for AS-201. It was planned to give a permanent record of the PTCS percentage readout via RCA 110A. Also, the final PTCS thumbwheel setting was to be calculated by predicting temperature/density at T-0. The fact that the hundredth percent flutter swamped the RCA 110A, caused the signals to be disconnected from the computer for AS-201. AS-204 was the first time they were reconnected. The program was revised to sample only once per ten seconds. The program has some shortcomings in that the temperatures are read to three places and the density is curve-fitted to the last two points. As long as the vehicle temperature has stabilized, this will give a satisfactory T-0 density prediction.

Minor problems were encountered but the program worked as planned. Loading was conducted using PTCS thumbwheel setting of 9001 based on an average temperature of 285.4°K (54°F) and 2% ullage. Adjust level drain was conducted to 3% ullage with PTCS set at 8819.

At T-50 minutes in the launch countdown, the S-IB fuel tanks were replenished to a 2% ullage level based on an average temperature of 287.3°K (57.4°F) with a PTCS setting of 8986. At T-28 minutes, the flight mass requirement was determined, based on a predicted T-0 temperature of 286.8°K (56.6°F) (density 807.747 kg/m³, 50.426 lbm/ft³). A setting of 8918 was entered into the PTCS Computer and an automatic adjust level drain sequence was accomplished. Final RP-1 levels as indicated by the PTCS Computer were: Automatic Mass Readout 99.99%, Manual Mass Readout 99.92%, and Delta Pressure 12.382 N/cm² diff. (17.959 psid). At T-10 minutes, the RP-1 transfer line and fuel mast were inerted for completion of the RP-1 System support requirement for launch.

5.4.2 LOX LOADING

The LOX system performed normally during dual loading operations and maintained flight mass to the S-IB and S-IVB stages until start of automatic sequence. Fill command was initiated at 1035 EST and proceeded normally until a LOX system manual revert was requested by the NASA Complex Lead Test Conductor (CLTC) because of a spacecraft Freon flow problem. The fill command was re-initiated at 1308 EST. The S-IB stage reached the replenish mode at 1340 EST and the S-IVB stage at 1403 EST. LOX boiloff of S-IB and S-IVB was replenished by the auto replenish system satisfactorily until LOX tank pressurization for launch.

5.4.3 LH₂ LOADING

S-IVB LH₂ loading was initiated at 1544 EST with chilldown of the heat exchanger. Slow fill rate was 0.019 m³/s (300 gpm) until 5% level was reached at 1615 EST, and fast fill was initiated. At 1642 EST 96% LH₂ mass was reached and slow fill to 100% LH₂ mass was begun, terminating at 1650 EST.

5.4.4 COLD HELIUM LOADING

The cold helium spheres were pressurized to approximately 655 N/cm² (950 psi) at T-11 hours 5 minutes. Prior to LOX load the spheres were pressurized to 879 N/cm² (1275 psi). At 92% LH₂ mass, the pressure was increased to 2124 N/cm² (3080 psi).

5.4.5 AUXILIARY PROPULSION SYSTEM PROPELLANT LOADING

Auxiliary propulsion system (APS) fuel and oxidizer loading was accomplished on January 15, 1968. Oxidizer tanks I and II were loaded to 24.99 cm (9.84 in) and 24.89 cm (9.80 in), respectively. Fuel loading was 24.77 cm (9.75 in) and 24.82 cm (9.77 in) for tanks I and II, respectively.

5.4.6 S-IB STAGE PROPELLANT LOAD

The propellant loading criteria for the S-IB-4 stage were based on environmental conditions expected during January. The propellant loading table provided a LOX weight and tanking differential pressure based on the criteria and a nominal LOX tank ullage volume of 1.5 percent. The loading table contained fuel tanking weights and differential pressures for fuel densities from 797.719 kg/m³ at 301°K (49.800 lbm/ft³ at 82°F) to 821.747 kg/m³ at 267°K (51.300 lbm/ft³ at 21°F). Figure 5-1 shows the temperature density relationship of the fuel. This relationship was determined by chemical analysis of fuel samples taken prior to flight.

Fuel was initially placed onboard the S-IB stage on January 14, and remained on board until launch. The desired fuel weight, obtained from the loading table, was 127,899.9 kg (281,971 lbm). The propellant tanking weights are shown in Table 5-III. The values shown in column 3 are the propellant weights expected at ignition from the loading table. The values shown in column 4 are the propellant weights indicated at ignition and were obtained by multiplying the weight requirements at ignition (column 3) by the PTCS mass readout indication just prior to automatic sequencing (99.99% for RP-1 and 100.04% for LOX). Column 5 propellant weights were calculated from discrete probe data in conjunction with Mark IV reconstruction.

The propellant discrete level instrumentation for this stage consisted of 15 probes in each of tanks OC, O1, O3, F1 and F3. The propellant levels in the other tanks were approximated by using data from the instrumented tanks. The reconstructed load is considered the best estimate of the propellants on board at stage ignition.

The LOX pump inlet temperatures monitored during flight indicated that the temperature of the LOX load at ignition was about 1.15°K (2.08°F) colder than predicted. The difference can be partially attributed to other than expected environmental conditions.

5.4.7 S-IVB STAGE PROPELLANT LOAD

Table 5-IV presents the S-IVB propellant load at S-IB ignition command. The best estimate includes loading determined from the PU system, engine analysis, and trajectory reconstruction.

5.5 HOLDDOWN

No known problems occurred during holddown. All functions occurred at nominal times.

The holddown arm release system was modified to give an explosive release backup to the pneumatic system. This modification installed ordnance to blow the release mechanism if the holddowns had not released a few milliseconds following commit command. The modification was not required as the pneumatics produced release. However, two of the eight charges did explode,

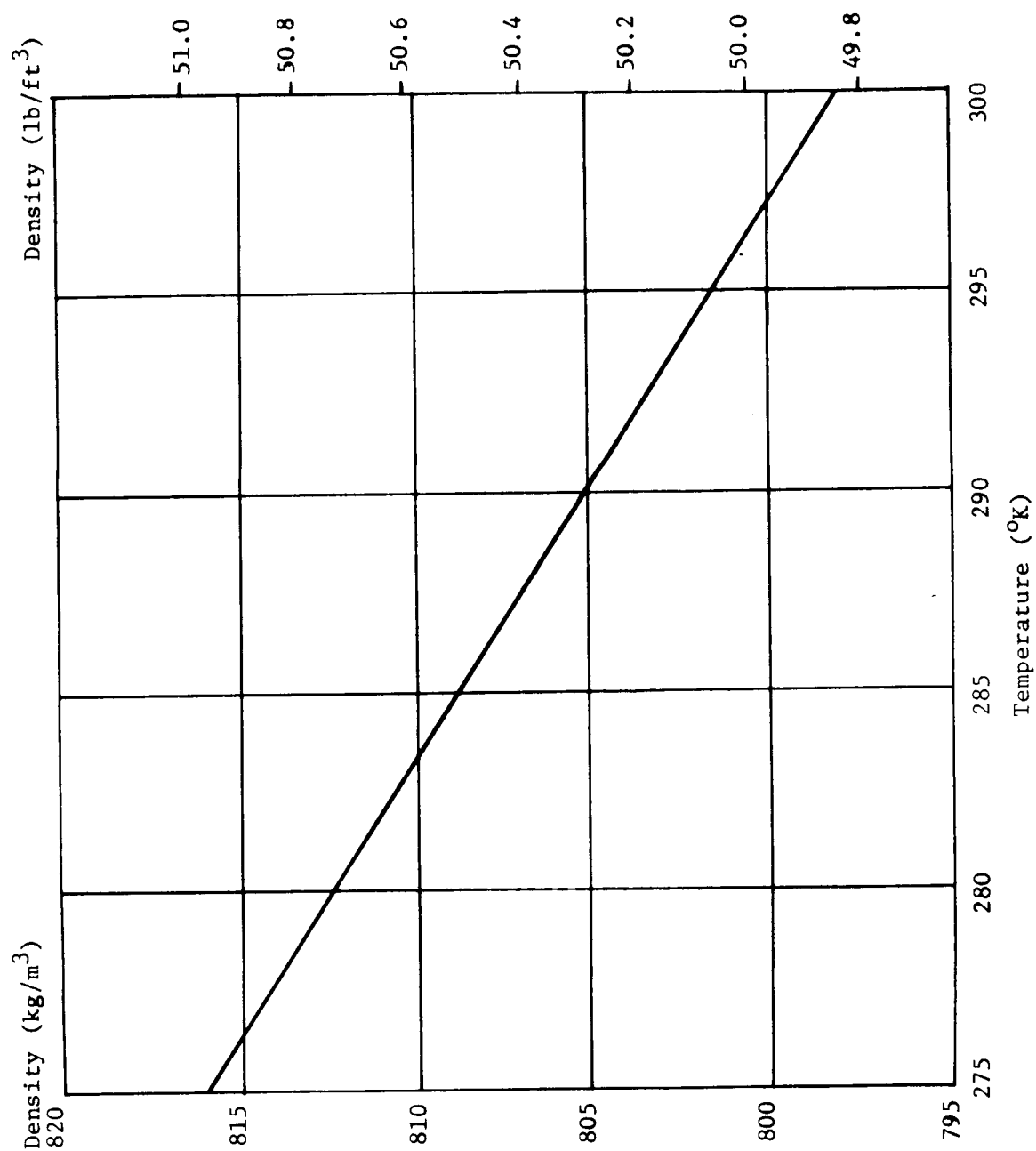


FIGURE 5-1 FUEL TEMPERATURE/DENSITY RELATIONSHIP

TABLE 5-III
AS-204 S-IB STAGE PROPELLANT WEIGHTS AT IGNITION COMMAND

Propellant	Units	Weight Requirements			Weight Indications		Weight Deviations			
		Predicted Prior to Launch (1)	Repredicted Prior to Launch (2)	Loading Table at Ignition (3)	KSC Mass Readout (4)	Reconstructed Load (5)	KSC Minus Ignition	Reconstructed Minus Ignition	Reconstructed Minus Predicted	Reconstructed Minus Repredicted
LOX	kg lbm %	285,985.9 630,491	285,656.1 629,764	285,656.1 629,764	285,770.5 630,016	285,876.6 630,250	114.3 252 0.04	220.4 486 0.08	-109.3 -241 -0.04	220.4 486 0.08
Fuel	kg lbm %	126,581.3 279,064	128,213.3 282,662	127,899.9 281,971	127,886.7 281,942	127,799.6 281,750	-13.2 -29 -0.01	-100.2 -221 -0.08	1,218.3 2,686 0.96	-413.6 -912 -0.32
Total	kg lbm %	412,567.2 909,555	413,869.4 912,426	413,556.0 911,735	413,657.2 911,958	413,676.2 912,000	101.1 223 0.02	120.2 265 0.03	1,109.0 2,445 0.27	-193.2 -426 -0.05

- (1) Predicted propellant weights were based on a nominal LOX density of 1085.51 kg/m³ (67.766 lbm/ft³) and a nominal fuel density of 802.04 kg/m³ (50.07 lbm/ft³). Predicted values were used in the operational flight trajectory.
- (2) Repredicted propellant weights were based on a nominal LOX density of 1126.47 kg/m³ (70.323 lbm/ft³) and a nominal fuel density of 809.25 kg/m³ (50.520 lbm/ft³). Repredicted values were used to generate the loading table. These densities correspond to those expected for a January launch and are documented in TB-P&VE-66-199B.
- (3) Propellant weights required at ignition were based on a nominal LOX density of 1126.47 kg/m³ (70.323 lbm/ft³) and a fuel density of 807.75 kg/m³ (50.426 lbm/ft³) determined immediately prior to launch.
- (4) KSC propellant weights are based on loading system pressure values immediately prior to propellant system pressurization.
- (5) Reconstructed propellant weights are based on discrete probe data in conjunction with the Mark IV reconstruction, and are a "best estimate" of the actual load.

TABLE 5-IV
AS-204 S-IVB STAGE PROPELLANT WEIGHTS AT S-IB IGNITION COMMAND

PROPELLANT	UNITS	WEIGHT REQUIREMENTS PREDICTED PRIOR TO LAUNCH	WEIGHT INDICATIONS		WEIGHT DEVIATIONS	
			LOADING SYSTEM	BEST ESTIMATE	LOADING SYSTEM MINUS PREDICTED	BEST EST MINUS PREDICTED
LOX	Kg	87,667.2	87,694.4	88,028.7	27.2	361.5
	lbm	193,273	193,333	194,070	60	797
	%				0.03	0.41
Fuel	Kg	16,982.5	16,960.7	16,925.4	-21.8	-57.1
	lbm	37,440	37,392	37,314	-48	-126
	%				-0.13	-0.34
Total	Kg	104,649.7	104,655.1	104,954.1	5.4	304.4
	lbm	230,713	230,725	231,384	12	671
	%				0.005	0.29

probably because the isolation system, which is intended to isolate the charges if pneumatic release is obtained, did not open the circuit as the holddowns released.

5.6 GROUND SUPPORT EQUIPMENT

The hydrogen burn pond vent system was modified to give a completely separate venting and burning system for the vehicle. Removing the helium heat exchanger vent from the vehicle vent reduced the GH_2 flow to the burn pond and prevented excessive back pressure to the S-IVB Hydrogen Tank. The ground pressure measurement indicated the highest back pressure was 0.5 N/cm^2 (0.8 psid).

An inspection of the spacecraft facility, GSE systems on the pad, and umbilical tower at Launch Complex 37 (LC-37), indicated no visible damage due to heat or blast effects during the launch. Damage to launch vehicle GSE and pad facilities was minor, being limited to superficial damage which was, in most cases, less than anticipated.

5.7 LAUNCH FACILITY MEASUREMENT

All redline values were met; however, fuel tank 3 temperature measurement failed. The fuel level is a redline requirement, but the measurement is not a redline requirement since the fuel temperature/density can be determined if two of the four measurements are working.

6.0 MASS CHARACTERISTICS

6.1 SUMMARY

Postflight analysis indicated that vehicle weights were significantly higher than predicted, ranging from 1,507.8 kg (3,324 lbm) at first motion to 1,368.0 kg (3,016 lbm) at S-IB outboard engine cutoff. Vehicle weight was 406.3 kg (896 lbm) higher at S-IVB engine start command and 99.8 kg (220 lbm) lower than predicted at guidance cutoff signal. Longitudinal center-of-gravity travel was essentially as predicted. Deviations of approximately 0.03 m (1.2 in) aft were noted throughout most of S-IB stage powered flight. Vehicle CG was 0.11 m (4.4 in) aft at outboard engine cutoff signal. Deviations during second stage powered flight ranged from 0.003 m (0.01 in) aft at start command to 0.06 m (2.36 in) forward at cutoff signal.

Comparison of vehicle moments of inertia indicated that both pitch and roll values were slightly higher than predicted during S-IB stage powered flight. During second stage flight moments of inertia were within 1% of predicted.

6.2 MASS ANALYSIS

Postflight mass characteristics are compared to the final predicted mass characteristics (Ref 1) which were used in determination of the final predicted trajectory (Ref 2). The postflight mass characteristics were determined from an analysis of all available actual and reconstructed data, from ground ignition through 5 hr: 33 min: 20 sec of launch vehicle flight. Dry weights of the S-IB stage, S-IVB stage, and vehicle instrument unit were based on an evaluation of the Weight and Balance Log Books (MSFC Form 998). Payload data were obtained from the Manned Spacecraft Center. S-IB stage propellant loading and utilization were evaluated from the S-IB propulsion system performance reconstruction. S-IVB propellant and service item loading and utilization were evaluated from a composite of Propulsion Utilization (PU) system, engine flow integral, reconstruction, and level sensor residuals.

Deviations in the dry or inert weights of most of the stages and the loaded spacecraft were within the predicted three sigma limits. The weight of the S-IB/S-IVB interstage exceeded this limit by 62.6 kg (138 lbm) and was due primarily to the use of additional insulation and sealing material required to replace and repair the original insulation which had aged and was no longer adhering properly. The total weight of the vehicle before the loading of any propellants and usable load items into the S-IB and S-IVB stages was 195.0 kg (430 lbm) higher than predicted.

At first motion the vehicle weight was 584,393.9 kg (1,288,368 lbm), which was 1,570.8 kg (3,324 lbm) higher than predicted. The primary reason for this increase was the loading of 1,218.3 kg (2,686 lbm) more RP-1 than anticipated in the predicted report. This fuel overload is a result of colder fuel temperature which is experienced in a January launch. The predicted report was based on a September launch. Additionally, the weight penalty for frost and ice, nominally estimated at 453.6 kg (1,000 lbm), had been increased to 680.4 kg (1,500 lbm) for this launch. A combination of factors including the extremely long hold period and a humidity conducive to frost formation contributed to the formation of much more frost and ice than is normally anticipated. The presence of large amounts of frost were also noted on films showing the launch and first few seconds of flight. The vehicle weight deviation noted at first motion remained essentially constant when compared on a time basis with the predicted data. Deviations of 1,754.9 kg (3,869 lbm) and 1,368.0 kg (3,016 lbm) were noted for the S-IB inboard and outboard cutoff events.

The vehicle weight at S-IVB engine start command was 134,732.7 kg (297,035 lbm), which was 406.3 kg (896 lbm) higher than predicted and is due primarily to a higher than anticipated propellant loading in the S-IVB stage. The vehicle weight at S-IVB stage cutoff command was 99.8 kg (220 lbm) lower than predicted and reflects lower than anticipated propellant residuals.

Vehicle flight sequence mass summary is presented in Table 6-I. Detailed vehicle masses are tabulated in Table 6-II. Graphical representations of these data, center-of-gravity, and mass moment of inertia histories, with respect to time, are illustrated in Figures 6-1 and 6-2 for the S-IB stage and S-IVB stage powered flight, respectively.

6.3 CENTER-OF-GRAVITY AND MOMENT OF INERTIA ANALYSIS

Comparison of the longitudinal center-of-gravity with the predicted data indicated aftward deviations ranging from 0.03 m (1.2 in) to 0.11 m (4.4 in). These deviations were caused principally by the higher weights of the S-IB stage propellant and ice loads, located aft of the vehicle center-of-gravity. Mass moments of inertia during S-IB stage powered flight were slightly higher than predicted, reflecting the higher vehicle weights.

Longitudinal center of gravity travel during S-IVB stage powered flight approximated the predicted values. The location at S-IVB stage cutoff command was 0.06 m (2.36 in) forward and reflected lower residuals. Mass moments of inertia were essentially as predicted with small deviations being caused by weight differences.

Weight, center-of-gravity, and moment of inertia data for the individual stages and the vehicle at significant events are presented in Table 6-III.

Weight data presented in this section are of masses under acceleration of one standard g. The sign convention used herein conforms to the Project Apollo mass properties coordinate system (Ref 3).

TABLE 6-1 AS-204 FLIGHT SEQUENCE MASS SUMMARY

MASS HISTORY	ACTUAL		PREDICTED	
	kg	lbm	kg	lbm
S-IB Stage at Ground Ignition	453,133.3	998,988	451,803.4	996,056
S-IB/S-IVB Interstage at Ground Ignition	3,103.5	6,842	3,018.2	6,654
S-IVB Stage at Ground Ignition	116,162.3	256,094	115,850.6	255,407
Vehicle Instrument Unit at Ground Ignition	2,088.8	4,605	2,086.5	4,600
Payload	16,577.4	36,547	16,484.5	36,342
First Flight Stage at Ground Ignition	591,065.3	1,303,076	589,243.2	1,299,059
S-IB Thrust Buildup Propellant	-6,671.4	-14,708	-6,357.1	-14,015
First Flight Stage at First Motion	584,393.9	1,288,368	582,886.1	1,285,044
S-IB Mainstage Propellant	-399,227.0	-880,145	-399,314.6	-880,338
S-IB Stage Frost	-680.4	-1,500	-453.6	-1,000
S-IVB Stage Frost	-45.4	-100	-45.4	-100
S-IB Stage Engine Seal Purge (N ₂)	-2.7	-6	-2.7	-6
S-IB Stage Gear Box Consumption (RP-1)	-323.0	-712	-323.8	-714
S-IB Stage Fuel Lubricant (Oronite)	-12.3	-27	-12.3	-27
S-IB Inboard Engine Thrust Decay Propellant	-973.4	-2,146	-972.0	-2,143
First Flight Stage at Outboard Engine Cutoff Signal	183,129.7	403,732	181,761.7	400,716
S-IB OETD to Separation Command	-717.6	-1,582	-736.2	-1,623
S-IVB Ullage Rocket Grain	-4.5	-10		
First Flight Stage at Separation Command	182,407.6	402,140	181,025.5	399,093
S-IB Stage at Separation Command	-44,525.5	-98,162	-43,631.0	-96,190
S-IB/S-IVB Interstage	-3,103.5	-6,842	-3,018.2	-6,654
S-IVB Separation Package	-15.4	-34	-16.3	-36
S-IVB Ullage Rocket Grain	-30.5	-67	-33.6	-74
Second Flight Stage at Ignition Command	134,732.7	297,035	134,326.4	296,139
S-IVB Thrust Buildup Propellant	-565.1	-1,246	-176.9	-390
S-IVB Ullage Rocket Grain	-45.4	-100	046.3	-102
S-IVB GH ₂ Start Tank	-1.8	-4	-1.8	-4
Second Flight Stage at 90% Thrust	134,120.4	295,685	134,101.4	295,643
S-IVB Mainstage Propellant	-102,163.5	-225,232	102,047.5	-224,976
S-IVB Ullage Rocket Cases	-100.7	-222	-97.5	-215
S-IVB Auxiliary Propellant (Power Roll)	-2.3	-5	-2.7	-6
Second Flight Stage at Cutoff Command	31,853.9	70,226	31,953.7	70,446
S-IVB Thrust Decay Propellant	-84.8	-187	084.3	-186
Second Flight Stage at End of Thrust Decay	31,769.1	70,039	31,869.4	70,260
Total S-IVB Stage	13,102.9	28,887	13,298.4	29,318
Vehicle Instrument Unit	2,088.8	4,605	2,086.5	4,600
Adapter (SLA)	1,750.4	3,859	1,750.4	3,859
Lunar Module	14,301.7	31,530	14,208.8	31,325
SLA Ring	41.3	91	41.3	91
Nose Cone	484.0	1,067	484.0	1,067

TABLE 6-IIa VEHICLE MASSES (KILOGRAMS)

FIRST FLIGHT STAGE

EVENT	GROUND IGNITION		FIRST MOTION		INBOARD ENGINE CUTOFF SIGNAL		OUTBOARD ENGINE CUTOFF SIGNAL		SEPARATION SIGNAL	
	Pred	Actual	Pred	Actual	Pred	Actual	Pred	Actual	Pred	Actual
RANGE TIME (sec)	-2.90	-2.97	0.20	0.20	139.34	138.97	142.34	142.25	143.64	143.50
S-IB Stage, Dry	38,699.1	38,688.7	38,699.1	38,688.7	38,699.1	38,688.7	38,699.1	38,688.7	38,699.1	38,688.7
LOX in Tanks	282,285.5	282,110.4	277,160.4	276,783.4	889.5	1,107.7				
LOX Below Tanks	3,700.4	3,766.2	3,905.9	3,924.9	3,854.6	3,871.8	1,557.2	1,526.3	1,320.9	1,289.6
LOX Ullage Gas	13.6	18.1	33.5	40.4	1,230.6	1,201.6	1,242.4	1,217.5	1,242.8	1,218.3
RP-1 in Tanks	124,403.2	125,605.6	122,524.8	123,657.0	2,121.5	3,169.7	425.5	1,350.3	31.3	959.8
RP-1 Below Tanks	2,178.1	2,194.0	2,599.1	2,617.2	2,599.1	2,617.2	2,388.1	2,405.4	2,282.0	2,314.2
RP-1 Ullage Gas	1.8	1.8	2.7	3.2	29.5	26.3	29.9	26.3	29.9	26.3
Nitrogen	6.8	6.8	6.8	6.8	4.1	4.1	4.1	4.1	4.1	4.1
Helium RP-1 Pressure Supply	33.6	33.6	32.7	32.2	5.9	9.1	5.5	9.1	5.5	9.1
Hydraulic Oil	12.7	12.7	12.7	12.7	12.7	12.7	12.7	12.7	12.7	12.7
Oronite	15.0	15.0	15.0	15.0	2.7	3.2	2.7	2.7	2.7	2.7
Frost	453.6	680.4	453.6	680.4						
Total S-IB Stage	451,803.4	453,133.3	445,446.3	446,461.9	49,449.3	50,712.1	44,367.2	45,243.1	43,631.0	44,525.5
S-IB/S-IVB Interstage, Dry	2,530.6	2,615.9	2,530.6	2,615.9	2,530.6	2,615.9	2,530.6	2,615.9	2,530.6	2,615.9
Retro Rocket Propellant	487.6	487.6	487.6	487.6	487.6	487.6	487.6	487.6	487.6	487.6
Total First Vehicle Stage	454,821.6	456,236.8	448,464.5	449,565.4	52,467.5	53,815.6	47,385.4	48,346.6	46,649.2	47,629.0
Total S-IVB Stage	115,850.6	116,162.3	115,850.6	116,162.3	115,805.3	116,116.9	115,805.3	116,116.9	115,805.3	116,112.4
Vehicle Instrument Unit	2,086.5	2,088.8	2,086.5	2,088.8	2,086.5	2,088.8	2,086.5	2,088.8	2,086.5	2,088.8
Payload	16,484.5	16,577.4	16,484.5	16,577.4	16,484.5	16,577.4	16,484.5	16,577.4	16,484.5	16,577.4
Total First Flight Stage	589,243.2	591,065.3	582,886.1	584,393.9	186,843.8	188,598.7	181,761.7	183,129.7	181,025.5	182,407.6

TABLE 6-IIb VEHICLE MASSES (POUNDS)

FIRST FLIGHT STAGE

EVENT	GROUND IGNITION		FIRST MOTION		INBOARD ENGINE CUTOFF SIGNAL		OUTBOARD ENGINE CUTOFF SIGNAL		SEPARATION SIGNAL	
	Pred	Actual	Pred	Actual	Pred	Actual	Pred	Actual	Pred	Actual
RANGE TIME (sec)	-2.90	-2.97	0.20	0.20	139.34	138.97	142.34	142.25	143.64	143.50
S-IB Stage, Dry	85,317	85,294	85,317	85,294	85,317	85,294	85,317	85,294	85,317	85,294
LOX in Tanks	622,333	621,947	611,034	610,203	1,961	2,442				
LOX Below Tanks	8,158	8,303	8,611	8,653	8,498	8,536	3,433	3,365	2,912	2,843
LOX Ullage Gas	30	40	74	89	2,713	2,649	2,739	2,684	2,740	2,686
RP-1 in Tanks	274,262	276,913	270,121	272,617	4,677	6,988	938	2,977	69	2,116
RP-1 Below Tanks	4,802	4,837	5,730	5,770	5,730	5,770	5,265	5,303	5,031	5,102
RP-1 Ullage Gas	4	4	6	7	65	58	66	58	66	58
Nitrogen	15	15	15	15	9	9	9	9	9	9
Helium RP-1 Pressure Supply	74	74	72	71	13	20	12	20	12	20
Hydraulic Oil	28	28	28	28	28	28	28	28	28	28
Oronite	33	33	33	33	6	7	6	6	6	6
Frost	1,000	1,500	1,000	1,500						
Total S-IB Stage	996,056	998,988	982,041	984,280	109,017	111,801	97,813	99,744	96,190	98,162
S-IB/S-IVB Interstage, Dry	5,579	5,767	5,579	5,767	5,579	5,767	5,579	5,767	5,579	5,767
Retro Rocket Propellant	1,075	1,075	1,075	1,075	1,075	1,075	1,075	1,075	1,075	1,075
Total First Vehicle Stage	1,002,710	1,005,830	988,695	991,122	115,671	118,643	104,467	106,586	102,844	105,004
Total S-IVB Stage	255,407	256,094	255,407	256,094	255,307	255,994	255,307	255,994	255,307	255,984
Vehicle Intrusment Unit	4,600	4,605	4,600	4,605	4,600	4,605	4,600	4,605	4,600	4,605
Payload	36,342	36,547	36,342	36,547	36,342	36,547	36,342	36,547	36,342	36,547
Total First Flight Stage	1,299,059	1,303,076	1,285,044	1,288,368	411,920	415,789	400,716	403,732	399,093	402,140

TABLE 6-IIc VEHICLE MASSES (KILOGRAMS)

SECOND FLIGHT STAGE

EVENT	S-IB STAGE GROUND IGNITION		ENGINE START COMMAND		90% THRUST		ENGINE CUTOFF COMMAND		END OF THRUST DECAY	
	Pred	Actual	Pred	Actual	Pred	Actual	Pred	Actual	Pred	Actual
RANGE TIME (sec)	-2.90	-2.97	145.04	144.90	148.34	148.20	598.35	593.35	599.75	594.74
S-IVB Stage, Dry	10,626.3	10,649.0	10,626.3	10,649.0	10,626.3	10,649.0	10,626.3	10,649.0	10,626.3	10,649.0
Separation Package	16.3	15.4								
Ullage Rocket Cases	97.5	100.7	97.5	100.7	97.5	100.7				
Ullage Rocket Grain	79.8	80.3	46.3	45.4						
LOX in Tank	87,500.7	87,862.2	87,500.7	87,859.9	87,354.2	87,397.2	1,334.9	1,197.9	1,280.5	1,143.5
LOX Below Tank	166.5	166.5	166.5	166.5	180.1	180.1	180.1	180.1	166.5	166.5
LOX Ullage Gas	16.8	13.6	16.8	15.9	17.2	16.3	166.9	139.7	166.9	139.7
LH2 in Tank	16,960.7	16,903.6	16,960.7	16,894.5	16,911.7	16,773.4	658.6	647.3	646.8	635.0
LH2 Below Tank	21.8	21.8	21.8	21.8	26.3	26.3	26.3	26.3	21.8	21.8
LH2 Ullage Gas	73.9	66.7	73.9	75.7	74.4	76.2	219.0	183.7	219.0	183.7
Cold Helium - LOX Pressure Supply	149.7	143.3	149.7	143.3	149.2	142.9	79.8	71.2	79.8	71.2
APS Propellant	59.4	58.5	59.4	58.5	59.4	58.5	56.7	56.2	56.7	56.2
Service Items	14.1	13.6	14.1	13.6	14.1	13.6	14.1	13.6	14.1	13.6
GH2 - Start Tank	2.2	2.2	2.2	2.2	0.5	0.5	0.5	3.2	0.5	3.2
Environmental Control Fluids	19.5	19.5	19.5	19.5	19.5	19.5	19.5	19.5	19.5	19.5
Frost	45.4	45.4								
Total S-IVB Stage	115,850.6	116,162.3	115,755.4	116,066.5	115,530.4	115,454.2	13,382.7	13,187.7	13,298.4	13,102.9
Vehicle Instrument Unit	2,086.5	2,088.8	2,086.5	2,088.8	2,086.5	2,088.8	2,086.5	2,088.8	2,086.5	2,088.8
Payload	16,484.5	16,577.4	16,484.5	16,577.4	16,484.5	16,577.4	16,484.5	16,577.4	16,484.5	16,577.4
Total Second Flight Stage	134,421.6	134,828.5	134,326.4	134,732.7	134,101.4	134,120.4	31,953.7	31,853.9	31,869.4	31,769.1

TABLE 6-IIId VEHICLE MASSES (POUNDS)
SECOND FLIGHT STAGE

EVENT	S-IB STAGE GROUND IGNITION		ENGINE START COMMAND		90% THRUST		ENGINE CUTOFF COMMAND		END OF THRUST DECAY	
	Pred	Actual	Pred	Actual	Pred	Actual	Pred	Actual	Pred	Actual
RANGE TIME (sec)	-2.90	-2.97	145.04	144.90	148.34	148.20	598.35	593.35	599.75	594.74
S-IVB Stage, Dry Separation Package	23,427	23,477	23,427	23,477	23,427	23,477	23,427	23,477	23,427	23,477
Ullage Rocket Cases	36	24	215	222	215	222				
Ullage Rocket Grain	176	177	102	100	192,583	192,678	2,943	2,641	2,823	2,521
LOX in Tank	192,906	193,703	192,906	193,698	397	397	397	397	367	367
LOX Below Tank	367	367	367	367	38	36	368	308	368	308
LOX Ullage Gas	37	30	37	35	37,284	36,979	1,452	1,427	1,426	1,400
LH2 in Tank	37,392	37,266	37,392	37,246	58	58	58	58	48	48
LH2 Below Tank	48	48	48	48	164	168	483	405	483	405
LH2 Ullage Gas	163	147	163	167	329	315	176	157	176	157
Cold Helium - LOX Pressure Supply	330	316	330	316	131	129	125	124	125	124
APS Propellant	131	129	131	129	31	30	31	30	31	30
Service Items	31	30	31	30	1	1	1	7	1	7
GH2 - Start Tank	5	5	5	5	43	43	43	43	43	43
Environmental Control Fluids	43	43	43	43						
Frost	100	100								
Total S-IVB Stage	255,407	256,094	255,197	255,883	254,701	254,533	29,504	29,074	29,318	28,887
Vehicle Instrument Unit	4,600	4,605	4,600	4,605	4,600	4,605	4,600	4,605	4,600	4,605
Payload	36,342	36,547	36,342	36,547	36,342	36,547	36,342	36,547	36,342	36,547
Total Second Flight Stage	296,349	297,246	296,139	297,035	295,643	295,685	70,446	70,226	70,260	70,039

TABLE 6-IIe VEHICLE MASSES (KILOGRAMS)

ORBITAL VEHICLE

EVENT	JETTISON NOSE CONE	DEPLOY SLA PANELS	LM/S-IVB SEPARATION	START LOX DUMP	END LOX DUMP	END PROGRAM
	Actual	Actual	Actual	Actual	Actual	Actual
RANGE TIME (sec)	638.51	1,193.51	3,235.24	8,774.31	8,894.51	20,000.00
RANGE TIME (hr:min:sec)	0:10:38.51	0:19:53.51	0:53:5.24	2:26:14.31	2:28:14.51	5:33:20.00
S-IVB Stage, Dry	10,649.0	10,649.0	10,649.0	10,649.0	10,649.0	10,649.0
LOX in Tank	1,135.8	1,122.6	1,075.4	946.2		
LOX Below Tank	166.5	166.5	166.5	166.5		
LOX Ullage Gas	105.2	118.4	165.5	294.8	252.7	
LH ₂ in Tank	624.2	484.0	155.6			
LH ₂ Below Tank	21.8	21.8	21.8			
LH ₂ Ullage Gas	183.7	182.8	343.4			
Cold Helium - LOX Pressure Supply	71.2	71.2	71.2	71.2	71.2	
APS Propellant	55.3	48.1	45.8	37.6	37.6	28.6
Service Items	13.6	13.6	13.6	13.6	13.6	13.6
GH ₂ - Start Tank	3.2	3.2	3.2	3.2	3.2	3.2
Environmental Control Fluids	19.5	19.5	19.5	19.5	19.5	19.5
Total S-IVB Stage	13,049.0	12,900.7	12,730.5	12,201.6	11,046.8	10,713.9
Vehicle Instrument Unit	2,088.8	2,088.8	2,088.8	2,088.8	2,088.8	2,088.8
Adapter (SLA)	1,750.4	1,750.4	1,750.4	1,750.4	1,750.4	1,750.4
Lunar Module	14,301.7	14,301.7				
Total Vehicle	31,189.9	31,041.6	16,569.7	16,040.8	14,886.0	14,553.1

TABLE 6-IIIf VEHICLE MASSES (POUNDS)

ORBITAL VEHICLE

EVENT	JETTISON NOSE CONE	DEPLOY SLA PANELS	LM/s-IVB SEPARATION	START LOX DUMP	END LOX DUMP	END PROGRAM
	Actual	Actual	Actual	Actual	Actual	Actual
RANGE TIME (sec)	638.51	1,193.51	3,235.24	8,774.31	8,894.51	20,000.00
RANGE TIME (hr:min:sec)	0:10:38.51	0:19:53.51	0:53:5.24	2:26:14.31	2:28:14.51	5:33:20.00
S-IVB Stage, Dry	23,477	23,477	23,477	23,477	23,477	23,477
LOX in Tank	2,504	2,475	2,371	2,086		
LOX Below Tank	367	367	367	367		
LOX Ullage Gas	232	261	365	650	557	
LH ₂ in Tank	1,376	1,067	343			
LH ₂ Below Tank	48	48	48			
LH ₂ Ullage Gas	405	403	757			
Cold Helium - LOX Pressure Supply	157	157	157	157	157	
APS Propellant	122	106	101	83	83	63
Service Items	30	30	30	30	30	30
GH ₂ - Start Tank	7	7	7	7	7	7
Environmental Control Fluids	43	43	43	43	43	43
Total S-IVB Stage	28,768	28,441	28,066	26,900	24,354	23,620
Vehicle Instrument Unit Adapter (SLA)	4,605	4,605	4,605	4,605	4,605	4,605
Lunar Module	3,859	3,859	3,859	3,859	3,859	3,859
Total Vehicle	68,762	68,435	36,530	35,364	32,818	32,084

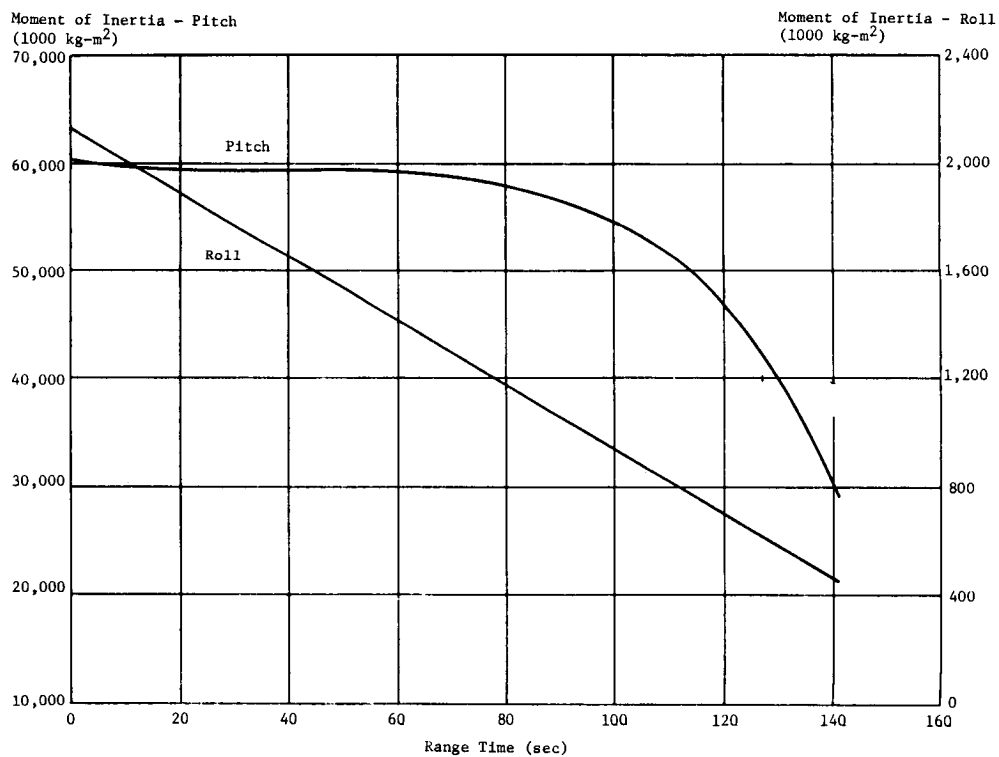
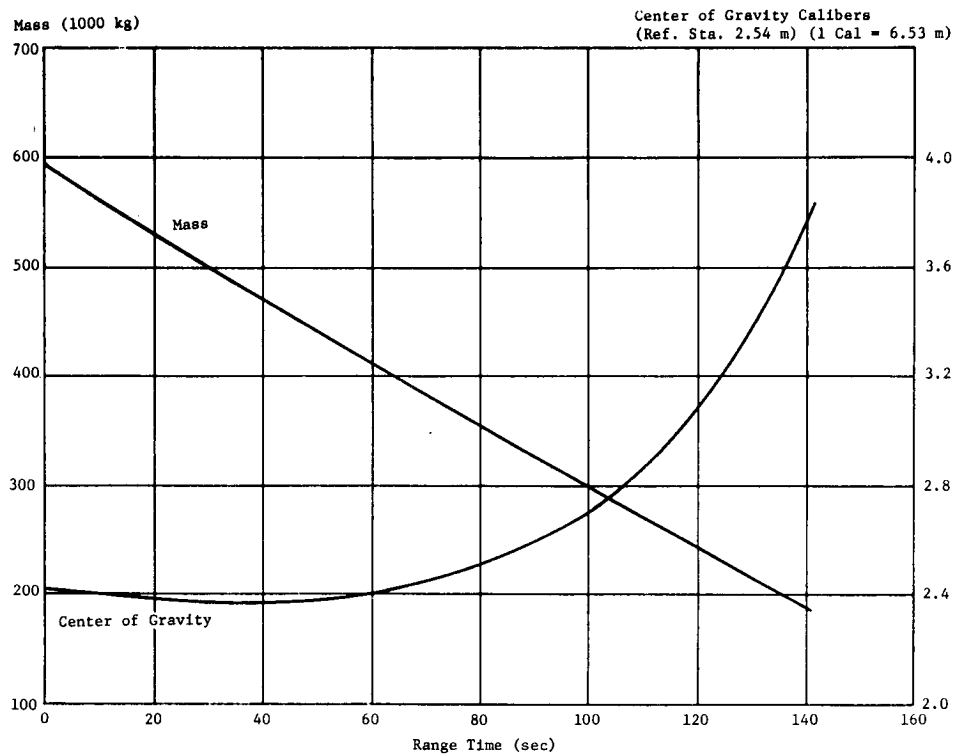


FIGURE 6-1 VEHICLE MASS, CENTER OF GRAVITY, AND MASS MOMENT OF INERTIA DURING S-IB STAGE POWERED FLIGHT

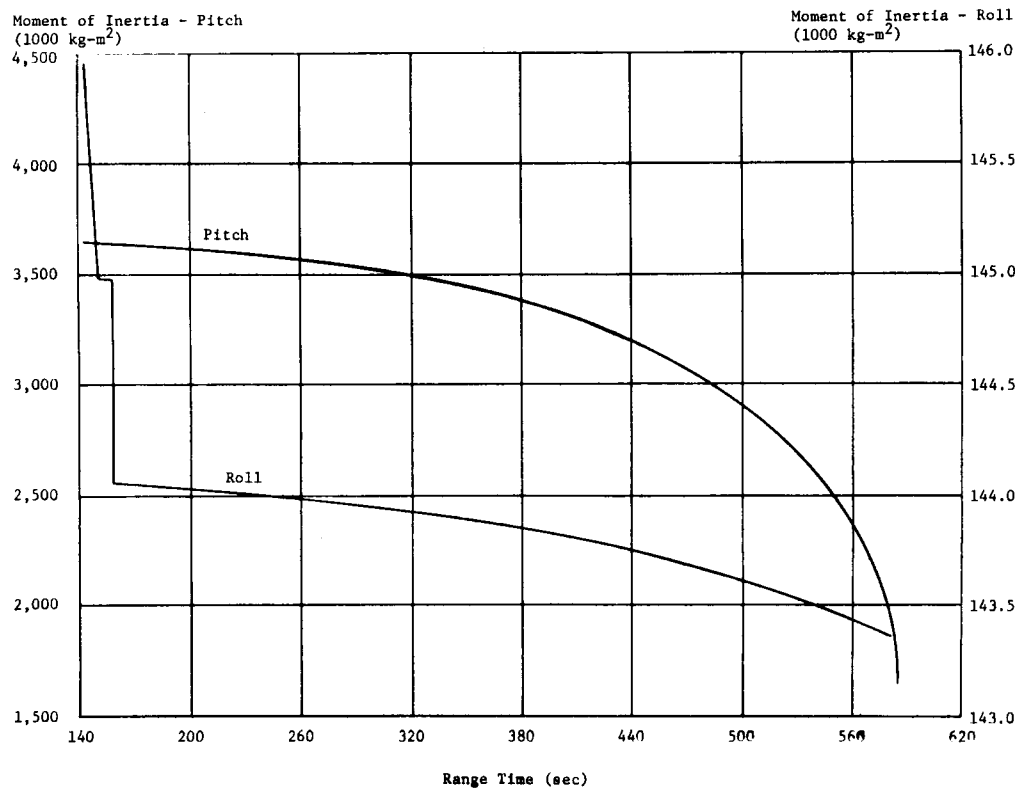
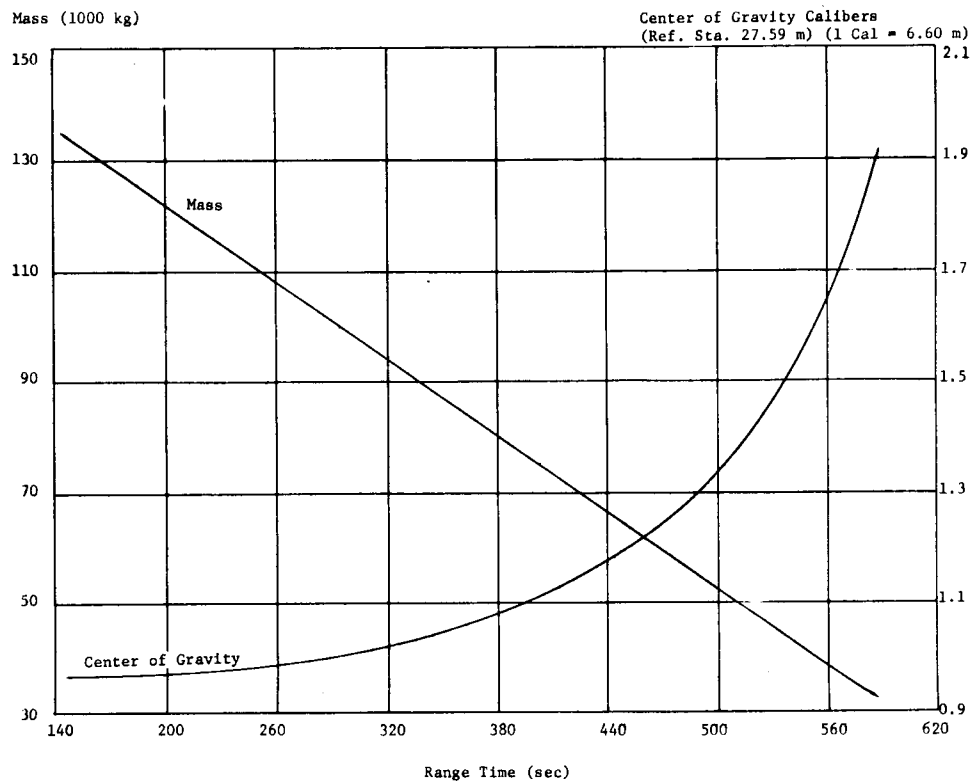


FIGURE 6-2 VEHICLE MASS, CENTER OF GRAVITY AND MASS MOMENT OF INERTIA DURING S-IVB POWERED FLIGHT

TABLE 6-IIIa MASS CHARACTERISTICS COMPARISON

EVENTS	MASS		LONGITUDINAL C.G. STATION		RADIAL C.G.		ROLL MOMENT OF INERTIA		PITCH MOMENT OF INERTIA		YAW MOMENT OF INERTIA	
	KILOGRAMS	% DEV.	METERS	INCHES	METERS	INCHES	Kg-M ²	% DEV.	Kg-M ²	% DEV.	Kg-M ²	% DEV.
S-IB STAGE, DRY	PRED	38,699.1	8.62	0.02	0.0	0.0	226,249	-0.03	2,615,512	-0.03	2,631,673	-0.03
	ACTUAL	38,688.7	8.62	0.02	0.0	0.0	226,190		2,614,806		2,630,967	
S-IB/S-IVB INTERSTAGE (INCLUDES RETRO ROCKET PROPELLANT)	PRED	3,018.2	26.64	0.06	0.03	0.0	33,323	2.82	23,438	2.85	23,840	2.84
	ACTUAL	3,103.5	26.67	0.06	1.0	0.0	34,264		24,105		24,517	
S-IVB STAGE, DRY (INCLUDES ULLAGE ROCKET CASES SEPARATION PACKAGE)	PRED	10,740.1	33.41	0.16	0.0	0.0	80,856	0.23	306,330	0.56	306,330	0.56
	ACTUAL	10,765.1	33.41	0.16	0.0	0.0	81,044		308,037		308,037	
VEHICLE INSTRUMENT UNIT	PRED	2,086.5	42.80	0.23	0.0	0.0	20,359	0.11	11,004	0.11	9,650	0.10
	ACTUAL	2,088.8	42.80	0.23	0.0	0.0	20,381		11,016		9,660	
PAYLOAD (LM-1, SLA, NOSE CONE)	PRED	16,484.5	45.67	0.04	-0.01	0.0	41,472	0.44	78,787	2.32	79,277	2.59
	ACTUAL	16,577.4	45.66	0.04	-0.3	0.0	41,653		80,613		81,329	
FIRST FLIGHT STAGE AT GROUND IGNITION	PRED	589,243.2	18.46	0.01	-0.03	0.0	2,154,528	0.67	60,269,070	0.13	60,267,910	0.11
	ACTUAL	591,065.3	18.43	0.01	-1.2	0.0	2,168,917		60,345,490		60,335,772	
FIRST FLIGHT STAGE AT FIRST MOTION	PRED	582,886.1	18.39	0.01	-0.03	0.0	2,120,947	0.59	60,298,110	0.14	60,297,050	0.13
	ACTUAL	584,393.9	18.36	0.01	-1.2	0.0	2,133,377		60,385,492		60,375,523	

TABLE 6-IIIB MASS CHARACTERISTICS COMPARISON

EVENTS		MASS		LONGITUDINAL C.G. STATION		RADIAL C.G.		ROLL MOMENT OF INERTIA		PITCH MOMENT OF INERTIA		YAW MOMENT OF INERTIA	
		KILOGRAMS POUNDS	% DEV.	METERS INCHES	ACT-PRED	METERS INCHES	ACT-PRED	Kg-M ²	% DEV.	Kg-M ²	% DEV.	Kg-M ²	% DEV.
FIRST FLIGHT STAGE AT INBOARD ENGINE CUTOFF SIGNAL	PRED	186,843.8 411,920	0.94	27.00 1,062.9	-0.15	0.02 0.9	0.0	451,264	2.85	30,583,060	2.37	30,581,680	2.34
	ACTUAL	188,598.7 415,789		26.85 1,057.2	-5.7	0.02 0.8	-0.1	464,106		31,306,910		31,297,648	
FIRST FLIGHT STAGE AT OUTBOARD ENGINE CUTOFF SIGNAL	PRED	181,761.7 400,716	0.75	27.59 1,086.3	-0.11	0.02 0.9	0.0	429,461	2.72	28,204,160	2.08	28,202,860	2.09
	ACTUAL	183,129.7 403,732		27.48 1,081.9	-4.4	0.02 0.8	-0.1	441,152		28,790,449		28,791,963	
FIRST FLIGHT STAGE AT SEPARATION COMMAND	PRED	181,025.5 399,093	0.76	27.68 1,089.9	-0.11	0.02 0.9	0.0	425,593	2.58	27,830,760	2.09	27,829,610	2.11
	ACTUAL	182,407.6 402,140		27.57 1,085.5	-4.4	0.02 0.8	-0.1	436,570		28,413,295		28,415,856	
S-1B AND INTERSTAGE AT SEPARATION	PRED	46,649.2 102,844	2.10	9.63 379.3	-0.09	0.02 0.9	0.0	285,674	1.98	3,700,951	2.15	3,699,817	2.26
	ACTUAL	47,629.0 105,004		9.54 375.6	-3.7	0.02 0.6	-0.3	291,316		3,780,708		3,783,425	
SECOND FLIGHT STAGE AT ENGINE START COMMAND	PRED	134,326.4 296,139	0.30	33.95 1,336.7	0.0	0.02 0.9	0.0	145,675	0.19	3,641,747	0.48	3,641,772	0.47
	ACTUAL	134,732.7 297,035		33.95 1,336.7	0.0	0.02 0.9	0.0	145,948		3,659,206		3,658,890	
SECOND FLIGHT STAGE AT CUTOFF COMMAND	PRED	31,953.7 70,446	-0.31	40.15 1,580.9	0.06	0.09 3.7	0.0	143,230	0.14	1,634,326	-0.05	1,633,830	-0.09
	ACTUAL	31,853.9 70,226		40.21 1,583.2	2.3	0.09 3.5	-0.2	143,426		1,633,534		1,632,290	

Note: Percent Deviation = (Deviation ÷ Predicted) x 100

7.0 TRAJECTORY

7.1 SUMMARY

The actual flight trajectory of the AS-204 vehicle was close to nominal. Launch azimuth, from pad 37B, was 90° east of north. After launch, the vehicle rolled into a flight azimuth of 72° east of north. Total space-fixed velocity was 3.3 m/s lower than nominal at OECO and 0.4 m/s lower than nominal at S-IVB cutoff. At S-IVB cutoff the altitude and surface range were 0.23 km higher than nominal and 30.99 km shorter than nominal, respectively. The cross range velocity deviated 6.4 m/s to the left of nominal at S-IVB cutoff.

The theoretical free flight trajectory utilizing the tumbling drag coefficient for the S-IB stage indicates that the impact ground range was 0.89 km greater than nominal. Impact, assuming the tumbling booster remained intact, occurred at 562.7 sec, 0.9 sec earlier than nominal.

Orbital insertion (S-IVB cutoff plus 10 sec) occurred at 603.35 sec, 5.00 sec earlier than nominal. The space-fixed velocity at this point was only 0.1 m/s less than nominal. The flight path angle relative to the local horizontal was 0.003 deg lower than nominal. S-IVB/LM-1 apogee altitude was 0.1 km higher than nominal and perigee was 0.2 km higher than nominal.

The parking orbit portion of the trajectory, from insertion to S-IVB/LM-1 separation, was close to nominal. Separation of the Lunar Module from the S-IVB/IU occurred at 3235.24 sec, 0.04 sec later than nominal.

7.2 TRACKING DATA UTILIZATION

Tracking data were available from first motion through the major portion of the powered flight. The only data received from high precision tracking systems, in time for utilization, were ODOP and GLOTRAC Station I. However, the final GLOTRAC data compared to within 40m in position components. Telemetered guidance information and measured meteorological data were also received and utilized in the postflight trajectory determination.

The initial launch phase trajectory was established by a least squares curve fit to the ODOP data. From 28 sec to orbital insertion, the trajectory was established by a composite fit of all tracking data available, utilizing the guidance velocity data as the generating parameters for fit of the tracking data through an 18 term guidance error model.

Orbital C-Band Radar tracking data are shown in Table 7-I. The data utilized in the orbital correction program to establish the insertion point are presented in Table 7-II. The orbital insertion conditions were determined by adjusting the estimated insertion parameters to fit the orbital tracking data in accordance with the respective weights assigned to the tracking data.

TABLE 7-I SUMMARY OF C-BAND TRACKING

Station	Type of Radar	Revolution						
		1	2	3	4	5	6	7
Bermuda	FPS-16M	X	X					
Canary	MPS-26	X						
California	FPS-16M	X	X	X				
Hawaii	FPS-16M		X					X
Tananarive	FPS-16M	X	X	X	X	X		X
Ascension	TPQ-18			X	X			
Patrick AFB	FPQ-6	X						
Grand Bahama	TPQ-18		X					
Pretoria	MPS-25M				X	X	X	X

TABLE 7-II INSERTION CONDITIONS DATA UTILIZATION

Station	Parameter	No. of Data Points	RMS Error
Bermuda	Azimuth	25	0.009 deg
	Elevation	25	0.015 deg
	Range	25	11m
Tananarive	Azimuth	20	0.006 deg
	Elevation	21	0.009 deg
	Range	22	6m
Grand Bahama	Azimuth	43	0.010 deg
	Elevation	43	0.009 deg
	Range	48	8m
Bermuda	Azimuth	39	0.013 deg
	Elevation	39	0.017 deg
	Range	44	17m

The most reasonable solutions had a spread of ± 200 meters in position components and ± 1.5 m/s in velocity components. The best solutions were reached using Bermuda (Rev. 1), Tananarive (Rev. 1), and Bermuda (Rev. 2), and the venting model.

7.3 TRAJECTORY ANALYSIS, POWERED FLIGHT

The actual flight trajectory was very close to nominal during the launch vehicle powered flight. Actual and nominal altitude, surface range, and cross range for the launch vehicle powered flight, are presented in Figure 7-1. The actual and nominal total earth-fixed velocities are shown in Figure 7-2. Comparisons of the actual and nominal parameters at the three cutoff events are shown in Table 7-III. The nominal trajectory is presented in Reference 1. In many of the figures, the actual and nominal parameters are nearly identical and appear as a single line.

Through the major portion of the powered flight, the altitude was slightly higher than nominal and the surface range was slightly less than nominal. The total inertial acceleration, shown in Figure 7-3, was very close to nominal for both the S-IB and S-IVB powered flight phases.

The combined burn time of the S-IB and S-IVB stages was 5.00 sec shorter than nominal. The S-IB stage was responsible for 0.09 sec of this deviation, as reflected in Table 7-III. This table presents the deviations from nominal in all trajectory parameters. Trajectory parameters at significant events are presented in Table 7-IV.

The S-IB stage OECO was issued by the LVDC at 142.25 sec as a result of LOX depletion and the S-IVB cutoff signal was given by the guidance computer at 593.35 seconds. The velocity increments imparted to the vehicle as a result of thrust decay impulse are given in Table 7-V.

TABLE 7-V THRUST DECAY VELOCITY GAIN

Event	Actual (m/s)	Nominal (m/s)
OECO	5.4	6.3
S-IVB CO	6.4	5.8

Mach number and dynamic pressure are shown in Figure 7-4. These parameters were calculated using measured meteorological data to an altitude of 60 km. Above this altitude the U. S. Standard Reference Atmosphere was used.

A theoretical free flight trajectory was computed for the discarded S-IB stage, using initial conditions at S-IB/S-IVB separation. The trajectory was

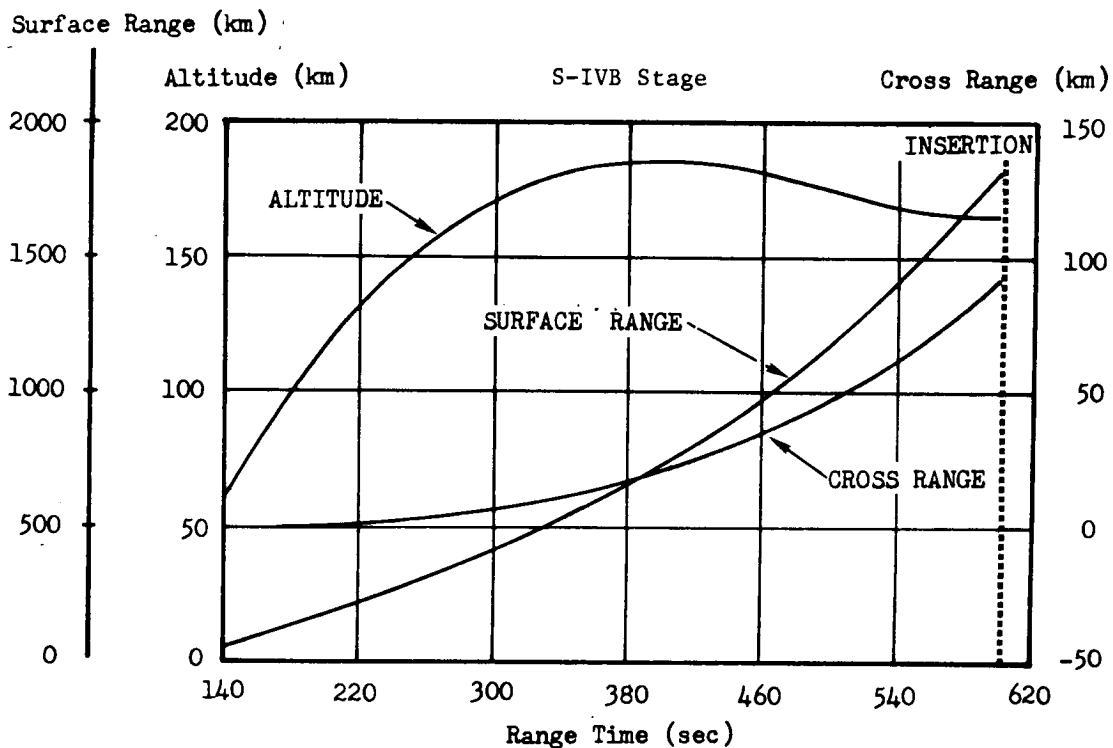
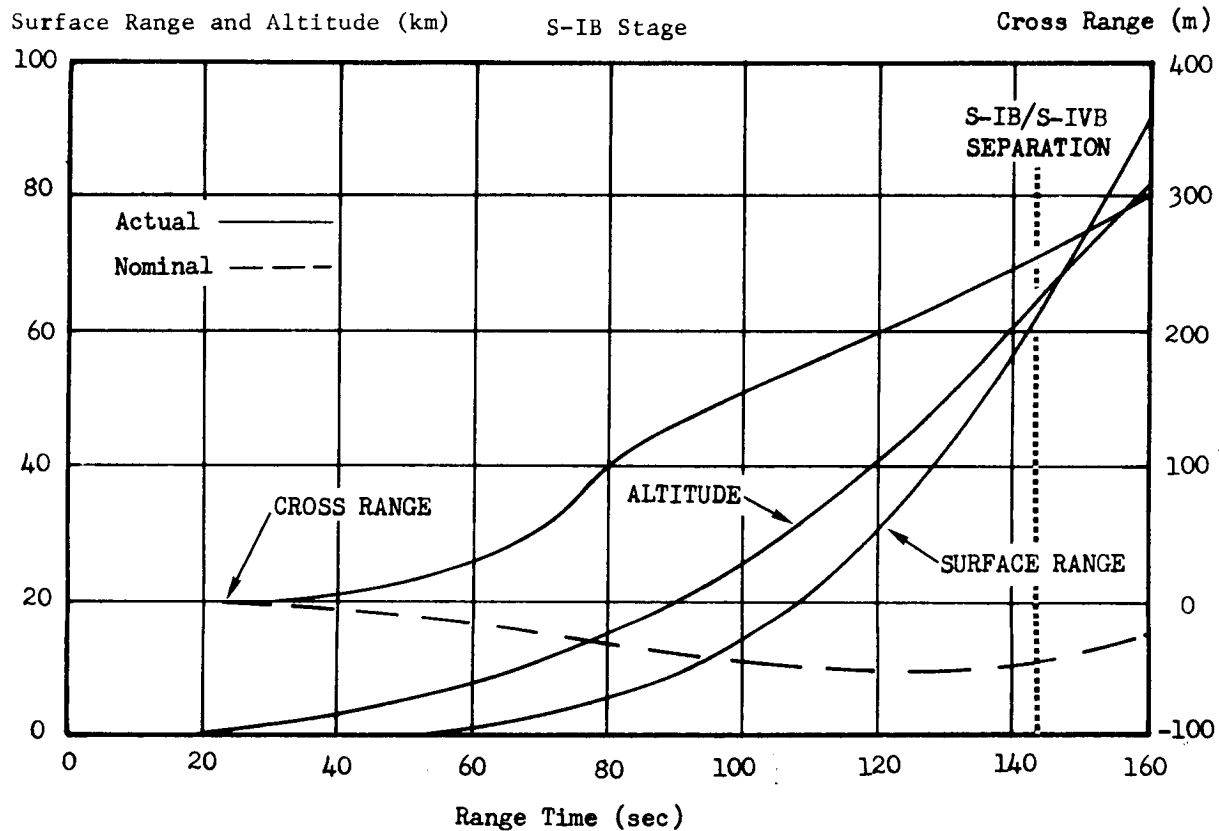


FIGURE 7-1 S-IB AND S-IVB TRAJECTORY

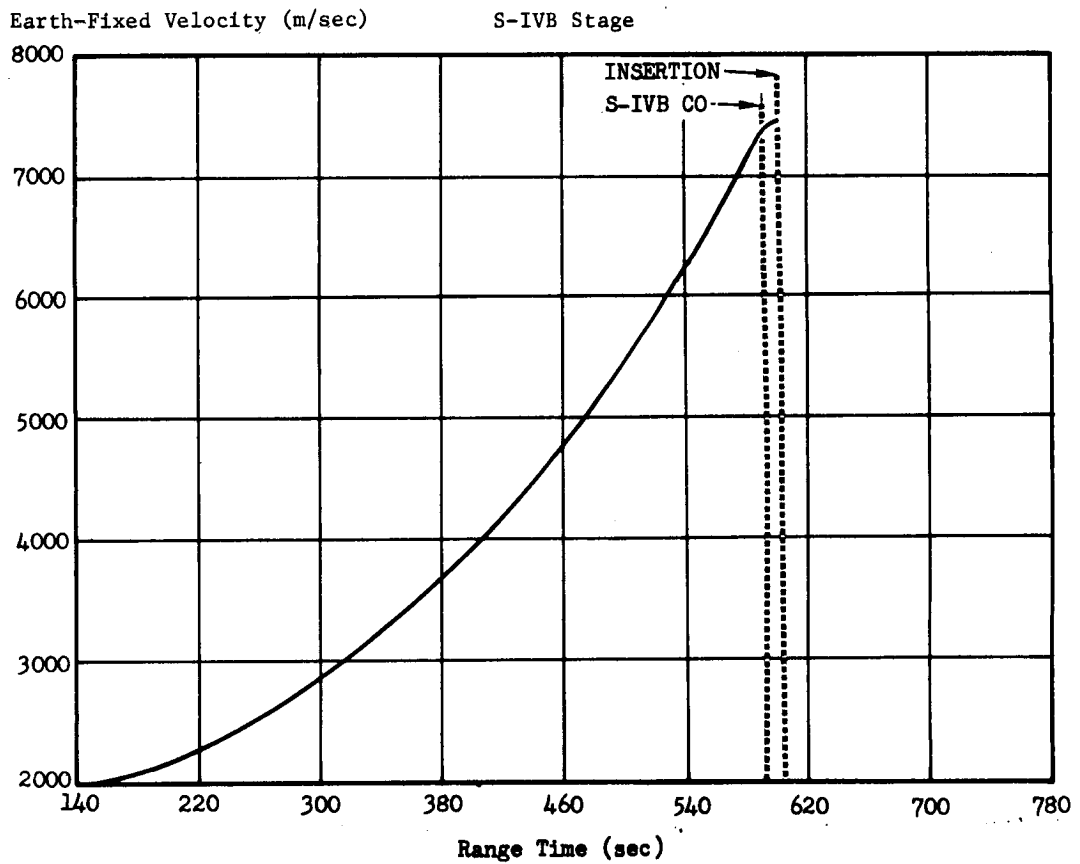
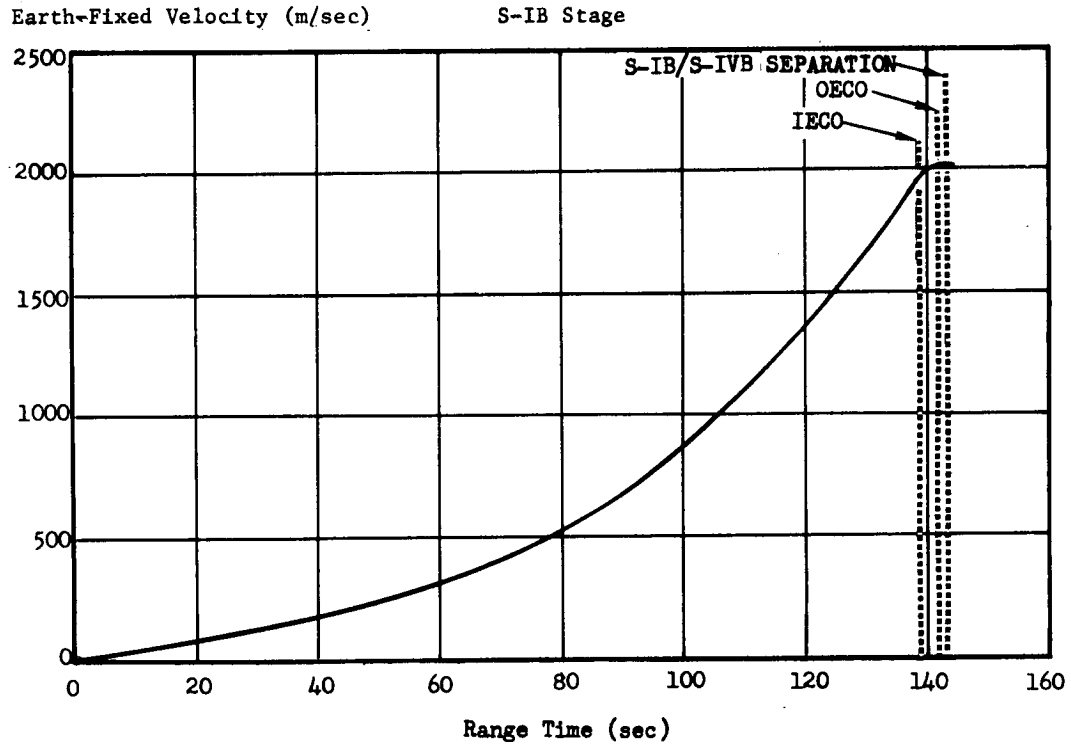


FIGURE 7-2 EARTH-FIXED VELOCITY

TABLE 7-III CUTOFF CONDITIONS

Parameter	Units	IECO			OEEO			S-IVB CO		
		Actual	Nominal	Act-Nom	Actual	Nominal	Act-Nom	Actual	Nominal	Act-Nom
Range Time	sec	138.97	139.34	-0.37	142.25	142.34	-0.09	593.35	598.35	-5.00
Altitude	km	59.20	58.82	0.38	62.79	62.08	0.71	163.42	163.19	0.23
Range	km	54.99	55.44	-0.45	60.41	60.43	-0.02	1765.21	1796.20	-30.99
Cross Range	km	0.24	-0.05	0.29	0.25	-0.05	0.30	87.57	90.88	-3.31
Cross Range Velocity	m/s	2.4	0.4	2.0	2.6	0.6	2.0	527.6	534.0	-6.4
Earth-Fixed Velocity Vector Elevation	deg	33.58	33.24	0.34	32.84	32.56	0.28	-0.01	0.0	-0.01
Earth-Fixed Velocity Vector Azimuth	deg	72.24	72.17	0.07	72.27	72.21	0.06	85.25	85.47	-0.22
Space-Fixed Velocity	m/s	2305.1	2309.9	-4.8	2365.4	2368.7	-3.3	7821.1	7821.5	-0.4
Total Inertial Acceleration	m/s ²	42.59	43.02	-0.43	18.71	19.70	-0.99	25.38	25.09	0.29
Earth-Fixed Velocity	m/s	1964.4	1968.3	-3.9	2022.4	2025.1	-2.7	7415.0	7415.7	-0.7

Earth-Fixed Velocity Accuracy

OEEO ± 0.3 m/s
S-IVB CO ± 0.5 m/s

Altitude Accuracy

OEEO ± 30 m
S-IVB CO ± 200 m

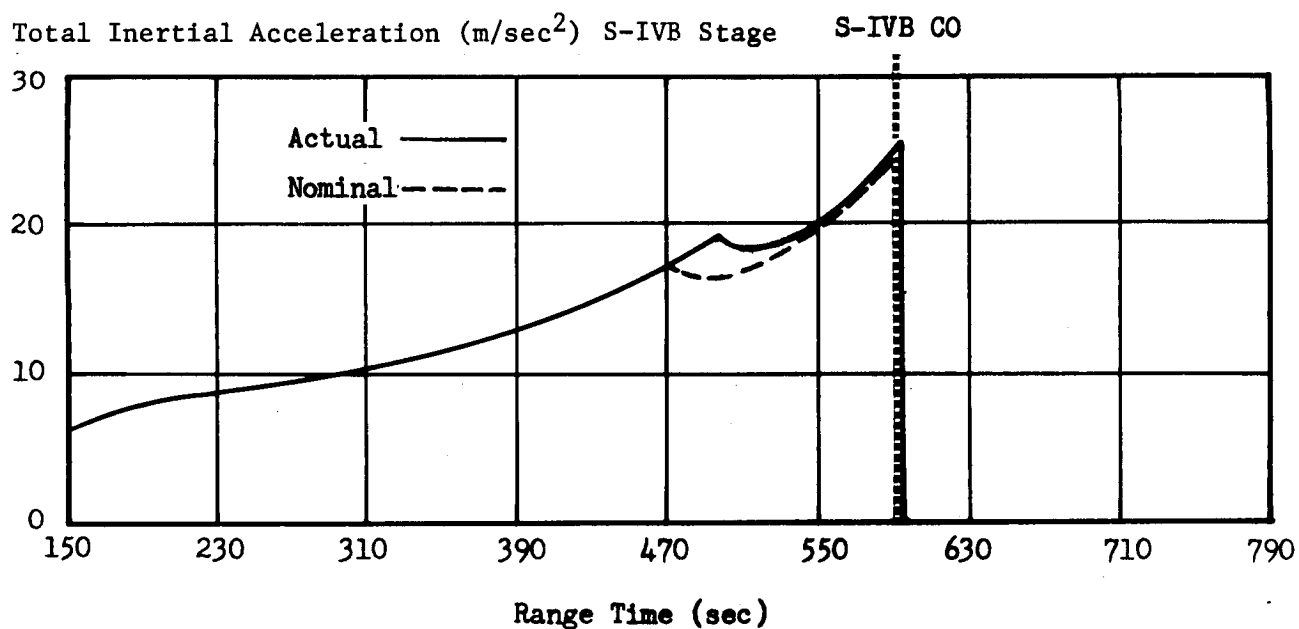
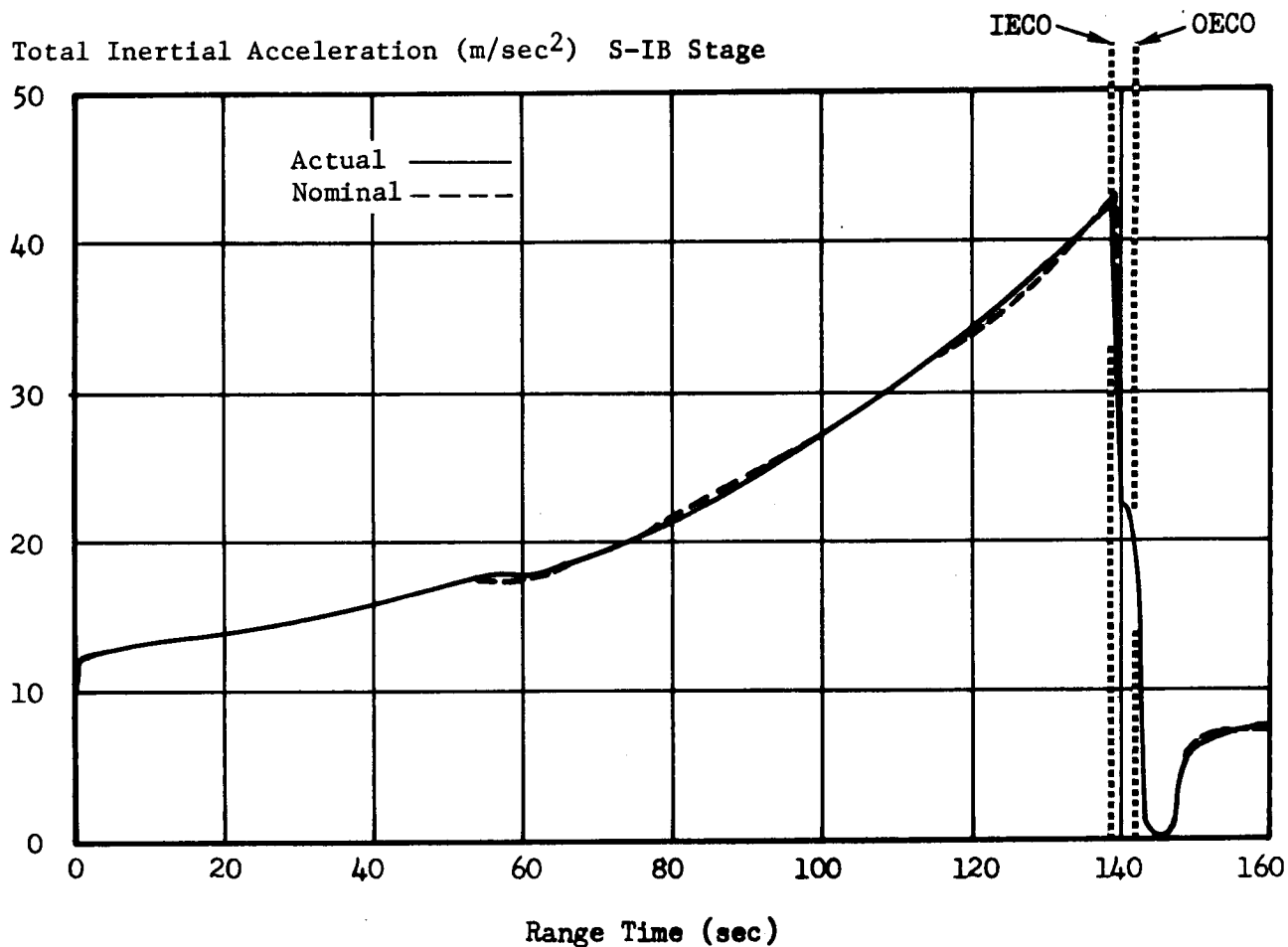


FIGURE 7-3 TOTAL INERTIAL ACCELERATION

TABLE 7-IV SIGNIFICANT EVENTS

Events	Parameter	Units	Actual	Nominal	Act-Nom
First Motion	Range Time	sec	0.20	0.20	0.00
	Total Inertial Acceleration	m/s ²	12.11	12.12	-0.01
Mach 1	Range Time	sec	59.56	60.18	-0.42
	Altitude	km	7.49	7.49	0.00
Maximum Dynamic Pressure	Range Time	sec	71.50	74.20	-2.70
	Dynamic Pressure	N/cm ²	3.13	3.27	-0.14
	Altitude	km	11.47	12.34	-0.87
Maximum Total Inertial Acceleration (S-IB Stage)	Range Time	sec	139.07	139.44	-0.37
	Acceleration	m/s ²	42.71	43.07	-0.36
Maximum Earth-Fixed Velocity (S-IB Stage)	Range Time	sec	142.6	142.7	-0.1
	Velocity	m/s	2025.0	2028.4	-3.4
S-IB/S-IVB Separation (Command)	Range Time	sec	143.50	143.64	-0.14
	Altitude	km	64.16	63.49	0.67
	Surface Range	km	62.52	62.63	-0.11
	Cross Range	km	0.25	-0.05	0.30
	Space-Fixed Velocity	m/s	2365.7	2369.8	-4.1
	Flight Path Angle	deg	27.39	27.16	0.23
Apex (S-IB Stage)	Range Time	sec	264.93	264.20	0.73
	Altitude	km	129.22	127.23	1.99
	Surface Range	km	261.02	261.16	-0.14
	Earth-Fixed Velocity	m/s	1652.7	1665.2	-12.5
Loss of Telemetry (S-IB Stage)	Range Time	sec	397.1	397.1	0.0
	Altitude	km	52.39	44.96	7.43
	Surface Range	km	496.96	477.64	-0.68
	Total Earth-Fixed Acceleration	m/s ²	-7.69	-12.21	-4.52
	Elevation Angle from Pad	deg	4.095	3.213	0.882
Impact (S-IB Stage)	Range Time	sec	562.7	563.6	-0.9
	Surface Range	km	523.64	522.75	0.89
	Geodetic Latitude	deg	29.85	29.87	-0.02
	Longitude	deg	75.39	75.41	-0.02
Maximum Total Inertial Acceleration (S-IVB Stage)	Range Time	sec	593.44	598.35	-4.91
	Acceleration	m/s ²	25.38	25.09	0.29
Maximum Earth-Fixed Velocity (S-IVB Stage)	Range Time	sec	595.0	599.9	-4.9
	Velocity	m/s	7422.5	7422.4	0.1

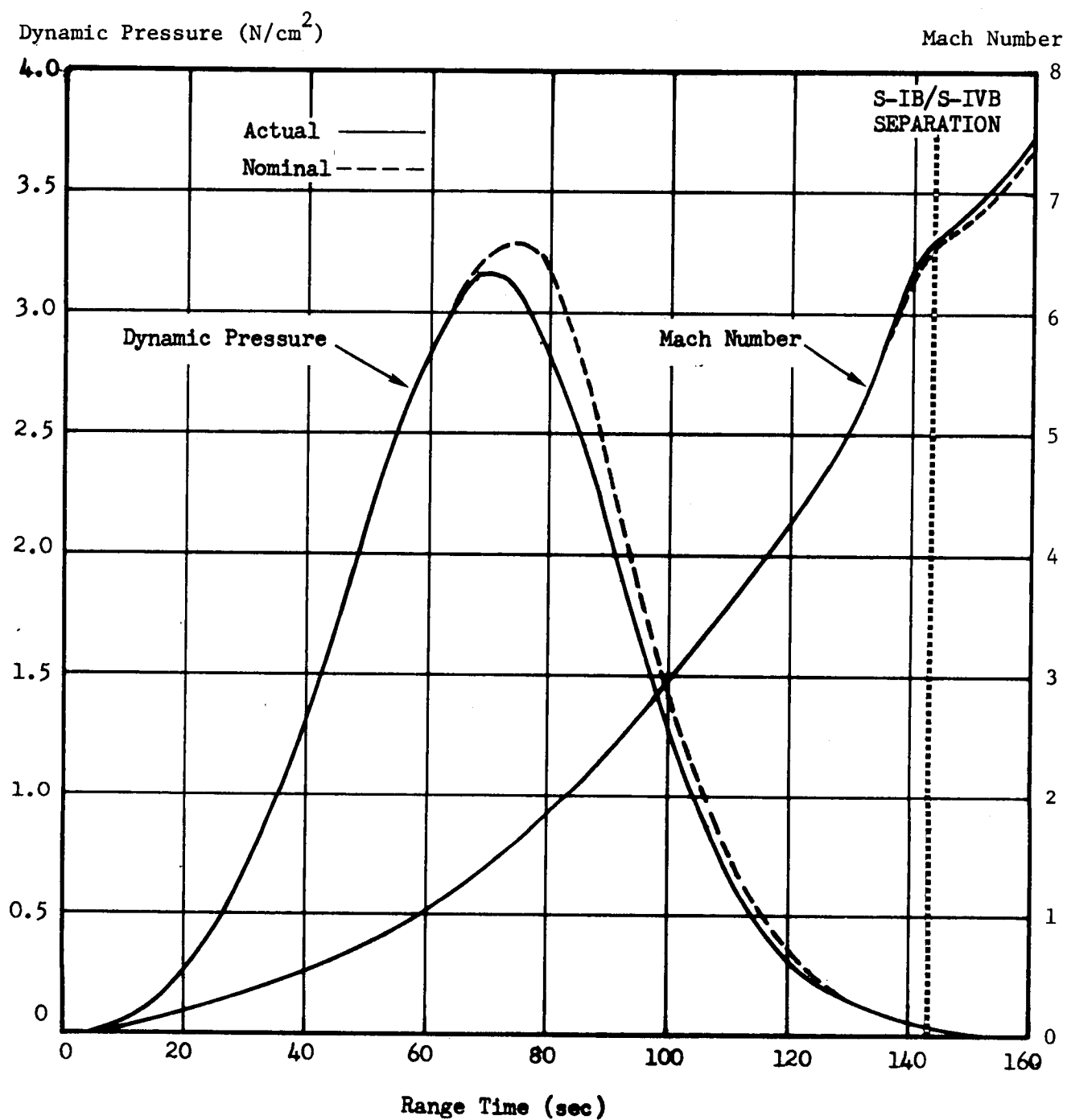


FIGURE 7-4 MACH NUMBER AND DYNAMIC PRESSURE

integrated from separation, assuming nominal retro rocket performance and outboard engine thrust decay. Tracking data were not available to confirm the results obtained.

The free flight trajectory utilizing the tumbling drag coefficient data was considered as the actual trajectory for the S-IB booster stage. Tracking on previous flights has proven this method to be a close approximation.

7.4 PARKING ORBIT TRAJECTORY

The parking orbit trajectory originates at S-IVB/LM-1 orbital insertion (603.35 sec) and continues until S-IVB/LM-1 separation (3235.24 sec). The trajectory parameters at orbital insertion were established by the best estimate trajectory in conjunction with the orbital correction program. The trajectory parameters for orbital insertion and S-IVB/LM-1 separation, as obtained from the orbital Correction Program, are presented in Tables 7-VI and 7-VII. The orbital ground track is presented in Figure 7-5.

7.5 S-IVB ORBITAL SAFING EXPERIMENT TRAJECTORY

The programmed S-IVB LOX and fuel dump was initiated at 2 hr: 26min: 14.31 sec (8774.31 sec) and was terminated at 2 hr: 31 min: 24.51 sec (9084.51 sec). The orbital parameters at these times were calculated from the integrated trajectory, utilizing the telemetered acceleration data. A trajectory was also initiated at the start of the LOX and fuel dump sequence and integrated through the sequence, assuming no accelerations due to dumping. This provides a theoretical calculated orbit, with no propellant dumping, as a basis for comparison. The orbital parameters at 2 hr: 31 min: 24.51 sec (9084.51 sec) from the theoretical trajectory are tabulated in Table 7-VIII under the no dump column. These parameters are compared to the parameters computed with the telemetered accelerations to determine the effects of the propellant dump on the orbit. This comparison is presented in Table 7-VIII. The apogee and perigee of the S-IVB orbital phase were changed, due to the safing experiment, by 5.867 km and -7.358 km, respectively.

TABLE 7-VI S-IVB INSERTION PARAMETERS

Parameter	Units	Actual	Nominal	Act-Nom
Range Time	sec	603.35	608.35	- 5.00
Space-Fixed Velocity	m/s	7828.5	7828.6	- 0.1
Altitude	km	163.44	163.22	0.22
Range	km	1837.56	1868.55	-30.99
Cross Range	km	92.87	96.24	- 3.37
Cross Range Velocity	m/s	532.7	539.0	- 6.3
Flight Path Angle	deg	0.005	0.008	- 0.003
Apogee	km	221.50	221.40	0.1
Perigee	km	157.60	157.40	0.2

TABLE 7-VII S-IVB/LM SEPARATION PARAMETERS

Parameter	Units	Actual	Nominal	Act-Nom
Range Time	sec	3235.24	3235.20*	0.04
Altitude	km	222.11	223.31	- 1.20
Space-Fixed Velocity	m/s	7759.1	7758.2	0.9
Flight Path Angle	deg	- 0.013	- 0.008	- 0.005
Heading Angle	deg	94.573	94.580	- 0.007

*From L/V operational trajectory

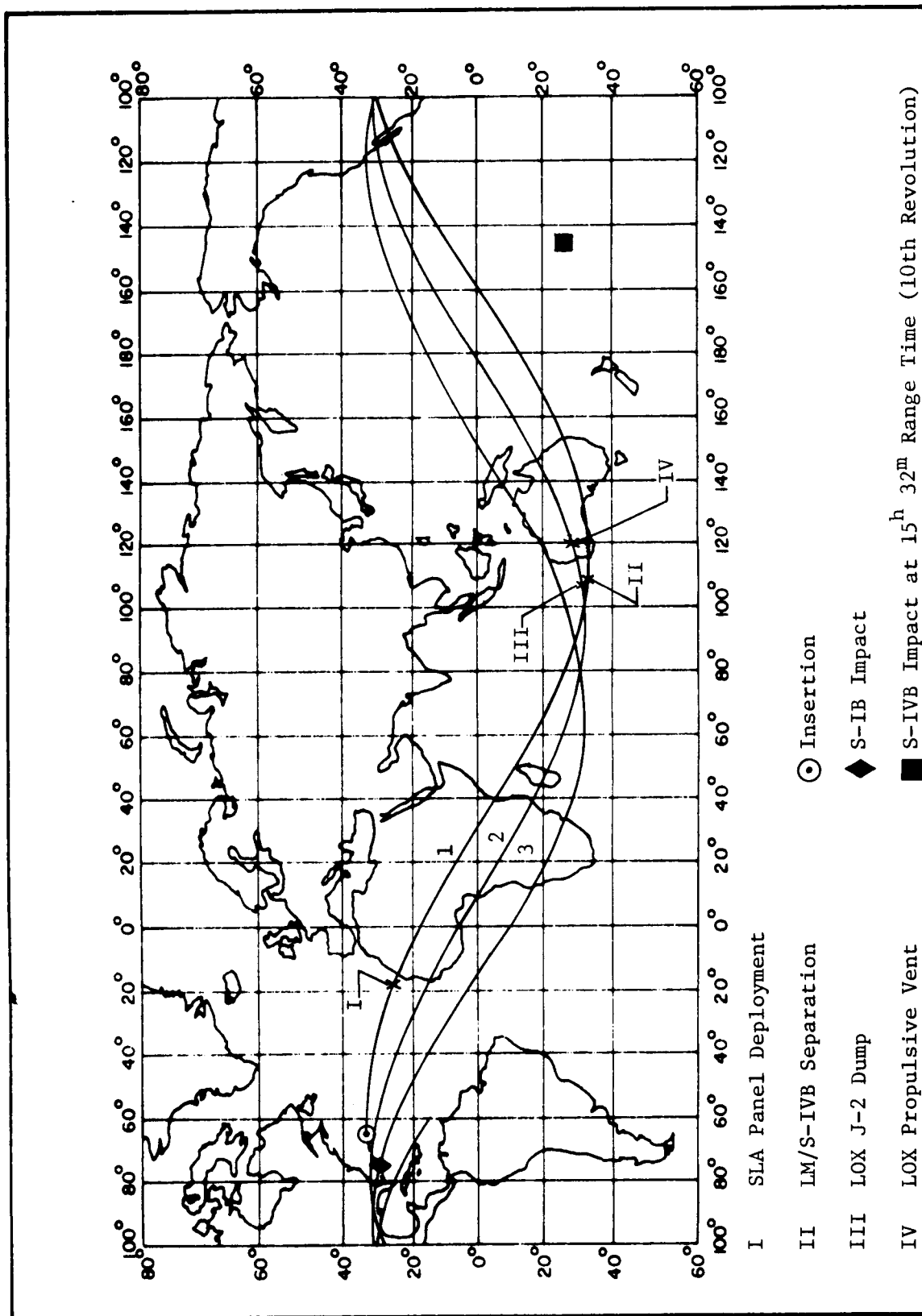


FIGURE 7-5 AS-204 GROUND TRACK

TABLE 7-VIII EFFECTS OF S-IVB ORBITAL SAFING EXPERIMENTS

Parameter	Unit	Before LOX Dump	After LH ₂ Dump	No Dump (Theoretical Orbit)	Orbital Effects (Dump - No Dump)
Range Time	sec	8774.31	9084.51	9084.51	----
Period	min	88.262	88.272	88.87	-0.015
Apogee	km	216.493	223.175	217.308	5.867
	nm	116.897	120.505	117.337	3.168
Perigee	km	160.492	154.777	162.135	-7.358
	nm	86.659	83.573	87.546	-3.973
Space-Fixed Velocity	m/s	7760.23	7771.64	7767.52	4.12
	ft/s	25459.76	25497.20	25483.68	13.52
Flight Path Angle	deg	-0.0893	-0.2629	-0.1721	-0.0908
Inclination	deg	31.6281	31.6388	31.6372	0.0016
Eccentricity	-	0.0043	0.0052	0.0042	0.0010

8.0 S-IB PROPULSION

8.1 SUMMARY

The S-IB propulsion system performed satisfactorily throughout flight.

On the basis of flight simulation: stage thrust, propellant flowrate, and specific impulse were 1.24%, 0.14%, and 1.10% higher than predicted, respectively.

Inboard engine cutoff (IECO) occurred 0.37 sec earlier than predicted. Outboard engine cutoff (OECO) was initiated 3.25 sec after IECO by the deactuation of the thrust OK pressure switches of engines 1 and 2 due to LOX starvation. The LVDC sensed OECO 0.03 sec later at 142.25 seconds.

Resequencing of the flight events resulted from S-IB-4 performance repredictions for which the propellants were loaded. Based on these repredictions, IECO occurred 2.54 sec early.

The fuel and LOX pressurization systems operated satisfactorily. The helium blowdown system was used successfully for the fourth consecutive flight in the fuel pressurization system.

Propellant utilization was satisfactory and close to predicted.

All mechanical systems functioned satisfactorily.

8.2 S-IB PROPULSION PERFORMANCE

Two separate analyses were used to determine the S-IB engine performance. The first method of determining the S-IB propulsion system flight performance was the reconstruction of the telemetered flight data with the Mark IV computer program. Calculated propellant residuals were also used as inputs to the program. The Mark IV program is a mathematical model of the Saturn IB stage propulsion system utilizing a table of influence coefficients to determine engine performance. A program option, RPM match, was used to arrive at engine power levels and propellant flowrates. The second method of determining S-IB engine performance utilized a trajectory simulation to generate multipliers that were enforced on the engine analysis results so that the resulting calculated trajectory fitted the actual observed trajectory.

The engine analysis evaluation of the flight performance of the S-IB-4 propulsion system is based upon the final prediction (reprediction) (Ref 4) for a January launch which was made with a revised table of influence coefficients. The previous prediction for a September launch as incorporated in the final operational trajectory (Ref 2) agrees more

closely with actual engine power levels and event times because of an unusually cold LOX condition experienced in this flight. Propellant loading operations at KSC were also consistent with the final prediction.

The predicted times used in the engine analysis portion of this section are shown in Table 8-I and were based on the repredicted parameters. These times are 2.17 sec later than those used in performing the flight simulation and those quoted in Section 4.0, which causes the deviations to be 2.17 sec greater when compared to the repredicted times.

Comparisons with both the predicted values from the MSFC preflight trajectory and the repredicted values are made in Table 8-IV where trajectory flight simulation analysis techniques were utilized.

8.2.1 STAGE PERFORMANCE

All eight H-1 engines ignited satisfactorily. The automatic ignition sequence, which schedules the engines to start in pairs with a 100 millisecond (ms) delay between each pair, began with ignition command at -2.968 seconds. The recorded individual engine ignition signals are shown in Table 8-II.

TABLE 8-II ENGINE START CHARACTERISTICS

Engine Position	Time from Ignition Command to Engine Ignition Signal (ms)	
	Actual	Programmed
5 and 7	12	10
6 and 8	112	110
2 and 4	212	210
1 and 3	312	310

Individual engine thrust buildup and stage thrust buildup are presented in Figure 8-1. The stage thrust shown is the sum of the individual engine thrusts and does not account for engine cant angles.

S-IB stage performance throughout flight was satisfactory. Figure 8-2 shows inflight stage longitudinal thrust and specific impulse determined from analysis of engine measurements. Stage inflight performance parameters are shown in Table 8-III. In this table, comparisons are made to repredicted values taken between first motion and IECO. The repredicted values were taken from the final propulsion predictions mentioned in Section 8.2. S-IB stage propellant mixture ratio and flowrate are shown in Figure 8-3. Stage LOX and fuel flowrates are shown

TABLE 8-I S-IB STAGE PROPULSION SYSTEM EVENT TIMES

Event	Actual Range Time (Sec)	Repredicted Range Time (Sec)	Act - Repred (Sec)
Engine Ignition Sequence			
Ignition Command	-2.968	-2.900	-0.068
Ignition Sequence 1 (Engines 5 & 7)	-2.956	-2.890	-0.066
Ignition Sequence 2 (Engines 6 & 8)	-2.856	-2.790	-0.066
Ignition Sequence 3 (Engines 2 & 4)	-2.756	-2.690	-0.066
Ignition Sequence 4 (Engines 1 & 3)	-2.656	-2.590	-0.066
First Motion	0.200	0.200	0.0
Start of Time Base 2	135.91	138.41	-2.50
Tank F2 Level Sensor Actuation (LSA)	137.62		
Tank F4 LSA	137.62		
Tank 02 LSA	135.90	138.41	-2.51
Tank 04 LSA	136.06		
Inboard Engine Cutoff	138.97	141.51	-2.54
Outboard Engine Cutoff (Engines 1,2,&3)	142.22	144.51	-2.29
Outboard Engine Cutoff (LVDC)	142.25		
Outboard Engine Cutoff (Engine 4)	142.28		

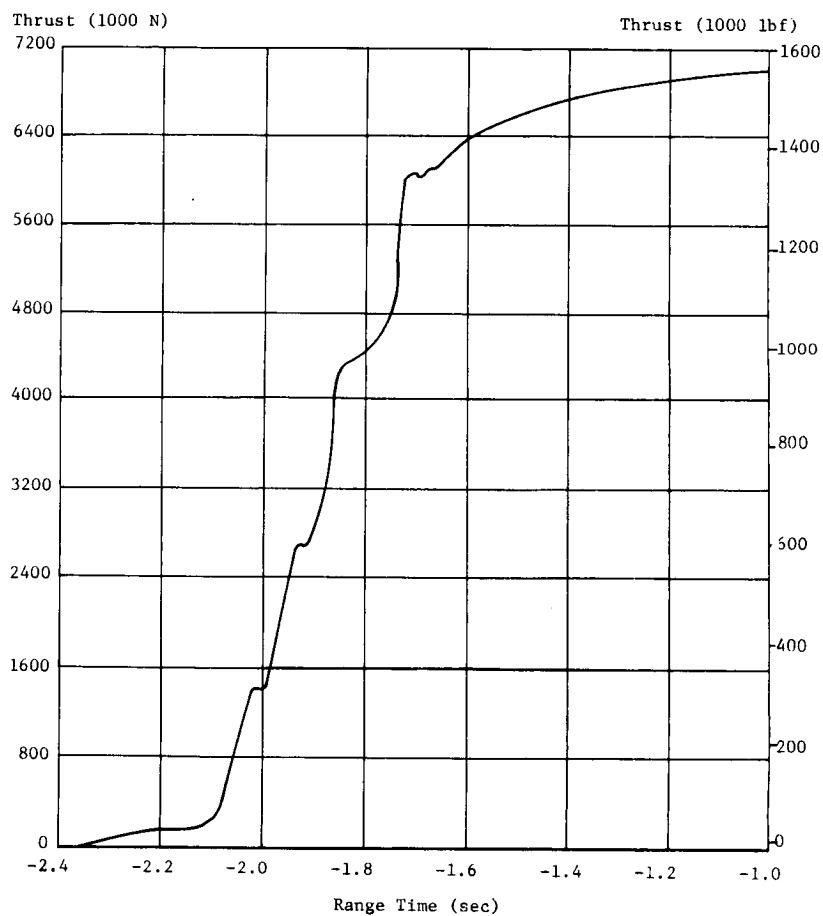
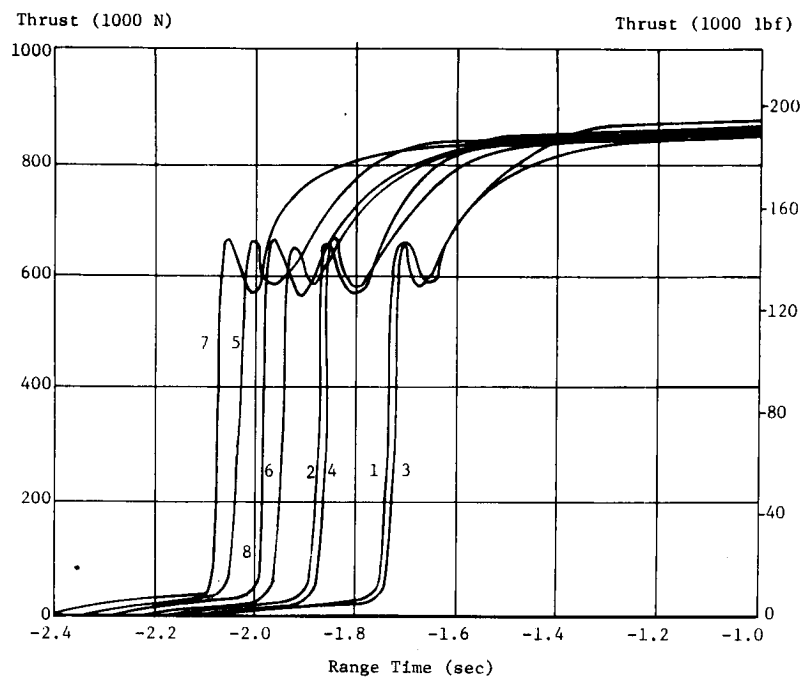


FIGURE 8-1 S-IB INDIVIDUAL ENGINE AND STAGE THRUST BUILDUP

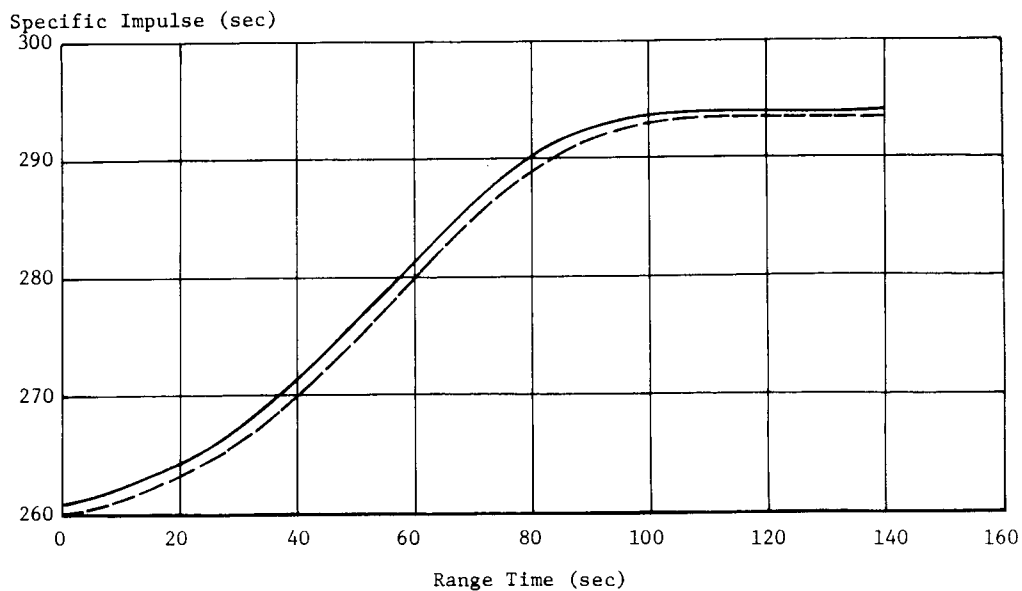
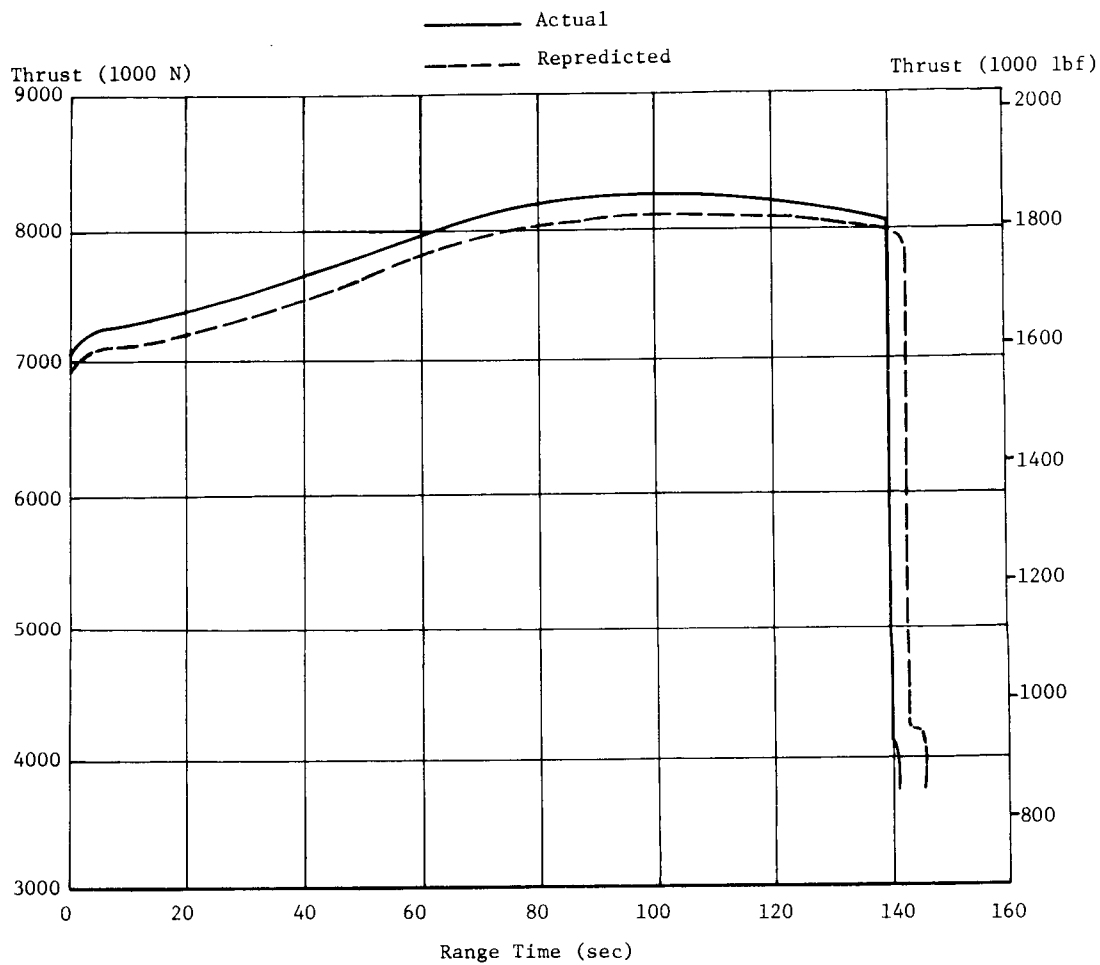


FIGURE 8-2 S-IB STAGE LONGITUDINAL THRUST AND SPECIFIC IMPULSE

TABLE 8-III S-IB STAGE INFLIGHT PERFORMANCE PARAMETERS

Parameters	Units	Actual Flight Engine Analysis	Repredicted	Flight Deviation From Repredicted	% Deviation
Thrust	N	7,870,674	7,733,322	137,352	1.78
	lbf	1,769,398	1,738,520	30,878	
Specific Impulse	sec	281.93	280.74	1.19	0.42
Stage Mixture Ratio	LOX/Fuel	2.2787	2.2524	0.0263	1.17
Total Propellant Flowrate	kg/s	2,846.7	2,808.9	37.9	1.35
	lbm/s	6,276.0	6,192.5	83.5	
LOX Flowrate	kg/s	1,978.5	1,945.2	33.3	1.71
	lbm/s	4,361.9	4,288.5	73.4	
Fuel Flowrate	kg/s	868.2	863.6	4.6	0.53
	lbm/s	1,914.1	1,904.0	10.1	

Note: Values listed are average altitude conditions which are not referenced to sea level conditions.

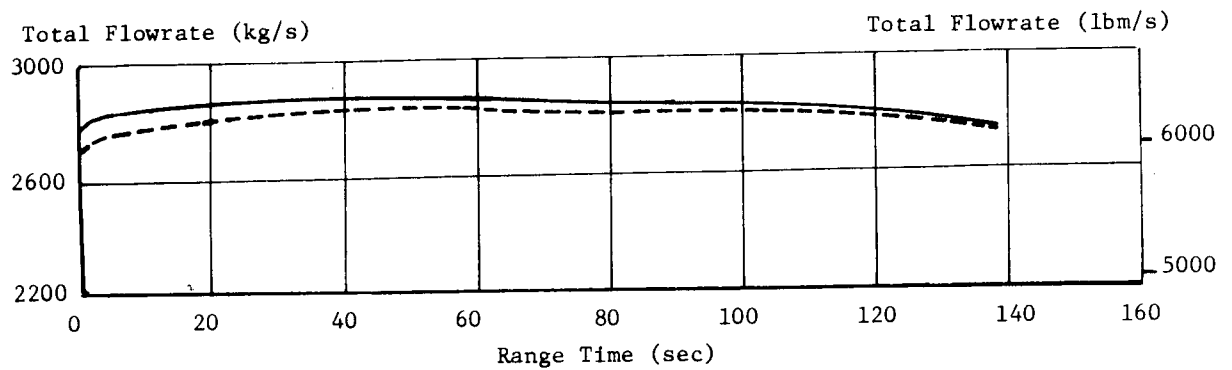
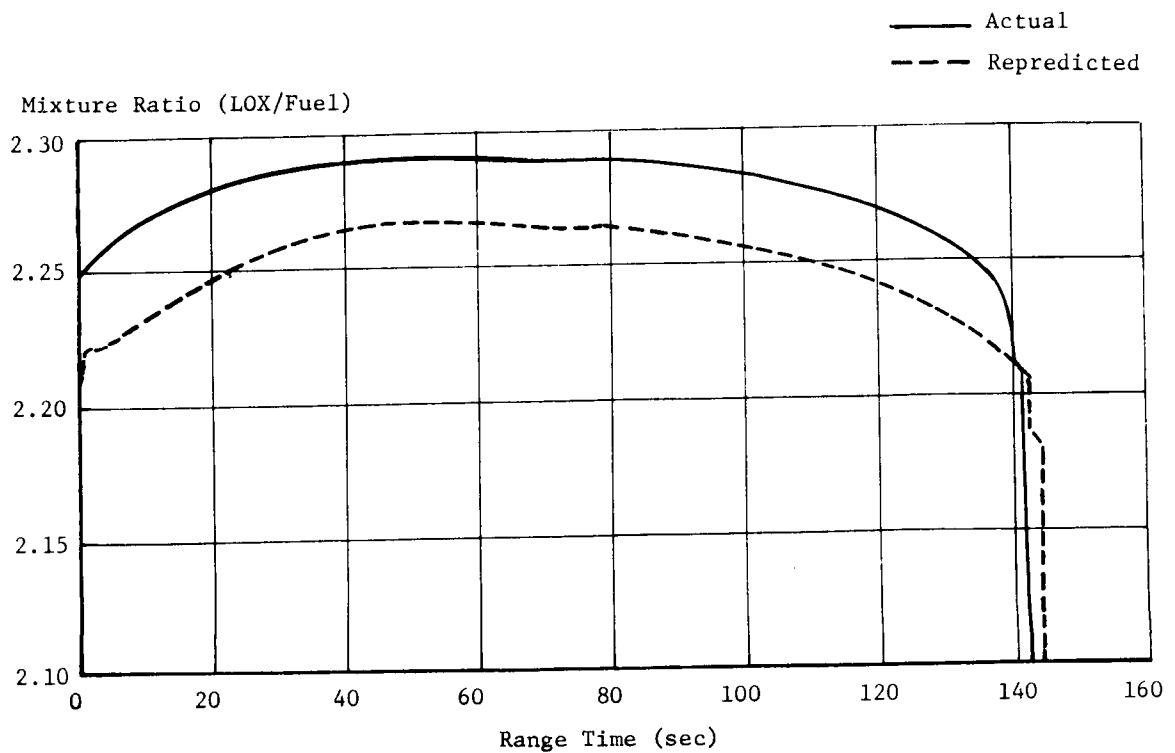


FIGURE 8-3 S-IB STAGE PROPELLANT MIXTURE RATIO AND FLOWRATE

in Figure 8-4. The performance parameters listed in Table 8-III and in the above mentioned figures are not reduced to sea level conditions. Reducing the thrust, specific impulse, and propellant flowrate in Table 8-III to sea level conditions yields the values in Table 8-IV. This table shows comparisons of predicted, repredicted, postflight engine analysis, and flight simulation propulsion values. Vehicle weights at first motion and IECO are also included in this table. The upper portion of Figure 8-5 shows the total longitudinal engine thrust, including the longitudinal component of the turbine exhausts. The curves show the official trajectory predicted thrust, repredicted thrust using an updated engine model, postflight engine thrust derived from engine analysis which incorporated telemetered propulsion measurements (reconstructed), and the thrust derived from flight simulation.

The higher than predicted performance can be explained by the flight deviations shown in Table 8-V. As can be seen from this table, the -1.16°K (-2.08°F) deviation from repredicted LOX temperature was the largest contributor to the higher performance. S-IB-4 was the second S-IB stage flown with a vent configuration providing vent valves in all five LOX tanks. The lack of experimental data with this new vent system, and the ambient loading conditions at KSC probably contributed most to the LOX density deviation. LOX pump inlet density throughout the flight is shown in the lower portion of Figure 8-5.

The mathematical model used to predict LOX density with the new vent configuration was formulated primarily from stage static test data of S-IB-1, S-IB-2, and S-IB-3, with only S-IB-3 having the same vent configuration as S-IB-4. Also, the LOX loading conditions during static tests are not entirely representative of those at KSC. The average LOX temperature during the S-IB-3 flight was 0.73°K (1.31°F) warmer than during the S-IB-4 flight. The LOX density prediction for S-IB-4 was influenced by the relatively high temperature data obtained from S-IB-3. Future predictions will incorporate the S-IB-4 flight results.

LOX density predictions are made for each flight from the projected ambient conditions of wind speed, humidity, temperature, and pressure that will occur statistically for that month. The accuracy of the prediction can be no better than the projected ambient conditions. The actual ambient conditions prior to launch accounted for 0.12°K (0.21°F) colder LOX than was predicted. The long (6 hour) hold of AS-204 may have contributed to colder LOX since launch observations indicated a thick layer of frost on the LOX tanks, which served as insulation. A survey of previous vehicle launch countdowns indicate that longer holds do contribute to colder LOX.

Another large contributor to the higher than repredicted performance was the fuel temperature and density variations. However, the 2.0°K (3.6°F) warmer than repredicted temperature is within the prediction accuracy expected for any launch.

The overall differences in engine calibration from predicted were some of the smallest ever experienced. Engine performance was

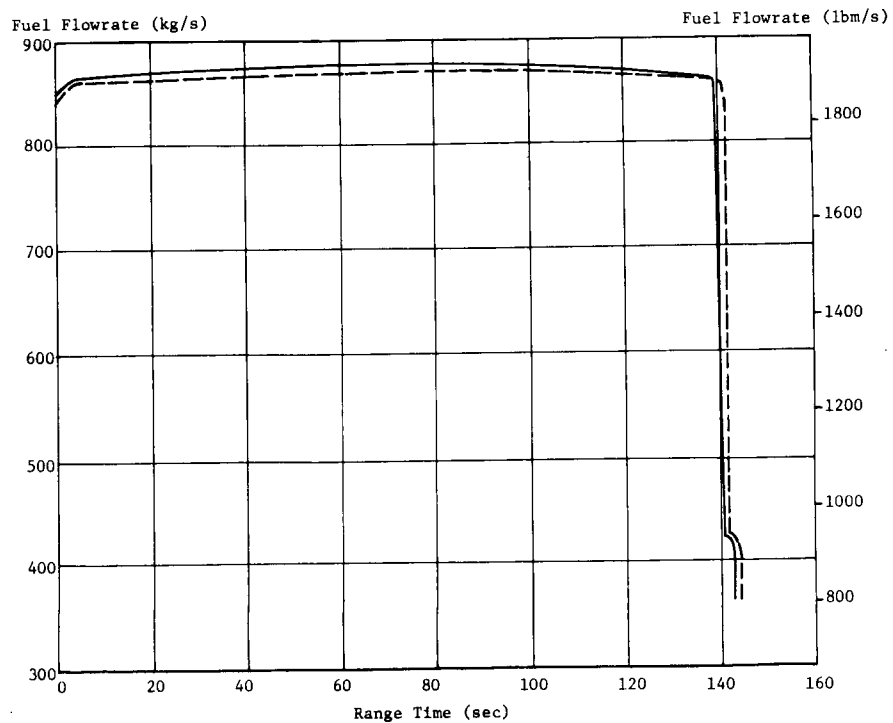
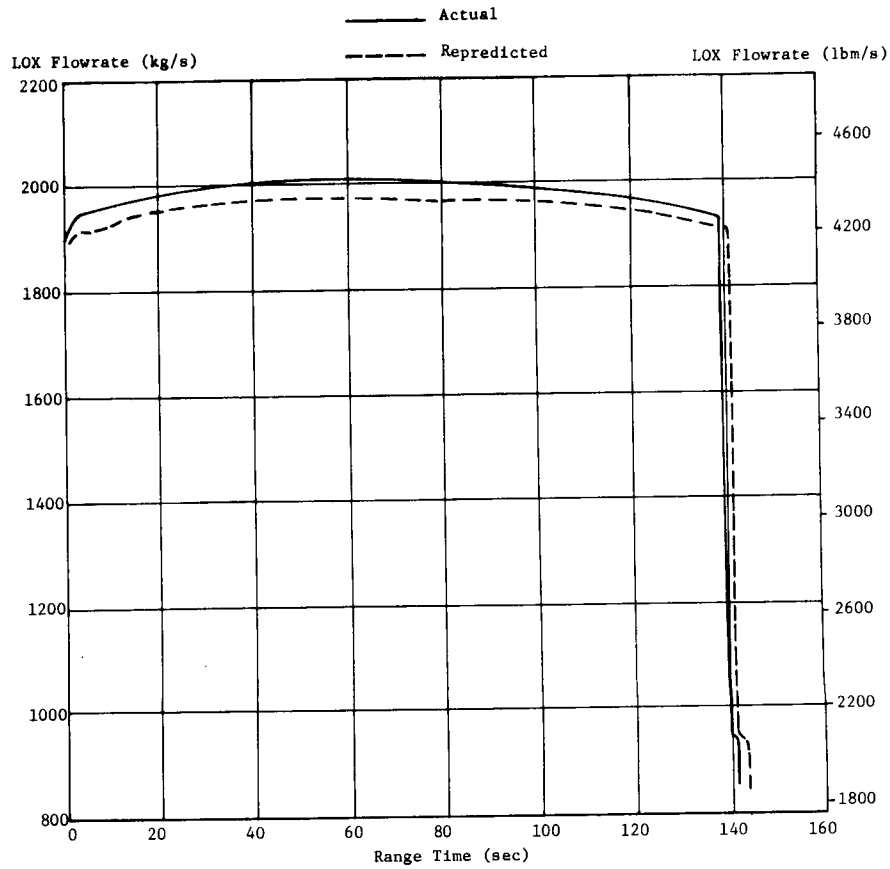


FIGURE 8-4 S-IB STAGE LOX AND FUEL FLOWRATES

TABLE 8-IV AVERAGE S-IB STAGE SEA LEVEL PROPULSION PARAMETERS

Parameters	Units	Predicted _{MLV}	Repredicted	% Dev. From Predicted	Flight Results			
					Engine Analysis	% Dev. From Predicted	Flight Simulation	% Dev. From Predicted
Sea Level Thrust	N	7,265,223*	7,194,896*	-0.97	7,327,213	0.85	7,355,610	1.24
	lbf	1,633,287*	1,617,477*		1,647,223		1,653,607	
Sea Level Specific Impulse	sec	260.62	261.21	0.23	262.47	0.71	236.48	1.10
Total Flowrate	kg/s	2,842.58	2,808.76	-1.19	2,846.70	0.14	2,846.70	0.14
	lbm/s	6,266.82	6,192.26		6,275.91		6,275.91	
First Motion Weight	kg	582,886	584,284	0.24	584,258	0.24	584,258	0.24
	lbm	1,285,044	1,288,126		1,288,069		1,288,069	
IECO Weight	kg	186,844	186,848	0.002	188,478	0.87	188,478	0.87
	lbm	411,920	411,929		415,522		415,522	

* Thrust levels do not include the 0.7% bias which was used in the final operational trajectory to account for "cluster effect".

Notes: (1) Propulsion parameters are average inflight values reduced to sea level ambient pressure conditions.

(2) Masses quoted in this table were used for establishing the flight simulation results and do not necessarily agree with those quoted in the final mass tables. The mass deviations are within 136 kg (300 lbm) and will not appreciably affect the simulation results.

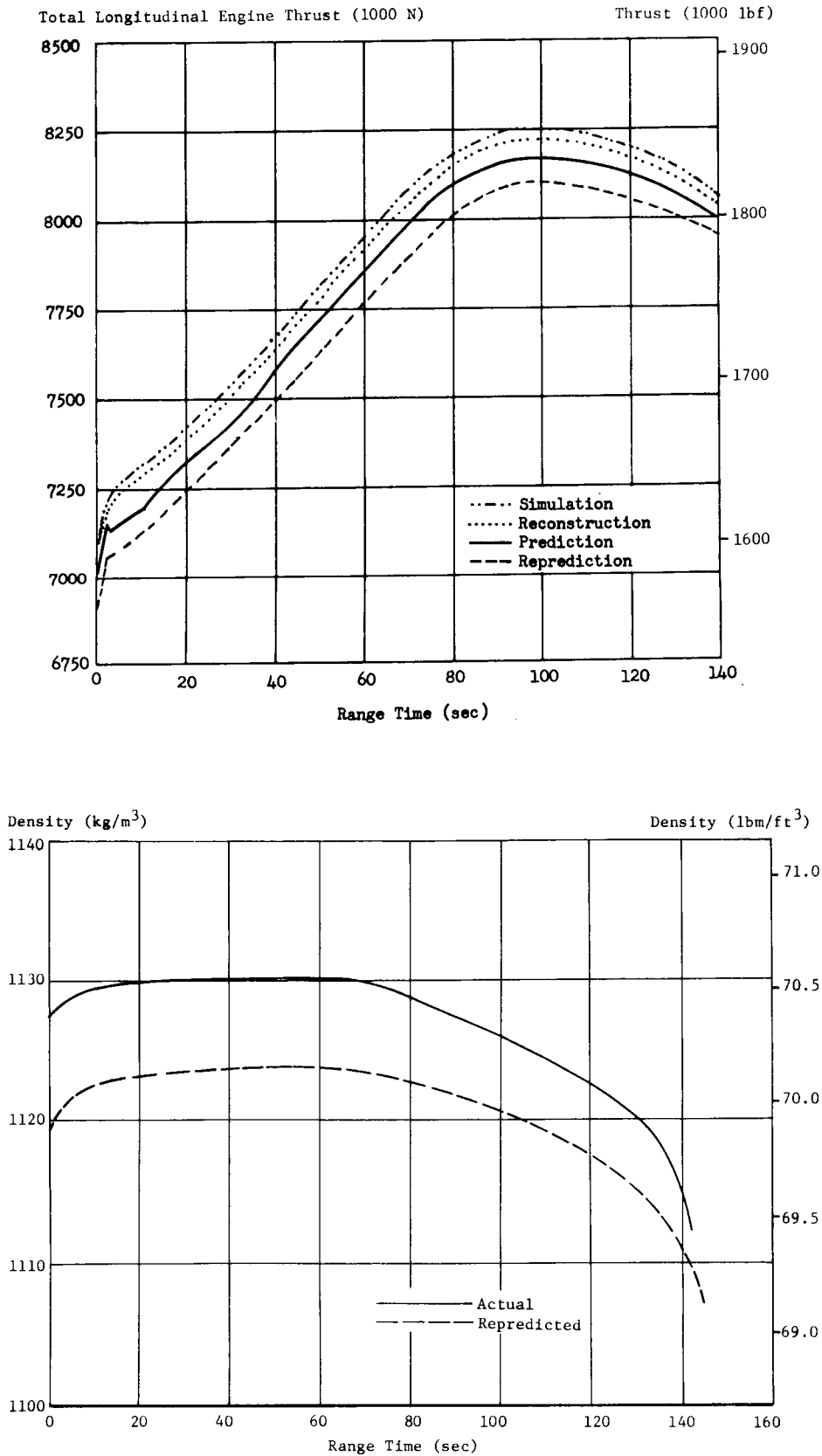


FIGURE 8-5 LONGITUDINAL ENGINE THRUST AND LOX DENSITY

TABLE 8-V INFLIGHT PERFORMANCE DEVIATION ANALYSIS

Error Contributor	Dev. from Repredicted	Percent Deviation From Repredicted			
		Thrust	Specific Impulse	Mixture Ratio	Burn-Time
LOX Pump Inlet Temperature	-1.16°K (-2.08°F)	1.07	0.20	0.92	-1.18
Fuel Temperature & Density	2.00°K (3.6°F)	0.27	0.05	0.24	-0.20
LOX Pump Inlet Pressure	-1.51 kg/m ³ (-0.094 lb/ft ³)	0.12	0.02	0.10	-0.13
Fuel Pump Inlet Pressure	0.55 N/cm ² (0.8 psi)	-0.02	0.02	-0.03	0.02
Engine Calibration	0.21 N/cm ² (0.30 psi)	0.34	0.22	-0.05	-0.11
Miscellaneous Effects			-0.09	-0.01	-0.20
Observed Deviation		1.78	0.42	1.17	-1.80

not predicted to be the same as either Rocketdyne or stage test data. Instead, a multiplier was enforced upon average data from the Rocketdyne single engine acceptance data so that results would be in accordance with the flight deviations from Rocketdyne test data experienced in S-IB-1, S-IB-2, and S-IB-3.

The S-IB stage received inboard engine cutoff signal 0.37 sec earlier than predicted, and the total earth fixed velocity at this time was 3.87 m/s lower than predicted. Flight simulation results were used to explain these time and velocity deviations. To explain the velocity deviations, an error analysis was made to determine the contributing parameters and the magnitude of the velocity deviation caused by each of these parameters. Table 8-VI lists the various error contributors and the cutoff velocity deviations associated with each one. The difference in velocity at IECO between the observed trajectory and the total error contributors was 1.07 m/s. This unexplained difference dropped to only 0.3 m/s just prior to IECO. This deviation in the unexplained differences was probably due to the transient area in the observed trajectory.

TABLE 8-VI VELOCITY DEVIATION ANALYSIS

Error Contributors	Dev. Fm. Pred. ΔV (m/s)
Prediction Thrust Bias (-0.7%)	-19.35
Guidance and Controls	-4.90
First Motion Mass (0.24%)	-13.85
Meteorological Data	6.44
Thrust (1.24%)	33.39
Flowrate (0.14%)	5.81
Axial Force Coefficient	1.67
Change in Burn Time (-0.37 sec)	-12.01
Total Contribution	-2.80
Observed	-3.87
Difference (total contrib. - observed)	1.07

Since inboard engine cutoff signal was given by a LOX level switch, the only quantities which affected the cutoff time are those which alter the level of LOX in the tanks. Table 8-VII lists the parameters which contributed to the deviation between the predicted and actual cutoff time, and the " Δt " contributions made by each.

TABLE 8-VII TIME DEVIATION ANALYSIS

Error Contributors	Dev. (Act-Pred) Δt (sec)
Initial LOX Load (-0.04%)	-0.05
LOX Consumed during Hold Down (0.09%)	-0.12
LOX Flowrate (0.07%)	-0.14
Excess LOX in Center Tank at IECO	-0.11
Total Contribution	-0.42
Observed	-0.37
Difference	0.05

The cutoff sequence on the S-IB stage began at 135.90 sec with the actuation of the LOX level cutoff probe in LOX tank 02. Inboard engine cutoff (IECO) was initiated 3.07 sec later by the Launch Vehicle Digital Computer (LVDC) at 138.97 seconds. IECO occurred 0.37 sec earlier than predicted. The shorter than predicted burn time to IECO was a result of a greater than predicted amount of LOX in the center tank at IECO, an increased LOX flowrate, and a longer holddown.

Thrust decay on each inboard engine was normal. The total inboard engine cutoff impulse was 1,193,485 N-s (268,306 lbf-s). Inboard engine total thrust decay is shown in the upper portion of Figure 8-6.

Outboard engine cutoff (OECO) occurred at 142.25 sec after the LVDC received deactuation of the thrust OK pressure switches of engines 1 and 2, as expected, when LOX starvation occurred. The expected time differential between IECO and OECO was 3.0 sec, with an actual time differential of 3.28 seconds. Total cutoff impulse for the outboard engines was 746,776 N-s (167,882 lbf-s). Outboard engine total thrust decay is shown in the lower portion of Figure 8-6.

8.2.2 INDIVIDUAL ENGINE CHARACTERISTICS

The performance of all eight engines was satisfactory. Thrust levels for all engines were higher than repredicted, with an average increase of 17,228 N (3,873 lbf) or 1.78% per engine. The average deviation from repredicted specific impulse was 1.19 sec or 0.42% higher than repredicted. Figure 8-7 shows the average deviation from repredicted thrust and specific impulse for engines 1 through 8 between first motion and IECO.

Individual engine flight performance data from the Mark IV reconstruction program were reduced to Sea Level Standard turbopump inlet

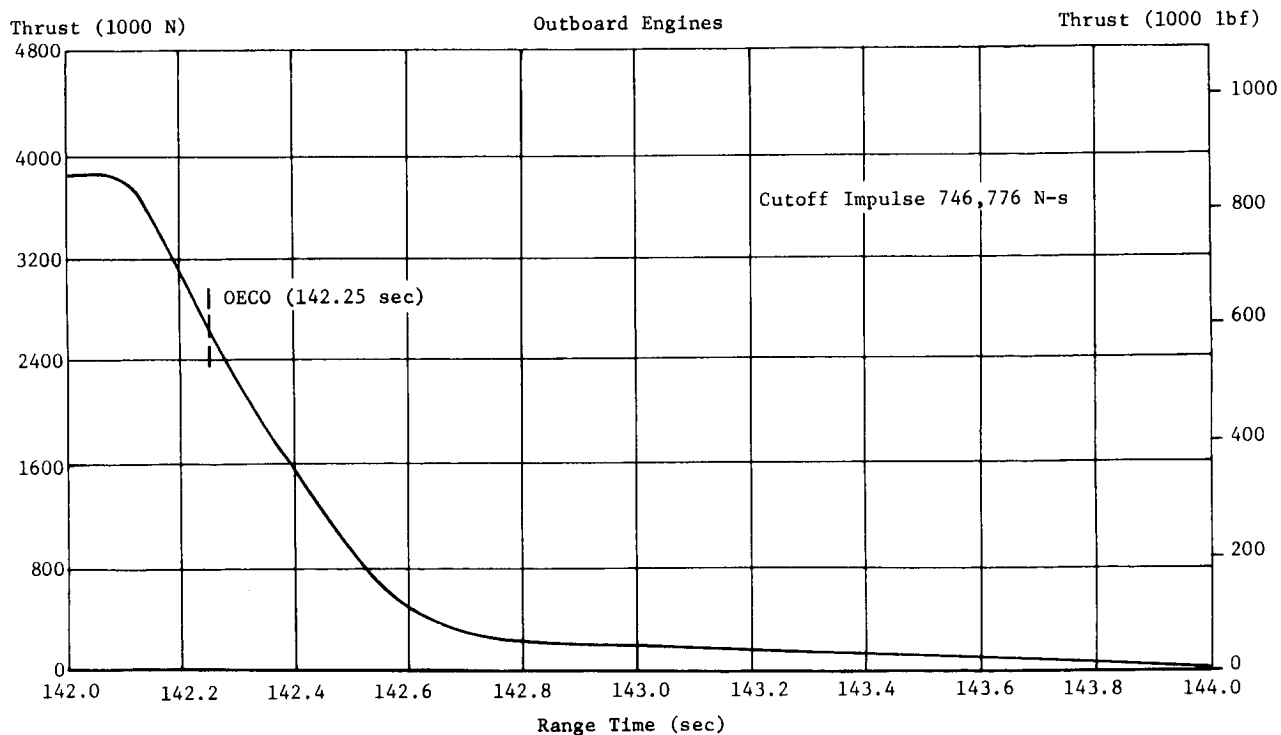
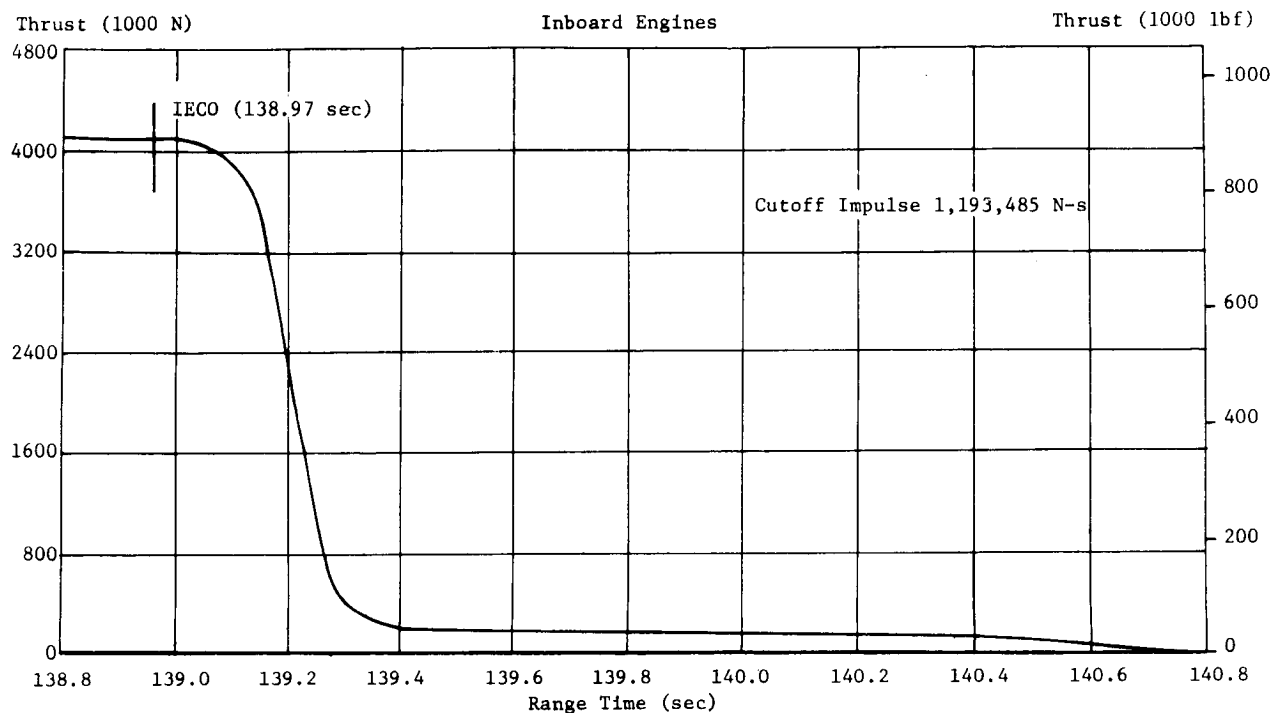
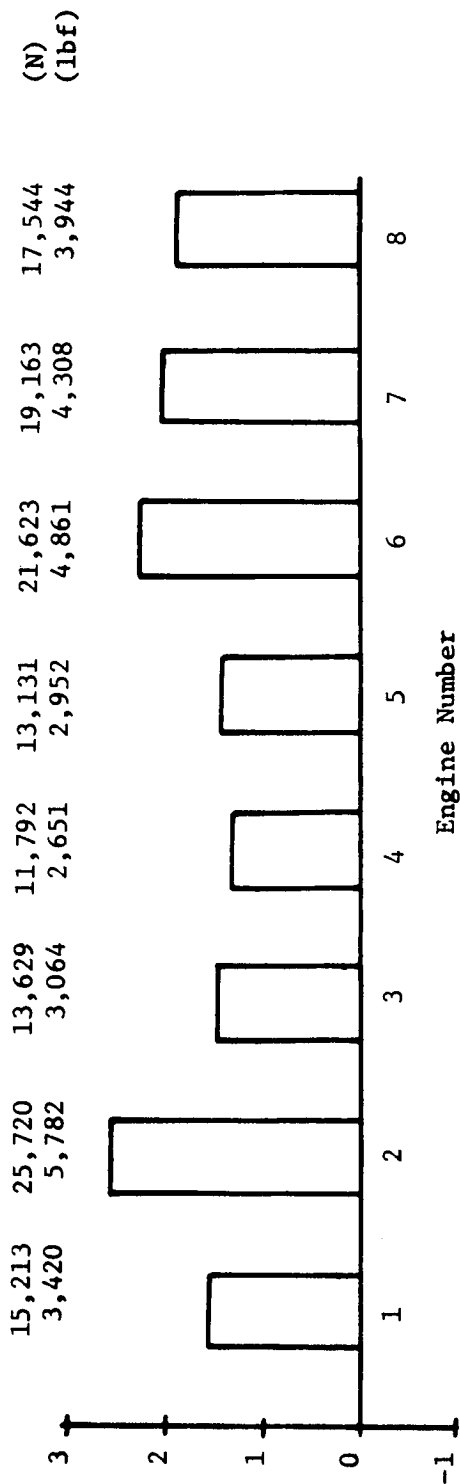


FIGURE 8-6 S-IB INBOARD AND OUTBOARD ENGINE THRUST DECAY

Average Deviation From Repredicted Thrust (%)



Average Deviation From Repredicted Specific Impulse (%)

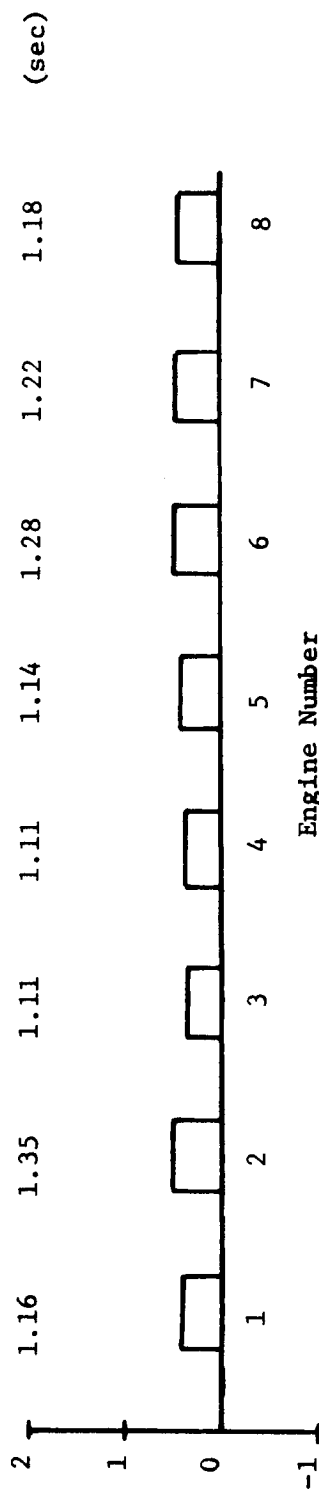


FIGURE 8-7 INDIVIDUAL ENGINE PERFORMANCE PARAMETERS

conditions to permit comparison of flight performance with predicted and preflight test performance. The reduction of engine data to Sea Level Standard conditions isolates performance variations due to engine characteristics from those attributable to engine inlet and environmental conditions.

The following discussion applies to the sea level performance at 30 seconds. This is the time period for which sea level performance is normally presented, and the flight prediction is based on test data obtained during this time period. Analysis of postflight data, along with static test data, indicates a pronounced increase in sea level performance occurring during the first 30 sec of flight, with a less pronounced increase occurring between this time and cutoff. The increase in sea level performance during the first 30 sec has been attributed to non-equilibrium engine operation and has been satisfactorily accounted for in the prediction. Sea level thrust, specific impulse, and mixture ratio are compared with repredicted values at a time slice of 30 sec in Table 8-VIII. At this time, the sea level thrust for engines 1 through 8 differed from repredicted by 0.194, 1.40, -0.144, -0.278, -0.028, 1.073, 0.443, 0.069 percent, respectively.

As can be seen from the above individual engine thrust deviations, only engine 2 and engine 6 show significantly higher than repredicted sea level thrust at 30 seconds.

The gas generator (GG) from engine 2 was removed to repair a leak in the LOX bellows surrounding the GG valve assembly LOX poppet. After successful repair of the bellows, a leak was found in the GG fuel poppet, which necessitated replacing the poppet. Subsequent component tests prompted the assessment that the engine, when reassembled with the repaired GG, would perform within the "normal run-to-run sigma" thrust deviation of 3,096 N (696 lbf).

Engine 6 was peculiar in that it resisted rotation during initial turbopump torque tests. The turbine was removed for repair which resulted in replacement of several non-aerodynamic parts such as seals and bearings. If the reassembly was closely controlled to maintain exactly the same blade-to-nozzle dimensions as on the original build, no change in engine performance would be expected. However, if the tolerances were not maintained, turbine power output and engine power would vary from previous tests. This could have caused the higher thrust levels on this engine. However, the turbine on engine 5 was also removed for repair which resulted in replacement of the same non-aerodynamic parts without a significant performance change.

8.3 S-IB PROPELLANT USAGE

Propellant usage is the ratio of propellant consumed to propellant loaded, and is an indication of the propulsion system performance and

TABLE 8-VIII
AS-204 AVERAGE INDIVIDUAL ENGINE PERFORMANCE AT 30 SECONDS

Sea Level Parameters	Units	Actual	Repredicted	Actual-Repredicted	% Deviation
Engine Thrust	N	901,567	898,478	3,078	0.34
Mixture Ratio	lbf	202,678	201,986	692	0.05
Specific Impulse	LOX/Fuel Sec	2.2353 262.76	2.2364 262.20	0.0011 0.56	0.21

the capability of the propellant loading system to load the proper propellant weights. The repredicted and actual (reconstructed) percentages of loaded propellants utilized during the flight are shown in Table 8-IX.

TABLE 8-IX PROPELLANT UTILIZATION

Propellant	Predicted (%)	Actual (%)
Total	99.13	98.94
Fuel	98.27	97.54
LOX	99.53	99.56

The planned mode of OECO was by LOX starvation. The LOX and fuel level cutoff probe heights and flight sequence settings were adjusted to yield a 3.1 sec time interval between any cutoff probe actuation and IECO, and a planned time interval between IECO and OECO of 3.0 seconds. OECO was to be initiated by the deactuation of two of the three thrust OK pressure switches on any outboard engine as a result of LOX starvation. It was assumed that approximately 0.284 m³ (75 gallons) of LOX in the outboard suction lines was usable. The backup timer (flight sequencer) was set to initiate OECO 10.1 sec after level sensor actuation. To prevent fuel starvation, fuel depletion cutoff probes were located in the F2 and F4 container sumps. The center LOX tank sump orifice was 48.3 ± 0.013 cm (19.0 ± 0.005 in) in diameter. Center LOX tank level was predicted to be 7.6 cm (3.0 in) higher than the LOX level in the outboard tanks at IECO.

The fuel bias for S-IB-4 was 453.6 kg (1000 lbm). This was included in the predicted residual and was available for consumption prior to IECO. An additional 3,885.5 kg (850 lbm) of the predicted residual was available for consumption prior to OECO if a significantly lower than predicted consumption ratio was experienced.

Data used in evaluating the S-IB propellant usage consisted of five discrete probe racks of 15 probes each in tanks 0C, 01, 03, F1, and F3; a continuous level probe in the bottom of each tank; cutoff level sensors in tanks 02, 04, F2, and F4; and fuel depletion probes in the F2 and F4 sumps.

The cutoff sequence on the S-IB was initiated by a signal from the LOX cutoff level sensor in tank 02 at 135.90 seconds. The IECO signal was received 3.07 sec later at 138.97 seconds. OECO occurred 3.25 sec after IECO at 142.22 sec due to LOX depletion on engines 1, 2, and 3. The LVDC initiated OECO at 142.25 sec or 0.03 sec later. Fuel depletion probes did not actuate prior to retrorocket ignition.

Based on continuous and discrete probe data, the liquid levels in the fuel tanks were nearly equal and approximately 69.6 cm (27.4 in)

above theoretical tank bottom at IECO (Figure 8-8). This level represents 5,747 kg (12,671 lbm) of fuel onboard. At that time, 4,954 kg (10,922 lbm) of LOX remained onboard. Corresponding LOX liquid height in the center tank was approximately 36.8 cm (14.5 in) and the average height in the outboard tanks was approximately 24.9 cm (9.8 in) above theoretical tank bottom. Propellants remaining above the main valves after outboard engine thrust decay were 1,250 kg (2,755 lbm) of LOX and 3,150 kg (6,945 lbm) of fuel. Repredicted values for these quantities were 1,337 kg (2,947 lbm) of LOX and 2,213 kg (4,878 lbm) of fuel.

Liquid levels illustrated in Figure 8-8 are based primarily on continuous level probe data. This data was not available beyond approximately 139.0 sec for the LOX tanks. Curves beyond these points are based on consumption rates from the Mark IV flight reconstruction and, as such, represent a best estimate. Since the cutoff mode was LOX depletion, LOX levels in the tanks beyond IECO were very low or below theoretical tank bottom; therefore, data on the exact heights are not considered to be critical for purposes of evaluation.

This was the first S-IB stage to fly with the shielded fuel depletion sensors in both tanks, and no premature actuation of the sensors was indicated. AS-202, the previous flight vehicle, had one sensor of the modified type and no abnormal operation was noted on that vehicle.

The cutoff probe signal times and setting heights from theoretical tank bottom are shown below:

TABLE 8-X CUTOFF PROBE ACTIVATION CHARACTERISTICS

Container	Height		Activation Time (sec)
	(cm)	(in)	
02	69.72	27.45	135.90
04	69.72	27.45	136.06
F2	84.77	33.375	137.62
F4	84.77	33.375	137.62

8.4 S-IB PRESSURIZATION SYSTEMS

8.4.1 FUEL PRESSURIZATION SYSTEM

The fuel tank pressurization system performed satisfactorily during the entire flight. The helium blowdown system used on this flight was identical to that used on S-IB-3, which included the 0.55 m³ (19.28 ft³) titanium spheres, lightweight tanks, and fuel vent valves. The measured absolute ullage pressure is compared with the predicted pressure in the upper portion of Figure 8-9. Measured ullage pressure compared favorably to the predicted pressure during the first half of the flight and never exceeded a difference of 1.0 N/cm² (1.5 psi). The Digital Events

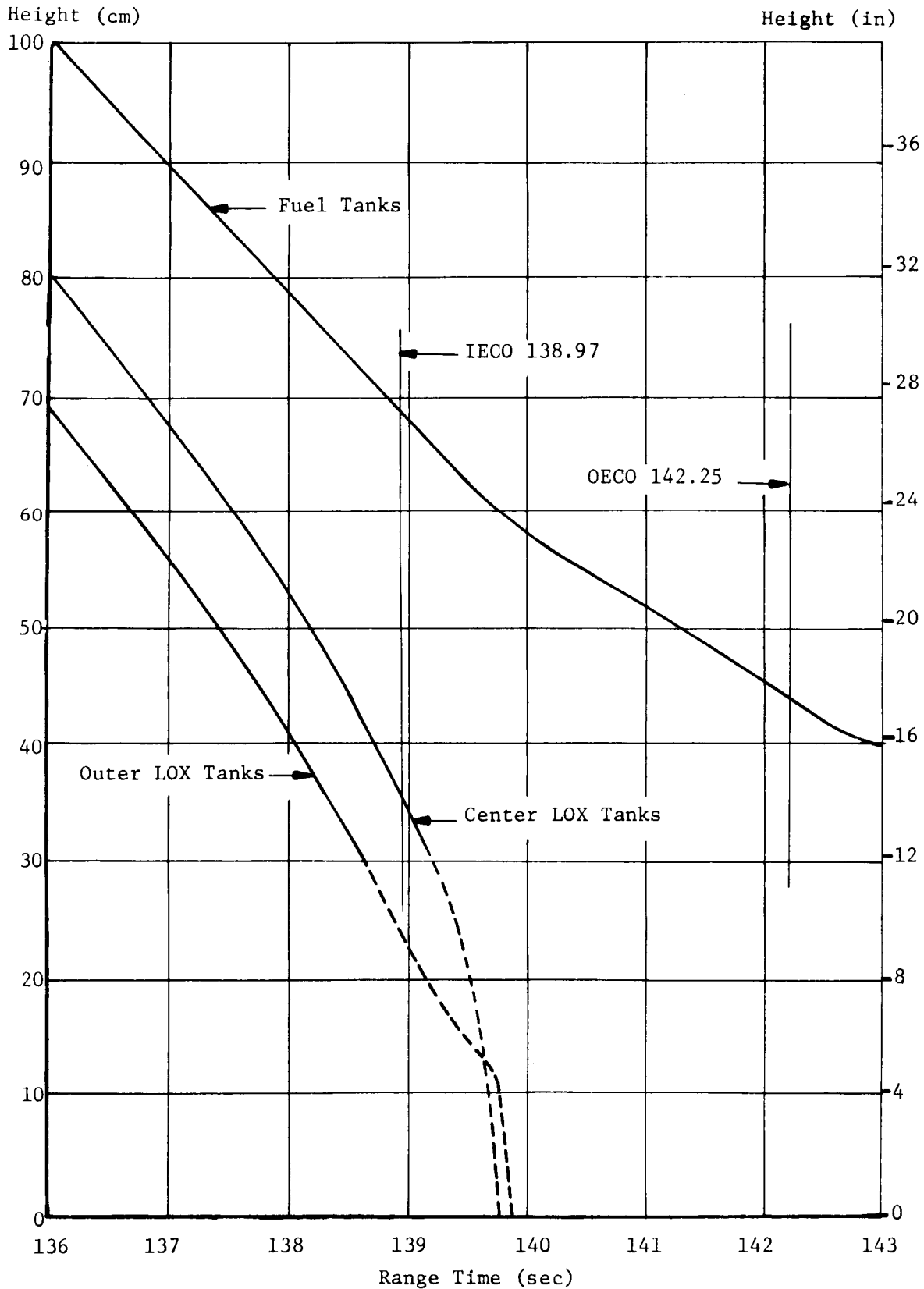


FIGURE 8-8 AVERAGE PROPELLANT LEVELS ABOVE THEORETICAL TANK BOTTOM

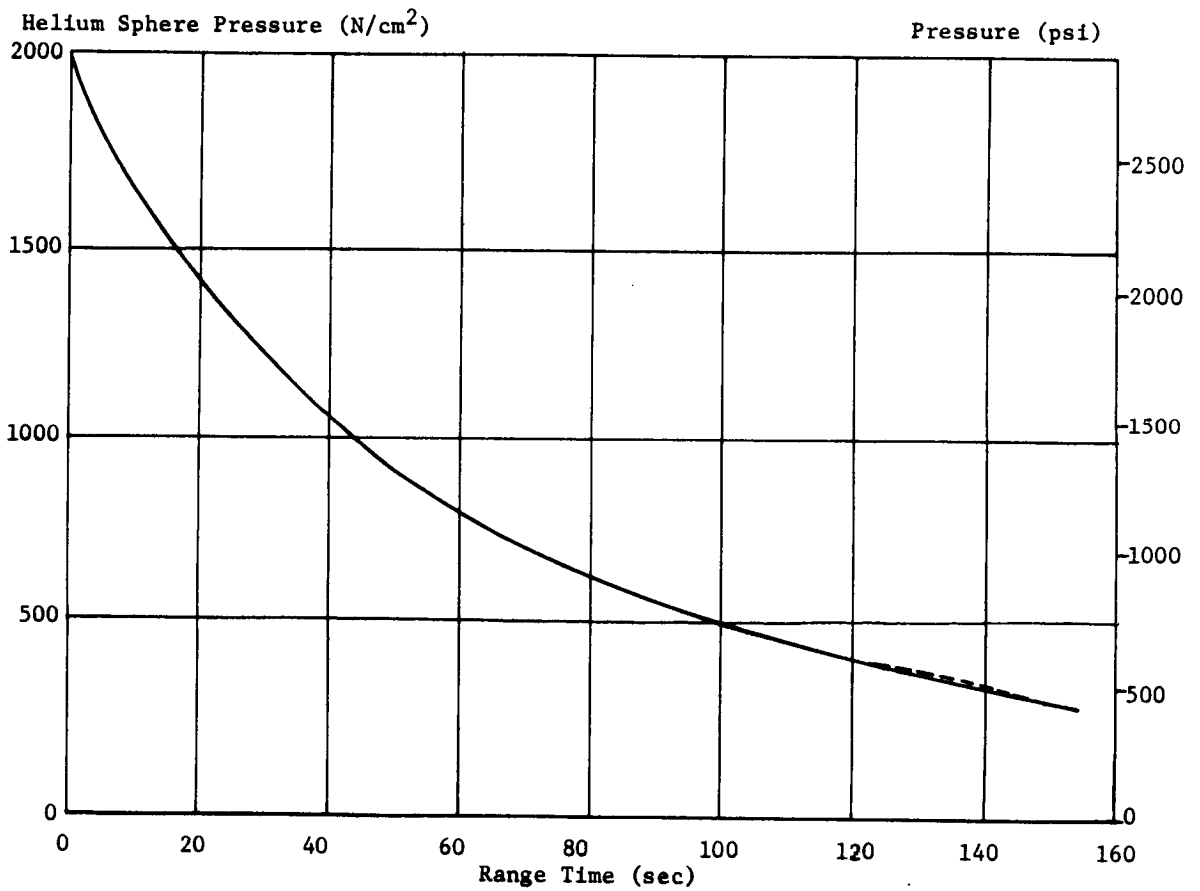
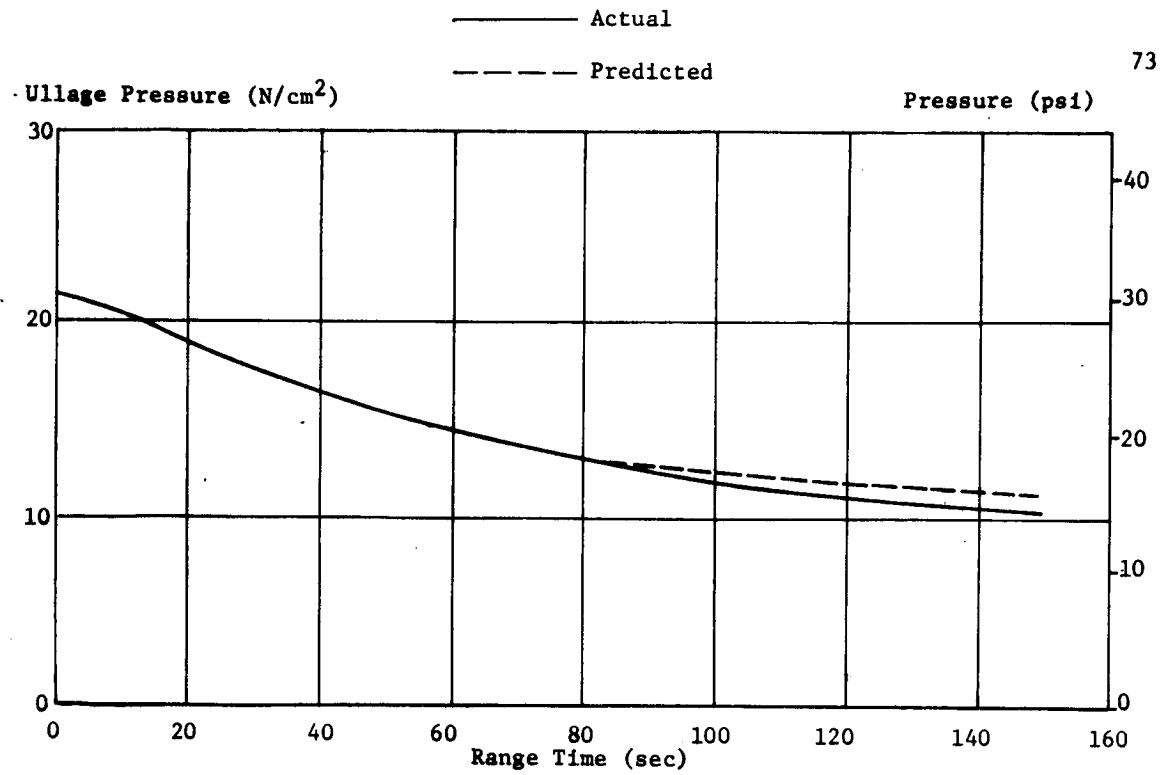


FIGURE 8-9 FUEL TANK ULLAGE AND HELIUM SPHERE PRESSURES

Recorder showed that fuel pressurization valves 1 and 2 closed at the beginning of the prepressurization sequence and remained closed. Due to cooling of the system, the pressurizing valves opened twice for repressurizing. This pressurization sequence was essentially the same as for S-IB-3.

The helium sphere pressure is shown in the lower portion of Figure 8-9, along with the predicted curve. Initial sphere pressure, which can vary from 1,941 to 2,206 N/cm² (2,815 to 3,200 psi), is the most significant factor affecting ullage pressure. Telemetry data shows it to be approximately 1,999 N/cm² (2,900 psi) at ignition, which was slightly lower than the initial predicted value.

Discrete probe data revealed the behavior of the fuel tank liquid levels during flight was very similar to that seen on AS-203. The maximum recorded difference between the levels in tanks F1 and F3 was 19.8 cm (7.8 in) at 11 seconds. The levels converged to a difference of 3.0 cm (1.2 in) at 93 sec and 2.8 cm (1.1 in) at 138 seconds.

8.4.2 LOX PRESSURIZATION SYSTEM

The LOX tank pressurization system performed satisfactorily during the AS-204 flight. The system configuration was the same as that flown on S-IB-3.

Pressurization of the LOX tanks provides increased structural rigidity and adequate LOX pump inlet pressures. Prelaunch prepressurization was achieved with helium from a ground source by utilizing a 0.290 cm (0.114 in) orificed line. From vehicle ignition command to liftoff, helium bypass flow was used to augment normal prepressurization flow. This maintained adequate pump inlet pressure during engine start.

The LOX tank pressurizing switch, which had an actuation range of 39.8 ± 0.6 N/cm² (57.7 ± 0.8 psi), actuated at 39.6 N/cm² (57.5 psi) for all seven prepressurizing cycles. Dropout occurred at 39.2 N/cm² (56.8 psi) for all cycles. Initial pressurization was started at -102.93 sec and continued for 62.59 seconds. Orifice bypass flow was initiated at -2.352 seconds.

In the upper portion of Figure 8-10, center LOX tank pressure during flight is compared with the predicted LOX tank pressure which was derived from static test data. The slight oscillation at about 10 sec was due to the GOX flow control valve (GFCV) response to the tank pressure drop during the ignition transient. The maximum pressure of approximately 36.5 N/cm² (53 psi) occurred at 33 sec, with tank pressure gradually decaying to 33.8 N/cm² (49 psi) at OECO.

The GFCV started to close at ignition and, after one oscillation, reached the full closed position at approximately 20 seconds. The valve

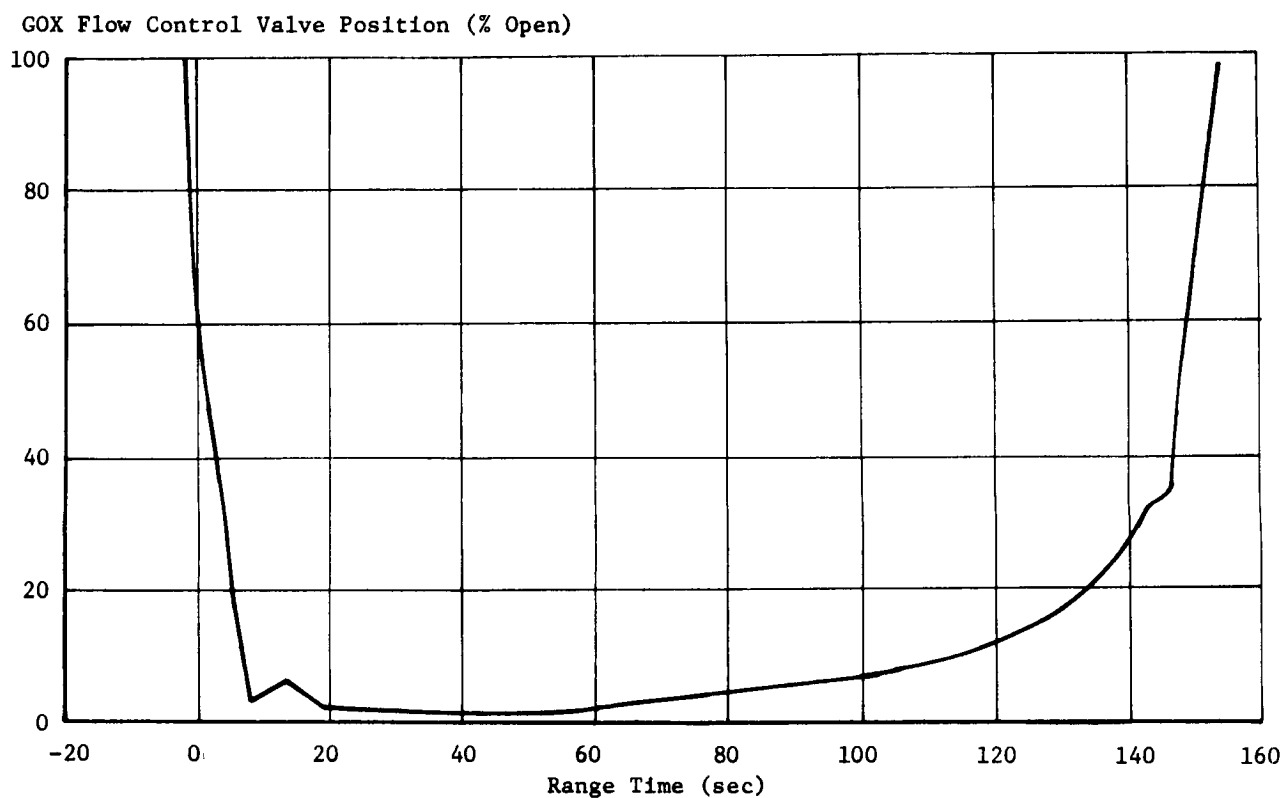
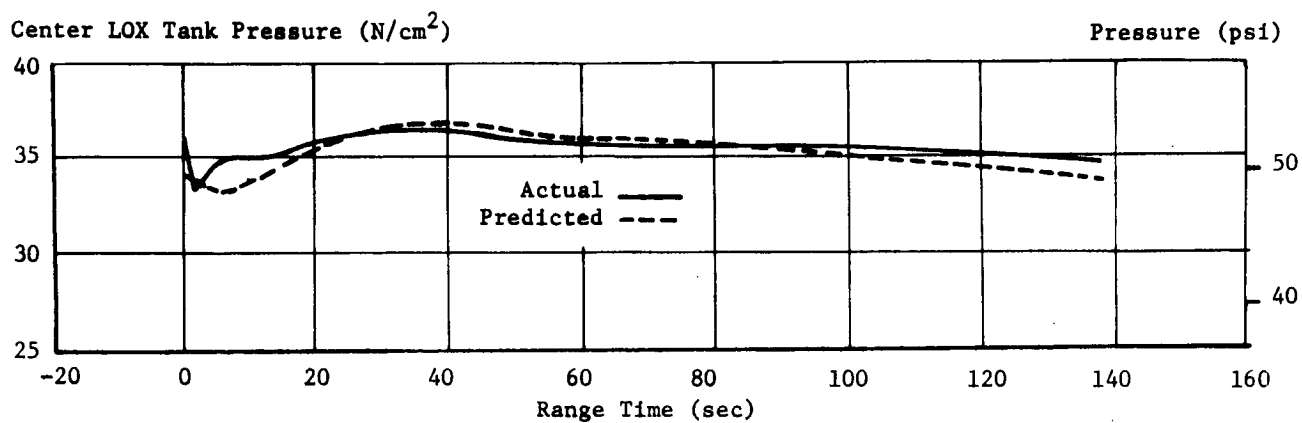


FIGURE 8-10 LOX PRESSURIZATION SYSTEM CHARACTERISTICS

remained in the closed position until 60 sec when decreased LOX tank pressure caused it to start opening. The GFCV position is shown in the lower portion of Figure 8-10. Predicted GFCV positions are not given because the original GFCV was replaced after static test of the stage due to an Engineering Change Proposal revising the seals. The pressure and temperature upstream of the GFCV were as expected and indicated nominal GOX flowrate.

8.4.3 CONTROL PRESSURE SYSTEM

The S-IB control pressure system supplied GN_2 at a regulated pressure of 531 to 541 N/cm^2 (770 to 785 psi) to pressurize the H-1 engine turbopump gearboxes and purge the LOX and lube seal cavities and the four radiation calorimeters. Regulated pressure was also available to operate one LOX vent and relief valve and was used to close the LOX and fuel prevalues at IECO and OECO.

System performance was satisfactory during prelaunch and flight. The flight sphere pressure history always remained within the acceptable band; however, the gas usage was slightly higher than predicted during the flight (Figure 8-11). The following factors contributed to the higher usage:

1. An increase in gearbox GN_2 flow on one engine not static tested was not accounted for in the prediction.

2. An ambient temperature difference of 27.8°K (50°F) between the stage static test and the time of launch resulted in a higher than predicted sphere gas temperature. This higher than predicted gas temperature could not be verified because it was not measured. The warmer GN_2 resulted in less mass in the stage storage sphere and, therefore, a slightly faster decay in supply pressure.

3. A minor leak could have occurred between the system leakage test and launch. The leakage possibility can not be evaluated because no comparative data is available.

The 517.1 N/cm^2 (750 psi) regulated pressure at liftoff was 534.3 N/cm^2 (775 psi). This pressure increased to 537.8 N/cm^2 (780 psi) at 140 sec but remained well within the prelaunch redline limits of 489.5 to 561.9 N/cm^2 (710 to 815 psi).

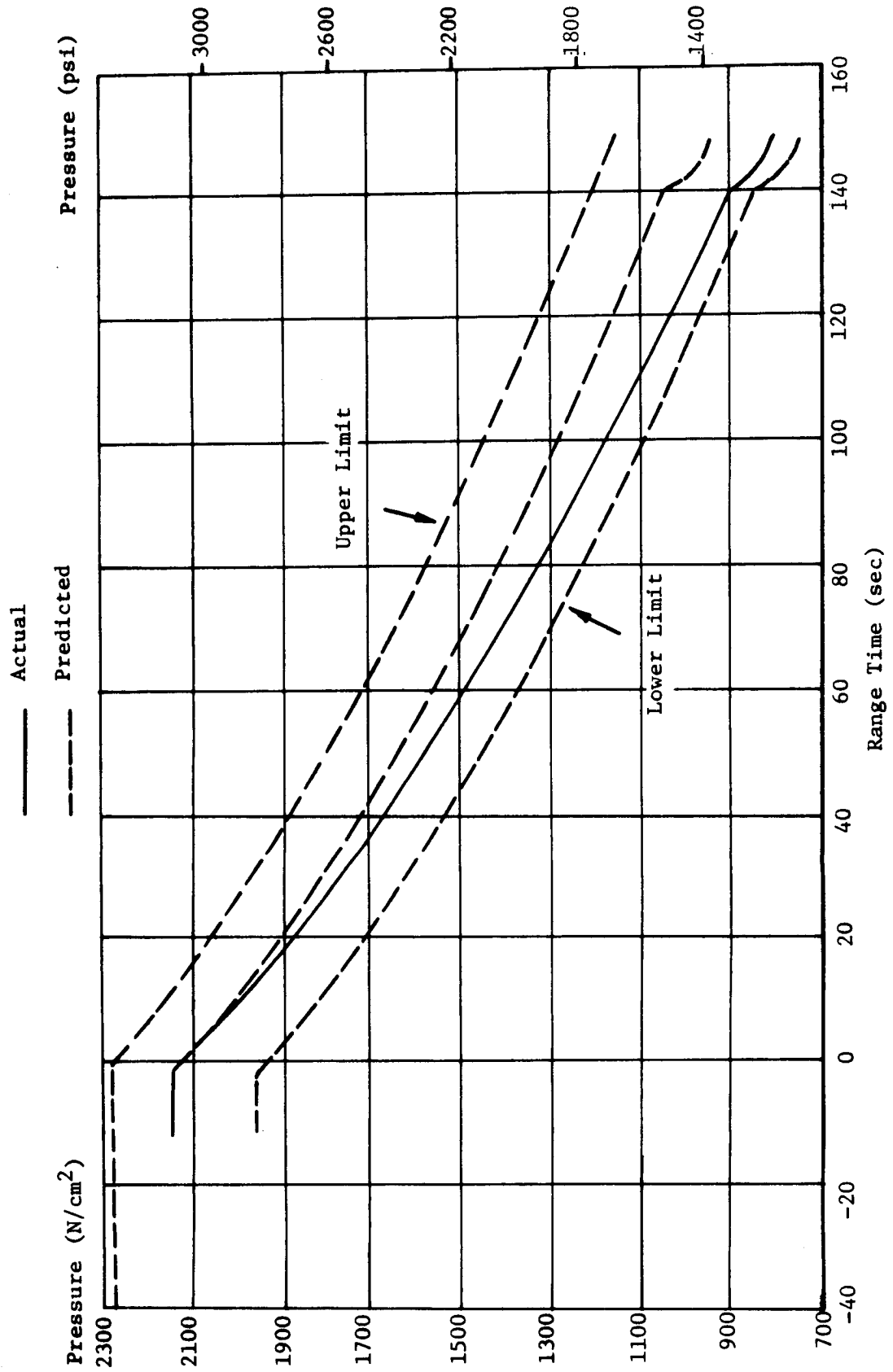


FIGURE 8-11 CONTROL SUPPLY PRESSURE

9.0 S-IVB PROPULSION AND ASSOCIATED SYSTEMS

9.1 SUMMARY

The performance of the S-IVB stage propulsion system was satisfactory throughout flight. All steady state performance values were within 1.66% of predicted.

On the basis of flight simulation, the overall average S-IVB thrust, mass loss rate, and specific impulse were 1.38% higher, 1.66% higher, and 0.30% lower than predicted, respectively. Guidance cutoff occurred at 593.35 sec, 5.00 sec earlier than predicted.

The PU system operated in the closed loop configuration and provided an average propellant mixture ratio of 5.5 to 1 during the high thrust period and 4.70 to 1 during the low thrust period. PU valve cutback occurred at 469.9 sec, 325.0 sec after J-2 start command. Cutback was 20.0 sec later than predicted. Propellant loading and utilization control by the PU system was satisfactory. The propellant load was within +0.41% LOX and -0.34% LH₂ of the desired load.

Operation of the propellant pressurization systems and pneumatic systems was satisfactory.

All portions of the orbital safing experiment were performed successfully, including propellant venting, propellant dump, cold helium dump, and stage and engine pneumatic supply dump. The GH₂ start bottle was not scheduled to dump.

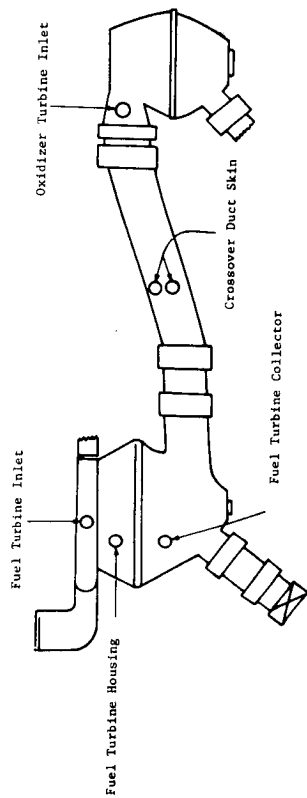
The LOX turbine inlet and the painted crossover duct temperatures in orbit were very close to expected.

9.2 S-IVB PROPULSION PERFORMANCE

9.2.1 ENGINE CHILLDOWN

Upon initiation of chillo down, the thrust chamber jacket temperature decreased normally. The temperature leveled off and was approximately 132°K (-222°F) at liftoff when chillo down was terminated (lower left portion of Figure 9-1). At S-IVB engine start command, 144.90 sec, the temperature was 143°K (-203°F), which was within the requirement of $133 \pm 28^\circ\text{K}$ ($-220 \pm 50^\circ\text{F}$).

The J-2 engine fuel turbine system and painted crossover duct temperatures were close to the expected range and are shown in Figure 9-1.



CROSSOVER DUCT MEASUREMENT LOCATIONS

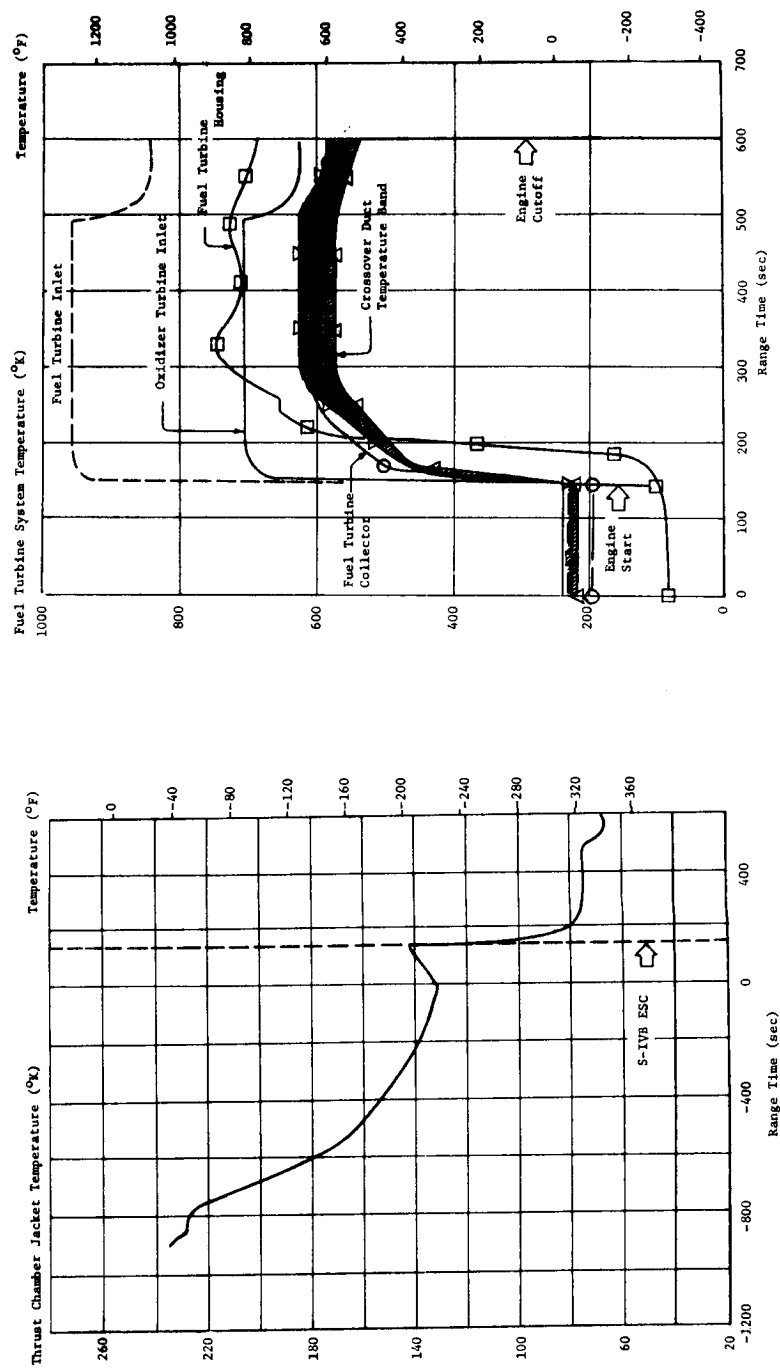


FIGURE 9-1 J-2 FUEL TURBINE SYSTEM AND THRUST CHAMBER JACKET TEMPERATURES

9.2.2 START CHARACTERISTICS

ESC occurred at 144.90 sec, 0.14 sec earlier than predicted. The engine start transient was satisfactory (Figure 9-2). The thrust buildup was within the limits set by the engine manufacturer and compared well with the altitude tests at Arnold Engineering Development Center. The PU system provided the proper null setting of the PU valve during the start transient until PU system activation. The thrust buildup to 90% performance [chamber pressure of 426 N/cm^2 (618 psi)] was much faster than during the sea level acceptance test and was within specifications. The faster thrust buildup resulted in less total impulse during the start transient (to 90% performance level) than during the acceptance test. The total impulse from ESC to 90% performance was 834,642 N-sec (187,635 lbf-sec) during flight compared to 1,193,457 N-sec (286,300 lbf-sec) during the acceptance test. Table 9-I briefly summarizes the start transient performance.

Performance of the GH_2 start sphere is discussed in paragraph 9.5.

TABLE 9-I START TRANSIENT PERFORMANCE

Parameter	Flight	Acceptance Test
Main Oxidizer Valve Open Time (Travel Time) (sec)	2.417	2.491
*Time from ESC to 90% Thrust (sec)	3.49	3.91
*Total Impulse to 90% Thrust (N-s)	834,642	1,193,457
(lbf-s)	187,635	268,300

*90% Thrust is defined as a chamber pressure of 426 N/cm^2 (618 psi)
 Note: ESC occurred at 144.90 seconds

9.2.3 MAINSTAGE ENGINE PERFORMANCE

Two separate analyses were employed in reconstructing S-IVB J-2 engine performance. The first method, engine analysis, utilized telemetered engine and stage data to compute longitudinal thrust, specific impulse, and stage mass flowrate. In the second method, flight simulation, a five-degree-of-freedom trajectory simulation was utilized to fit engine analysis results to the trajectory. Performance values and deviations

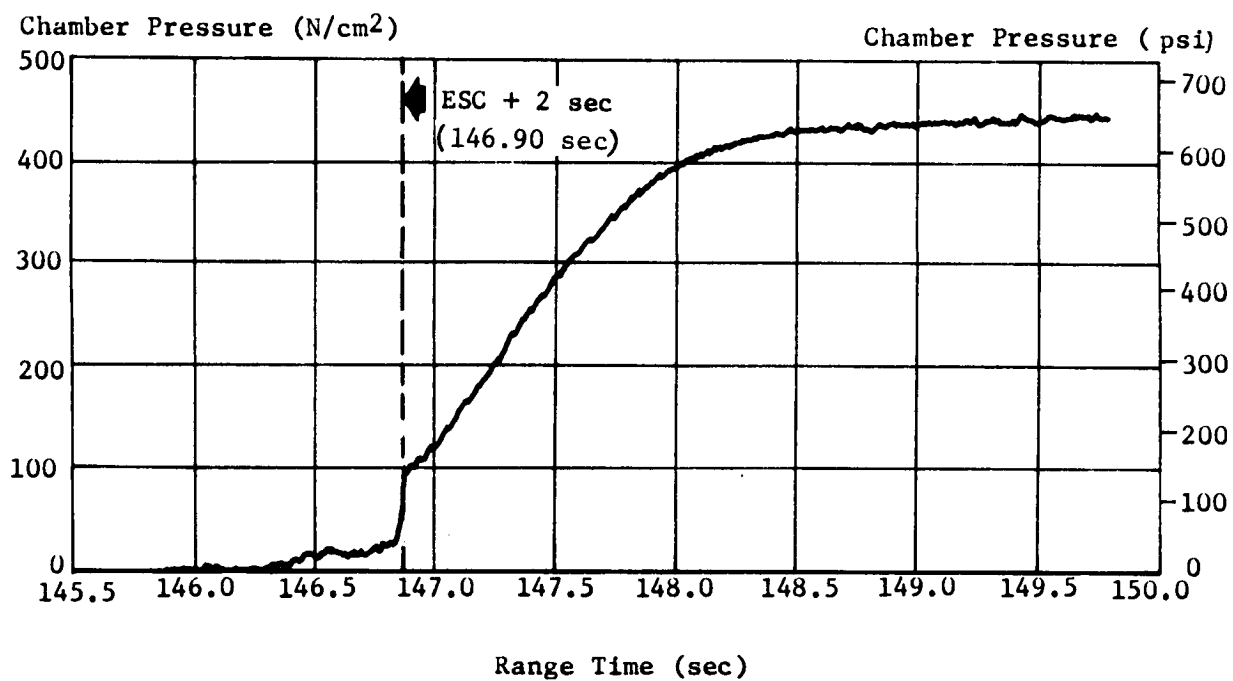
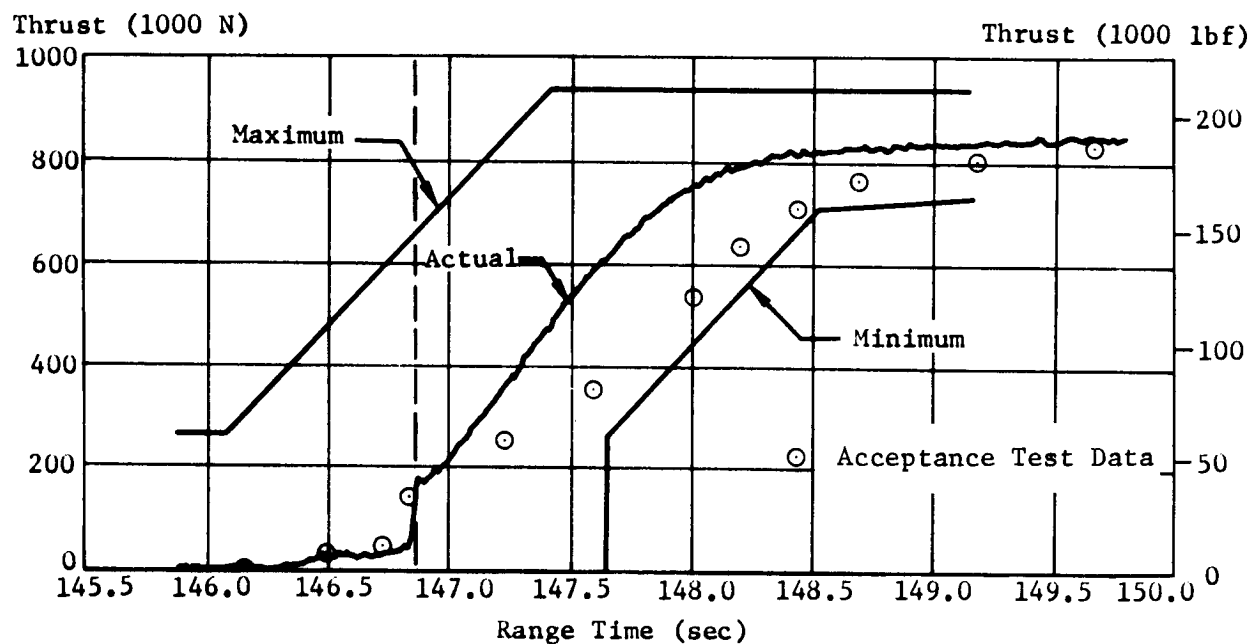


FIGURE 9-2 S-IVB START TRANSIENT

from predicted for both methods are summarized in Table 9-II.

Thrust, specific impulse, total flowrate, and engine mixture ratio during J-2 engine steady-state performance, based upon engine analysis, are depicted in Figure 9-3. Figure 9-4 shows the LOX and LH₂ flowrates separately. On the basis of engine analysis, the overall average S-IVB stage thrust, mass loss rate, and specific impulse were 1.01% higher, 1.42% higher, and 0.44% lower than predicted as a result of the late PU valve cutback. These performance levels were satisfactory.

A five-degree-of-freedom trajectory simulation program was employed to adjust the S-IVB propulsion performance analysis results generated by the engine analysis. Using a differential correction procedure, this simulation determined adjustments to the engine analysis thrust and mass flow histories to yield a simulated trajectory which closely matched the observed mass point trajectory. These results were obtained by a hunting procedure adjustment which resulted in an increase of 0.37% in thrust and an increase of 0.24% in mass flowrate from the engine analysis results.

On the basis of flight simulation, the overall average S-IVB stage thrust, mass loss rate, and specific impulse were 1.38% higher, 1.66% higher, and 0.30% lower than predicted (Table 9-II). Contributing factors causing these deviations were a 4.86 sec shorter than predicted burn time and the 20.0 sec later than predicted cutback of the PU valve.

The mass flowrate determined by flight simulation, combined with the mass at any point in time on the trajectory, allows an accurate determination of the vehicle mass history. The flight simulation solution of the second flight stage mass resulted in a mass of 134,614 kg (296,772 lbm) at S-IVB ESC and a mass of 31,889 kg (70,304 lbm) at S-IVB engine cutoff command (ECC). These masses are not considered best estimate masses.

9.2.4 CUTOFF CHARACTERISTICS

The engine cutoff transient was satisfactory and agreed well with acceptance test results (Figure 9-5). The thrust decreased to 5% of rated thrust (50,042 N or 11,250 lbf) 0.453 sec after guidance cutoff signal was received at the engine and reached essentially zero thrust 2 sec later. The cutoff impulse to 5% of rated thrust was 171,292 N-s (38,508 lbf-s), which was somewhat higher than during stage acceptance test [151,315 N-s (34,017 lbf-s)] but lower than predicted [179,584 N-s (40,372 lbf-s)].

The higher cutoff impulse, compared to the stage acceptance test, resulted because the PU valve was at -11.8 deg at cutoff during flight and was -23.5 deg during the stage acceptance test. In addition, the

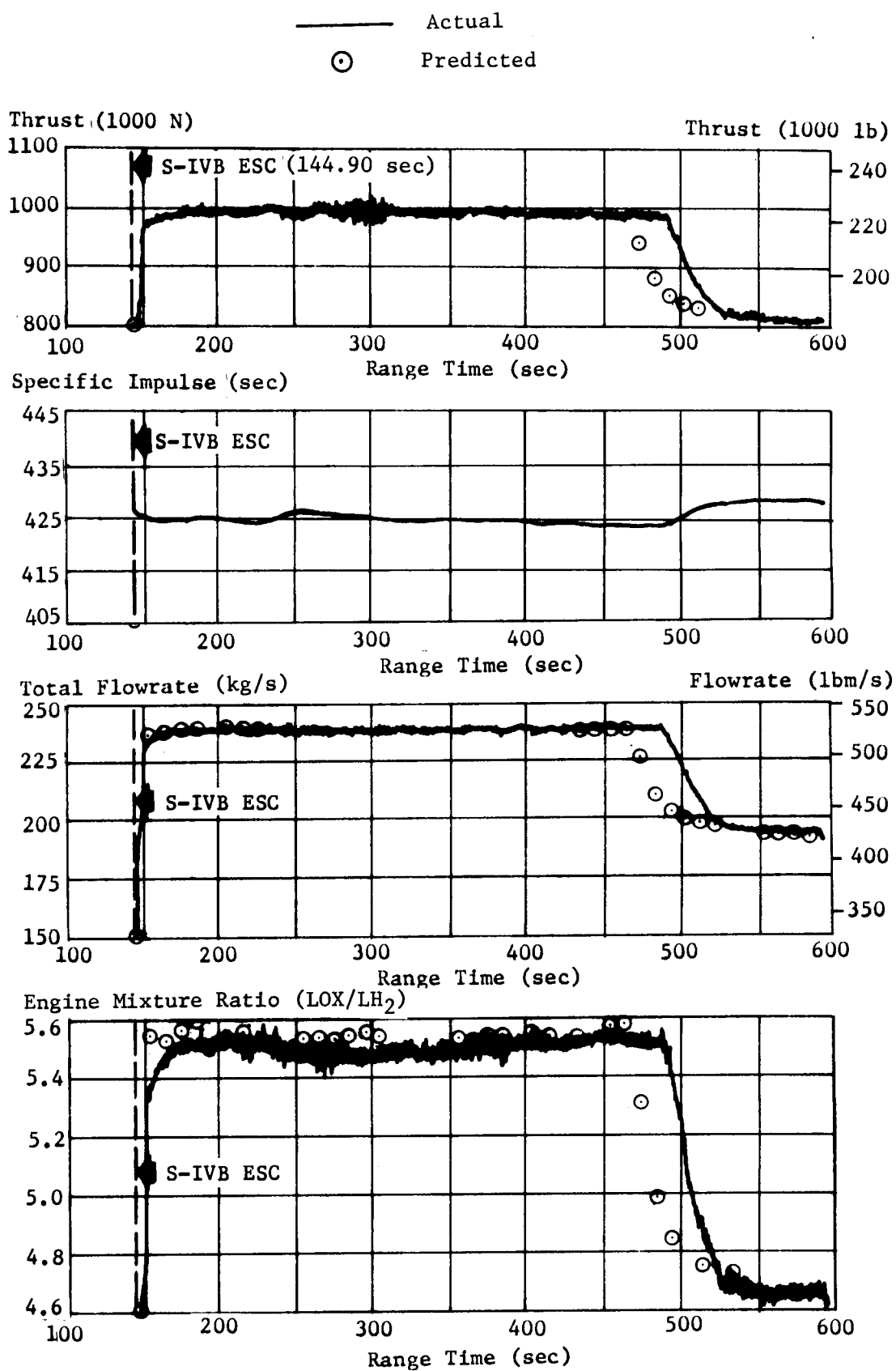


FIGURE 9-3 S-IVB STEADY-STATE OPERATION (ENGINE ANALYSIS)

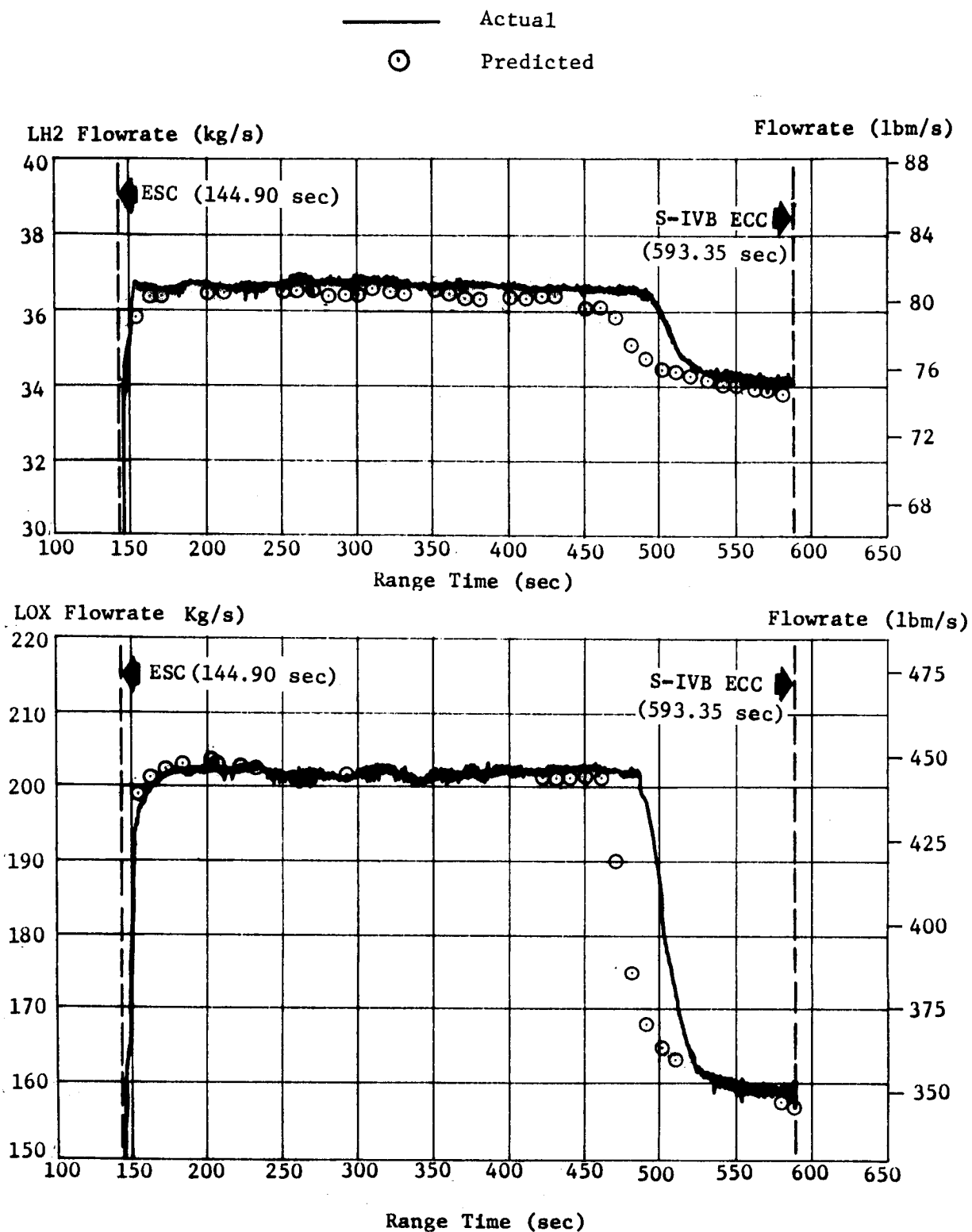


FIGURE 9-4 S-IVB PROPELLANT FLOWRATES

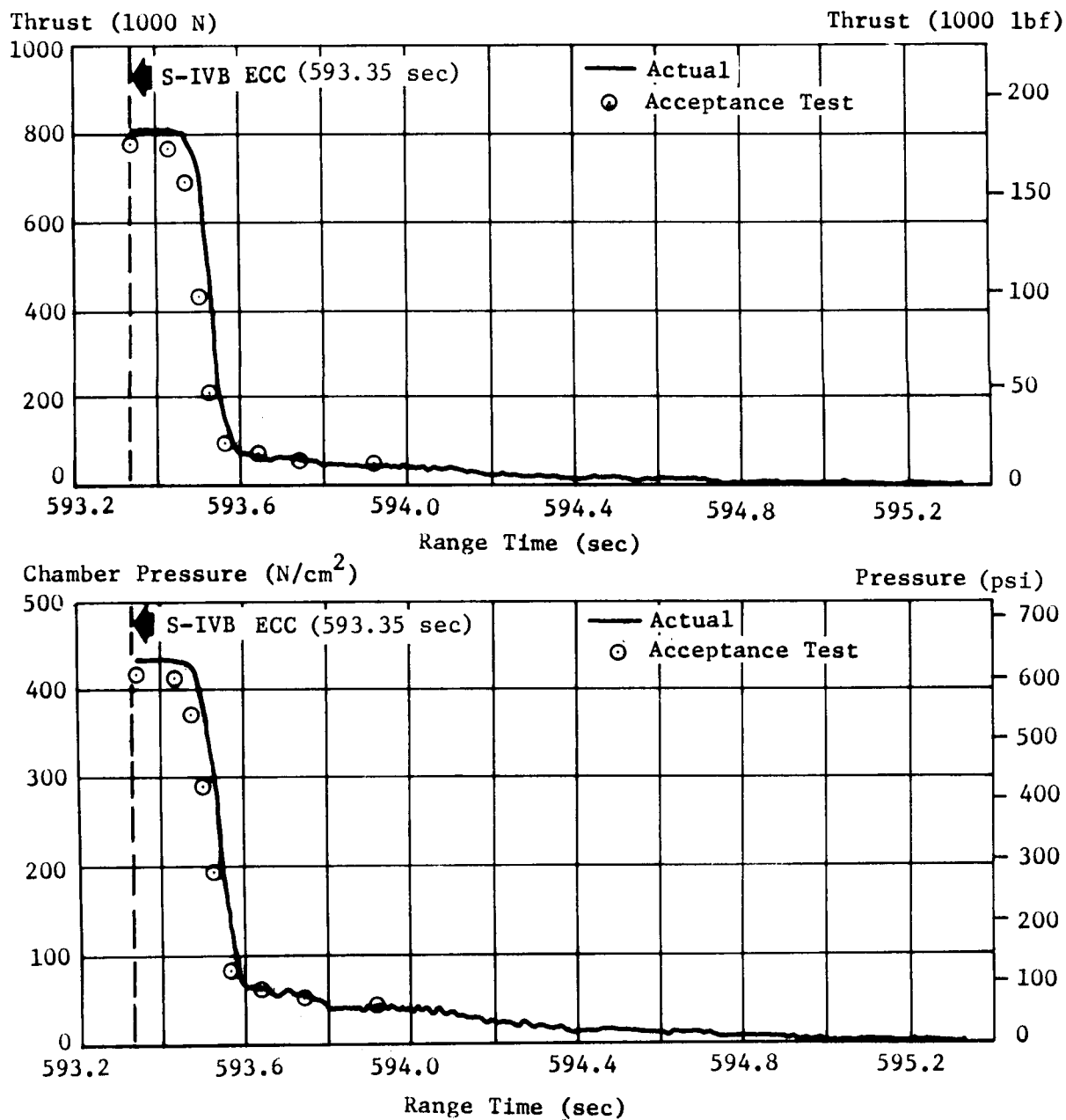


FIGURE 9-5 S-IVB CUTOFF TRANSIENT

main oxidizer valve closed slightly later and slower during flight than during the acceptance test.

Table 9-III summarizes S-IVB cutoff transient performance. The total cutoff impulse and associated velocity increase agree well with predicted. All cutoff impulses in the table are to zero thrust unless otherwise noted.

9.3 S-IVB STAGE PROPELLANT UTILIZATION

9.3.1 PROPELLANT MASS ANALYSIS

The propellant utilization system successfully accomplished the requirements associated with propellant loading and with management during S-IVB burn. The best estimate of propellant mass values at ESC were 88,026 kg (194,065 lbm) LOX and 16,916 kg (37,294 lbm) LH₂, as compared to predicted mass values of 87,667 kg (193,273 lbm) LOX and 16,982 kg (37,440 lbm) LH₂. These values were 0.41% higher LOX and 0.39% lower LH₂ than predicted. The deviations were well within the required $\pm 1.12\%$ loading accuracy. The indicated loading computer propellant-load values at liftoff (not corrected for flight conditions) were 87,694 kg (193,333 lbm) LOX and 16,961 kg (37,392 lbm) LH₂, very close to desired values.

Figure 9-6 presents the second flight stage best estimate ignition and cutoff masses. At ESC the mass was 134,733 kg (297,035 lbm) and was 31,854 kg (70,226 lbm) at ECC.

A comparison of propellant mass values at critical flight events, as determined by various analyses, is presented in Table 9-IV. Best estimate of residuals were 1,378 kg (3,038 lbm) LOX and 674 kg (1,485 lbm) LH₂ as compared to the predicted values of 1,501 kg (3,310 lbm) LOX and 681 kg (1,501 lbm) LH₂. This was 9.0% lower LOX and 1.1% higher LH₂ than predicted. Residuals were determined at ECC.

Extrapolation of propellant residuals to depletion indicated that a LOX depletion would have occurred 7.46 sec after velocity cutoff with a usable LH₂ residual of 65.3 kg (144 lbm). 61.7 kg (136 lbm) of the usable residual resulted from the intentional LH₂ bias. The extrapolated residual yielded a PU system efficiency of 99.94 percent.

9.3.2 PU VALVE RESPONSE AND THRUST FLUCTUATIONS

The PU valve position history is illustrated in Figure 9-7. The PU valve was positioned at null prior to J-2 start and remained there until PU system activation at ESC + 6 seconds. At activation the PU valve was commanded to the full-closed position (high EMR). The PU valve reached the full-closed position at ESC + 7.8 sec, as compared to the predicted time of ESC + 10.5 seconds. The deviation between the predicted and actual valve position slope following PU activation was due

TABLE 9-III S-IVB CUTOFF TRANSIENT PERFORMANCE

Parameter	Predicted	Acceptance Test		Flight	
		Stage	Engine	Engine Data	Guidance Data
Total Cutoff Impulse (N-s)	198,168	151,315*	169,789	202,261	204,116
(lbf-s)	44,550	34,017*	38,170	45,470	45,887
Velocity Increase (m/s)	7.1**	4.75	-	6.34	6.4
(ft/s)	23.3**	15.6	-	20.81	21.0

* Cutoff Impulse to 5 Percent Thrust

** Approximately 0.25 m/s (0.82 ft/s) of the predicted velocity increase is attributed to venting during the cutoff impulse.

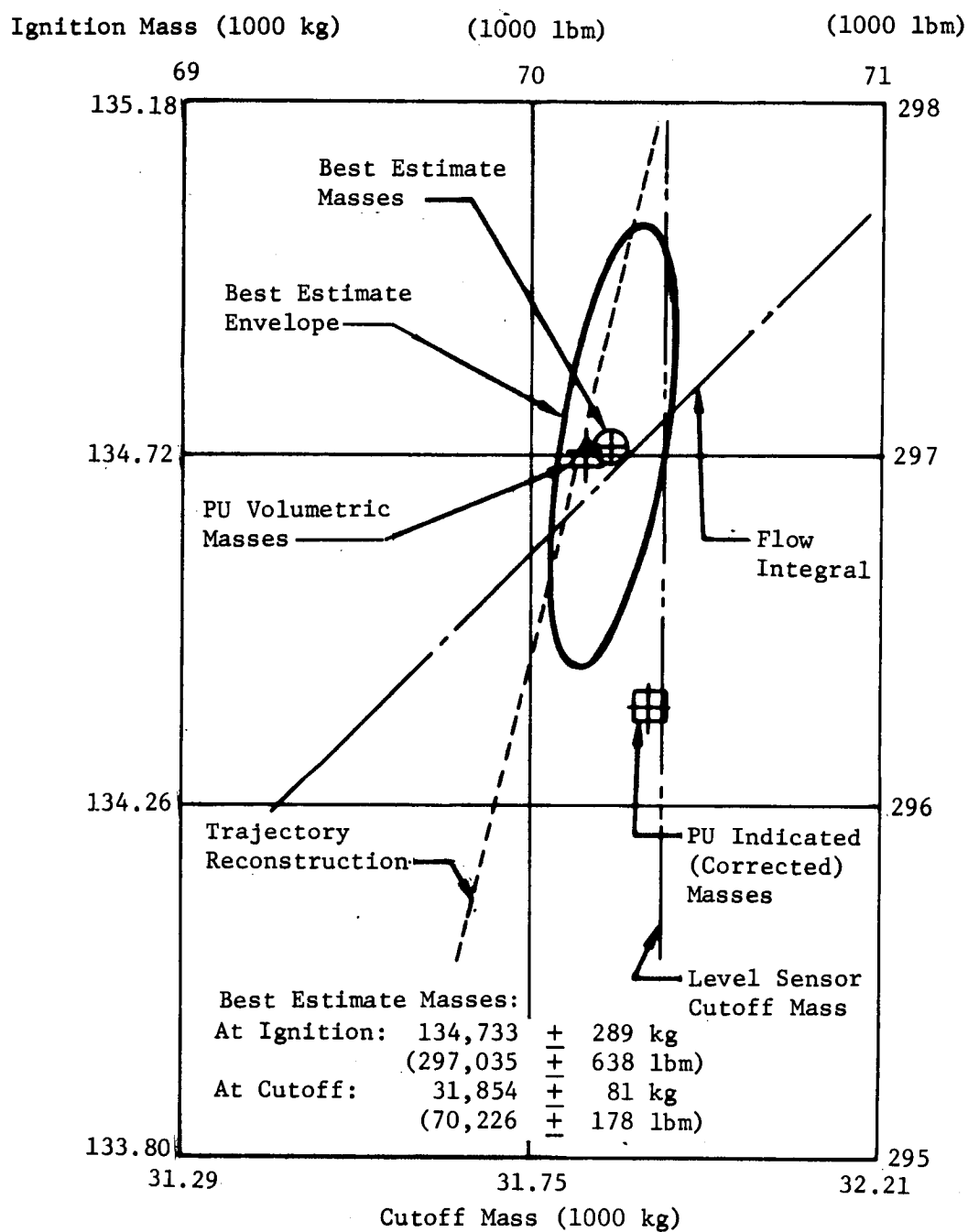


FIGURE 9-6 SECOND FLIGHT STAGE BEST ESTIMATE MASSES

TABLE 9-IV S-IVB PROPELLANT MASS HISTORY

Event	Units	Predicted		PU System (1)		PU Volumetric		Engine Flow Integral (2)		Statistically WTD Average (3)	
		LOX	LH ₂	LOX	LH ₂	LOX	LH ₂	LOX	LH ₂	LOX	LH ₂
S-IB Liftoff	kg lbm	87,667 193,273	16,982 37,440	87,694 193,333	16,961 37,392	88,071 194,163	16,911 37,282	87,997 194,000	16,949 37,367	88,029 194,070	16,925 37,314
S-IVB ESC	kg lbm	87,667 193,273	16,982 37,440	87,674 193,287	16,928 37,320	88,050 194,117	16,883 37,220	87,997 194,000	16,949 37,367	88,026 194,065	16,916 37,294
PU Valve Cutback	kg lbm	26,637 58,725	5,855 12,908	22,772 50,204	5,111 11,268	23,108 50,944	5,008 11,041	22,847 50,370	5,024 11,076	---	---
Residuals Above Main Propellant Valves at ECC (4)	kg lbm	1,501 3,310	681 1,501	1,389 3,062	714 1,575	1,332 2,937	686 1,513	1,431 3,154	665 1,467	1,378 3,038	674 1,485

- (1) PU System indicated mass corrected for inflight tank geometry variations and center-of-gravity offset.
- (2) Composite of engine analysis programs
- (3) Composite of PU System, PU volumetric, engine flow integral, trajectory reconstruction, and level sensor residuals (last two items are shown in Figure 9-6).
- (4) Weighted average residuals include level sensor residuals of 1,921 kg (4,235 lbm) LOX and 730 kg (1,610 lbm) LH₂.

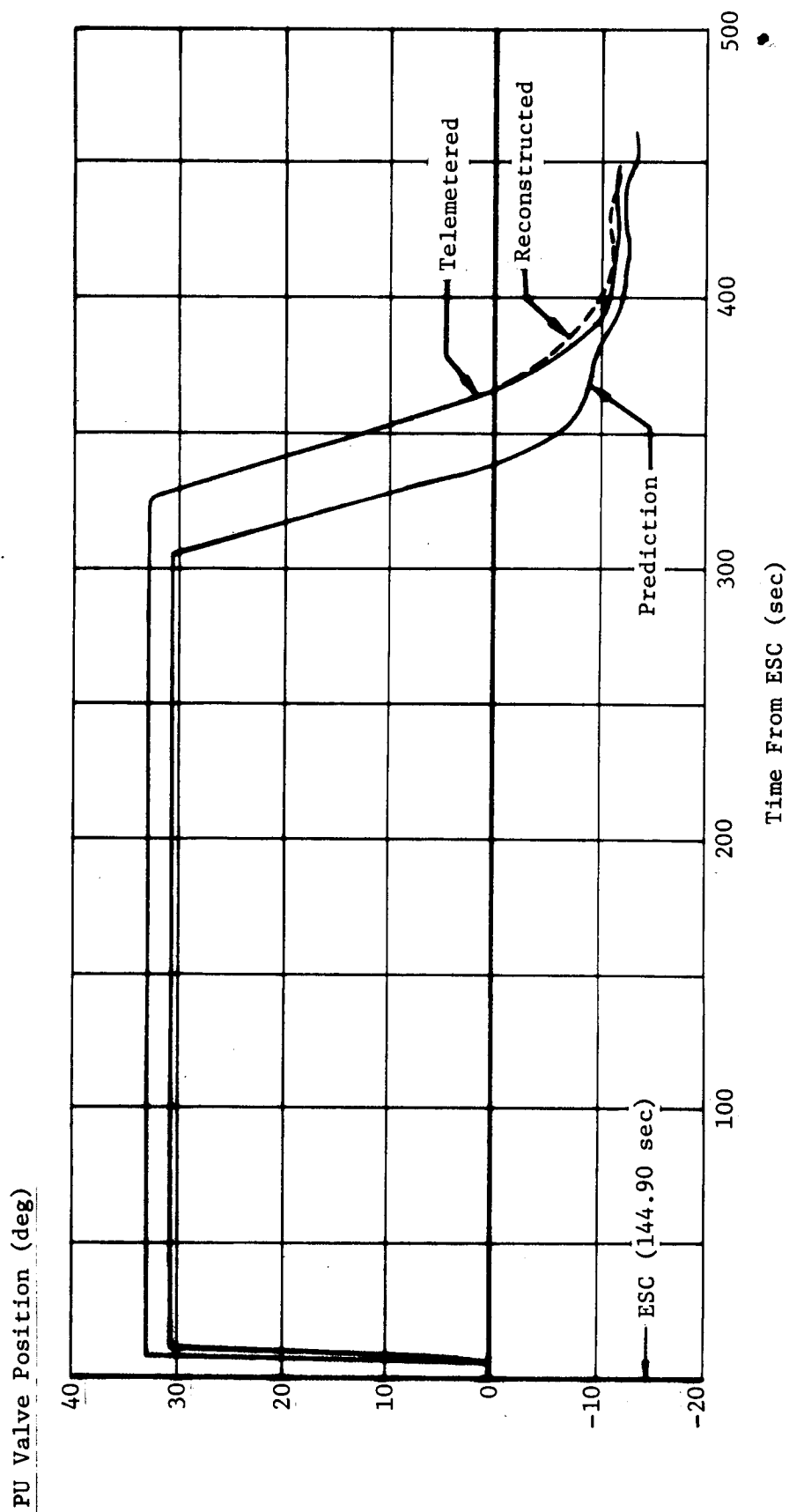


FIGURE 9-7 S-IVB-204 PU VALVE POSITION HISTORY

to a difference between the method used to activate the PU system in the simulation model and the actual method used for activation in flight.

After PU system activation, the PU valve remained at the fully closed position until 469.9 sec (ESC + 325.0 seconds). PU valve cutback was 20.0 sec later than the predicted time of ESC + 305 sec but was well within the ± 45 sec tolerance. The PU system deviations between reconstructed and predicted flight performance which caused the later than predicted PU valve cutback are shown in Table 9-V. These deviations are in satisfactory agreement with the observed 20.0 sec late cutback and 1.2 deg high PU valve position.

TABLE 9-V PU SYSTEM DEVIATIONS

Error Source	Cutback Time Deviation (sec)	Valve Position Shift at High EMR (deg)
1. Loading	-3.5	0
2. Updated J-2 Engine Influence Coefficients and Auxiliary Drive	5.0	0.5
3. Engine Tag Values	0	-1.0
4. Mismatch (engine flowmeter)	-3.2	0
5. Calibration (engine flowmeter)	12.7	1.5
6. Engine Performance	11.5	0.2
7. Simulation	<u>-2.5</u>	<u>0</u>
Total Observed Deviation	20.0	1.2

The items in Table 9-V and/or references to the items are discussed below:

1. Loading errors of +0.41% LOX and -0.34% LH₂ are discussed in paragraph 9.3.1.

2. This error is the result of updating the values predicted by the engine contractor.

3. This error is the result of run-to-run variations in engine tag values.

4. The PU system LH₂ and LOX nonlinearities (LH₂ and LOX tank-to-sensor mismatches) are shown in Figure 9-8.

5. This error is the result of calibration errors in the engine propellant flowmeters.

6. The errors caused by the flowrate during the high thrust period of flight are due to the effects of the differences between the predicted and actual pump inlet condition pressurization and to the boiloff rate. These conditions extended the cutback time by 11.5 seconds.

7. Flight Simulation errors are due to the computer program not operating as fast as the valve. This deviation resulted from a difference between the method used to activate the PU system in the simulation model and the actual implementation of PU activation in flight.

Inflight tank geometry variations deviated from predicted but caused only a small effect on total PU system nonlinearities. Total fuel and LOX nonlinearities are shown in Figure 9-8.

The redesigned forward shaping-network slosh-filter successfully removed the effects of propellant sloshing on the PU valve. Propellant sloshing, within a 0.2 to 0.6 Hz range, was present in the mass signals and in the PU summing point error signal. However, the added filter attenuation removed the slosh effects on the signal fed to the PU valve servo.

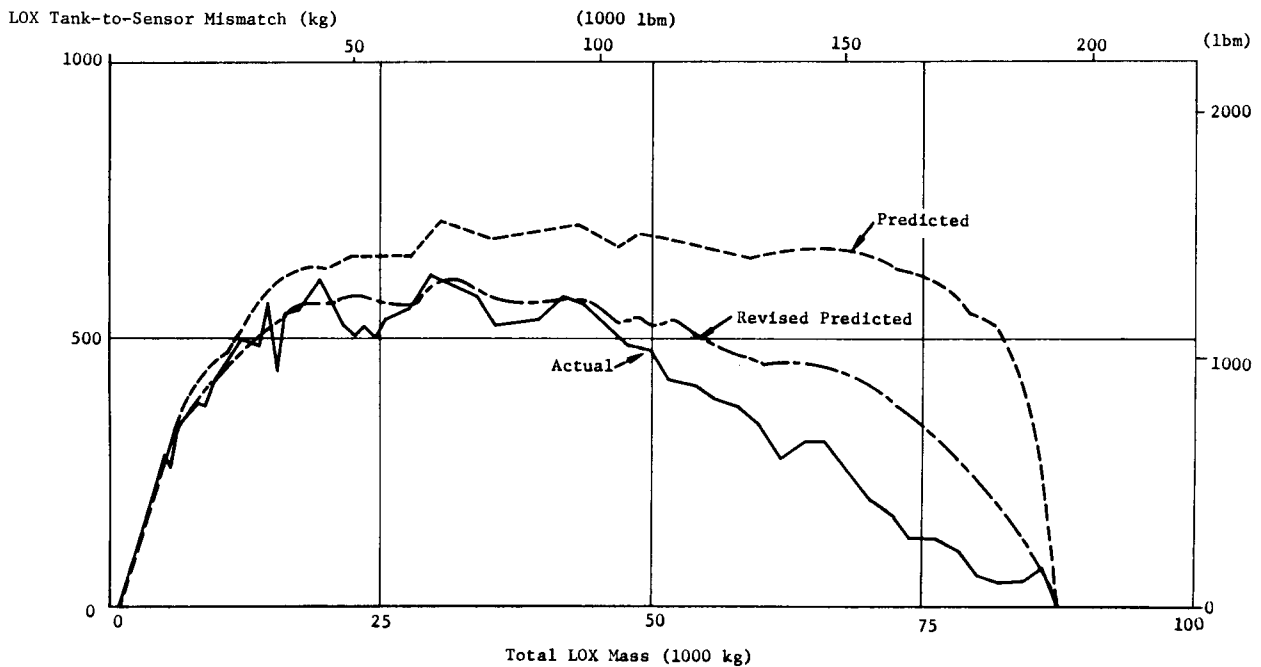
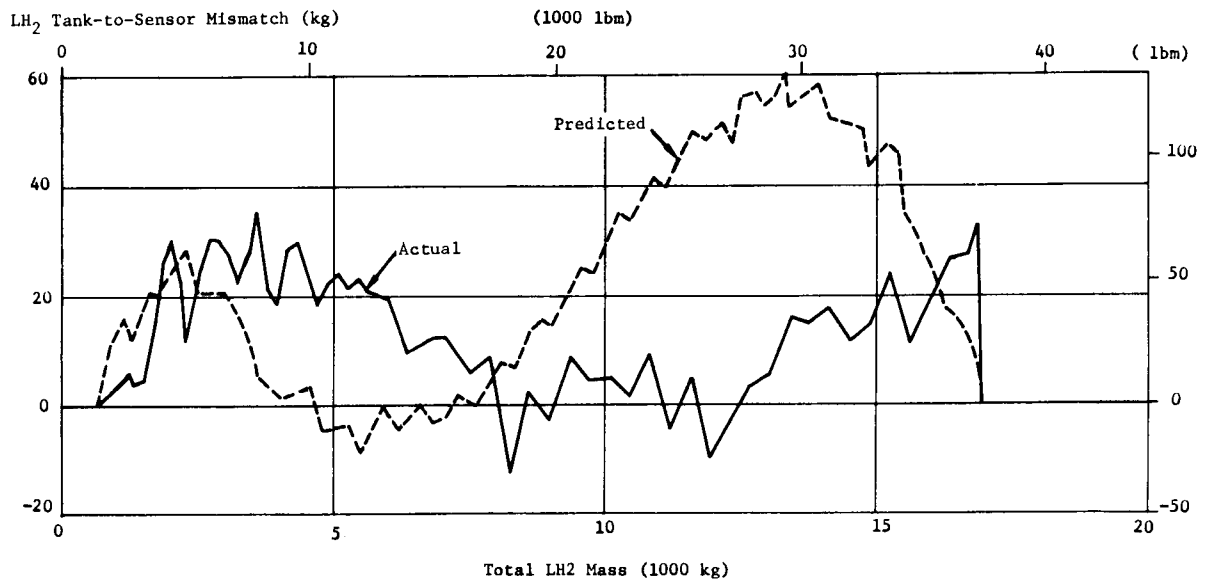
The thrust level change from high EMR operation (before PU valve cutback) to Reference Mixture Ratio (RMR) operation was 995,957 N (233,900 lbf) before cutback to 836,457 N (188,043 lbf) after cutback. The EMR before PU valve cutback was 5.5 to 1 (same as predicted) and was 4.70 to 1 (4.702 to 1 predicted) during RMR. This resulted in a thrust level change of 159,500 N (35,857 lbf). Thrust variations were within specification limits throughout the flight.

9.4 S-IVB PROPELLANT PRESSURIZATION SYSTEMS

9.4.1 FUEL PRESSURIZATION SYSTEM

The fuel pressurization system performance was satisfactory throughout flight, supplying LH₂ to the engine pump inlet within the specified operating limits. The NPSP at the engine LH₂ pump inlet was maintained above the allowable minimum throughout S-IVB powered flight. The minimum NPSP was 10.3 N/cm² (14.9 psi) at 444.4 sec and was 5.9 N/cm² (8.6 psi) above the allowable minimum. Pressurization control and step pressurization were normal and within predicted limits.

The LH₂ pressurization command was received at approximately -113 seconds. The LH₂ "tank pressurized" signal was received 46 sec

FIGURE 9-8 S-IVB PU SYSTEM LH₂ AND LOX NONLINEARITIES

later, when the LH₂ tank ullage pressure reached 23.3 N/cm² (33.8 psi). However, the ullage pressure continued to increase until S-IVB ESC (lower portion of Figure 9-9).

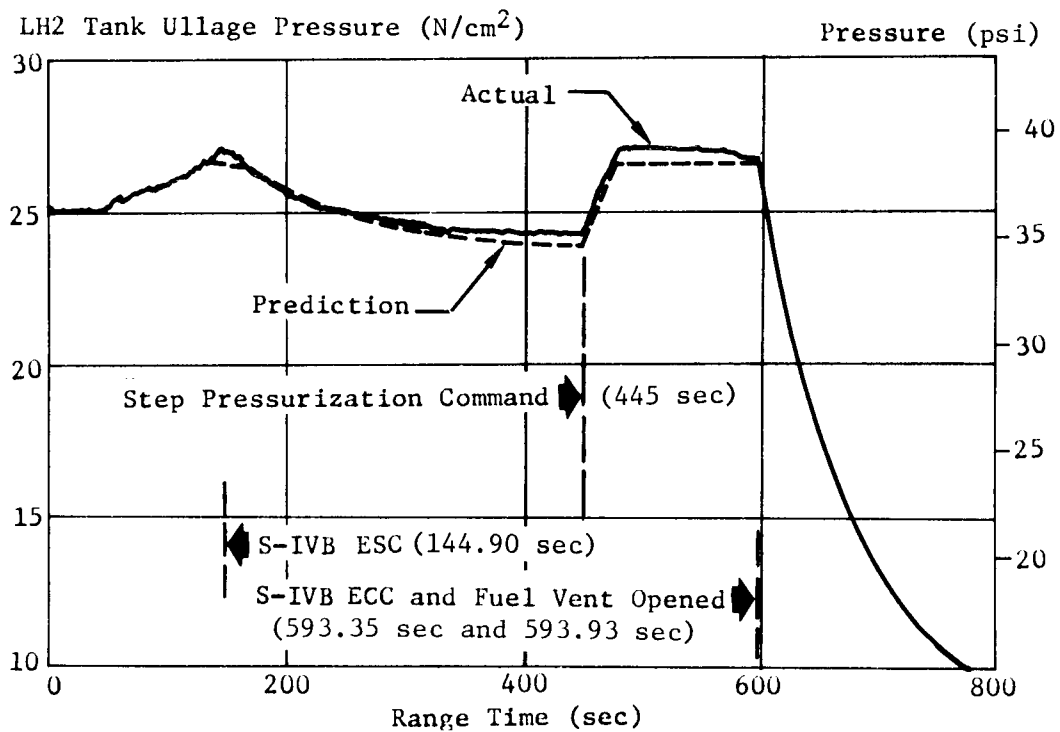
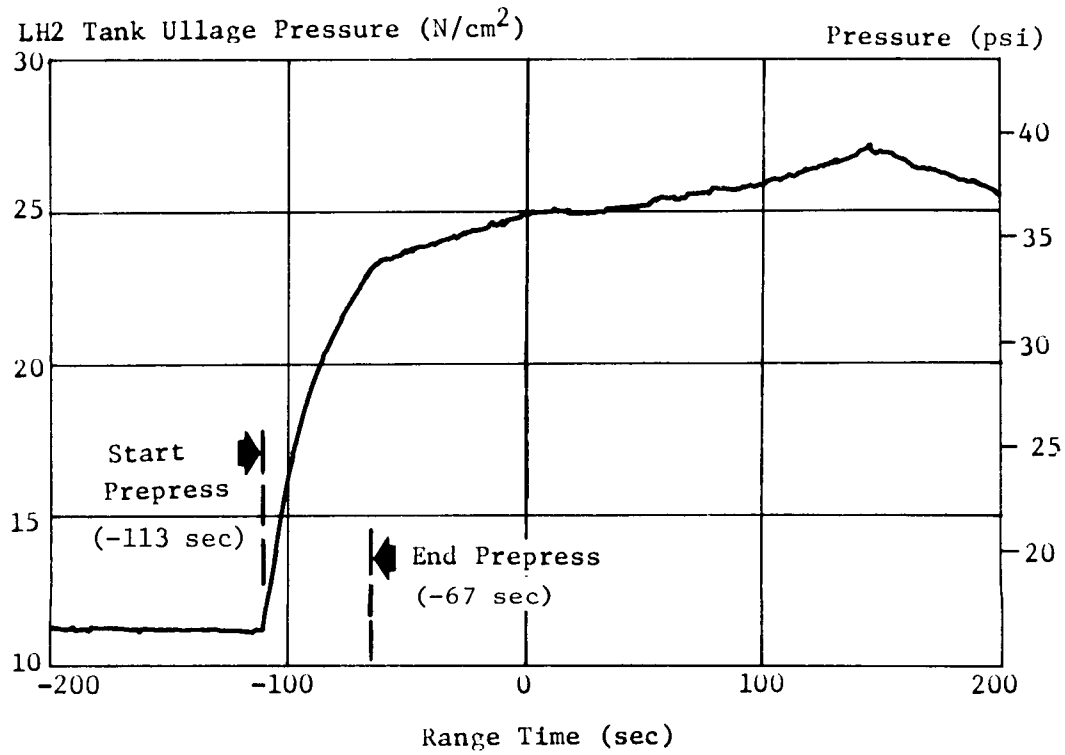
At S-IVB ESC, the LH₂ tank ullage pressure was approximately 27.0 N/cm² (39.2 psi). Between S-IVB ESC and approximately 145.69 sec, GH₂ bleed from the engine flowed into the LH₂ tank through the normal pressurization orifice, the control pressurization orifice, and the step pressurization orifice. The control and step pressurization orifices are normally opened at S-IVB ESC and closed 2.6 sec later. Therefore, a momentary high flow of GH₂ entered the LH₂ tank at S-IVB ESC. However, the effect on the ullage pressure was negligible. When the control and step pressurization orifices were closed, the ullage pressure began a normal decrease to a minimum of 24.4 N/cm² (35.4 psi) at 445 sec (lower portion of Figure 9-9). The actual profile was close to that predicted, with the ullage pressure being maintained above 24.1 N/cm² (35 psi) up to step pressurization.

Step pressurization was initiated automatically at 445 sec to provide adequate LH₂ pump NPSP until S-IVB ECC. At step pressurization command, both the control and step-pressurization orifices were opened to permit additional pressurant flow into the LH₂ tank. The ullage pressure increased from 24.3 N/cm² to 27.2 N/cm² (35.2 psi to 39.4 psi) during step pressurization and decreased to 26.8 N/cm² (38.9 psi) at ECC.

Approximately 20 sec after ECC, the ullage temperatures at 20% and 30% of full LH₂ tank level decreased sharply. The sharp temperature drop was due to slosh caused by the S-IVB cutoff vibrations and a pitch down that started at S-IVB ECC. Simultaneously, the ullage pressure was decreasing due to the programmed vent that ended 1260 sec after S-IVB ECC (Figures 9-9 and 9-16).

The GH₂ pressurization flowrates were 0.234 to 0.270 kg/s (0.536 to 0.596 lbm/s) until step pressurization. After step pressurization was initiated, the GH₂ flowrates were 0.587 and 0.512 kg/s (1.294 and 1.128 lbm/s) during high EMR and RMR, respectively. These values were nearly equal to the predicted values and indicated that, from S-IVB ESC to S-IVB ECC, 161.5 kg (356 lbm) of GH₂ was added to the ullage. The collapse factor varied from 0.71 to 0.88 during steady-state operation. Calculations based on the LH₂ tank ullage pressures and temperatures at S-IVB engine start command and engine cutoff indicated negligible LH₂ boiloff during S-IVB powered flight.

LH₂ tank venting did occur during the last 115 sec of powered flight. The GH₂ vented flowrate varied between 0.211 and 0.270 kg/s (0.466 and 0.596 lbm/s) during the venting period. The data does not indicate whether the GH₂ was vented through the vent and relief valve or through the backup relief valve. The crack pressures based upon stage contractor production acceptance testing for the vent and relief valve and the backup relief valve were 26.54 and 27.23 N/cm² (38.5 and 39.5 psi), respectively. The fuel tank ullage pressure was 27.03 N/cm² (39.2 psi) when the venting

FIGURE 9-9 LH₂ TANK PRESSURIZATION PERFORMANCE

began. The GH_2 flowrate (calculated) could have been vented by either of the two valves.

It is believed that relief was through the vent and relief valve. Preliminary analysis of the valve GH_2 flow path indicates that considerable flow goes around the main piston due to the metering grooves in the side of the valve. If the vented GH_2 had passed through the vent and relief valve, the stroke of the valve main piston should have been sufficient to cause a loss of the closed valve position indication. Loss of the closed valve position was never received; however, test data on the valve indicates the closed valve position microswitch may not be tripped if the tank pressure rise rate is less than 0.14 N/cm^2 (0.2 psi/sec). During flight the pressure rise rate was $0.0800 \text{ N/cm}^2/\text{sec}$ (0.116 psi/sec). The indicated high relief pressure of 27.03 N/cm^2 (39.2 psi) was found to be within the valve crack pressure range when the accuracy of instrumentation is considered. The quoted crack pressures have an inaccuracy range of $\pm 0.41 \text{ N/cm}^2$ ($\pm 0.6 \text{ psi}$) while the ullage pressures have an inaccuracy of approximately $\pm 0.69 \text{ N/cm}^2$ ($\pm 1.0 \text{ psi}$). No impact upon future flights is anticipated.

LH₂ Supply Condition

The LH₂ pump inlet NPSP was calculated from the pump inlet temperature and total pressure. These values indicated that the NPSP at S-IVB ESC was about 14.4 N/cm^2 (20.9 psi), as shown in the upper portion of Figure 9-10. It reached a minimum of 10.3 N/cm^2 (14.9 psi) at 444.4 sec just before step pressurization. This was 5.9 N/cm^2 (8.6 psi) above the required NPSP at that time. The NPSP agreed closely with predictions.

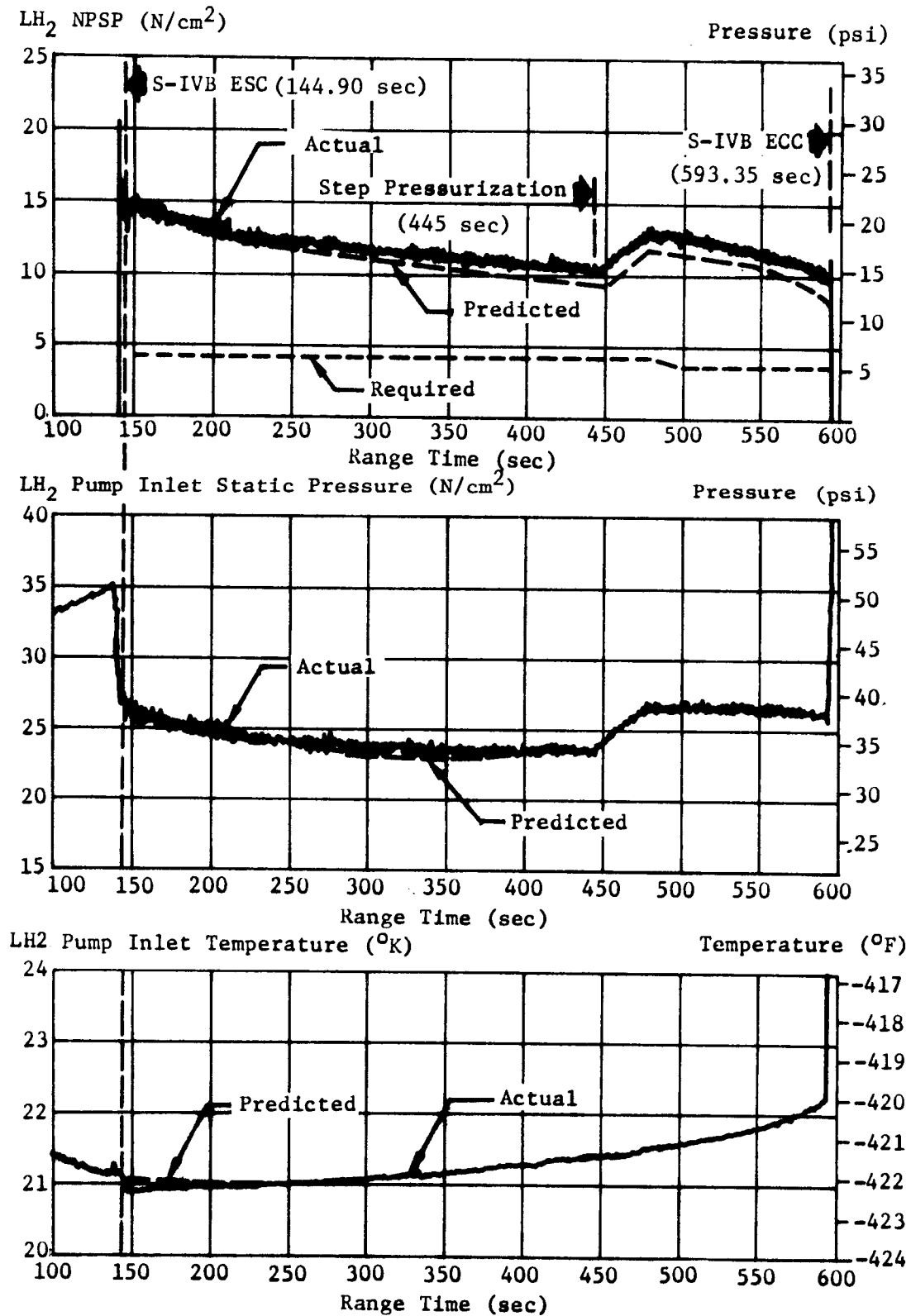
The LH₂ pump inlet static pressure (middle portion of Figure 9-10) followed the LH₂ tank ullage pressure closely (lower portion of Figure 9-9). Values ranged from about 23.8 to 26.9 N/cm^2 (34.5 to 39 psi) during the burn and were close to predicted. The LH₂ pump inlet temperature (lower portion of Figure 9-10) followed predicted values very closely.

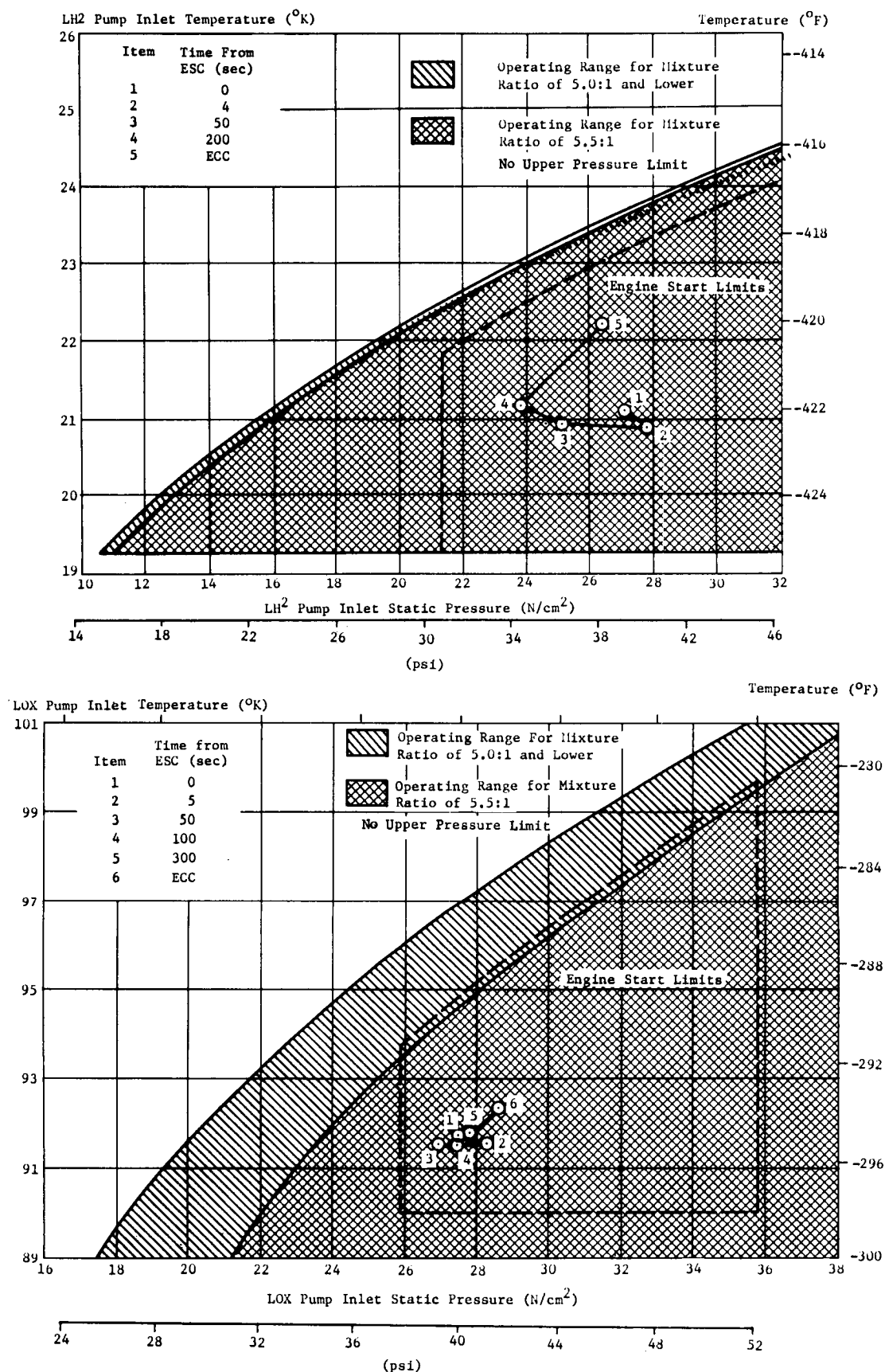
The LH₂ system recirculation chilldown was adequate. At S-IVB ESC, the LH₂ pump inlet static pressure and temperature were 27.4 N/cm^2 (39.8 psi) and 21.0°K (-421.9°F), respectively. This was well within engine start requirements (upper portion of Figure 9-11).

9.4.2 LOX PRESSURIZATION SYSTEM

The LOX pressurization system performance was satisfactory throughout the flight, supplying LOX to the engine pump inlet within the specified operating limits. Prepressurization and pressurization control were normal and within predicted limits.

LOX tank prepressurization was initiated at 163.3 sec, and increased the LOX tank ullage pressure from 10.6 N/cm^2 (15.38 psi) to 27.8 N/cm^2

FIGURE 9-10 LH₂ PUMP CONDITIONS

FIGURE 9-11 LH₂ AND LOX PUMP INLET START REQUIREMENTS

(40.3 psi) within 13.8 sec (upper portion of Figure 9-12). One makeup cycle was required prior to liftoff to maintain the LOX tank ullage pressure above the control pressure switch minimum of 25.9 N/cm^2 (37.5 psi). By -111 sec the ullage gas temperature had stabilized. The ambient helium purges of the ullage pressure sense line and of the tank vent and relief valve caused a gradual rise in ullage pressure to 29.8 N/cm^2 (43.2 psi) at -31 seconds.

The ullage pressure began increasing after S-IB cutoff; this has been observed on previous flights and was caused by ullage compression as the S-IVB stage acceleration level dropped during IB separation. Following ESC, the LOX pressurization system was activated before the LOX began flowing to the engine, resulting in an additional ullage pressure rise prior to engine ignition.

During S-IVB powered flight (lower portion of Figure 9-12), the ullage pressure cycled seven times and remained between 26.0 and 27.3 N/cm^2 (37.7 and 39.6 psi) except during the start transient, at which time the ullage pressure dropped momentarily to 24.0 N/cm^2 (34.8 psi) at 165 seconds. This value compared closely with the predicted value of 23.6 N/cm^2 (34.2 psi) and resulted in a NPSP that was above the minimum requirement.

The LOX tank pressurization total flowrate, excluding the first 10 sec transient period, varied from 0.168 to 0.191 kg/s (0.37 to 0.42 lbm/s) during over-control, and from 0.122 to 0.141 kg/s (0.27 to 0.31 lbm/s) during under-control system operation. This variation is normal because the bypass orifice inlet temperature changes as it follows the heat exchanger temperature. The calculated helium mass, based upon flow integration during S-IVB powered flight, was 68 kg (149 lbm). The cold helium pressure measurement was biased because of irregular measurement behavior prior to liftoff and because of suspected lower than actual readings. Readings were suspected to be low based upon other stage system pressure levels. Calculations using the biased pressure agree reasonably well with flow integration calculations. Using the biased pressure, the helium mass loaded was 151.5 kg (334 lbm).

The J-2 engine heat exchanger outlet temperature increased from 357°K (183°F) to 533°K (499°F) during the 65 sec start transient period. Throughout the remainder of the high engine mixture ratio portion of S-IVB powered flight, the heat exchanger outlet temperature varied between 537 and 557°K (507 and 543°F) on the over-control and 550 and 586°K (530 and 595°F) on under-control operation. These temperatures were 15 to 30°K (27 to 54°F) higher than those recorded during the S-IVB-204 acceptance testing. This difference was caused by the absence of atmospheric convective heat transfer loss through the uninsulated

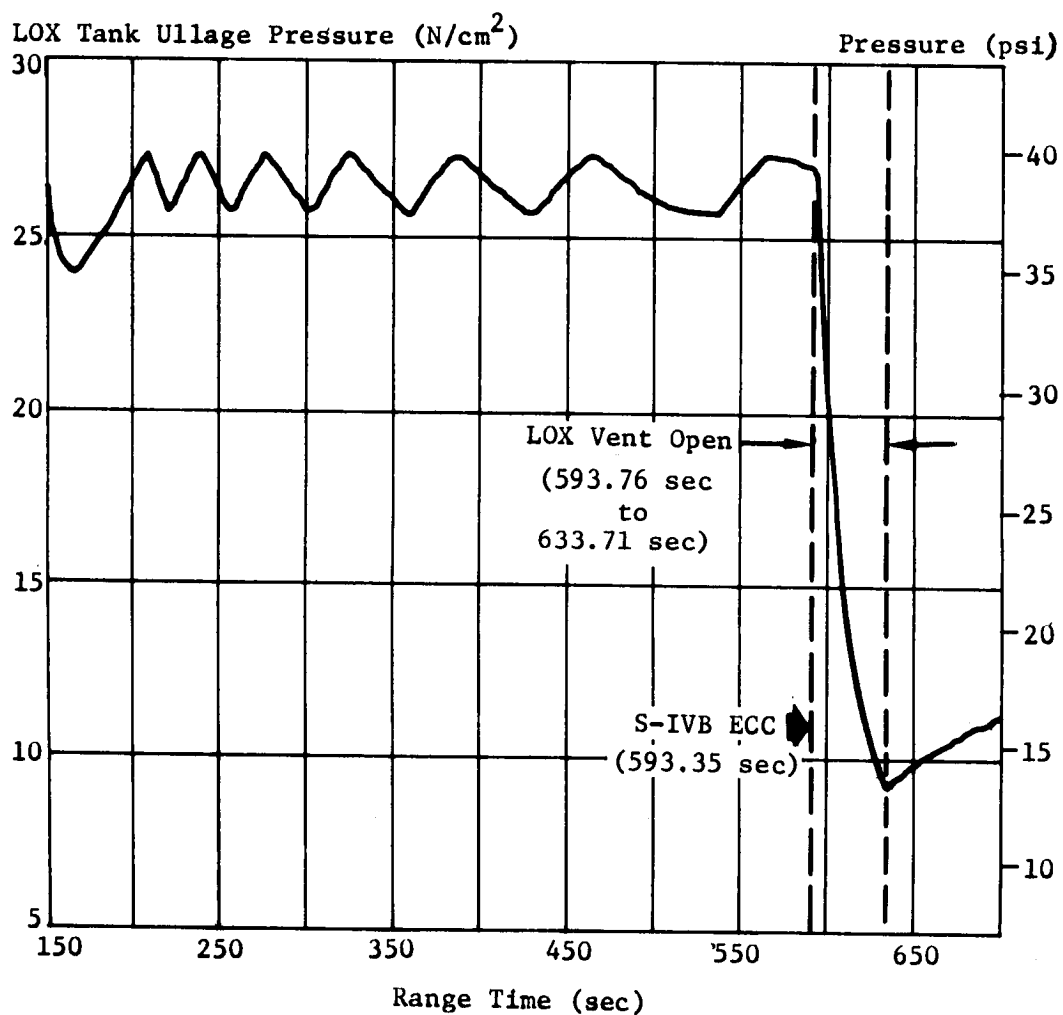
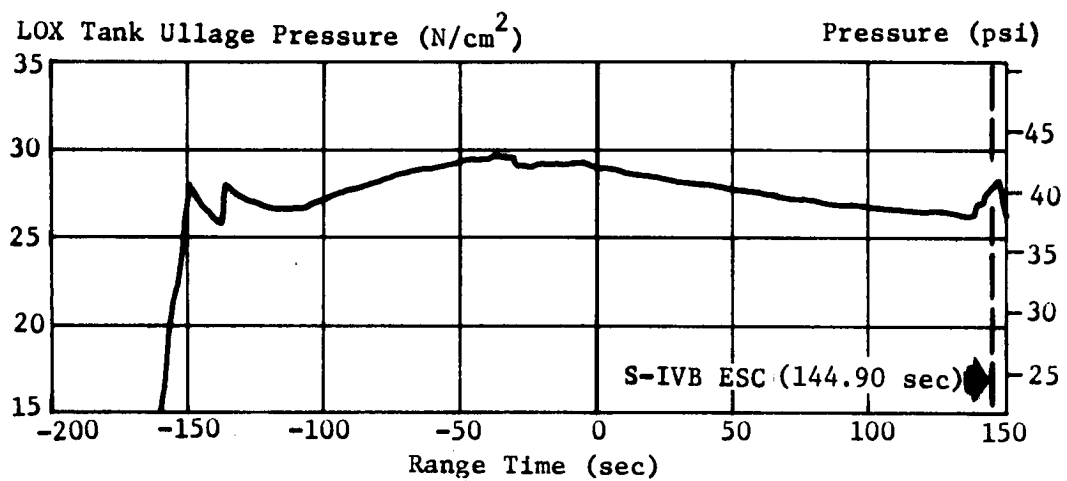


FIGURE 9-12 LOX TANK ULLAGE PRESSURE

part of the pressurization line during flight, and by differences between the actual and the predicted engine mixture ratio. The helium flow through the heat exchanger was relatively constant at 0.086 kg/s (0.19 lbm/s) during over-control and at 0.032 kg/s (0.07 lbm/s) during under-control operation.

After S-IVB ECC, the ullage pressure remained momentarily at 27.1 N/cm² (39.3 psi) until the programmed LOX vent occurred at 593.76 seconds. The LOX vent valve was commanded closed at 633.71 sec, at which time the ullage pressure was at a low reading of 9.17 N/cm² (13.3 psi).

LOX Supply Conditions

The NPSP, calculated at the LOX pump inlet, was 15.7 N/cm² (22.8 psi) at S-IVB ESC (upper portion of Figure 9-13). The NPSP decreased after S-IVB ESC and reached a minimum value of 15.0 N/cm² (21.8 psi) at 164 seconds. This was 0.69 N/cm² (1.0 psi) above the required NPSP at that time. The NPSP then increased and followed the pump inlet pressure closely throughout S-IVB powered flight, since there was small variation in LOX temperature. The NPSP was slightly less than predicted, but was greater than required.

The LOX system chilldown circulation was satisfactory. As programmed, the chilldown valve was not closed until just prior to S-IVB ECC. At S-IVB ESC, the LOX pump inlet static pressure (middle portion of Figure 9-13) was 27.6 N/cm² (40.0 psi) and the temperature was 91.5°K (-294.9°F) (lower portion of Figure 9-13). This was well within the start requirements (lower portion of Figure 9-11). The NPSP at ESC was 15.7 N/cm² (22.8 psi).

The LOX pump inlet static pressure (middle portion of Figure 9-13) followed the cyclic trends of the LOX tank ullage pressure. Values ranged from 25.5 N/cm² (37 psi) at 164 sec to 30.3 N/cm² (44.0 psi) immediately after ESC, with quasi-steady cycling around 27.6 N/cm² (40 psi). The LOX pump inlet temperature (lower portion of Figure 9-13) was slightly above the expected level.

9.5 S-IVB PNEUMATIC SYSTEMS

The following three S-IVB pneumatic systems performed satisfactorily: (1) stage pneumatic control and purge system, (2) GH₂ start tank system, and (3) engine pneumatic control system.

Stage Pneumatic Supply

The pneumatic control and purge system performed satisfactorily throughout flight. The helium supply to the system was adequate for both pneumatic valve control and purging. The regulated pressure was maintained within acceptable limits and all components functioned normally.

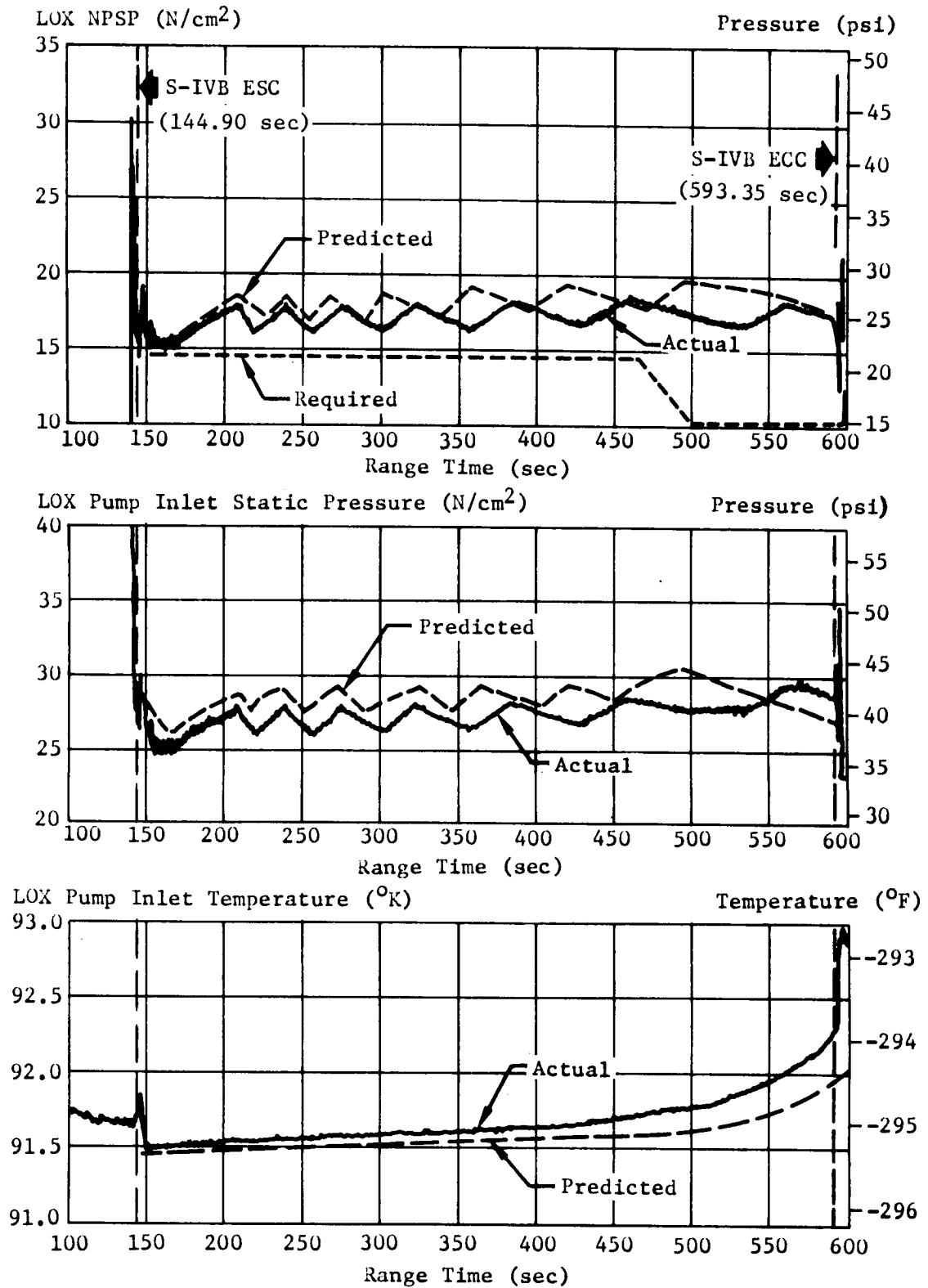


FIGURE 9-13 LOX PUMP CONDITIONS

The middle portion of Figure 9-14 shows that the pneumatic control helium sphere pressure was approximately 2090 N/cm^2 (3032 psi) at liftoff. The sphere pressure decreased to 2076 N/cm^2 (3011 psi) by S-IVB ESC. During S-IVB powered flight, the pressure rose due to thermal increase and the pressure was 2096 N/cm^2 (3040 psi) at S-IVB ECC. The upper portion of Figure 9-14 shows that the sphere temperature was 255°K (0°F) at liftoff. The temperature decreased to 253°K (-5°F) at S-IVB ESC. By S-IVB ECC, the sphere temperature had increased to 256°K (1°F).

At liftoff, the pneumatic helium sphere contained 4.49 kg (9.89 lbm). The helium mass in the sphere at S-IVB ESC was 4.49 kg (9.89 lbm) and 4.48 kg (9.88 lbm) remained at S-IVB ECC. The helium mass usage rates are compared to S-IVB-203 in Table 9-VI.

TABLE 9-VI STAGE PNEUMATIC HELIUM USAGE

PORTION OF POWERED FLIGHT	S-IVB-204		S-IVB-203	
	SCCS	SCFM	SCCS	SCFM
S-IB Stage	0.0	0.0	585	1.24
S-IVB Stage	6.3	0.013	194	0.41

Note: SCCS is Standard Cubic Centimeter Per Second
SCFM is Standard Cubic Feet Per Minute

All stage pneumatic control valves responded properly throughout the countdown and flight. The pneumatic control helium regulator operated satisfactorily and maintained an output pressure of 365 to 390 N/cm^2 (530 to 565 psi). During the period of high pneumatic system use at S-IVB engine cutoff, the control pressure dropped to 282 N/cm^2 (409 psi). Such drops occurred during acceptance testing and were expected.

GH₂ Start Bottle

Chilldown and loading of the engine GH₂ start bottle were accomplished satisfactorily. GH₂ mass in the sphere at liftoff was 1.64 kg (3.62 lbm). The warmup rate after the sphere was pressurized, until liftoff, was 0.94°K/min (1.7°F/min). At S-IVB ESC, the temperature was 153°K (-185°F) and the pressure was 913 N/cm^2 (1325 psi); these values were well within the requirements of $161 \pm 17^\circ\text{K}$ ($-170 \pm 30^\circ\text{F}$) and $914 \pm 52 \text{ N/cm}^2$ (1325 \pm 75 psi), respectively. The mass diminished during start sphere blowdown to 0.39 kg (0.85 lbm); the total mass utilized was 1.26 kg (2.78 lbm).

Figure 9-15 shows the GH₂ start bottle performance from ESC to initiation of LOX dump in orbit. Fuel pump spin-up, as the result of

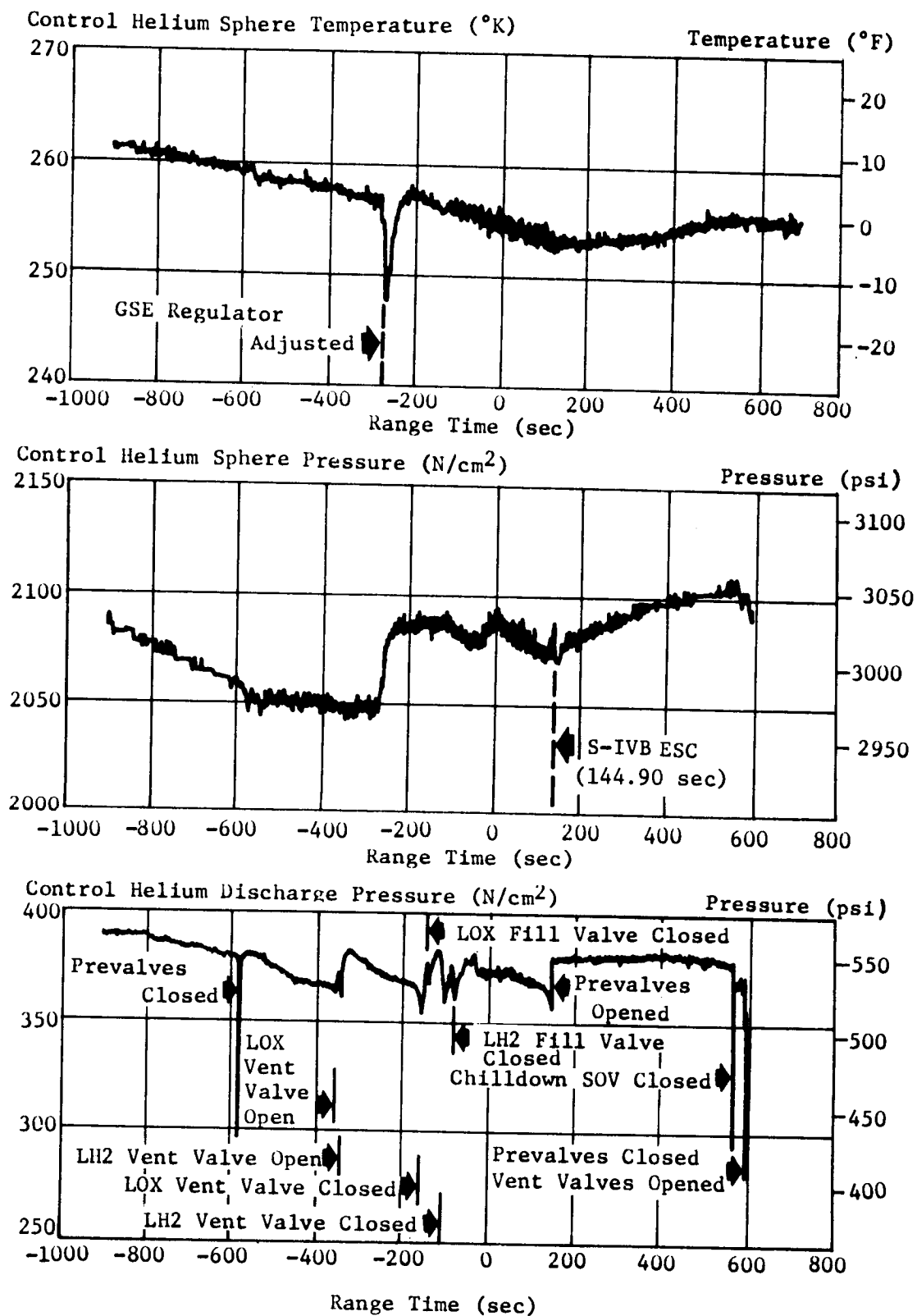


FIGURE 9-14 STAGE PNEUMATIC CONTROL AND PURGE SYSTEM PERFORMANCE

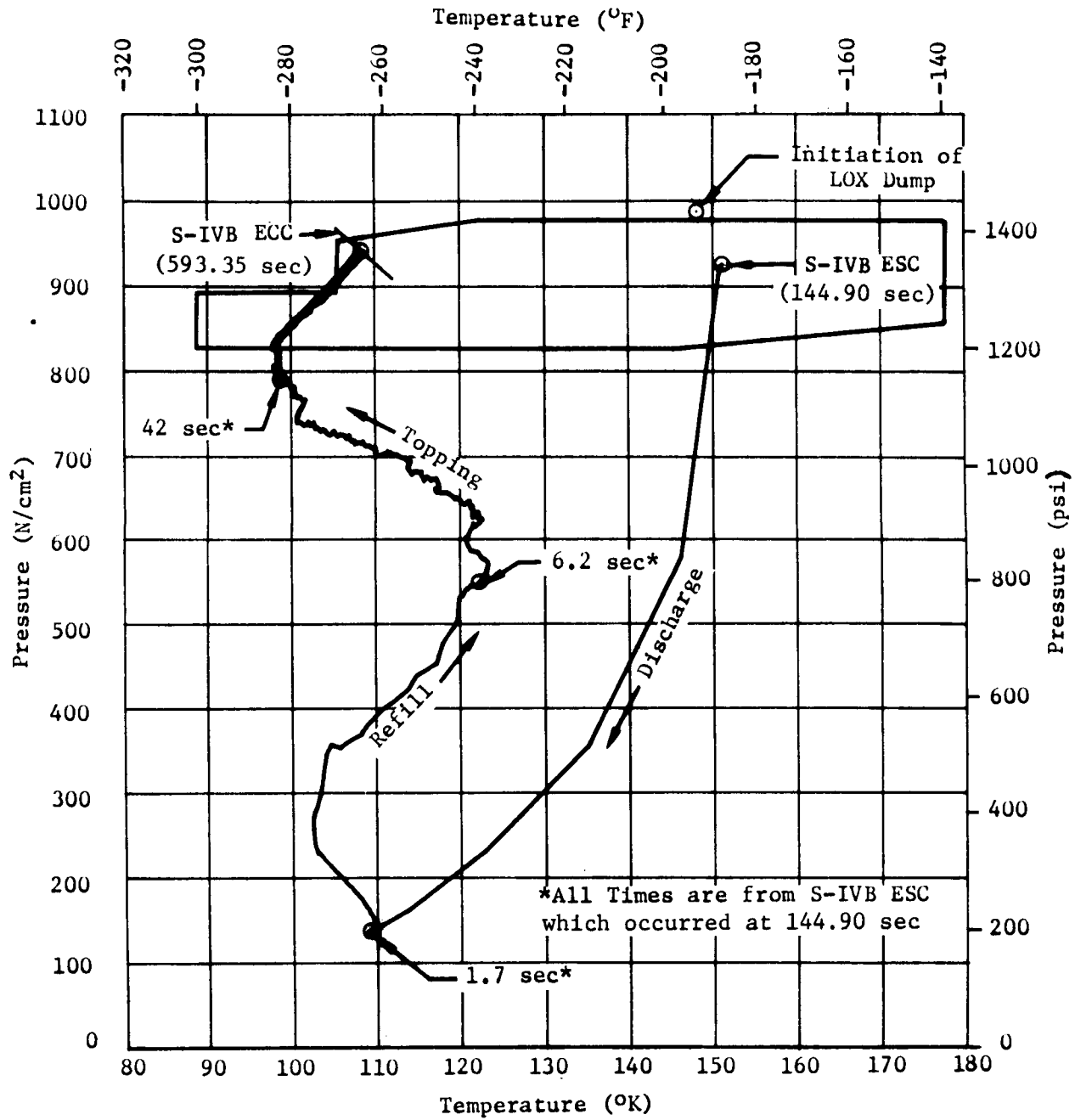


FIGURE 9-15 J-2 START BOTTLE PERFORMANCE

GH₂ discharge from the start tank, was completed by ESC + 1.7 seconds.

No modifications to provide for J-2 engine restart capability were made to the S-IVB-204 start tank and its refill system, since restart was not a requirement on S-IVB-204. In absence of these modifications, the start tank recharge was much faster than that experienced during the S-IVB-501 mission. Gas flow from the injection manifold was terminated at ESC + 6.2 sec as compared to ESC + 10 sec for S-IVB-501. When corrected for the differences in fuel lead, the comparative values are 5.2 sec and 7 sec for S-IVB-204 and -501, respectively. The S-IVB-204 topping process was completed at ESC + 42 sec, when the pressure in the start tank was 804 N/cm² (1167 psi). A similar pressure balance between the start tank and fuel pump discharge was not reached until ESC + 64 sec during the S-IVB-501 mission. The rapid refill and the relatively long burn period (compared to the S-IVB-501 first burn) caused the pressure, due to heat input, to increase to the cutoff level of 924 N/cm² (1340 psi).

Engine Control Sphere

The helium control system for the J-2 engine performed satisfactorily during mainstage operation. The engine pneumatic control sphere conditioning was satisfactory. At S-IVB ESC, the sphere pressure was 2106 N/cm² (3055 psi), the temperature was 155°K (-181°F), and the mass was 0.90 kg (1.99 lbm). Pressure and temperature specifications of the sphere at ESC are 1931 to 2379 N/cm² (2800 to 3450 psi) and 88.9 to 177.8°K (-300 to -140°F). The mass remaining after engine cutoff was 0.72 kg (1.59 lbm); 0.18 kg (0.40 lbm) was consumed. The pressure in the control sphere was lower than predicted at cutoff, but within the allowable band. The low pressure was probably due to temperature effects caused by the rapid GH₂ start bottle refill.

9.6 S-IVB ORBITAL SAFING EXPERIMENT

9.6.1 EXPERIMENT PURPOSE AND EVENTS

After the S-IVB had accomplished its planned mission of inserting the spacecraft into orbit, an experiment was performed to determine the capability of venting the high pressure gasses and of dumping propellants in orbit. This experiment was performed to obtain information relative to safing S-IVB stages during orbital coast on subsequent missions. All portions of the experiment were performed successfully, yielding valuable data for future study and analysis.

The manner and sequencing in which the experiment was performed is presented in Table 9-VII.

TABLE 9-VII ORBITAL EVENTS SUMMARY

Event	Duration (sec)	Range Time			
		Time Started		Time Completed	
	(sec)	(sec)	hr:min:sec	(sec)	hr:min:sec
LOX Tank Vent 1	39.95	593.76	00:09:53.76	633.71	00:10:33.71
LH ₂ Tank Vent 1	1260.00	593.93	00:09:53.93	1853.93	00:30:53.43
LH ₂ Tank Vent 2	1200.00	3398.51	00:56:38.51	4598.51	01:16:38.51
LH ₂ Tank Vent 3	600.00	6143.51	01:42:23.51	6743.51	01:52:23.51
LOX Dump	120.20	8774.31	02:26:14.31	8894.51	02:28:14.51
LH ₂ Dump	180.20	8904.31	02:28:24.31	9084.51	02:31:24.51
LH ₂ Tank Vent 4	2558.00	9094.31	02:31:34.31	11651.51	03:14:11.51
LOX Tank Vent 2	2556.80	9094.51	02:31:34.51	11651.31*	03:14:11.31
Cold Helium Open to LOX Tank	1301.60	10349.51	02:52:29.51	11651.11	03:14:11.11
LH ₂ Tank Vent 5	2764.00	14216.51	03:56:56.51	16980.51	04:43:00.51
LOX Tank Vent 3	2764.00	14216.71	03:56:56.71	16980.71	04:43:00.71
Ambient Helium Sphere Vent	300.00	16985.91	04:43:05.91	17285.91	04:48:05.91

*See paragraph 9.6.2 for clarification of LOX tank vent closure.

9.6.2 LH₂ AND LOX TANK VENTING

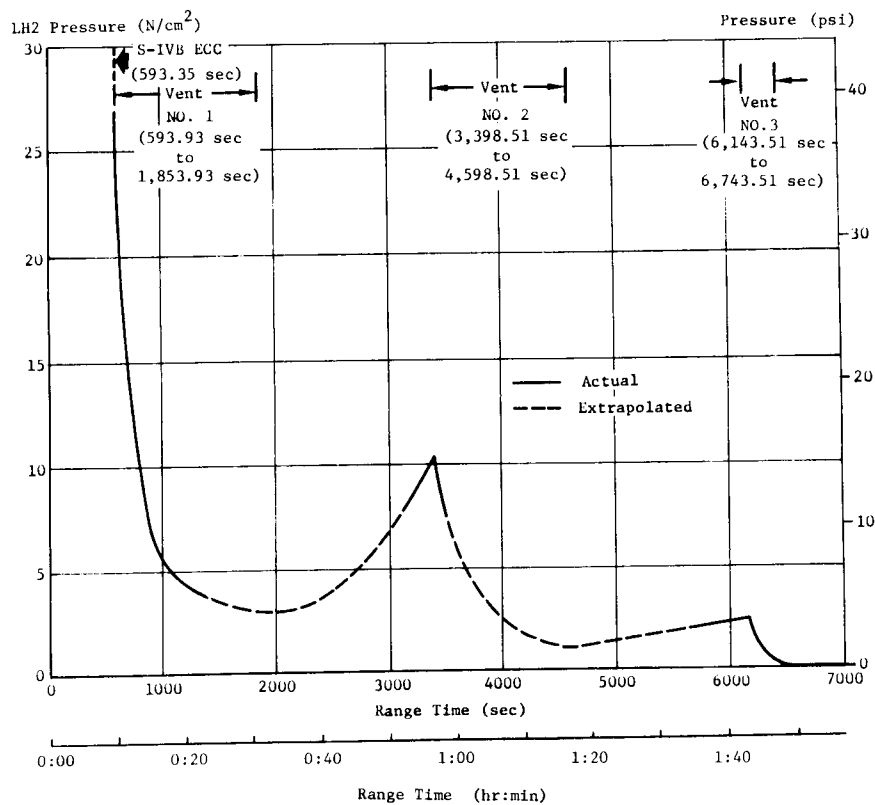
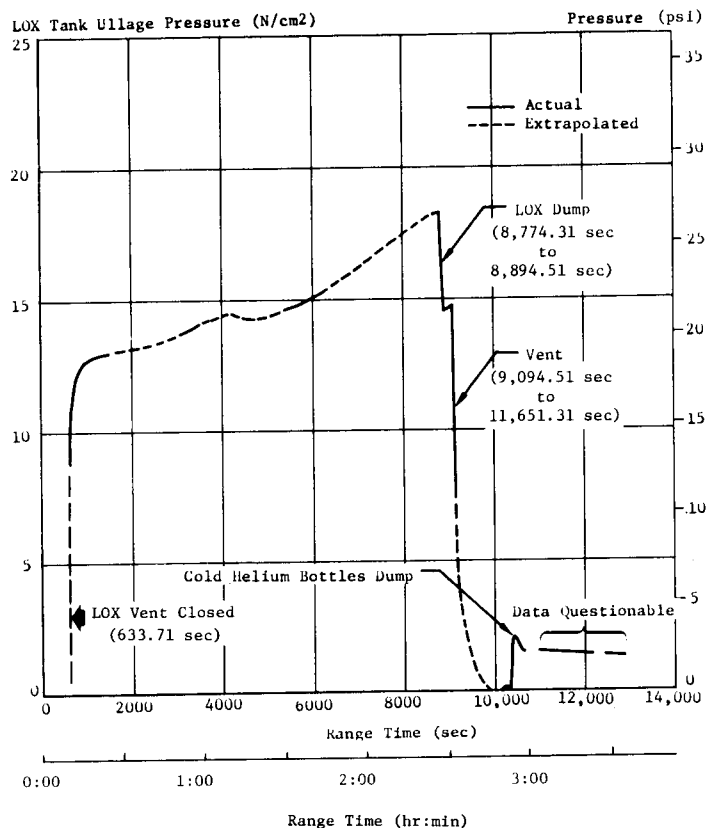
The LH₂ tank venting operations were performed as planned and were satisfactorily accomplished. The vent and relief valve inconsistencies discussed in paragraph 9.4.1 had no effect on the operation. The LH₂ tank pressure during the first 7000 sec of orbital coast is shown in the lower portion of Figure 9-16. The tank ullage pressure at the end of the third programmed vent was 0.0 N/cm² (0.0 psi) and remained at that level for the remainder of the flight. Safing of the stage was accomplished at the end of the third vent, since all residual LH₂ had boiled off and had been vented during the programmed vent sequence.

The LOX tank orbital venting operations were satisfactorily accomplished. The only irregularities observed were those following the cold helium dump when the ullage pressure decay rate was much lower than expected and the vent valve closed indication picked up 18.90 min after the close command at 3hr:33min:5sec range time. Neither of these irregularities impaired the mission success. The LOX tank ullage pressure is shown in the upper portion of Figure 9-16.

Three programmed LOX vents occurred during orbit, as shown in the upper portion of Figure 9-16. The first vent occurred immediately after J-2 engine cutoff and dropped the ullage pressure from 27.0 to 9.3 N/cm² (39.2 to 13.5 psi) in 40 seconds. The second vent began shortly after propellant dump at 2hr:31min:34.51sec (9094.51 sec) and terminated after the cold helium dump at 3hr:14min:11.31sec (11,651.31 sec). The third LOX vent began at 3hr:56min:56.71sec (14,216.71 sec) and ended at 4hr:43min:00.71sec (16,980.51 sec).

During the cold helium dump the LOX tank ullage pressure indicated that the vent path was partially blocked; further analysis revealed that the vent effective flow area was at maximum when the ullage pressure began to decay, and then decreased during the remainder of the dump. Since the vent valve appeared to be fully open during this period (the open indication did not drop out and no abnormal pneumatic gas usage occurred), the restriction may have been due to the formation of snowy or solid oxygen in the vent system (upper portion of Figure 9-17).

Evidence exists that this formation may have occurred at the LOX vent valve. When the LOX vent valve was commanded closed at the end of the cold helium dump at 3hr:14min:11.11sec (11,651.11 sec), the open indication dropped out, but the closed indication was not received until 3hr:33min:5sec (12,785 sec). The blockage may have formed around the vent valve piston. When the valve was commanded closed, the valve may not have closed completely. As the oxygen formation changed states, the valve finally closed at 3hr:33min:5sec (12,785 sec). This theory is supported by the ullage pressure data, which begins increasing very slightly at 3hr:14min:11.11sec (11,651.11 sec), indicating that partial sealing had occurred. At 3hr:33min:5sec (12,785 sec) the rise rate increased, indicating that a

FIGURE 9-16 LH₂ AND LOX TANK ULLAGE PERFORMANCE IN ORBIT

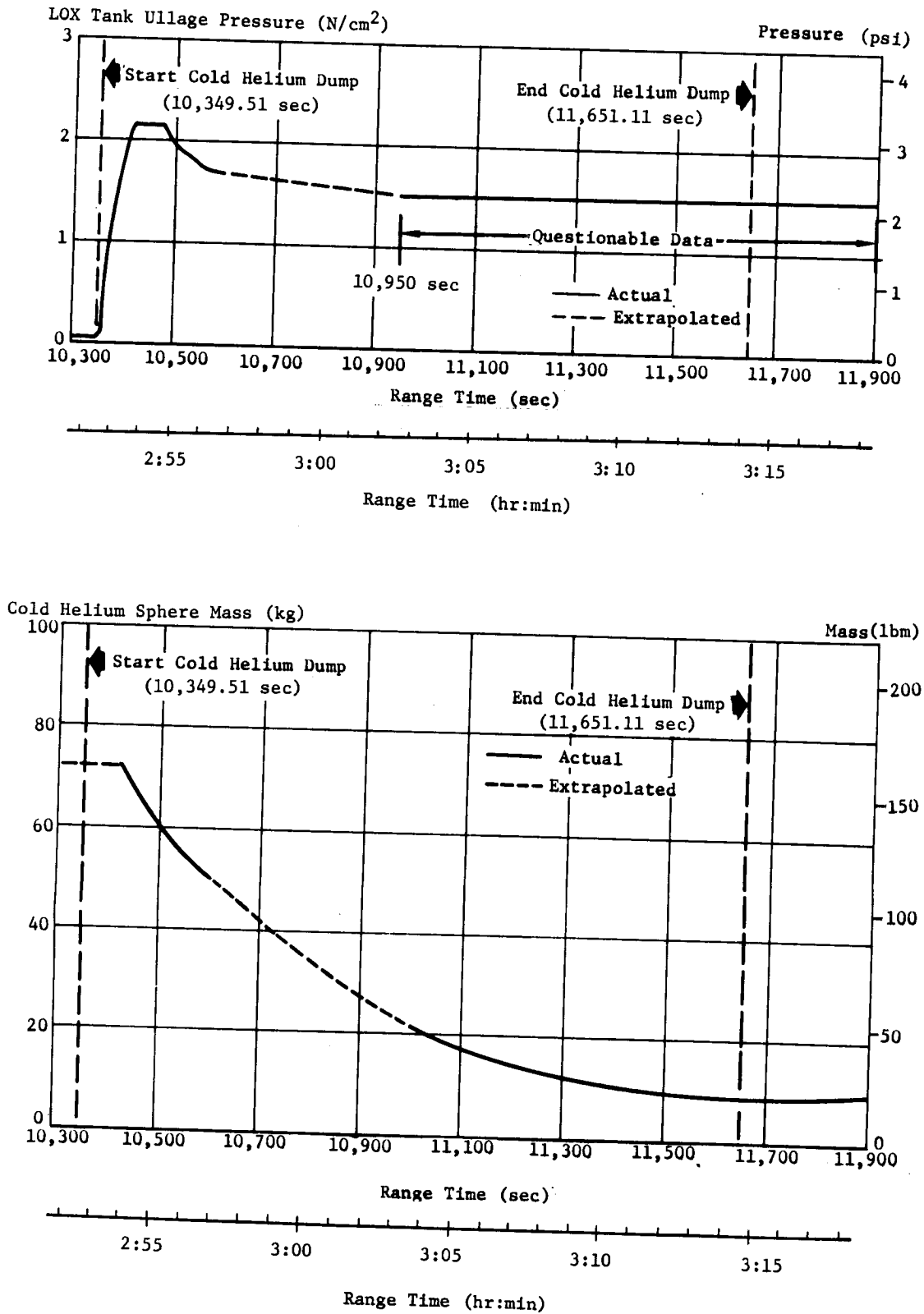


FIGURE 9-17 COLD HELIUM DUMP PERFORMANCE

complete seal had probably occurred.

The restriction was absent when the vent valve was commanded open for the third vent at 3hr:56min:56.71sec (14,216.71 sec). The vent effective flow area was normal, and the ullage pressure decreased rapidly from 1.7 N/cm² (2.5 psi) towards 0 psi.

9.6.3 PROPELLANT DUMP

By the time the LH₂ tank propellant dump was programmed to occur, all the liquid in the tank had been boiled off and vented overboard. Consequently, no data applicable to dumping liquid hydrogen through the J-2 engine were obtained.

The LOX tank dump was accomplished satisfactorily as planned. Ullage pressure data during LOX dump is shown in the upper right portion of Figure 9-18. Approximately 65 sec after LOX dump was initiated, the ullage pressure began decreasing, indicating that gas ingestion had begun. This was verified by acceleration data, which reflected a sharp decrease in thrust commencing 55 sec after LOX dump initiation. It is probable that gas ingestion began at this time, with the ullage pressure data lagging by some 10 seconds. The ullage pressure continued to decrease until end of the dump.

Calculations indicate that approximately 868 kg (1913 lbm) of the liquid residual was dumped, with the remainder vaporizing and then being vented shortly afterwards (see paragraph 9.6.2). The lower right portion of Figure 9-18 shows the LOX mass, both liquid and gaseous oxygen, during LOX dump. The thrust resulting from the LOX dump is shown in the left-hand portion of Figure 9-18. A maximum thrust of 3,415 N (768 lbf) resulted at 8830 seconds. See paragraph 12.4.2.2 for resulting velocity changes.

9.6.4 COLD HELIUM DUMP

At ECC, the cold helium temperatures ranged from 27 to 31°K (-411 to -404°F), indicating that all the bottles were no longer covered with liquid hydrogen. By 58min:20sec (3500 sec), the bottle temperatures had decreased to a range of 23 to 25°K (-419 to -415°F). During this time, the pressure had also decreased, from 868 N/cm² (1259 psi) at ECC to 517 N/cm² (750 psi) at 58min:20sec (3500 sec). Using the bias applied during boost and burn, these conditions indicate a mass loss of 13.6 kg (30 lbm). Similar indicated mass losses occurred in AS-501 during orbital coast. It is not believed that mass losses actually occurred, and sphere instrumentation is thought to be responsible for the indicated mass losses.

By the beginning of cold helium dump, the sphere temperature had increased to a range of 35 to 37°K (-397 to -393°F) and the pressure had increased to 818 N/cm² (1187 psi). The biased data indicated a mass of 73.5 kg (162 lbm). Bottle conditions indicated that the mass dumped

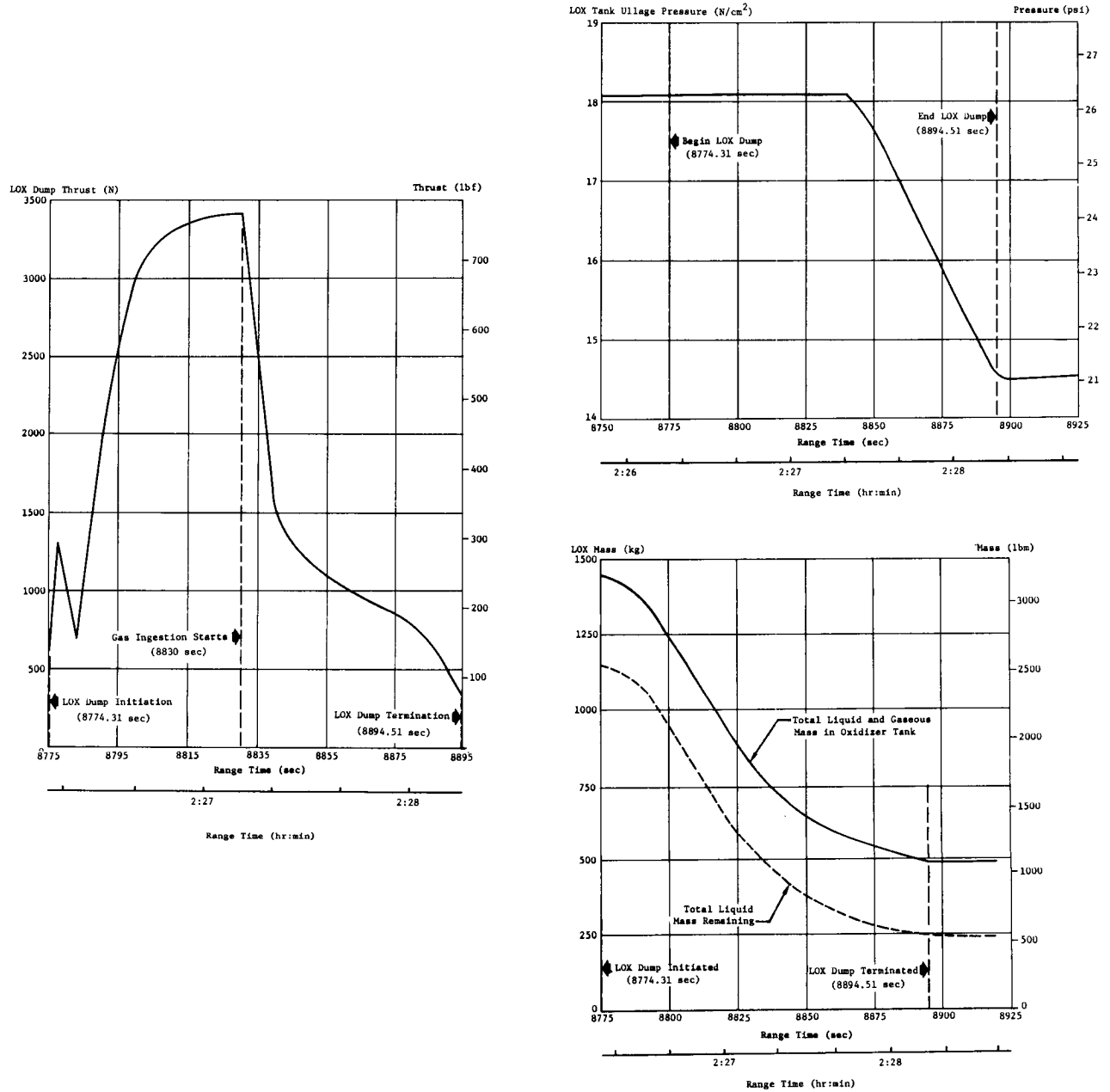


FIGURE 9-18 LOX DUMP PERFORMANCE

was approximately 68 kg (150 lbm) as shown in the lower portion of Figure 9-17. The indicated bottle pressure and temperature at the end of the dump were 28 N/cm^2 (40 psi) and 16°K (-430°F), respectively. All data indicates that safing of the cold helium bottle was successfully accomplished.

9.6.5 PNEUMATIC SPHERES

Stage Pneumatic Sphere (Ambient Helium)

The stage pneumatic helium usage was much lower than predicted. This, plus the orbital heatup that was not predicted, resulted in a higher than predicted supply pressure. Most of the predicted usage was for vent valve actuations. A prediction based on the observed heatup and on no vent valve actuation leakage agrees closely with actual data. During the period between ECC and initiation of safing, the sphere supply temperature increased from 256°K (1°F) to 290°K (63°F). The pressure accordingly increased from 2103 N/cm^2 (3050 psi) to 2282 N/cm^2 (3310 psi) during the same period. These changes indicate a mass loss of 0.195 kg (0.43 lbm) during the same time period.

The pressure decreased from 2282 N/cm^2 (3310 psi) to 1034 N/cm^2 (1500 psi) during safing of the sphere. The temperature decreased from 290°K (63°F) to 218°K (-67°F) during the same period. The predicted pressure at initiation of safing was 1193 N/cm^2 (1730 psi), based upon nominal leakage (upper portion of Figure 9-19). The pressure, from the initial level, was expected to decrease to 834 N/cm^2 (1210 psi) during the preprogrammed 5-minute vent.

The rate and manner in which the sphere was vented were demonstrated to be satisfactory. When required on future flights, the duration of safing can be revised to compensate for anticipated conditions. The Clary actuation control modules used on S-IVB-204 will be replaced by the Sterer modules on S-IVB-205.

GH₂ Start Bottle

The relief setting of the start tank vent and relief valve was 958.4 N/cm^2 or 1390 psi at $116.7 \pm 27.8^\circ\text{K}$ ($-250 \pm 50^\circ\text{F}$). The valve relieved continuously from cutoff, and the pressure was 986.0 N/cm^2 (1430 psi) approximately 1.75 hours after cutoff. The relief valve performed adequately, allowing the pressure to decay to 951.5 N/cm^2 (1380 psi) at ECC + 6 hours. As usual, the measured start tank temperature was erratic during orbital coast but the normal corrections indicated that, near the end of stage life, the temperature was approximately 139°K (-210°F) with a corresponding pressure of 948 N/cm^2 (1375 psi). The degree of data accuracy near the end of the stage life is not known. The GH₂ start bottle pressure up to LOX dump initiation is shown in Figure 9-15. No safing of the start sphere was attempted, since it was not modified on S-IVB-204 to permit safing.

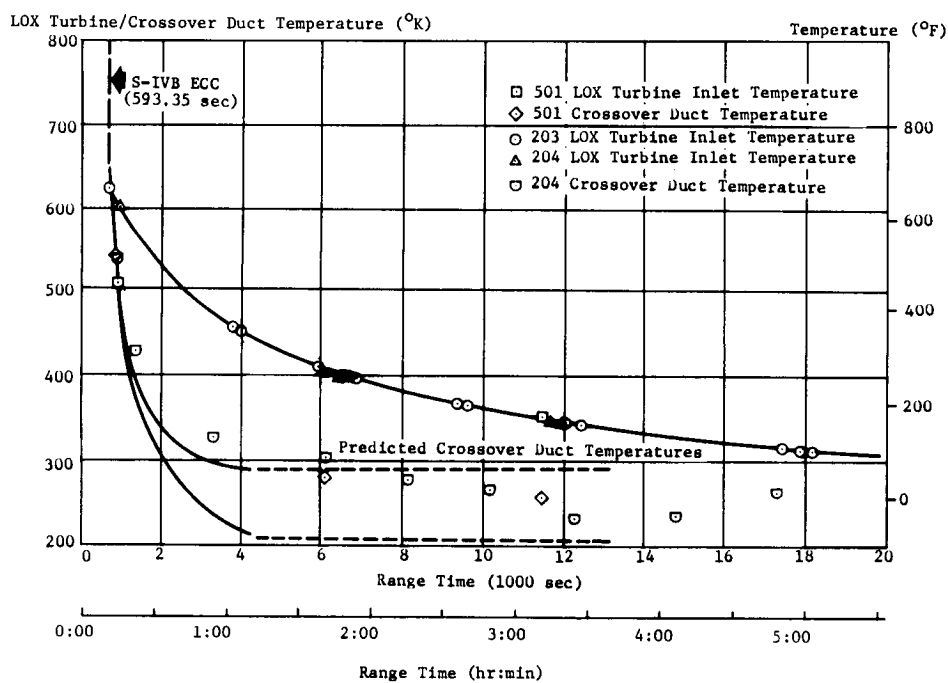
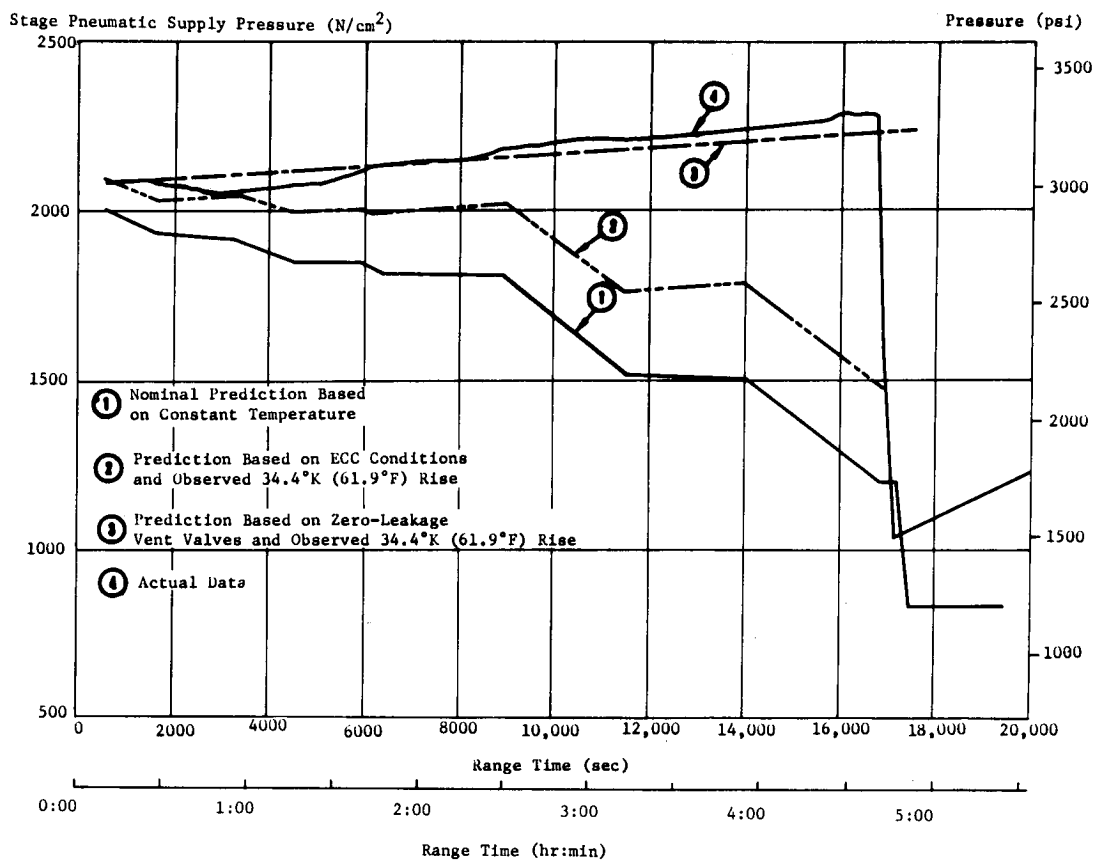


FIGURE 9-19 S-IVB STAGE PNEUMATIC SUPPLY PRESSURE AND LOX TURBINE/CROSSOVER DUCT TEMPERATURES

Engine Control Sphere

The control sphere temperature and pressure were 106.8°K (-267.5°F) and 1096 N/cm² (1590 psi) after the 1 sec post cutoff blowdown. Immediately prior to the safing experiment, the measured temperature and pressure were 138.7°K (-210°F) and 3103 N/cm² (1890 psi); which, considering the erratic nature of the temperature measurement during orbital coast, was consistent with pressure, volume, and temperature relationships, and a non-leaking system.

No consideration was given to the initial pressure decay required to fill the void downstream of the regulator or to temperature effects. Therefore, upon initiation of the safing experiment, the pressure decayed outside (to lower than) the predicted band (Figure 9-20). As the LOX dump continued, the reduced temperature caused the pressure decay rate to decrease and, at the end of the LOX dump, the pressure in the control sphere was above the predicted band. The control sphere pressure decay during the fuel dump was as predicted. At the end of the fuel dump, the pressure was 62 N/cm² (90 psi), as predicted. There was no significant pressure recovery due to heat input during the remainder of the stage life.

9.6.6 CROSSOVER DUCT AND LOX TURBINE TEMPERATURES

The LOX turbine inlet and the painted turbine crossover duct temperatures in orbit were very close to values obtained during S-IVB-203 and -501 orbital flight periods (lower portion of Figure 9-19). The S-IVB-204 data was within or near the predicted band. These results add a large degree of confidence to the repeatability of the turbine hardware temperature conditions during orbital coast.

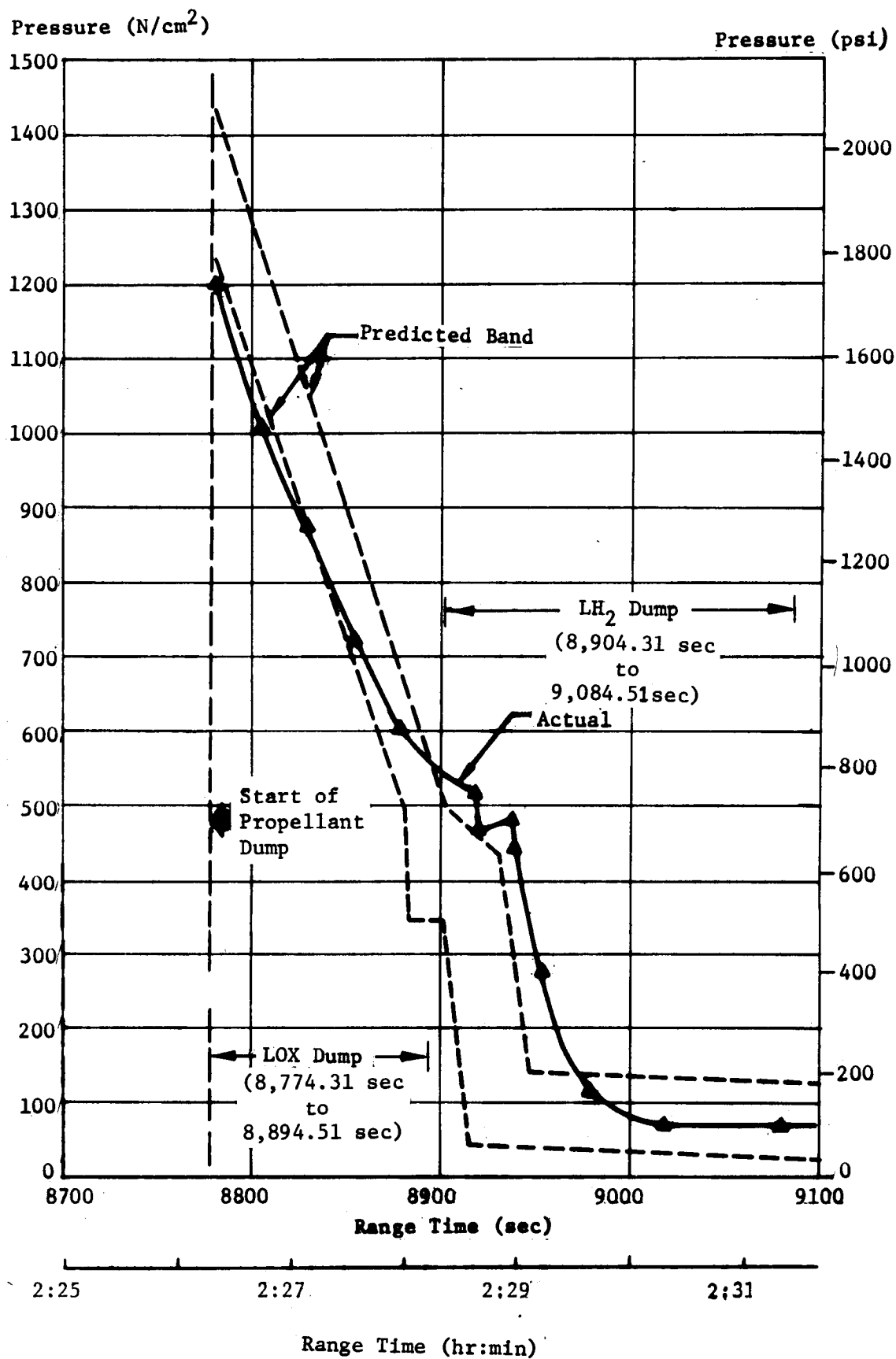


FIGURE 9-20 ENGINE CONTROL SPHERE PRESSURE DURING DUMP EXPERIMENT

10.0 AUXILIARY PROPULSION SYSTEM

10.1 SUMMARY

The performance of each motor in the two Auxiliary Propulsion System (APS) modules was as expected. The average specific impulses of Modules 1 and 2 during powered flight were 211 and 205 sec, respectively.

The APS functioned properly to provide roll control during S-IVB powered flight and to provide pitch, yaw, and roll control following S-IVB engine cutoff. By 6 hr: 16 min: 40 sec (22,600 sec), 55% of the available oxidizer and 57.5% of the available fuel were used. Of the available propellants, 4.5% was required for roll control during S-IVB powered flight.

10.2 APS PERFORMANCE

10.2.1 PROPELLANT AND PRESSURIZATION SYSTEMS

Modules 1 and 2 oxidizer and fuel systems operated properly. The quantities of propellants remaining in each module during the flight and the propellant temperatures are presented in Figure 10-1. The propellant masses consumed during the major phases of flight are shown in Table 10-1 and Figure 10-2.

The APS propellant usage was slightly higher than predicted during the first two LH₂ vents and during the pitch to retrograde maneuver. The actual and predicted propellant usage for attitude control is presented in Figure 10-2 for Module 1 and Module 2.

The high propellant usage can be attributed to three effects:

- (1) The high steady-state roll torque during powered flight resulted in high usage. (The roll torque was higher than the mean but less than the predicted three-sigma. See section 12.0.)
- (2) The possible venting of liquid LH₂ during the first two LH₂ vents, resulting in a high rate of usage during the time of these vents.
- (3) Aerodynamic moments were much larger than predicted. At large angles-of-attack, the aerodynamic moments produced by the open SLA panels are significant. (See Section 12.0.)

Before APS activation, the Module 1 oxidizer temperature was 307°K (92°F) and the mass was 17.7 kg (39.1 lbm); the Module 2 oxidizer temperature was 300°K (80°F) and the mass was 17.9 kg (39.5 lbm). At

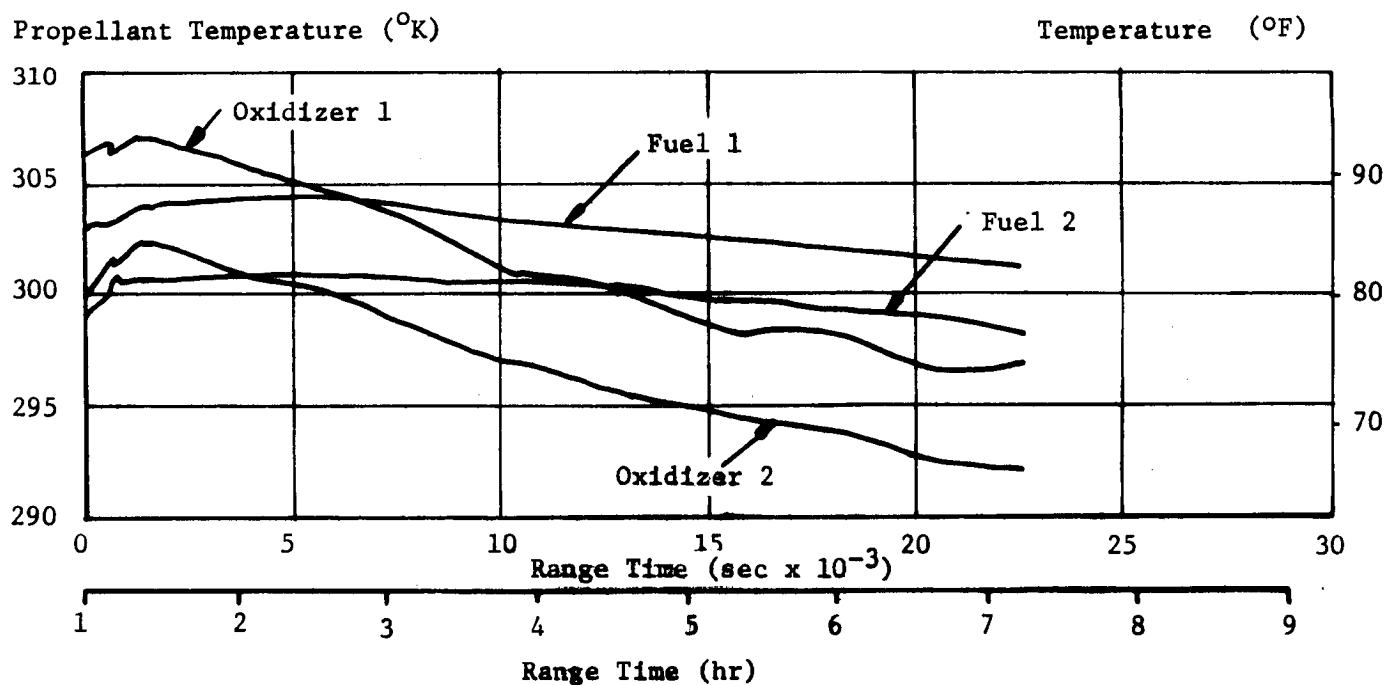
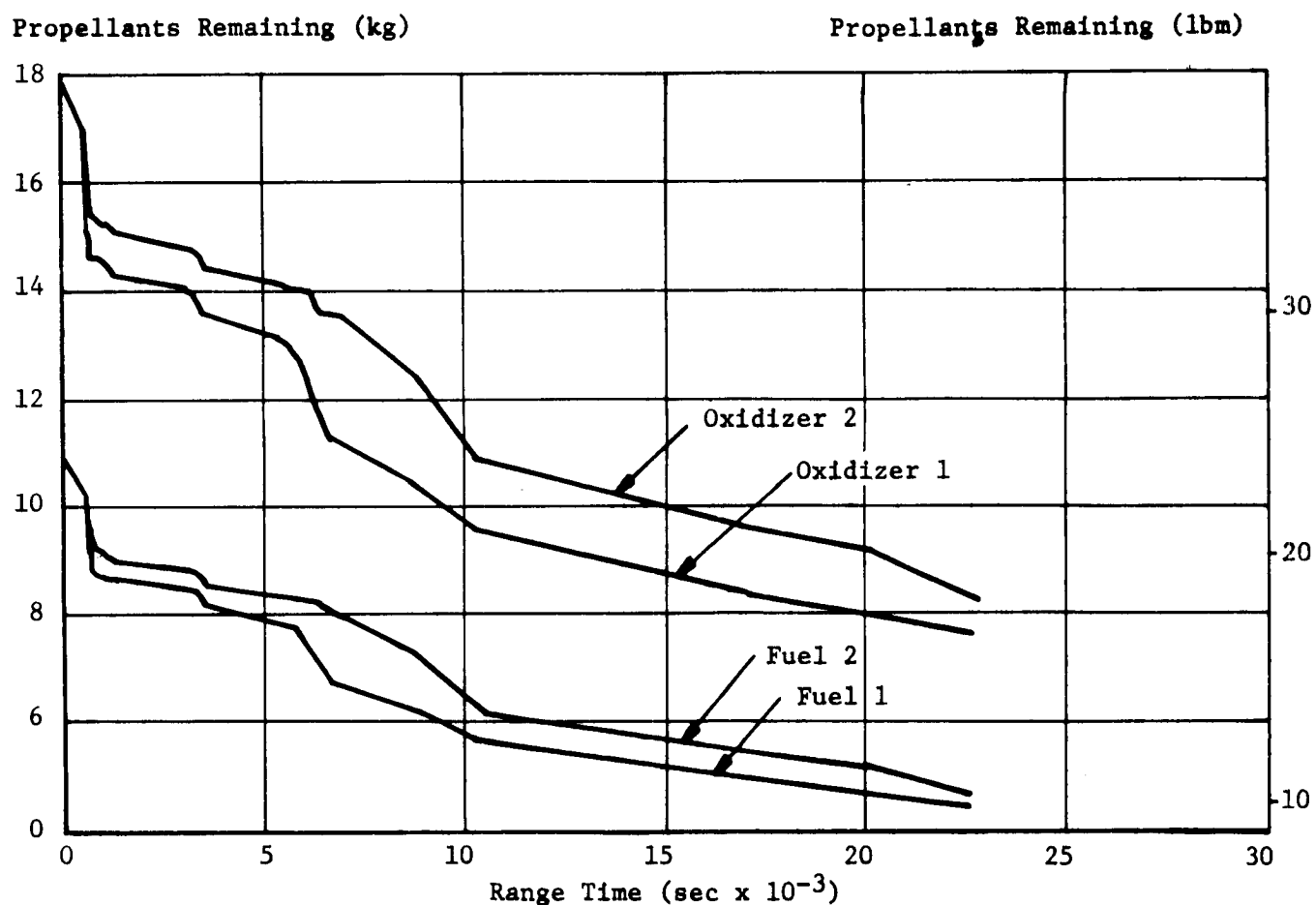


FIGURE 10-1 APS PROPELLANT REMAINING AND TEMPERATURES

TABLE 10-I AS-204 APS PROPELLANT USAGE

EVENTS	MODULE 1					MODULE 2				
	Oxid Quant Used	% of Ox Used	Fuel Quant Used	% of Fuel Used	Oxid Quant Used	% of Ox Used	Fuel Quant Used	% of Fuel Used	Oxid Quant Used	% of Ox Used
Powered Roll Control	0.73 kg (1.6 lbm)	4.09%	0.50 kg (1.1 lbm)	4.62%	0.77 kg (1.7 lbm)	4.30%	0.59 kg (1.3 lbm)	5.44%		
Pitch To Local Horizontal Initial Convergence, LH ₂ Vent Disturbance LOX Vent Disturbance	2.45 kg (5.4 lbm)	13.78%	1.50 kg (3.3 lbm)	13.92%	1.77 kg (3.9 lbm)	9.87%	1.09 kg (2.4 lbm)	10.0%		
Limit Cycle Prior to S-IVB/LM Separation	0.50 kg (1.1 lbm)	2.81%	0.32 kg (0.7 lbm)	2.95%	0.54 kg (1.2 lbm)	3.04%	0.36 kg (0.8 lbm)	3.36%		
Separation Disturbances, Maneuvers, and Limit Cycle Operation Following Separation	2.86 kg (6.3 lbm)	16.07%	1.77 kg (3.9 lbm)	16.45%	1.27 kg (2.8 lbm)	7.09%	0.82 kg (1.8 lbm)	7.56%		
Maneuver to Propellant Dump Attitude, and Propellant Dump	0.91 kg (2.0 lbm)	5.10%	0.59 kg (1.3 lbm)	5.42%	1.18 kg (2.6 lbm)	6.58%	0.82 kg (1.8 lbm)	7.56%		
LOX And LH ₂ Vent, And Limit Cycle Operation 22,600sec	2.63 kg (5.8 lbm)	14.80%	1.63 kg (3.6 lbm)	15.19%	4.04 kg (8.9 lbm)	22.53%	2.50 kg (5.5 lbm)	23.11%		
Totals	10.08 kg (22.2 lbm)	56.78%	6.31 kg (13.9 lbm)	58.38%	9.57 kg (21.1 lbm)	53.41%	6.18 kg (13.6 lbm)	56.90%		

EMR Average Module 1 = 1.61
EMR Average Module 2 = 1.55

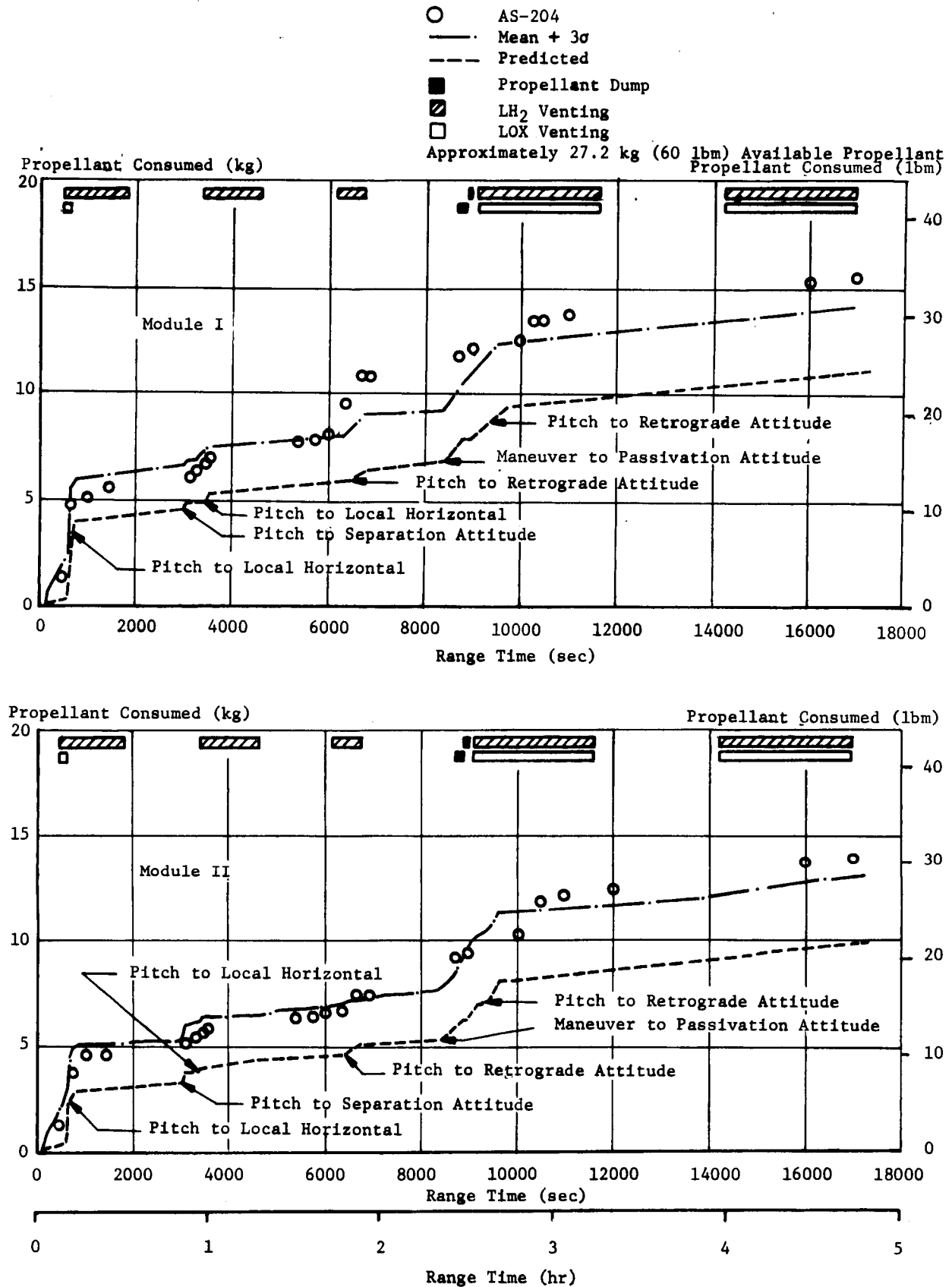


FIGURE 10-2 APS. PROPELLANT USAGE

the end of S-IVB burn, Module 1 contained 17.0 kg (37.5 lbm) of oxidizer and Module 2 contained 17.1 kg (37.8 lbm). Thus the oxidizer consumption during powered flight was 0.73 kg (1.6 lbm) from Module 1 and 0.77 kg (1.7 lbm) from Module 2. At 6 hr: 16 min: 40 sec (22,600 sec), the Module 1 oxidizer temperature was 299°K (79°F) and the mass was 7.7 kg (16.9 lbm); the Module 2 temperature was 292°K (66°F) and the mass was 8.3 kg (18.4 lbm). Module 1 used 57% of the oxidizer mass and Module 2 used 53%.

Before APS activation, the Module 1 fuel temperature was 303°K (86°F) and the mass was 10.80 kg (23.81 lbm); the Module 2 fuel temperature was 299°K (79°F) and the mass was 10.84 kg (23.90 lbm). At the end of S-IVB burn, 10.30 kg (22.71 lbm) of fuel remained in Module 1 and 10.25 kg (22.6 lbm) remained in Module 2. Thus 0.50 kg (1.1 lbm) and 0.59 kg (1.3 lbm) of fuel were consumed from Modules 1 and 2, respectively, during powered flight. At 6 hr: 16 min: 40 sec (22,600 sec), the Module 1 fuel temperature was 301°K (82°F) and the mass was 4.49 kg (9.9 lbm); the Module 2 fuel temperature was 298°K (78°F) and the mass was 4.67 kg (10.3 lbm). Module 1 used 58% of the fuel mass and Module 2 used 57%.

APS helium pressurization systems functioned satisfactorily throughout the flight.

Before APS activation, the Module 1 helium sphere pressure was 2062 N/cm² (2990 psi) at 304°K (91°F) and the mass was 0.133 kg (0.293 lbm). At 22,600 sec, the Module 1 pressure was 1517 N/cm² (2200 psi) at 297°K (75°F) and the remaining mass was 0.103 kg (0.228 lbm). After achieving altitude reference pressure, the Module 1 regulator outlet pressure varied from 136.5 to 137.2 N/cm² (198 to 199 psi). This was within the desired range of 133.1 to 137.2 N/cm² (193 to 199 psi).

Before APS activation, the Module 2 helium sphere pressure was 2055 N/cm² (2980 psi) at 300°K (80°F) and the mass was 0.135 kg (0.297 lbm). At 22,600 sec, the Module 2 pressure was 1524 N/cm² (2210 psi) and the remaining mass of 0.105 kg (0.232 lbm) had a temperature of 292°K (67°F). After achieving altitude reference pressure, Module 2 regulator outlet pressure varied from 133.8 to 134.4 N/cm² (194 to 195 psi). This was within the desired range of 133.1 to 137.2 N/cm² (193 to 199 psi).

10.2.2 APS MOTOR PERFORMANCE

APS motor performance was satisfactory throughout the flight. It is evident from the coincidence of the APS motor pulses and the flight events that the APS firings were of satisfactory frequency and duration. The longest pulse recorded was 0.551 sec on the pitch motor of Module 1 during establishment of orbital pitch rate.

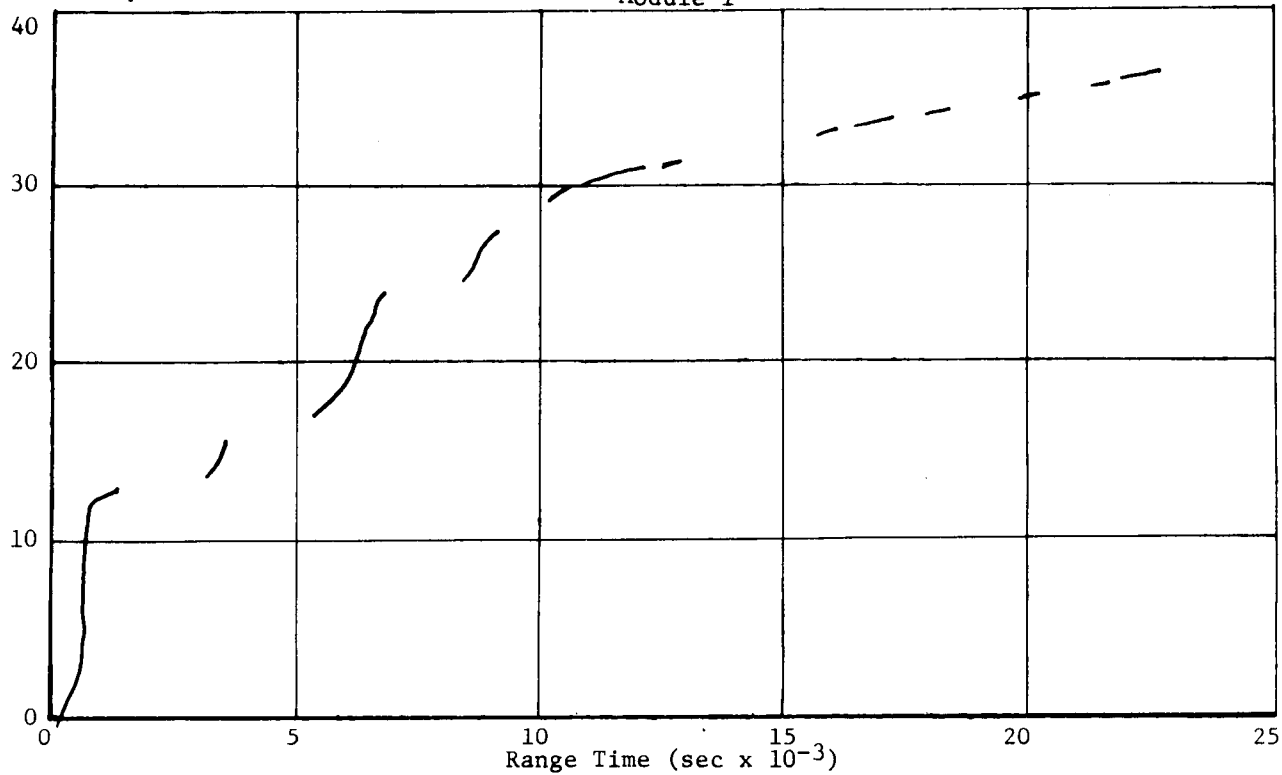
After the propellant supply pressures decreased to the nominal orbital level (regulator at vacuum reference), the APS motor chamber

pressures were in the 62.0 to 65.5 N/cm² (90 to 95 psi) range. The chamber pressure traces exhibited normal start, transient, and cutoff characteristics.

During S-IVB powered flight, Module 1 supplied 2531 N-s (569 lb-s) of total impulse and Module 2 supplied 2731 N-s (614 lb-s). Roll control required 80 pulses each from engines I_{II} and III_{IV}. The specific impulse during this period was 211 sec for Module 1 and 205 sec for Module 2. These values are as expected for minimum impulse bits. The integrated total impulses for Modules 1 and 2 as a function of mission time are presented in Figure 10-3. The Modules 1 and 2 total impulse for various events throughout the flight is presented in Table 12-III (APS Event Summary in Section 12). The average engine mixture ratio (EMR) of Module 1 was 1.61:1; and of Module 2, 1.55:1.

124 Total Impulse (1000 N-s)

Module 1



Module 2

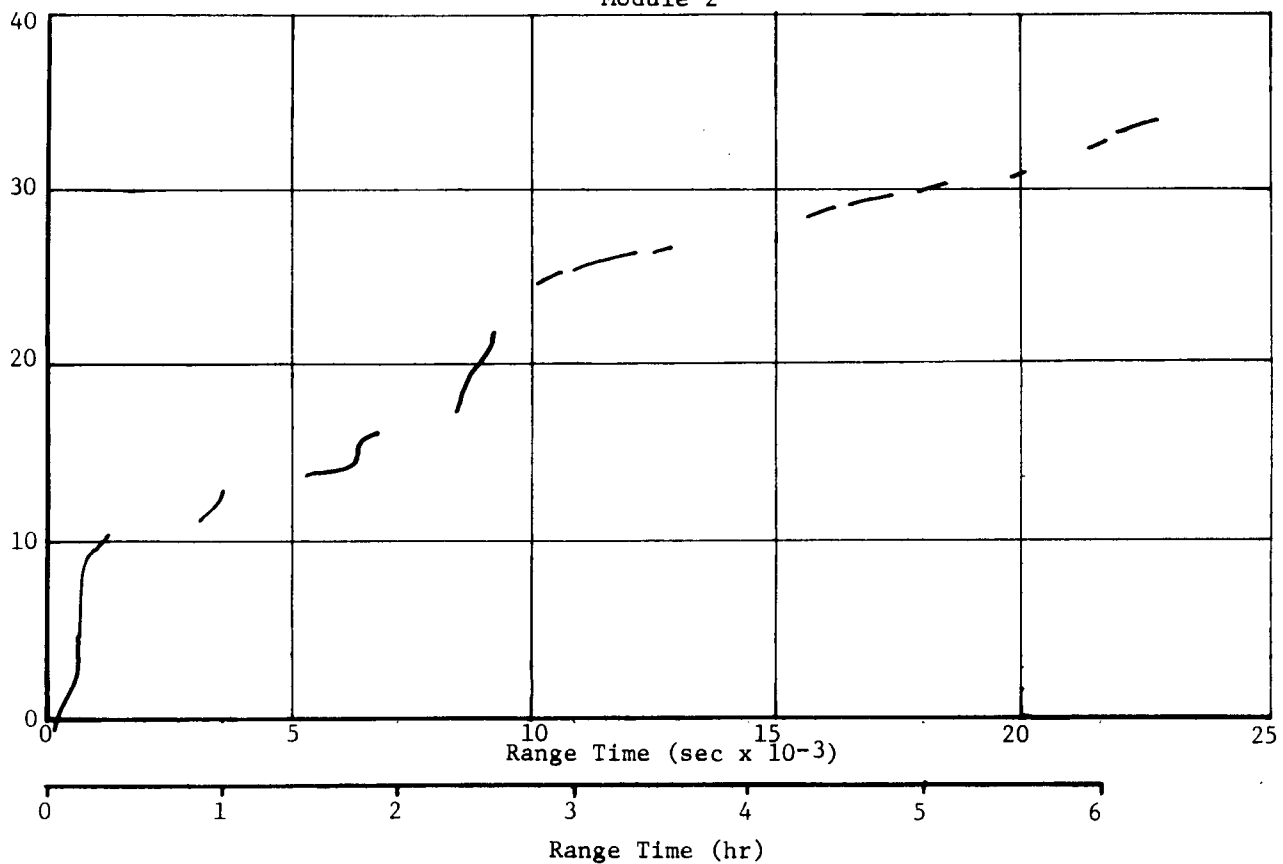


FIGURE 10-3 APS TOTAL IMPULSE

11.0 HYDRAULIC SYSTEM

11.1 SUMMARY

The vehicle's hydraulic systems performed satisfactorily throughout powered flight and during orbital control mode. Pressure, oil levels, and temperatures remained within acceptable limits.

11.2 S-IB STAGE HYDRAULIC SYSTEM

The four outboard H-1 engines are gimbal-mounted to the S-IB stage thrust structure. Controlled positioning of these engines by means of hydraulic actuators provides thrust vectoring for vehicle attitude control. The force required for actuator movement is provided by four independent closed-loop hydraulic systems.

The system pressure levels were satisfactory during the flight and were similar to those of the S-IB-3 flight. At liftoff, the system pressures ranged from 2258 to 2275 N/cm²g (3275 to 3300 psig) from engine to engine. The pressure decreased about 34.5 N/cm² (50 psi) on each engine during the flight. This normal pressure decrease was due to the main pump temperature increase during flight.

Reservoir oil levels were also similar to those of the S-IB-3 flight. There was an approximately 3% rise in each level from 0 to 142 sec, indicating about 11°K (20°F) rise in each hydraulic system's average oil temperature (not to be confused with reservoir oil temperature).

The reservoir oil temperatures were satisfactory during flight. Liftoff temperatures for S-IB-4 averaged 334°K (141°F) as compared to an average of 326°K (127°F) for the four S-IB-3 hydraulic systems. The average temperature decrease during the flight was 10.6°K (19°F) for S-IB-4 as compared to an average of 8°K (16°F) for the four S-IB-3 hydraulic systems.

Figure 11-1 shows hydraulic oil pressure, reservoir level, and temperature as measured during the flight.

11.3 S-IVB STAGE HYDRAULIC SYSTEM

The S-IVB hydraulic system performed satisfactorily throughout the flight. Thermal expansion of oil was not sufficient to cause overboard venting. System internal leakage of 0.0027 m³/min (0.72 gpm) was within the allowable range of 0.0015 to 0.003 m³/min (0.4 to 0.8 gpm) and the expected range of 0.0023 to 0.003 m³/min (0.6 to 0.8 gpm).

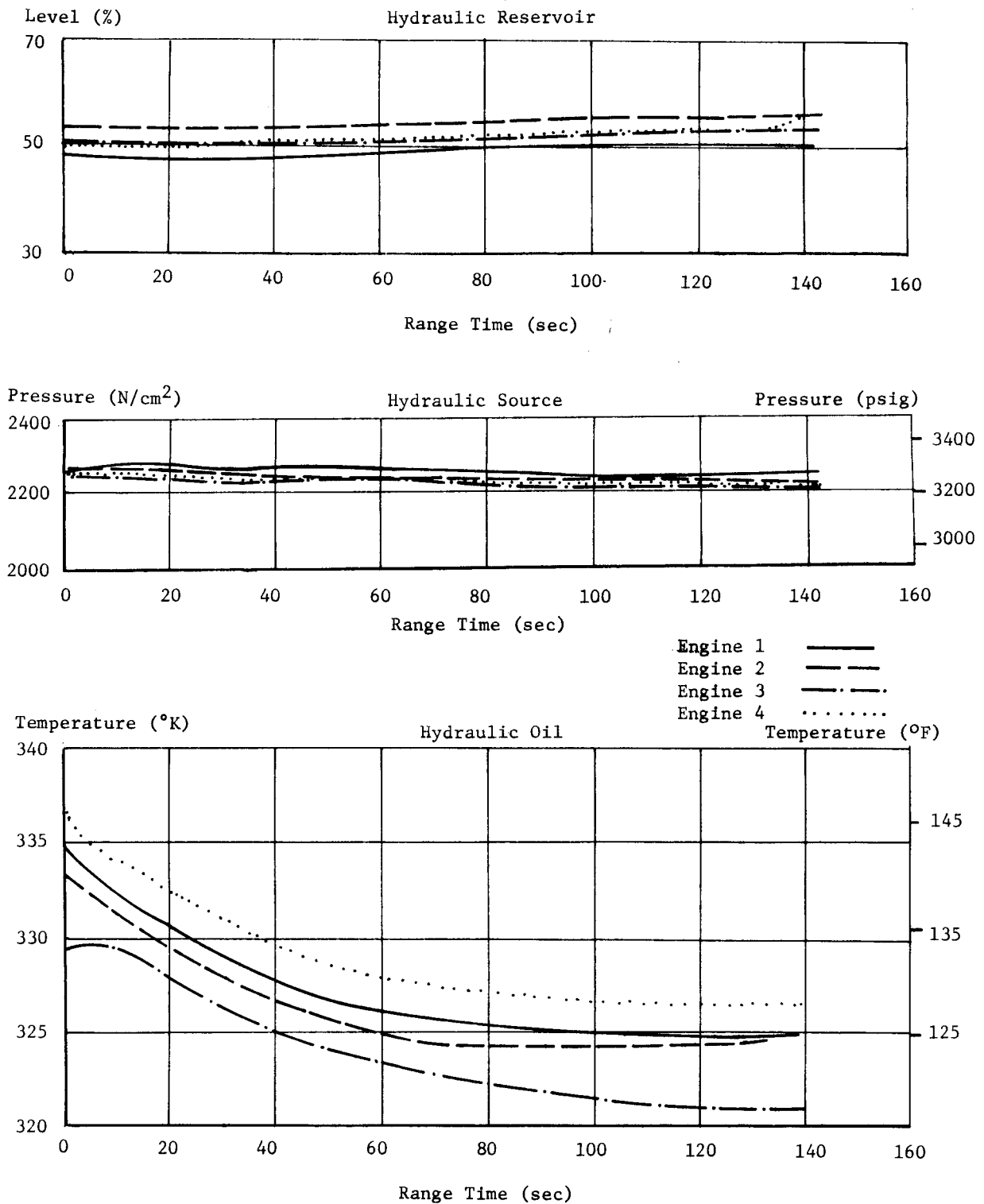


FIGURE 11-1 S-IB HYDRAULIC OIL LEVEL, PRESSURE, AND TEMPERATURE

Hydraulic system pressures during various phases of flight are presented in Table 11-I. Reservoir oil level and system fluid temperatures are shown by curve plots during liftoff and powered flight, and also during orbit and passivation experiment (Figures 11-2 thru 11-4).

The main pump discharge pressure setting was approximately 10 N/cm^2 (15 psi) higher than that of the auxiliary pump, but less than 0.5 percent. Reservoir fluid level rose from 24 percent at liftoff to 30 percent at the end of engine burn due to increased oil temperature. The reversion to 93 percent static level occurred after the auxiliary pump Flight Mode Off command. After command, when pump pressure had decreased to zero, the accumulator oil volume was forced back into the reservoir by the accumulator gas precharge, bringing the reservoir level up to 93 percent. The main (engine driven) hydraulic pump extracted 4.9 horsepower during engine burn mode.

After S-IVB ECO, the main pump inlet oil temperature continued to rise due to the transfer of heat from the LOX turbine housing to the pump manifold. Inlet temperature peaked at 358°K (185°F) at 3500 seconds. The auxiliary hydraulic pump was activated prior to the LOX dump experiment to provide gimbal control.

Immediately after the auxiliary hydraulic pump start, the inlet oil temperature dropped to the reservoir temperature level. Accumulator gas and reservoir oil temperatures rose by small amounts as the hydraulic pump warmed the oil. The reservoir oil level dropped to a minimum of 32% after pump start as 0.0015 m^3 (92 in^3) of oil volume was pumped into the accumulator. When the pump stopped, the reservoir was refilled to the 90% level. Actuator temperatures dropped to a minimum of 262°K (12°F) during orbital coast. There were no thermal cycles by the auxiliary pump during orbital coast.

During the passivation experiment, the maximum excursions of the pitch and yaw actuators were -0.85 deg at 8834.8 sec and -1.20 deg at 8825.9 sec, respectively. The pitch actuator differential pressure developed a torque of 1571.8 N-m ($14,000 \text{ lbf-in}$) during this activity.

Pitch actuator transient loads during engine start were negligible as were the loads throughout the flight. Proper operation of the pitch actuator dynamic pressure feedback mechanism is indicated by the actuator differential pressure traces. The hydraulic servo actuators responded properly to incoming IU signals. Good correlation was observed between the S-IVB actuator position data and the IU actuator command data throughout powered flight.

TABLE 11-1 S-IVB HYDRAULIC SYSTEM PRESSURES

Pressures	Units	Predicted During Pump Operation	Liftoff	Powered Flight	Parking Orbit	Passivation
System Oil	N/cm ² (psi)	2420 to 2520 (3500 to 3650)	2500 (3625)	2510 (3640)	- -	2505 (3630)
Accumulator Gas	N/cm ² (psi)	2420 to 2520 (3500 to 3650)	2500 (3625)	2520 (3650)	1590 (2300)	2500 (3625)
Reservoir Oil	N/cm ² (psi)	114 to 128 (165 to 185)	119 (172)	128 (185)	49.7 (72)	117 (170)
Auxiliary Pump Air Tank	N/cm ² (psi)	173 to 310 (250 to 450)	259 (375)	269 (390)	294 (426)	297 (430)
Auxiliary Pump Motor Air	N/cm ² (psi)	10.4 to 24 (15 to 35)	19 (28)	20 (29)	14.5 (21)	9.3 (13.5)

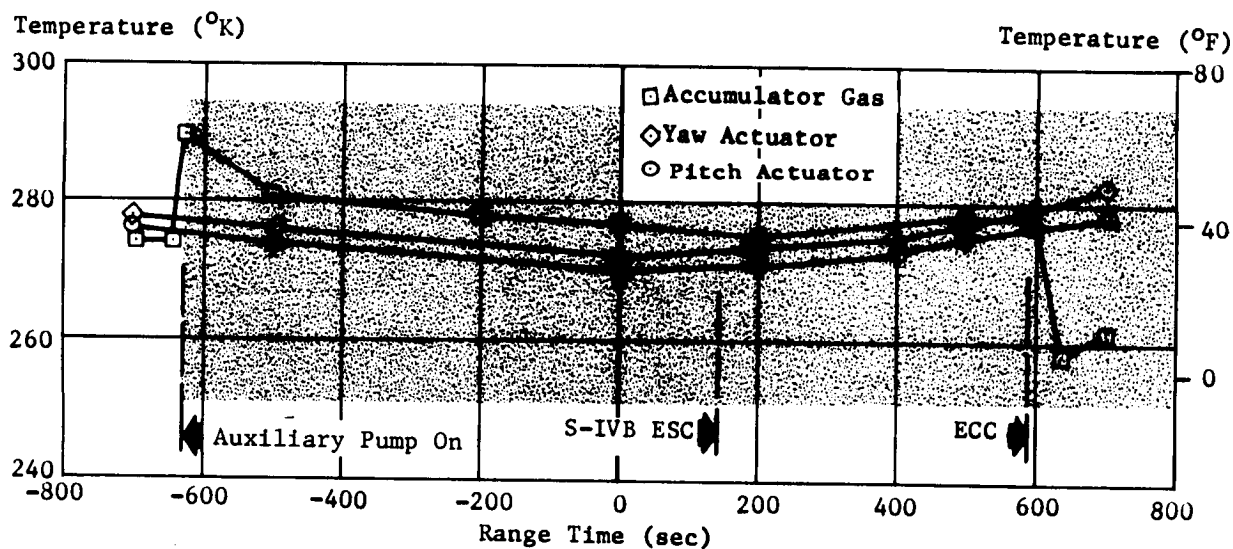
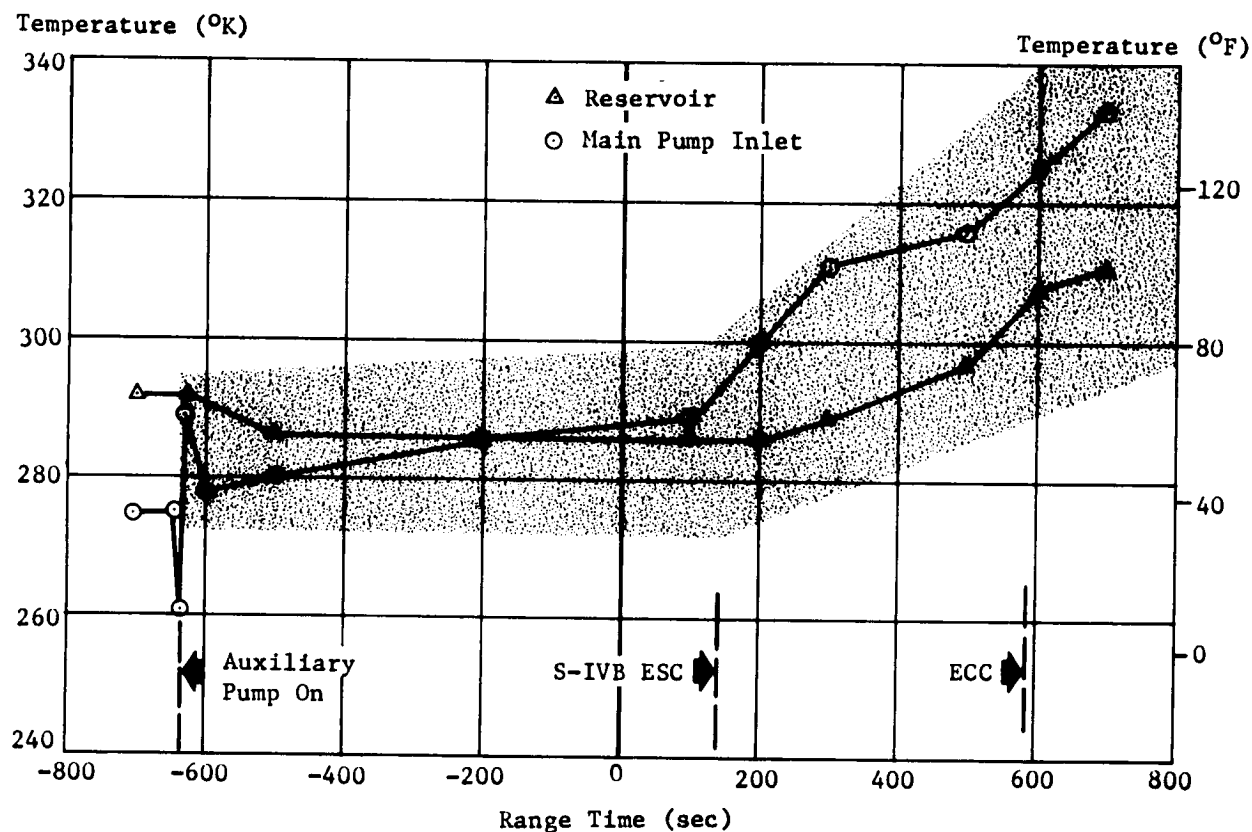


FIGURE 11-2 S-IVB HYDRAULIC SYSTEM TEMPERATURES
 DURING LIFTOFF AND POWERED FLIGHT

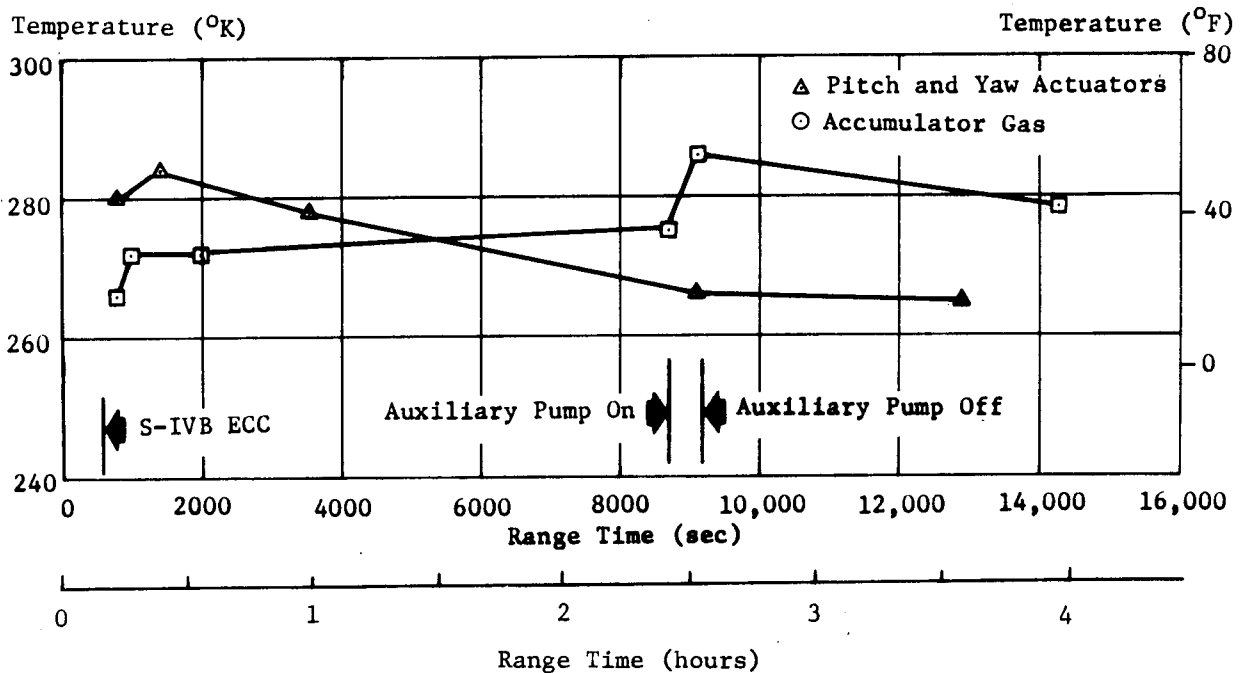
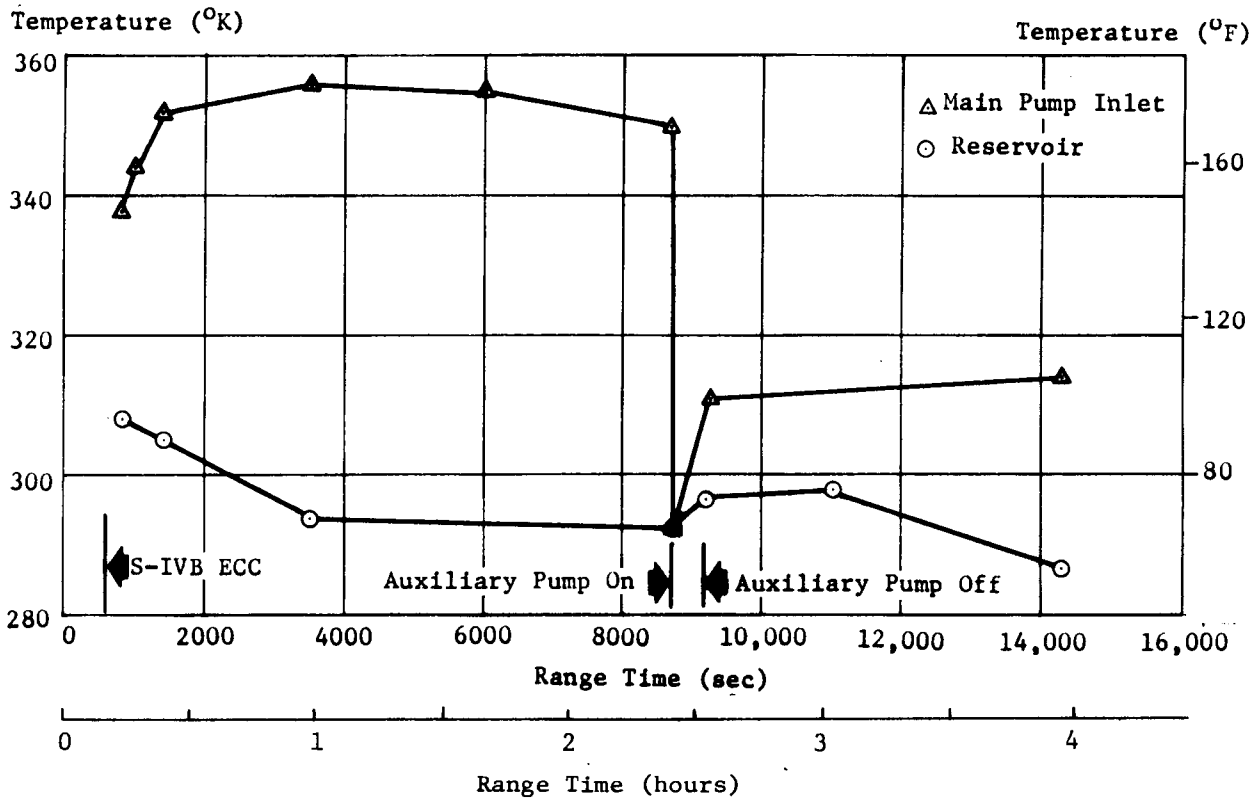
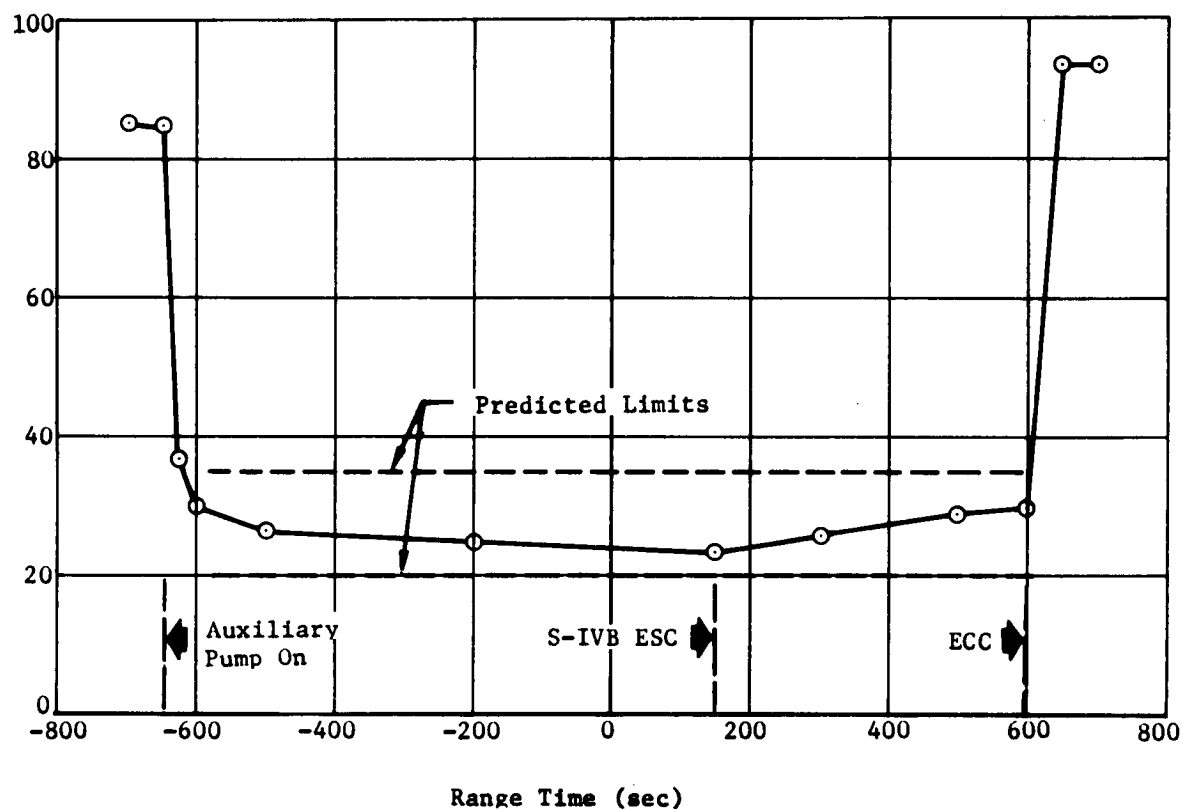


FIGURE 11-3 S-IVB HYDRAULIC SYSTEM TEMPERATURES DURING ORBITAL COAST

Reservoir Oil Level (%)



Reservoir Oil Level (%)

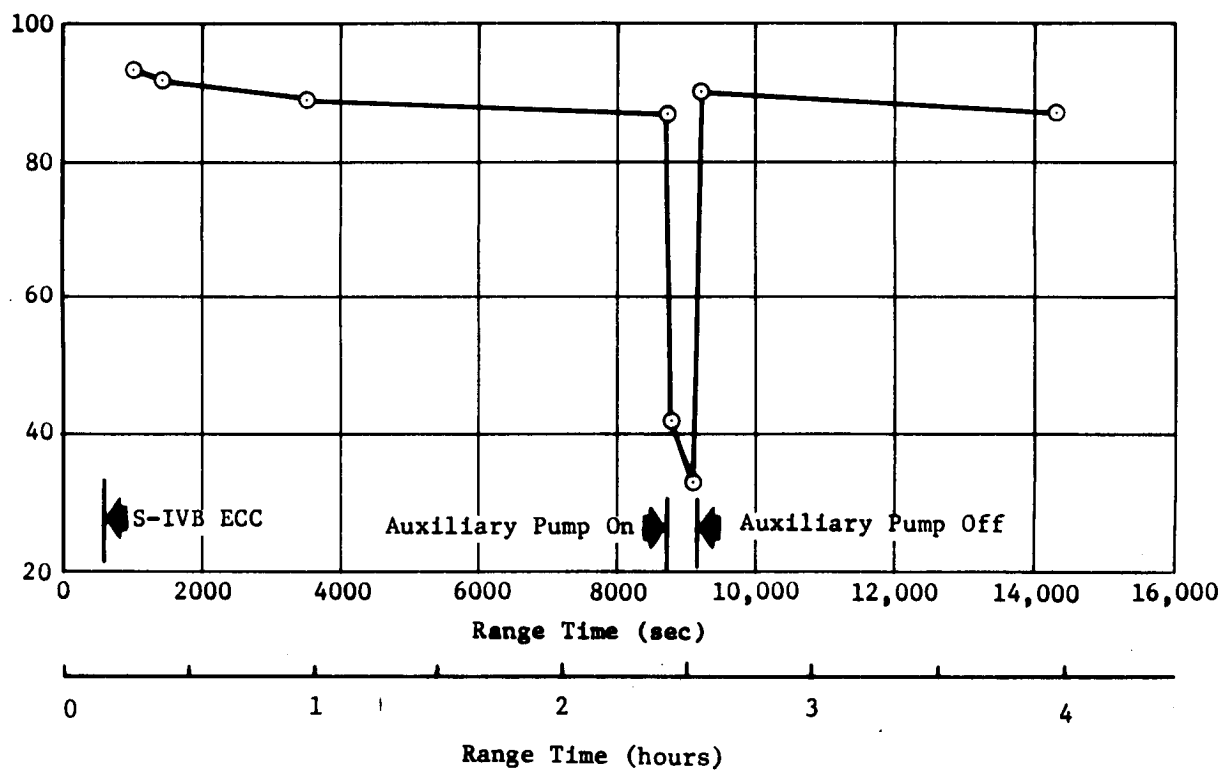


FIGURE 11-4 S-IVB HYDRAULIC RESERVOIR OIL LEVELS
DURING LIFTOFF, POWERED FLIGHT, AND ORBITAL COAST

12.0 GUIDANCE AND CONTROL

12.1 SUMMARY

In general, the performance of the guidance and control system was satisfactory and as expected. The cross range (Y) accelerometer exceeded a reasonableness test value prior to liftoff, resulting in a velocity bias error of 0.45 m/s throughout flight. A -1.5 deg yaw offset developed at S-IVB ullage ignition and remained throughout powered flight. Neither of the foregoing events significantly affected end conditions at S-IVB cutoff. Orbital maneuvers were executed as planned.

The control system functioned properly. The maximum values observed for the control parameters, near the maximum dynamic pressure region, were attitude errors of 1.8 deg in pitch, -1.1 deg in yaw, and -1.0 deg in roll; and angle-of-attack (calculated from FPS-16 radar data) of -2.5 deg in pitch and 1.5 deg in yaw. Control system transients occurred at S-IB/S-IVB separation, guidance initiation, gain change, artificial tau and chi bar guidance modes, chi freeze, and J-2 engine cutoff. These transients were expected and well within the capabilities of the control system. A 17-18 Hz oscillation on the roll rate signal during the first 80 sec after S-IB/S-IVB separation affected the Auxiliary Propulsion System (APS) roll control, permitting a 2.3 deg maximum roll attitude error during that period. The roll rate oscillation caused the roll dead band to increase from the nominal ± 1 degree. The APS corrected for a constant roll torque throughout the remainder of S-IVB powered flight which created an attitude error of approximately 0.5 degrees. During orbit, transients resulted from programmed maneuvers, LOX and LH₂ venting, LM separation, and the propellant removal experiment. All transients were well within the capabilities of the control system.

12.2 SYSTEM DESCRIPTION

12.2.1 CHANGES FOR SATURN IB AS-204

The Saturn AS-204 vehicle was the first vehicle to use the Apollo Standard Coordinate System (SE 008-001-1) in the flight program, and the first Saturn vehicle to have live navigation update capability in the navigation, guidance and control system. All system components were flight qualified on previous Saturn vehicles.

The navigation, guidance, and control system was the same as those flown on AS-201, AS-202, and AS-203 except for minor component and functional changes, see Appendix A, to improve reliability. In addition to the changes in Appendix A, the following changes were incorporated to eliminate an accelerometer problem experienced on previous flights caused by vehicle vibration:

1. The accelerometer reasonableness test constant was changed from 6.0 to 0.3 meters per second from Guidance Reference Release (GRR) to time base 1 plus ten seconds ($T_1 + 10 \text{ sec}$), in order to detect and eliminate erroneous accelerations caused by vibration.

2. The accelerometer float stops were changed from ± 3.0 deg of freedom to ± 6.0 deg of freedom to prevent the float striking the mechanical stops during periods of high vibration levels at critical frequencies.

12.2.2 FUNCTION AND HARDWARE DESCRIPTION

A block diagram of the navigation, guidance, and control system is shown in Figure 12-1.

The stabilized platform (ST-124M-3) is a three gimbal configuration with gas bearing gyros and accelerometers mounted on the stable element to provide a space-fixed coordinate reference frame for attitude control and for navigation measurements. Vehicle accelerations and rotations are sensed relative to this stable element. Gimbal angles are measured by resolvers which have fine and coarse outputs, and inertial velocity is obtained from accelerometer head rotation in the form of encoder outputs which have redundant channels.

The Launch Vehicle Data Adapter (LVDA) is an input-output device for the Launch Vehicle Digital Computer (LVDC). These two components are digital devices which operate in conjunction to carry out the flight program. This program performs the following functions: (1) processes the inputs from the (ST-124M-3), (2) performs navigation calculations, (3) provides first stage tilt program, (4) calculates Iterative Guidance Mode (IGM) steering commands, (5) resolves gimbal angles and steering commands into the vehicle system for attitude error commands, and (6) issues cutoff and sequencing signals.

The Control/Emergency Detection System (Control/EDS) rate gyro package contains 9 gyros (triple redundant in 3 axes). Their outputs go to the Control Signal Processor (CSP), where they are voted and sent to the Flight Control Computer (FCC). In the FCC the rate signals, the control accelerometer signals, and the attitude error command signals are processed and combined to generate control command signals for the engines actuators and the S-IVB APS.

The switch selectors are used to relay discrete commands from the LVDC to other locations in the vehicle. The cutoff signal and time based events are issued through the switch selectors.

12.2.3 NAVIGATION SCHEME DESCRIPTION

Guidance during S-IB powered flight was provided by programs

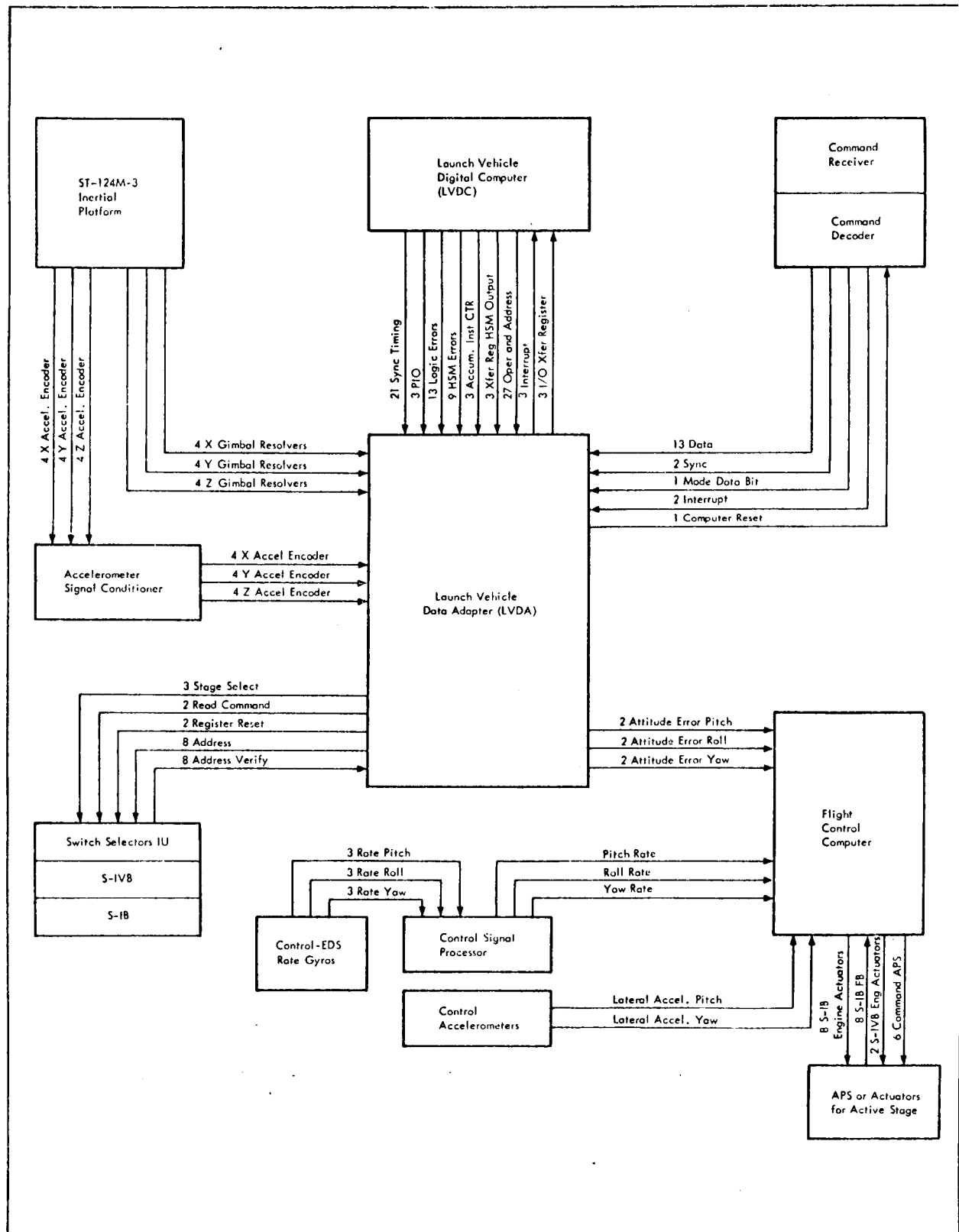


FIGURE 12-1 NAVIGATION, GUIDANCE, AND CONTROL SYSTEM BLOCK DIAGRAM

stored in the LVDC and may be broken into three time periods:

1. GRR to 10 sec after liftoff ($T_1 + 10$ sec).
2. $T_1 + 10$ to $T_1 + 133$ sec.
3. $T_1 + 133$ sec to IGM initiation.

In period 1, pitch and yaw steering commands were zero. The roll steering command was set to -18 deg to prevent the removal of the initial -18 deg roll attitude.

In period 2, the yaw command remained zero, roll was set to zero (rate limiting prevented the command from exceeding 1 deg/s), and the pitch command was computed from one of three third degree time polynomials.

In period 3, the steering commands were arrested at their final values from period 2.

The S-IVB stage was guided by a modification of the multi-stage three-dimensional form of the IGM. IGM is an optimal scheme based on the optimum steering function derived from the Calculus of Variations. This approximate thrust vector steering function was implemented in both the pitch and yaw planes of motion.

Near optimum vehicle performance dictates the use of two thrust levels during S-IVB burn. The desired thrust level change is achieved by a Propellant Mixture Ratio Shift (PMRS) which causes rapid variations in Force-to-Mass (F/M) ratio. The IGM scheme is very sensitive to acceleration changes. In particular, τ , a time term in the IGM equation, varies as the reciprocal of F/M. To smooth the steering commands of these disturbances, IGM inputs are supplemented by two acceleration levels of artificial τ . At detection of PMRS or if PMRS is forced a 35 second artificial τ mode is entered. If PMRS is not detected before nominal PMRS time an additional artificial τ mode is implemented. This additional artificial τ mode is used until PMRS is detected or until 60 sec has elapsed at which time PMRS is forced. The PMRS is detected by a decrease in measured platform acceleration over two computation cycles twice in succession.

The sensitivity of the scheme to F/M changes increases as the terminal conditions are approached, requiring the use of a terminal scheme utilizing only the velocity constraint terms. This mode is the chi bar steering mode. During this mode, beginning 15 sec before S-IVB cutoff, the altitude constraint terms in pitch are set to zero and the yaw terms are frozen at their last values. Three seconds prior to S-IVB cutoff, all IGM commands are frozen. The S-IVB stage cutoff signal is given by the program when the desired terminal velocity is reached. To obtain an accurate cutoff velocity, a high-speed program loop is entered just

prior to cutoff.

The orbital guidance routine, initiated 15 sec after T_4 , controls the computation of the commanded platform gimbal angles during orbit. Nine maneuvers comprise the orbital attitude time line as follows:

Start	Stop	Maneuver
$T_4 + 0$	$T_4 + 90$	Attitude freeze
$T_4 + 90$	GRR + 3005	Vehicle longitudinal axis parallel to local horizontal reference
GRR + 3005	GRR + 3420	Attitude freeze for LM separation
GRR + 3420	GRR + 5490	Vehicle longitudinal axis parallel to local horizontal reference
GRR + 5490	GRR + 6360	Attitude freeze for second chance LM separation
GRR + 6360	$T_4 + 7840$	Vehicle longitudinal axis parallel to local horizontal reference, retro-grade
$T_4 + 7840$	$T_4 + 8157$	Vehicle longitudinal axis parallel to local vertical reference, nose down, 85 deg roll
$T_4 + 8157$	$T_4 + 8800$	Vehicle longitudinal axis parallel to local vertical reference, nose down, antenna pointing at Carnarvon
$T_4 + 8800$	-----	Vehicle longitudinal axis parallel to local horizontal reference, retro-grade

Ground command processing is accomplished by the command receiver interrupt with the Digital Command System (DCS) routine. The vehicle state vector (position and velocity) can be updated via the DCS any time after $T_4 + 15$ sec by uplinking a state vector consisting of three position and three velocity components and the time when the vector will be valid. When the specified time occurs, the LVDC state vector is replaced by the uplinked vector and navigation continues.

12.3 LAUNCH VEHICLE FLIGHT CONTROL

12.3.1 S-IB STAGE CONTROL ANALYSIS

The S-IB stage control system performed satisfactorily in the pitch,

yaw, and roll planes. Table 12-I presents the control parameters maximum values with corresponding flight times in the high dynamic pressure region. The actuator position and angular rate responses for the AS-204 flight were generally lower than the AS-203 flight but higher than the AS-202 flight. The angles-of-attack were higher on this flight than on AS-202 or AS-203 and are attributed to the high winds in the maximum dynamic pressure region.

Figure 12-2 shows the vehicle attitudes in the roll and pitch planes compared to the programmed attitudes. The vehicle response to the pitch program started at 9.70 sec and was arrested at 133.50 sec at an attitude of -59.4 deg from the space-fixed-vertical. The vehicle response to the roll program started at 10.67 sec and was completed at 28.67 sec after rolling 18.0 degrees. The pitch and roll programs presented were taken from LVDA ladder reduced telemetry data. These commanded maneuvers were properly executed by the vehicle.

Since no Q-ball was used on AS-204, the angles-of-attack in pitch and yaw were taken from an elastic body planar simulation and from calculations using the FPS-16 winds (Figure 12-3). The winds used in both the simulation and the calculations were taken from the final Meteorological Data Tape and are FPS-16 winds for the first 85 sec and rawinsonde winds thereafter sampled every 250 meters. Good agreement is observed in yaw but the pitch simulation values are slightly lower than the FPS-16 calculated values. This is attributed to the predicted pitch tilt program that was used in the simulation which differs slightly with the LVDC reduced tilt program used in the FPS-16 calculated angle-of-attack. Both methods have demonstrated high sensitivity (± 0.5 deg) to the tilt program in the past. Figure 12-3 also shows the total angle-of-attack.

Figure 12-4 shows attitude errors in pitch, yaw, and roll. These signals are nominal and in good agreement.

Figure 12-5 shows angular rates in pitch, yaw, and roll. There was a noise level of about 0.4 to 0.5 deg/s at a frequency of 1.4 to 1.5 Hz present in the 100 sample per second digitized control rate gyro signals. An examination of continuous oscillograms of these signals showed that this low frequency noise was not present on the analog tapes and therefore was attributed to data reduction processing. The signals presented were filtered by a 1 Hz low-pass filter to eliminate this low frequency noise.

At IECO, a positive roll rate was evident which peaked at 0.8 deg/s at 139 seconds. Roll rates at this time also appeared on AS-201, AS-202, and AS-203 and are possibly due to non-simultaneous thrust decay of the inboard engines or inboard engine thrust misalignments. The roll rate decreased to null at 140.5 seconds.

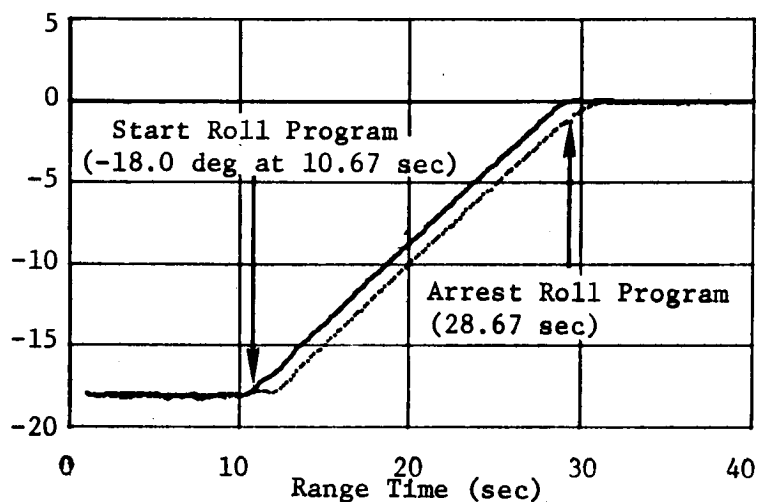
Figure 12-6 shows control accelerations in pitch and yaw. Very

TABLE 12-I MAXIMUM CONTROL PARAMETERS
(Near the maximum dynamic pressure region and during Roll Maneuver)

Parameters	Units	Pitch Plane		Yaw Plane	
		Magnitude	Range Time (sec)	Magnitude	Range Time (sec)
Attitude Error	deg	1.85	84.5	-1.14	75.6
Angle-of-Attack (FPS-16 Calculated)	deg	-2.54	72.3	1.53	72.8
Angular Rate	deg/s	-1.15	85.0	-0.45	74.0
Normal Acceleration	m/s ²	-0.93	72.1	0.83	72.5
Average Actuator Position	deg	-1.61	80.6	1.40	73.0
Angle-of-Attack Dynamic Pressure Product	deg-N/cm ²	7.99	72.3	4.83	72.8
Roll Plane					
		During Roll Maneuver		After Roll Maneuver	
		Magnitude	Range Time (sec)	Magnitude	Range Time (sec)
Attitude Error	deg	-1.38	14.0	-1.00	81.0
Angular Rate	deg/s	1.09	28.7	-0.45	74.8
Engine Deflection	deg	-0.18	11.7	-0.22	76.1

..... Vehicle Attitude
 ————— Command Attitude

Roll Program and Attitude (Space Fixed) (deg)
 (+CW Viewed From Rear)



Pitch Program and Pitch Attitude (Space Fixed) (deg)
 (- Nose Down From Vertical)

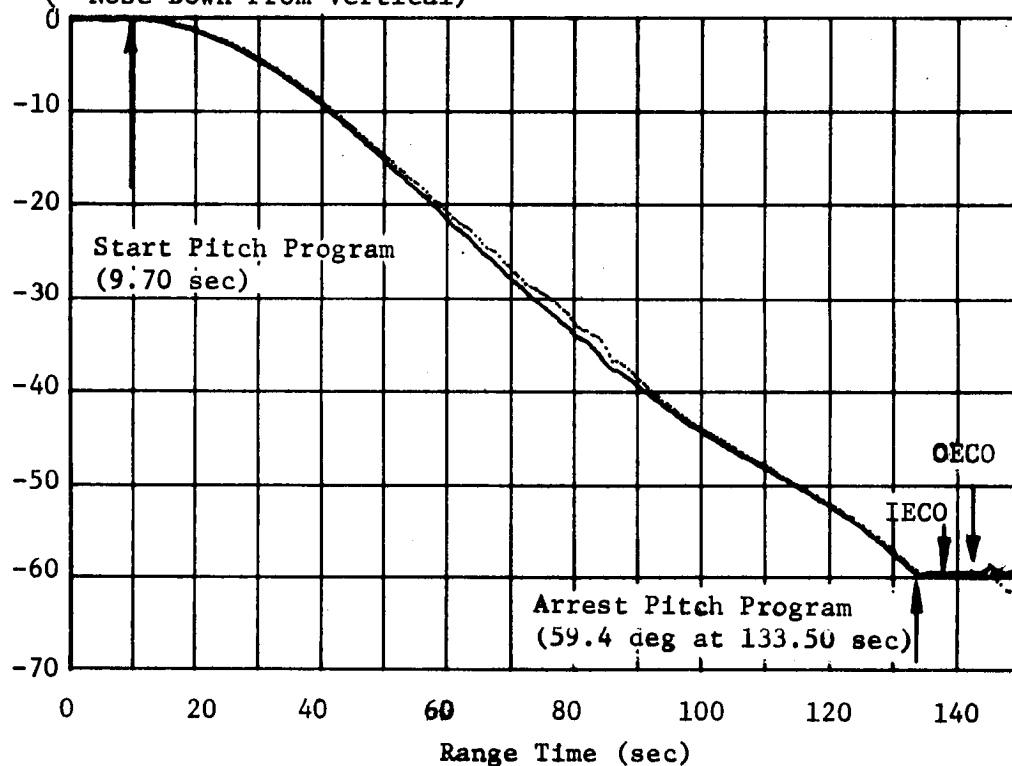
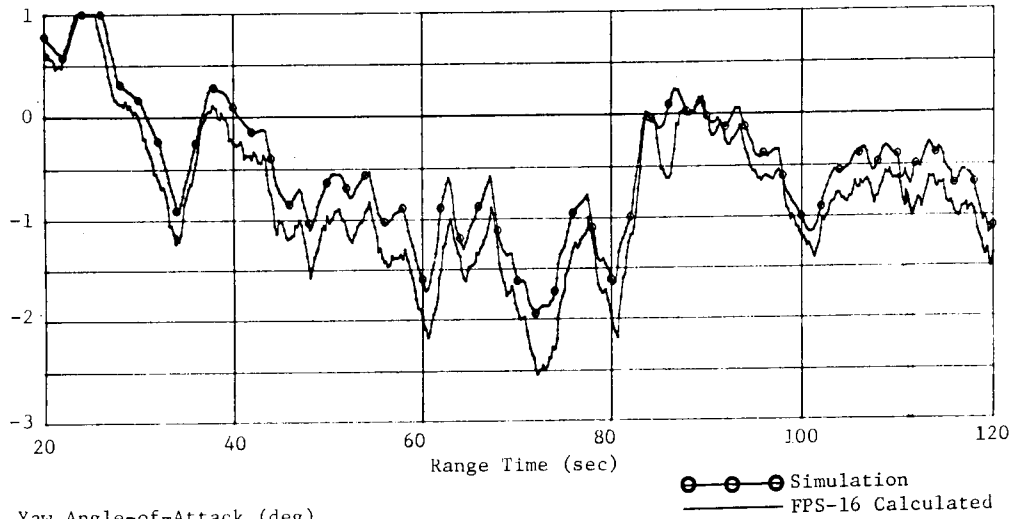


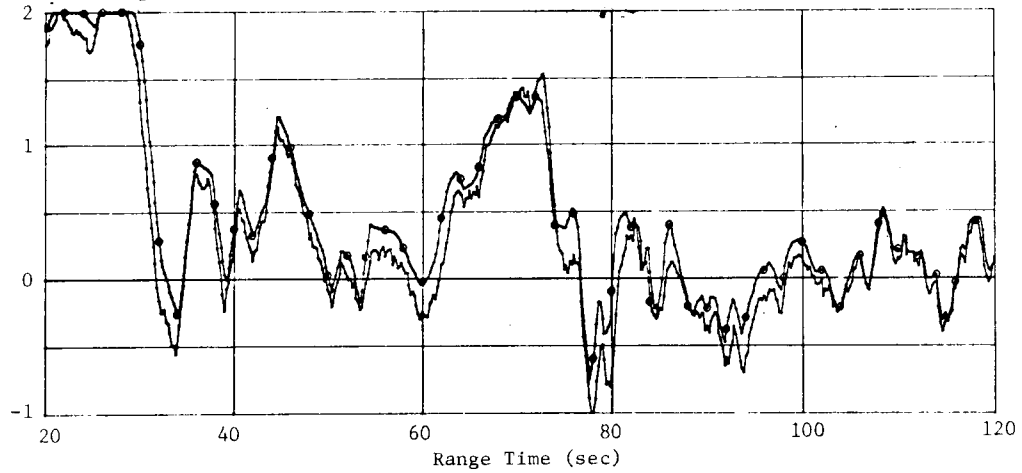
FIGURE 12-2 S-IB STAGE COMMAND ANGLES

140

Pitch Angle-of-Attack (deg)
(+ Nose Above Relative Velocity Vector)



Yaw Angle-of-Attack (deg)
(+ Nose Right of Relative Velocity Vector)



Resultant Angle-of-Attack (deg)

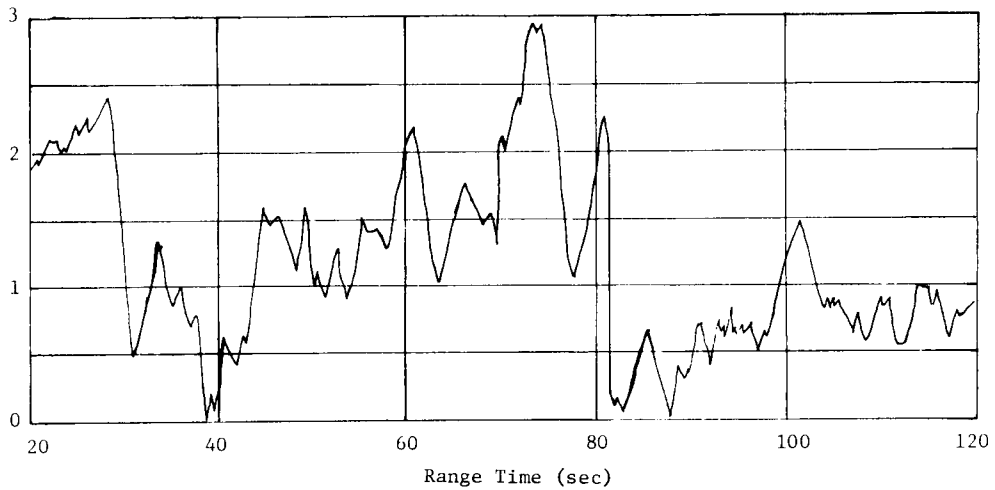


FIGURE 12-3 FREE STREAM ANGLE-OF-ATTACK

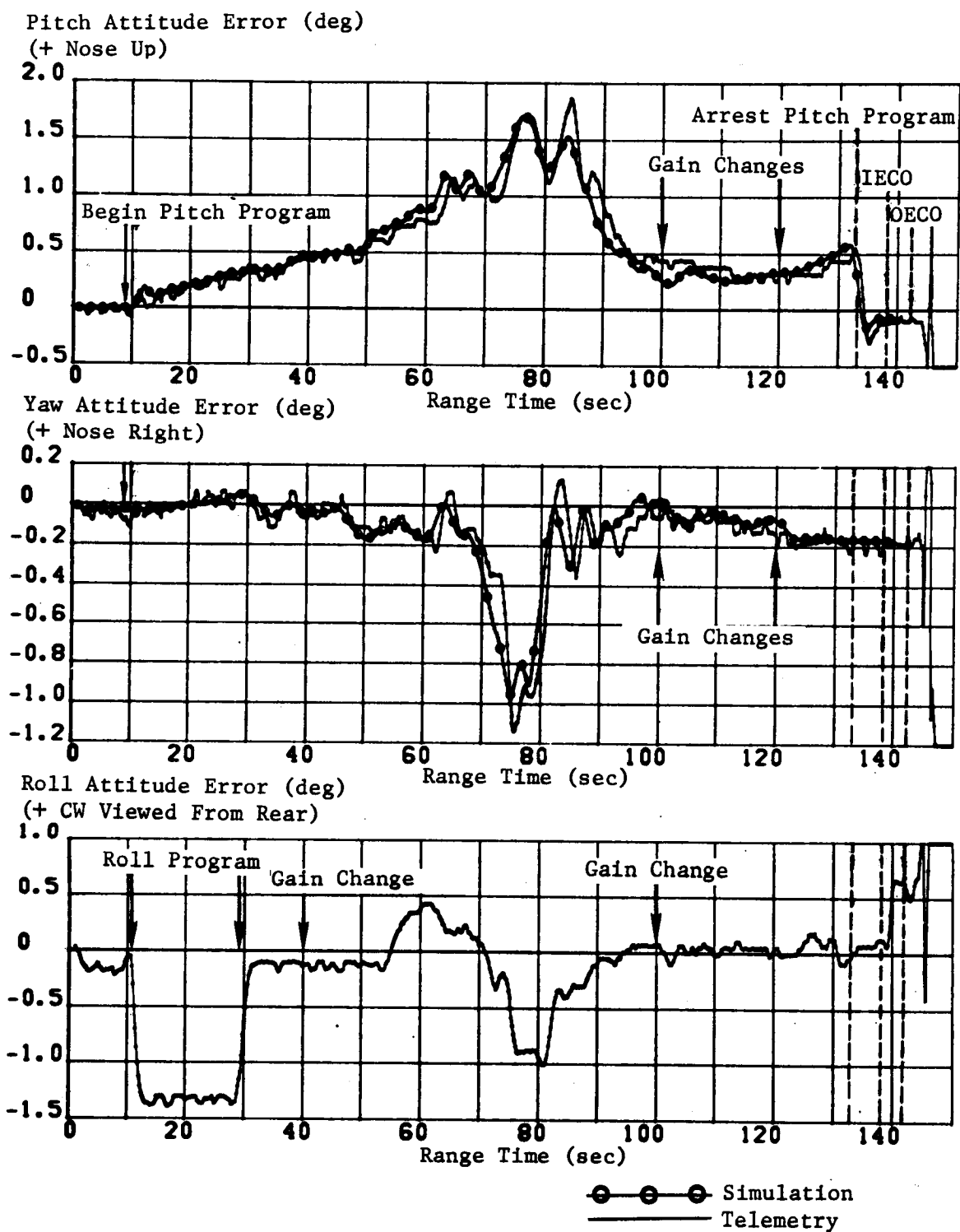


FIGURE 12-4 ATTITUDE ERROR S-IB POWERED FLIGHT

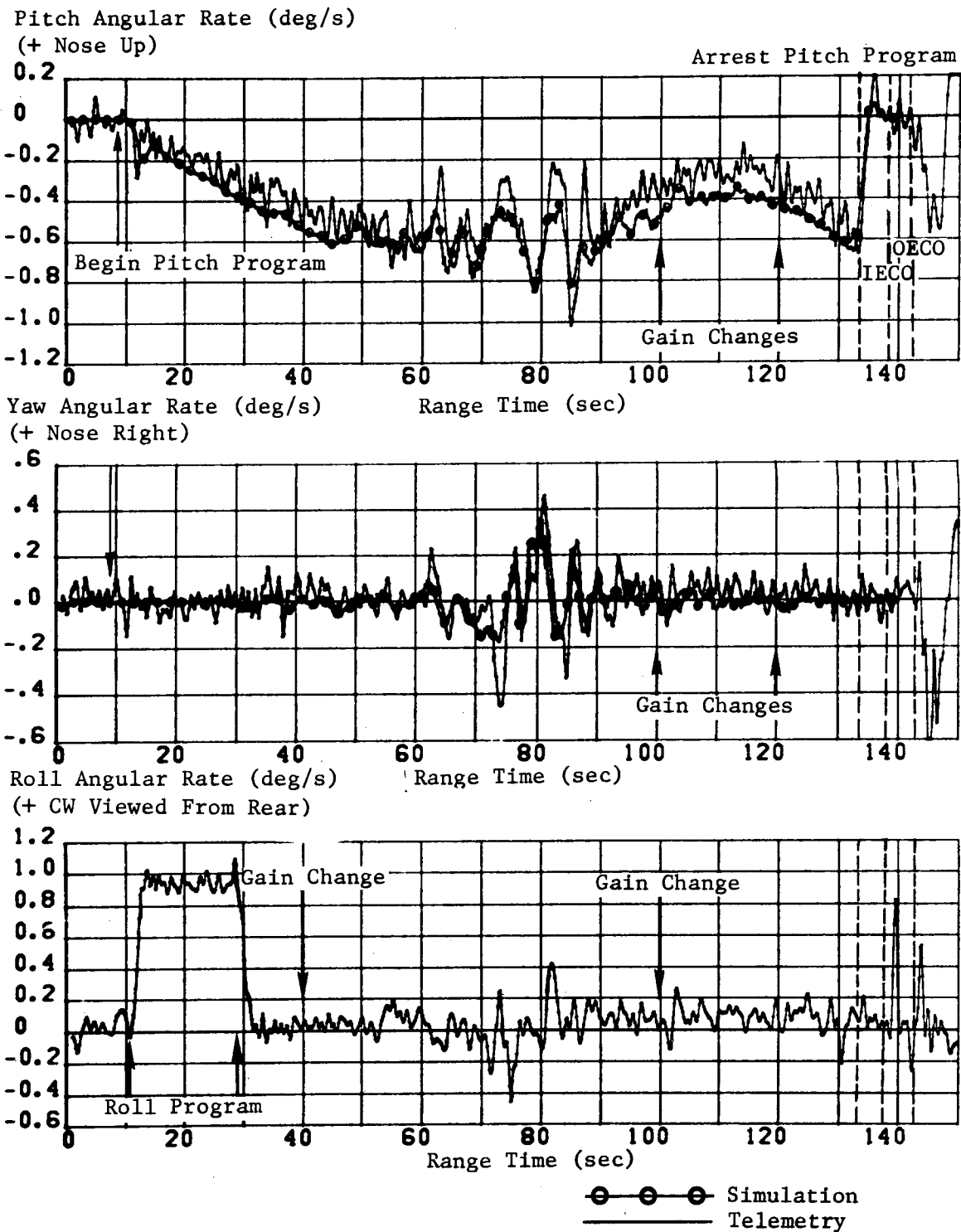
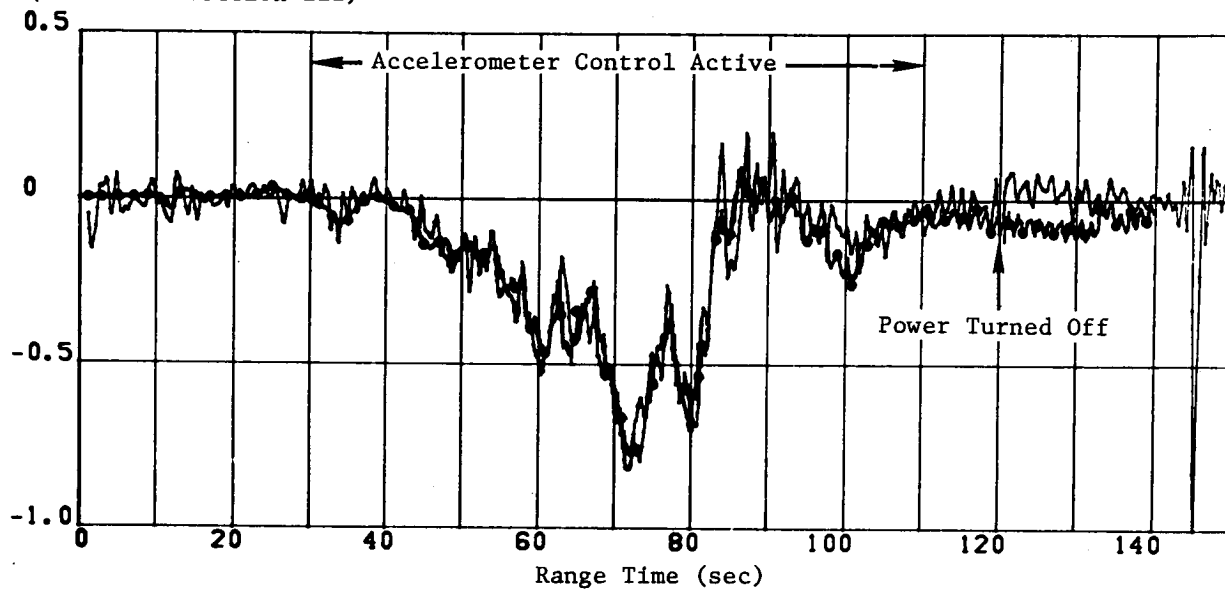


FIGURE 12-5 ANGULAR RATES S-IB POWERED FLIGHT

Pitch Control Acceleration (m/s^2)
(+ Toward Position III)



Yaw Control Acceleration (m/s^2)
(+ Toward Position IV)

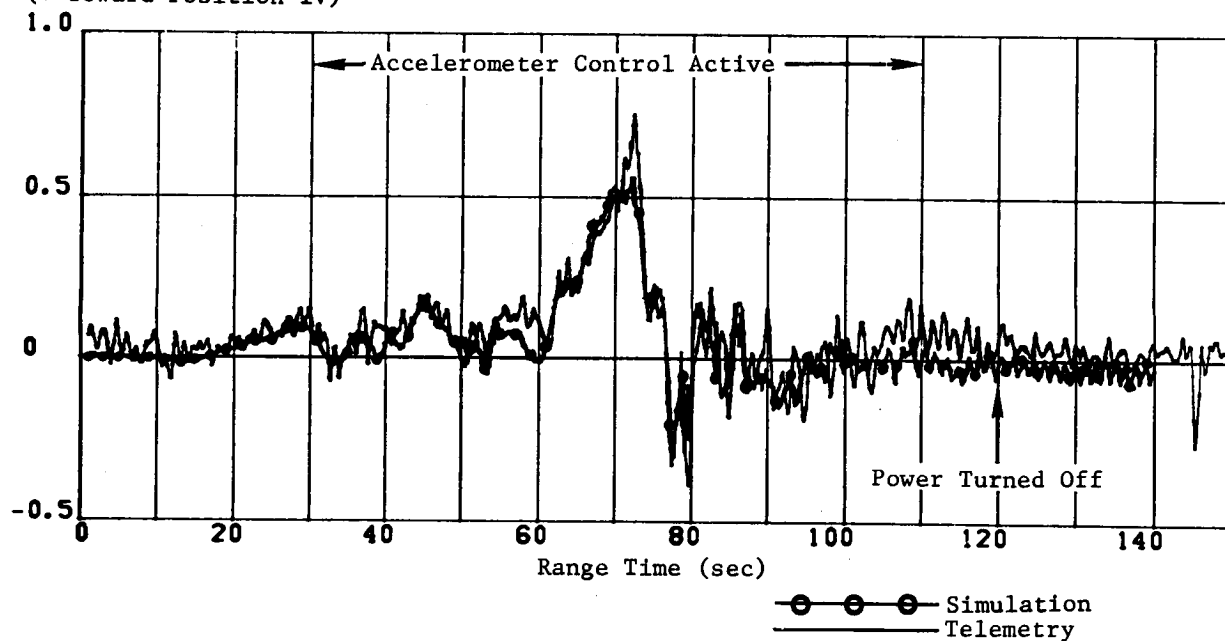


FIGURE 12-6 CONTROL ACCELERATION S-IB POWERED FLIGHT

good agreement with the simulation is noted. These signals also contained erroneous low frequency noise as experienced on the angular rate signals and it was necessary to filter them with a 1 Hz low-pass digital filter for presentation purposes. The low frequency noise level on the 100 sample per second signal was about 0.2 m/s^2 double amplitude at 1.4 to 1.5 Hertz.

On this flight the yaw control accelerometer, and to a lesser extent the yaw rate gyro, showed a distinct response to what appears to be the vehicle first bending mode between 75 and 80 seconds. This acceleration response, not evident in the plots because of filtering, had a peak-to-peak magnitude of approximately 0.9 m/s^2 at a frequency of 2.51 Hertz. This corresponds quite closely to the predicted coupled first bending frequency of 2.48 Hz at 80 seconds.

The average actuator positions in pitch, yaw, and roll are shown in Figure 12-7. Good agreement with the simulation is noted.

Figure 12-8 presents the sloshing analysis during S-IB powered flight. The top plot on the left side of the figure shows the peak-to-peak sloshing amplitude in degrees from the S-IVB LH₂ PU probe signal with and without the hydrodynamic attenuation factor. Although LH₂ sloshing on this flight was higher than on the AS-202 flight it was about the same order of magnitude as the AS-203 flight and is considered to be low. No analysis of the S-IVB LOX amplitudes was made because the LOX PU probe and the liquid surface intersection were practically on the centerline of the tank for this flight. On the basis of sloshing occurring about the centerline of the tank, no rational amplitude readings from the PU probe can be expected during S-IB powered flight.

The bottom graph on the left side shows predominant sloshing frequencies from the S-IVB LOX and LH₂ PU probe measurements compared to their predicted coupled natural frequencies.

The top graph on the right side of Figure 12-8 shows the predominant sloshing frequencies based on power spectral densities using 20 sec time slices of the actuator signals in the pitch and yaw directions compared to the predicted first mode coupled frequencies of the most influential tanks. It is apparent that the S-IVB LH₂ is the major contributor to sloshing frequencies in both pitch and yaw.

The lower two graphs on the right side of Figure 12-8 show the individual contributions to engine deflections from the S-IVB LOX and LH₂ in pitch and yaw. Again it is evident that the LH₂ tank is the major contributor in both planes.

Table 12-II presents control parameter values at S-IB/S-IVB separation. The values are considered nominal and indicate adequate performance of the attitude control system.

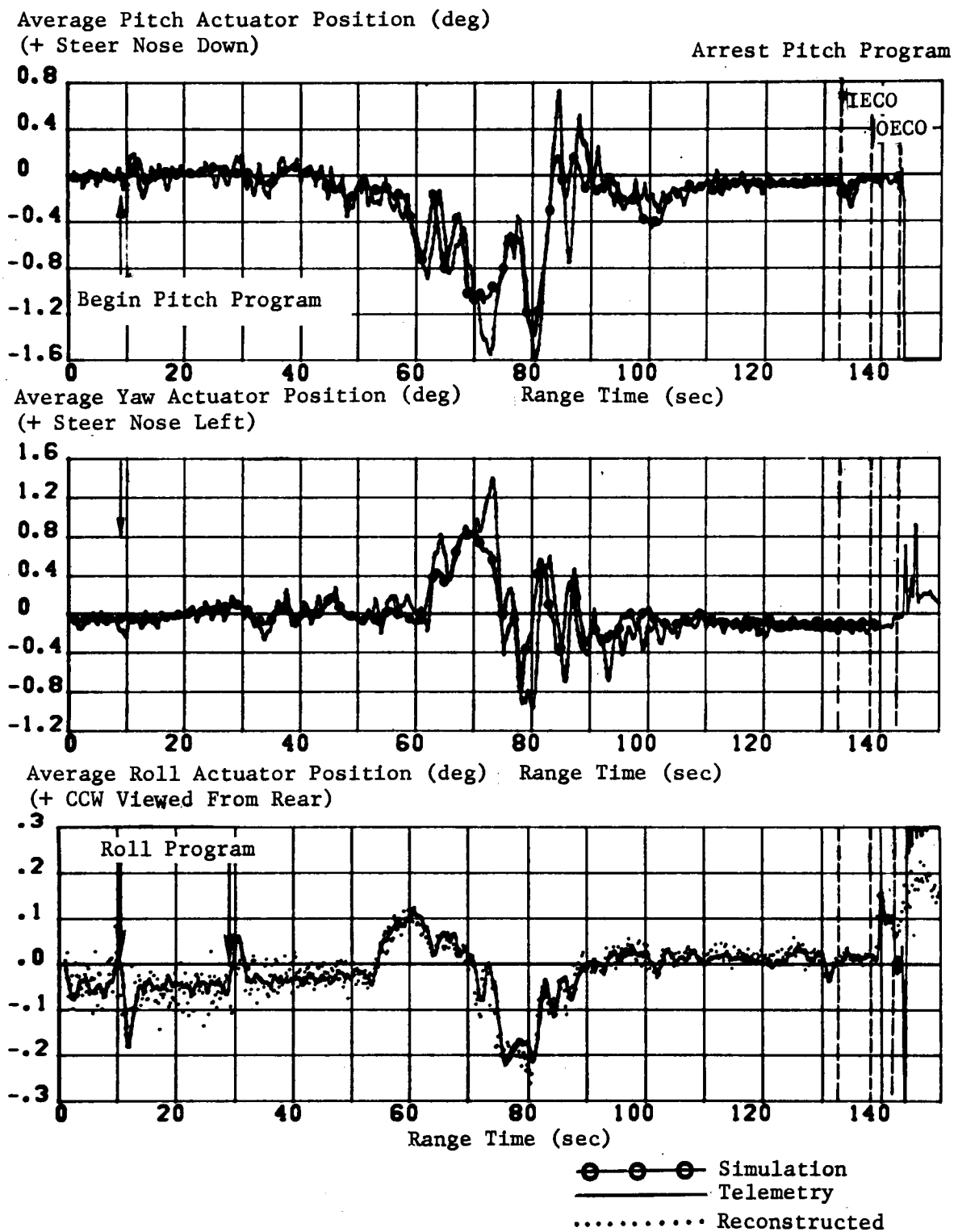


FIGURE 12-7 S-IB AVERAGE ACTUATOR POSITION

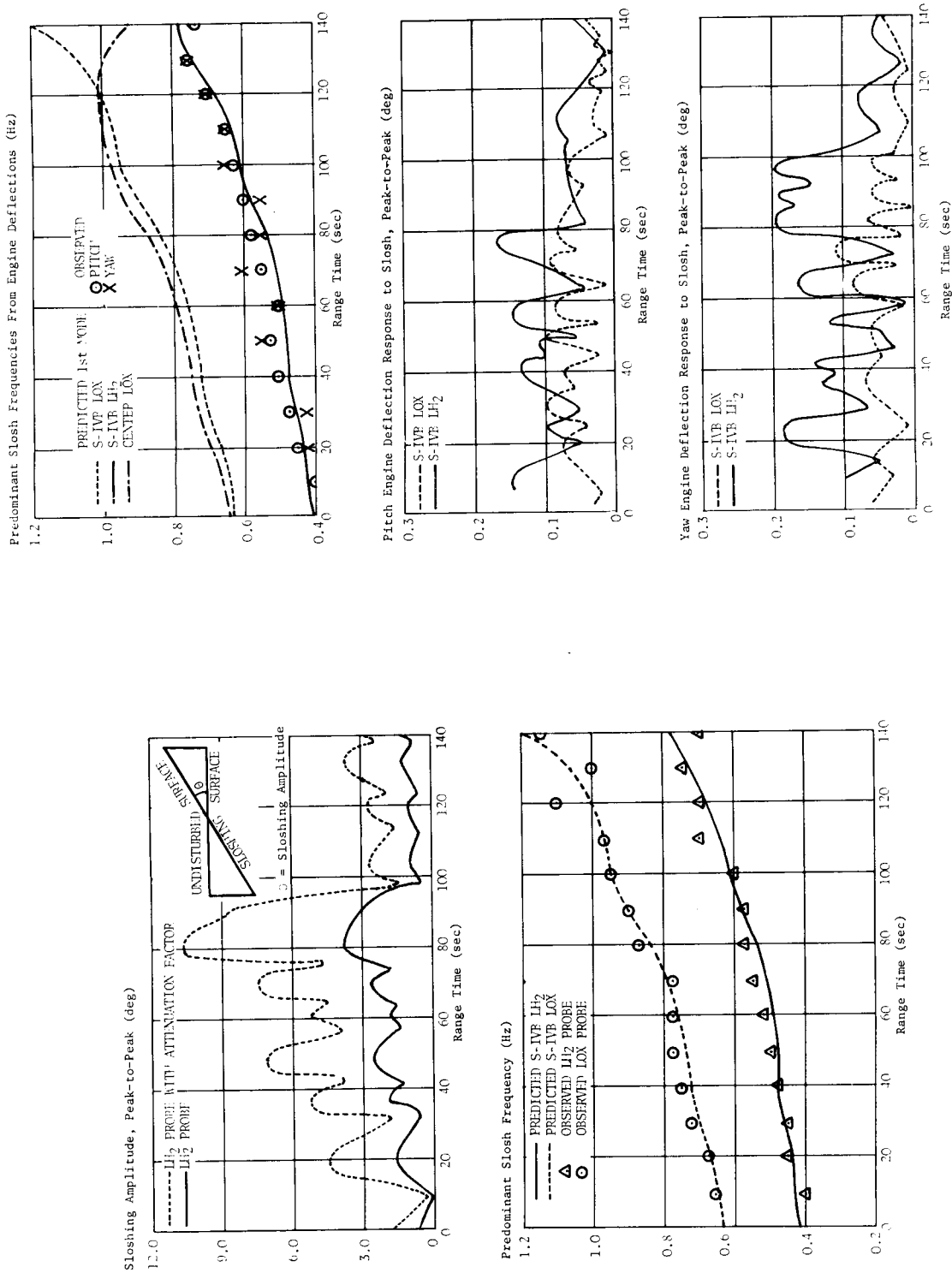


FIGURE 12-8 SLOSH DURING S-1B POWERED FLIGHT

TABLE 12-II
S-IB STAGE SEPARATION PARAMETERS

Parameter	Units	Pitch	Yaw	Roll
Attitude Error	deg	-0.08	-0.16	0.51
Attitude Rate	deg/s	-0.08	0.05	0.02

12.3.2 S-IVB STAGE CONTROL ANALYSIS

The S-IVB J-2 engine control system provided satisfactory control in the pitch and yaw planes during S-IVB powered flight and during the first 80 sec of the LOX dump of the propellant removal experiment. The Auxiliary Propulsion System (APS) control performance in the roll plane during S-IVB burn and in the pitch, yaw, and roll planes during orbit was satisfactory.

During S-IVB powered flight, control system transients occurred at S-IB/S-IVB separation, guidance initiation, gain change, artificial tau and chi bar guidance modes, chi freeze, and J-2 engine cutoff. These transients were expected and were well within the capabilities of the system.

The thrust vector control system provided satisfactory pitch and yaw control in response to guidance commands issued by the LVDC. Figures 12-9 and 12-10 show the vehicle attitudes in the pitch and yaw planes respectively, compared to the commanded attitudes. Event times are indicated on the figures and include the high acceleration level of artificial tau initiated at the predicted time, and the low acceleration level of artificial tau initiated when PMRS was sensed. The attitude errors and APS engine firings, angular rates, and actuator positions during powered flight are presented in Figures 12-11 through 12-13. The maximum pitch attitude error, angular rate, and actuator position during powered flight were 2.4 deg, -1.4 deg/s, and 0.7 deg, respectively. The respective parameters in yaw were -4.2 deg, 1.1 deg/s, and -0.95 degrees. The effective thrust vector misalignment necessary to match simulated and flight data was 0.21 deg in pitch and -0.36 deg in yaw. A summary of maximum flight control parameters is presented in Table 12-III.

The roll attitude error and angular rate during powered flight are presented in Figures 12-11 and 12-12, respectively. The maximum roll attitude error and angular velocity during powered flight were 2.3 deg and -0.4 deg/s, respectively. Roll disturbances were corrected by APS Engines I_{II} and III_{IV} throughout powered flight. The frequency of engine firings was higher than experienced on previous Saturn IB flights. This is attributed to a higher steady-state roll torque [approximately 36.6 N-m

- | | |
|---|-----------------------------------|
| 1. Guidance Initiation | 5. End of Artificial TAU Guidance |
| 2. Attitude Error and Rate Gain Change | 6. CHI Bar Guidance Mode |
| 3. Predicted Artificial TAU Guidance Mode | 7. CHI Freeze |
| 4. Guidance Sensed PMRS | |

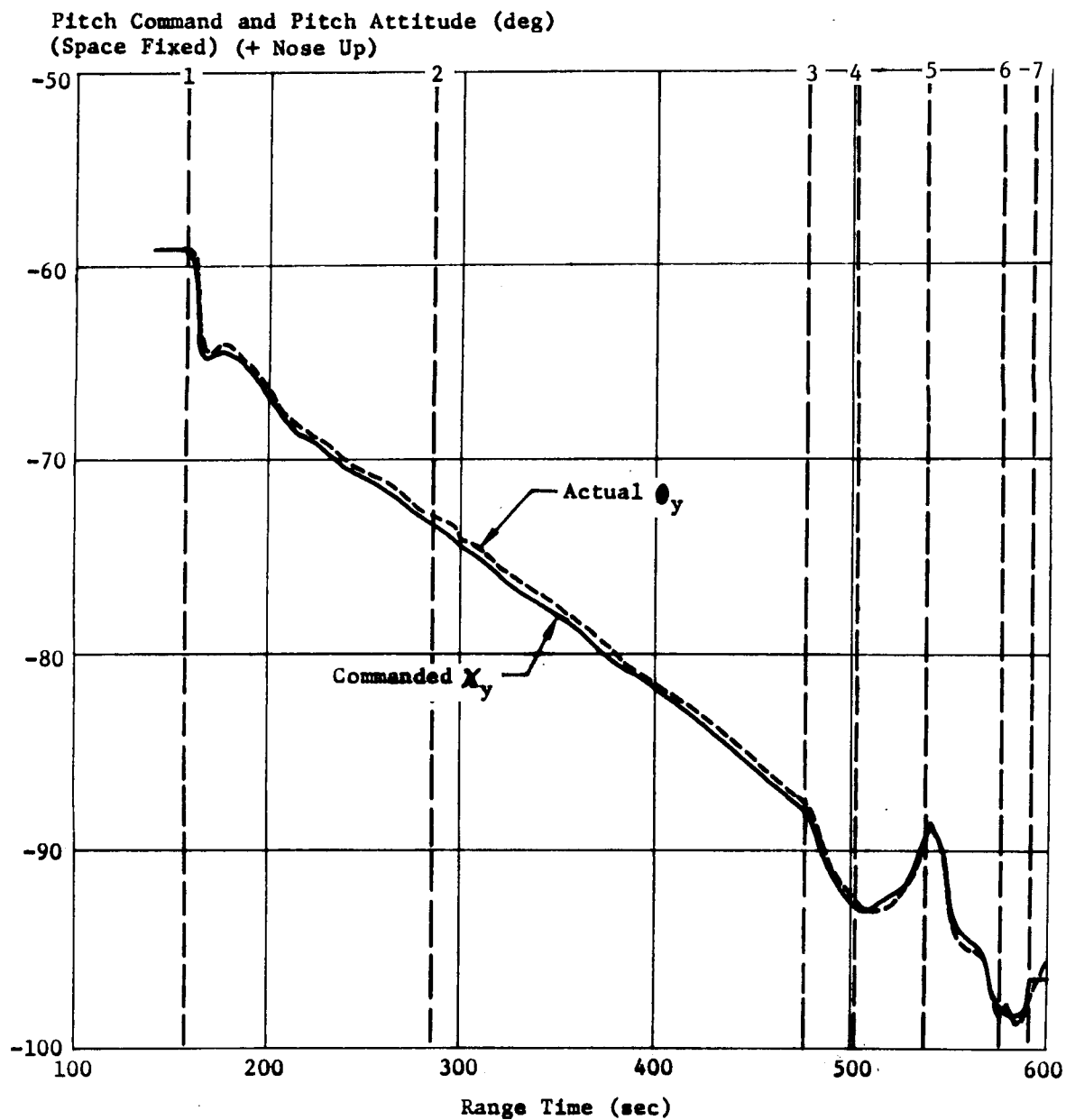


FIGURE 12-9 S-IVB STAGE COMMAND ANGLES-PITCH

1. Guidance Initiation
2. Introduction of Misalignment Correction Term
3. Attitude Error and Rate Gain Change
4. Guidance Sensed PMRS
5. CHI Bar Guidance Mode
6. CHI Freeze

Yaw Command and Yaw Attitude (deg)
(Space Fixed) (+ Nose Right)

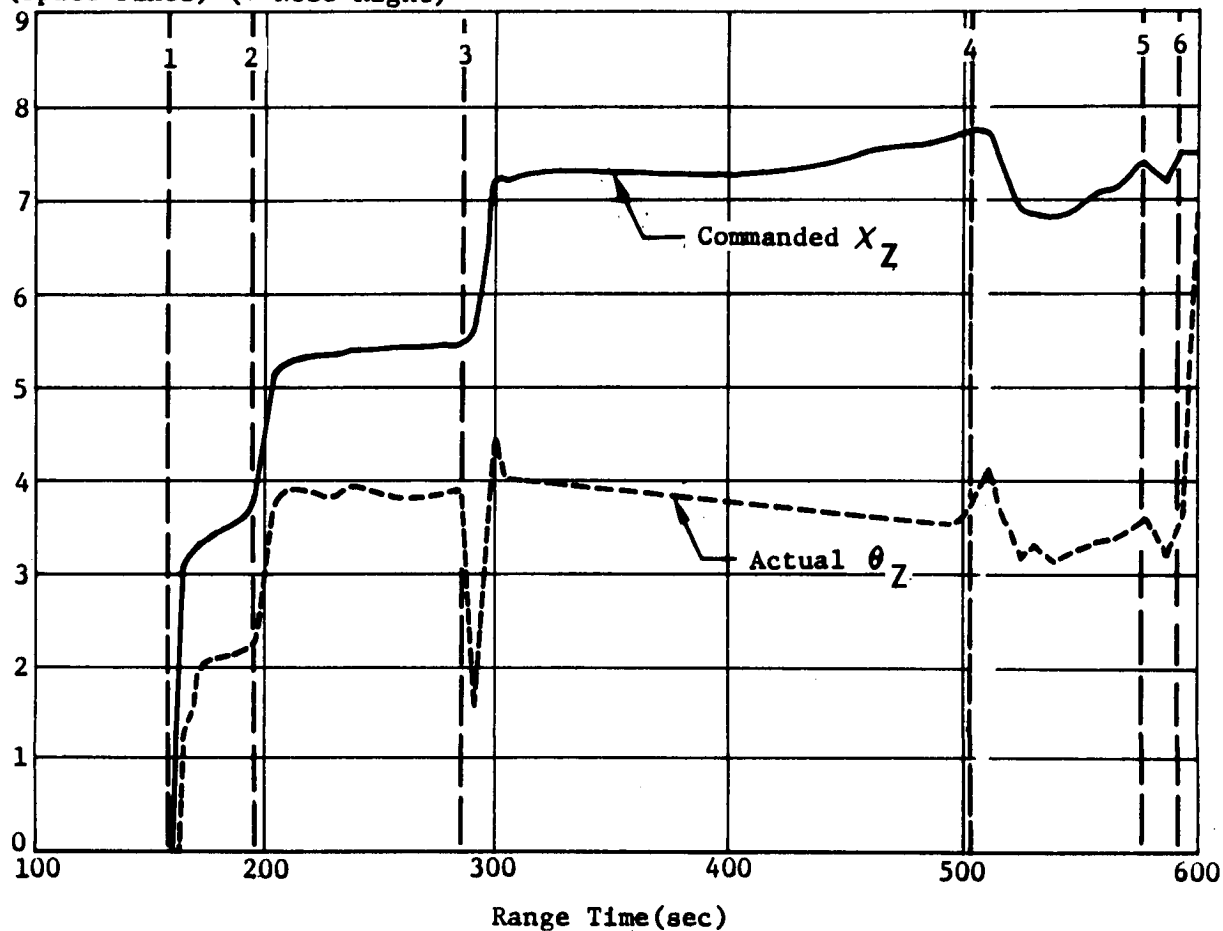


FIGURE 12-10 S-IVB STAGE COMMAND ANGLES - YAW

- | | |
|---|---|
| 1. S-IB/S-IVB Separation | 5. Predicted Artificial TAU Guidance Mode |
| 2. Guidance Initiation | 6. Guidance Sensed PMRS |
| 3. Introduction of Misalignment Correction Term | 7. End of Artificial TAU Guidance |
| 4. Attitude Error and Rate Gain Change | 8. CHI Bar Guidance Mode |
| | 9. CHI Freeze |
| | 10. J-2 Engine Cutoff |

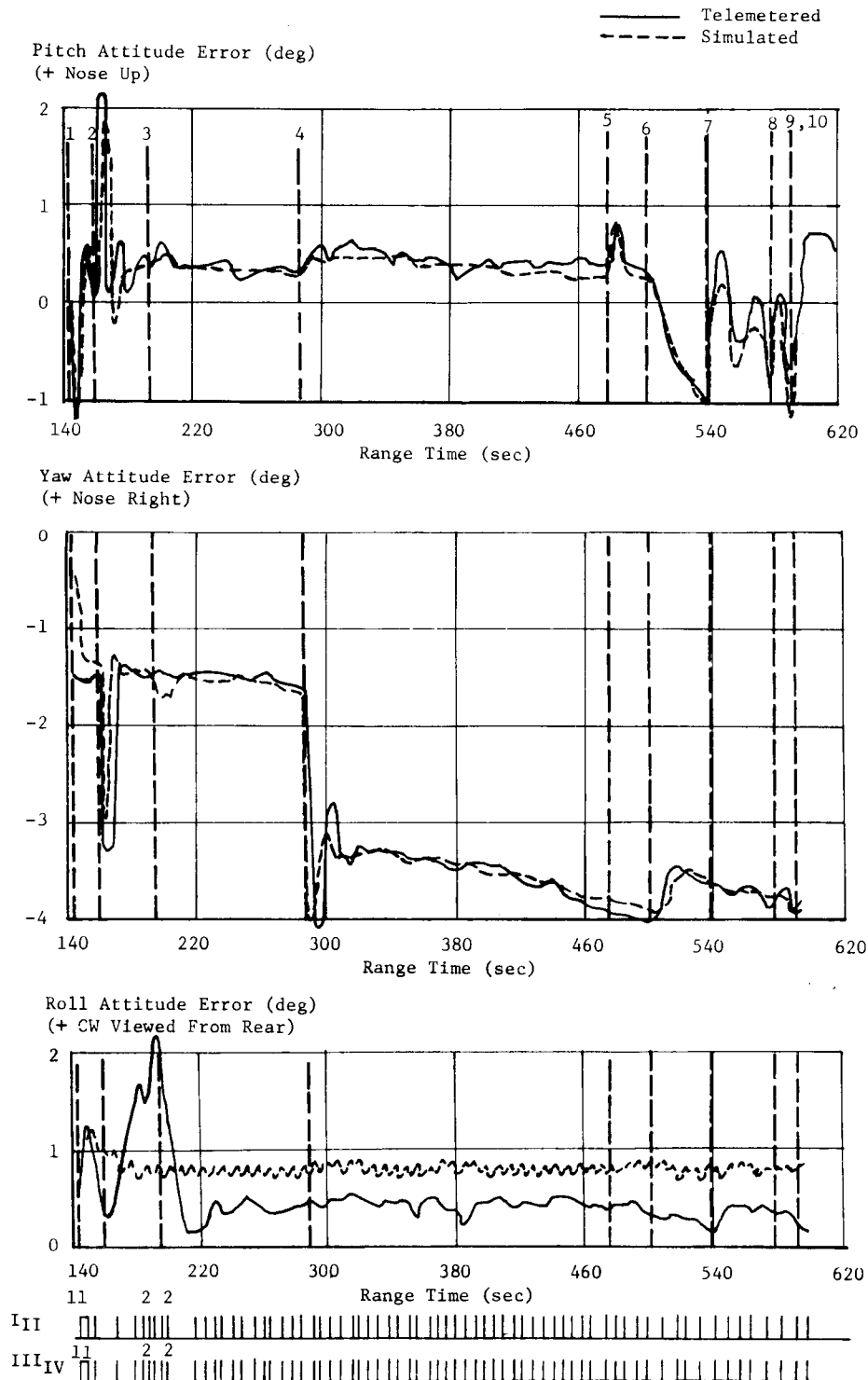


FIGURE 12-11 ATTITUDE ERRORS AND APS FIRINGS DURING S-IVB POWERED FLIGHT

- | | |
|---|---|
| 1. S-IB/S-IVB Separation | 5. Predicted Artificial TAU Guidance Mode |
| 2. Guidance Initiation | 6. Guidance Sensed PMRS |
| 3. Introduction of Misalignment Correction Term | 7. End of Artificial TAU Guidance |
| 4. Attitude Error and Rate Gain Change | 8. CHI Bar Guidance Mode |
| | 9. CHI Freeze |
| | 10. J-2 Engine Cutoff |

151

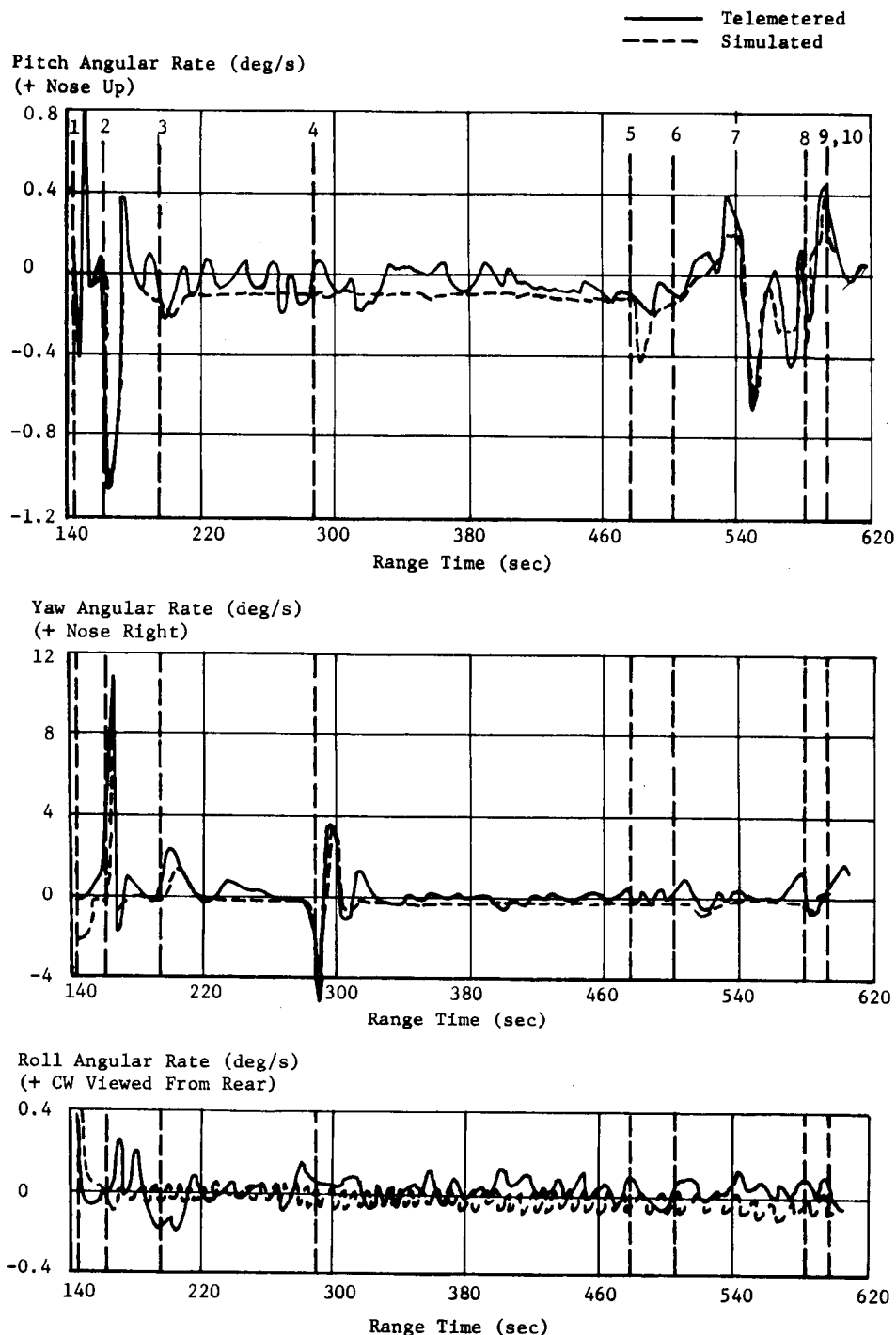


FIGURE 12-12 ANGULAR RATE GYROS DURING S-IVB POWERED FLIGHT

- | | |
|--|---|
| 1. S-IB/S-IVB Separation | 5. Predicted Artificial TAU Guidance Mode |
| 2. Guidance Initiation | 6. Guidance Sensed PMRS |
| 3. Introduction of Misalignment | 7. End of Artificial TAU Guidance |
| Correction Term | 8. CHI Bar Guidance Mode |
| 4. Attitude Error and Rate Gain Change | 9. CHI Freeze |
| | 10. J-2 Engine Cutoff |

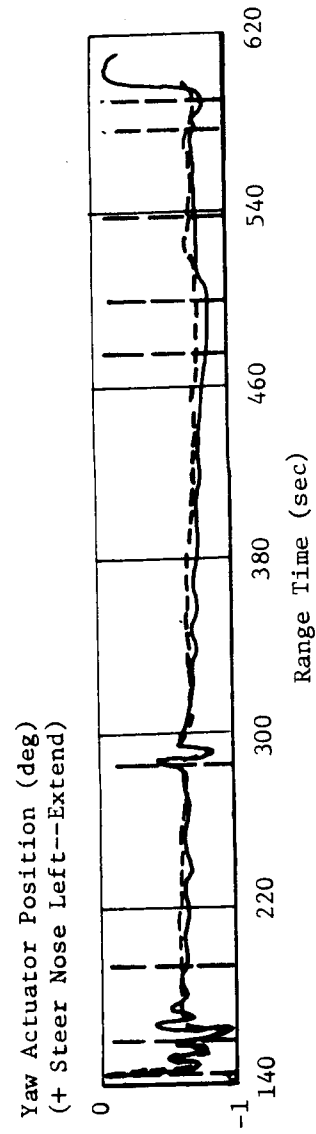
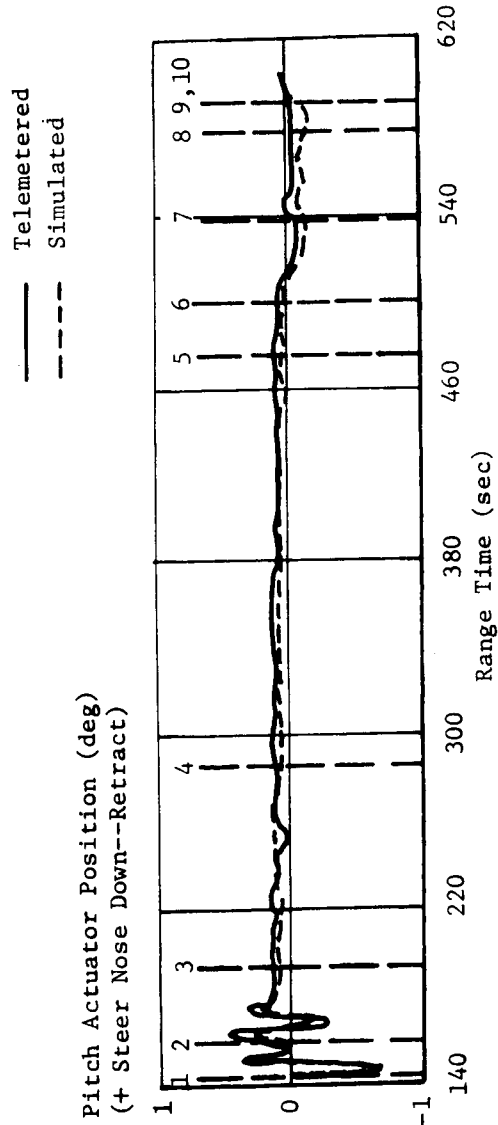


FIGURE 12-13 S-IVB PITCH AND YAW ACTUATOR POSITION

TABLE 12-III
MAXIMUM VALUES OF CRITICAL FLIGHT CONTROL PARAMETERS

Parameters	S-IVB/S-IB Separation	Guidance Initiation	Flight Control Computer Gain Change	Artificial Tau Guidance	Chi Bar Guidance Mode	Chi Freeze & J-2 Engine Cutoff
Attitude Error (deg)						
Pitch	- 1.7	+ 2.4	+ 0.8	- 0.9	- 0.8	- 1.1
Yaw	- 1.8	- 3.4	- 4.2	- 3.9	- 3.9	- 4.0
Roll	+ 1.3	+ 2.3	+ 0.6	+ 0.5	+ 0.44	+ 0.3
Angular Rate (deg/s)						
Pitch	+ 0.7	- 1.4	- 0.3	- 0.7	+ 0.4	+ 0.5
Yaw	- 0.6	+ 1.1	- 0.6	+ 0.25	- 0.35	+ 0.6
Roll*	- 0.4	+ 0.2	- 0.3	+ 0.2	- 0.3	- 0.5
Actuator Position (deg)						
Pitch	- 0.63	+ 0.7	+ 0.36	+ 0.25	+ 0.32	+ 0.14
Yaw	- 0.75	- 0.95	- 0.81	- 0.85	- 0.79	- 0.82

*Determined from filtered rate gyro data.

(27 lbf-ft) in a clockwise direction]. The highest steady-state roll torque experienced previously was 23.0 N-m (17 lbf-ft) on AS-202.

APS propellant requirements for roll control during powered flight were approximately 2.6 kg (5.7 lbm) from both modules. This represents approximately 4.5% of the total propellant available for attitude control and is within the expected range of propellant usage for roll control during powered flight. Table 12-IV presents a summary of the APS impulse usage for the events of powered flight and orbital maneuvers. For the total period shown in the table, the propellant requirements were approximately 12.2 kg (27 lbm) for Module 1 and 9.5 kg (21 lbm) for Module 2. This represents approximately 42.9% and 33.1% of the total propellant available in the respective modules.

High frequency oscillations (17 Hz) were observed on the pitch and roll rate gyros until 80 sec after S-IB/S-IVB separation. The maximum rate observed during this interval was approximately 1.75 deg/second. The effect of this roll rate oscillation was to cause the roll dead band to increase from the nominal ± 1 deg, thereby causing the vehicle to maintain an attitude error in excess of 1 deg for a period of approximately 30 seconds. The roll attitude error decreased to a nominal operating value after the high frequency oscillations damped out. See Section 12.3.4.2 for further discussion of this phenomenon.

LH₂ sloshing was observed on PU sensor fine mass data. The slosh frequency and amplitude during S-IVB burn are shown in Figure 12-14. The slosh frequency correlated well with the LH₂ predicted first mode natural frequency. Previous Saturn IB flights have exhibited an LH₂ slosh frequency near the first mode natural frequency. The slosh amplitudes are presented as indicated by the PU sensor, corrected for sensor attenuation, and extrapolated to the LH₂ tank wall. The maximum slosh amplitude at the PU sensor was approximately 10.16 cm (4 in) zero to peak (0 - P) which is comparable to LH₂ slosh amplitudes experienced on previous Saturn IB flights.

Oscillations, low in frequency and amplitude (approximately 0.2 deg peak-to-peak maximum at 0.35 Hz), were observed on the pitch actuator position data during S-IVB powered flight. The frequency and amplitude of these oscillations were comparable to those experienced on AS-201. These oscillations were easily discernible on the pitch actuator position, differential pressure, and rate gyro measurements until approximately 145 sec after engine start command when the attitude error and rate gain change was introduced. The oscillations remained at a very low amplitude for the remainder of the S-IVB powered flight.

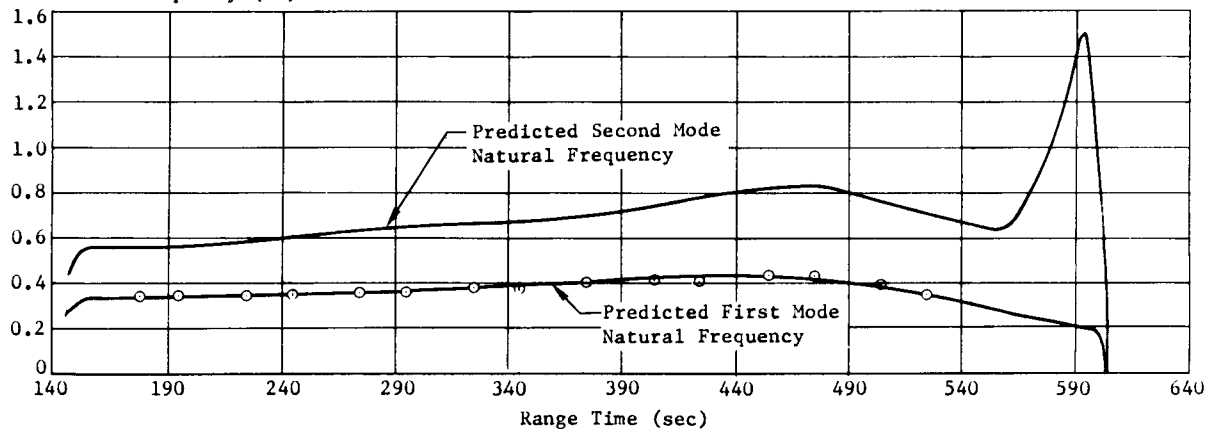
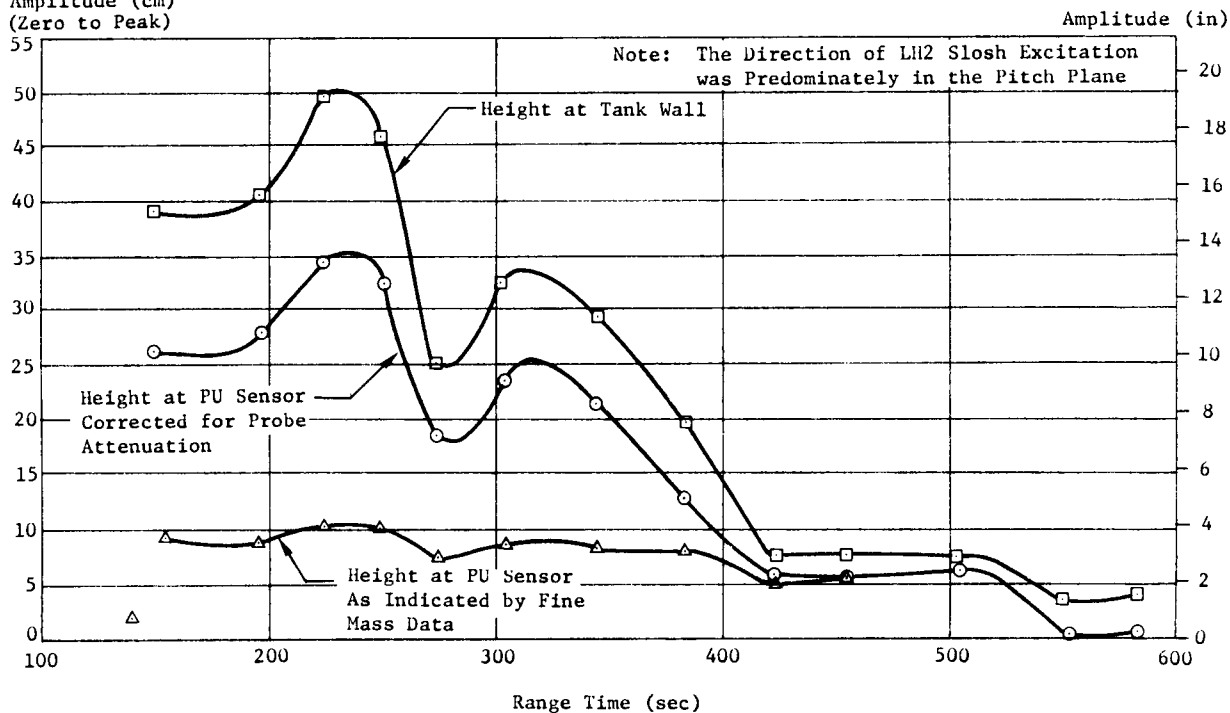
The most probable cause of the noted oscillations in the J-2 engine control system appears to be a combination of LH₂ and LOX sloshing. This phenomenon was experienced on AS-201 and has been simulated in preflight control system studies. The oscillations as experienced on AS-201 and AS-204

TABLE 12-IV APS IMPULSE SUMMARY

155

Event	Units	Module 1	Module 2	APS Engine					
				I _{IV}	I _p	I _{II}	III _{II}	III _p	III _{IV}
Powered Flight: Separation, Guidance Initiation and Ullage RKT JETT 144 to + 210 seconds	lbf-s	180.9	180.2	0	0	180.9	0	0	180.2
	N-s	804.5	801.7	0	0	804.5	0	0	801.7
	lbf-s	428.5	422.1	0	0	428.5	0	0	422.1
	N-s	1905.9	1877.5	0	0	1905.9	0	0	1877.5
Limit Cycle Operations for Remaining Burntime 210 to 594 seconds	lbf-s	1575.0	1020.0	0	517.5	1057.5	1020.0	0	0
	N-s	7006.0	4537.2	0	2302.0	4704.0	4537.2	0	0
Initial Recovery Following J-2 Cutoff: 595 to 638 seconds (Includes LOX & LH ₂ Venting)	lbf-s	379.8	341.3	112.3	173.1	94.4	119.1	139.7	82.5
	N-s	1689.4	1518.2	499.5	770.0	419.9	529.8	621.4	367.0
Alignment to Local Horizontal Following J-2 Cutoff 638 to 680 seconds (Includes LH ₂ Venting)	lbf-s	72.5	102.0	27.7	0	44.8	57.0	0	45.0
	N-s	322.5	453.7	123.1	0	199.4	253.5	0	200.2
SLA Panel Deployment: 1194 to 1200 seconds (Includes LH ₂ Venting)	lbf-s	65.4	55.5	0	0	65.4	55.5	0	0
	N-s	290.7	247.0	0	0	290.7	247.0	0	0
LEM Separation: 3231 to 3250 seconds	lbf-s	65.4	55.5	0	0	65.4	55.5	0	0
	N-s	290.7	247.0	0	0	290.7	247.0	0	0
Alignment to Local Horizontal Following LEM Separation: 3415 to 3540 seconds (Includes LH ₂ Venting)	lbf-s	405.0	337.5	37.5	255.0	112.5	165.0	142.5	30.0
	N-s	1801.5	1501.3	166.8	1134.3	500.4	734.0	633.9	133.4
Inertial Hold (From 5480 to 6356 seconds) LH ₂ Venting at 6133 through 6356 seconds	lbf-s	963.2	125.3	52.0	874.3	36.9	73.6	22.5	29.2
	N-s	4284.5	557.4	231.3	3889.1	164.1	327.4	100.1	129.9
Maneuver to Retrograde: 6356 to 6645 seconds (Includes LH ₂ Venting)	lbf-s	530.1	343.4	97.8	330.0	102.3	113.2	130.7	99.5
	N-s	2357.9	1527.5	435.0	1467.9	455.0	503.5	581.4	442.6
LOX Removal During TVC Only: 8774 to 8856 seconds	lbf-s	14.8	14.6	7.6	0	7.2	7.5	0	7.1
	N-s	65.8	65.0	33.6	0	32.2	33.4	0	31.6
Recovery from LOX Removal: 8856 to 8904 seconds	lbf-s	98.8	70.2	24.2	37.4	37.1	41.6	0	28.6
	N-s	439.3	312.3	107.6	166.5	165.2	185.2	0	127.1
LH ₂ Removal: 8904 to 9085 seconds	lbf-s	36.5	118.	14.4	0	22.1	15.2	88.9	14.3
	N-s	162.3	526.9	63.9	0	98.4	67.7	395.5	63.7
Initiate Pitch to Retrograde Following LH ₂ Removal: 9105 to 9180 seconds (Includes LOX and LH ₂ Venting)	lbf-s	43.9	242.7	36.7	0	7.2	139.5	103.2	0
	N-s	195.2	1079.7	163.4	0	31.8	620.6	459.1	0
Total Impulse Expended	lbf-s	4794.2	3373.3						
	N-s	21325.5	15005.4						

LH2 Slosh Frequency (Hz)

LH2 Slosh Amplitudes
Amplitude (cm)
(Zero to Peak)FIGURE 12-14 LH₂ SLOSH DURING S-IVB POWERED FLIGHT

did not appreciably affect control system operation.

LOX slosh frequencies and amplitudes obtained from PU sensor fine mass data are shown in Figure 12-15. The LOX slosh frequency data correlated well with the predicted second mode natural frequency. The maximum slosh height seen at the PU sensor was approximately 1.65 cm (0.65 in) (0 - P). This slosh height compares favorably with AS-201 and AS-202 flight data. AS-203 LOX sloshing was slightly higher at 6.35 cm (2.5 in) (0 - P).

12.3.3 CONTROL DURING ORBIT

During orbit, the S-IVB Stage experienced transients resulting from programmed maneuvers, LOX and LH₂ venting, LM separation, and the propellant removal experiment. All transients encountered in orbit were well within the capabilities of the control system.

Control system data indicates that proper attitude control during orbit was maintained. Following S-IVB cutoff, an inertial attitude hold was maintained until approximately 90 sec after cutoff, during which time the launch vehicle nose cone was jettisoned (approximately 45 sec after S-IVB cutoff). Relatively small disturbances were experienced during the nose cone separation. Following the inertial attitude hold, the attitude control system maneuvered the vehicle to the local horizontal and established the desired orbital pitch rate. The commanded and actual vehicle attitudes following S-IVB cutoff are shown in Figure 12-16. Correlation between the commanded and actual vehicle attitudes indicates normal attitude control following S-IVB cutoff. The APS impulse usage is included in Table 12-IV.

The commanded and actual vehicle attitudes during LM separation are shown in Figure 12-17. The pitch, yaw, and roll attitude errors and rates during this period are shown in Figures 12-18 and 12-19, respectively, and Table 12-V presents the maximum control system parameters. The disturbances resulting from the separation of the LM were well within the capabilities of the APS. The APS impulse usage during this time interval is included in Table 12-IV.

TABLE 12-V

LM SEPARATION PARAMETERS

Parameter	Units	Pitch	Yaw	Roll
Attitude Error	deg	0.75	-1.11	-1.0
Attitude Rate	deg/s	0.0	-0.1	0.2

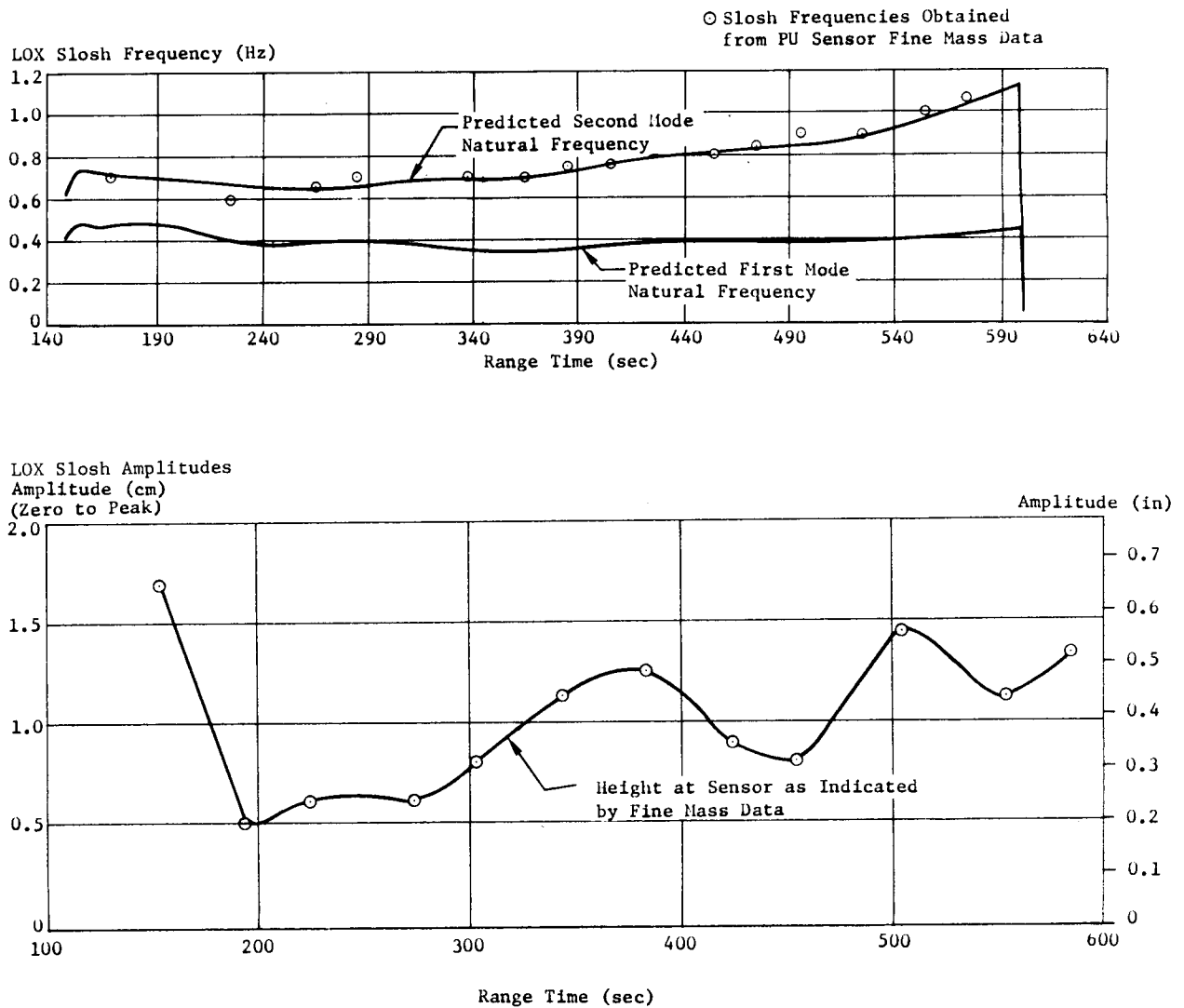


FIGURE 12-15 LOX SLOSH DURING S-IVB POWERED FLIGHT

1. LOX Vent OFF
2. Nose Cone Separation
3. Maneuver to Local Horizontal

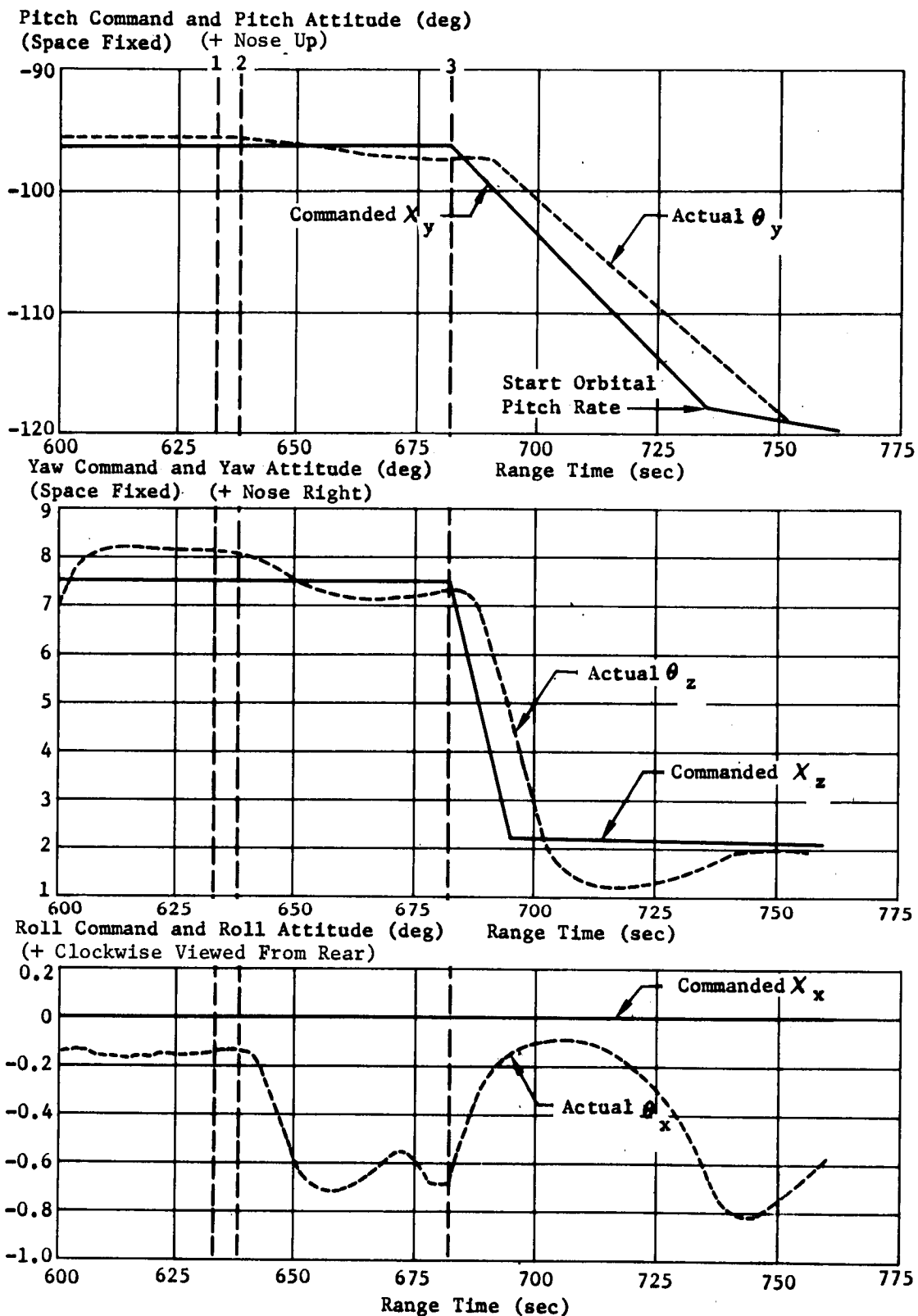


FIGURE 12-16 S-IVB STAGE COMMAND ANGLES FOLLOWING S-IVB CUTOFF

1. LM Separation
2. LH2 Vent Valve Open
3. Alignment to Local Horizontal

Pitch Command and Pitch Attitude (deg)
(Space Fixed) (+ Nose Up)

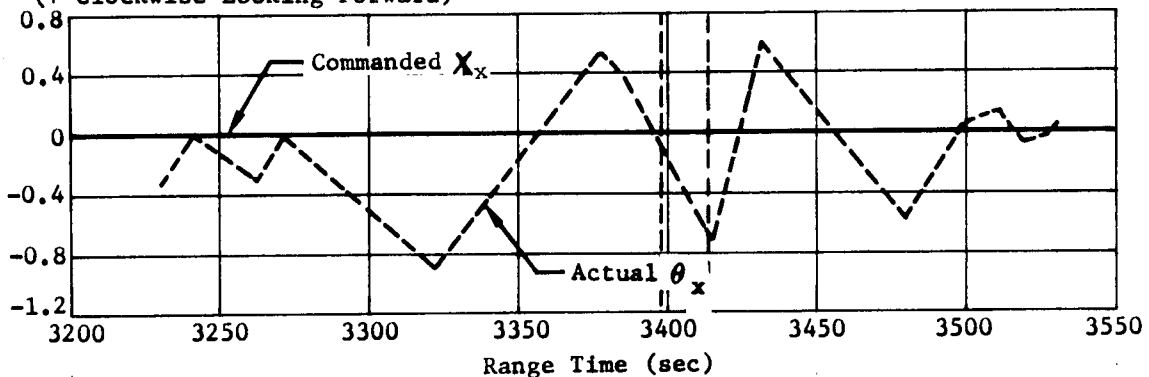
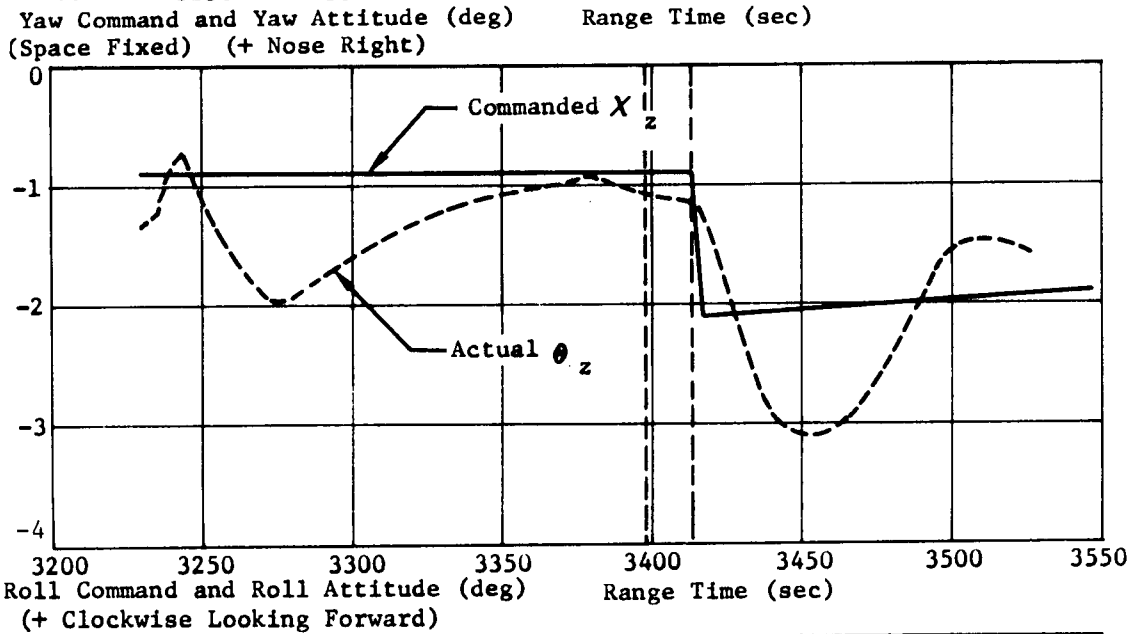
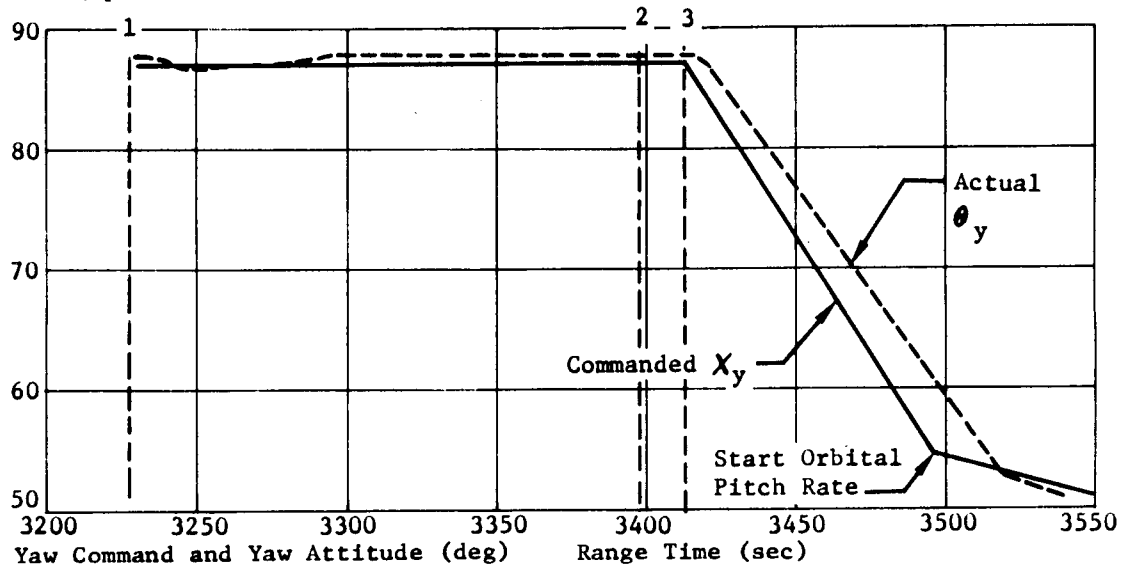


FIGURE 12-17 S-IVB STAGE COMMAND ANGLES DURING
LM SEPARATION

1. LM Separation Command
2. Initiate LH2 Tank Vent
3. Alignment to Local Horizontal

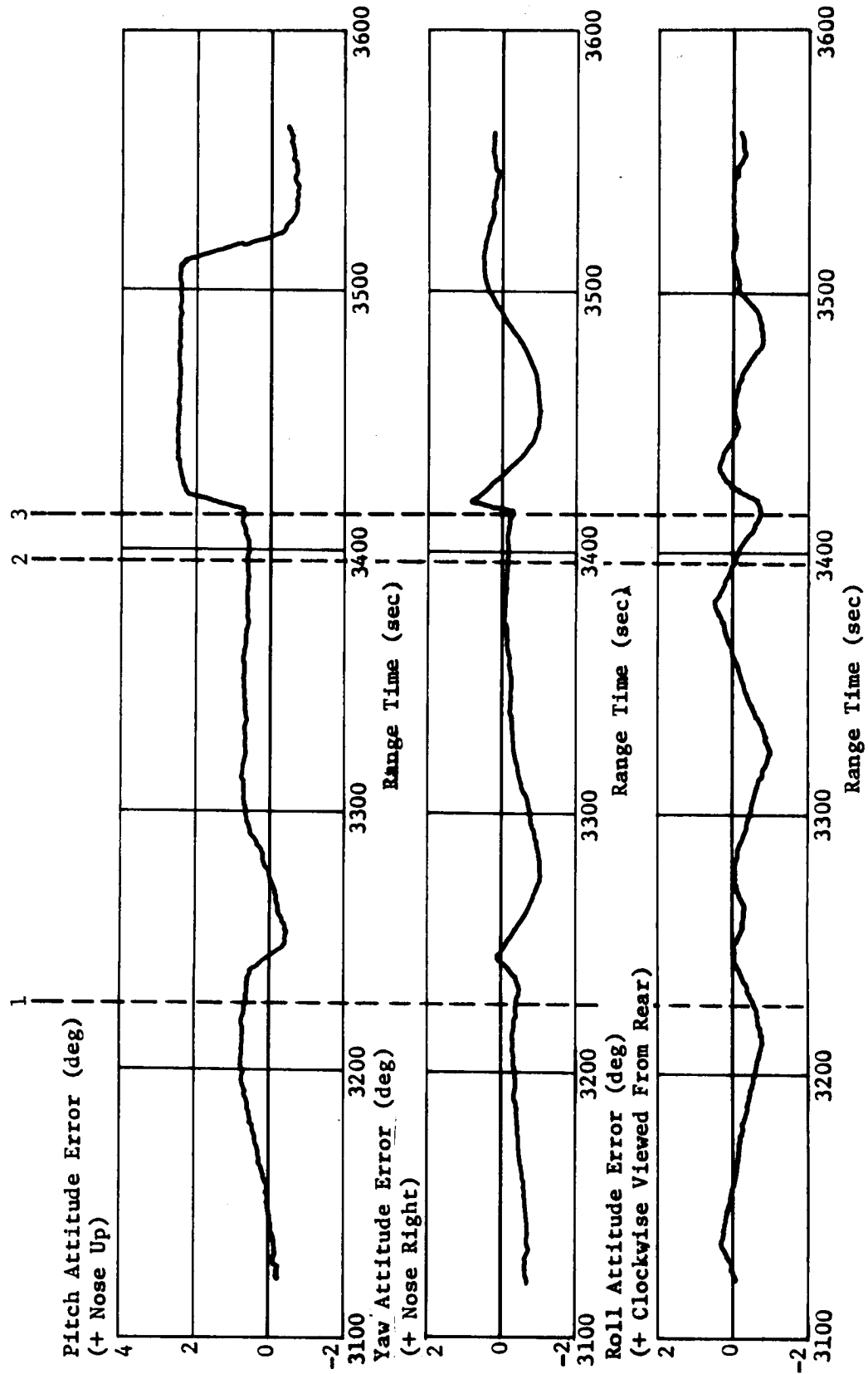


FIGURE 12-18 S-IVB ATTITUDE ERRORS DURING LM SEPARATION

1. LM Separation Command
2. Initiate LH2 Tank Vent
3. Alignment to Local Horizontal

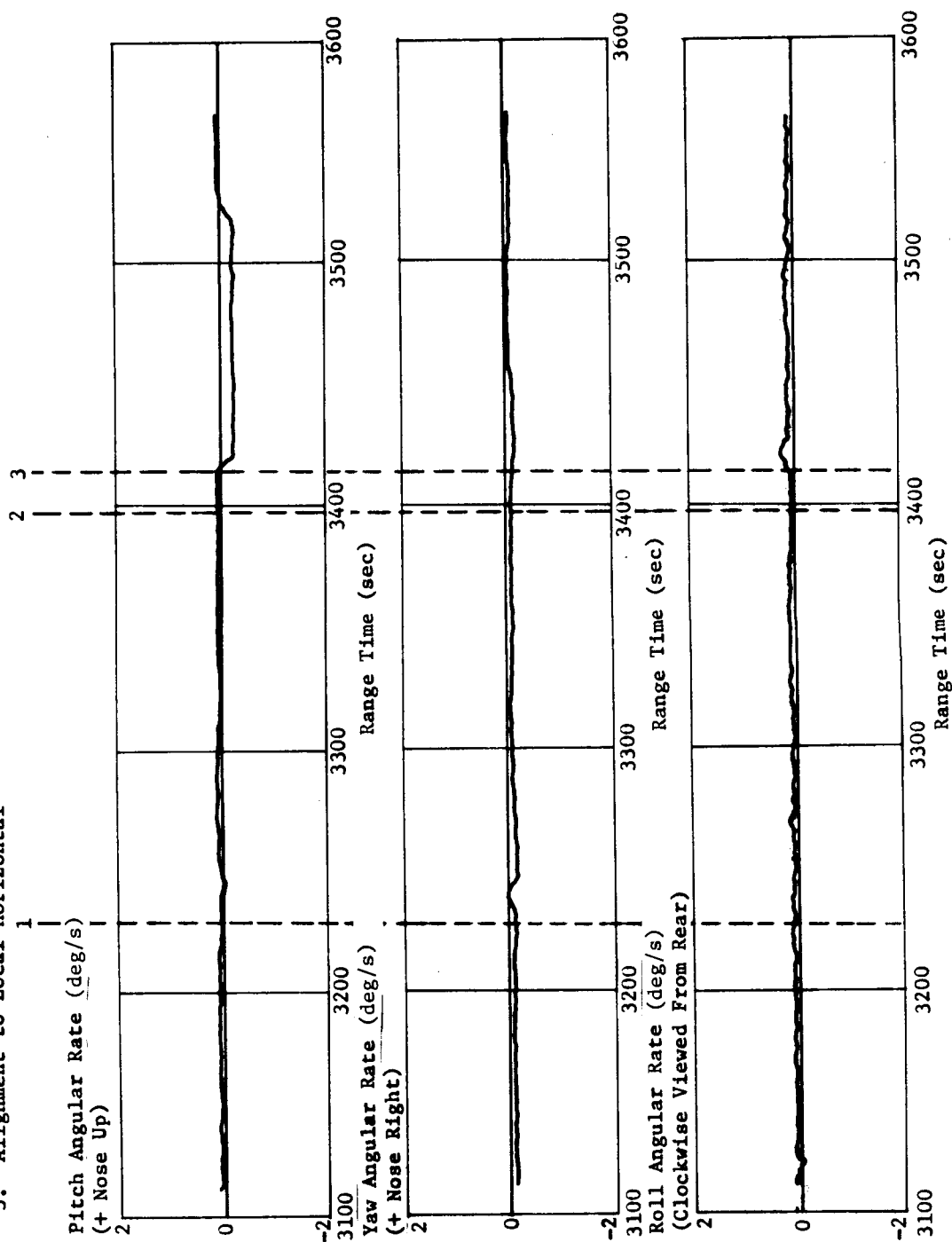


FIGURE 12-19 S-IVB ANGULAR RATE GYROS DURING LM SEPARATION

At approximately 5,485 sec, guidance commands were frozen, allowing the vehicle to rotate approximately 60 deg nose up with respect to the local horizontal. The aerodynamic moments increased appreciably as the vehicle angle-of-attack increased, requiring an impulse usage of approximately 3889.1 N-s (874.3 lbf-s) from APS engine I_p. At 6356 sec, a pitch maneuver was initiated to place the stage in a retrograde attitude. The attitude errors and rates during the retrograde maneuver are presented in Figures 12-20 and 12-21. The APS impulse usage during this time interval is included in Table 12-IV.

The J-2 engine control system provided satisfactory control during the first 80 sec of the LOX dump during the propellant removal experiment. The APS provided control for the remainder of the experiment. The commanded angles and actual pitch, yaw, and roll gimbal angles are presented in Figure 12-22. The pitch, yaw, and roll attitude errors and APS firings are presented in Figures 12-23 and 12-24. Angular rates are presented in Figure 12-25. The pitch and yaw actuator positions during the propellant removal experiment are shown in Figure 12-26. The maximum pitch attitude error, angular rate, and actuator position were -5.3 deg, +0.3 deg/s, and -0.8 deg, respectively. The same parameters in yaw were -5.5 deg, -0.25 deg/s, and -1.1 degrees. The maximum roll attitude error and rate during the propellant removal experiment were 2.3 deg and -0.28 deg/s, respectively. The APS impulse usage during this time interval concludes the data in Table 12-IV. The actual propellant consumption was slightly higher than predicted (see Section 10).

The vehicle was commanded to maintain a retrograde position with the local horizontal at 9393.8 sec after completion of the programmed attitude maneuvers and the propellant removal tests. The vehicle maintained this attitude until 33,451 seconds. At this time, LVDC computer time (TAS) became negative during counter overflow from orbital guidance initiation, TB₄ + 90 seconds. When this occurred, the pitch, yaw and roll chi values were frozen in the flight program and the vehicle remained in a fixed attitude for the remainder of orbited life and/or loss of APS control. At 33,451 sec, chi values were frozen at -4.7 deg in pitch, 0.4 deg in yaw, and 0.0 deg in roll. Figure 12-27 depicts the vehicle gimbal angles during this period. Data up to 38,073 sec is compressed data with a reading each 100 seconds. The curves were constructed from a best fit. Data after 38,073 sec is real time data from over Hawaii (Rev 7).

Figure 12-27 shows that at approximately 37,235 sec, stability of the vehicle was lost. The vehicle entered a coning oscillation.

Figure 12-28 is a graph of the composite gimbal angle changes in the pitch-yaw plane. Vehicle attitude oscillations appear as follows:

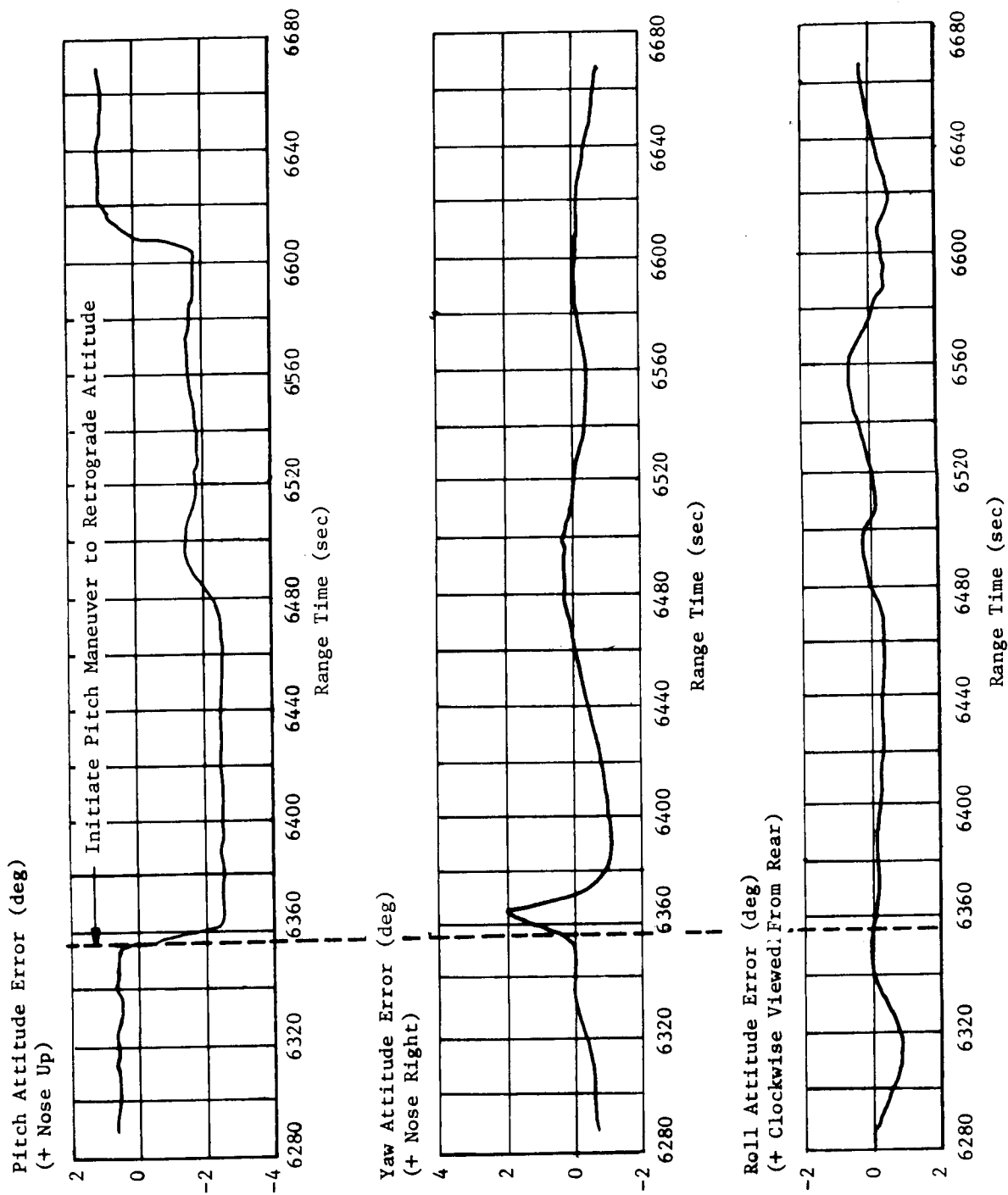


FIGURE 12-20 S-IVB ATTITUDE ERRORS DURING MANEUVER TO RETROGRADE ATTITUDE

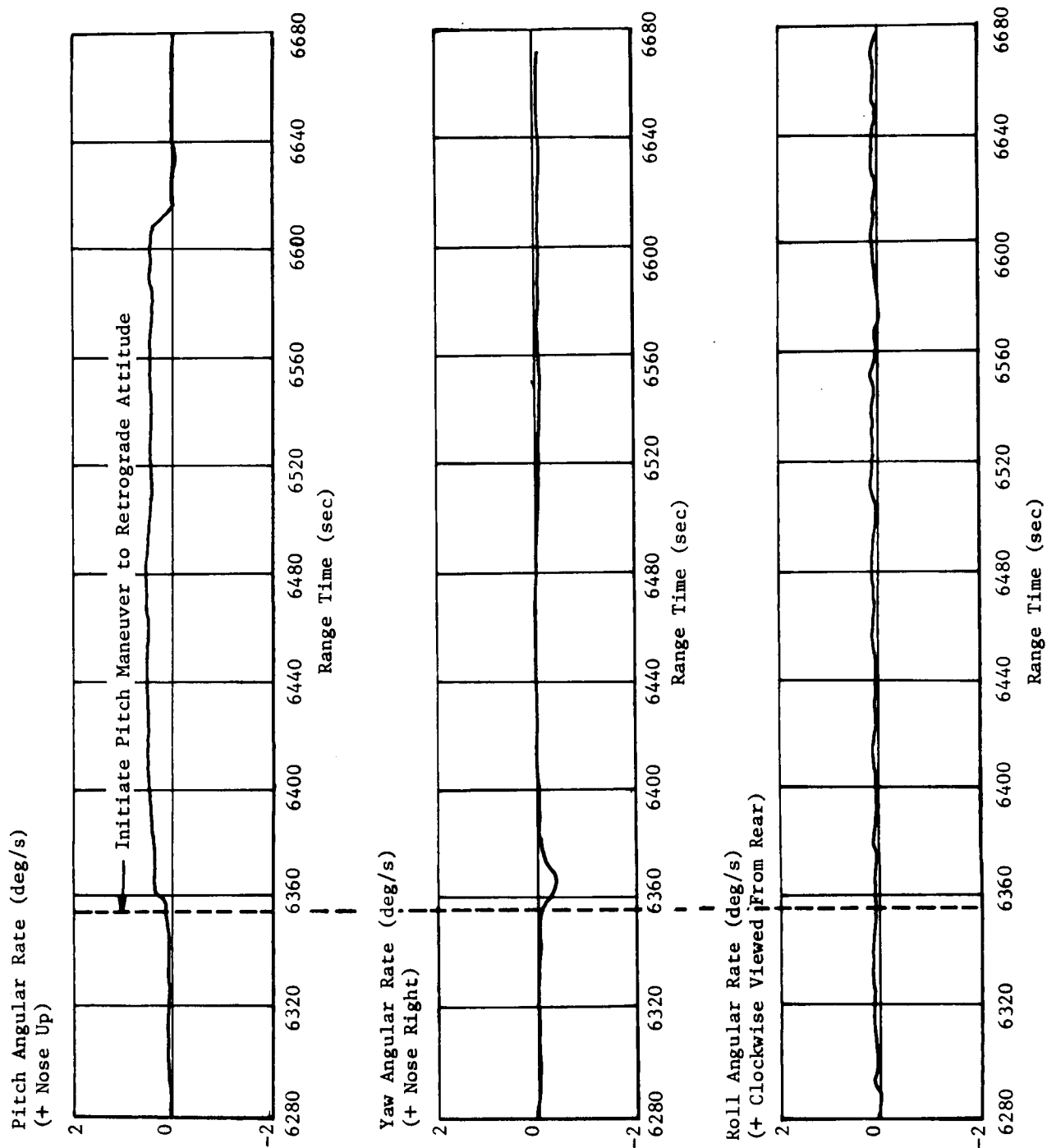
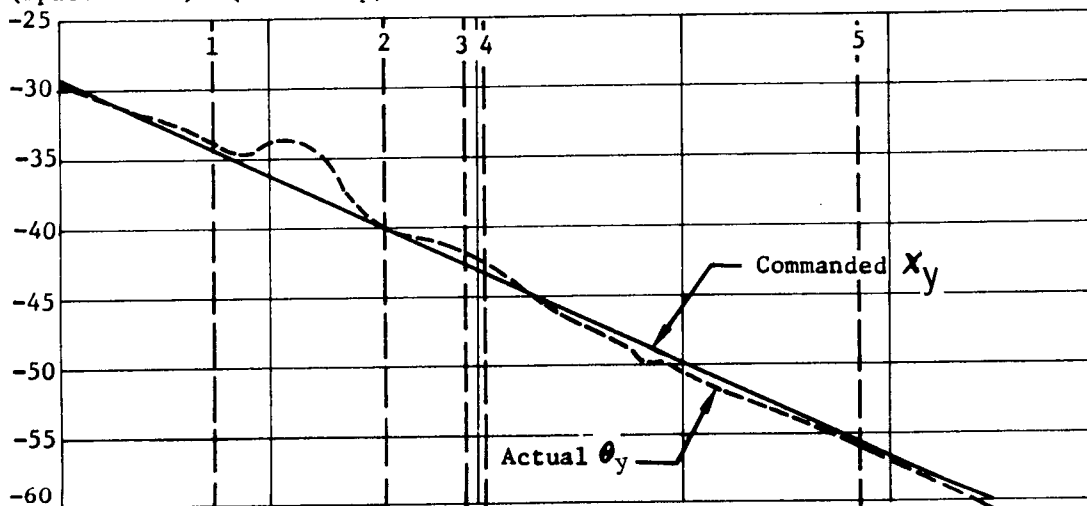


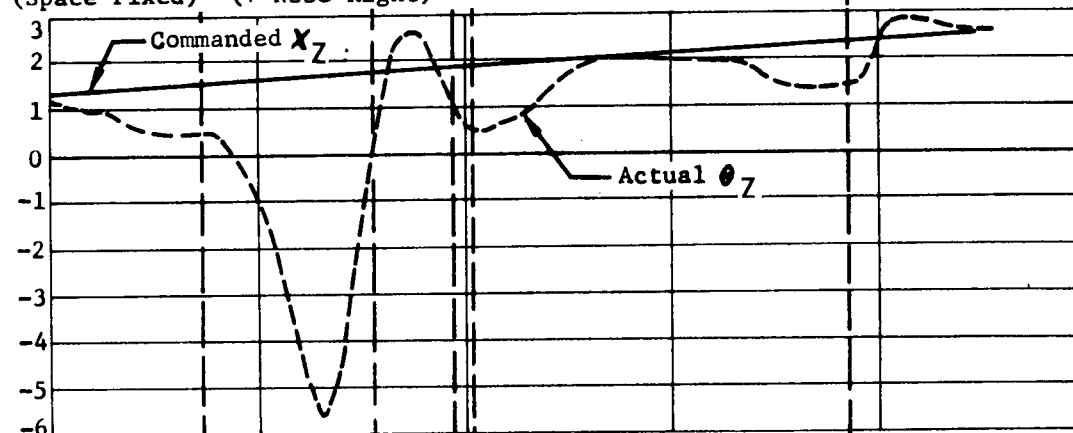
FIGURE 12-21 S-IVB ANGULAR RATE GYROS DURING MANEUVER TO RETROGRADE ATTITUDE

1. LOX Dump On, Burn Mode On
2. Burn Mode Off
3. LOX Dump Off
4. LH2 Dump On
5. LH2 Dump Off

Pitch Command Pitch Attitude (deg)
(Space Fixed) (+ Nose Up)



Yaw Command and Yaw Attitude (deg)
(Space Fixed) (+ Nose Right)



Roll Command and Roll Attitude (deg)
(+ Clockwise Viewed From Rear)

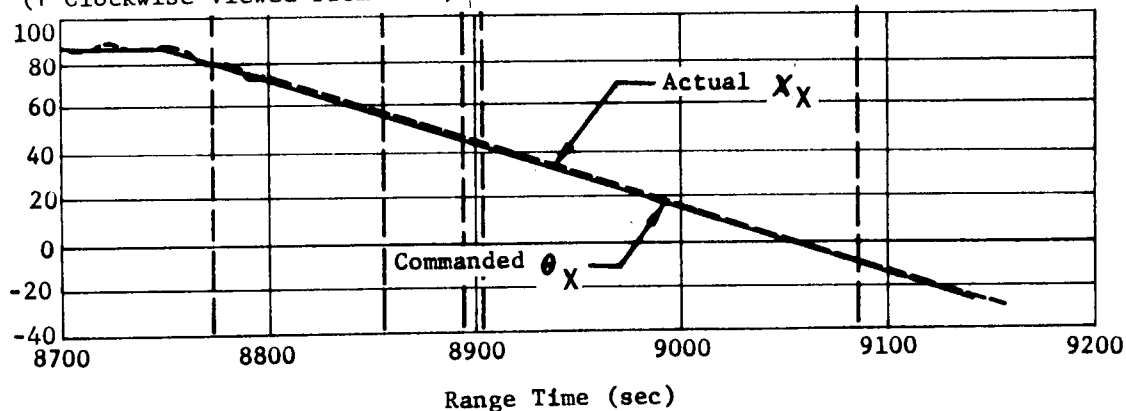


FIGURE 12-22 S-IVB STAGE COMMAND ANGLES DURING PROPELLANT REMOVAL TEST

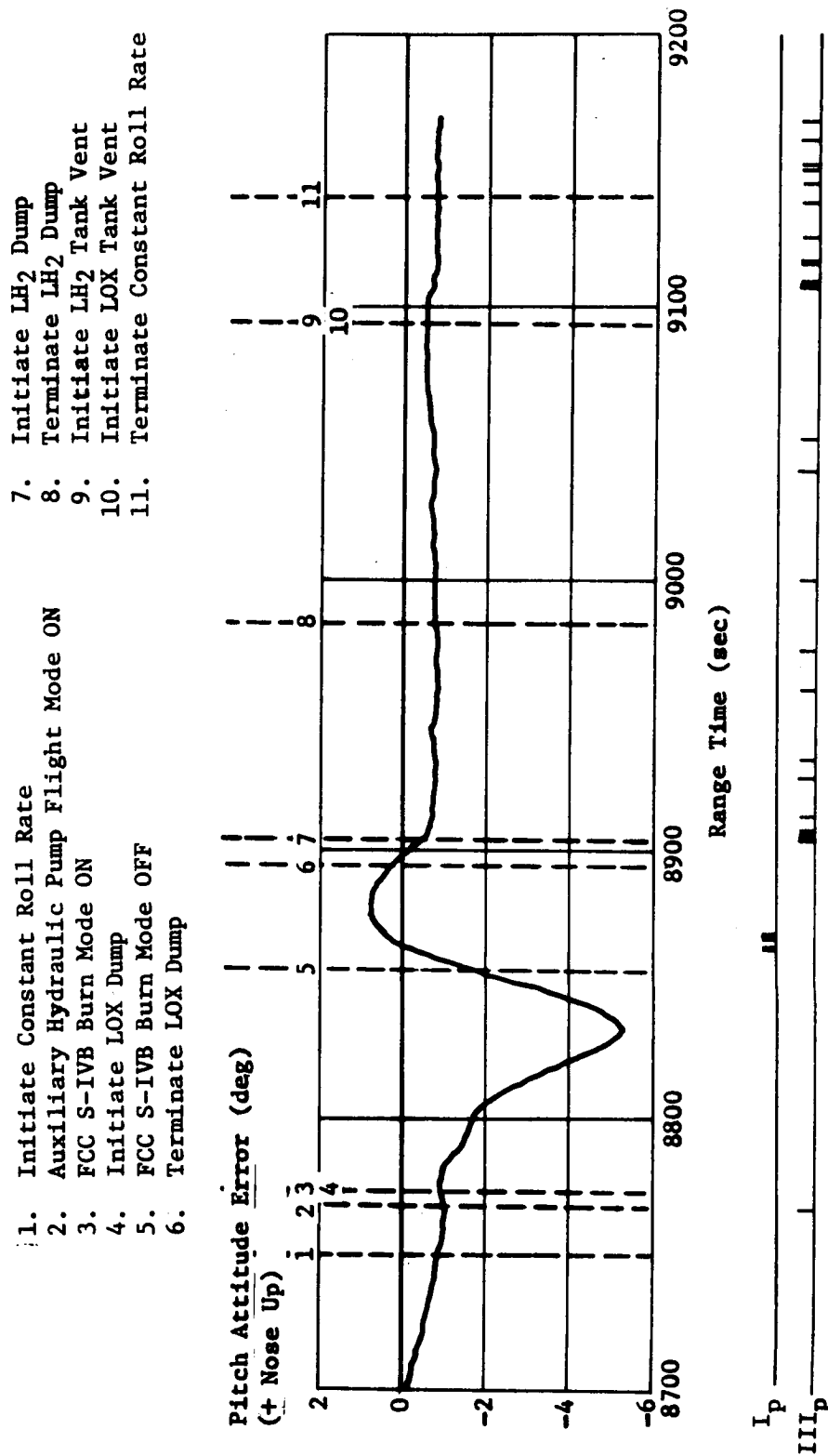


FIGURE 12-23 S-IVB ATTITUDE ERRORS AND APS FIRINGS DURING PROPELLANT REMOVAL TEST

- | | |
|--|----------------------------------|
| 1. Initiate Constant Roll Rate | 7. Initiate LH2 Dump |
| 2. Auxiliary Hydraulic Pump Flight Mode ON | 8. Terminate LH2 Dump |
| 3. FCC S-IVB Burn Mode ON | 9. Initiate LH2 Tank Vent |
| 4. Initiate LOX Dump | 10. Initiate LOX Tank Vent |
| 5. FCC S-IVB Burn Mode OFF | 11. Terminate Constant Roll Rate |
| 6. Terminate LOX Dump | |

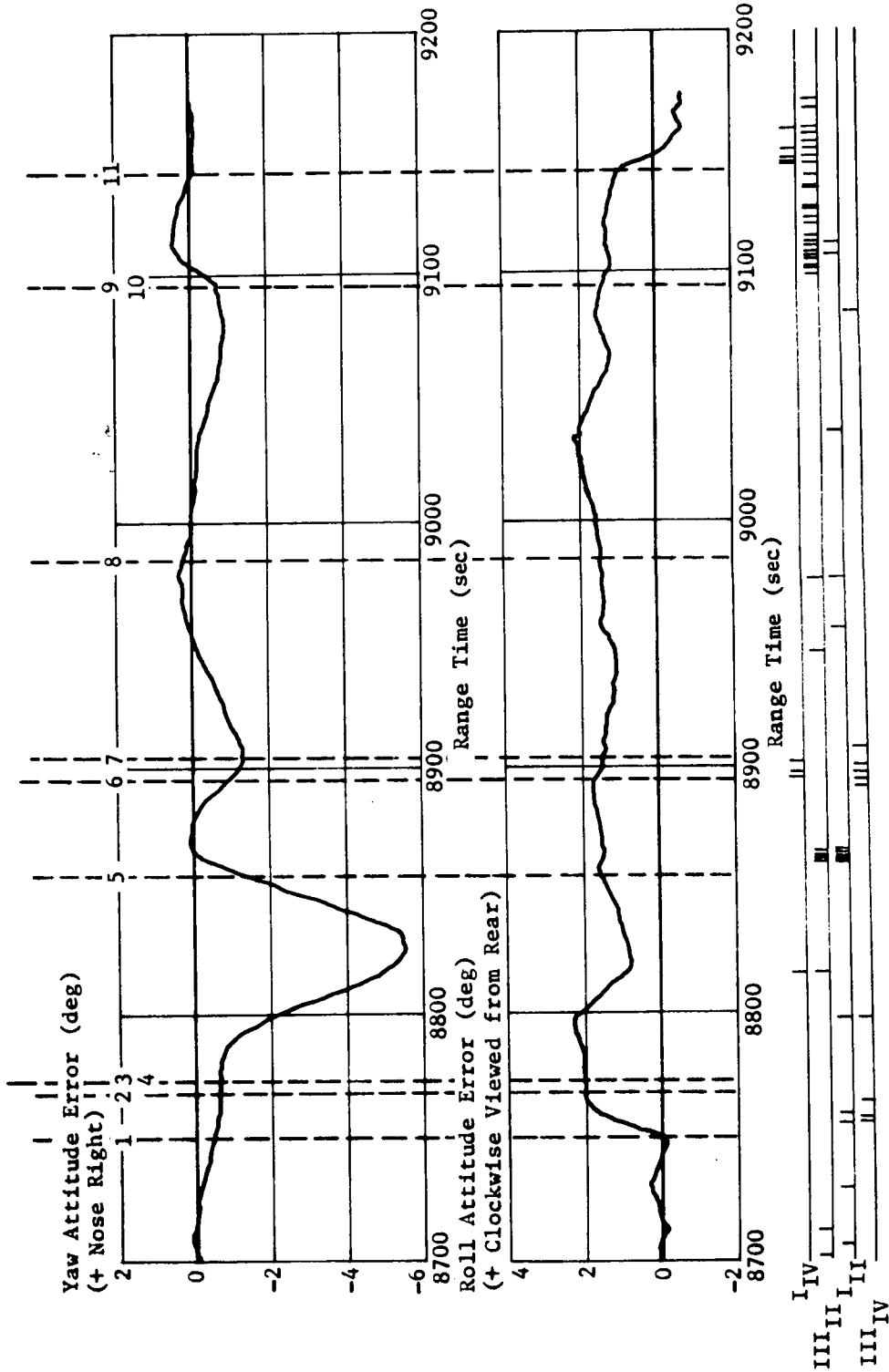


FIGURE 12-24 S-IVB ATTITUDE ERRORS AND APS FIRINGS DURING PROPELLANT REMOVAL TEST

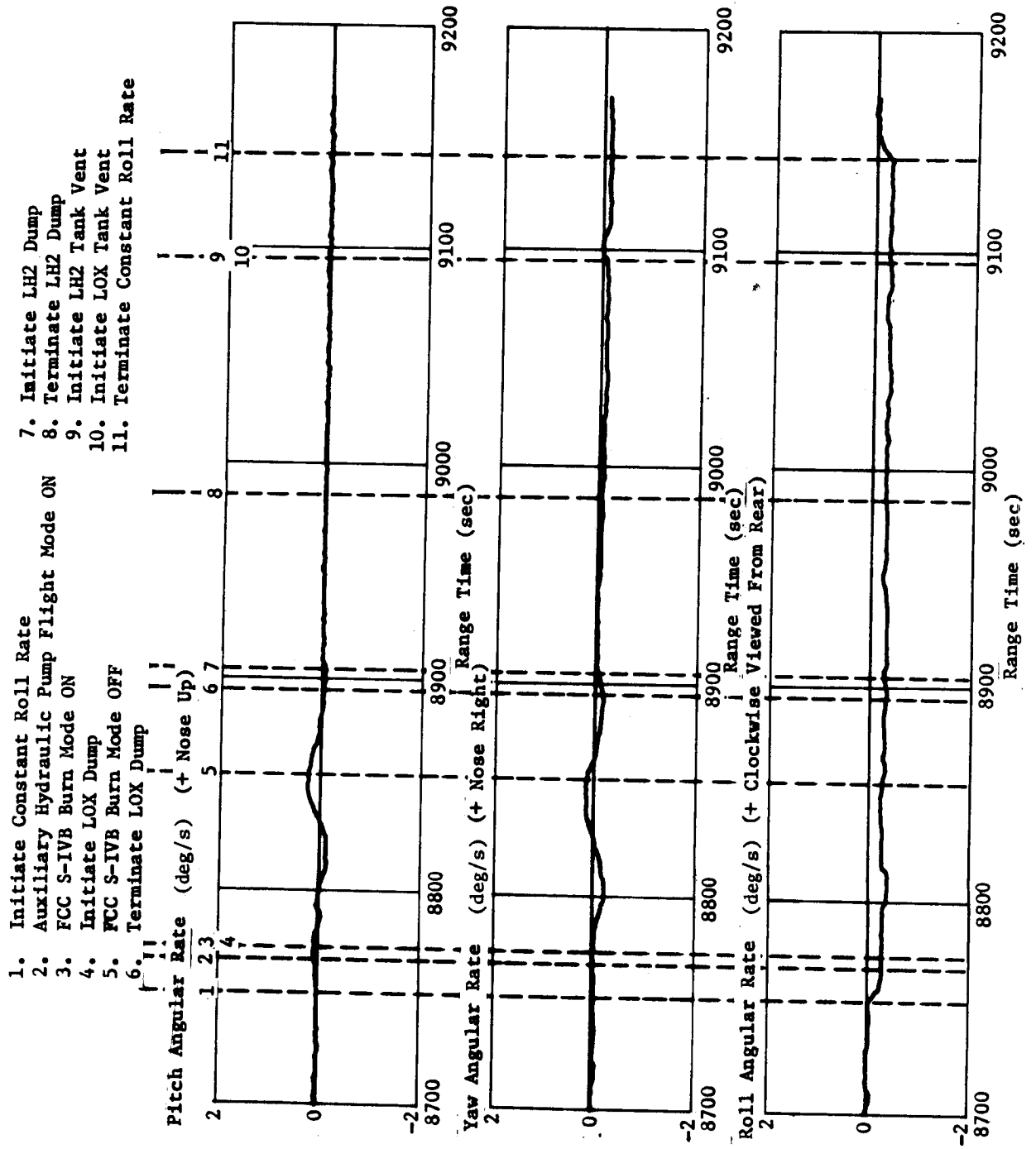


FIGURE 12-25 S-IVB ANGULAR RATE GYROS DURING PROPELLANT REMOVAL TEST

1. Auxiliary Hydraulic Pump Flight Mode ON
2. FCC S-IVB Burn Mode ON
3. Initiate LOX Dump
4. FCC S-IVB Burn Mode OFF

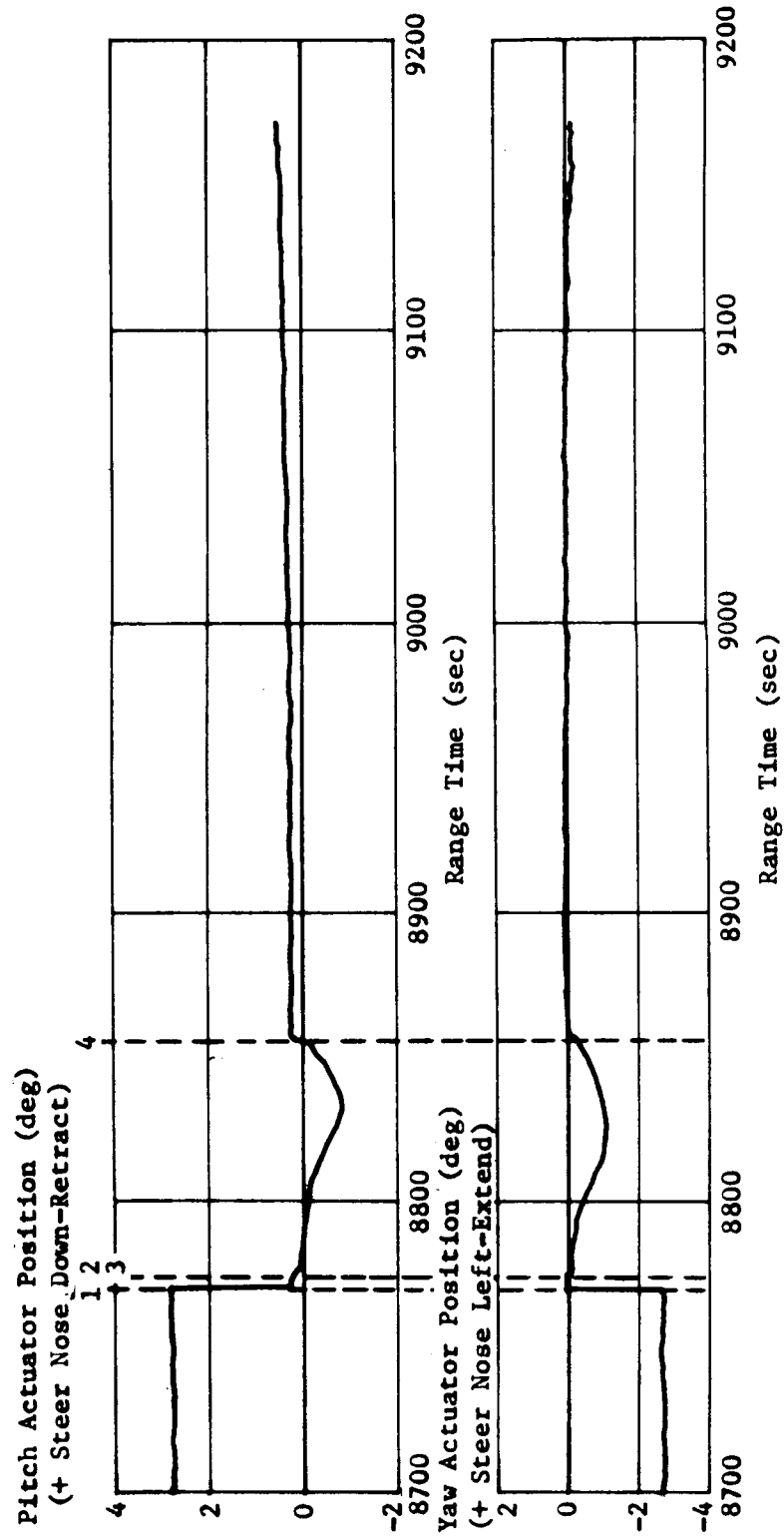


FIGURE 12-26 S-IVB ACTUATOR POSITION DURING PROPELLANT REMOVAL TEST

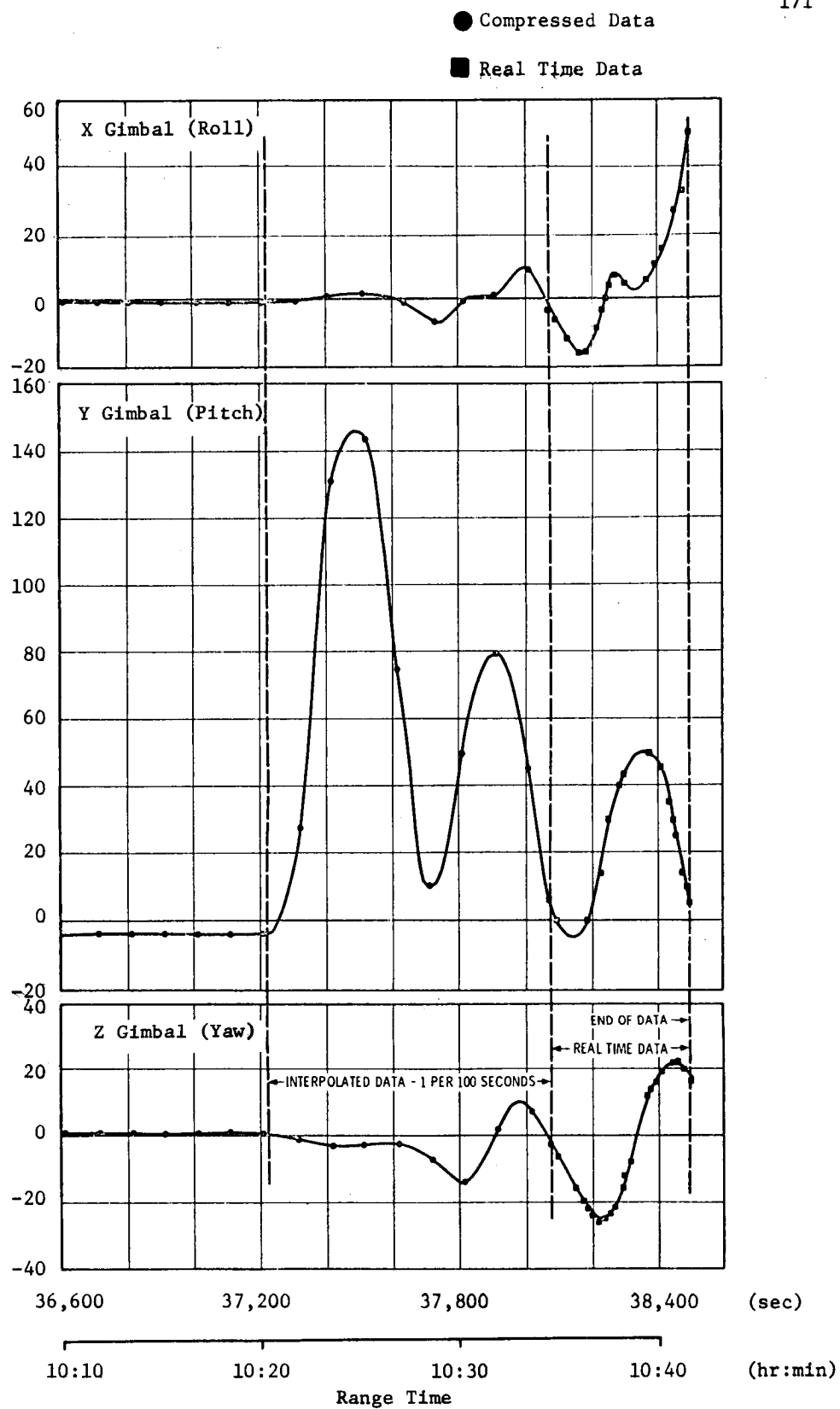


FIGURE 12-27 S-IVB PITCH, YAW, ROLL GIMBAL ANGLES (HAWAII, REV 7)

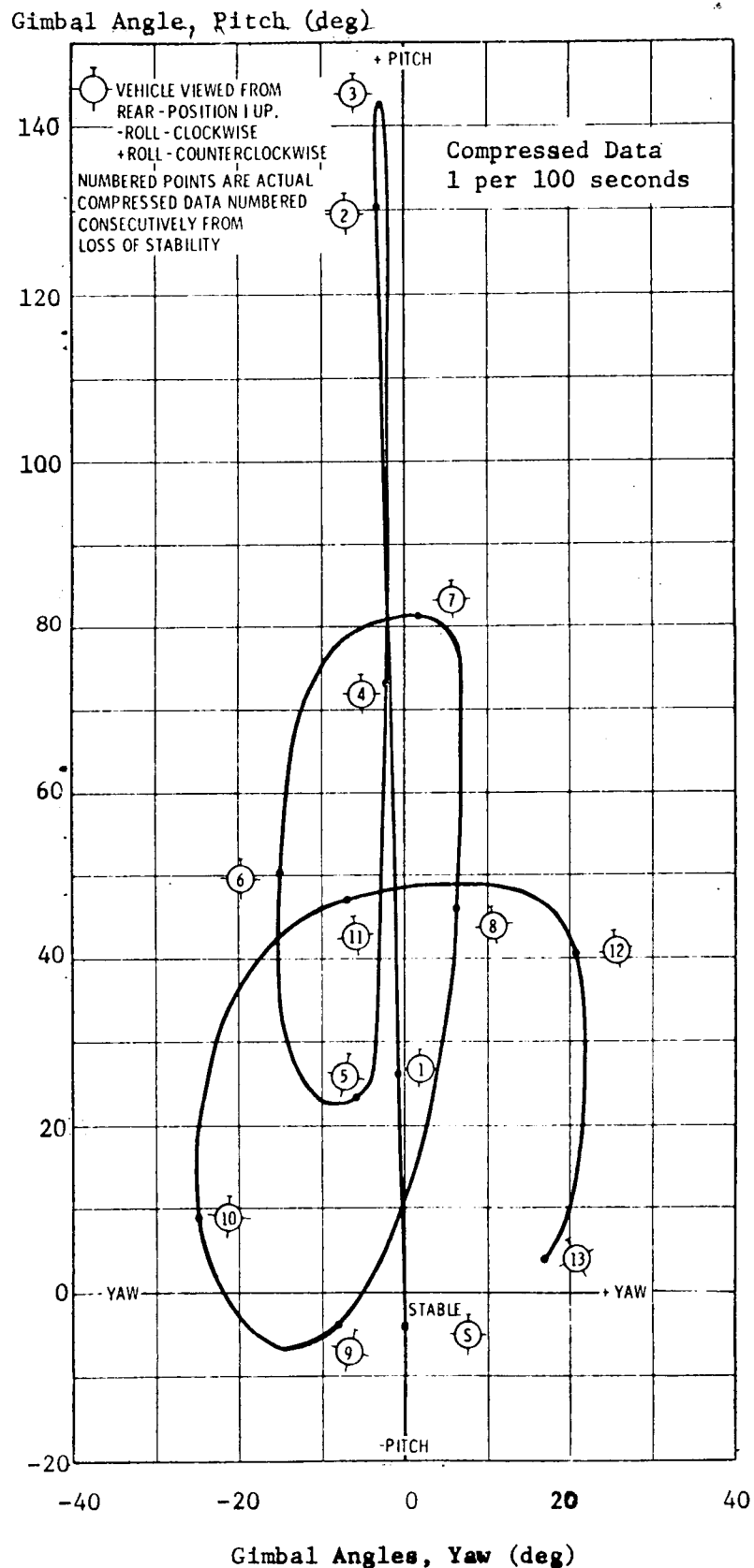


FIGURE 12-28 S-IVB COMPOSITE GIMBAL ANGLES (HAWAII, REV 7)

Axis	Rate (deg/s)	Amplitude (deg)	Period (sec)
Pitch	± 0.25	± 27	440
Yaw	± 0.23	± 25	440
Roll	± 0.17	Increasing	Continuous

Analyses to determine the exact cause for loss of attitude control on the spent stage between 37,208 sec and 37,308 sec have been hampered by lack of precise trajectory data for altitude and attitude time histories during this time interval. The S-IVB telemetry was not operating at this time and it was not possible to determine whether the APS had depleted propellant or ceased operating due to other causes. When the loss of control occurred, the vehicle was flying at a constant space-fixed attitude and the local angle-of-attack was approximately 80 deg (nose up).

The best trajectory available, based on a state vector established at 9117 sec (immediately after passivation), shows that perigee shifted and occurred between Tananarive and Hawaii at an altitude of approximately 141 kilometers. An investigation of the aerodynamics involved indicated that even at 141 km there is enough moment to cause the observed motion and that between 120 km and 140 km the aerodynamic forces would have been more than sufficient to cause the observed disturbance. Since the orbit would have had to decay to an altitude of about 105 km for aerodynamic forces to overcome the APS, the most probable cause for the loss of attitude control was APS propellant depletion coupled with aerodynamic forces. The APS had provided attitude control considerably in excess of the guaranteed lifetime.

12.3.4 CONTROL COMPONENT ANALYSIS

12.3.4.1 CONTROL ACCELEROMETERS

The two body-fixed control accelerometers located in the Instrument Unit (to provide load relief in the pitch and yaw planes from 30 to 110 seconds) functioned properly. The pitch control accelerometer maximum output was -0.93 m/s^2 at 72.1 seconds. The yaw control accelerometer reached a maximum of 0.83 m/s^2 at 72.5 seconds. Data from the control accelerometers are given in Figure 12-6. The telemetered data were filtered by a digital filter while the flight simulation data are the output of the control system filter in the analysis.

12.3.4.2 RATE GYROS

A triple redundant, $\pm 10 \text{ deg/s}$ range, 3 axis, rate gyro package located in the Instrument Unit was used to provide pitch, yaw, and roll

angular rate information for vehicle control throughout flight (Figures 12-5, 12-12, 12-19, 12-21, and 12-25). Analyses of the data indicate that the performance was nominal.

The pitch and roll rate gyros had a high frequency (17-18 Hz) content during the first 80 sec of the S-IVB flight. Examination of detailed S-IB oscillograms showed some 17-18 Hz signals in the roll channel during and immediately after liftoff but during the remainder of the S-IB stage flight only 23-26 Hz content of above noise level was noted.

The thrust vector control systems and the emergency detection system were unaffected by this 17-18 disturbance due to filters within these systems. In the APS System, used for roll control during S-IVB powered flight, the signals are not filtered and the system was affected.

The APS System is an on-off system fired by a combined signal of attitude error from the LVDC and control rate gyro output. The combined signals are summed and fed to a spatial amplifier that modulates the signal to produce APS firing commands. This system is non-linear and will not fire if the rate gyro input has a sufficiently high frequency and amplitude content to widen the spatial amplifier deadband to values above the LVDC attitude error output. Additionally if the amplitude is sufficient to saturate the spatial amplifiers such that an attitude error signal greater than 3.5 deg is required from the LVDC, then roll control authority can be lost.

From around 145 sec to 225 sec the roll rate gyros exhibited a 17-18 Hz oscillation that peaked around 185 sec at an amplitude of approximately 3.5 deg/s P-P. During this period of time, APS firings did not occur as frequently as required to maintain the roll attitude error within the nominal ± 1 deg operating limit. Laboratory test results indicate that the deadband is widened to approximately 4.6 deg for the peak amplitude stated above; i.e., the allowable LVDC commanded attitude error would have to be raised from 3.5 deg to 4.6 deg in order for the APS engines to fire. The roll attitude error input and rate input are shown in Figure 12-29.

The cause of the 17-18 Hz frequency is unknown but was observed on other instrumentation such as some S-IVB forward skirt vibration measurements and the ST-124M-3 platform accelerometers. This frequency is in the range of IU shell modes determined from dynamic tests.

Oscillations of 17-22 Hz have been observed on the rate gyro outputs of all Saturn IB and V flight tests. However, the amplitude and duration of oscillations were greater during AS-204 S-IVB burn than previously observed.

Action taken for AS-502 only was a software change; the LVDC roll attitude error limit was changed to ± 15.3 deg from the ± 3.5 deg previously utilized. The need for any action on vehicles subsequent to AS-502 is being investigated.

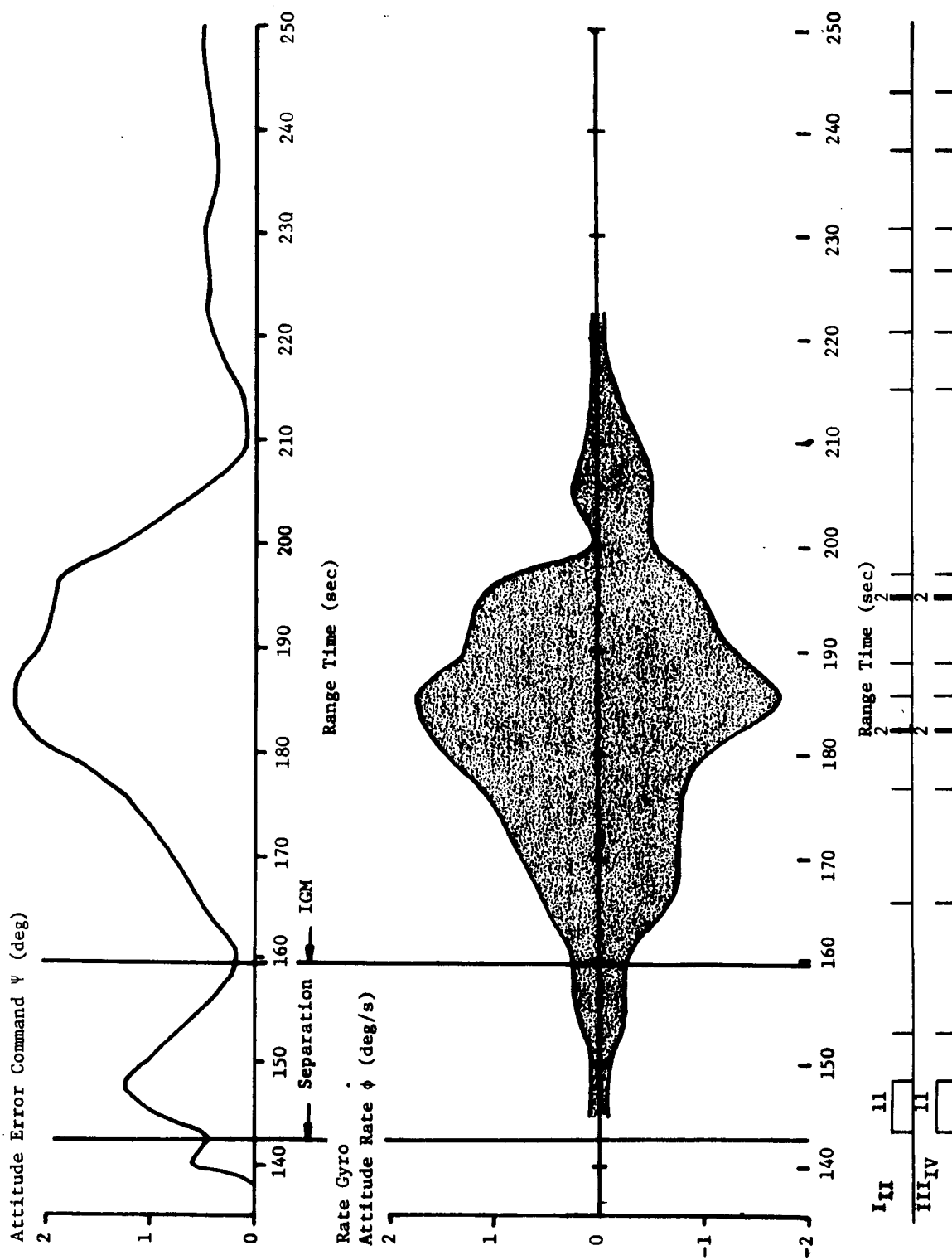


FIGURE 12-29 ROLL ATTITUDE ERROR AND ROLL RATE GYRO OUTPUT

12.3.4.3 ACTUATOR PERFORMANCE

All eight actuators performed smoothly during S-IB stage flight. In general, actuator activity was similar to AS-202. The maximum pitch gimbal angle of -1.76 deg occurred on engine 4 at 80.5 sec, and is 22% of the maximum 8 deg deflection. Engine 2 yaw actuator had the largest yaw gimbal angle, 1.47 deg at 72.8 sec or 18.4% of the maximum. The gimbal rates observed on AS-204 were considerably less than those on AS-203 and comparable with AS-202. The largest gimbal rate observed on AS-204 was on engine 3 pitch actuator, which reached 2.34 deg/s, 12.8% of the design loaded velocity limit of 18.3 deg/second.

The average actuator loads on AS-204 were less than those on AS-203 and more than AS-202. The largest torque observed on AS-204 was -16,218 N-m (11,962 lbf-ft) on engine 4 pitch at 80.3 seconds. This load is approximately 52% of the 31,184 N-m (23,000 lbf-ft) design torque for the component and 35% of the 46,369 N-m (34,200 lbf-ft) stall torque. The differential currents to the servo valves ranged from 6.8 to 10.3 percent of rated 12 ma current during S-IB stage flight. The largest differential current observed was on engine 2 pitch actuator and was 1.24 ma at 84.5 seconds.

The maximum values of each pitch and yaw performance parameter for any single actuator during liftoff, max Q, outboard engine cutoff, and S-IB stage flight are presented in Table 12-VI. It should be noted that, due to the physical mounting of the servo actuators, the polarity of their position in degrees may not agree with the polarity of the average actuator positions illustrated in Figure 12-7.

Both actuators of the S-IVB stage performed satisfactorily throughout the flight. The engine positioning commands from the control computer were correct and well within the load, gimbal rate, and torque capabilities of the actuators. The maximum actuator deflection was -1.1 deg during the propellant dump experiment on the yaw actuator, which also had the largest valve current, 7.4 ma, at that time. The maximum torque observed was 14,236 N-m (10,500 lbf-ft) which is 27% of the 53,555 N-m (39,500 lbf-ft) nominal design torque for the component. Table 12-VII presents the maximum of each pitch and yaw parameter during ignition, cutoff, flight and propellant dump.

12.4 LAUNCH VEHICLE NAVIGATION AND GUIDANCE

The overall performance of the navigation and guidance system (ST-124M-3 stabilized platform system, launch vehicle digital computer, and launch vehicle data adapter) was very satisfactory. An analysis of the telemetered guidance data is discussed in subsequent parts of this section.

TABLE 12-VI
S-IB ACTUATOR MAXIMUM PERFORMANCE DATA*

177

Parameters	Units	Axis	Liftoff	max Q	OECO	Flight
Gimbal Angle	deg	Pitch	-0.18	-1.41	-0.11	-1.76
		Yaw	-0.27	0.96	-0.26	1.47
Gimbal Rate	deg/sec	Pitch	1.24	-0.30	0.26	2.34
		Yaw	-1.52	0.46	0.78	1.90
Torque	N-m	Pitch	-13236	-13826	-7441	-16,218
		Yaw	-4505	-8482	4024	-10,020
	lb-ft	Pitch	-9763	-10197	-5488	-11,962
		Yaw	-3323	-6256	2967	-7,390
Valve Current	ma	Pitch	-0.74	-0.20	0.26	1.24
		Yaw	0.99	-0.80	0.33	-1.03

*The values represent the maximum from the 4 pitch and 4 yaw actuators and are not necessarily from the same actuator for any parameter or event.

TABLE 12-VII
S-IVB ACTUATOR MAXIMUM PARAMETERS

Parameters	Units	Axis	Ignition	Cutoff	Flight	Propellant Dump
Gimbal Angle	deg	Pitch	-0.16	0.20	-0.64	-0.8
		Yaw	-0.30	-0.80	-0.96	-1.1
Gimbal Rate	deg/s	Pitch	0.14	0.03	0.35	0.044
		Yaw	0.15	0.0	0.33	0.040
Torque	N-m	Pitch	295.4	0	14,236	1167
		Yaw*				
	lbf-ft	Pitch	291.6	0	10,500	1582
		Yaw*				
Valve Current	ma	Pitch	-2.0	-0.4	-5.7	-5.4
		Yaw	-2.0	1.3	2.5	7.4

*No Values Obtained Due to Malfunction of Transducer D45

12.4.1 NAVIGATION AND GUIDANCE SCHEME PERFORMANCE ANALYSIS

The flight program performance was normal. The navigation and guidance schemes functioned properly. The control calculations were correct, and orbital operation was as expected.

The cross range (Y) accelerometer exceeded a reasonableness test value just prior to liftoff which resulted in the accumulation of a 0.45 m/s velocity bias error which remained throughout the flight (Figure 12-30). A very strict reasonableness test constant (0.3 m/s) had been imposed near liftoff as an interim fix to limit the magnitude of erroneous accelerations caused by vibration as encountered on previous flights. Vehicle navigation and orbital insertion goals were not affected by the velocity bias error.

A yaw offset of -1.5 deg developed during the S-IVB stage ullage ignition (Figure 12-31). Initiation of active control approximately 0.2 sec later moved the engine to correct for the negative yaw. With a considerable increase in thrust at S-IVB stage ignition, a yaw overshoot to 2.1 deg occurred. The vehicle returned to 1.6 deg in yaw offset when IGM was initiated. IGM guidance commanded the vehicle to 3.5 deg yaw but the vehicle responded to only 2.0 deg because of center-of-gravity offset and thrust misalignment. Increased yaw and proper guidance resulted when the yaw Steering Misalignment Corrections (SMCZ) were initiated and increased the chi value. The negative yaw offset remained throughout S-IVB stage burn. With the proper execution of the SMCZ calculations, navigation and orbital insertion conditions were not impaired as a result of the yaw offset.

At S-IVB stage cutoff, a 7.5 deg yaw chi command existed in the control system. This yaw command was the final chi value computed for the IGM freeze period prior to S-IVB stage cutoff. It was the accumulation of a 3.5 deg desired yaw command and a 2.0 deg yaw steering correction multiplied by a factor of two after the FCC switch point 4 for the control gain change program at 285.8 seconds. A positive yaw rate of 0.7 deg/s was developed immediately following S-IVB stage cutoff. Indications are that this perturbation was primarily caused by LOX venting with contributions from J-2 engine thrust decay. The perturbation yawed the vehicle to 8.1 degrees. The APS stabilized the vehicle at the final chi command of 7.5 degrees. Even without the perturbation, the APS would have yawed the vehicle to the final chi value.

The vehicle end conditions at S-IVB stage guidance cutoff as determined from LVDC telemetry and compared to preflight predicted values (actual-predicted) were -0.018 km in radius, 0.01 m/s in space-fixed velocity vector, and -0.008 deg in path angle from the local horizontal.

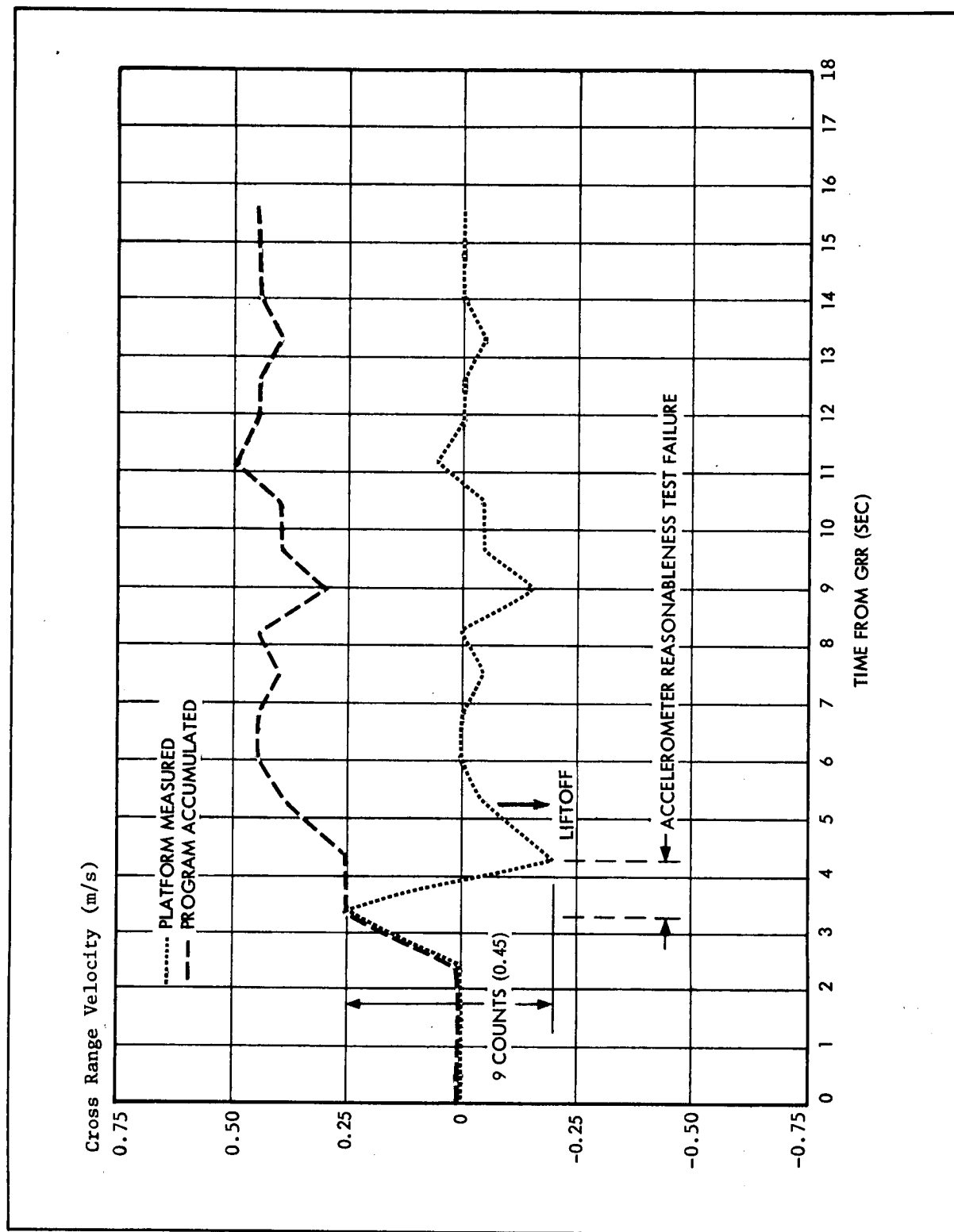


FIGURE 12-30 CROSSRANGE (Y) COMPONENT OF INERTIAL VELOCITY

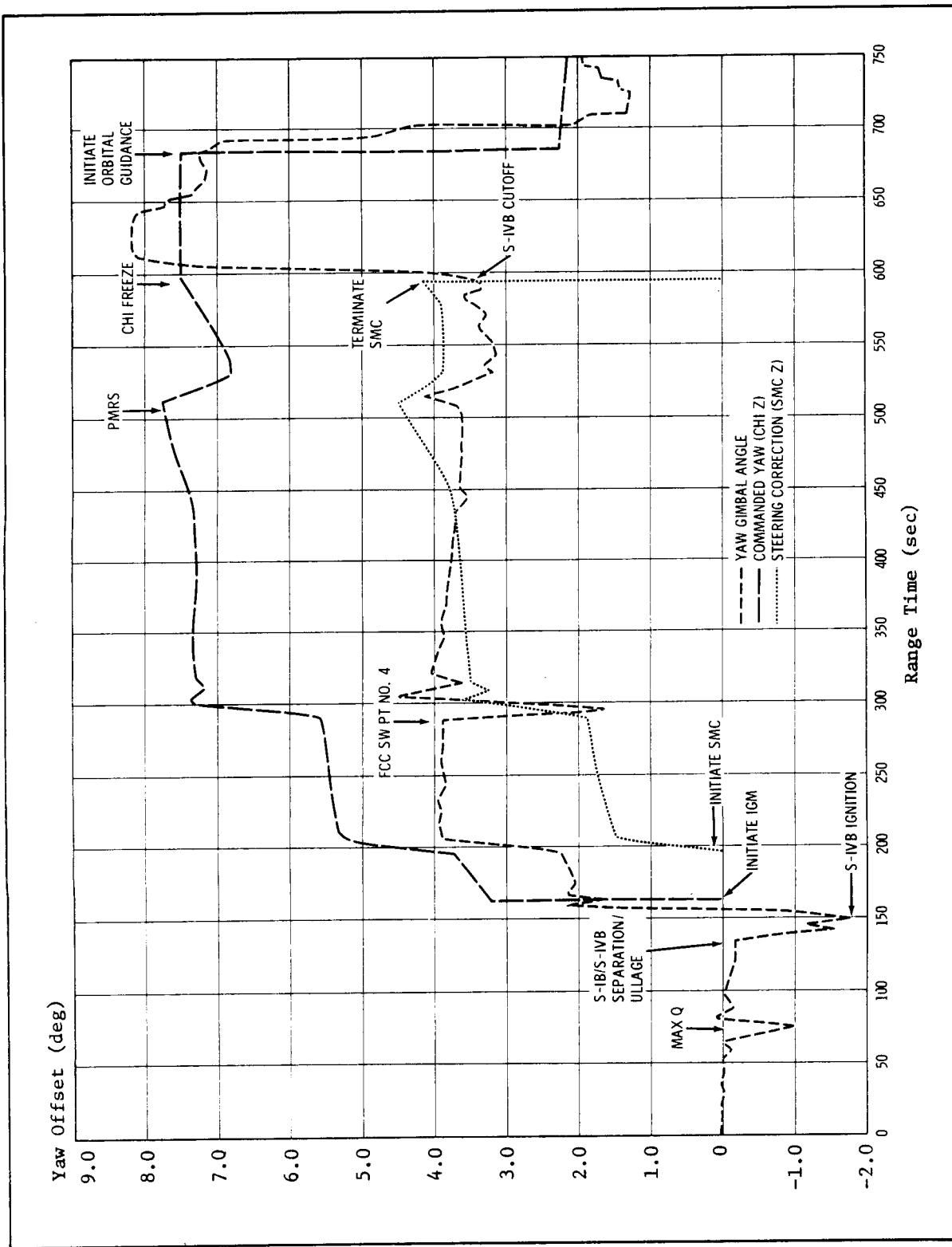


FIGURE 12-31 YAW OFFSET AND S-IVB STAGE CUTOFF CONDITIONS

The programmed orbital maneuvers were completely satisfactory during orbital guidance. Table 12-VIII depicts the start and completion times of the commanded maneuvers and the vehicle attitudes achieved. Pitch attitudes are referenced to the local horizontal. The times indicated are times when the maneuver was started and when the vehicle was restabilized. The position achieved were within the 1 deg limit of the calculated commands. The commands were calculated on insertion conditions. The predicted attitudes were obtained from the preflight operational trajectory.

12.4.2 NAVIGATION AND GUIDANCE COMPARISON

12.4.2.1 POWERED FLIGHT COMPARISON

Comparisons between the final post-flight trajectory and the telemetered guidance platform velocities are shown for the powered flight in Figure 12-32. The differences shown for the pitch plane, X and Z velocity differences, indicated very good agreement with the trajectory. The differences are well within the accuracy of the data compared.

The telemetered cross range velocity was adjusted by 0.45 m/s for the invalid velocity accumulated prior to liftoff. The differences shown for cross range velocity are larger than desired, however, the value at S-IVB cutoff is within 1 m/s of the error expected from preflight hardware measurements.

Orbital telemetry from about 640 sec to 3150 sec was used to determine bias associated with the individual accelerometers. The bias errors were small and may be compared with values presented in memorandum R-ASTR-G-339-66, "Test Data From S/N 8 Platform System For AS-204." The X bias term was about one third the magnitude and opposite in sign, the Y bias term was about the same magnitude and opposite sign, and the Z bias term was approximately equal the referenced value. The test data do not necessarily apply to the platform system flown on AS-204 since accelerometer change-out occurred, it is given as a reference only.

The guidance platform measured velocities, along with corresponding data from both the post-flight and operational trajectories, are shown at significant powered flight events in Table 12-IX. The differences between the telemetered velocities and preflight (operational) data are the results of nonstandard flight performance and conditions. The differences between the telemetered and post-flight trajectory velocities are relatively small and reflect tracking errors in addition to small guidance hardware errors. The differences are within the accuracy of the data compared except for cross range velocity which is insignificant



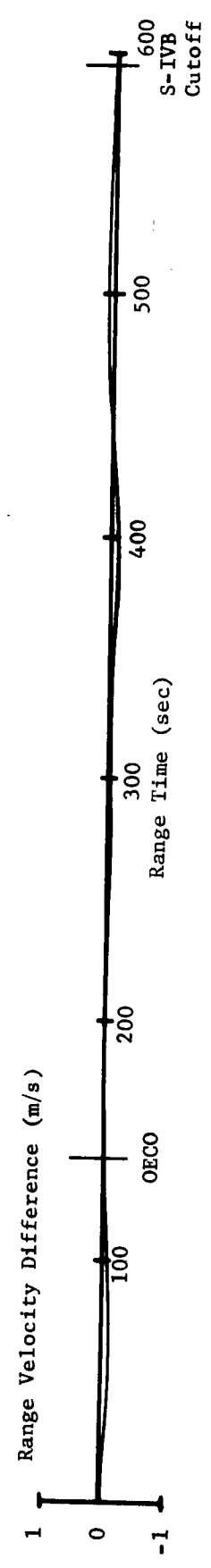
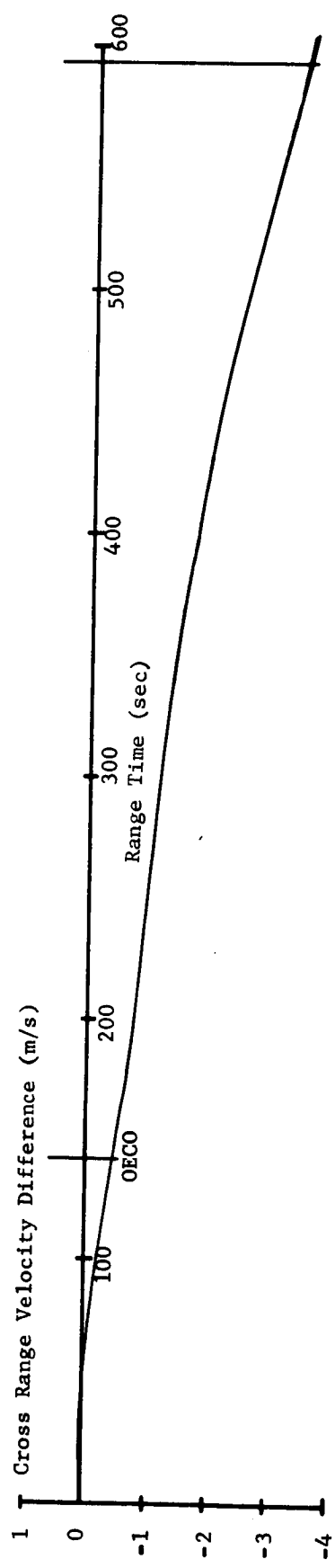
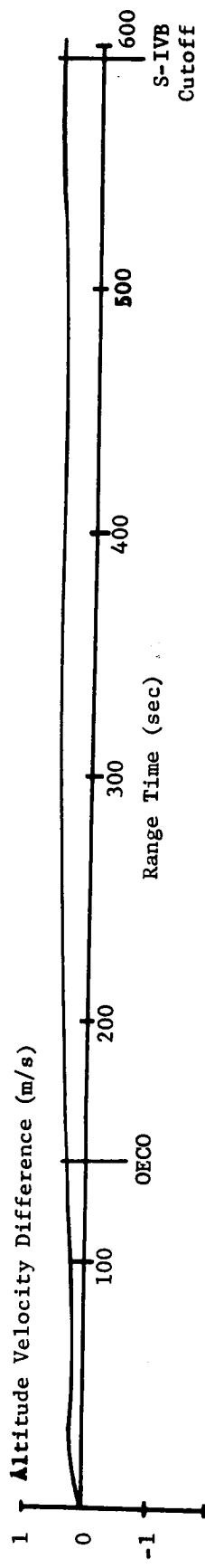


FIGURE 12-32 GUIDANCE VELOCITY DIFFERENCES
(TRAJECTORY MINUS MEASURED)

TABLE 12-IX
GUIDANCE INERTIAL PLATFORM VELOCITY COMPARISON

Events Range Time (sec)	*	Telemetered	Trajectory	
		Accelerometer **	Postflight	Preflight
O E C O 142.25	X_m	2496.13	2496.42	2489.01
	Y_m	-1.35	-1.87	-3.98
	Z_m	1713.17	1731.03	1738.36
I G M 159.48	X_m	2541.95	2542.27	2534.67
	Y_m	-3.85	-4.49	-4.96
	Z_m	1809.48	1809.45	1816.69
S-IVB C O 593.35	X_m	3188.10	3188.64	3195.31
	Y_m	332.62	328.84	333.47
	Z_m	7605.93	7605.60	7609.16
Insertion 603.35	X_m	3187.20	3187.70	3194.17
	Y_m	332.95	329.23	333.84
	Z_m	7613.35	7613.37	7616.28

* X_m Altitude Velocity (m/s)

Y_m Cross Range Velocity (m/s)

Z_m Range Velocity (m/s)

**Telemetered cross range velocity was adjusted by 0.45 m/s to compensate for velocity accumulated prior to liftoff.

with respect to the necessary end conditions for insertion into orbit. The telemetered cross range velocity values shown were taken from LVDA telemetry and do not include the 0.45 m/s accumulated error prior to liftoff. However, this error is reflected in the navigation data shown in Table 12-X.

Velocity increase due to thrust decay after S-IVB cutoff was very close to the expected value. The measured velocity vector increase was 6.4 m/s compared with the predicted 5.8 m/s increase.

Navigation parameters are presented in Table 12-X for S-IB separation, S-IVB cutoff, and orbital insertion (S-IVB cutoff + 10 sec). Telemetered values are shown along with predicted and post-flight trajectory data. Since S-IB powered flight utilizes open-loop guidance with attitude control only, the guidance measurements do not necessarily agree with the operational trajectory at stage separation. After IGM is initiated, the guidance system computes and issues commands to guide the vehicle to the prescribed conditions for S-IVB cutoff to insure the desired orbit. Comparison of the telemetered and predicted position, velocity vector, and path angle indicate that the guidance system performed well within tolerances. The actual cutoff velocity, as indicated by guidance, was within 0.01 m/s of the prescribed value. At insertion the velocity difference was 0.2 m/s, which reflects differences between actual and predicted thrust decay and propulsive LOX venting during this 10 sec period. The guidance data are in very good agreement with the post-flight trajectory data except in cross range which does include the initial 0.45 m/s error. The difference between the telemetered and post-flight trajectory cutoff velocity was only 0.36 m/second.

12.4.2.2 MEASURED VELOCITY CHANGES DURING ORBIT

Figure 12-33 presents the measured and predicted inertial velocity change from S-IVB cutoff through about 40 sec of LOX venting, LM separation, LOX and LH₂ passivation with about 500 sec of LOX vent after passivation, and LOX venting with the helium valve open. Predicted values were not available for the LM separation and the helium valve open.

Velocity changes which include venting effects following S-IVB cutoff are referenced to cutoff time as the common base for both actual and predicted values. The total change includes thrust decay as well as venting effects. The LOX tank vent valve opened 0.4 sec after cutoff and closed after about 40 sec of venting. At cutoff plus 2 sec the actual velocity change was about 0.2 m/s greater than predicted but when the vent valve closed the predicted value was about 0.1 m/s greater than actual. This indicates a slightly greater velocity increase due to engine thrust decay and less venting effect than predicted. The overall effect was essentially the same as predicted.

TABLE 12-X
NAVIGATION COMPARISON

Event	Parameter	Symbol	Units	Envelope Tolerance	Guidance Computer	Trajectory	
						Post Flight	Predicted
S-IB Stage Separation	Position						
	Altitude	X_S	km	NA	6436.246	6436.283	6435.696
	Cross Range	Y_S	km	NA	35.826	35.774	35.477
	Range	Z_S	km	NA	115.965	115.970	116.174
	Radial Distance	R_S	km	+3.06 -4.16	6437.38	6437.427	6436.843
	Velocity						
	Altitude	\dot{X}_S	m/s	NA	1049.48	1049.86	1042.34
	Cross Range	\dot{Y}_S	m/s	NA	121.03	120.33	118.28
	Range	\dot{Z}_S	m/s	NA	2116.54	2116.53	2124.72
	Total Velocity	V_S	m/s	+58.1 -70.1	2365.49	2365.67	2369.58
	Path Angle	θ	deg	+2.51 -3.94	27.38	27.39	27.15
S-IVB Cutoff	Position						
	Altitude	X_S	km	NA	6217.098	6217.402	6206.692
	Cross Range	Y_S	km	NA	140.249	139.198	142.015
	Range	Z_S	km	NA	2010.283	2010.224	2042.110
	Radial Distance	R_S	km	± 1.07	6535.531	6535.784	6535.549
	Velocity						
	Altitude	\dot{X}_S	m/s	NA	-2413.07	-2412.20	-2450.10
	Cross Range	\dot{Y}_S	m/s	NA	411.53	407.64	411.04
	Range	\dot{Z}_S	m/s	NA	7428.55	7428.65	7416.46
	Total Velocity	V_S	m/s	± 5.9	7821.50	7821.14	7821.49
	Path Angle	θ	deg	± 0.063	-0.012	-0.009	-0.004
Orbital Insertion	Position						
	Altitude	X_S	km	NA	6192.513	6192.828	6181.739
	Cross Range	Y_S	km	NA	144.359	143.268	146.120
	Range	Z_S	km	NA	2084.497	2084.435	2116.190
	Radial Distance	R_S	km	± 1.07	6535.532	6535.787	6535.557
	Velocity						
	Altitude	\dot{X}_S	m/s	NA	-2502.60	-2501.76	-2539.69
	Cross Range	\dot{Y}_S	m/s	NA	409.97	406.13	409.49
	Range	\dot{Z}_S	m/s	NA	7406.72	7406.82	7393.86
	Total Velocity	V_S	m/s	± 5.9	7828.82	7828.46	7828.60
	Path Angle	θ	deg	± 0.063	0.002	0.005	0.008

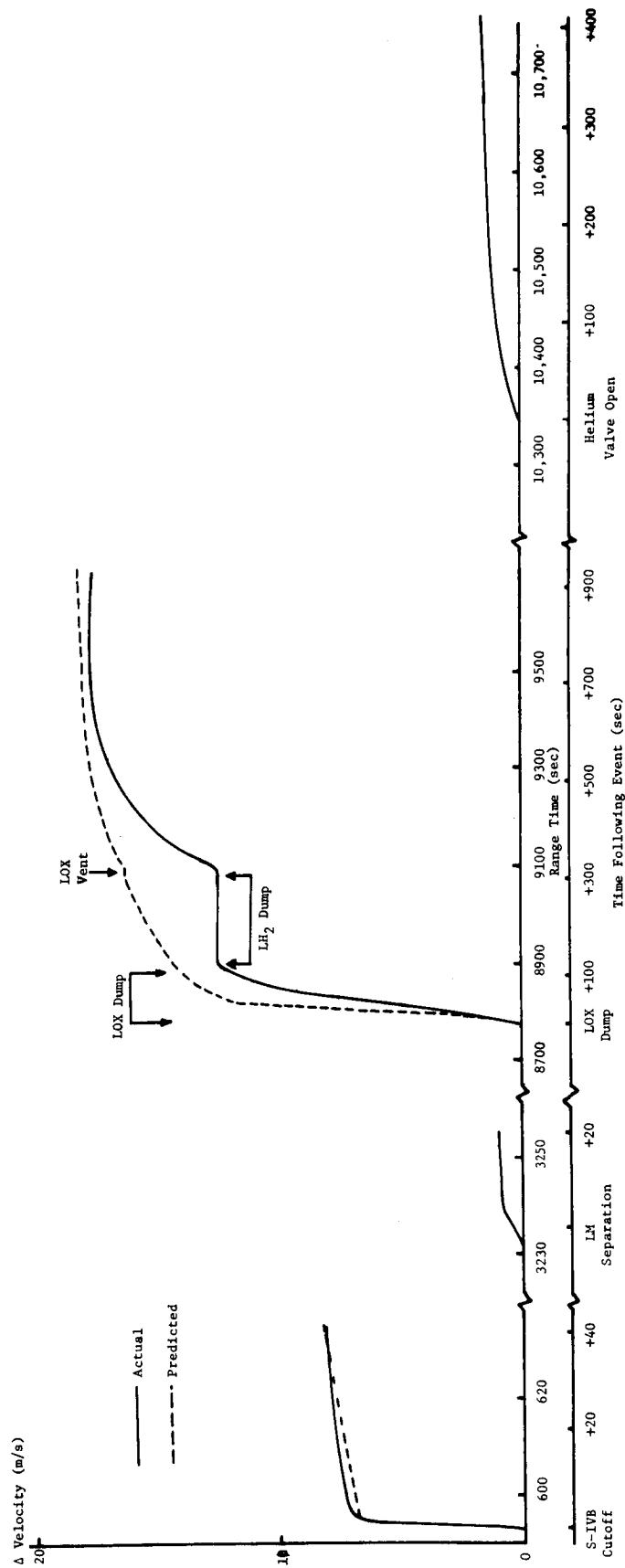


FIGURE 12-33 MEASURED VELOCITY CHANGE ORBITAL EVENTS

Spacecraft Lunar Module Adapter (SLA) Panel deployment A and B occurred at 1193.51 and 1193.71 sec range time, respectively. Telemetry coverage was received from Canary Island from about 1022 sec to 1415 second. During this 393 sec period only one velocity pulse (0.05 m/s) was noted in each of range and cross range accelerometer outputs and no change was noted in the altitude accelerometer output. The pulse outputs of the range and cross range accelerometers cannot be attributed to the SLA deployment. A small bias error of $1.3 \times 10^{-4} \text{ m/s}^2$ would cause a velocity output of 0.05 m/s during this period of time.

The velocity change due to LM separation was essentially all along the range accelerometer axis for a total of about 1.0 m/second. One pulse (0.05 m/s) change was observed from the altitude accelerometer. Since the vehicle pitch attitude at the time of LM separation (3235.24 sec) was about 177.6 deg from the platform range axis, the measured 1.0 m/s velocity change was positive, indicating a deceleration.

LOX purge began with engine mainstage control valve open at 8774.31 sec and ended 120.20 sec later. The measured velocity change during LOX purge was 12.5 m/s compared with a predicted value of 14.1 m/second. The difference was probably due to variation in the propellant mass onboard to be dumped (see Section 9.6.3).

Engine ignition phase control valve open occurred at 8904.31 sec and closed at 9084.51 sec range time. LH_2 purge occurred during this period. However, prior to this time all the liquid in the tank evidently had boiled off and vented overboard. The velocity change during this 180 sec period was less than 0.1 m/s compared with a predicted value of about 2.3 m/second. At 9094.51 sec the LOX tank vent valve opened. The velocity increase during 500 sec of LOX venting was 5.2 m/s compared to 1.8 m/s predicted. The velocity change during the first 40 sec of this vent was 1.8 m/s compared to 1.1 m/s due to venting immediately following S-IVB cutoff. The average acceleration from 9095 to 9135 sec was 0.044 m/s^2 , which indicates a force of about 641 N (144 lbf) from the propulsive LOX vent. The average acceleration between end of thrust decay and S-IVB cutoff plus 40 sec was 0.026 m/s^2 which indicates a force of about 827 N (186 lbf) from the propulsive vent.

LOX tank pressurization shutoff valves opened at 10349.51 seconds. The helium gas escaped through the LOX vent valve, generating a small thrust. The velocity change from 10349.51 to 10660 sec was 1.27 m/second. The average acceleration over this time period was 0.0049 m/s^2 which indicates an average force of about 53 N (12 lbf) from the propulsive helium purge.

Velocity changes shown in Figure 12-33, both actual and predicted, are root sum square (RSS) values of changes in platform measured velocity components (vector differences).

12.4.3 GUIDANCE SYSTEM COMPONENT ANALYSIS

12.4.3.1 LVDC/LVDA ANALYSIS

The LVDC and LVDA performed satisfactorily and as predicted for the AS-204 flight. No valid error monitor words and no-self test error were observed that indicate any deviation from correct operation of the LVDC.

Five error monitor words were observed on compressed data which indicate apparent disagreements in the TMR Orbital Check Ready (OCR) latch associated with the LVDA Computer Interface Unit (CIU) interrupt logic. The apparent disagreement is attributed to a difference between rise delay times for the TMR interrupt input logic channels. The disagreement did not impact mission requirements. With the exception of the error monitor words, no deviation from correct operation of the LVDA was observed.

12.4.3.2 ST-124M-3 STABILIZED PLATFORM ANALYSIS

The performance of the ST-124M-3 inertial platform and associated equipment was nominal. The accelerometer pickup and servo amplifier output signals indicated normal loop operation. The oscillations seen in the accelerometer signals were typical vibration response characteristics noted in all previous vehicles. The gyro pickup and servo amplifier output signals indicated that inertial reference was maintained throughout the entire mission. The accelerometer servo loops maintained the accelerometer float within the measuring head stops (± 6 deg) throughout the flight. The accelerometer encoder outputs indicated that the accelerometers correctly measured thrust acceleration throughout the boost phase of flight. The effects of vibration on the ST-124M-3 inertial platform were minimal. There were no malfunctions due to vibrations as noted on AS-202 and AS-203. The vibration profile of the AS-204 ST-124M-3 inertial platform most nearly resembled that of AS-203, and was significantly lower than AS-202 during critical flight periods. The stabilization and accelerometer loops were operating normally through the pass over telemetry station Hawaii in revolution seven (10 hr: 30 min: 27 sec range time).

13.0 SEPARATION

13.1 SUMMARY

S-IB/S-IVB separation was accomplished as planned and the sequence executed in the desired time period. The S-IVB engine cleared the interstage approximately 0.97 sec following the separation command. Separation transients were small and within the design requirements.

LV/LM-1 separation occurred at 3235.24 seconds. Small transients were imparted to the S-IVB during separation but were within design requirements.

13.2 S-IB/S-IVB SEPARATION

13.2.1 ULLAGE MOTOR PERFORMANCE

Three Thiokol TX-280 solid propellant motors equally spaced circumferentially provide a positive acceleration to the S-IVB stage to settle propellants for J-2 engine start.

Ullage motor performance was satisfactory. The ullage rocket ignition command was given at 143.30 sec, with the jettison command at 155.21 seconds. Table 13-I presents the individual rocket motor performance parameters as defined by the specification. A comparison of these data with nominal performance limits indicates that the three motors performed within design specifications. Figure 13-1 presents the thrust profiles during firing.

13.2.2 RETROROCKET PERFORMANCE

The S-IB-4 stage retrorockets are solid propellant Thiokol TE-M-29-5 Recruits which provide a one-retrorocket-out capability as scheduled for S-IB-3 and subsequent stages. Because of a possible retrorocket case burn-through on S-IB-2, the following modifications were made: (1) insulation was added to the inside of the motor case at the nozzle end, before loading of the propellant grain; (2) the cut surface of the propellant grain at the nozzle end was coated with an inhibitor to prevent burning of the cut surface (end burning); and (3) the space between the nozzle adapter and the propellant grain was filled with sealant.

Performance of the retrorockets was satisfactory. The retrorocket ignition command was given at 143.50 sec and ignition was at 143.58 seconds. Performance parameters of the retrorockets are shown in Table 13-II. Figure 13-2 presents retrorocket thrust versus time of each rocket.

TABLE 13-I ULLAGE MOTOR PERFORMANCE

Parameter	Units	Motor 1 (Pos I-II)	Motor 2 (Pos II-III)	Motor 3 (Pos IV-I)	Nominal Performance Limits	
					Maximum	Minimum
Action Time*	(Sec)	5.83	5.80	5.82	6.08	5.01
Burn Time**	(Sec)	3.84	3.80	3.83	4.10	3.54
Maximum Chamber Pressure	N/cm ²	714	721	726	841	621
	psi	1035	1045	1053	1220	900
Maximum Ignition Chamber Pressure	N/cm ²	722	741	757	1014	---
	psi	1047	1075	1098	1470	---
Average Action Time Chamber Pressure	N/cm ²	516	518	525	607	469
	psi	748	752	762	880	680
Average Burn Time Chamber Pressure	N/cm ²	690	698	705	758	614
	psi	1001	1012	1022	1100	890
Maximum Thrust	N	15,974	16,129	16,254	18,460	11,565
	lbf	3591	3626	3654	4150	2600
Maximum Ignition Thrust	N	16,160	16,592	16,948	22,686	---
	lbf	3633	3730	3810	5100	---
Average Action Time Thrust	N	11,552	11,605	11,761	13,545	10,431
	lbf	2597	2609	2644	3045	2345
Average Burn Time Thrust	N	15,444	15,618	15,778	16,841	13,749
	lbf	3472	3511	3547	3786	3090
Action Time Total Impulse	N-sec	67,337	67,302	68,458	69,370	63,765
	lbf-sec	15,138	15,130	15,390	15,595	14,335
Burn Time Total Impulse	N-sec	59,308	59,344	60,429	60,451	55,603
	lbf-sec	13,333	13,341	13,585	13,590	12,500

* The time interval between 10% of maximum chamber pressure during the start transient and 10% of maximum chamber pressure during the cutoff transient.

** The time interval between 10% of maximum chamber pressure during the start transient and 75% of maximum chamber pressure during the cutoff transient.

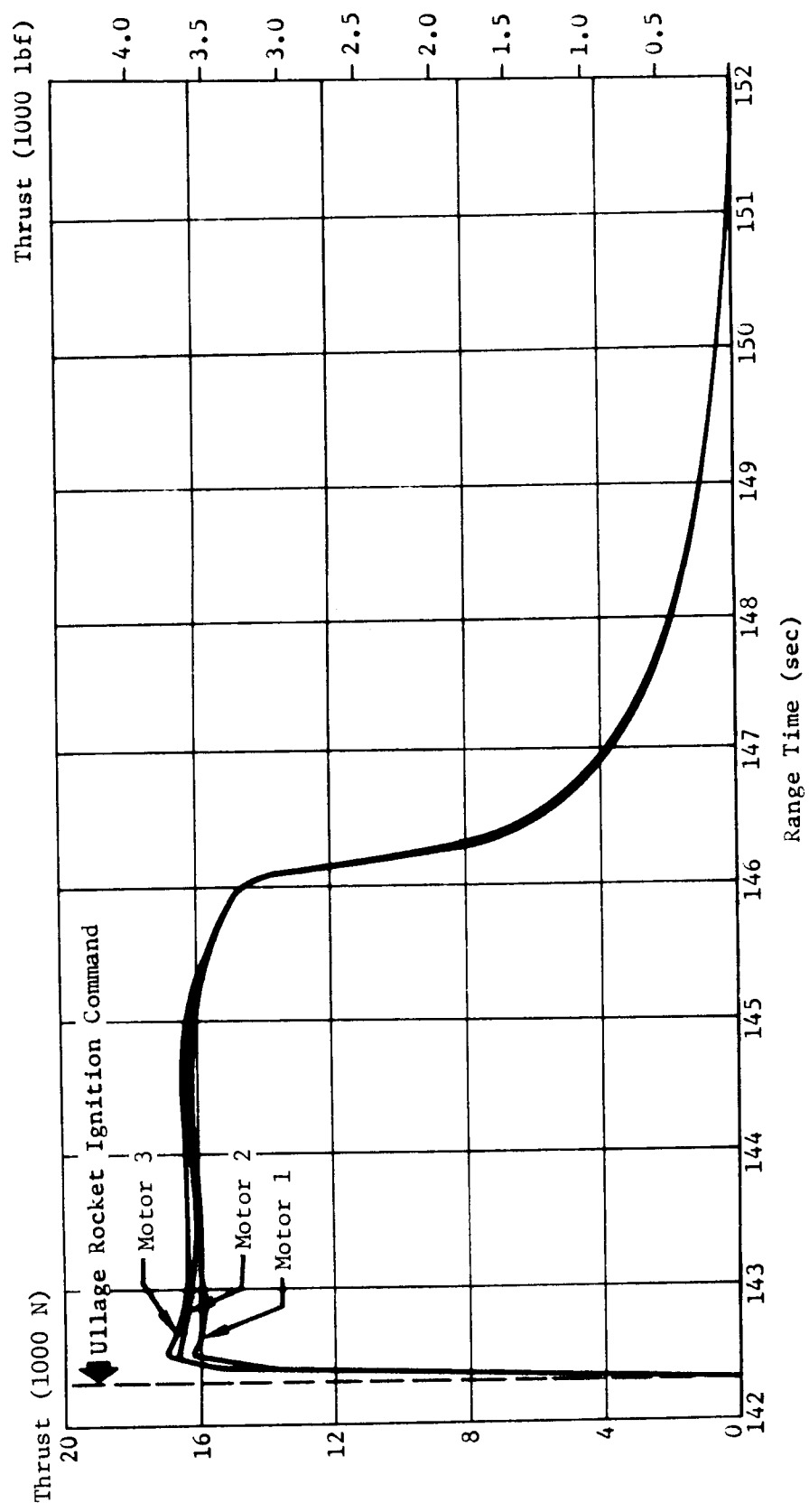


FIGURE 13-1 S-IVB ULLAGE MOTOR PERFORMANCE

TABLE 13-II RETROCKET PERFORMANCE

Parameters	Units	Rockets				Average	Nominal*
		1	2	3	4		
1. Burning Time	sec	1.510	1.536	1.542	1.541	1.532	1.508
2. Average Pressure	N/cm ² psi	1211 1756	1182 1714	1182 1714	1186 1720	1190 1726	1208 1752
3. Average Thrust	N lbf	170,247 38,273	166,119 37,345	166,128 37,347	166,604 37,454	167,275 37,605	169,170 38,031
4. Total Impulse	N-s lbf-s	257,072 57,792	255,159 57,362	256,169 57,589	256,734 57,716	256,284 57,615	255,110 57,351

1. Burning Time; The interval between the time at which the pressure attains 10% of the maximum pressure during the buildup portion of the pressure curve, and the time at which the bisector of an angle formed by the intersection of a line tangent to the pressure curve just prior to decay and a line tangent to the descending portion of the pressure curve intersects the pressure curve.

2. Average Pressure; Average of pressure during the burning time.

3. Average Thrust; Average of the thrust during the burning time.

4. Total Impulse; Area under the thrust-versus-time curve during the burning time.

*The results of one firing of the TE-M-29-5 solid motor with a grain temperature of 288.71°K (60°F) were extrapolated to vacuum conditions to obtain the nominal values.

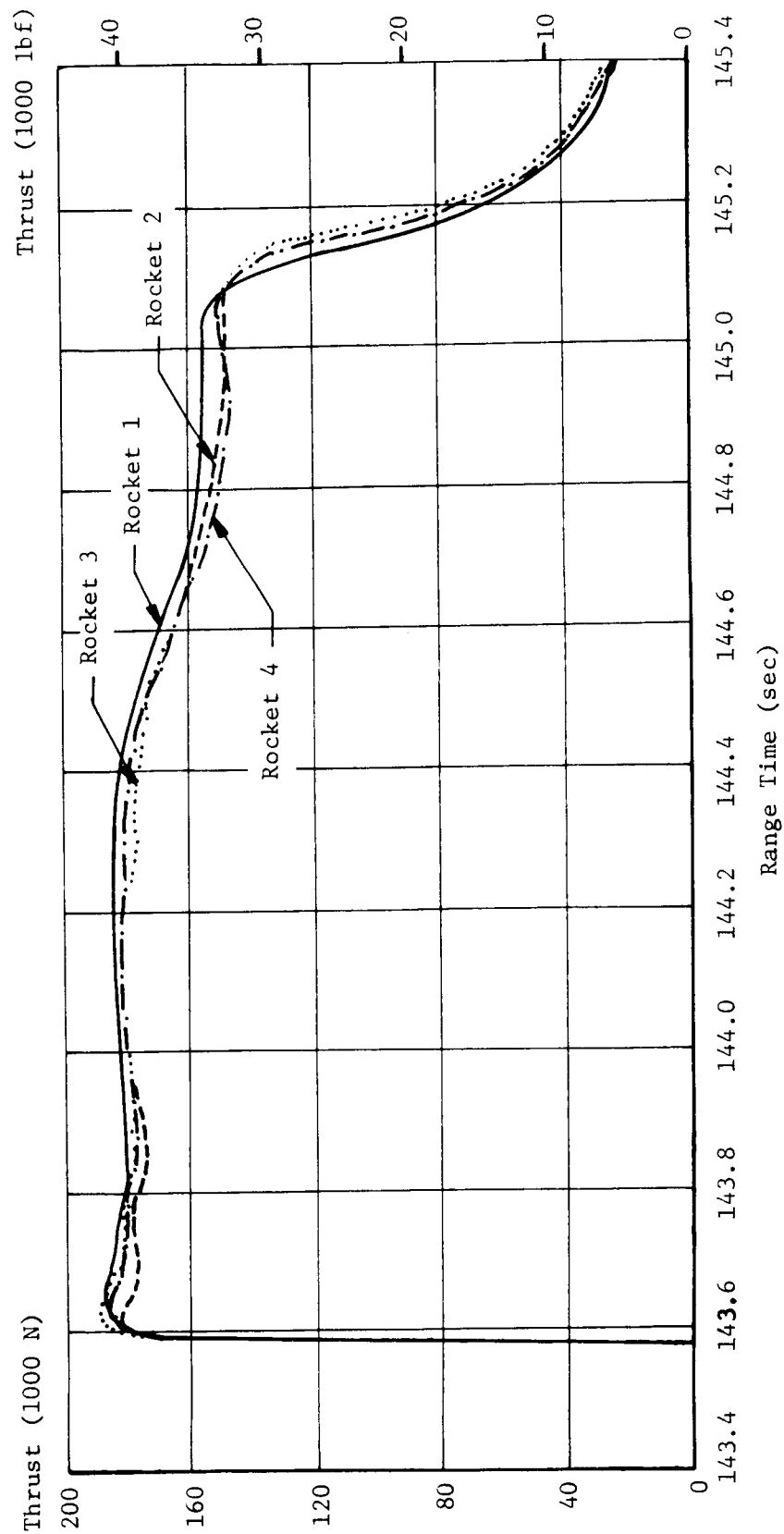


FIGURE 13-2 RETROROCKET THRUST

AS-204 was the last flight scheduled for the chamber pressure measurements. Retrorocket performance for S-IB-5 and subsequent stages will be evaluated on an average or total basis using longitudinal acceleration data.

13.2.3 SEPARATION DYNAMICS

S-IB/S-IVB separation was completed at 144.47 sec when the S-IVB J-2 engine cleared the interstage, 0.97 sec after separation command. Pertinent separation sequence of events is presented in Table 13-III. Separation acceleration and relative velocities (Figure 13-3) were determined from the accelerometer data and agree closely with predicted.

The lateral accelerations during separation are presented in Figure 13-4. The longitudinal translation between S-IB and S-IVB stages, shown in Figure 13-5, agrees quite well with predicted. During S-IB/S-IVB separation only 0.05 m (2 in) of the available 2.032 m (80 in) lateral clearance was used.

During and immediately following separation, the attitude errors and angular rates remained relatively low and no problems were encountered in controlling the S-IVB through these transients. The maximum angular velocities measured during separation were: 0.7 deg/s nose up in pitch, at approximately 149.9 sec; -0.6 deg/s nose left in yaw, at approximately 149.9 sec; and -0.4 deg/s clockwise (looking forward) in roll, at approximately 147.0 seconds. The maximum attitude errors were: -1.7 deg in pitch, at approximately 148.1 sec; -1.8 deg in yaw, at approximately 155.4 sec; and 1.3 deg in roll, at 148.2 seconds. During these transients, the Auxiliary Propulsion System (APS) corrected roll properly. At J-2 engine steady-state thrust attainment, the thrust vector control system began correcting the pitch and yaw transients. S-IVB stage attitude errors and angular rates during and following separation are presented in Section 12-0, Figures 12-11 and 12-12.

13.3 LV/LM-1 SEPARATION

The Lunar Module (LM) was successfully separated from the S-IVB/IU at 3235.24 seconds. The separation caused very little disturbance and resulted in maximum attitude errors of 0.75 deg nose up in pitch, 1.4 deg nose left in yaw, and 1.0 deg counter clockwise (looking forward) in roll.

TABLE 13-III SEPARATION EVENTS

Event	Range Time		Time from Sep. Command	
	Predicted	Actual	Predicted	Actual
Inboard Engine Cutoff Command	139.34	138.97	-4.30	-4.53
Outboard Engine Cutoff Command	142.34	142.25	-1.30	-1.25
Ullage Motor Ignition Command	143.44	143.30	-0.20	-0.20
Separation Command (Retro-rocket Ignition Command)	143.64	143.50	0	0
Retrorocket Ignition	143.69	143.576	0.05	0.076
Retrorocket 90% Thrust	143.74	143.59	0.10	0.09
First Axial Motion	143.76	143.59	0.12	0.09
Separation Complete	144.65	144.47	1.01	0.97
J-2 Engine Start Command	145.04	144.90	1.40	1.40

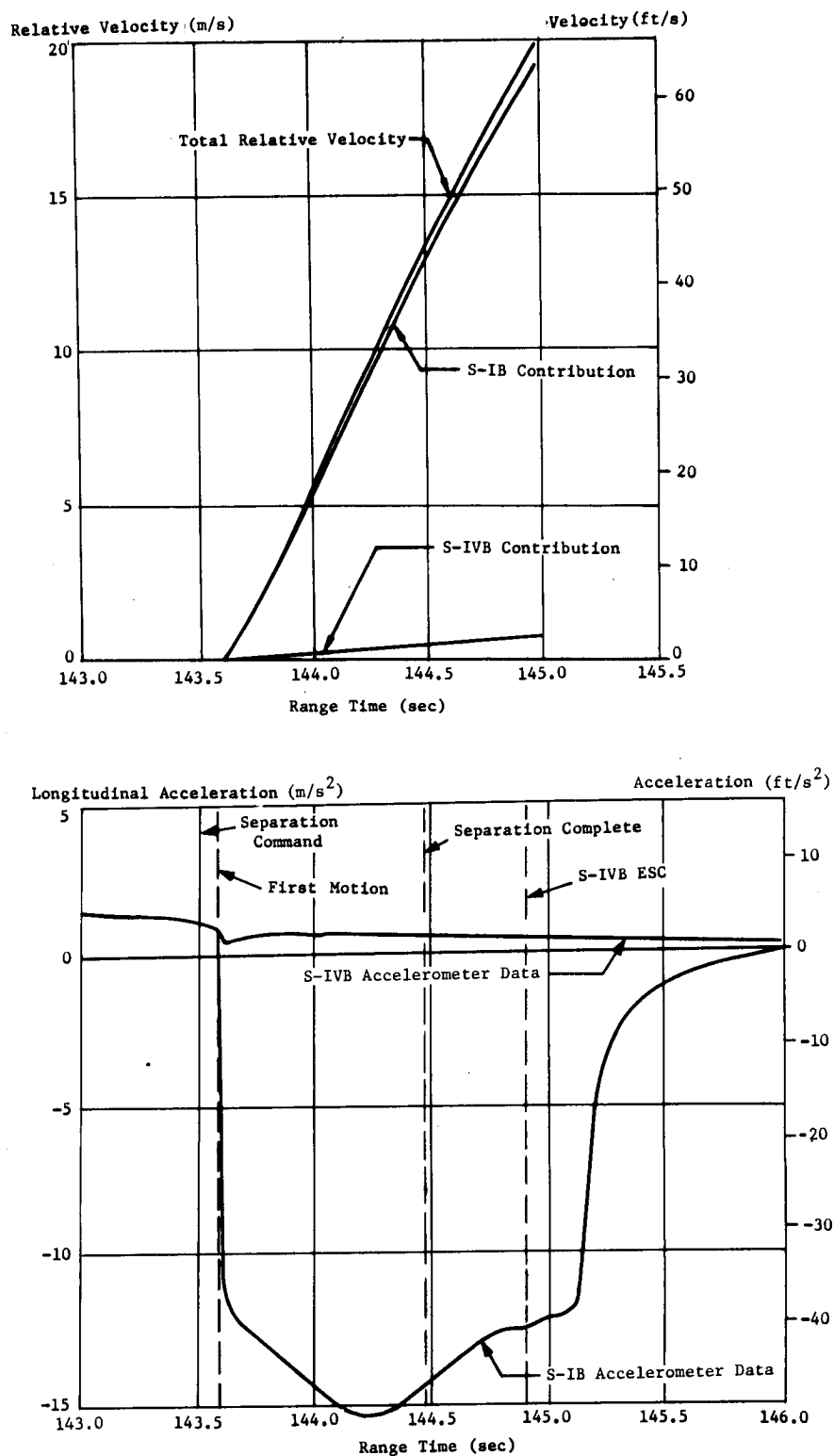


FIGURE 13-3 S-IB/S-IVB RELATIVE VELOCITY AND LONGITUDINAL ACCELERATION

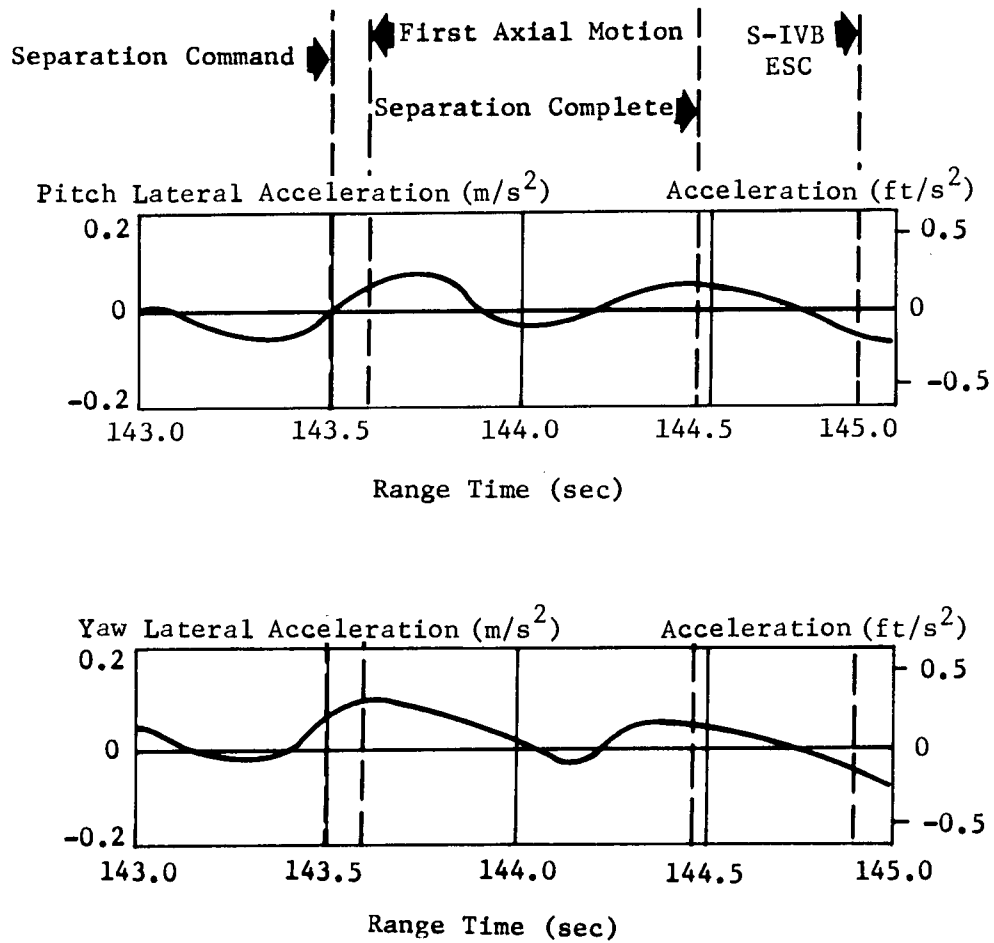


FIGURE 13-4 LATERAL ACCELERATIONS DURING S-IB/S-IVB SEPARATION

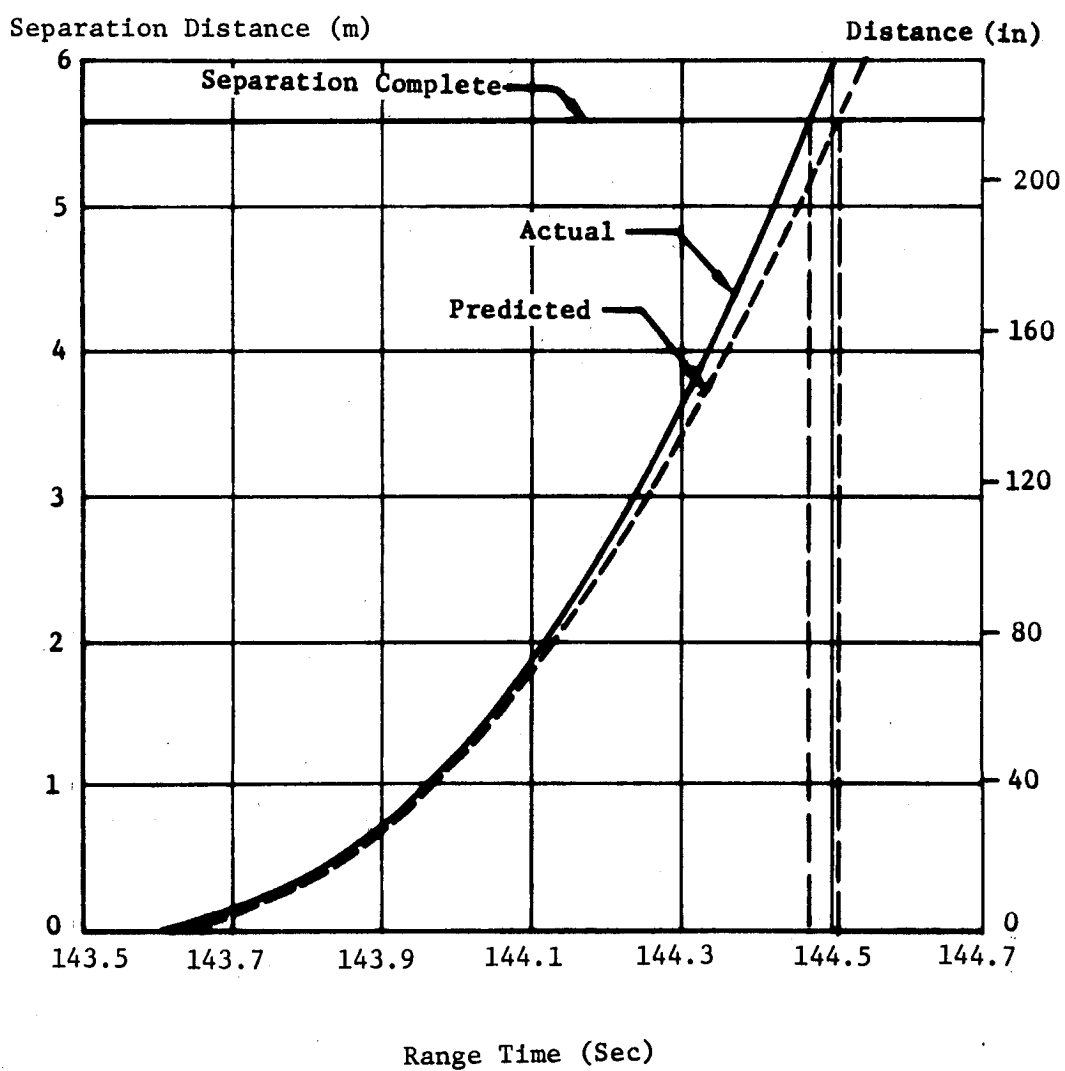


FIGURE 13-5 S-IB/S-IVB SEPARATION DISTANCE

14.0 VEHICLE ELECTRICAL SYSTEMS

14.1 SUMMARY

The electrical systems of the AS-204 launch vehicle operated satisfactorily during the entire flight. Battery performance - including voltages, currents, and temperatures - was satisfactory and remained within predicted tolerances. The master measuring voltage supplies performed satisfactorily. The secure command system and range safety decoder were operable during flight. All Exploding Bridge Wire (EBW) firing units responded correctly. Battery life-time met mission requirements.

14.2 S-IB STAGE ELECTRICAL SYSTEM

Inflight power for the S-IB stage is supplied by two 28 volt, zinc-silver batteries, designated 1D10 and 1D20. Each battery is rated at 2000 amp-minutes. The power and distribution system consists of batteries, measurement voltage supplies, distributors, plug J-Boxes, and interconnecting circuitry. Three master measuring voltage supplies are utilized to furnish a precisely regulated reference voltage to the telemetry system. Each power supply converts 28 vdc to a regulated 5 vdc reference voltage for use in the instrumentation measuring system. Differences in configuration between AS-202 and AS-204 are discussed in Appendix A.

The S-IB-4 stage electrical system performed as expected throughout normal flight periods, and all mission requirements were met. Battery performance - including voltages, currents, and temperatures - was satisfactory and remained within predicted tolerances. The Secure Command System and Range Safety Decoder were operable during flight. All Exploding Bridge Wire (EBW) firing units responded correctly.

All Thrust OK Pressure Switches and EBW units functioned properly. The average charge time for the retro rocket EBW units was 0.66 second. The charge time for the separation EBW was 0.84 second. The destruct EBW units indicated no charge.

The voltage for each battery averaged 27.8 vdc throughout the normal flight period. Battery voltage drops and current loads correlated with significant vehicle events. The most pronounced power drains were caused at S-IB cutoff by conjoint conax firing and prevalve operation. The current on batteries 1D10 and 1D20 averaged approximately 30 amps throughout powered flight. Power consumption did not approach the specification limit of 120 hours continuous activation. The voltage and current profiles for the batteries are presented in Figure 14-1.

The Master Measuring Voltage Supplies performed satisfactorily, and remained within the allowable tolerance of 5.000 ± 0.0125 vdc.

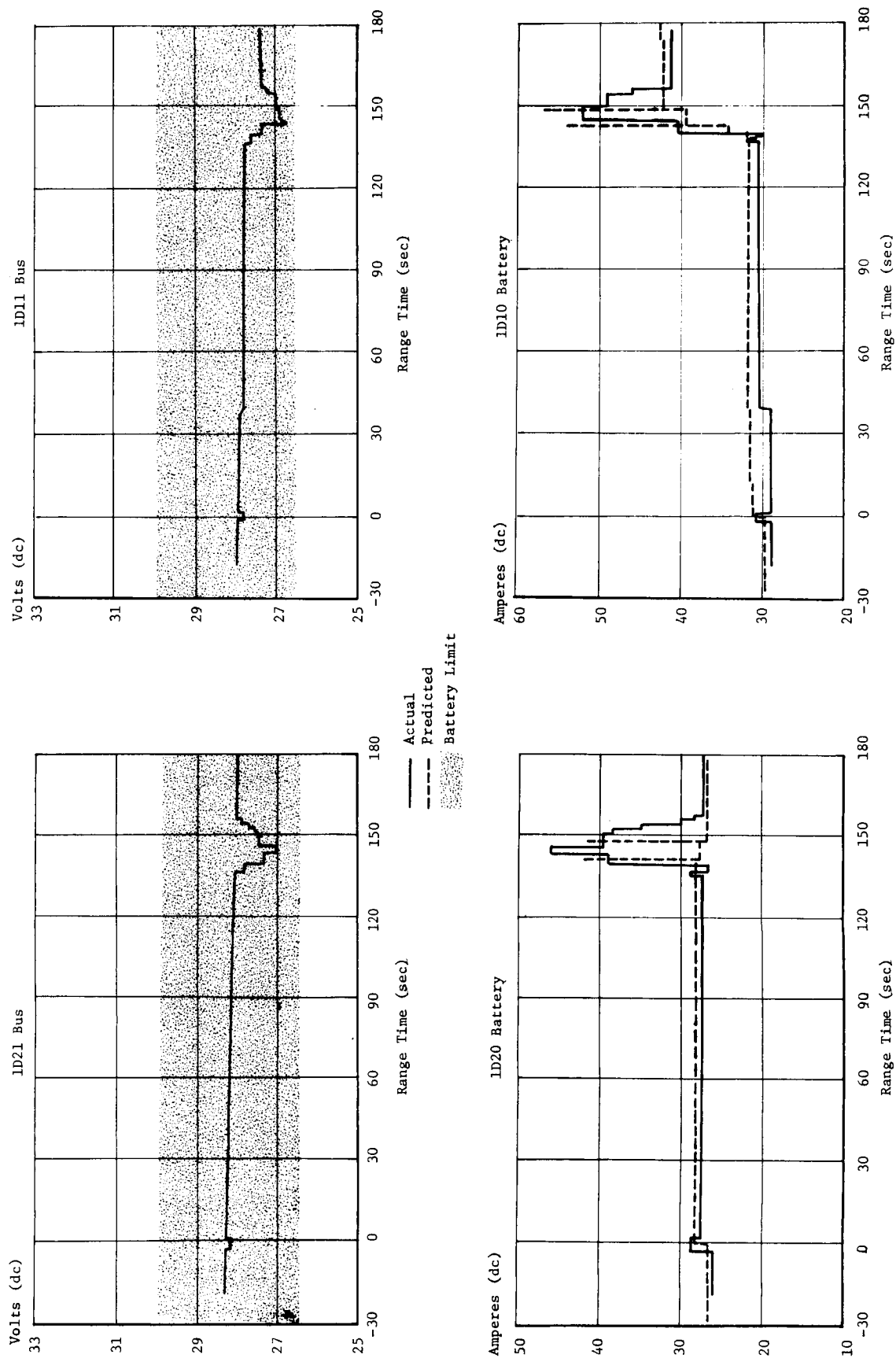


FIGURE 14-1 S-IB STAGE CURRENT AND VOLTAGE

The following tabulation indicates battery power consumption from liftoff in amp-min and as a percent of rated capacity:

<u>Battery</u>	<u>Capacity (amp-min)</u>	<u>Consumption (amp-min) to Separation</u>	<u>Consumption (amp-min) through Playback</u>
1D10	2000	85.8 (4.2%)	193 (9.6%)
1D20	2000	59.1 (2.9%)	114.4 (5.7%)

14.3 S-IVB STAGE ELECTRICAL SYSTEM

The AS-204 S-IVB stage electrical power system consisted of four batteries, one LOX and one LH₂ chilldown inverter, a static inverter-converter, three 5 vdc excitation modules, and fifteen 20 vdc excitation modules. Differences in configuration between AS-202 and AS-204 are covered in Appendix A.

Forward 1 and 2 batteries were rated at 300 and 4 amp-hours, respectively. Aft 1 and 2 batteries were rated at 70 and 25 amp-hours, respectively. The following tabulation indicates battery power consumption in amp-hours and as a percent of rated capacity:

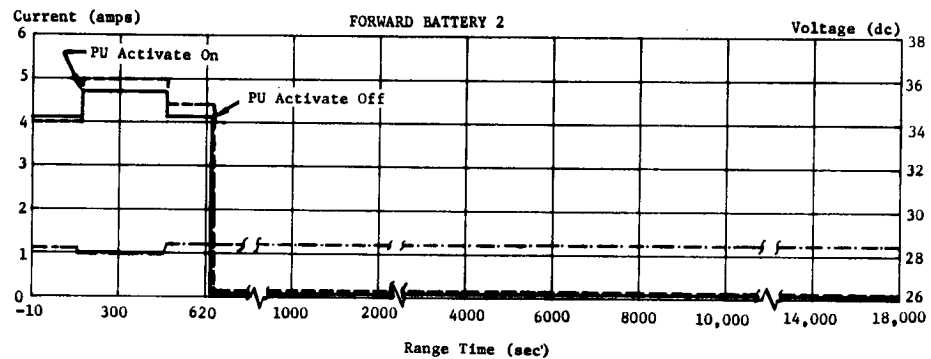
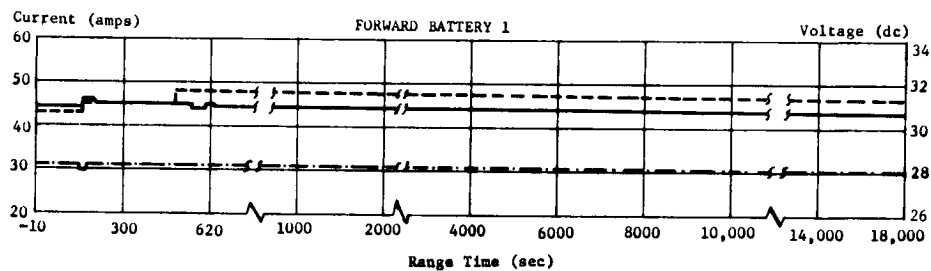
<u>Battery</u>	<u>Capacity (amp-hours)</u>	<u>Amp-Hours Used at 7.54 hr</u>	<u>Percent Con- sumed at 7.54 hr</u>
Fwd. 1	300	125*	41.6
Fwd. 2	4	0.8	20
Aft 1	70	14	20
Aft 2	25	9.4	37.6

*Voltage level too low for TM system after 7.54 hours.

Battery voltage and current profiles for the entire flight are presented in Figure 14-2. The composite average temperature of the batteries from the switch to internal power until S-IVB engine start command was 312°K (101°F). Battery temperatures remained below the 347°K (169°F) limit. The temperature of each battery at S-IVB engine cutoff and the maximum and minimum temperatures of each battery for the duration of the flight are shown in Figure 14-3. The battery temperature histories indicate normal heat rise during battery loading and proper cycling of the heater circuits to maintain battery temperature. Temperature limits of 347°K (169°F) during powered flight and 366°K (199.1°F) in orbit were not approached. Forward battery 1 reached a high temperature of 341°K (154.1°F) shortly before the close of second orbit, but stabilized gradually to 336°K (144.1°F).

— Actual Current (amps)
 - - - Predicted Current (amps)
 - - - Actual Voltage (dc)

203



Note: Random APS Firings from ESC Throughout Mission

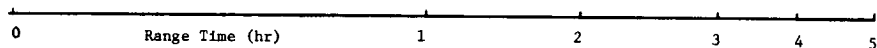
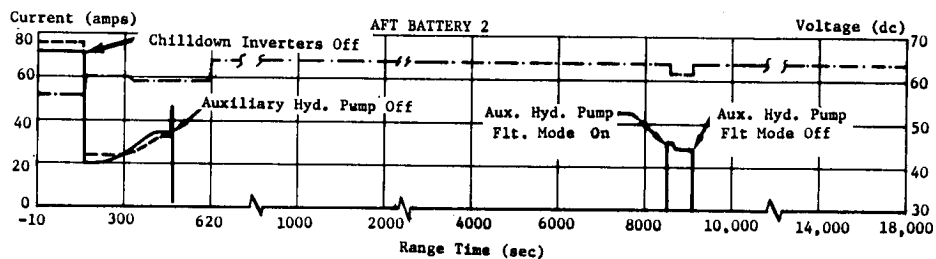
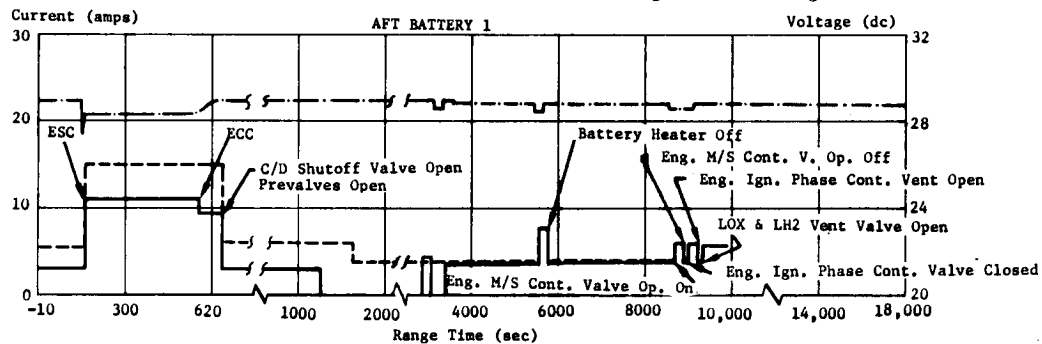


FIGURE 14-2 S-IVB BATTERY CURRENT AND VOLTAGE

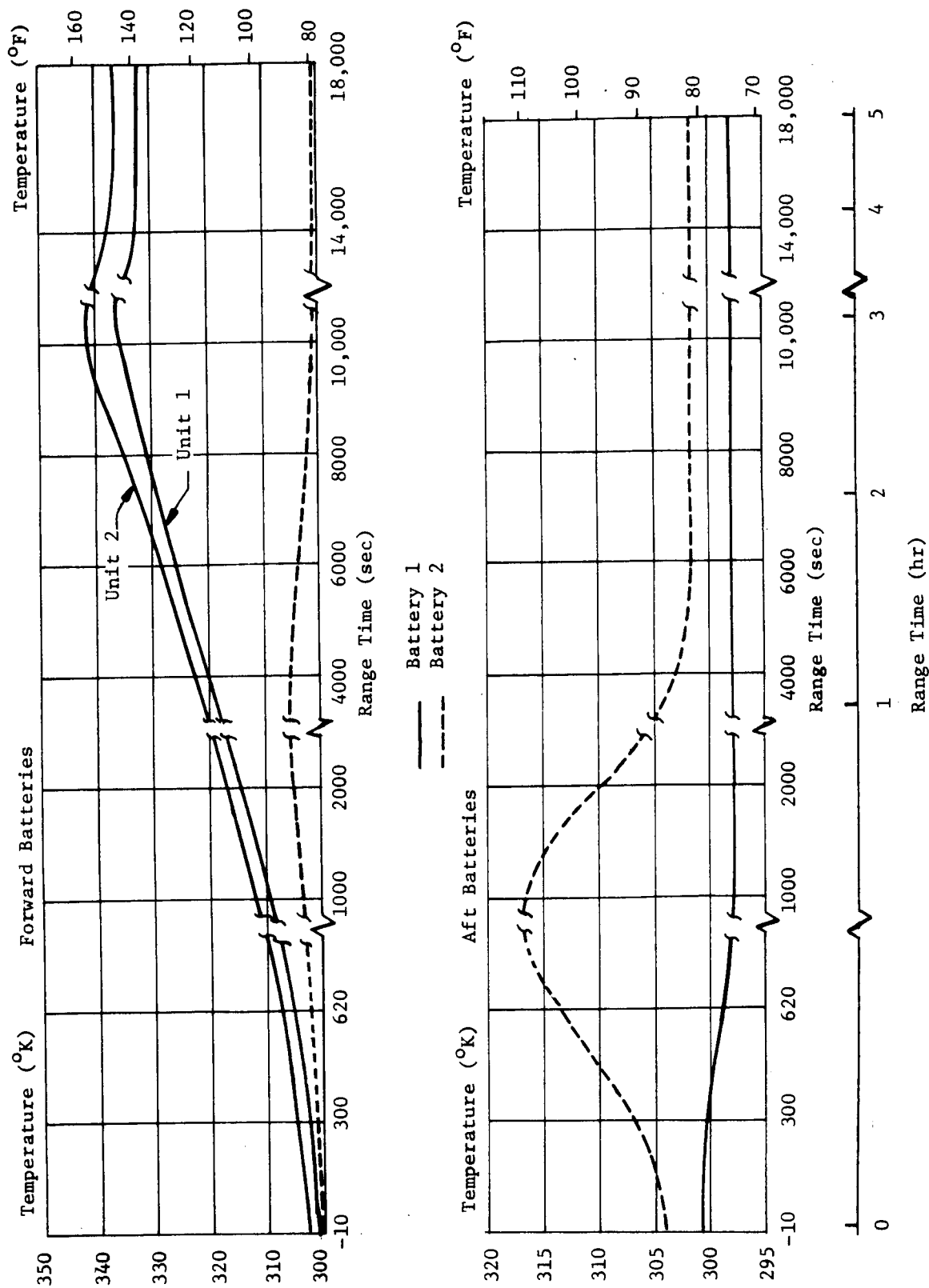


FIGURE 14-3 S-IVB BATTERY TEMPERATURES

The static inverter-converter and the chilldown inverters performed satisfactorily. At umbilical disconnect, the static inverter-converter voltage was 114.8 vac; the voltage remained at this level through PU system activate to S-IVB engine cutoff. The LH₂ chilldown inverter supplied power satisfactorily to the LH₂ chilldown pump; the voltage was a nominal 56.5 v at 401.0 Hz, and the operating temperature range was 277°K (39°F) to 282°K (47°F). The LOX chilldown inverter supplied power satisfactorily to the LOX chilldown pump; the voltage was a nominal 56.5 v at 400.2 Hz, and the operating temperature range was 266°K (20°F) to 288°K (55°F).

All EBW firing units performed satisfactorily. The ullage rocket ignition EBW units were charged at 139.88 sec; and the normal ullage rocket ignition occurred, on command, at 143.30 seconds. The ullage rocket jettison EBW units were charged at 152.41 sec and were discharged at 155.52 seconds. This and other data indicated that all three ullage rockets were jettisoned satisfactorily.

The electrical portions of the S-IVB control system responded properly to the commands generated by the sequencer and the Instrument Unit. The S-IVB stage switch selector performed as expected. Telemetry data indicated that both range safety receivers functioned properly during the entire flight.

The Electrical Control and Electrical Power Systems operated satisfactorily to provide the necessary control functions and electrical power during the Dump Experiment. The LOX Tank Vent Valve event indication did not fully respond to the close command which was exercised at 11,651.35 seconds. However, it operated properly during the subsequent LOX Vent Valve command.

Data after the Dump Experiment were analyzed to evaluate the Launch Vehicle orbital coast lifetime. Forward battery 1, which provides power to the TM system, decreased below the level required to operate the system on the fifth revolution. The voltage was 29 volts at Tel-4 (22680 sec), dropped to 17 volts at Hawaii (27150 sec), and was indicating 0 volts at Guaymas (27800 sec). The voltages for Forward 2, Aft 1, and Aft 2 batteries were at normal levels at 27150 seconds. However, since the TM battery voltage was below the level required to operate the system, no data are available to determine the life of these three batteries after 7 hrs 32 min (27150 sec).

14.4 INSTRUMENT UNIT ELECTRICAL SYSTEM

The Electrical Subsystem functioned normally from liftoff through at least 10.7 hours.

The IU electrical system consisted of four batteries (designated 6D10, 6D20, 6D30, 6D40), two power supplies, four types of distributor, and a switch selector. The four batteries, each rated at 350 ampere-hours, provided the 28-vdc power for the IU. These 20-cell batteries were composed of alkaline silver-zinc cells with potassium hydroxide electrolyte. The two power supplies converted the unregulated 28 vdc from the batteries to regulated 56 vdc required for stabilized platform electronics and to highly regulated 5 vdc used as

excitation and reference voltage for transducers and signal conditioning equipment. The four types of distributor provided power/signal distribution and switching for IU components. The switch selector decoded the flight sequence commands issued by the LVDC/LVDA and activated the proper circuits to execute the commands.

The 56-volt power supply voltage remained within the tolerance limits of 56 ± 2.5 vdc for a 1.1 to 8 ampere load. The 5-volt measuring voltage supply remained within the 5 ± 0.005 vdc tolerance for a 1 ampere load. The distributors performed without discrepancy.

The battery voltages and internal temperatures were as anticipated throughout the mission. There was a slight rise in the voltages of all four batteries due to the increase in internal temperatures associated with current discharge. The largest temperature rise occurred in the 6D20 battery. Figure 14-4 shows battery voltages, currents, and temperature trends throughout the flight. The following tabulation indicates battery power consumption in amp-hours and as a percent of rated capacity:

<u>Battery</u>	<u>Amp Hrs Used at 10.7 Hours</u>	<u>% Used</u>	<u>Hours Remaining</u>
6D10	264	75.4	3.48
6D20	293	83.7	2.1
6D30	203	58.0	7.74
6D40	176	50.3	10.54

Bus currents agreed with predictions to within 10 percent for the initial 22,000 sec of flight. The largest divergence between predicted and actual data was on the 6D20 and 6D30 buses. 6D20 current was higher and 6D30 current was lower than predicted. Between 920 and 5800 sec, the 6D20 bus current rose from 5.3 percent to 9.4 percent above the predicted. The 6D10 and 6D40 bus currents were within 4 percent of the expected values for the initial 22,000 seconds.

The usual excursion was observed on the 6D20 battery voltage and current at liftoff. A voltage excursion was also present on the 6D30 battery at this time. The usual spike in the 6D10 bus current occurred at liftoff and is attributed to the 56 vdc converter. Staging at 145 sec produced the expected spikes in the 6D10, 6D30, and 6D40 bus currents. The control accelerometer turnoff at 120 sec was reflected in a 0.5 ampere decrease in the 6D40 bus current. The opening of the water solenoid valve at 180 sec produced a slight decrease in 6D20 bus current. The opening and closing of this valve at 17,200 and 22,350 sec, respectively, was also observed in this manner. The 6D30 bus current increased 1 ampere reflecting "tape recorder record On" at 136 sec, with "tape recorder record Off" at 161 sec reducing the current by 1 ampere. The IU Tape Recorder playback was also indicated in the 6D30 bus current by a 1.0-ampere rise between 597 and 625 seconds. At 285 sec, there was a 0.5-ampere increase in the 6D30 bus current due to gain changes in the Flight Control Computer with a corresponding decrease in the 6D30 bus voltage. The 6D30 bus measurements (M14-601 and M18-601) also reflect Azusa power-off as a decrease of 4.2 amperes at 880 seconds. The SLA Panel deployment was observed on the 6D10 battery bus parameters at 1193.3 seconds.

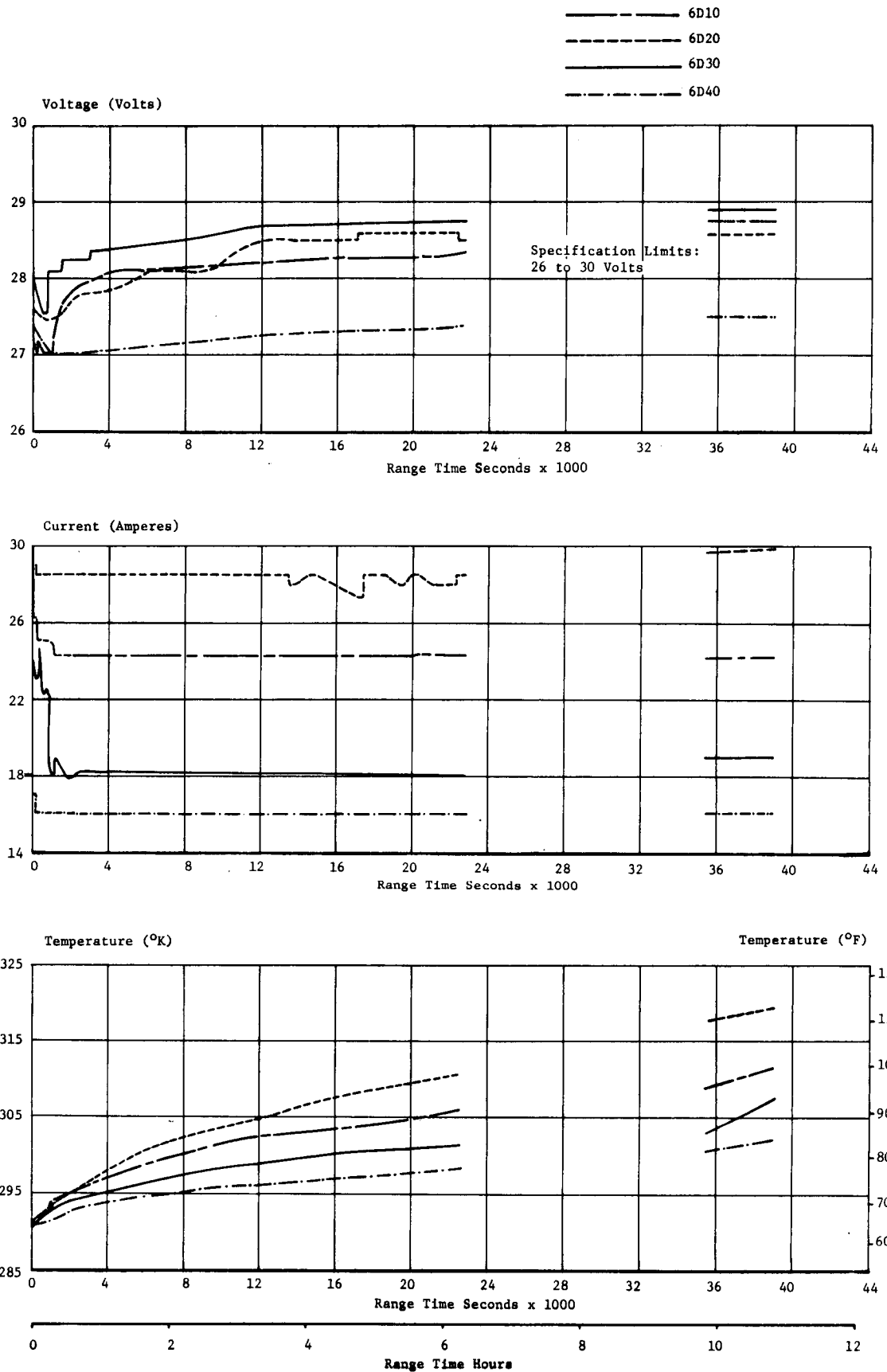


FIGURE 14-4 INSTRUMENT UNIT BATTERY VOLTAGE, CURRENT, AND TEMPERATURE

15.0 RANGE SAFETY AND COMMAND SYSTEMS

15.1 SUMMARY

Secure Range Safety Command Destruct Systems (RSCDS) were fully operational and could have performed the destruct function at any time during powered flight. The Digital Command System (DCS) performed satisfactorily. Seven switch selector mode commands from MILA during the third orbital pass were not issued in proper form to obtain the desired DCS response.

15.2 COMMAND DESTRUCT SYSTEMS

Identical RSCDS were operational on the S-IB-4 and S-IVB-204 stages. Each stage carried two RSCDS installations that operated independently in response to a common ground command, thus affording a very high degree of reliability. Three types of range safety command were provisioned:

1. Arm/Cutoff - Arming of the Exploding Bridge Wire (EBW) and thrust termination.
2. Destruct - Firing of the EBW.
3. Safe - Disconnecting the command decoding equipment from its power supply.

No arm/cutoff and no destruct commands were required. During the AS-204 flight, telemetry indicates that the command antenna, receivers/decoders, destruct controllers, and EBW firing units would have performed satisfactorily if needed. The low level field measurements for the command-destruct receivers indicated that they had adequate signal strength throughout the flight. EBW firing unit data indicated that the units were in the required state of readiness. The receivers turned off at 629.3 sec, as observed in the data from Bermuda.

15.3 DIGITAL GUIDANCE COMMAND SYSTEM

DCS performance was completely satisfactory. The limiter test voltage requirements for the system indicated its steady receipt of a good signal level.

Table 15-I contains a list of significant DCS events. The Command Received Pulse (CRP) issued by the LVDC at 609.28 sec was an automatic function to reset the Command Decoder register at the initiation of orbital guidance. The SLA panel deployment commands were issued as a backup, beginning at 1272.48 sec, inasmuch as the SLA panel deployment, which occurred actually at 1193.5 sec, had not been verified. Seven switch selector mode commands issued by MILA during the third orbital pass, to effect LOX Vent Valve closing, did not include the expected data words; hence, the commands could not be effectuated. DCS and LVDC response was, however, proper under the circumstances.

Range Time (Sec)	Pulse Transmitted	Command Word Received	Remarks
609.28	CRP		Issued by LVDC during orbital initialization
1272.48	AVP	Sw Sel Mode Command	SLA Panel Deploy A
1272.51	CRP		
1272.79	AVP	First Data Word	
1272.80	CRP		
1273.07	AVP	Second Data Word	
1273.09	CRP		
1273.38	AVP	Sw Sel Mode Command	
1273.40	CRP		
1273.68	AVP	First Data Word	
1273.69	CRP		
1273.96	AVP	Second Data Word	SLA Panel Deploy B
1273.98	CRP		
11707.01	AVP	Sw Sel Mode Command	
11707.03	CRP		
11707.65	AVP	Sw Sel Mode Command	
11708.20	AVP	Sw Sel Mode Command	
11708.80	AVP	Sw Sel Mode Command	
11717.80*	AVP	Sw Sel Mode Command	
11718.10*	AVP	Sw Sel Mode Command	
11718.40*	AVP	Sw Sel Mode Command	
11718.70*	AVP	Sw Sel Mode Command	
AVP: Address Verification Pulse			
CRP: Command Received Pulse			
*Approximate Times			

16.0 EMERGENCY DETECTION SYSTEM

16.1 SUMMARY

Only the launch vehicle portion of the Emergency Detection System (EDS) was flown on AS-204. The EDS sensors and logic functioned properly, and all abort parameters remained below Saturn IB abort limits.

16.2 SYSTEM DESCRIPTION

The AS-204 launch vehicle portion of the EDS was the same as on previous Saturn IB vehicles. The absence of a Command and Service Module dictated an "open loop" configuration. In addition, the Q-Ball, which is a launch vehicle sensor, was not flown on AS-204. The Saturn IB automatic abort parameters are: angular overrates and two or more S-IB engines-out. The Saturn IB manual abort parameters are: angle-of-attack, LV attitude reference failure, S-IB and S-IVB stage thrust, angular overrates, and attitude error (spacecraft sensed). Of these parameters, all except angle-of-attack and attitude error were monitored on AS-204.

16.3 EDS BUSES

The EDS buses - 6D91, 6D92, and 6D93 - are supplied by the IU batteries 6D10, 6D30, and 6D40, respectively. The EDS buses were energized properly throughout the mission. The IU battery voltages, shown in Section 14, represent the respective EDS bus voltages.

16.4 EDS EVENT TIMES

Tables 16-I and 16-II list the event times associated with the Emergency Detection System. All timed EDS events occurred properly.

16.5 THRUST OK INDICATIONS

The H-1 engine has three discrete thrust chamber pressure sensors and the J-2 engine has two. Loss of thrust indication from two of the three Thrust OK switches on the H-1 engine results in indication of engine-out to the crew. Before automatic abort deactivation, loss of thrust on two or more S-IB engines results in energizing the 6D95 (automatic abort) bus. There was no indication of S-IB engine-out from ignition to inboard cutoff and, therefore, no indication of the automatic abort bus having been energized.

S-IVB engine thrust is indicated to the crew for a manual abort cue. The logic is such that, if either thrust OK switch actuates, indication is given to the crew. The performance of the thrust sensors and associated logic on AS-204 was nominal. Table 16-III gives the thrust OK switch actuation times for AS-204 flight.

TABLE 16-I

EDS/SWITCH SELECTOR EVENTS	
<u>Function</u>	<u>Range Time (sec)</u>
LV Engines EDS Cutoff Enable	60.31
Excessive Rate Auto-Abort Inhibit	132.03
Two Engines Out Auto-Abort Inhibit	132.42
Inboard Engines Cutoff	138.97
Auto-Abort Enable Relays Reset	139.18
Outboard Engines Cutoff	142.25
S-IB/S-IVB Separation Command	143.50

TABLE 16-II

EDS/DISCRETE EVENTS		
<u>Meas. No.</u>	<u>Event</u>	<u>Range Time (sec)</u>
K18-602	EDS/Manual Cutoff Armed	40.52
K9-602&K11-602	EDS S-IB One or More Engines Out	139.26
K63-602	S-IB Physical Separation	143.89

TABLE 16-III

THRUST OK SWITCH OPERATING TIMES				
<u>Stage</u>	<u>Engine</u>	<u>Switch</u>	<u>Closed</u>	<u>Open</u>
S-IB	1	1	- 1.50	142.24
S-IB	1	2	- 1.50	142.24
S-IB	1	3	- 1.55	142.27
S-IB	2	1	- 1.67	142.24
S-IB	2	2	- 1.67	142.24
S-IB	2	3	- 1.65	142.27
S-IB	3	1	- 1.50	142.32
S-IB	3	2	- 1.51	142.32
S-IB	3	3	- 1.45	142.27
S-IB	4	1	- 1.67	142.24
S-IB	4	2	- 1.67	142.32
S-IB	4	3	- 1.65	142.27
S-IB	5	1	- 1.83	139.24
S-IB	5	2	- 1.84	139.24
S-IB	5	3	- 1.80	139.18
S-IB	6	1	- 1.75	139.24
S-IB	6	2	- 1.76	139.24
S-IB	6	3	- 1.72	139.18
S-IB	7	1	- 1.83	139.24
S-IB	7	2	- 1.84	139.24
S-IB	7	3	- 1.90	139.18
S-IB	8	1	- 1.75	139.24
S-IB	8	2	- 1.76	139.22
S-IB	8	3	- 1.86	139.18
S-IVB	1	1	147.67	593.35
S-IVB	1	2	147.67	593.35

16.6 EDS RATE GYROS

The triple redundant rate gyros for sensing angular overrate provide for automatic abort during first stage flight and a cue for manual abort during second stage flight. Abort indication occurs if two or more gyros in any one axis sense an overrate. The limit settings on AS-204 were ± 5 deg/s in the pitch and yaw axis and ± 20 deg/s in the roll axis. The maximum rates experienced during first stage flight on AS-204, after liftoff, were -0.9 deg/sec pitch (at 85 sec), $+0.7$ deg/sec yaw (at 86 sec), and $+1.2$ deg/sec roll (at approximately 20 sec). Near liftoff, rates were observed of 1.25 deg/sec pitch and 2 deg/sec roll. Maximum noise, witnessed at liftoff, could have contributed significantly to the rates observed. All rates were measured before being filtered. The overrate switches operate as a function of the filtered gyro rate outputs. As these rates were well below limit setting, there were no indications of overrate switch closures.

16.7 LAUNCH VEHICLE ATTITUDE REFERENCE MONITORING

If the ST-124 platform fails in such a fashion that the platform achieves unreasonable gimbal angles in a given time increment, a discrete indication is given to the spacecraft. On AS-204, the platform functioned properly; therefore, no reference failures were indicated. The platform gimbal angle rate reached a maximum of 36 percent of the rate which results in a failure indication.

16.8 EDS DISTRIBUTOR

The EDS Distributor functioned normally throughout the flight. The thrust-OK voting logic functioned normally during S-IB stage engines ignition and cutoff. The Switch Selector command for inboard engines cutoff was issued at 138.97 sec, and the discretes monitoring one and two S-IB engines-out came on at 139.25 seconds. The time delay from the Switch Selector command to the engine-out discrete was therefore 0.28 sec, which is nominal for this function. Since no overrate conditions were experienced on this flight, the overrate voting circuitry within the EDS Distributor was not exercised.

17.0 STRUCTURES

17.1 SUMMARY

The postflight predicted longitudinal load and bending moment for the AS-204 vehicle compares favorably with the flight measured accelerometer and strain data. Vehicle loads due to the combined longitudinal load and bending moment were below limit design values and, therefore, the stress levels in key structural members were below their limit design value. Measured vehicle first and second bending mode data compare favorably with dynamic test data. There was no indication that POGO occurred.

The fin bending and torsion mode frequencies measured on AS-204 compare well with those from AS-202 and AS-203. The S-IB, S-IVB, and IU stage structure and component vibrations were as expected. H-1 and J-2 engine vibrations were as expected. Vibration levels on the structure and internally mounted components of the IU were within the design criteria.

The S-IVB forward skirt panel dynamic strain measurements gave no indication of flutter on 12 of the 16 measurements. On the remaining measurements a complex periodic wave shape was observed between 80 and 87 sec that was characteristic of limited amplitude flutter, as expected. The measured composite strain signal was insignificant for AS-204 in both amplitude and duration.

17.2 TOTAL VEHICLE LOADS AND MOMENTS

17.2.1 LONGITUDINAL LOADS

Vehicle postflight predicted longitudinal force distributions were computed using the mass characteristics of AS-204 and the applied forces from the flight trajectory data recorded during S-IB stage burn. The longitudinal accelerations obtained from the analysis show agreement with values measured during flight at all time points and reached a maximum of 42.1 m/s^2 at 138.97 sec, the time of IECO.

Comparisons between the postflight predicted longitudinal force and that derived from the strain measurements at station 23.9 m are present in Figure 17-1 for the conditions of maximum bending and maximum compression, which occurred at 72.5 and 138.97 sec, respectively. These comparisons show consistent results.

The longitudinal load at Station 23.9 m was 5,965,510 N (1,341,100 lbf) at IECO and is 7.3% greater than the design loads analysis value of 5,558,137 N (1,249,525 lbf) based on R-P&VE-SL-212-63. This difference is acceptable, since combined longitudinal and bending moment loads are below limit design values, and occurred due to weight increase above Sta. 23.9 m for the AS-204 configuration as compared to the configuration used in the design loads analysis. The AS-201 and AS-202 vehicles longitudinal load values were greater than the loads analysis values by

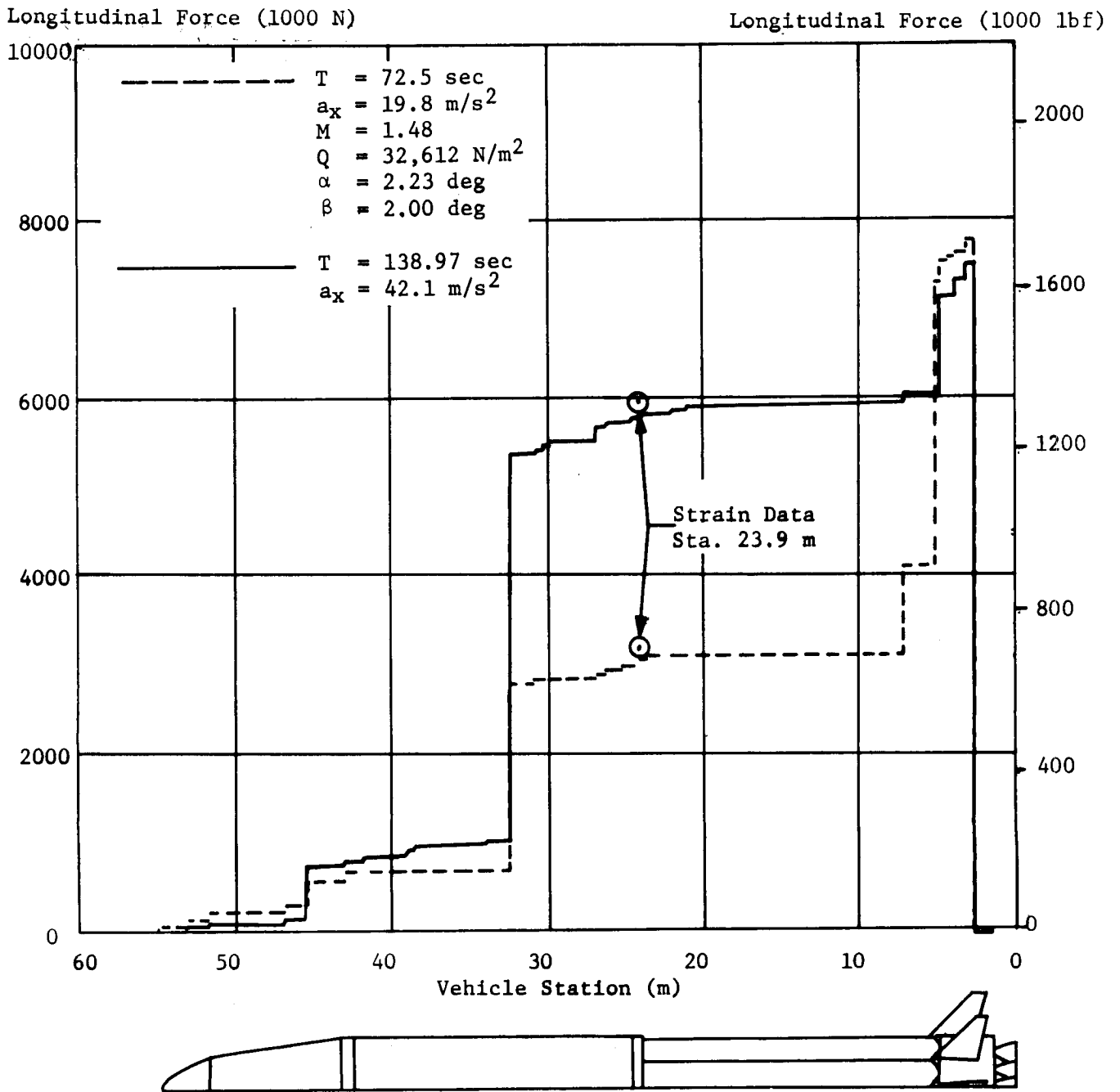


FIGURE 17-1 VEHICLE LONGITUDINAL FORCE DISTRIBUTION

3% and 6%, respectively. The AS-203 vehicle values were less than loads analysis values.

The AS-204 longitudinal load time history at Sta. 23.9 m, obtained from strain data, is compared to the time histories for vehicles AS-202 and AS-203 in Figure 17-2.

17.2.2 BENDING MOMENTS

The AS-204 maximum pitch moment of 1,145,900 N-m (10,142,100 lb-in) occurred at time point $T = 72.3$ sec and the maximum yaw moment of -1,160,000 N-m (-10,267,000 lb-in) occurred at 72.5 seconds. The maximum resultant moment of 1,593,950 N-m (14,107,700 lb-in), occurring at 72.5 sec, represents 25% of the design criteria of 6,361,000 N-m (56,300,000 lb-in). The resultant vehicle postflight bending moment for 72.5 sec versus vehicle station is presented in Figure 17-3. The measured strain data at Stations 23.9 m and 32.0 m is derived from 24 and 16 strain gauges, respectively. The strain data at sta. 23.9 m does not include effect of the 2.67 m (105 in) LOX tank. The results from two instrumented vehicles showed this to be about 10%.

17.2.3 BODY BENDING OSCILLATIONS

The first and second vehicle bending modes determined from the AS-204 flight data compared favorably with those predicted by dynamic analysis, as presented in Reference 5. The response amplitude at the vehicle bending frequencies was low, but generally higher than that measured on previous Saturn IB flights. The amplitudes at both the first and second vehicle bending frequencies were considerably higher in the yaw than in the pitch direction. The greatest amplitude response recorded was $0.111 G_{rms}$, measured from 1 to 4 sec of flight at the second vehicle bending frequency at Station 22.7 m (895 in) in the pitch direction. The data was analyzed from 0 to 25 Hz using a 0.677 Hz bandwidth filter. Figure 17-4 shows the vehicle bending frequency time histories from AS-204 flight data compared to dynamic analysis time histories. Little deviation between measured and predicted values is indicated. Figure 17-5 shows response amplitudes at the first and second vehicle bending frequencies in the pitch and yaw directions for each station measured. These amplitudes display the expected relative maxima during liftoff, Mach 1 - max Q portion of the flight, and separation.

17.2.4 LONGITUDINAL DYNAMIC ANALYSIS (POGO)

A RAVAN analysis was performed on selected lateral data for time points prior to liftoff and on longitudinal data at selected time points throughout first stage flight to determine predominant frequencies in the 0 to 25 Hz range and their rms amplitudes. The predominant frequencies are shown in Table 17-I.

During first stage flight, various data were investigated to determine if coupling between structural and fluid vibrations, as evidenced by the engine chamber pressure measurements, was present.

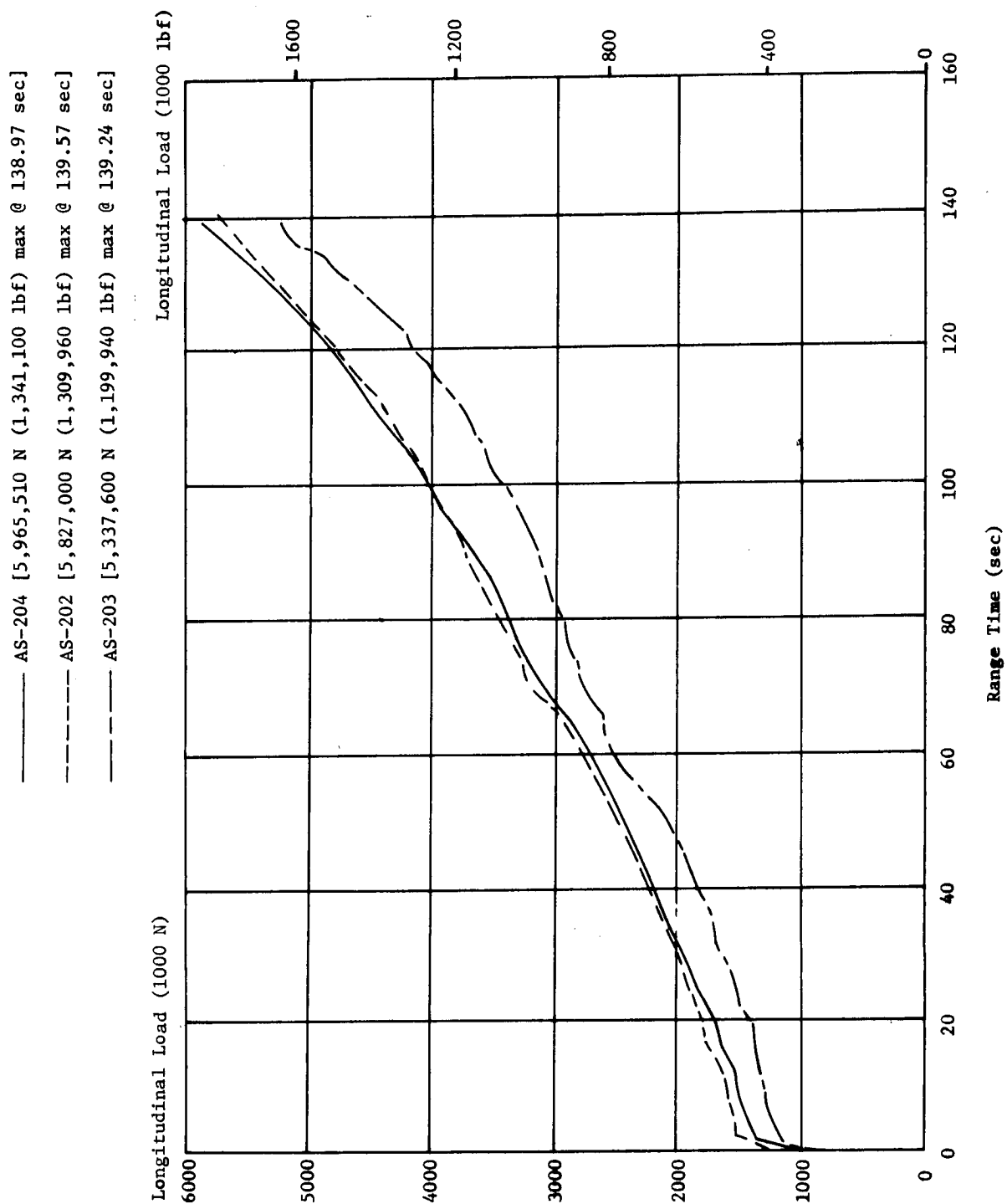


FIGURE 17-2 LONGITUDINAL LOAD (FROM STRAIN DATA AT STA. 23.9 M)

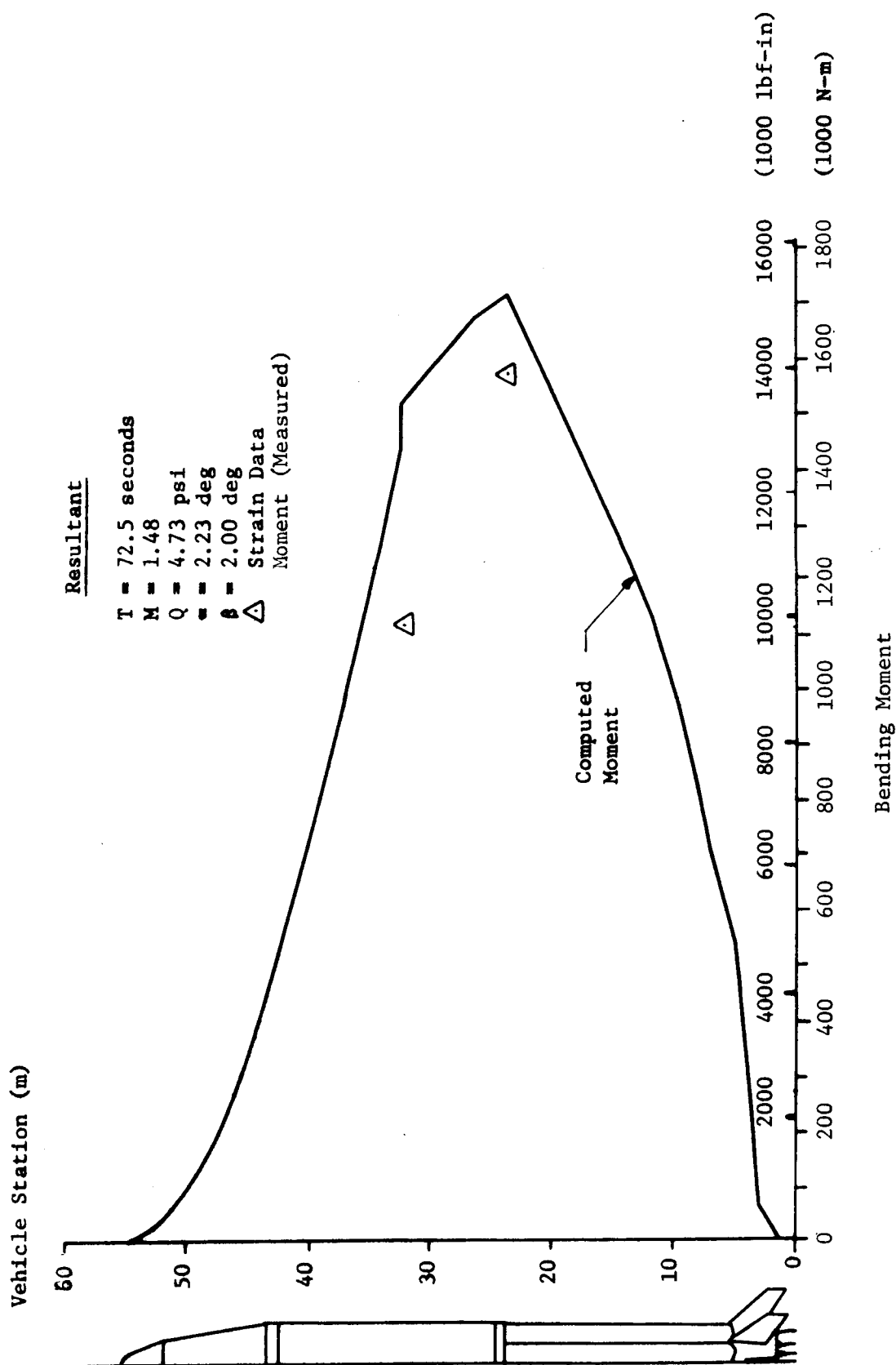


FIGURE 17-3 VEHICLE BENDING MOMENT

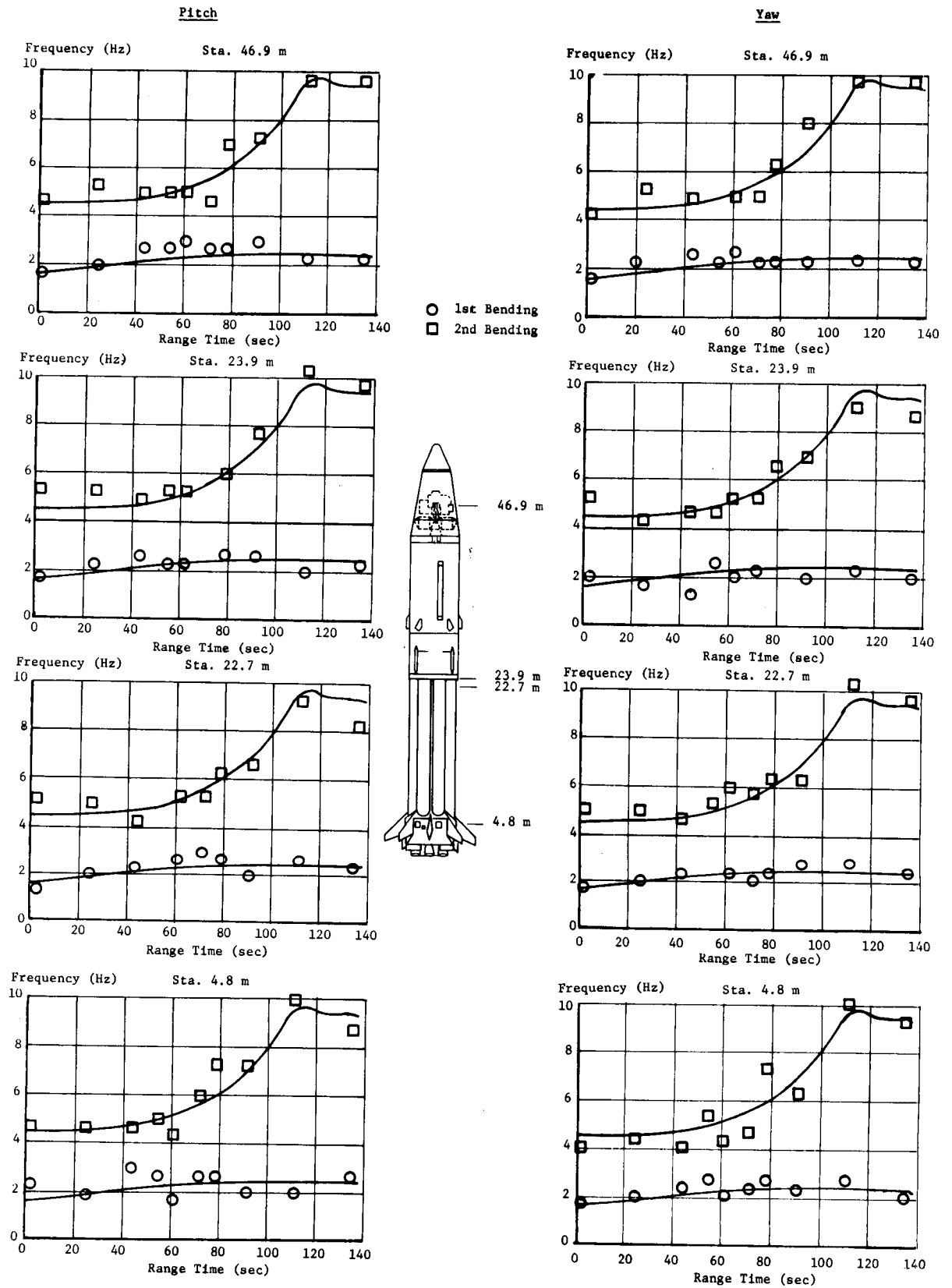


FIGURE 17-4 VEHICLE BENDING MODES

220

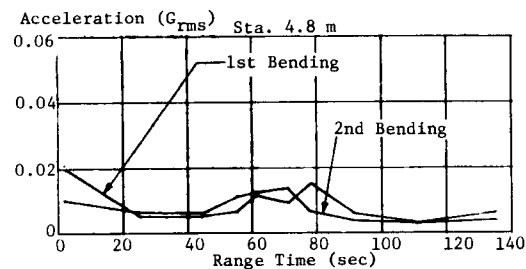
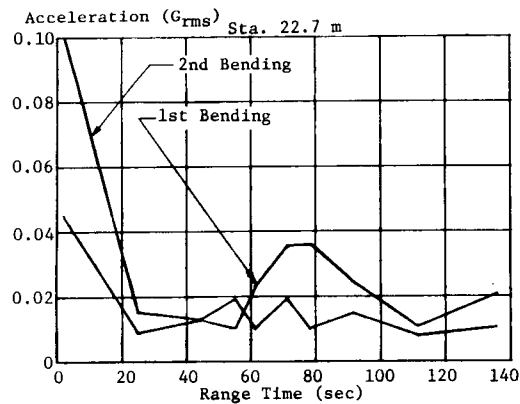
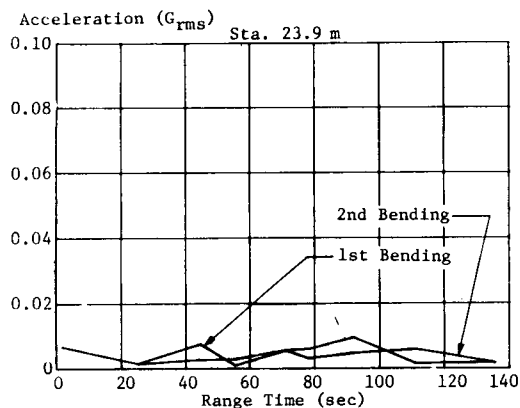
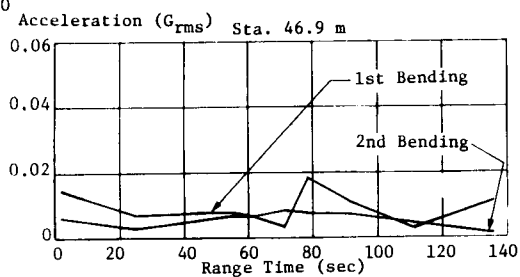
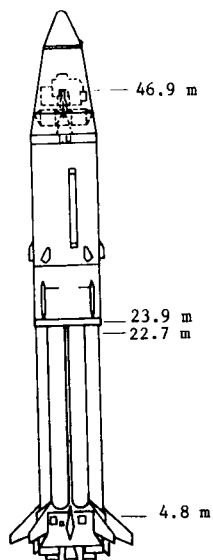
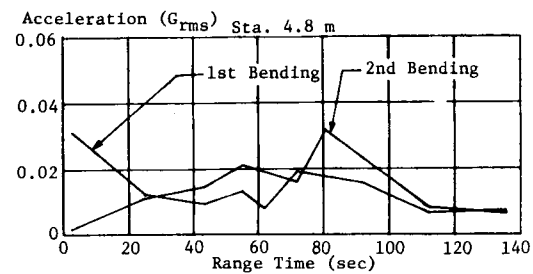
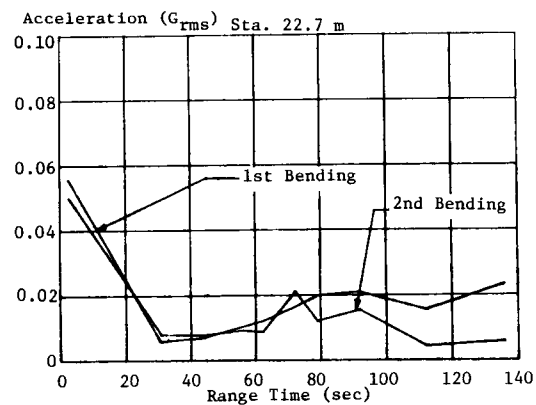
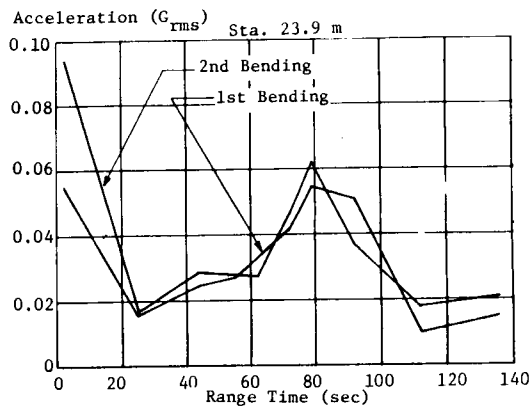
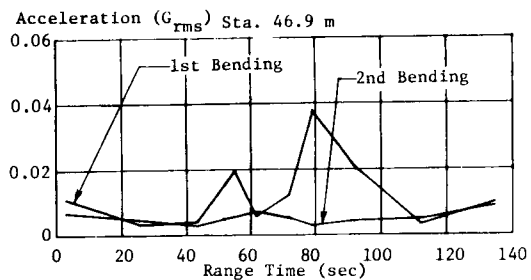
PitchYaw

FIGURE 17-5 VEHICLE BENDING AMPLITUDES

TABLE 17-I RESPONSE FREQUENCIES

Predominant Frequencies (Hz)										
	Lateral	Longitudinal								
Time (sec)	-2.7 to 0.3	-1.0 to 1.0	1.0 to 3.0	3.0 to 5.0	5.0 to 7.0	60.0 to 62.0	71.0 to 73.0	124.0 to 126.0	137.0 to 139.0	140.0 to 142.0
Freq. (Hz)	2.0	3.0	5.0	2.0	4.0	5.0	2.0	4.5	3.0	5.0
	3.0	11.0	10.0	7.0	5.5	8.0	4.0	7.0	6.0	7.0
	4.5	17.5	13.0	8.0	8.5	10.0	7.0	10.0	7.0	9.0
	6.5	20.0	15.5	17.5	11.0	16.0	9.0	12.5	8.0	13.0
	8.0			20.0	14.0	18.0	12.0	15.5	12.0	17.0
	9.5				19.0		14.5	17.5	15.0	20.0
	12.0						16.0		17.0	
	15.0						18.5		19.0	
							20.0			

No coupling and subsequent response buildup, which could be termed a longitudinal instability phenomenon or POGO, was noted.

The dynamic load factor for the S-IB stage engine buildup transient was determined to be 1.11, using simplified total thrust force and the total holddown arm force (see Figure 17-6). Actual thrust buildup curves are presented in Section 8. The values obtained from this analysis compare favorably with AS-202 and give an indication of adequate timing between firing of engine pairs.

17.3 S-IB STAGE ANALYSIS

17.3.1 S-IB FIN BENDING AND TORSION

The fin bending and torsion characteristics were measured during flight. Due to clipped data at liftoff, Mach 1, and max Q portion of flight, the evaluation was limited to defining predominant frequencies only. The results agree favorably with previous flights. A frequency range of 0 to 80 Hz was analyzed for various time periods. The predominant frequencies versus vehicle velocity for fins 5 and 7 are presented in Figure 17-7. These frequency values confirm the analysis predictions that no flutter conditions would exist during critical flight periods. The first bending and torsion mode frequencies are approximately the same as those recorded on AS-202 and AS-203 flights. The maximum amplitude response of the fins could not be determined due to the data being clipped. It was expected that maximum amplitude would have occurred during the Mach 1/max Q portion of flight. The data confirms this, since the large amplitudes which caused the data clipping did occur at these time periods.

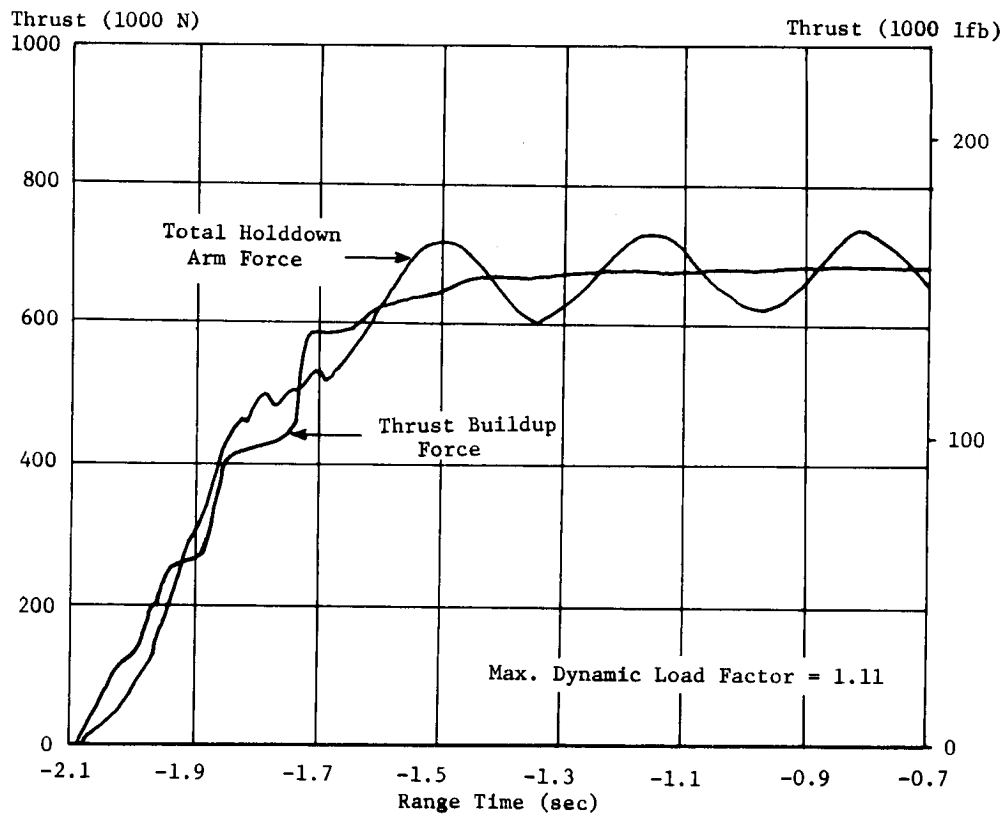
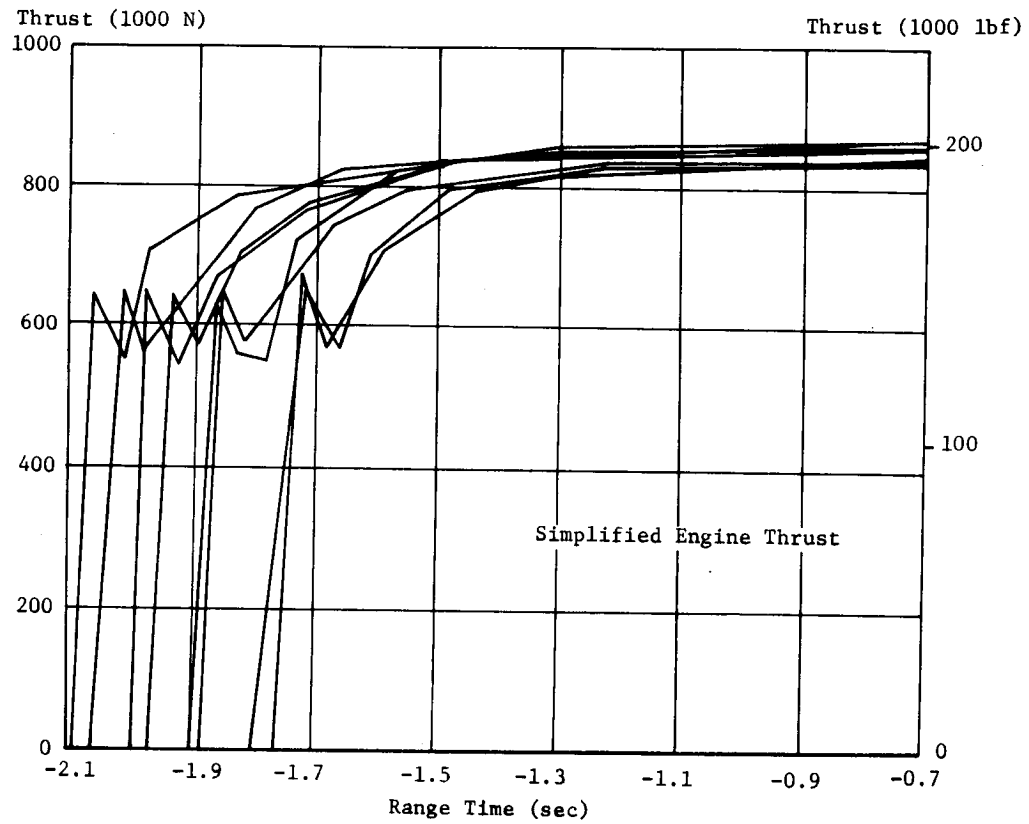
17.3.2 S-IB STAGE VIBRATIONS

The S-IB stage vibration environments were normal and did not exceed expected levels. Valid data was received from 21 of the 22 measurements which recorded the structural and component vibration environments. The vibration environment obtained is summarized in Table 17-II. Vibration envelopes for the S-IB stage structure and components are presented in Figures 17-8 and 17-9, respectively.

The vibration envelopes for the S-IB fin tip structure are shown in Figure 17-10. The data on which these envelopes are based did not reveal any unusual levels.

17.3.3 H-1 ENGINE VIBRATIONS

The envelopes of H-1 engine vibrations, presented in Figure 17-11, are resulting composite levels recorded by a total of fifteen measurements that were located on the S-IB stage engines. These envelopes are normal for these measurements and expected levels were not exceeded.



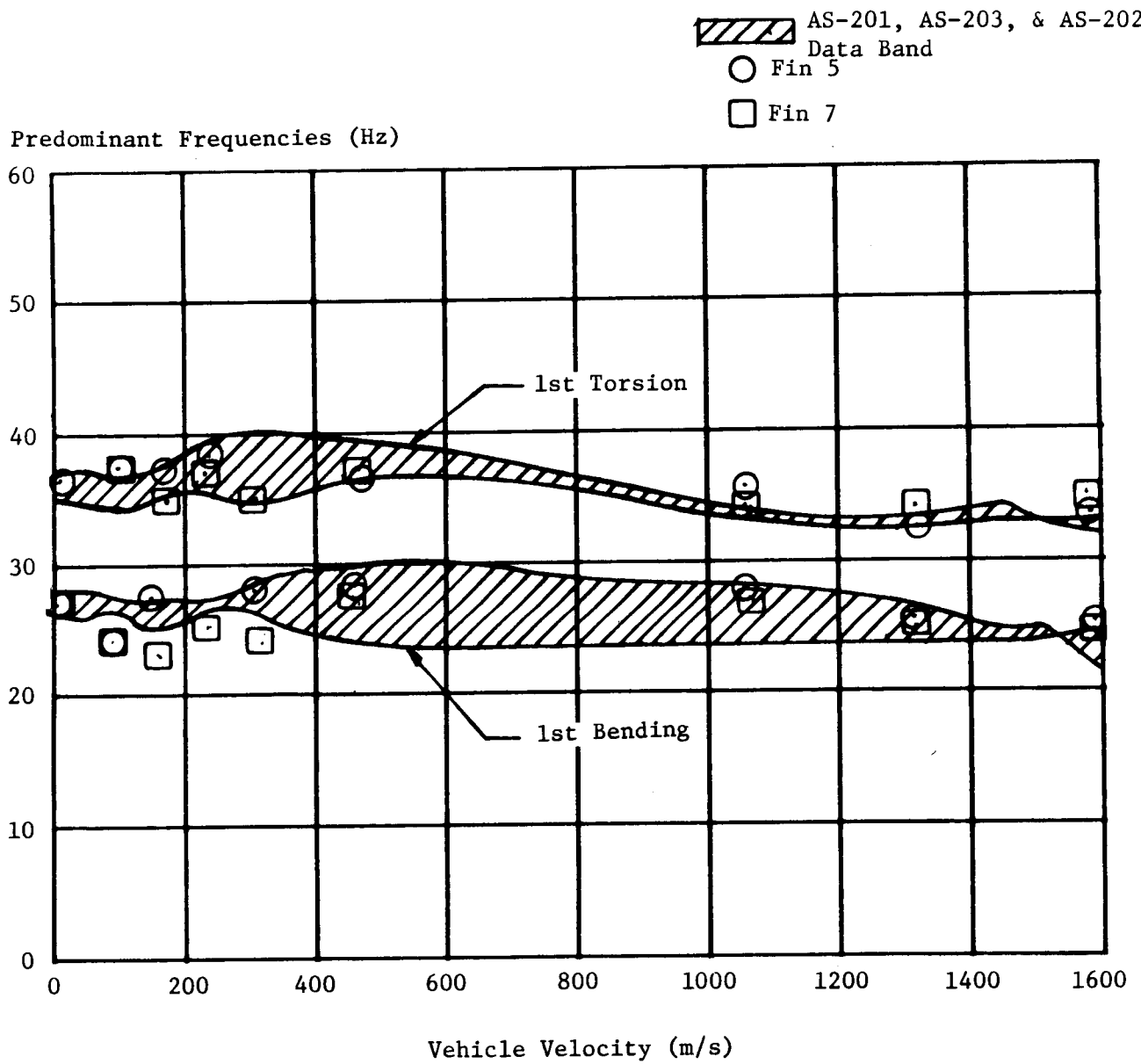


FIGURE 17-7 FIN BENDING AND TORSION MODES

TABLE 17-II S-IB VIBRATION SUMMARY

Area Monitored		Max. Level (G _{rms})	Range Time (sec)	Remarks
STRUCTURE	<u>Upper Structure</u> E226-11, E227-11	3.5	4.0	Level of 3.5 G _{rms} at liftoff and 0.5 to 2.5 G _{rms} throughout flight are approximately the same as AS-201 values.
	<u>Spider Beam</u> E504-11, E505-11	11.0	-1.0	Liftoff level 3.0 G _{rms} greater than AS-201. Flight levels comparable.
	<u>Engine Thrust Beam</u> E500-4, E501-4, E502-9, E503-9	5.5	-2.0	Liftoff level and flight levels same as AS-201.
ENGINE	<u>Thrust Cham. Dome</u> <u>Longitudinal</u> E33-1, E33-3, E33-5, E33-7	6.0	25.0	Liftoff and flight levels are 1 G _{rms} lower than AS-201 values. Measurement being investigated. (E33-3)
	<u>Lateral</u> E11-2, E11-4 E11-6, E11-8	8.0	4.0	Liftoff and flight levels same as AS-201.
	<u>Turbine Gear Boxes</u> E12-1 thru E12-8	27.5	130	Liftoff and flight levels are slightly higher than the AS-201 values, ranging from 15 to 27 G _{rms} .
COMPONENT	<u>Instrument Panel F-II</u> E101-12, E102-12, E103-12	4.2	0	Levels are approximately the same as AS-201 values. Max level of 4 G _{rms} at liftoff.
	<u>Distributor 9A3</u> E521-9, E522-9, E523-9	6.5	2.0	Liftoff levels are 3.5 G _{rms} higher than AS-201. Flight levels are higher by 1.5 G _{rms} .
	<u>Engine #4 Actuators</u> E271-4, E272-4, E273-4, E274-4, E275-4, E275-4	5.5	5.0	Approximately the same as level recorded on SA-6. Levels ranged from 0.5 to 5.5 G _{rms} throughout S-IB powered flight.
FIN	<u>Fin Tip</u> E530-20, E530-22	24.5	-1.0	Liftoff levels approximately 7 G _{rms} higher than AS-201. Flight levels agree with AS-201.

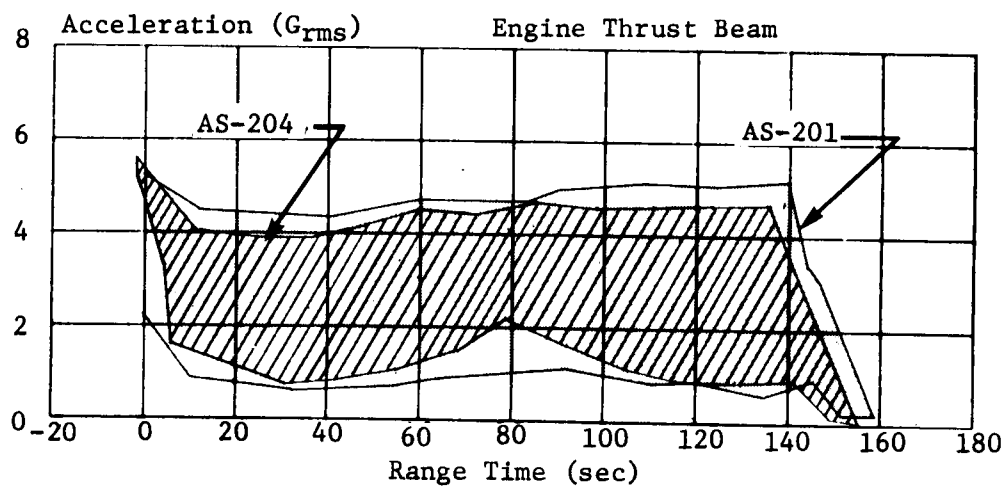
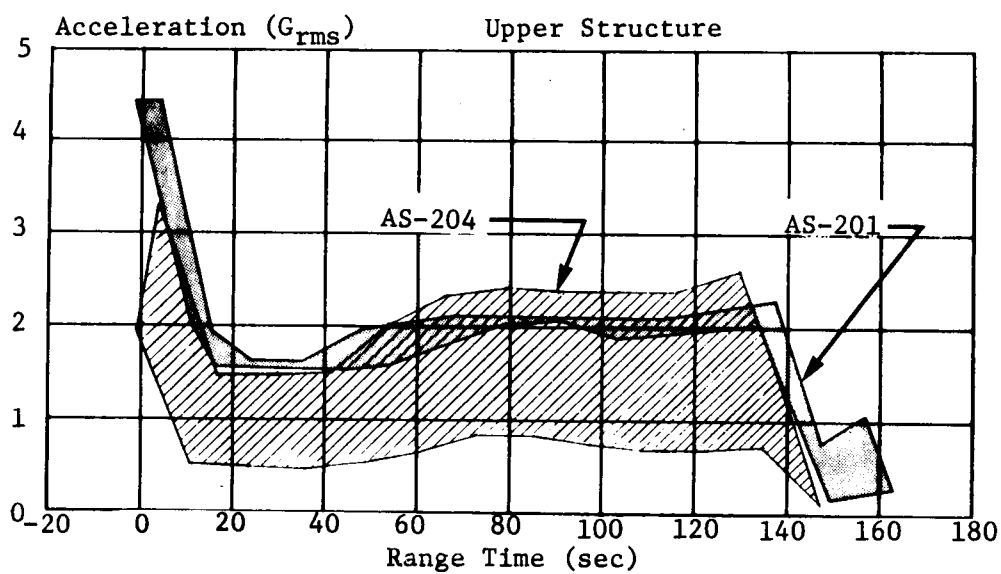
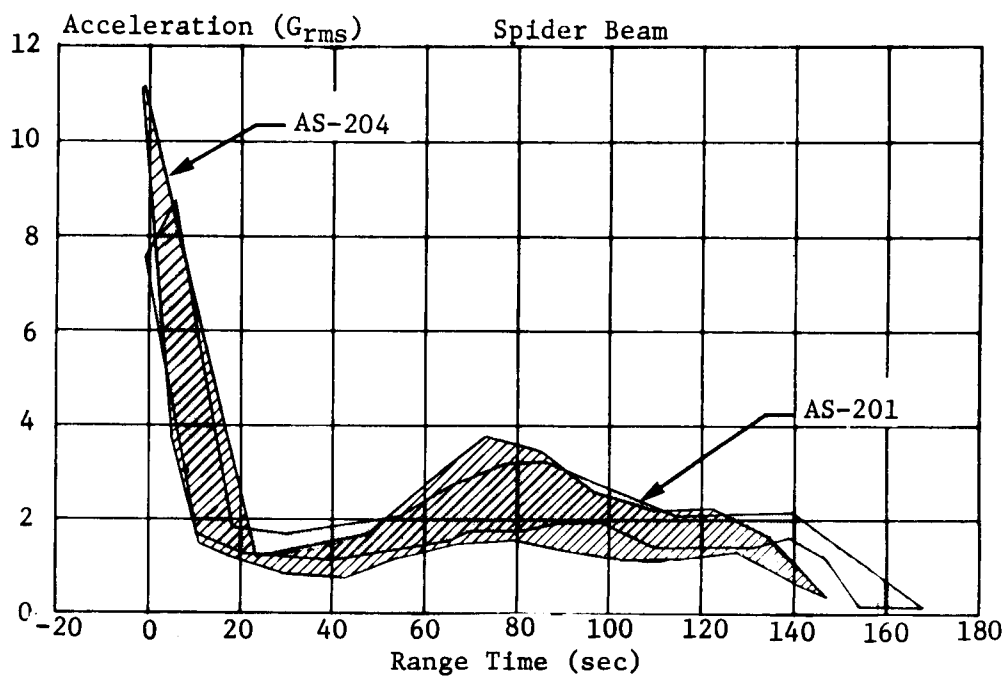


FIGURE 17-8 S-IB STRUCTURE VIBRATION ENVELOPES

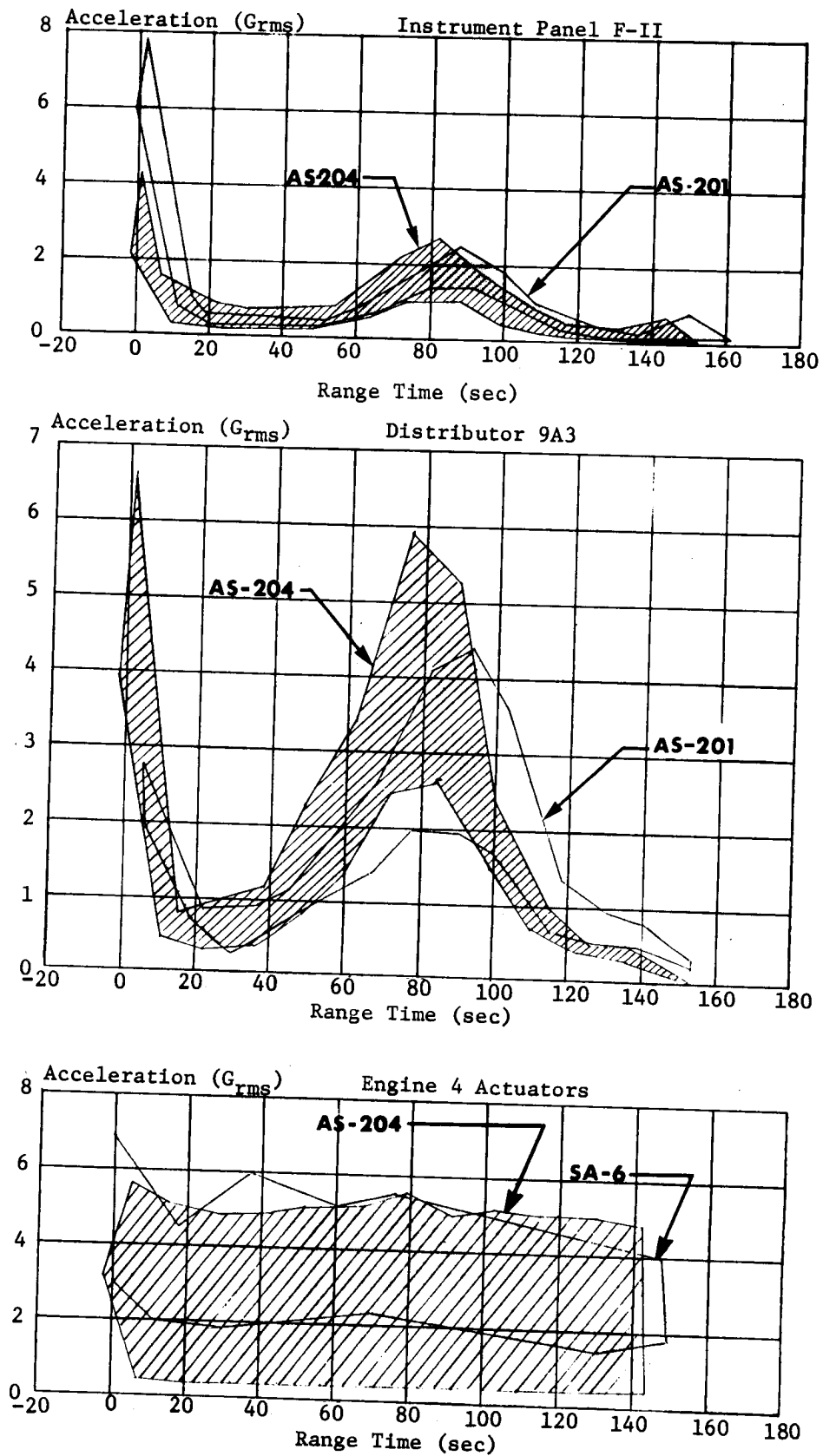


FIGURE 17-9 S-1B COMPONENT VIBRATIONS

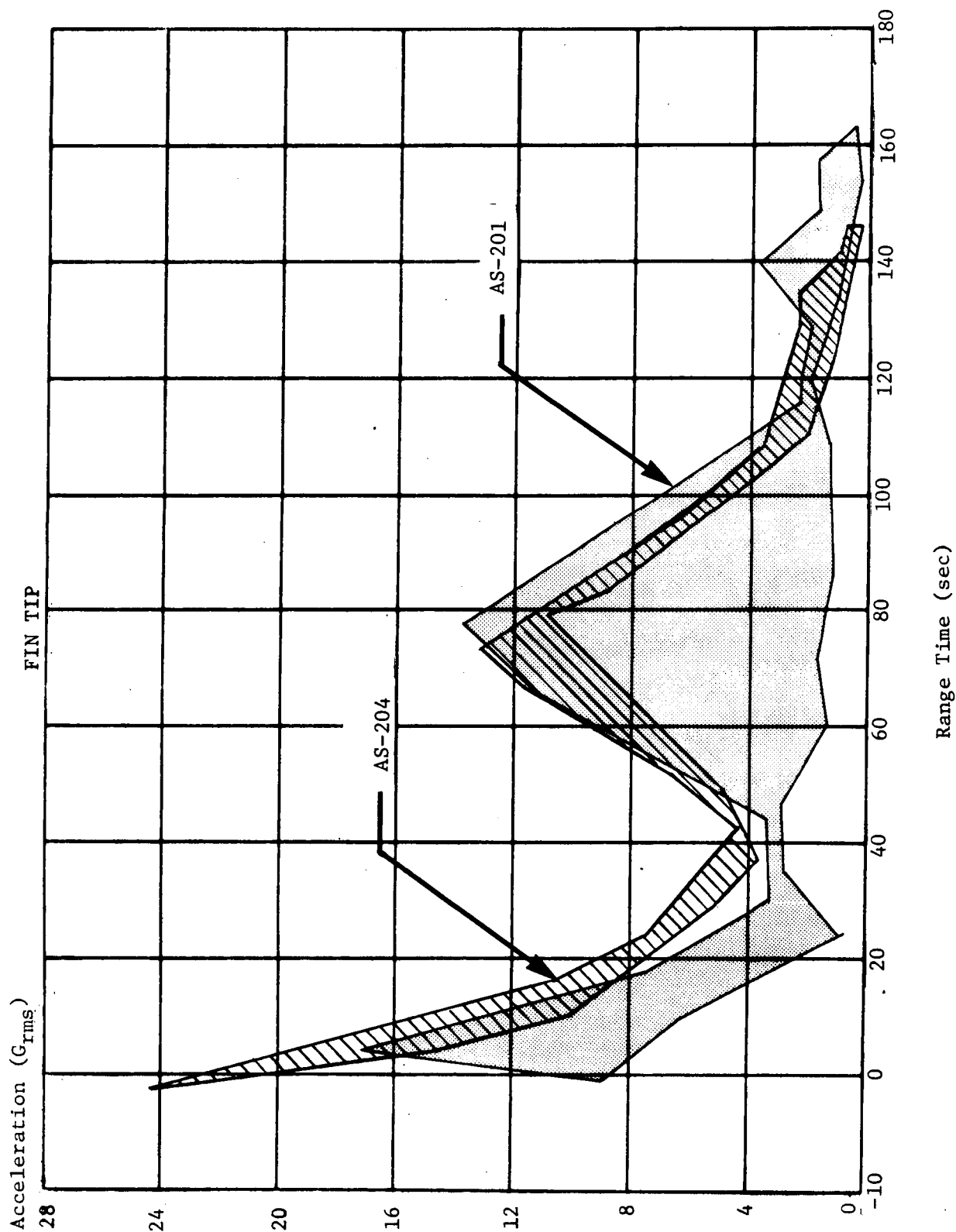


FIGURE 17-10 S-IB FIN VIBRATION ENVELOPES

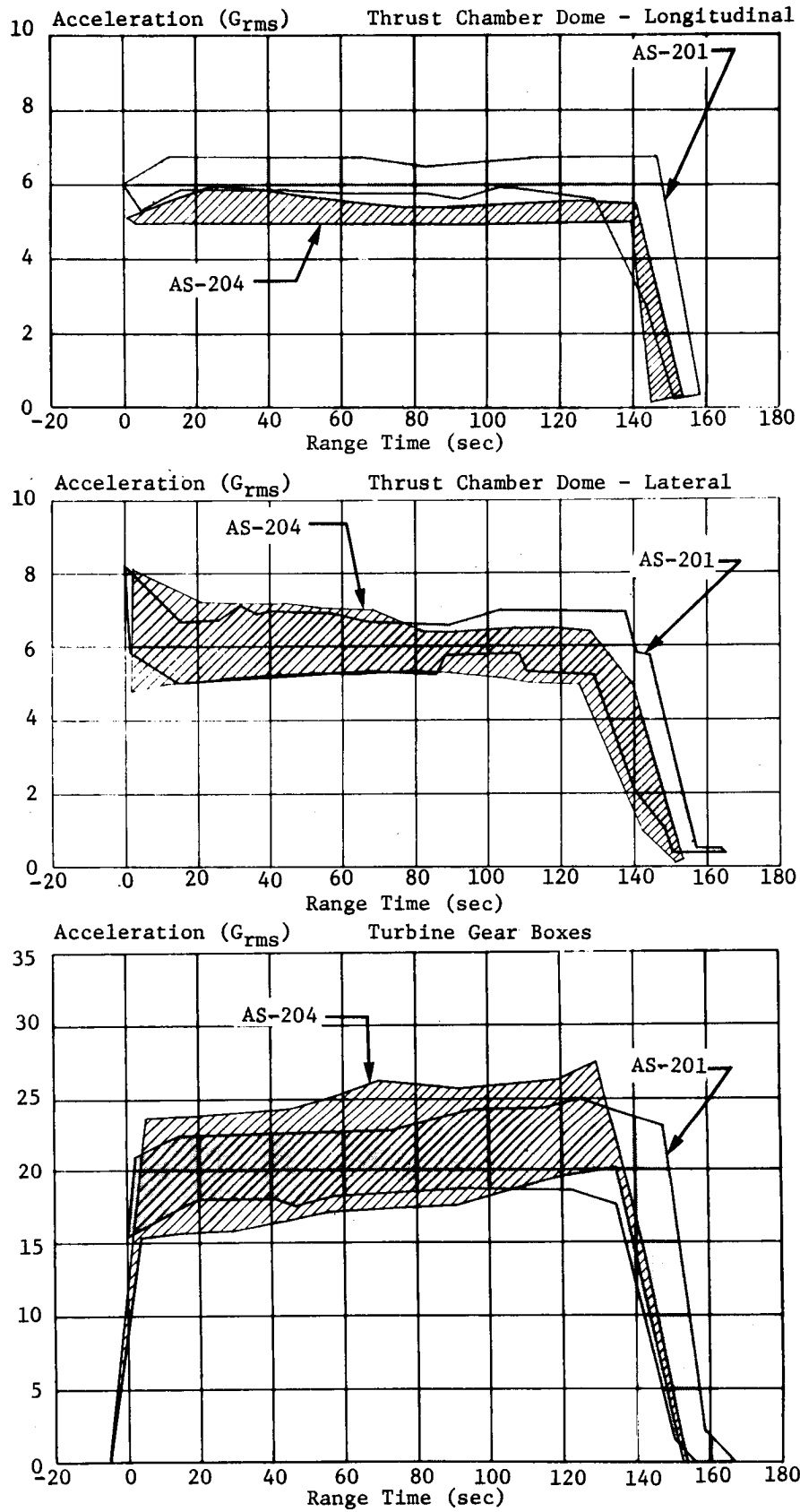


FIGURE 17-11 H-1 ENGINE VIBRATION ENVELOPES

17.4 S-IVB STAGE ANALYSIS

17.4.1 S-IVB VIBRATIONS

Six structural, twenty-one component, and two engine measurements were included in the S-IVB stage vibration evaluation. Time histories of the maximum and minimum composite levels for the structural components and engine measurements are shown in Figure 17-12 and the maximum composite levels are summarized in Table 17-III. Time histories are compared with comparable measurements made during AS-203 flight.

17.4.2 J-2 ENGINE VIBRATIONS

The LOX turbopump measurement was inoperative prior to flight and the LH₂ turbopump measurement became inoperative after approximately 150 sec of the S-IVB J-2 engine operation. The measured S-IVB-204 stage vibration environment during flight was comparable to the measured S-IVB-203 stage vibration environment. A time history of the composite (50 to 3000 Hz) vibration levels during S-IVB powered flight, compared to S-IVB-203, is shown in Figure 17-12.

17.4.3 S-IVB FORWARD SKIRT IN-FLIGHT FLUTTER EXPERIMENT

Sixteen dynamic strain gage measurements were placed on the AS-204/S-IVB forward skirt for the purpose of investigating possible panel flutter characteristics during the supersonic flight regime. These measurements were located at vehicle station 40.024 m (1575.75 in) and placed approximately every 22.5 deg around the circumference of the skirt section. The measurement numbers were S-0086 thru S-0101. Positioning of each strain gage was such that it was mounted along the streamwise center-line of the respective panel 10.16 cm (4 in) forward of the panel trailing edge. This location was chosen because data was obtained at the same point during earlier full-scale wind tunnel tests. Figure 17-13 shows the flight measurement locations and the corresponding identification system.

Two of the more important parameters affecting the susceptibility for panel flutter are:

1. Loading history of the panels; i.e., superimposing the bending moments due to angle-of-attack on the axial loading.
2. Differential pressure across the panels.

The total angle-of-attack history versus range time is shown in Section 12, for Figure 12-3. For angles-of-attack smaller than two deg, all the panels are assumed to be buckled due to axial loads alone (for higher angles-of-attack, the tensile loading on the windward side tends to reduce the buckling amplitude).

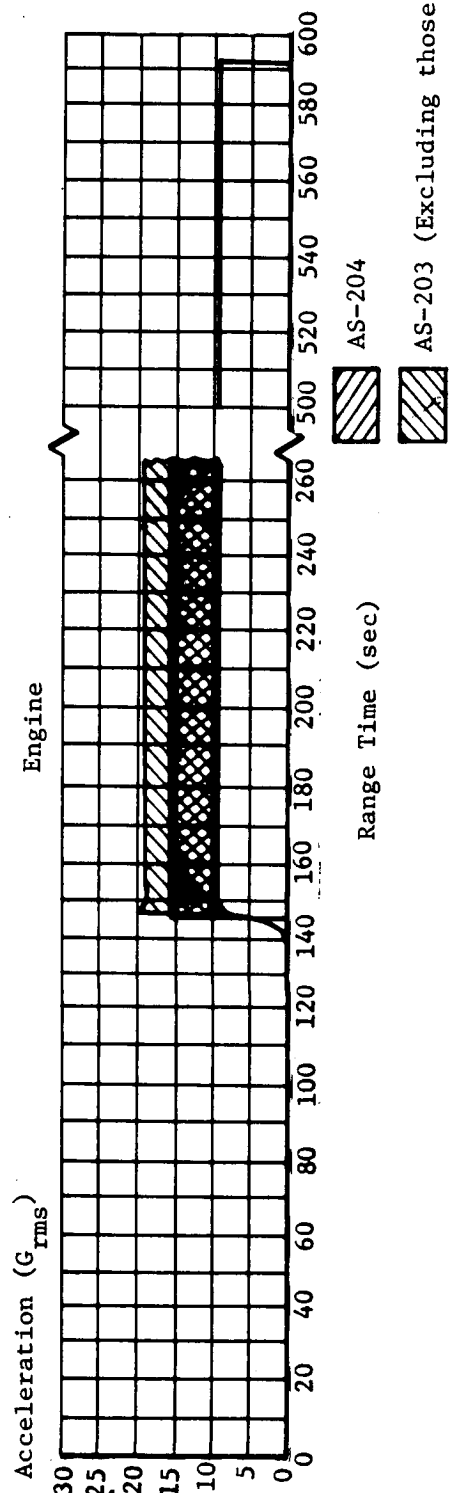
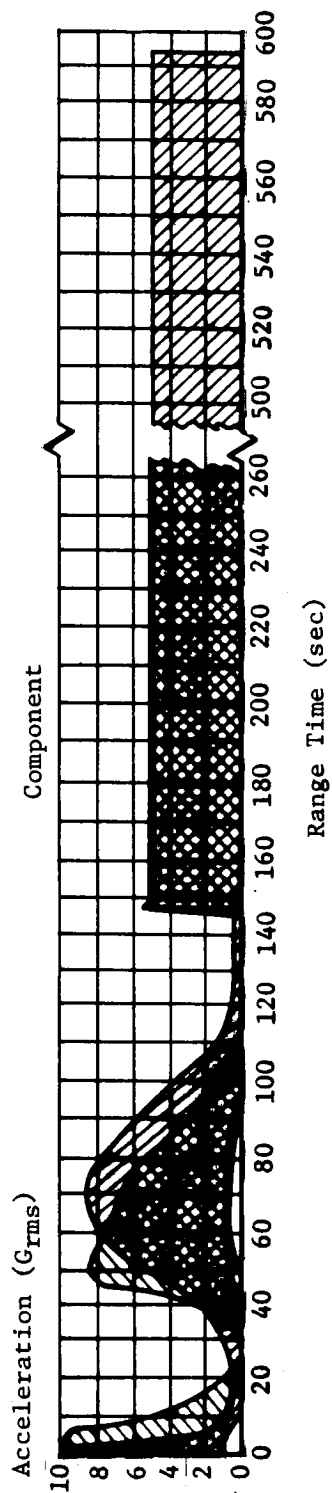
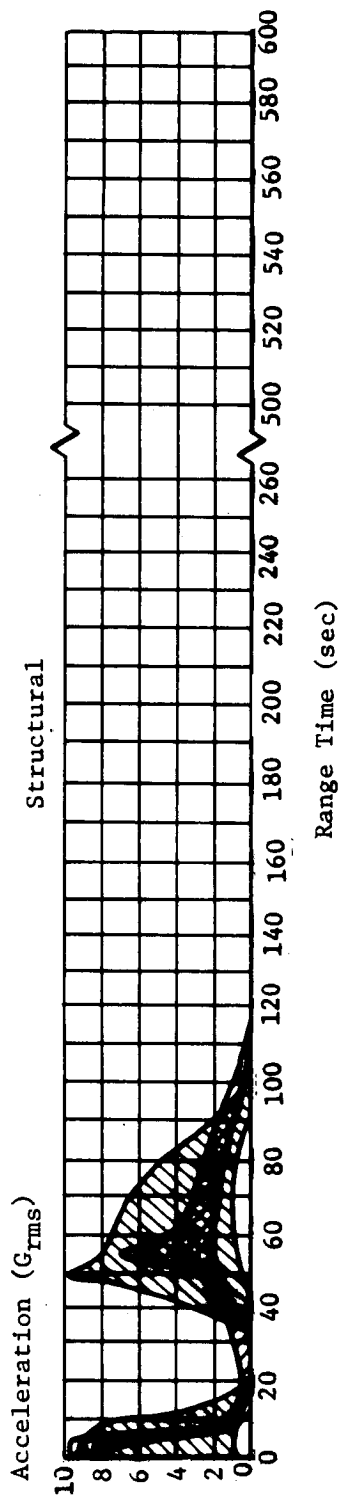


FIGURE 17-12 S-IVB VIBRATION ENVELOPES

TABLE 17-III S-IVB VIBRATION SUMMARY

Area Monitored		Max Level (G _{rms})	Range Time (sec)	Remarks
Structure	Forward Field Splice, Pos II-Thrust	1.6	79	
	Forward Field Splice, Pos II-Tangential	6.2	-1	
	Forward Field Splice, Pos II-Radial	6.1	0	
	LH ₂ Tank Cylinder at Sta. 43.8m (1436in)			
	Between Pos II and Pos III-Radial	9.4	3	
	At Position III Radial and Between Pos III and Pos IV Radial	8.6 7.3	3 -1	
Engine	Combustion Chamber Dome Thrust	7.6	570	
	LH ₂ Turbopump - Radial	14.8	170	The LH ₂ turbopump measurement became degraded at about 300 seconds probably due to loosened connector.
	LOX Turbopump - Radial	-	-	The LOX turbopump measurement was deleted prior to launch due to damaged connector.
Component	<u>Forward Skirt</u>			
	Telemetry Antenna-Tangential	3.9	56	
	Telemetry Antenna-Radial	11.3	0	
	LH ₂ Tank Vent Valve-Thrust	2.8	-1	
	LH ₂ Tank Vent Valve-Radial	6.2	4	
	<u>Tank Cylinder</u>			
	Helium Spheres-Radial	3.2	80	
	<u>Aft Skirt</u>			
	LOX Tank Vent Valve-Normal to Flow	1.2	0	The LOX tank vent valve normal to flow measurement registered 2.3 G's at about 610 seconds. This is about 12 seconds after the S-IVB J-2 engine cutoff and may be due to normal venting.
	LOX Feedline at Tank-Thrust	2.5	2	
	LOX Feedline at Tank-Radial	1.1	3	
	LOX Feedline at Engine-Thrust	6.7	565	
	LOX Feedline at Engine-Radial	2.5	570	
	LOX Feedline at Tank-Thrust	2.8	565	
	LH ₂ Feedline at Tank-Radial	4.9	4	
	LH ₂ Feedline at Engine-Thrust	3.4	155	
	LH ₂ Feedline at Engine-Radial	4.6	570	
	Auxiliary Hydraulic Pump-Thrust	3.8	568	
	APS Mod 1 Aft Attach Point-Thrust	5.9	68	
	APS Mod 1 Aft Attach Point-Radial	7.4	68	
	APS Mod 1 Fwd. Attach Point-Radial	7.6	73	
	Retrorocket Center Attach Point-Thrust	3.3	1	
	Retrorocket Forward Attach Point-Radial	3.2	68	
	Retrorocket Fwd. Attach Point-Tangential	3.3	4	
				Note:
				The maximum vibration occurs in one of three intervals. One at liftoff due to high sound pressure, second near maximum dynamic pressure due to turbulence, and third during J-2 engine operation.

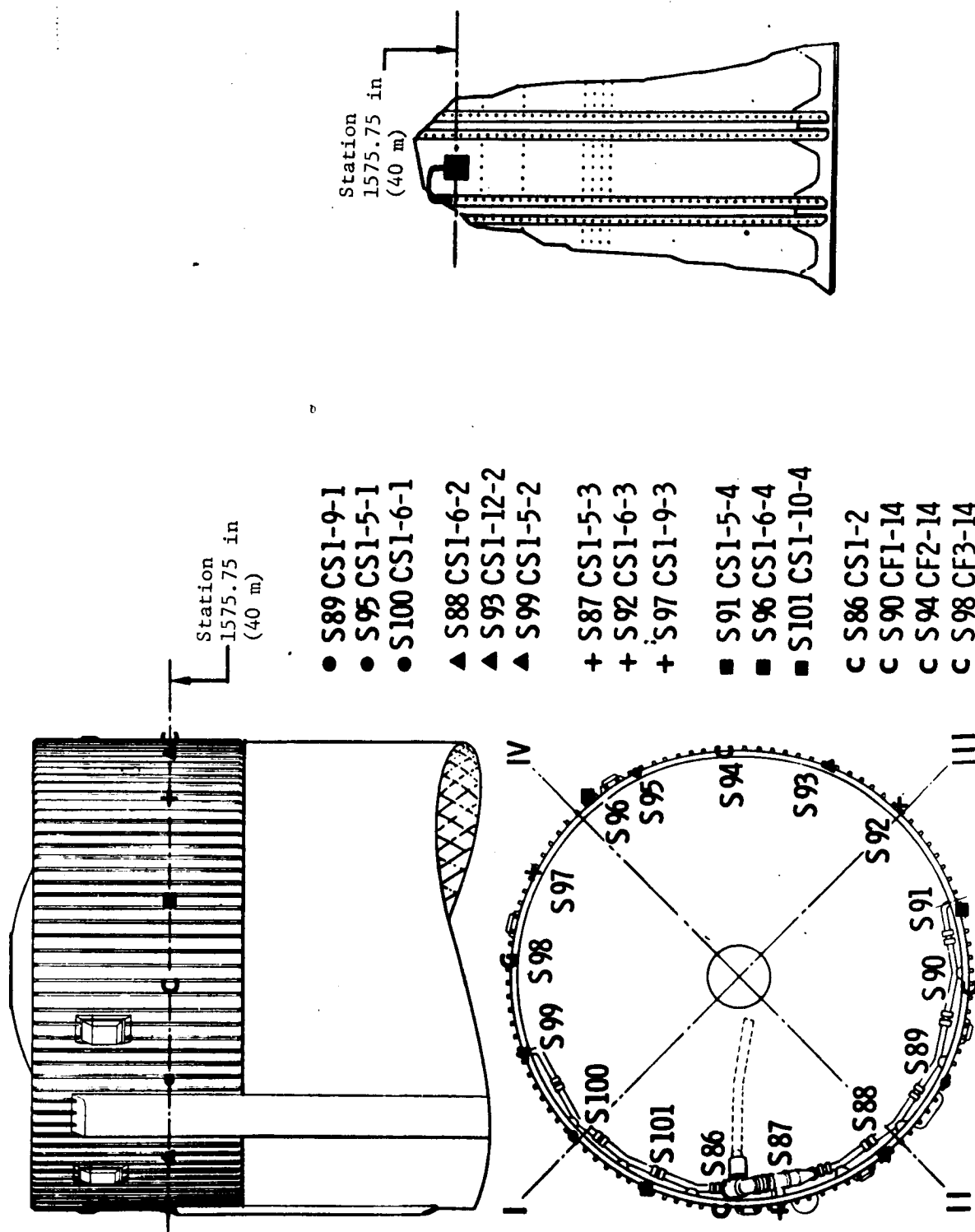


FIGURE 17-13 S-IVB FORWARD SKIRT DYNAMIC STRAIN MEASUREMENTS

The differential pressure time history across the panels is shown in Figure 17-14. The differential pressure loads were calculated by using two internal pressure measurements and two of the three external measurements located at Station 40.21 m (1583 in). A third external measurement was disregarded due to its being located adjacent to a protuberance. The differential pressure at 86 sec was $0.58 \pm 0.04 \text{ N/cm}^2$ ($0.84 \pm 0.05 \text{ psid}$), and the correlation between corresponding measurements was excellent. The presence of a pressure differential across a panel will tend to decrease the flutter potential and/or suppress the resulting panel flutter stress amplitudes. Similarly, angles-of-attack greater than about 2 deg will decrease the differential pressure loading on panels on the windward side of the vehicle, making conditions more favorable for flutter to occur.

Most of the observed data were random in nature, showing no indications of panel flutter. This random response is typical of response which results from engine acoustic excitation or boundary layer pressure fluctuations. The dominant response modes (320 - 600 Hz), indicated by the flight data, were observed in the wind tunnel data when the panels were responding to the random fluctuating pressures in the boundary layer during periods when panel flutter was not occurring. The wave form of the random response flight data, which is similar to the wind tunnel data during periods when panel flutter was not occurring, was that of narrow-band, random vibration. This wave form is typical of panel response to acoustic noise or pressure fluctuations due to random turbulence in the boundary layer (see Figure 17-15, T = 2 sec). However, four measurements exhibited a complex periodic strain amplitude time history within a time interval of 80 to 87 seconds. These measurements were S-90, S-92, S-98, and S-100. The amplitude time histories were of the type which is characteristic of buckled panel flutter. Measurement S-92 exhibited this complex periodic amplitude for approximately 3 sec near Mach 2.1 at the significantly high differential pressure value quoted above. A trace, obtained from a high speed oscillogram, is shown in Figure 17-15.

Time histories of the maximum and minimum composite strain levels measured at each location, which are relevant only to the specific location, are shown in Figure 17-16. The measured maximum amplitude of the dynamic strain during flight was $\pm 600 \mu \text{ in/in}$ at approximately 80 sec as compared to a maximum value of $\pm 700 \mu \text{ in/in}$ measured at liftoff. The measured maximum amplitude of the composite strain signal of measurement S-92 is $\pm 400 \mu \text{ in/in}$, which is insignificant for AS-204 in both amplitude and duration.

It is concluded from the limited amount of flutter instrumentation and the fact that a high value of ΔP was present during the AS-204 flight that the majority of the panel loading was due to random excitation but that evidence of limited amplitude flutter was present as expected. Both types of loading were insignificant with respect to the AS-204 panels. Additional in-flight flutter measurements are to be made on the S-IVB stage of Saturn V, 502 flight.

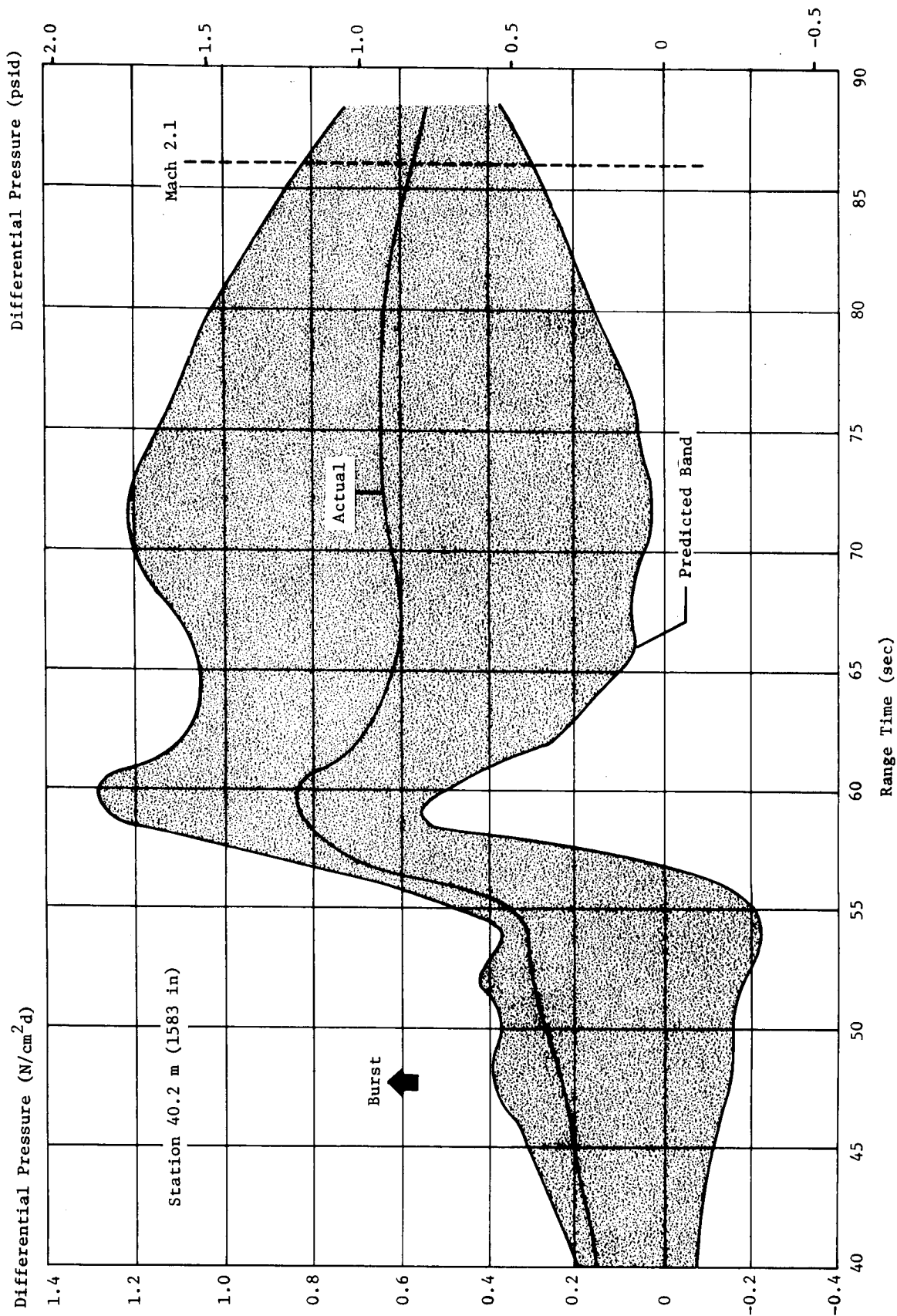
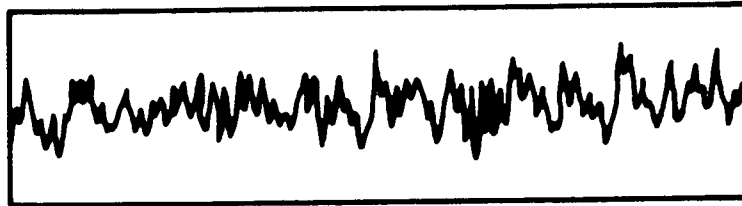
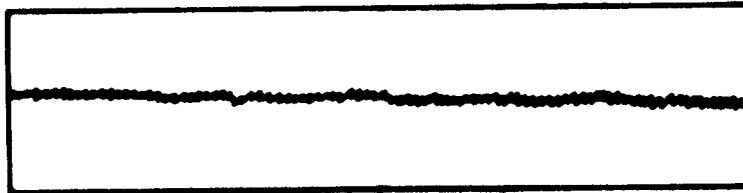


FIGURE 17-14 DIFFERENTIAL PRESSURE ACROSS PANELS



2 sec Time Slice

84.5 to 87.5 sec Time Slice
2.05 to 2.25 Mach Number

96.5 sec Time Slice

FIGURE 17-15 TIME SLICES OF DYNAMIC STRAIN OUTPUT FOR MEASUREMENT S-92

17.4.4 S-IVB INTERNAL ACOUSTICS

The S-IVB stage internal acoustic environment was measured in the aft skirt near position IV approximately 0.79 m (31 in) forward of the separation plane. Time histories for the composite levels are shown in Figure 17-16. The time histories for the composite levels of the external acoustic environment are provided to indicate transmissibility of the aft skirt structure. The levels measured at a comparable location during the AS-203 flight are also shown. No significant difference between the environments of the AS-203 and AS-204 is portrayed.

17.5 INSTRUMENT UNIT VIBRATION

Data was received from all 23 vibration measurements and the one acoustic measurement. However, data from two measurements have been declared invalid since the vibration peak levels exceeded the circuit capability of 120% and 100%, respectively, of full scale during liftoff.

As shown in Figure 17-17, the maximum vibration levels for S-IU-204 occurred during liftoff and lasted for approximately five seconds.

The seven valid measurements monitoring S-IU-204 structural vibration (Figure 17-17) at the upper and lower interface rings indicated a lower environment existed during this flight than on S-IU-202. At liftoff the S-IU-204 structural vibration levels exceeded those of S-IU-202 by approximately 10 percent. This deviation is within the accuracy of the telemetry system. The fifteen Instrument Unit component vibration measurements indicate that the S-IU-204 component vibration level was lower than that of S-IU-202.

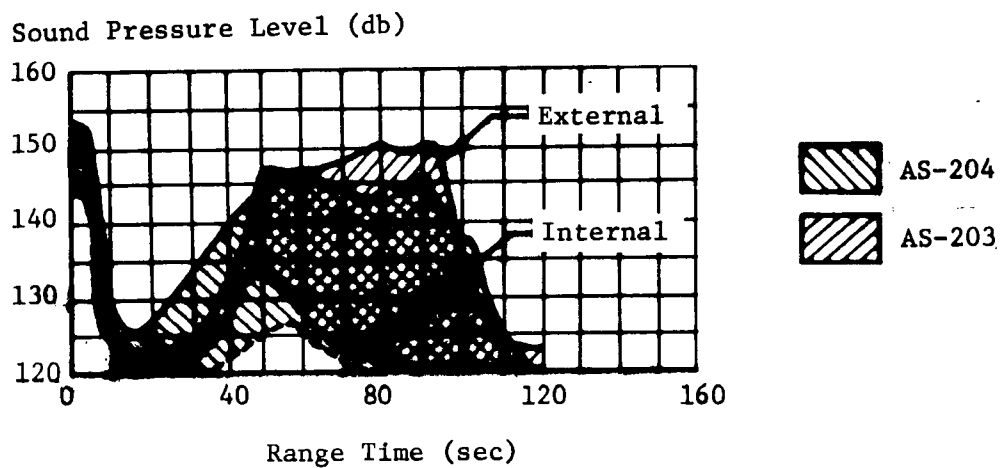
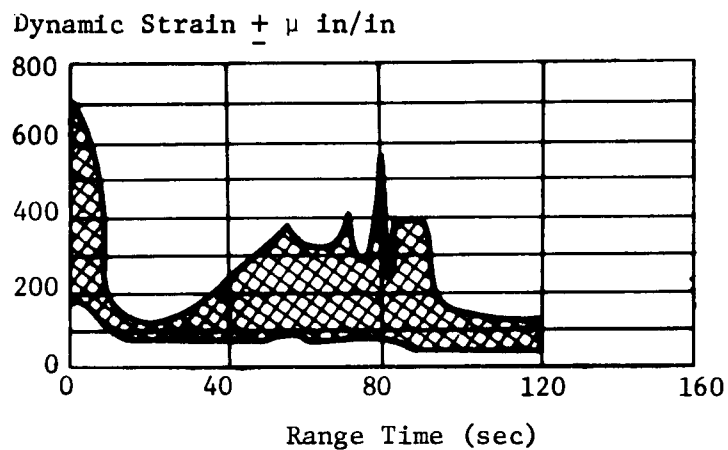


FIGURE 17-16 S-IVB FORWARD SKIRT DYNAMIC STRAIN AND SOUND PRESSURE LEVEL

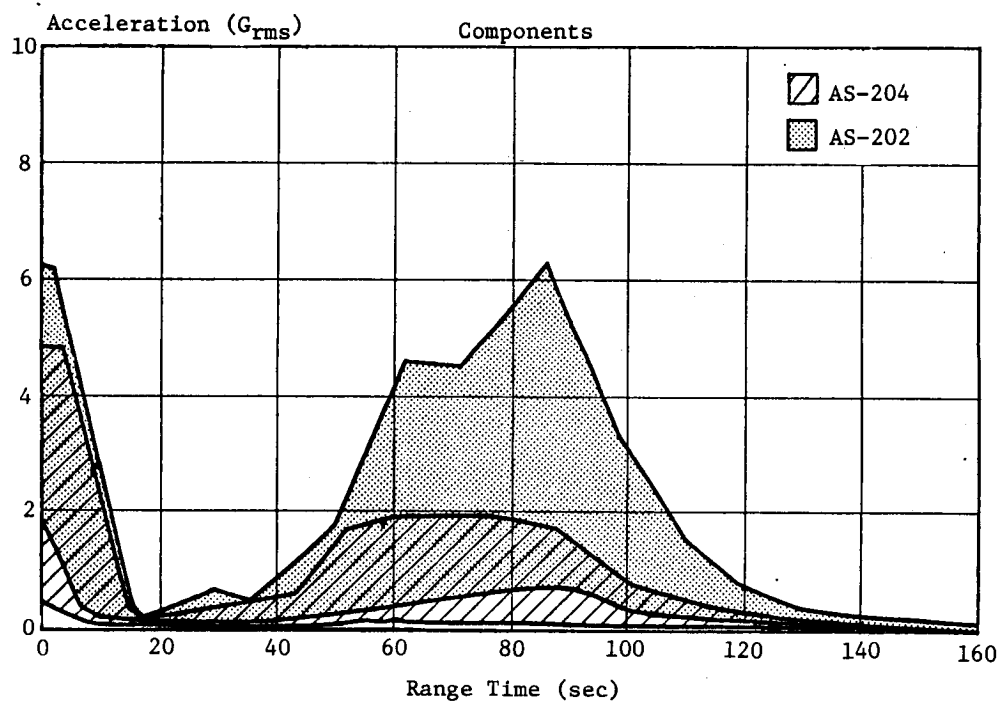
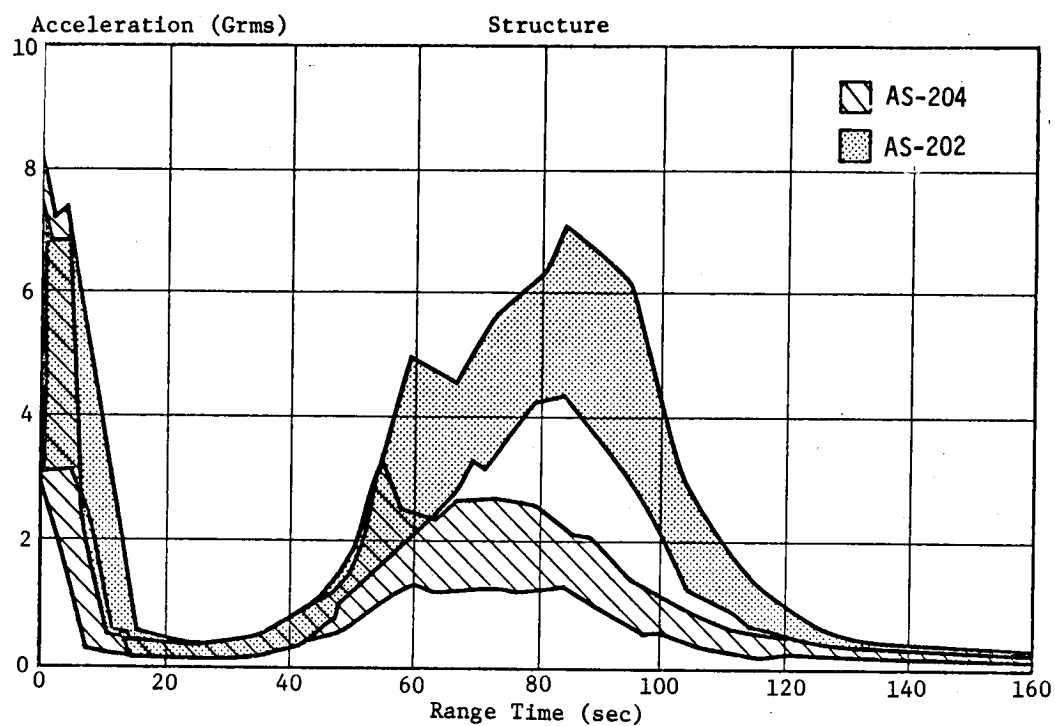


FIGURE 17-17 IU VIBRATION ENVELOPES

18.0 PRESSURE AND THERMAL ENVIRONMENT

18.1 SUMMARY

The measured S-IB stage pressure and thermal environment was in general agreement with preflight predictions and previous S-IB flight data. The base pressures were slightly higher than on previous flights; however, the higher levels present no design problems.

The S-IVB-204 pressure and thermal environment was as expected. The forward and aft compartment pressure differentials were well within their design limits. Aerodynamic heating and the protuberance-induced heating rates were lower on AS-204 than on AS-203.

Overall sound pressure levels on AS-204 were slightly lower than those measured on previous flights.

Analysis of the Thermal Conditioning System indicated deviations in three performance parameters. These were low water flowrates during sublimator startup, low sublimator water inlet pressures, and excessive GN₂ consumption. The low water pressure and flowrate did not affect the performance of the Thermal Conditioning System as measured by system temperatures. The excessive GN₂ consumption has been attributed to leakage.

The Gas Bearing System maintained temperature within specification. The differential pressure across the gas bearings was slightly higher than the specified value. There were no adverse effects to the platform from this higher differential pressure.

18.2 VEHICLE PRESSURE AND ACOUSTIC ENVIRONMENT

18.2.1 EXTERNAL SURFACE PRESSURES

Pressures measured on the LOX tank 03 forward skirt and fuel tank F1 aft skirt, shown in Figure 18-1, were as expected. The LOX tank 03 forward skirt pressures were generally lower than those experienced on previous flights after 71 seconds.

The 60 deg tank fairing pressure loading was similar to previous flight data and well within design specifications (see Figure 18-21). The external surface pressure on the 60 deg tank fairing was obtained by combining the differential pressure across the tank fairing with the thrust frame compartment pressure. The resultant pressure coefficient, as shown in the bottom half of Figure 18-2, is in good agreement with wind tunnel and previous flight data.

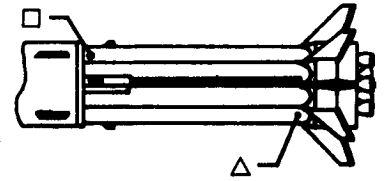
--- Wind Tunnel Data

— AS-201

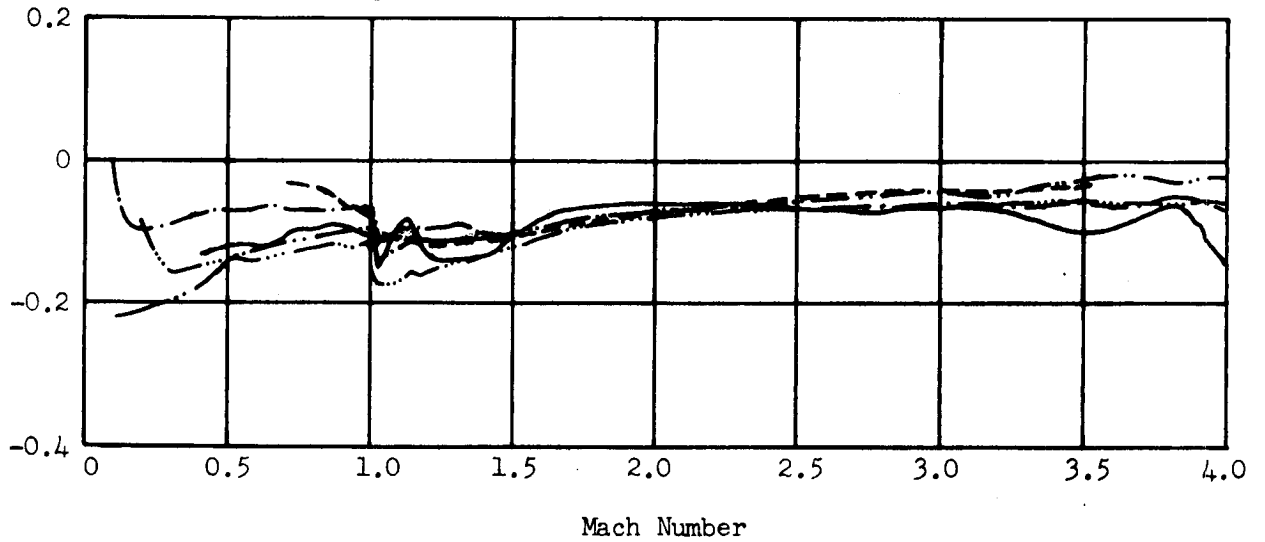
... AS-202

... AS-203

— AS-204



LOX Tank 3 Forward Skirt
Pressure Coefficient, (C_p)



Fuel Tank 1 Aft Skirt
Pressure Coefficient, (C_p)

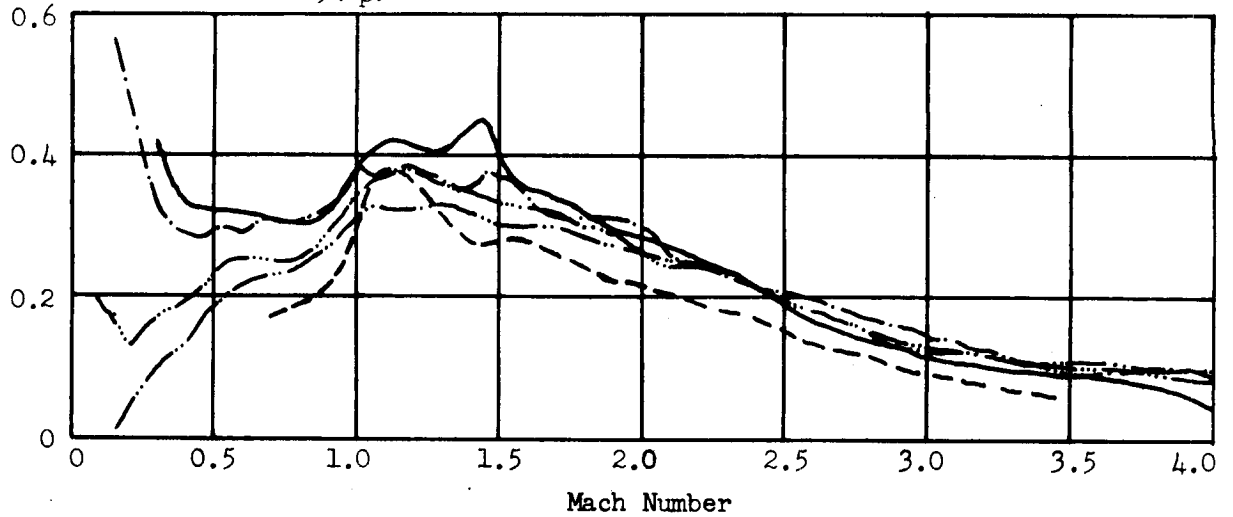


FIGURE 18-1 S-IB STAGE TANK SURFACE PRESSURE ENVIRONMENT

--- Wind Tunnel Data

— AS-201

· · AS-202

· · · AS-203

— AS-204

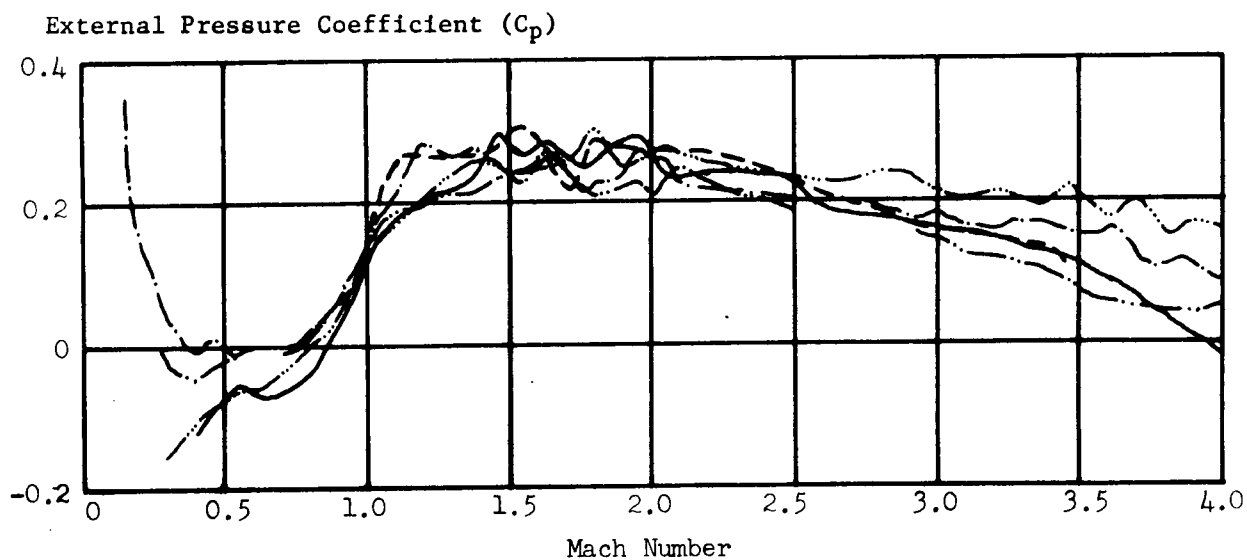
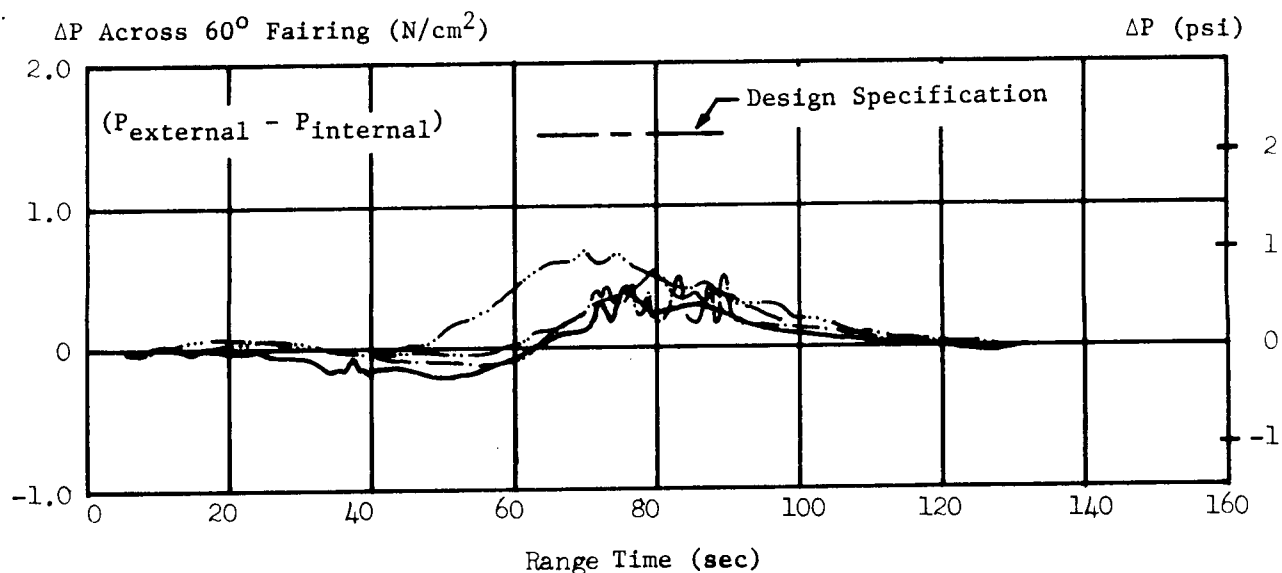
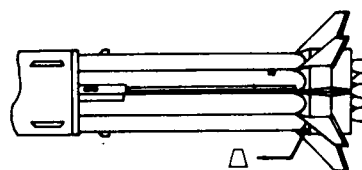


FIGURE 18-2 SURFACE PRESSURE ENVIRONMENT ON 60° FAIRING

18.2.2 EXTERNAL ACOUSTICS

Three external acoustic measurements were flown on AS-204; one on the IU, one on the aft skirt of the S-IVB stage, and one on the lower tail shroud of the S-IB stage. The IU measurement location was coincident with those on AS-201 and AS-202. The S-IB stage measurement was the same as on all previous Saturn IB vehicles and the S-IVB measurement was coincident with AS-203. All measurements yielded valid data through first stage powered flight with the exception of the S-IB stage lower shroud, which became questionable after 28 seconds.

Figure 18-3 presents the AS-204 acoustic environment at liftoff. The overall sound pressure level (OASPL) between 10 and 3000 Hz is presented as a function of vehicle station and compared to previous flight data and the predicted band. The upper portion of Figure 18-3 presents acoustic spectra at liftoff and compares the spectrum levels to the acoustic design specifications. All data were within the design specifications with the exception of some frequencies around 200 Hz on the IU. This condition also existed on AS-202 and is not considered serious.

The OASPL during flight at the three instrument positions is presented in Figure 18-4. The data for these instruments were reduced every 3 or 4 sec, hence any data pulses between reduction points were lost. Check points with a one second integration time are indicated. At 54 sec, which corresponds to 0.83 Mach number, an increase in amplitude was indicated on the oscillogram. The 0.83 Mach number is approximately the Mach number at which wind tunnel data indicates an unsteady shock wave would exist at Station 42.8m. A spectral breakdown at 54 sec did not correspond to typical unsteady shock spectra from AS-201 and AS-202. The OASPL of 147.5 db for this location is 10 db lower than the unsteady shock levels on AS-201 and AS-202.

The fluctuating pressure coefficient ($\Delta C_{p_{rms}}$) for the IU measurement at Sta. 42.8 m (1685 in) is presented in the upper portion of Figure 18-5. AS-204 data shown for Mach 0.79 (52.5 sec) to Mach 0.89 (56 sec) indicate the non-agreement of the unsteady shock spectra. The AS-204 fluctuating pressure spectra at Mach 1 are compared to AS-202 and AS-203 in the middle portion of Figure 18-5. Payload configuration differences are believed to be the reasons for the difference in the fluctuating pressure coefficient and in unsteady shock spectra above Mach 0.8 and Mach 1.0. The lower portion of Figure 18-5 compares AS-203 and AS-204 fluctuating pressure at Mach 1 on the aft skirt of the S-IVB stage. Good agreement is shown for this location even though there is a difference in dynamic pressure values (middle portion of Figure 18-5), indicating a non-dependence on dynamic pressure.

The flight telemetry response of external acoustics measurements is from 50 to 3000 Hz with signals attenuated at 200 Hz by 0.4 db and 4dB at 50 Hz. Data should be disregarded below 50 Hz. All sound pressure

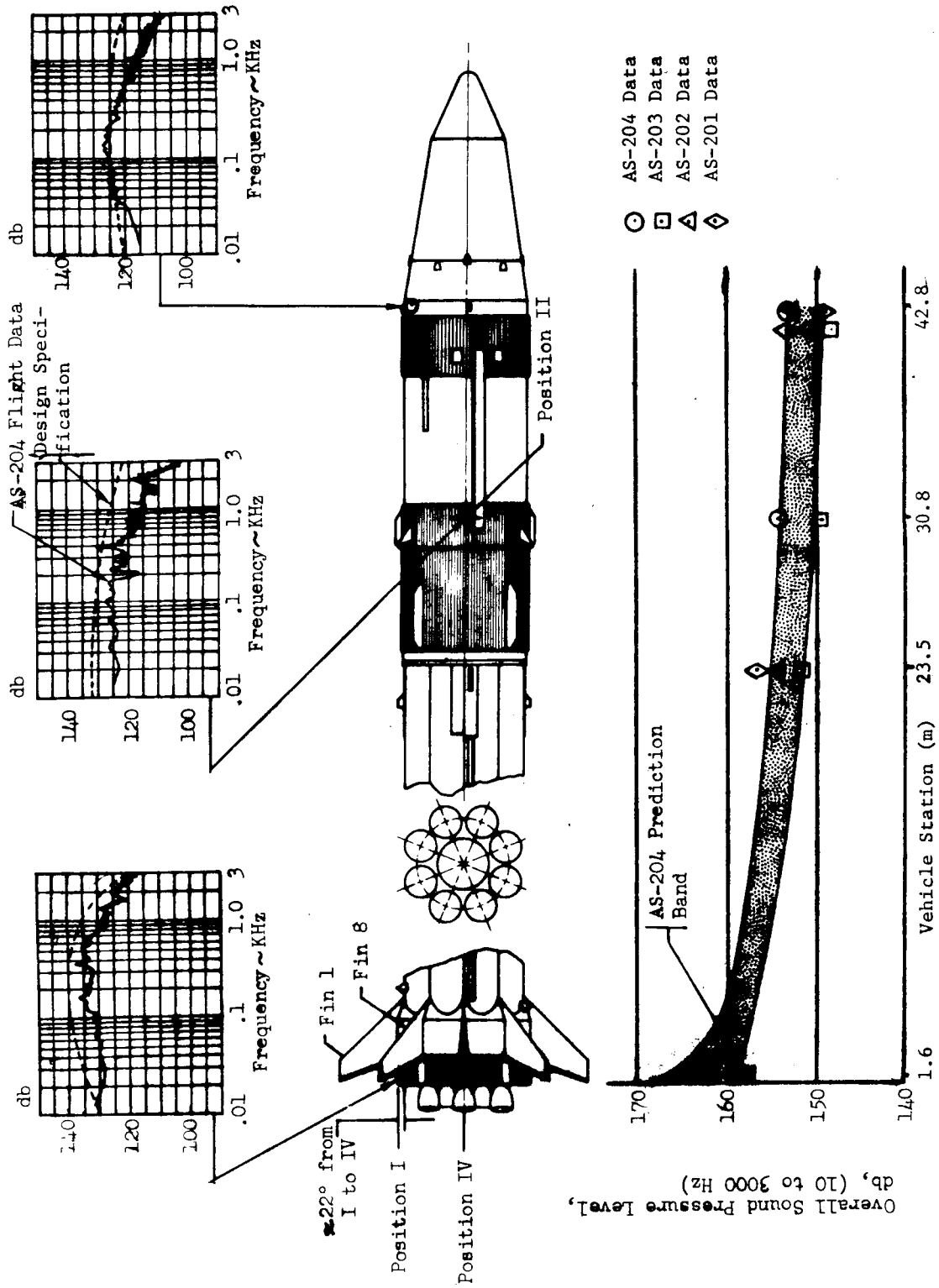


FIGURE 18-3 VEHICLE NOISE ENVIRONMENT AT LIFTOFF

NOTE: Overall Sound Pressure Level (db) is referenced to 0.00002 N/cm²

Overall Sound Pressure Level contains the energy from 10 to 3000 Hz. Data obtained every 3 to 4 seconds.

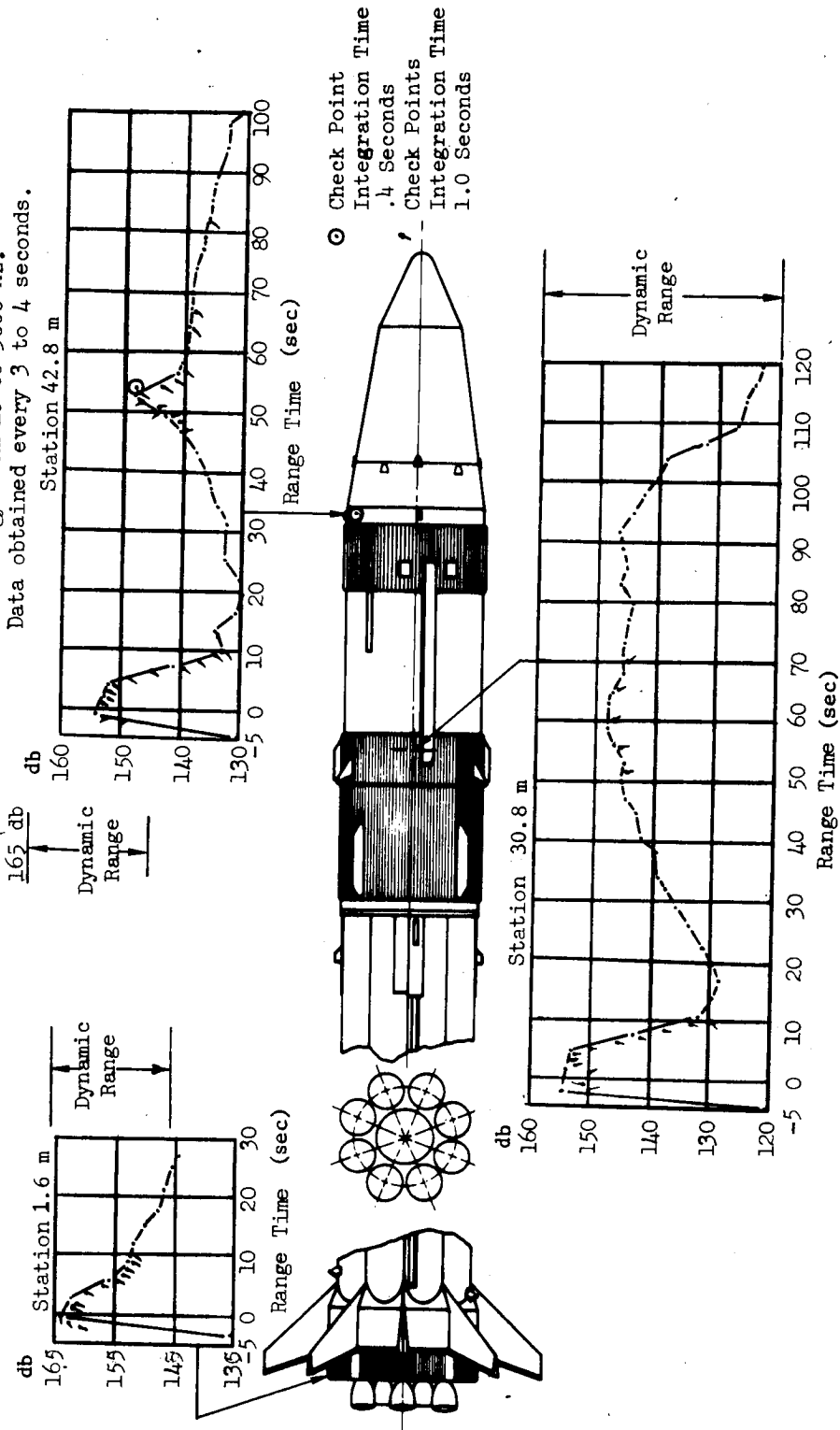


FIGURE 18-4 OVERALL SOUND PRESSURE LEVEL AT VARIOUS LOCATIONS

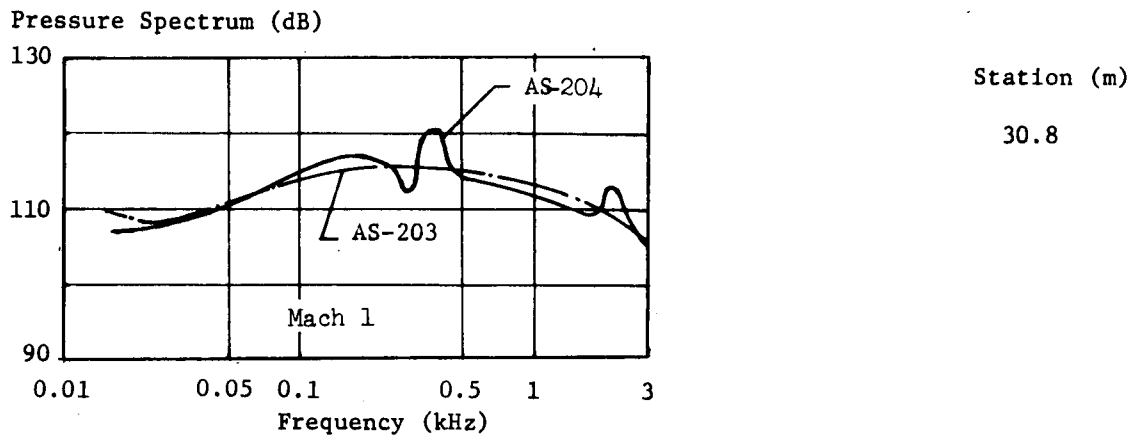
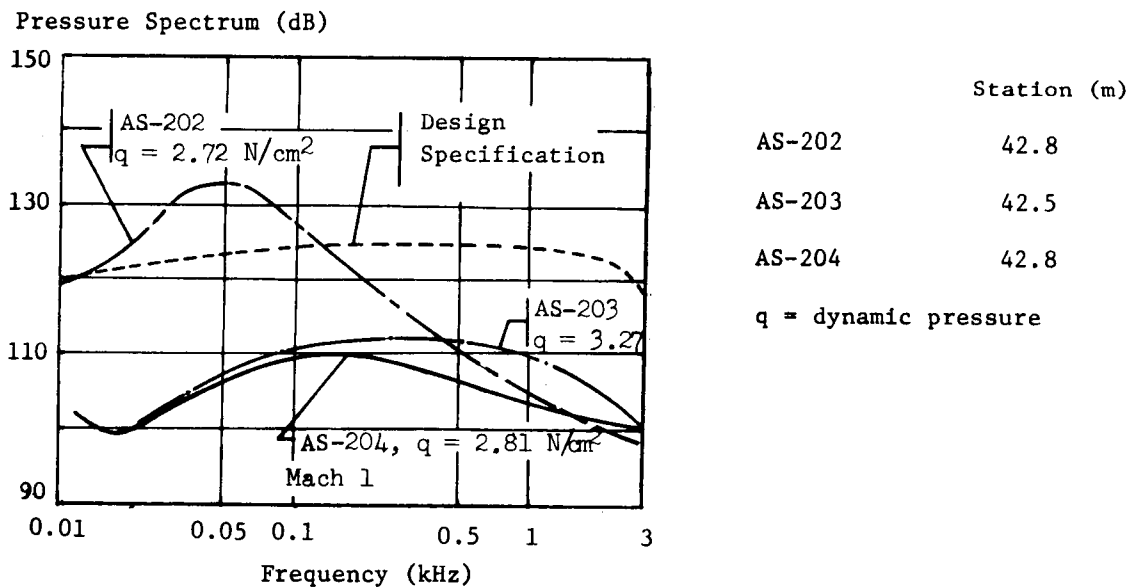
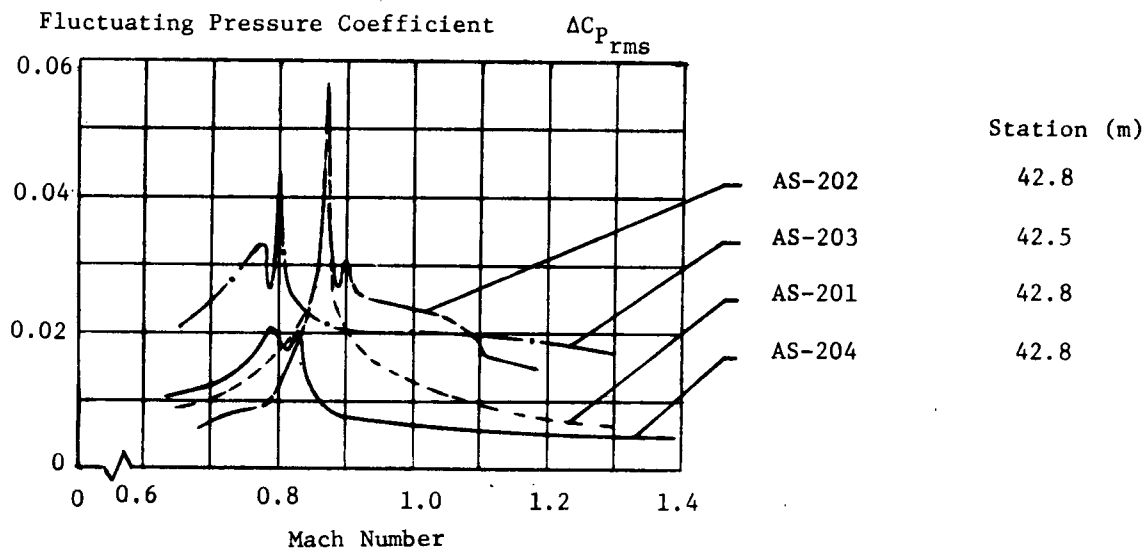


FIGURE 18-5 FLUCTUATING PRESSURE COEFFICIENT AND MACH 1 ACOUSTIC SPECTRA

levels are expressed as decibels (dB) and are referenced to 0.00002 N/cm^2 .

All pressure spectra presented were obtained from a random vibration analysis (RAVAN) program for use with a digital computer. The spectra obtained from this program utilized a 10 Hz filter bandwidth and are presented in terms of Hanned decibel (dB). All data were corrected for sample length utilizing the method developed by Hann. The program obtains the spectrum from the Fourier transform of the auto-correlation function. All flight data were digitized at 8,000 samples per second. Measurement accuracy is generally within 10% of full scale.

18.2.3 S-IB STAGE INTERNAL PRESSURES

Pressures measured in the shear panel compartment and referenced to ambient pressure are compared to the preflight prediction in Figure 18-6. Flight data exceeded the predicted band between 2 and 9 km (33 to 64 sec), but this was of little consequence since the maximum pressure difference was lower than the predicted maximum.

18.2.4 S-IB STAGE BASE PRESSURE

The measured loading on the heat shield was within the predicted band and was similar to that of the previous flights. Maximum heat shield loading, as seen in the lower part of Figure 18-6, was lower than design specification.

Heat shield pressures (Figure 18-7) were slightly higher than those recorded on previous flights. These higher base region pressures did not increase the heat shield loading significantly, but did produce a reduction in base drag.

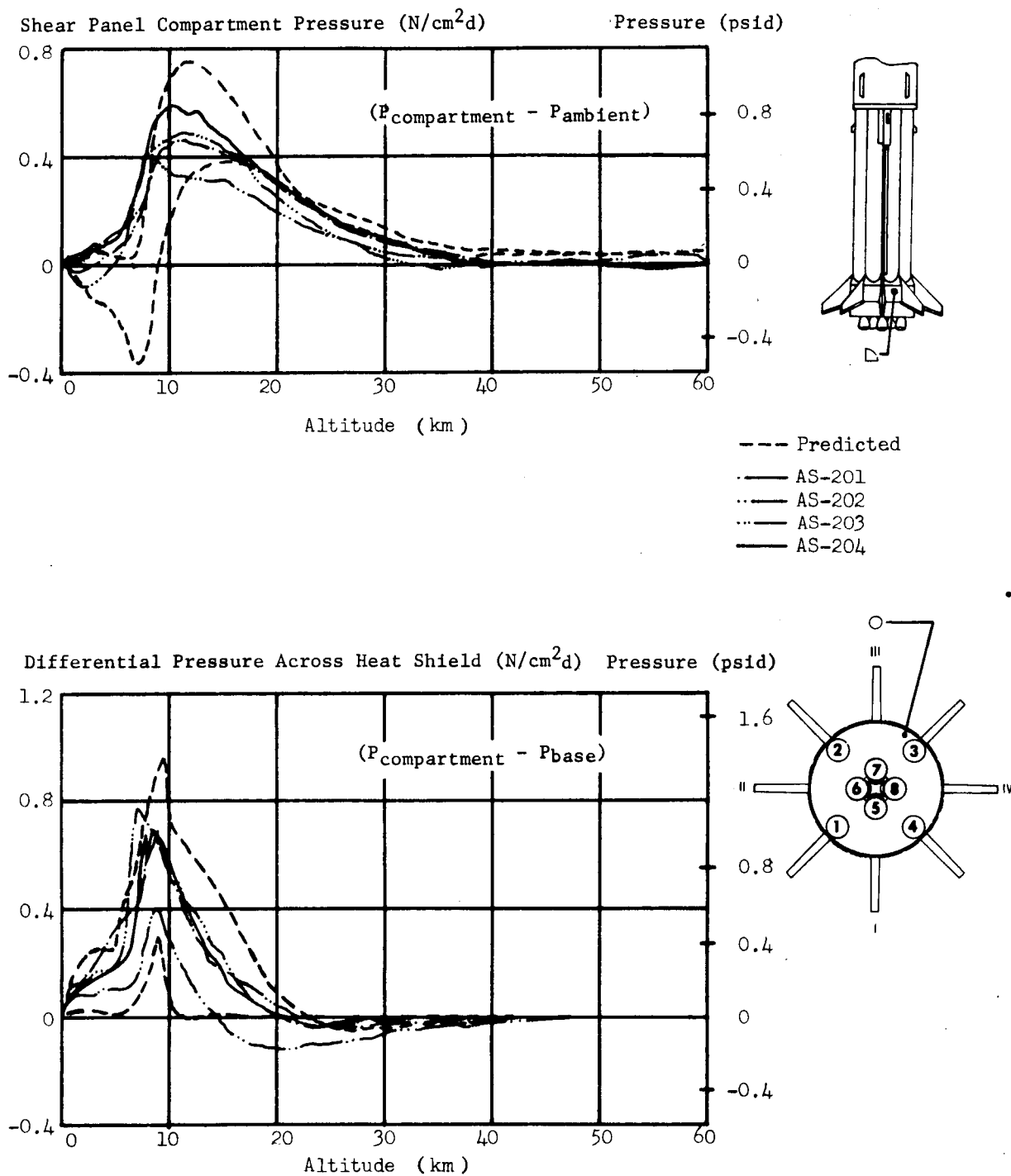
The AS-204 flame shield differential ($P_{\text{base}} - P_{\text{ambient}}$) pressure (shown on the left of Figure 18-8) were also slightly higher than on previous flights. Differential pressure loading on the flame shield ($P_{\text{flame shield}} - P_{\text{base}}$) was lower than on AS-203 and about 1 N/cm^2 below the design limit as shown in the right portion of Figure 18-8.

18.2.5 S-IB/S-IVB INTERSTAGE ENVIRONMENT

Figure 18-9 presents the S-IB/S-IVB interstage pressure environment and the S-IB stage seal plate loading. Agreement with previous flight and predicted was good.

18.2.6 S-IVB STAGE PRESSURE DIFFERENTIAL

The forward and aft compartment pressure differentials were within design levels and similar to those measured on AS-203. This is as expected since the vent areas were the same (0.097 m. or 3.8 in) and there were only minor configuration differences. Figure 18-10 shows the preflight predicted



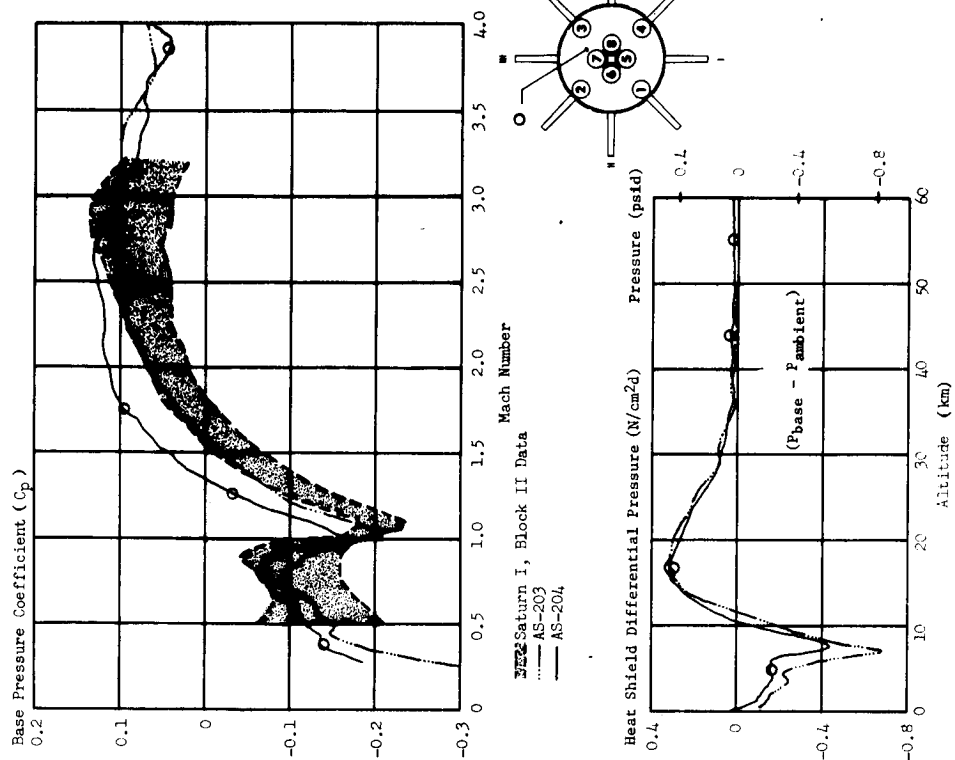
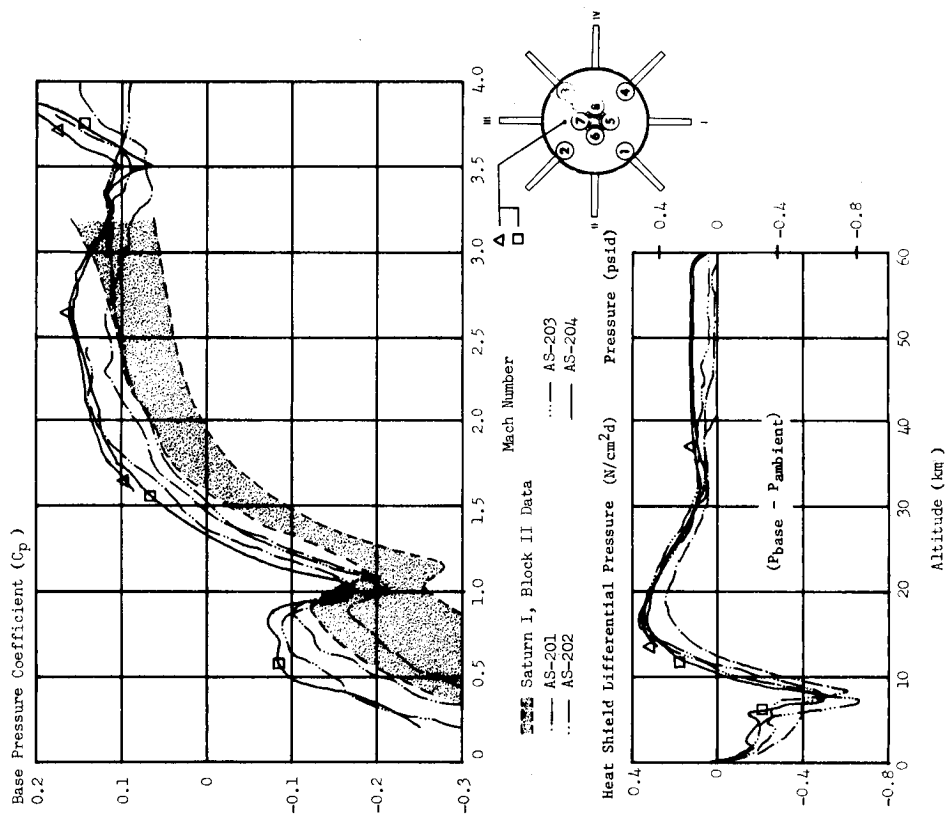


FIGURE 18-7 S-1B STAGE BASE PRESSURES

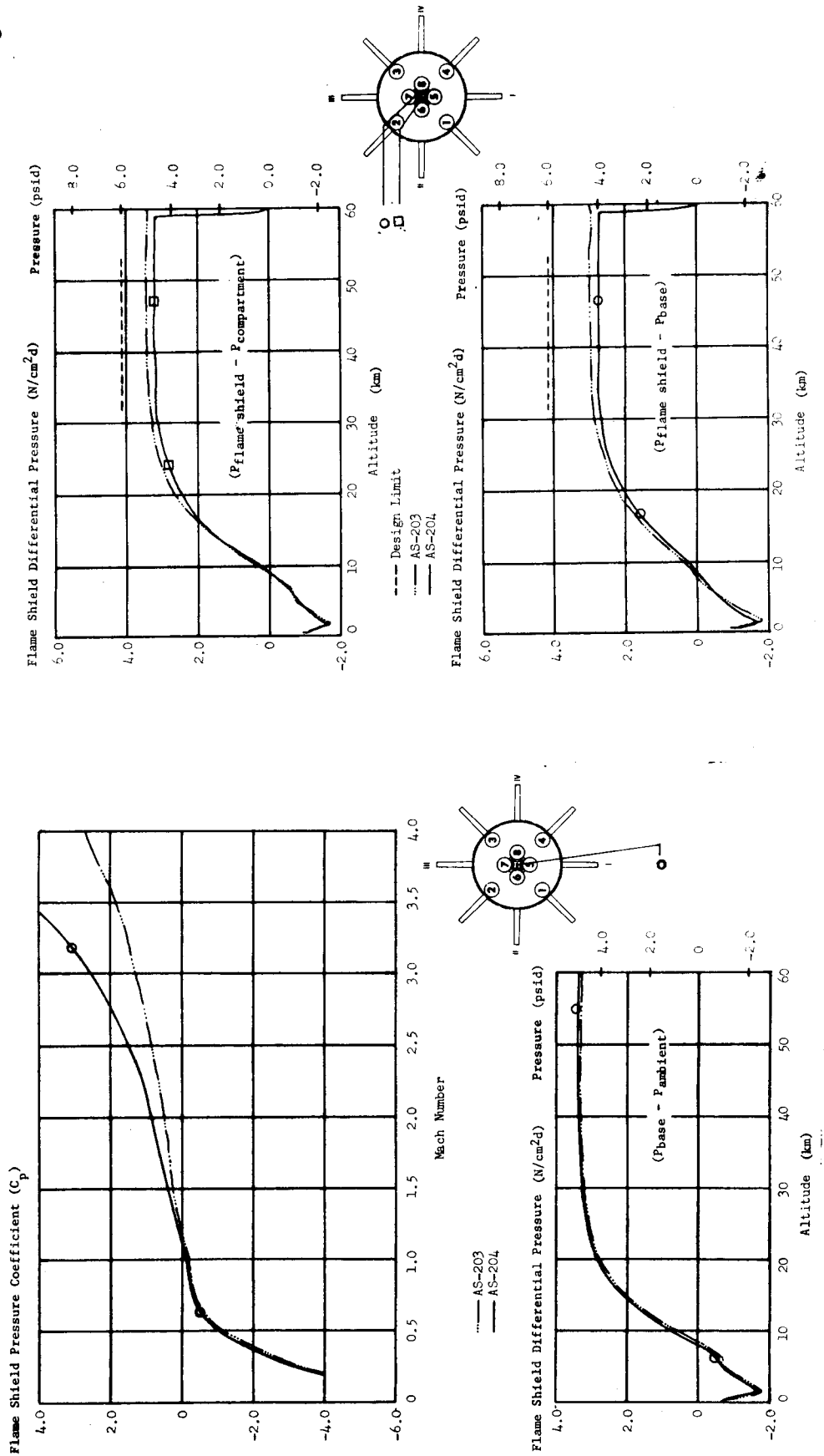


FIGURE 18-8 FLAME SHIELD PRESSURE ENVIRONMENT

--- Predicted
 — AS-201
 - - - AS-202
 ... AS-203
 — AS-204

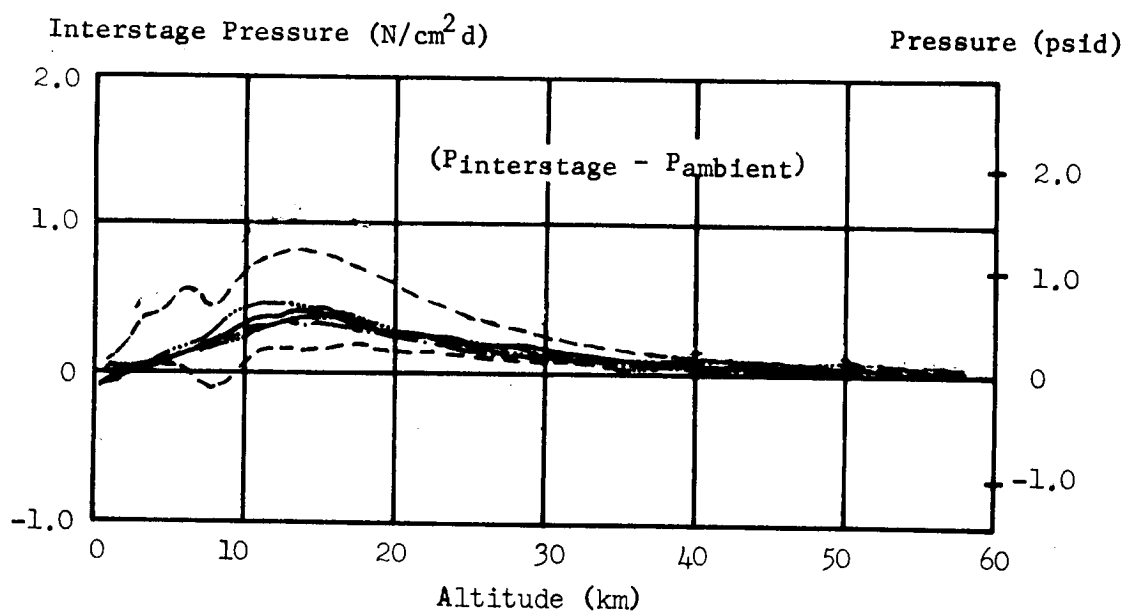
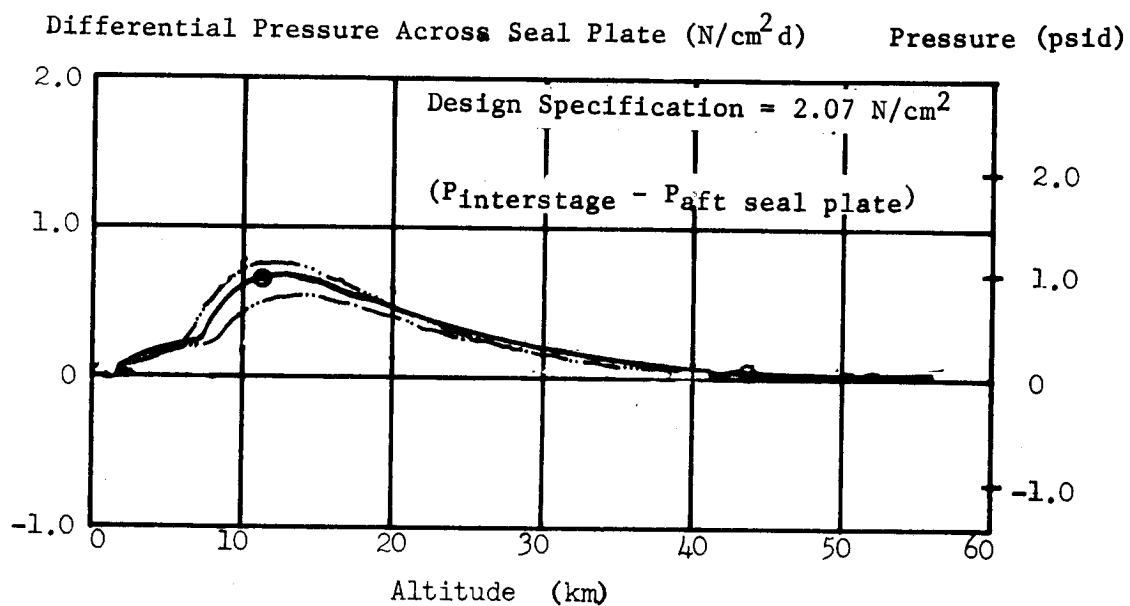
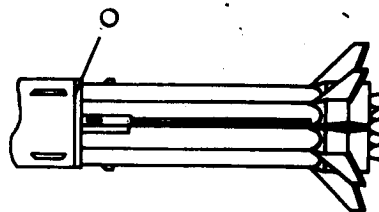


FIGURE 18-9 S-IB/S-IVB INTERSTAGE PRESSURE ENVIRONMENT

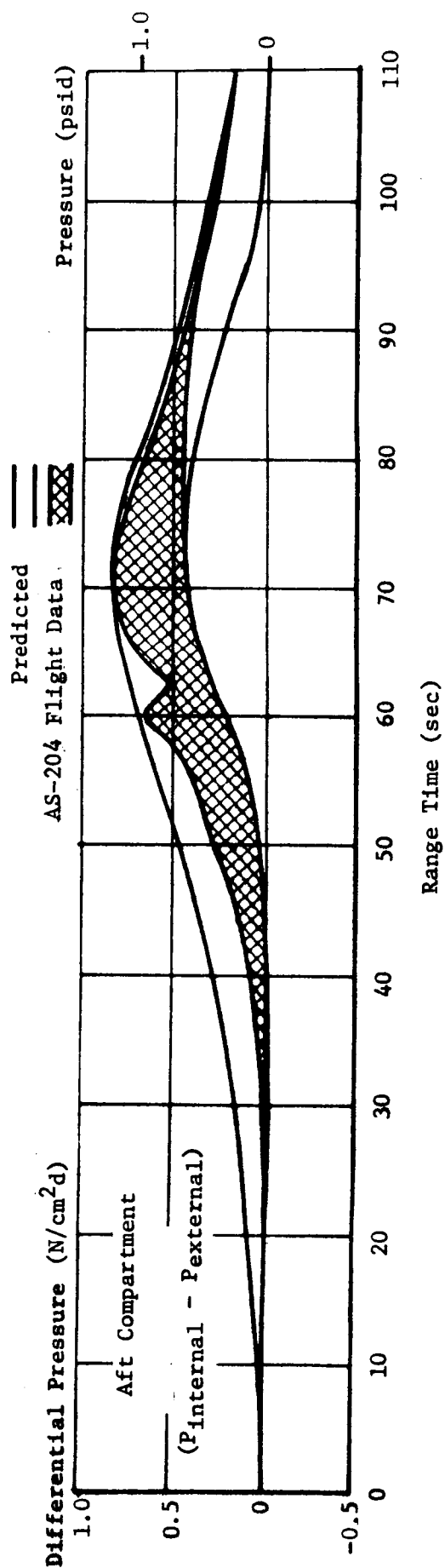
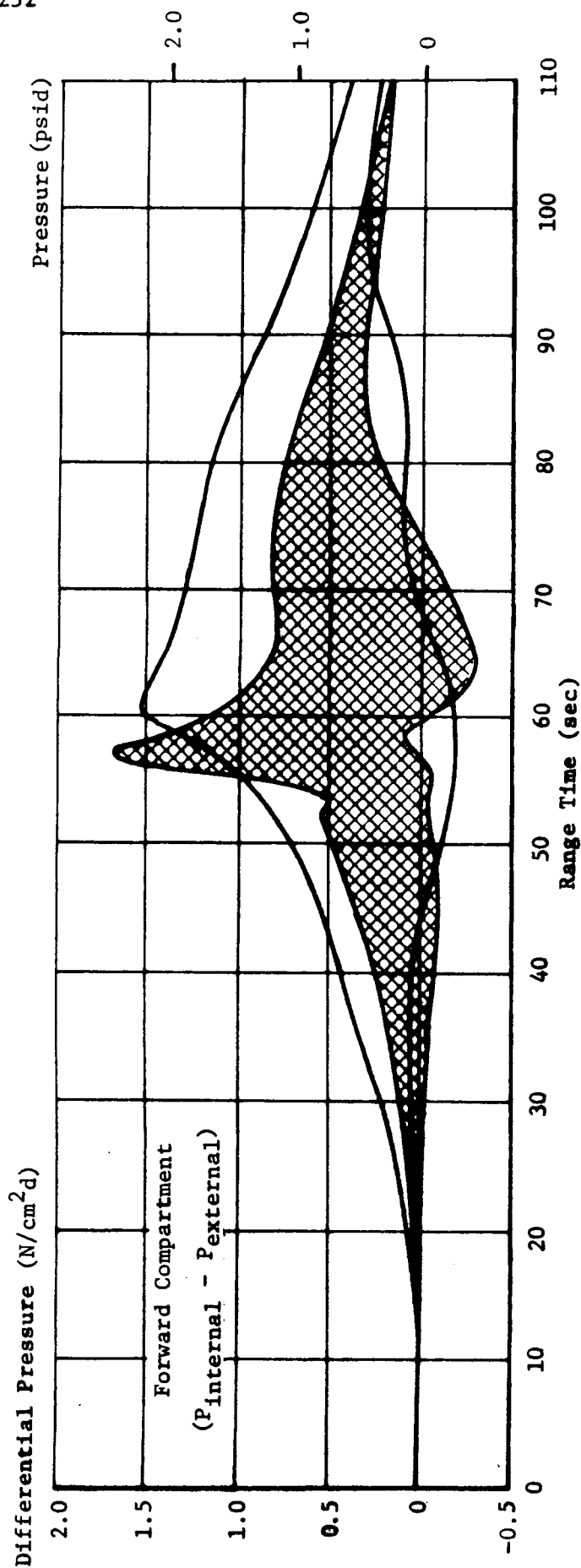


FIGURE 18-10 S-IVB FORWARD AND AFT COMPARTMENT DIFFERENTIAL PRESSURES

and measured flight pressure differentials. The maximum measured bursting and crushing pressures were 1.69 and 0.29 N/cm²d (2.45 and 0.42 psid), respectively, for the forward compartment as compared to predicted values of 1.52 and 0.17 N/cm²d (2.21 and 0.25 psid). Aft compartment measured values were 0.827 N/cm²d (1.20 psid) bursting and 0.035 N/cm²d (0.5 psid) crushing as compared to 0.827 and 0.0 N/cm²d (1.20 and 0.0 psid) predicted values.

Predicted pressure band limits were established by analyzing external and internal pressure profiles for future flights. Internal pressure distributions were derived from a consideration of structural leakage, drain and vent locations, and anticipated low and high pressure regions for Saturn IB stage configuration.

The maximum predicted pressure differentials histories presented in Figure 18-10 were obtained by assuming a maximum compartment volume, minimum compartment temperature at liftoff, and specified allowable leakage. All predicted data are for zero angle-of-attack.

18.3 VEHICLE THERMAL ENVIRONMENT

18.3.1 S-IB STAGE AERODYNAMIC HEATING

There were two aerodynamic heating skin temperature measurements on the S-IB stage of AS-204. Both measurements, one on the upper tail shroud and one on the lower tail shroud, indicated an aerothermodynamic environment less severe than experienced on AS-203.

Upper tail shroud skin temperatures are compared to comparable AS-203 data and the AS-204 predicted temperatures in Figure 18-11 (upper portion). The AS-204 flight data are in good agreement with the predicted until approximately 100 seconds. The actual and predicted both began at the same initial temperature of 268°K (23°F); however, the predicted was about 100°K higher (492°K or 426°F) at 140 seconds. This could be due to the lower than expected exhaust plume radiation.

The lower tail shroud skin temperatures all show good agreement with the predicted and AS-203 data in the lower portion of Figure 18-11. The initial temperature for actual and predicted was 283°K (50°F) and the final temperature of both was 426°K (307°F) at 140 seconds.

18.3.2 S-IVB STAGE AERODYNAMIC HEATING

The forward skirt skin temperature measurement was located in the same position as on previous flights. Maximum temperatures recorded were 339°K (150°F), approximately 2°K (3.6°F) higher than AS-201 and 52°K (93.5°F) lower than AS-203. Figure 18-12 (upper portion) shows the sensor temperature history and correlation using the post-flight trajectory. All correlations use $T_w/T_r = 0.5$ as boundary layer transition

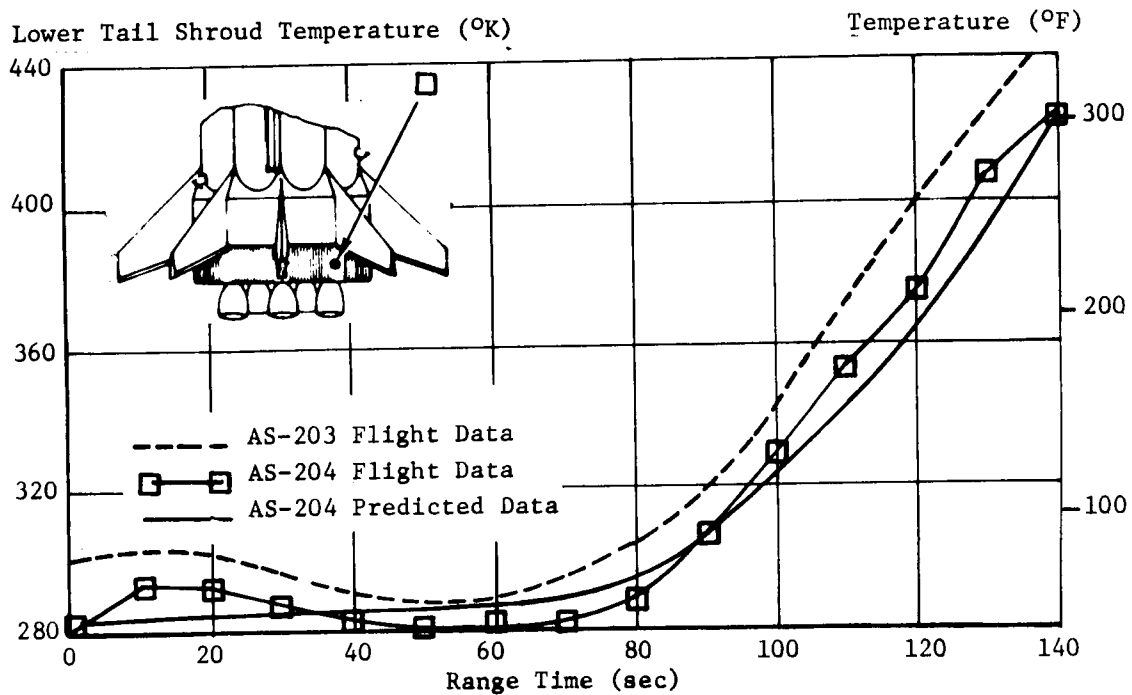
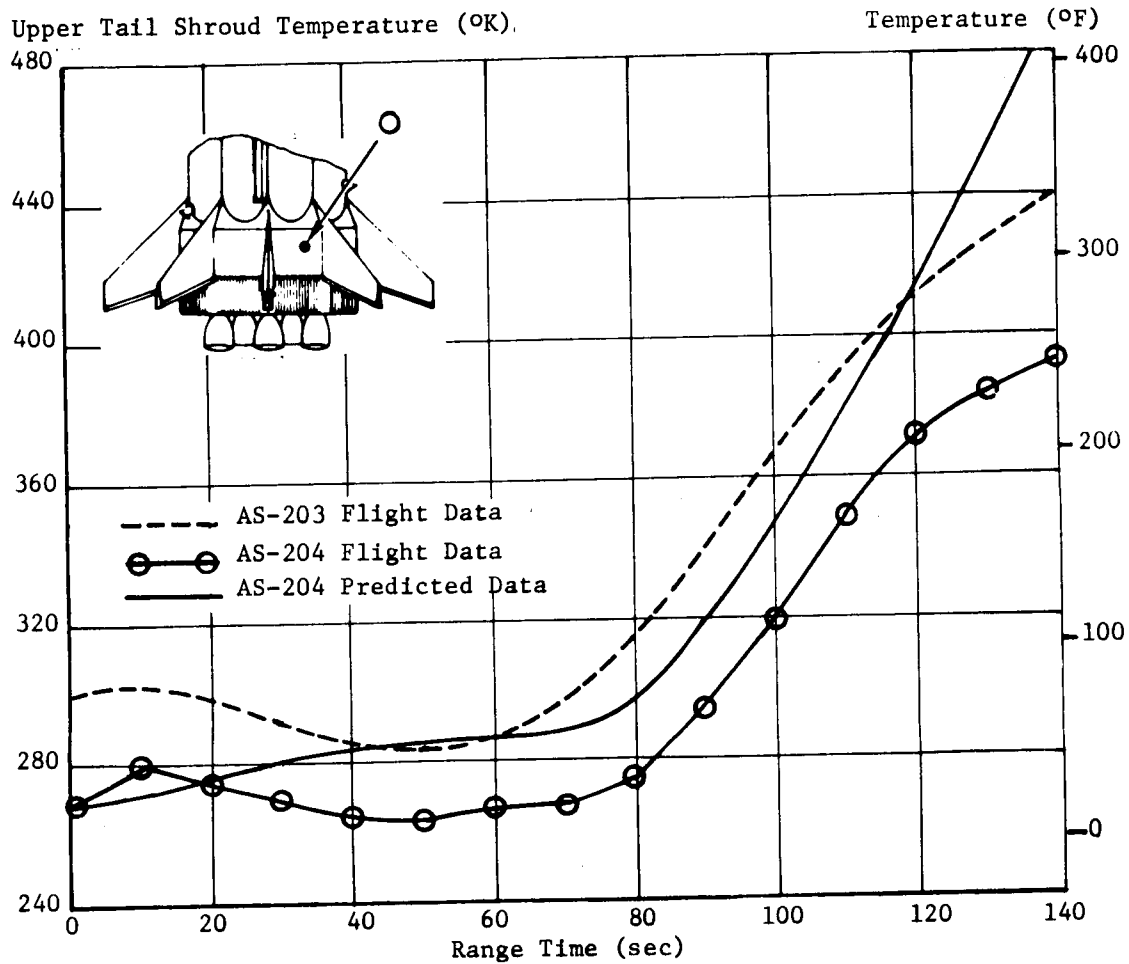


FIGURE 18-11 UPPER AND LOWER TAIL SHROUD TEMPERATURES

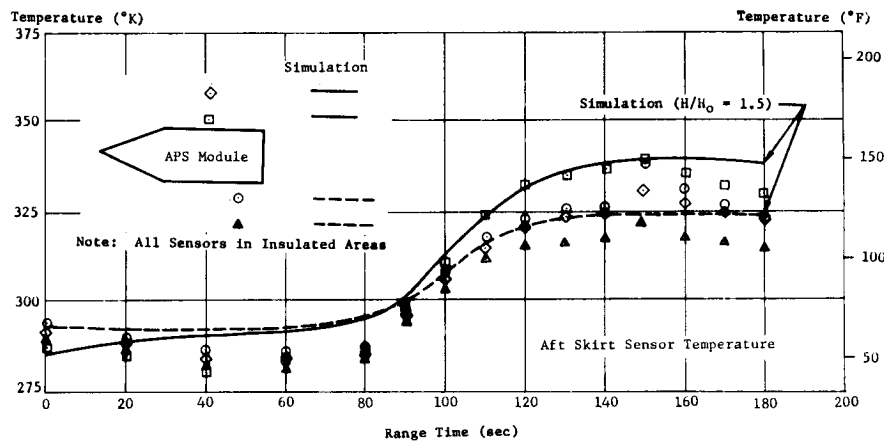
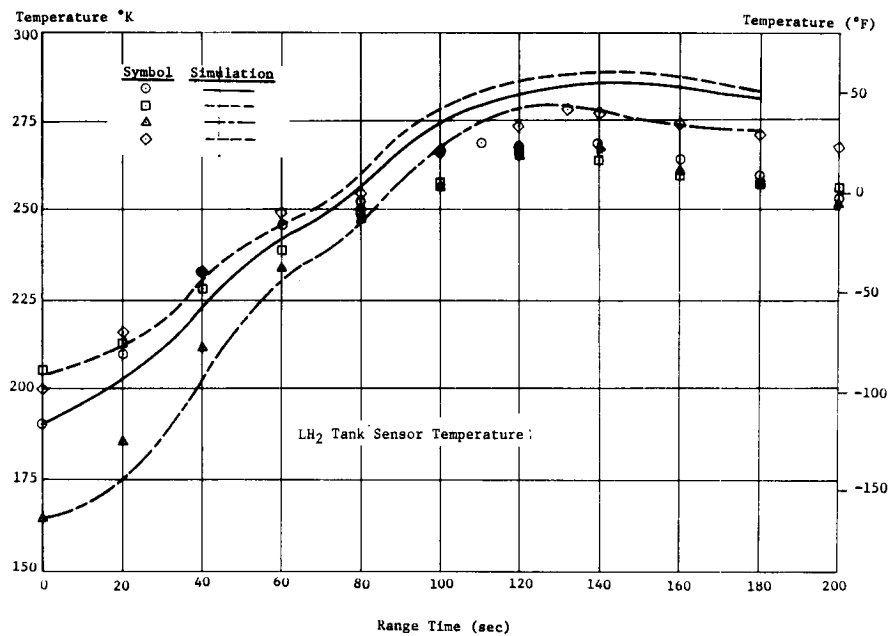
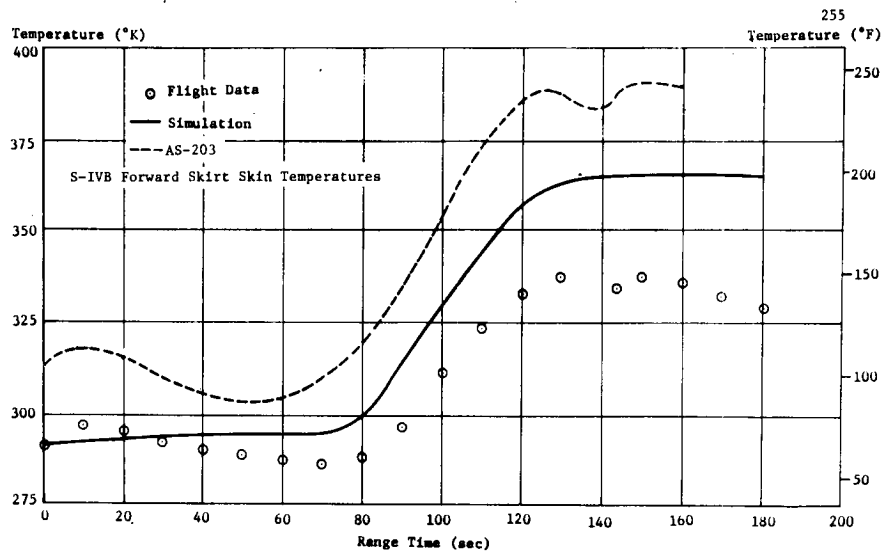


FIGURE 18-12 S-IVB STAGE AERODYNAMIC HEATING ENVIRONMENT

criterion. S-IVB-204 assumed a design coefficient of zero. The pressure coefficient from liftoff through the maximum heating period is negative, so the result of using the assumed value of zero is an increase in heating rates and over-prediction of the sensor temperature of 27°K (48.5°F).

Instrumentation on the LH₂ tank was identical to previous flights; however, the data was not directly comparable due to the wide range of temperatures at liftoff and the presence of ice or frost on the tank skin. The middle portion of Figure 18-12 presents selected measurements on the LH₂ Tank and their correlations using the post-flight trajectory. The correlations were better than expected due to the fact the ice and frost were removed during the initial flight phase. The maximum temperature recorded on the tank was 281°K (45°F), approximately 51°K (92°F) lower than the maximum for S-IVB-203.

Aft skirt instrumentation on S-IVB-204 was the same as on the previous vehicles; however, the measurements are not comparable to AS-201 and AS-202 since the aft skirt on those vehicles was not insulated. All aft skirt measurements on AS-204 were in protuberance-induced heating areas and were insulated. The four measurements near APS Module II and their correlation are shown in Figure 18-12 (lower portion). As noted on previous flights and wind tunnel tests, the measurements nearer the APS were subjected to higher heating rates. The correlations utilized a protuberance heating factor (h/h_0) of 1.5 and match the data quite well for the two measurements nearer the APS. The maximum recorded temperature was 336°K (145°F), approximately 15°K (27°F) lower than the S-IVB-203 maximum. The measurements on the left side of the fairing are near a frame, which accounts for their lower temperatures.

18.3.3 APS AND FORWARD AND AFT SKIRT TEMPERATURES

All APS components were within their desired temperature range of 267 to 325°K (20 to 125°F). Table 18-I presents minimum and maximum measured temperatures for the AS-204 and AS-203 flights. Both the minimum and maximum temperatures for AS-204 occurred on the oxidizer tank forward hemisphere. The maximum was 3.3°K (6°F) higher and the minimum was 10.5°K (19°F) lower than the same measurement on AS-203.

All forward and aft skirt component temperatures remained within acceptable limits. During this time the LOX chilldown inverter approached its minimum limit of 262°K (10°F). A summary of the maximum and minimum temperatures for the instrumented components is presented in Table 18-II along with comparisons to previous flights.

18.3.4 S-IB STAGE BASE THERMAL ENVIRONMENT

Twenty-seven measurements, composed of membrane calorimeters and gas, skin, and structural thermocouples, were used to measure the S-IB stage base thermal environment. Of these, only one (an inboard engine turbine exhaust temperature) failed to produce usable data.

TABLE 18-I S-IVB 204 APS COMPONENT TEMPERATURES
(MODULE II)

MEASUREMENT NO.	LOCATION	RECORDED TEMPERATURE °K (°F)				TEMPERATURE LIMITS °K (°F)
		AS-203		AS-204		
		MIN	MAX	MIN	MAX	
C0258	Fuel line at tank outlet	299 (78)	305 (89)	293 (67)	298 (76)	267-326 (20-127)
C0259	Fuel line between propellant control module and engine 2	292 (66)	308 (94)	298 (76)	304 (87)	267-326 (20-127)
C0260	Ox line near support bracket	293 (67)	320 (116)	294 (69)	306 (71)	267-326 (20-127)
C0261	Ox line between control module and engine 2	298 (76)	311 (100)	298 (76)	303 (85)	267-326 (20-127)
C0262	Ox tank fwd hemisphere	298 (76)	314 (105)	287 (57)	317 (111)	267-326 (20-127)
C0263	Fuel tank constant sect	298 (76)	306 (91)	293 (67)	304 (87)	267-326 (20-127)
C0264	Fuel (propellant control module)	298 (76)	307 (93)	298 (76)	302 (83)	267-326 (20-127)
C0265	Oxidizer (propellant control module)	298 (76)	314 (105)	299 (78)	302 (83)	267-326 (20-127)
C0266	Fuel line between control module and engine 3	298 (76)	310 (98)	299 (78)	305 (89)	267-326 (20-127)
C0267	Ox line between control module and engine 3	298 (76)	312 (102)	299 (78)	305 (89)	267-326 (20-127)

TABLE 18-II S-IVB 204 COMPONENT TEMPERATURES

MEASUREMENT NO.	LOCATION	RECORDED TEMPERATURES °K (°F)				QUALIFICATION TEMPERATURE LIMITS OK (°F)
		PREVIOUS FLIGHTS		AS-204		
		MIN	MAX	MIN	MAX	
C0061	Static inverter-converter	279 (42)	303 (85)	281 (46)	294 (69)	278-317 (40-111)
C0017	PU assembly	280 (44)	299 (78)	285 (53)	297 (75)	278-317 (40-111)
C0139	LOX chilldown inverter	246 (-17)	298 (76)	262 (12)	292 (66)	262-340 (12-152)
C0140	LH2 chilldown inverter	248 (-14)	300 (80)	266 (19)	291 (64)	262-340 (12-152)
C0233	Bridge module - fwd skirt	284 (51)	292 (66)	290 (62)	294 (69)	220-345 (-64-161)
C0234	Bridge module - fwd skirt	283 (49)	292 (66)	290 (62)	286 (55)	220-345 (-64-161)
C0235	Bridge module - fwd skirt	281 (46)	292 (66)	283 (49)	288 (58)	220-345 (-64-161)
C0236	Bridge module - aft skirt	250 (-10)	283 (49)	258 (4)	267 (21)	220-345 (-64-161)
C0237	Bridge module - aft skirt	242 (-24)	281 (46)	233 (-41)	249 (-12)	220-345 (-64-161)
C0238	Bridge module - aft skirt	235 (-37)	292 (66)	250 (-10)	280 (44)	220-345 (-64-161)

Heat shield outer region radiation heat fluxes are shown to be generally lower than similar AS-203 data in the upper portion of Figure 18-13. An unusual decay of heating rates at 110 sec (33 km), as recorded by one of the two instruments, was conceivably caused by some blackening of the calorimeter window. Outer region total heat flux and outer region gas temperatures are compared to AS-203 data in the middle and lower parts of Figure 18-13.

Comparison of the heat shield inner region thermal environments of AS-204 and AS-203 (Figure 18-14) shows the initial radiation heat flux of AS-204 to be slightly lower and becoming slightly higher after about 25 km. Gas temperatures were higher initially on AS-204 and lower than AS-203 later in the flight.

Data for the non-honeycomb portion of the heat shield shows little difference between AS-204 and AS-203 (upper portion of Figure 18-15). The heat shield inner region honeycomb differential temperatures and the water saturation curve for AS-204 are presented in the middle part of Figure 18-15. As shown, the honeycomb forward (cold) face recorded the ice point temperature 273°K (32°F) at liftoff and then continued to drop to the lower limit of the thermocouple range from approximately 30 to 90 seconds. A probable explanation of this phenomenon is that frost dropped from the bottom of the LOX lines or tanks and affected the instrument. After the frost melted and left a residue of moisture, the temperature rose until the water saturation temperature was encountered. The data then followed the water saturation temperature curve until the water boiled off and then continually increased to the end of flight. This analysis is supported by the high ambient dew-point temperature recorded before launch and the large amount of frost formation over the entire vehicle. The honeycomb aft face shows the effect of the temperatures experienced by the cold face. The data did not intersect the water saturation temperature curve until about 65 sec and then followed along the curve to approximately 100 seconds. For the remainder of the flight, the data remained relatively steady. Similar data for the heat shield outer region (Figure 18-15) indicates no frost effect was noted. At 20 sec of flight, the hot face data intersected the water saturation curve and continued along it until 45 sec, at which time the moisture effect was eliminated. The cold face temperature curve shows no indication of moisture.

Radiation and total heating rates measured on the AS-204 flame shield (Figure 18-16) were slightly higher than those recorded on AS-203, while the gas temperatures were initially higher and became lower than AS-203 by the end of the flight. Flame shield skin temperatures remained almost constant 290°K (62°F) throughout the flight.

Flame shield access chute structural temperatures, as shown in Figure 18-17, were considerably higher than AS-203. This condition is probably due to a difference in mounting or insulating methods.

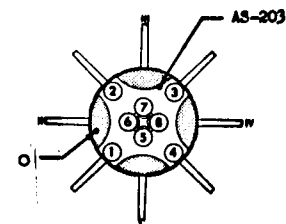
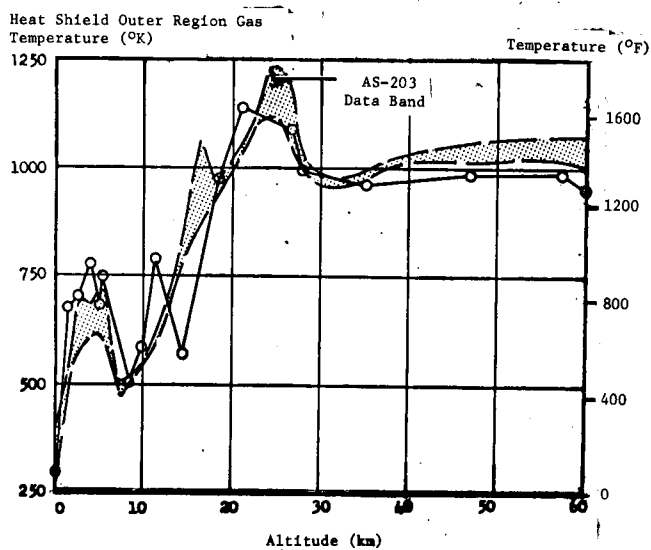
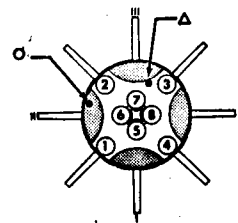
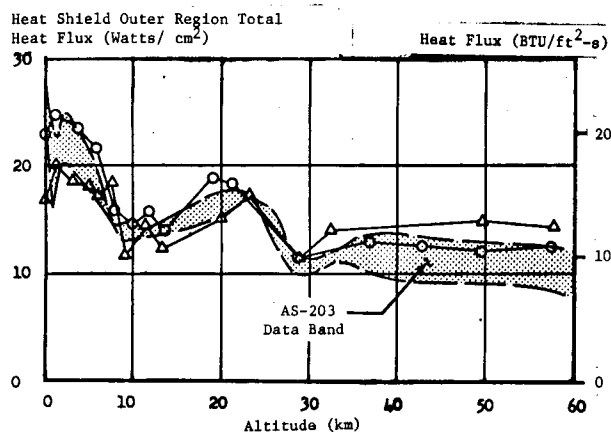
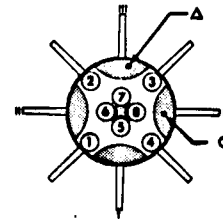
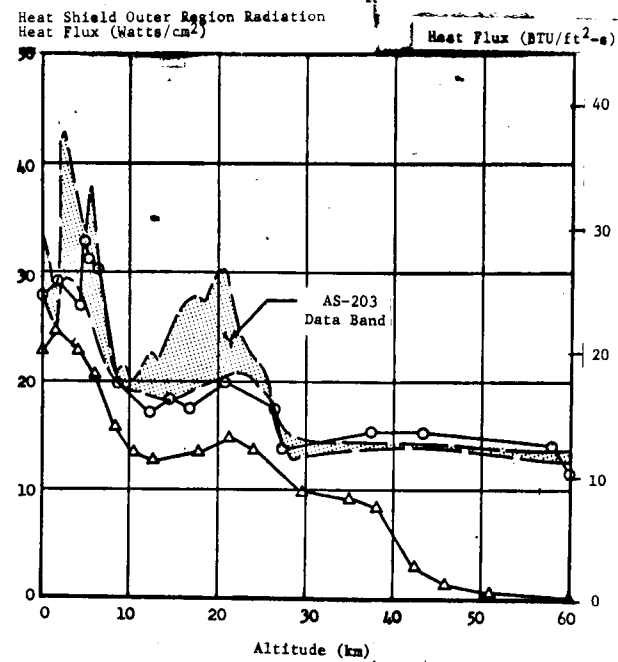


FIGURE 18-13 HEAT SHIELD OUTER REGION THERMAL ENVIRONMENT

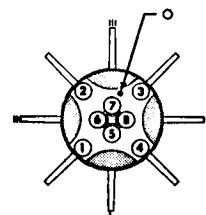
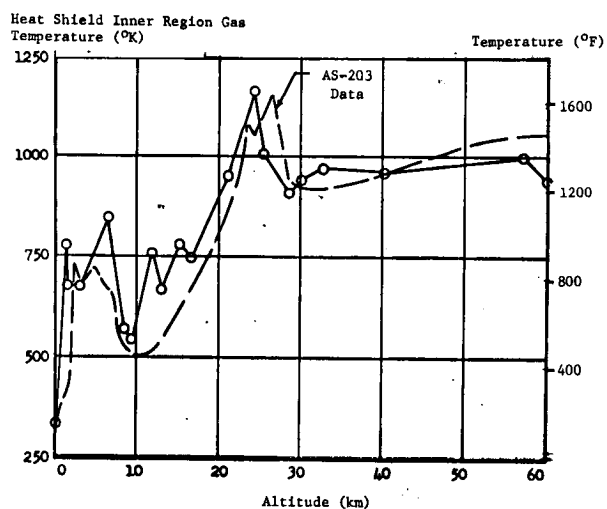
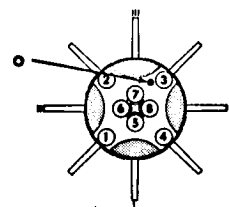
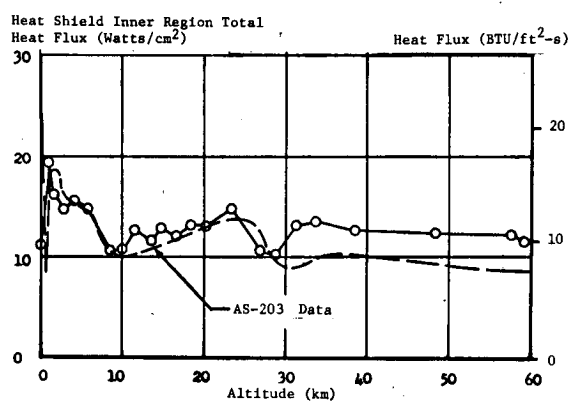
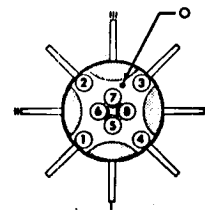
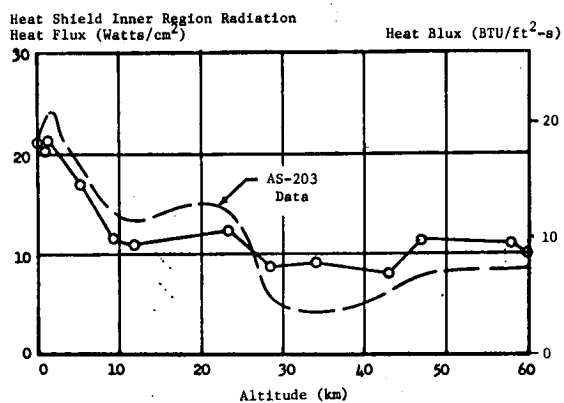


FIGURE 18-14 HEAT SHIELD INNER REGION THERMAL ENVIRONMENT

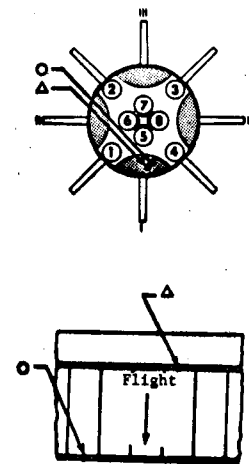
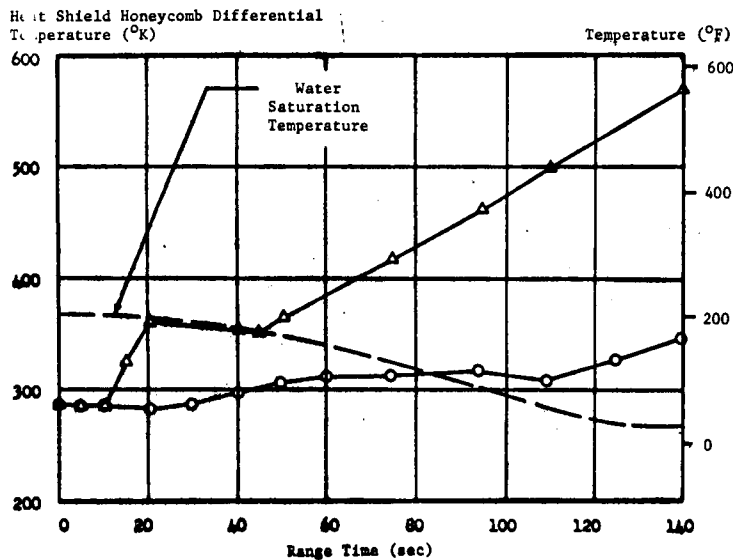
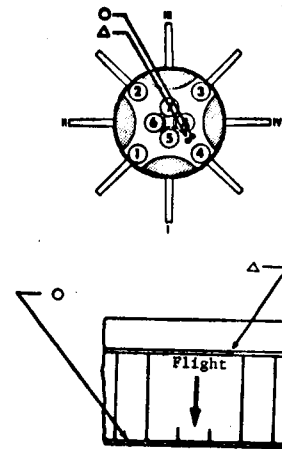
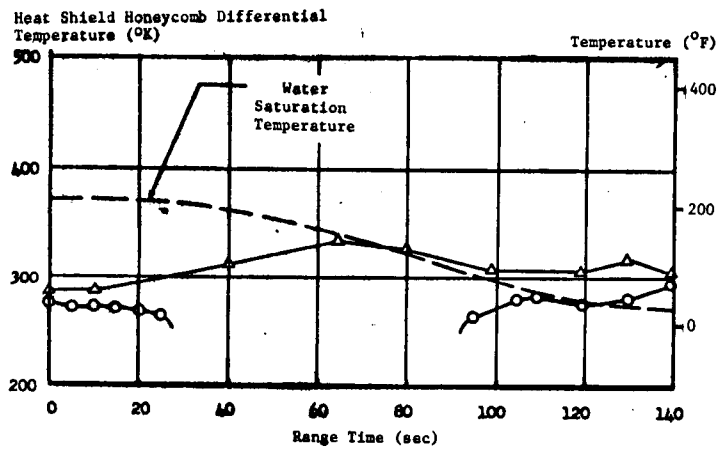
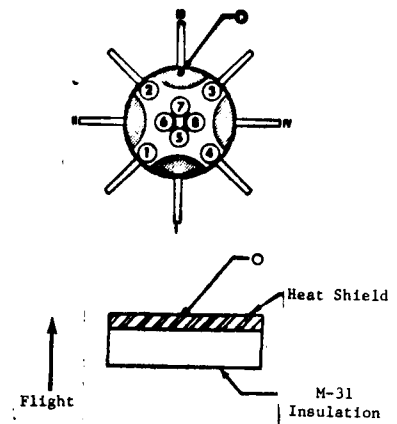
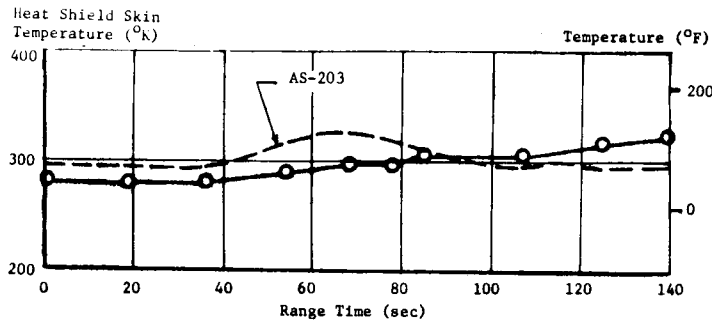
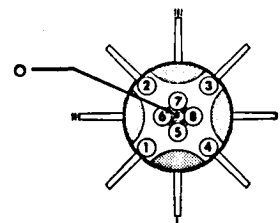
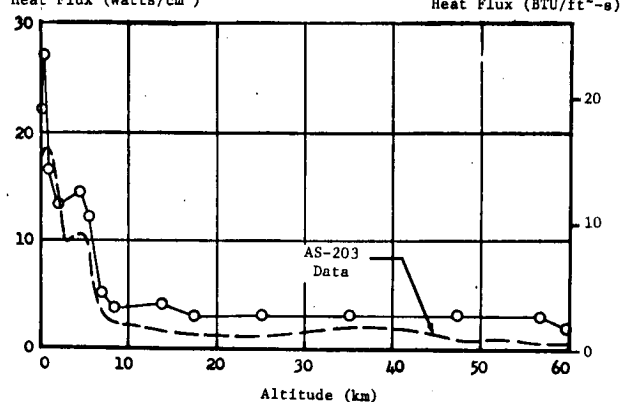
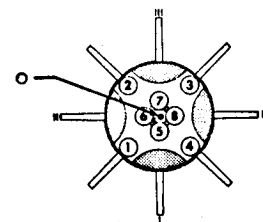
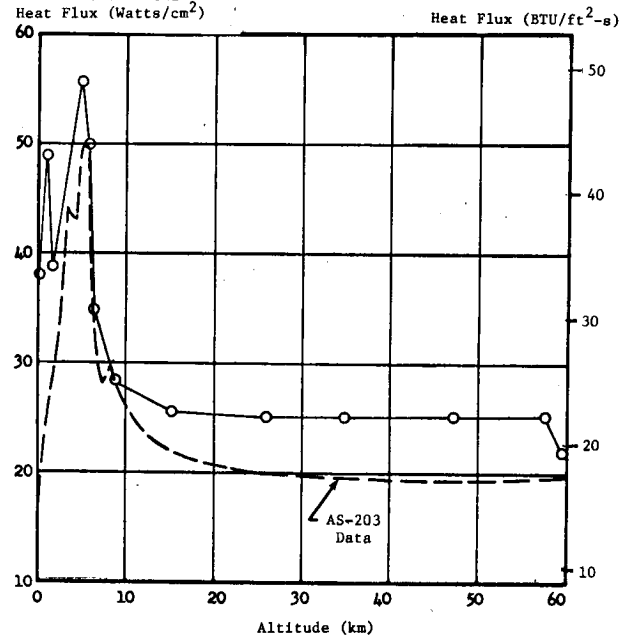


FIGURE 18-15 HEAT SHIELD SKIN AND DIFFERENTIAL TEMPERATURES

Flame Shield Radiation
Heat Flux (Watts/cm²)



Flame Shield Total
Heat Flux (Watts/cm²)



Flame Shield Gas
Temperature (°K)

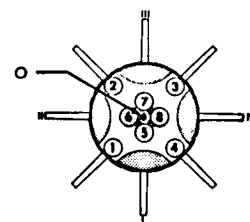
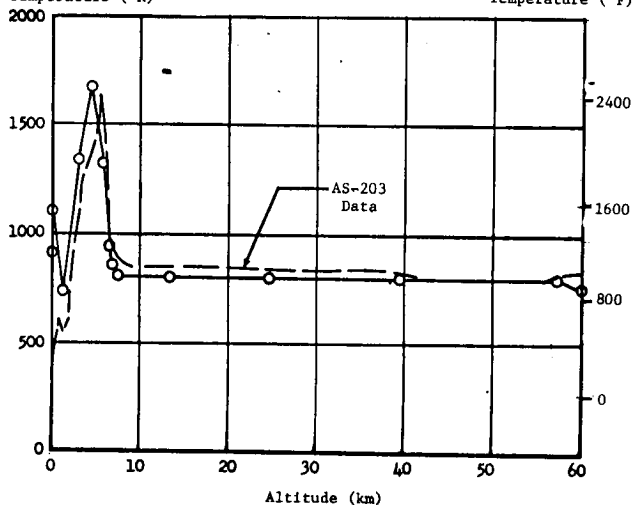


FIGURE 18-16 FLAME SHIELD THERMAL ENVIRONMENT

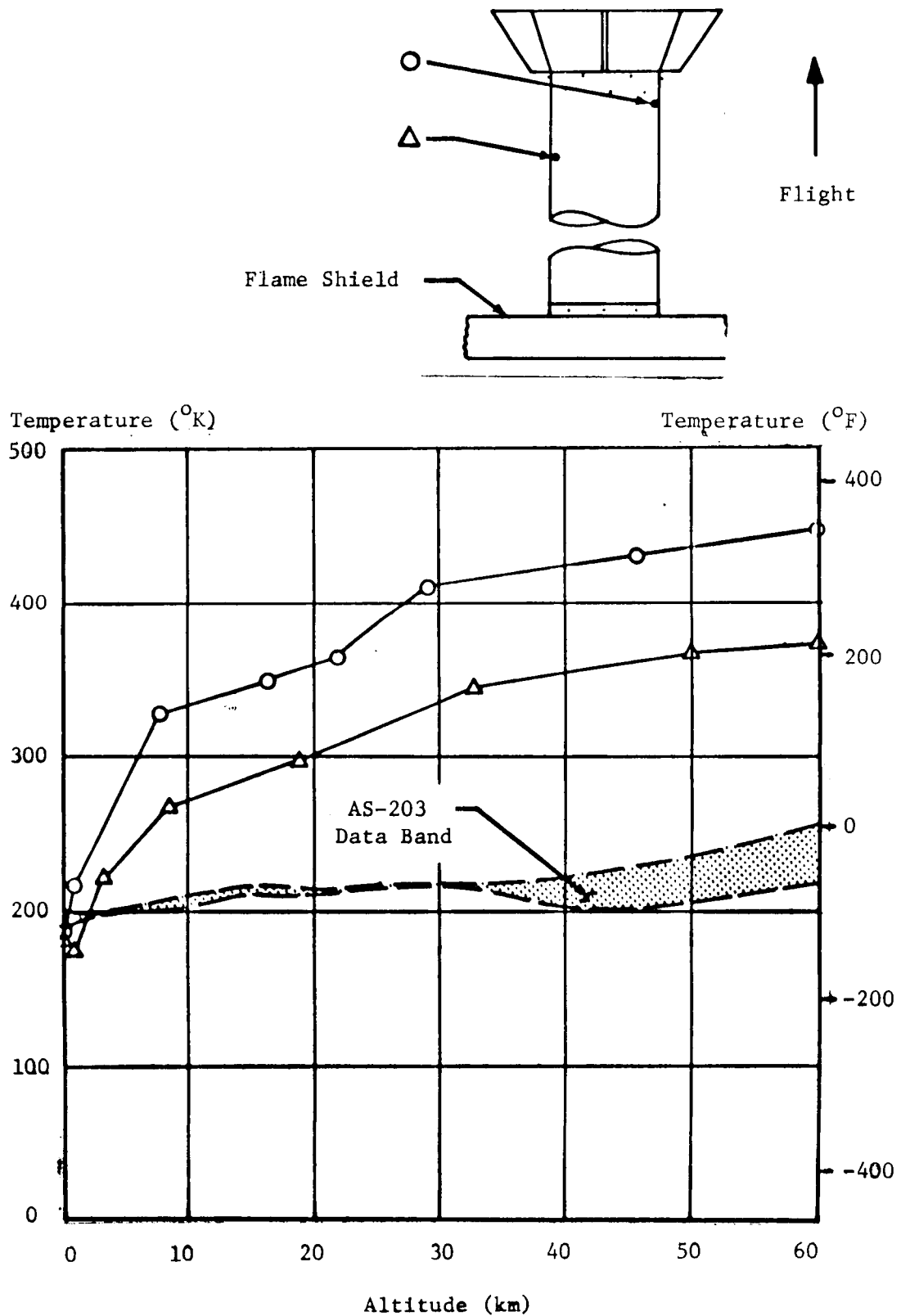


FIGURE 18-17 FLAME SHIELD ACCESS CHUTE STRUCTURAL TEMPERATURES

The outboard engine aspirator body gas temperature was measured for the first time on AS-204. As shown in the top of Figure 18-18, the data has a similar trend as measured heat shield gas temperatures; however, the data values are dissimilar, as expected.

Total heating rates to the turbopump aspirator of Engine 3 were within the data band of the previous flights until an altitude of 20 km. After that time the AS-204 rates showed only a slight increase as compared to an approximate increase of 30 watts/cm² on the previous vehicles (middle of Figure 18-18). Total heating rates on the neck of the outboard engine aspirator agreed very well with data taken from AS-203 (bottom of Figure 18-18).

Comparison of the inboard engine nozzle and turbine exhaust duct total heating rates presents good agreement with AS-203 in Figure 18-19. The only noticeable deviation from the AS-203 data is that one of the turbine exhaust duct measurements dropped below the AS-203 data between 20.5 and 22.5 km.

The eight H-1 engine compartment ambient temperatures showed only slight change throughout the flight. Approximate maximum and minimum values recorded were 294°K and 233°K (69.5 and 40.3°F), respectively.

18.4 INSTRUMENT UNIT ENVIRONMENTAL CONTROL SYSTEMS

18.4.1 THERMAL CONDITIONING SYSTEM

The Thermal Conditioning Subsystem (TCS) maintains a 60 percent methanol/40 percent water coolant solution at a stable temperature and circulates this coolant through IU and S-IVB coldplates and through four IU components having integral coolant passages (Figure 18-20). Each of the coldplates is capable of dissipating 420 watts. The heat removed from components with integral coolant passages depends on the heat transfer characteristics of the individual component and the coolant solution flowrate through the component. The flowrates are controlled by fixed orifices.

Following liftoff, no onboard cooling occurs until after 180 sec when water from the water accumulator is allowed to enter the flight heat exchanger (sublimator). Water is supplied to the sublimator where, under vacuum conditions, water sublimation removes heat from the onboard methanol/water (M/W) coolant.

A TCS pressurization system pressurizes the M/W accumulator and water accumulator. The associated pressure regulators maintain M/W and water accumulator pressures for coolant pump and sublimator operation, respectively.

The temperature of the coolant is controlled from 180 to 4320 sec

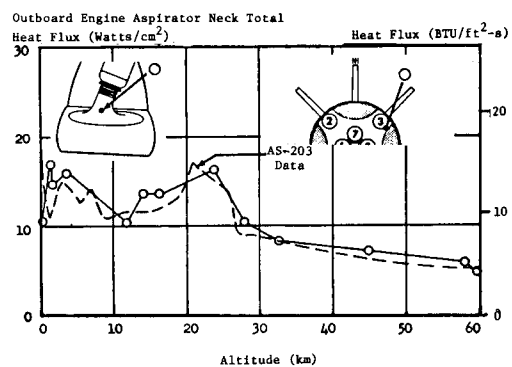
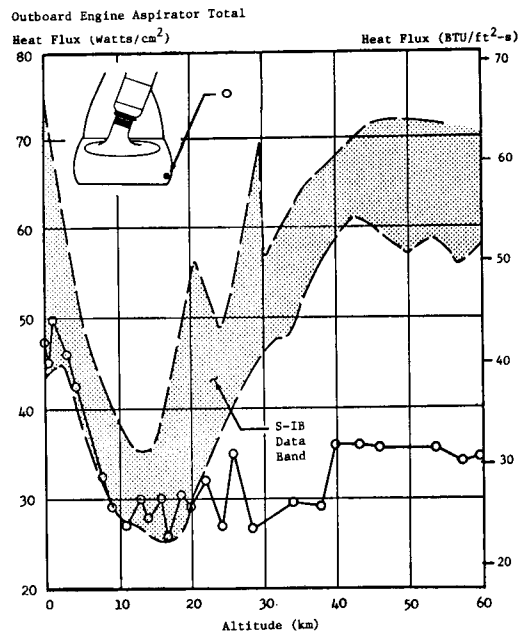
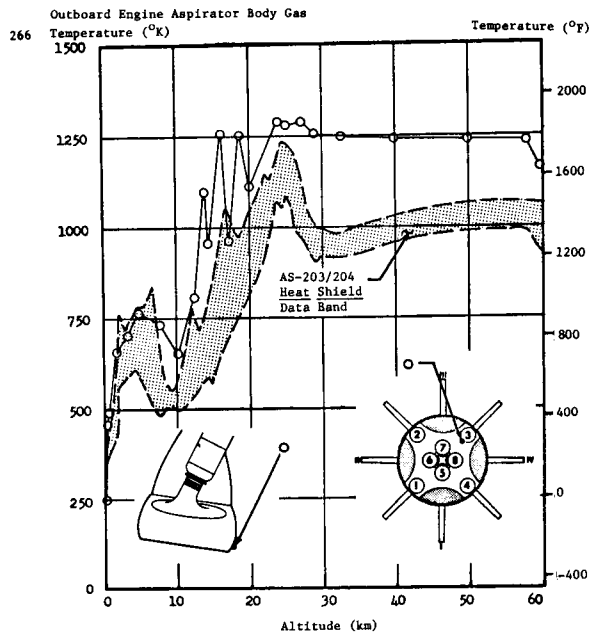
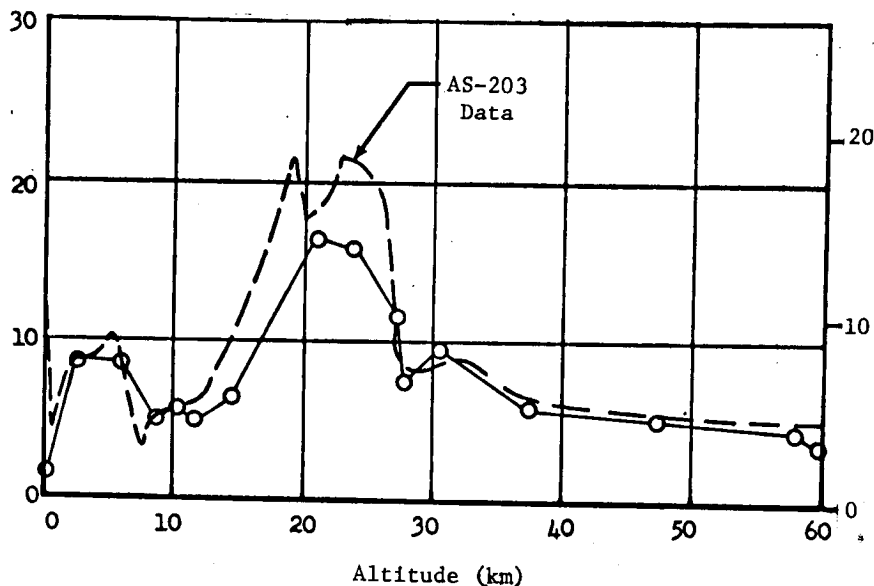


FIGURE 18-18 OUTBOARD ENGINE ASPIRATOR ENVIRONMENT

Inboard Engine Nozzle Total
Heat Flux (Watts/cm²)

Heat Flux (BTU/ft²-s)

267



Inboard Engine Turbine Exhaust Duct Total
Heat Flux (Watts/cm²)

Heat Flux (BTU/ft²-s)

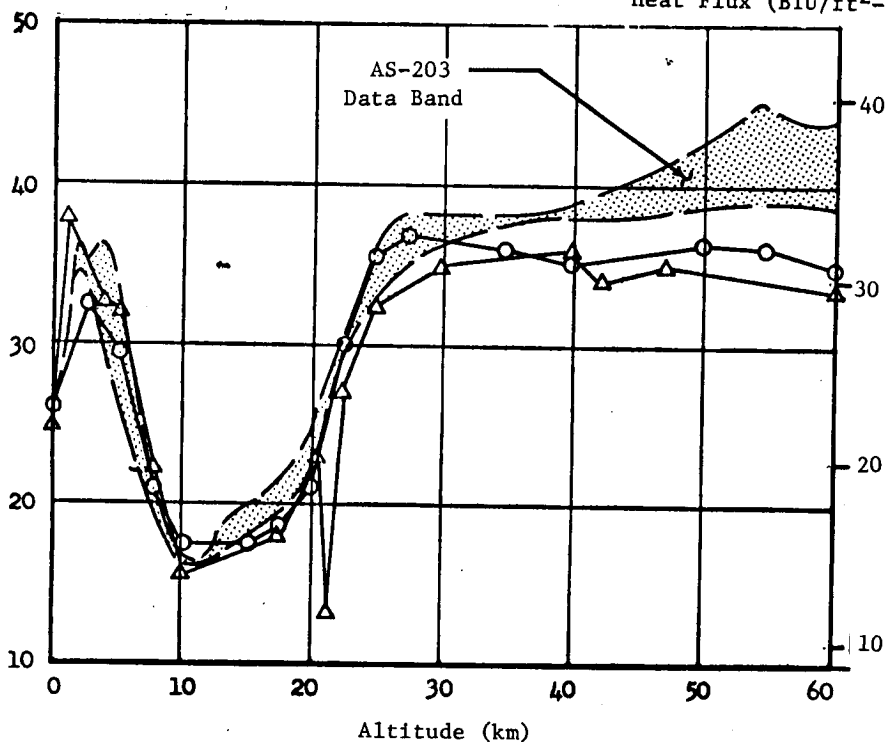


FIGURE 18-19 INBOARD ENGINE NOZZLE AND EXHAUST DUCT HEATING RATES

FIGURE 18-20 ENVIRONMENTAL CONTROL SYSTEM MECHANICAL DIAGRAM

by varying the amount of coolant flowing through the sublimator through use of the Modulating Flow Control Valve (MFCV). The valve position is controlled by the electric controller assembly, which senses any coolant temperature change and outputs a signal to adjust the MFCV position. The MFCV allows more or less coolant to bypass the sublimator depending upon temperature decreases or increases, respectively.

At 4320 sec the sensor bias is enabled and the MFCV is set at zero bypass and all coolant is forced to flow through the sublimator. After 4420 sec the coolant condition is sampled every 300 seconds. If the temperature of the coolant is above the upper temperature setting, (286.4°K, 56.2°F) the water coolant valve is opened, allowing sublimator cooling. For coolant temperatures below the lower limit (286.4°K, 55.9°F), the water coolant valve is closed, stopping the sublimator operation.

The TCS temperature requirement for the primary mission (liftoff to 72 min) was to maintain an average temperature from 280.8°K to 289.2°K (46 to 61°F). During this time period, control by M/W modulation was employed and requirements for this phase were met as shown in Figure 18-21. However, the data indicates that the water flowrate was not operating within predicted limits at this time. The water mass flowrate was predicted to be from 20.9 to 28.1 kg/hr (46 to 62 lbm/hr) during sublimator fill (5 to 10 minutes after opening the water solenoid valve at 180 sec). The sublimator inlet pressure differential was predicted to be approximately 0.69 N/cm²d (1.0 psid) during this time period. Figure 18-21 shows the pressure differential was only slightly below the 0.69 N/cm²d (1.0 psid) predicted value, but the mass flowrate ranges from 0 to 13.6 kg/hr (0 to 30 lbm/hr) before stabilizing at 13.6 kg/hr (30 lbm/hr) at approximately 600 seconds. The flowrate data appears reasonable at 1200 and 3300 sec of flight.

Figure 18-22 presents sublimator startup from liftoff through orbital inseriton. Increasing M/W temperature caused the MFCV to position to full sublimator flow. The calculated sublimator heat rejection reached a maximum of only 3.0 kw, with the control temperature remaining above the 288.0°K (59°F) control temperature. The AS-203 sublimator was removing 9.0 kw of heat at this time and AS-202 had reached 4.0 kw by 300 seconds. It is indicated that the slow sublimator startup was due to low water flowrates.

Available temperature control parameters for the TCS verification portion of the mission indicated close correlation with predictions (Figure 18-23). The maximum temperature extreme exceeded the maximum predicted value of 287.4°K (58°F) by 0.55°K (1°F) at 4hr:25min:0sec (15,900 sec) and 3.0°K (5.5°F) at 5hr:58min:20sec (21,500 sec).

Sublimator startups were indicated at 4hr:45min:0sec (17,100 sec) and 6hr:15min:0sec (22,500 sec). At 4hr:45min:0sec (17,100 sec) the start was confirmed by increasing water flow and water inlet pressure at increasing

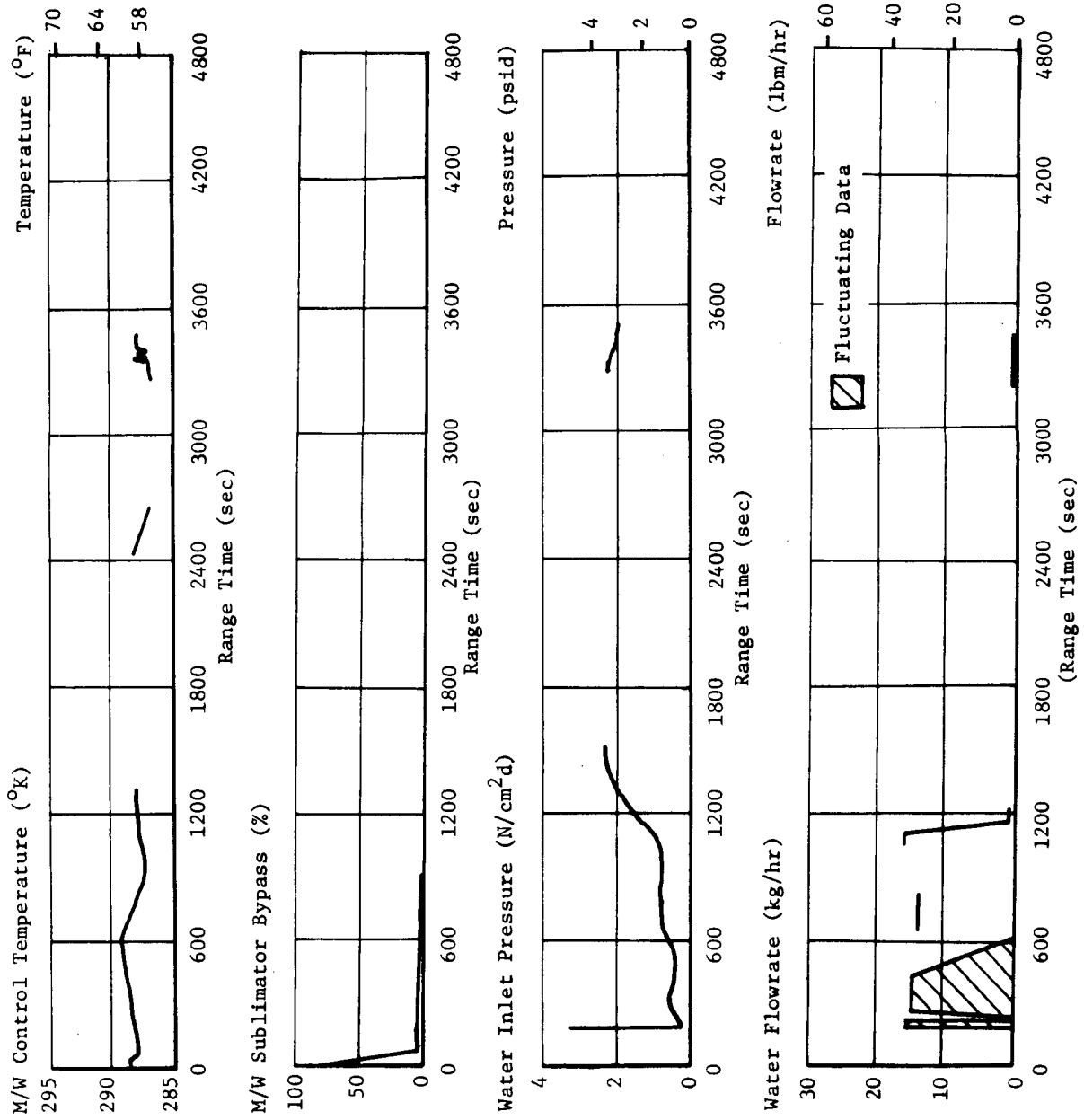


FIGURE 18-21 PRIMARY MISSION TEMPERATURE CONTROL PARAMETERS

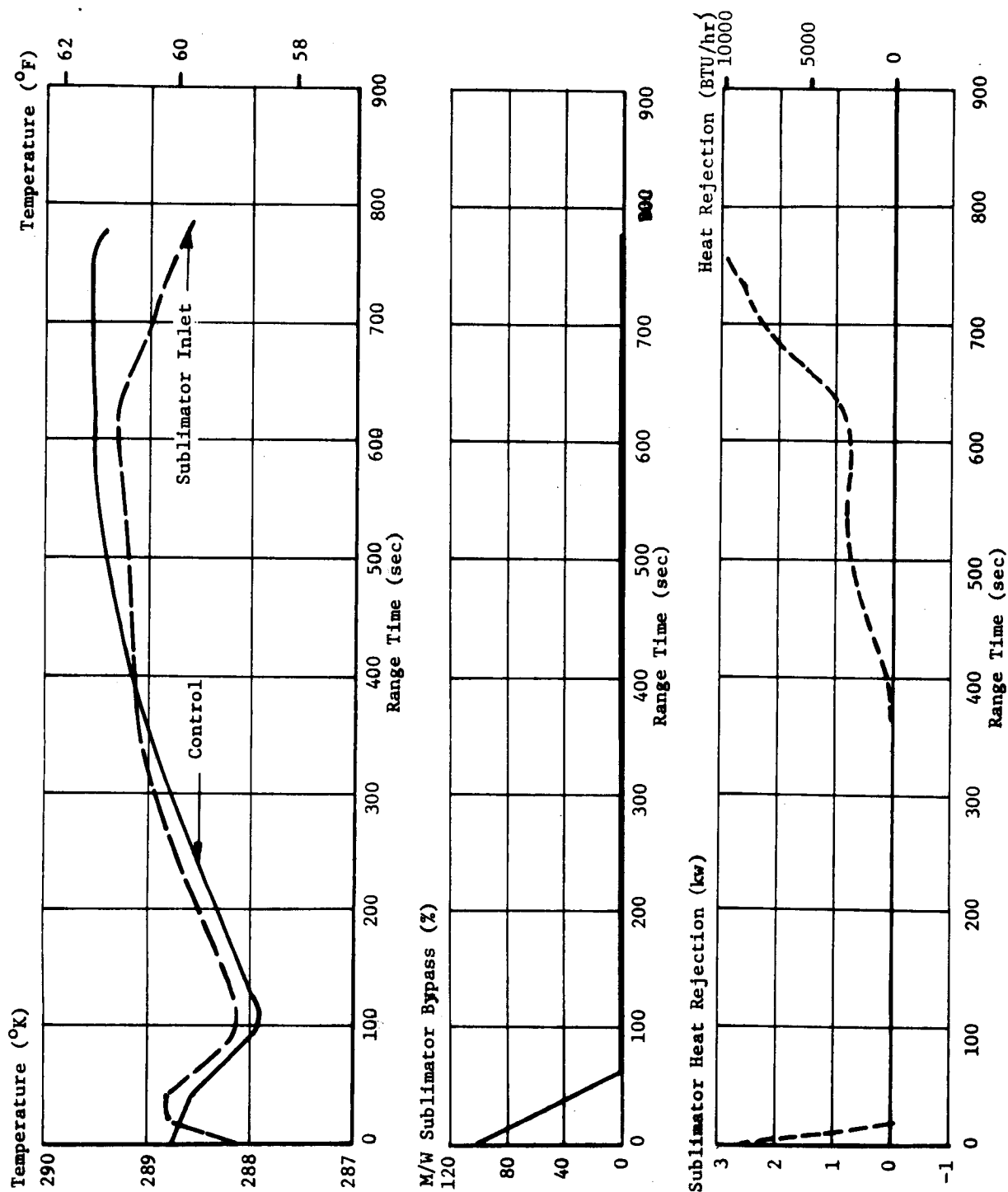
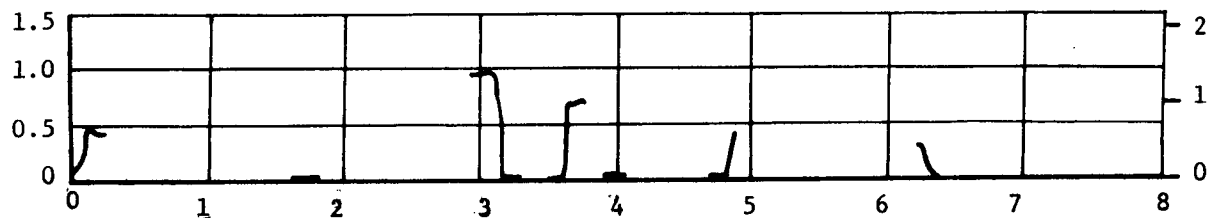


FIGURE 18-22 SUBLIMATOR START-UP PARAMETERS

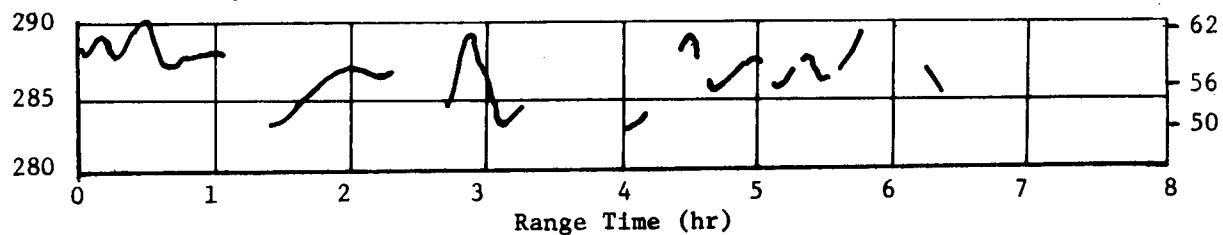
Water Inlet Pressure (N/cm²d)

Pressure (psid)



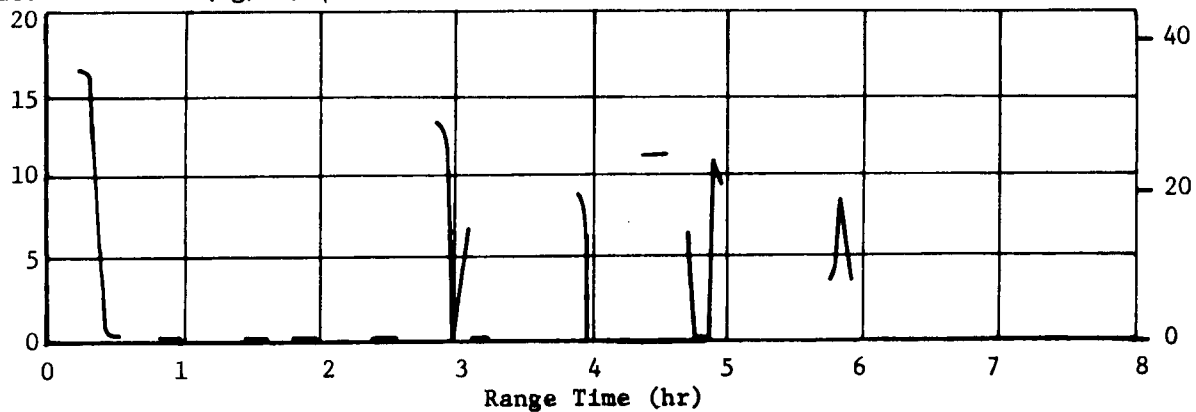
M/W Control Temperature (°K)

Temperature (°F)



Water Flowrate (kg/hr)

Flowrate (lbm/hr)



Sublimator Heat Rejection (kw)

Heat Rejection (BTU/hr)

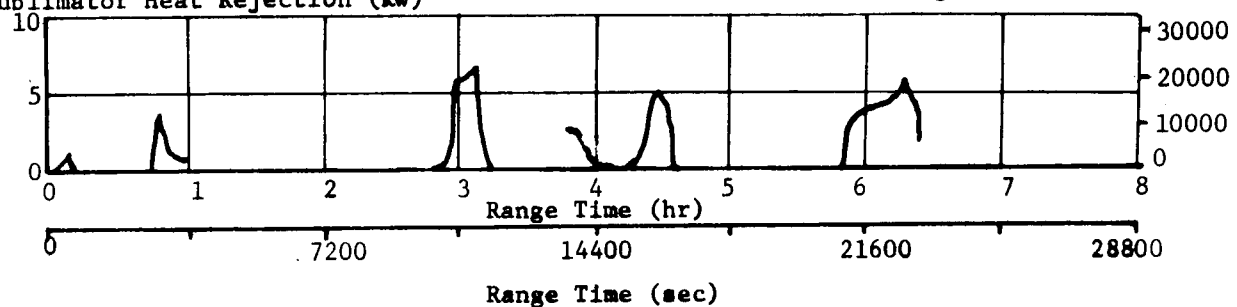


FIGURE 18-23 TCS VERIFICATION TEMPERATURE CONTROL PARAMETERS

coolant temperature through the thermal switch set point of 286.3°K (56°F) (Figure 18-23). Water inlet pressure fell with decreasing temperature at 6hr:15min:0sec (22,500 sec) indicating the end of a cycle. Switch Selector data indicating valve opening and closing has verified these cycles.

The water inlet pressure differential is shown in Figure 18-23 to be a maximum of 0.35 N/cm²d (0.5 psid). The minimum predicted value was 0.69 N/cm²d (1.0 psid). For the measured inflight water mass flow-rates of 0 to 13.6 kg/hr (0 to 30 lbm/hr), the expected pressure range is 1.4 to 3.2 N/cm²g (2.0 to 4.75 psig).

Water flowrate and longitudinal acceleration are shown in Figure 18-24. Generally, the water flow is erratic, decreases with increasing acceleration, and does not stabilize to a nominal until after the acceleration is over at approximately 600 seconds. If the water accumulator pressure had been within the specified range of 2.1 to 4.1 N/cm² (3 to 6 psi), water flow should not have been affected by the G loads experienced on AS-204. The water inlet temperature (Figure 18-24) indicates a low water flowrate. At 200 sec the temperature rises sharply as water is forced into the tube between the water accumulator and sublimator. This temperature should maintain a stable value throughout the period from 180 to 600 seconds. The subsequent drop and rise again at 600 sec follows the same general pattern as the water flowrate.

The TCS GN₂ storage sphere pressure decay curve (Figure 18-25) closely follows the maximum predicted GN₂ use rate. The maximum specified in-flight GN₂ use rate is 0.044 kg/hr (0.097 lbm/hr), including leakage, and can occur only for GN₂ temperatures of 221°K (-60°F). The predicted use rate for S-IU-204 based on measured data and the GN₂ temperature was 0.036 kg/hr (0.08 lbm/hr) as compared with an actual in-flight use rate of 0.048 kg/hr (0.106 lbm/hr). Assuming the orifice regulator was within specification, only leakage could cause this excess GN₂ consumption.

GN₂ leakage associated with the orifice regulator or the water accumulator appeared to be caused by the low water flowrate, low sublimator inlet pressure, and the high GN₂ consumption. These deviations did not materially affect the TCS performance as measured by system temperatures which were maintained within the specification limits.

18.4.2 GAS BEARING SUPPLY SYSTEM

The gas bearing subsystem (GBS) supplies gaseous nitrogen (GN₂) at a regulated pressure and temperature to the ST-124M-3 Inertial Platform for preflight and flight operation.

During system operation (preflight and flight), GN₂ flows from the storage sphere, through a filter, to a pressure regulator which maintains a 10.35 ± 0.345 N/cm²d (15 ± 0.5 psid) differential pressure across the

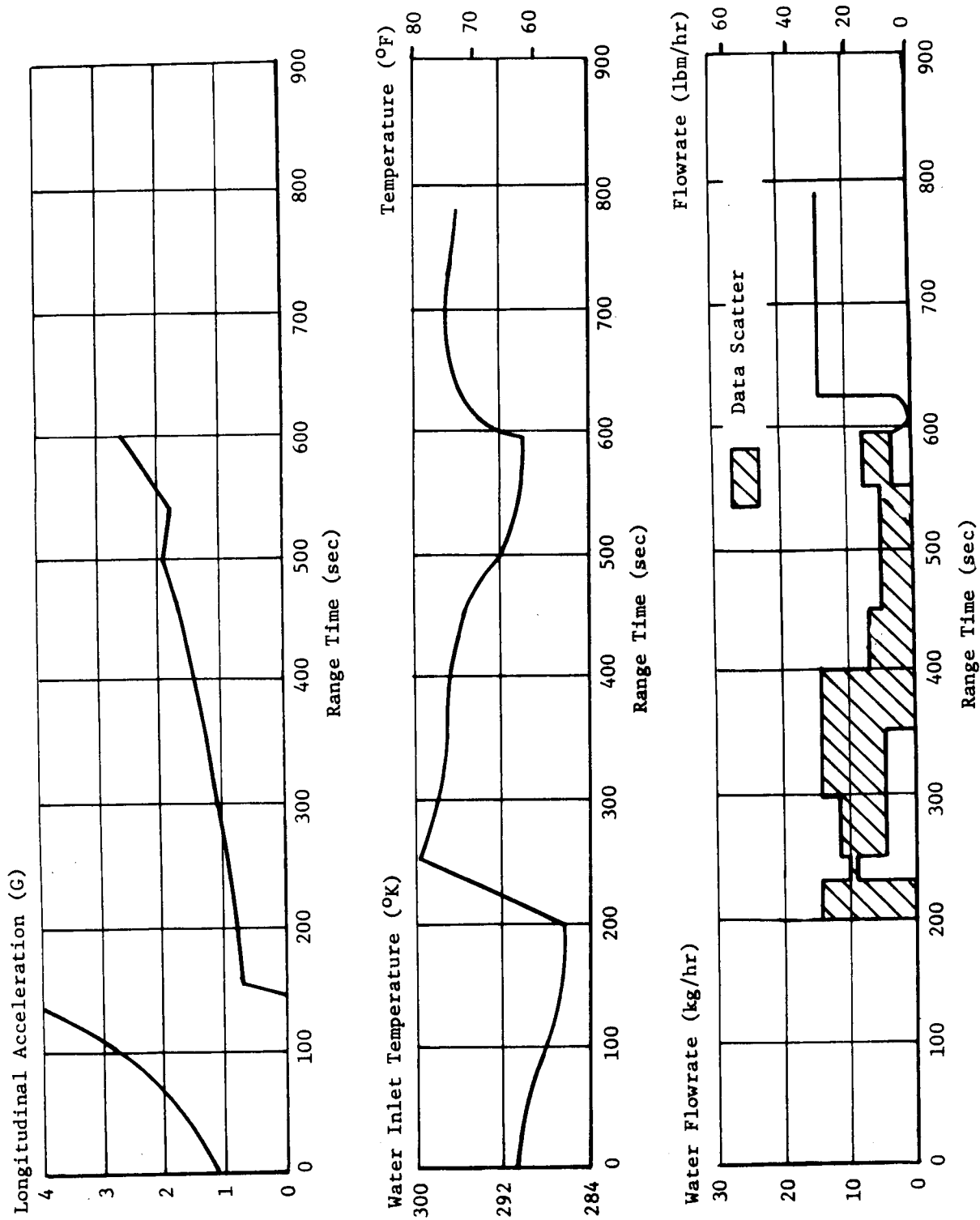
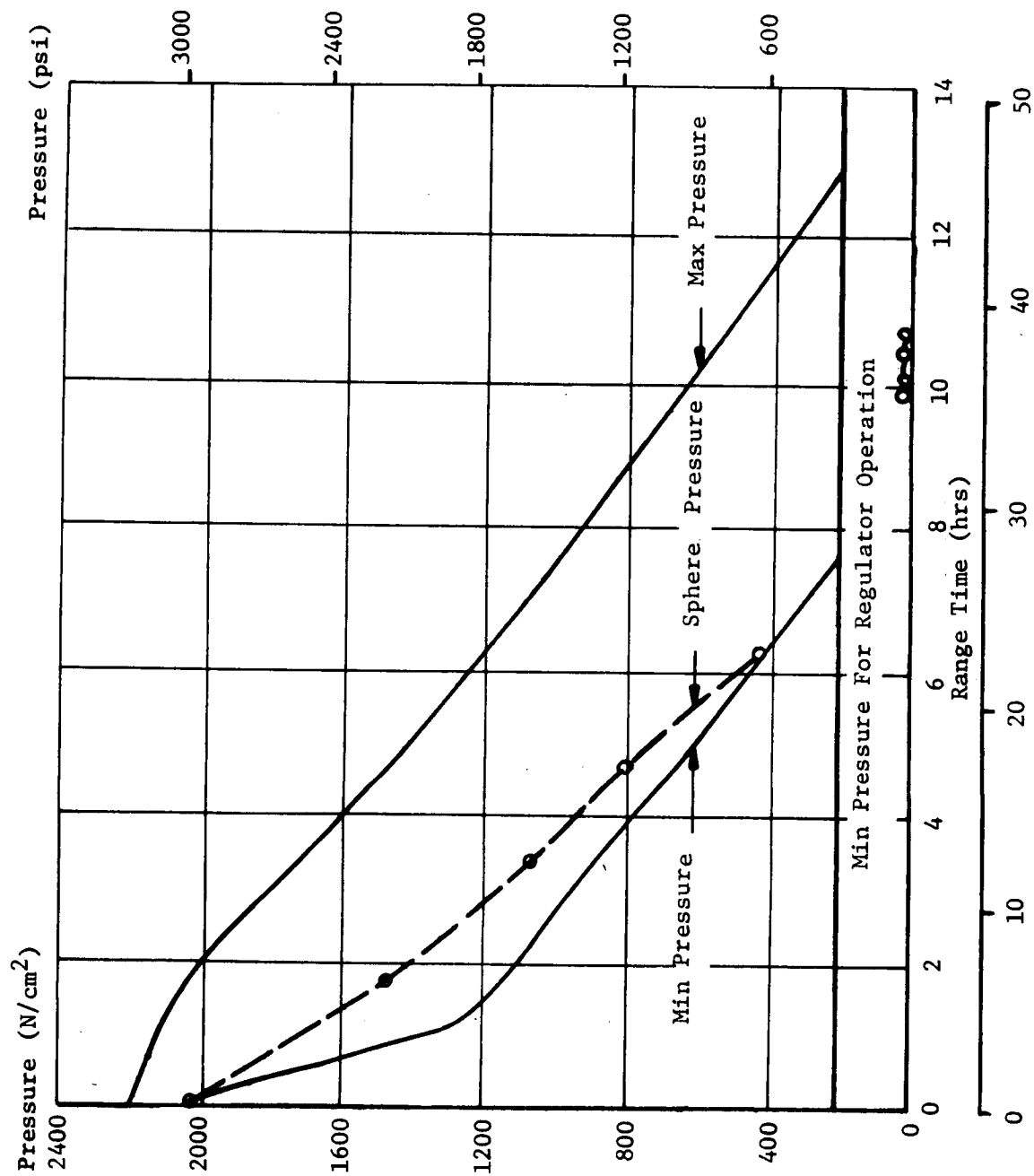


FIGURE 18-24 WATER SYSTEM FLOWRATE OPERATION DURING START-UP



Range Time (sec x 10⁻³)

FIGURE 18-25 PREDICTED AND ACTUAL TCS GN₂ PRESSURES

gas bearings. The GN_2 then flows through the gas bearing heat exchanger and a second filter to the gas bearing inlet. The heat exchanger thermally conditions the GN_2 for use by the Inertial Platform (Figure 18-20).

The GBS maintained temperature within specifications. The differential pressure across the gas bearings was not maintained within the specified tolerances. The differential pressure rose $0.276 \text{ N/cm}^2\text{d}$ (0.4 psid) above the maximum specified value at 0.25 hours and achieved steady state at $10.97 \text{ N/cm}^2\text{d}$ (15.9 psid) at approximately 3.25 hours (Figure 18-26). The internal platform ambient is shown to drop from 12.4 N/cm^2 (18 psi) at liftoff to 8.28 N/cm^2 (12 psi) in flight, however, this is within the regulator design range and should not cause the set point drift.

The undesirable temperature drift characteristics of the regulator GN_2 inlet temperature experienced on previous flights did not occur on AS-204 due to modifications resulting in better sealing of the regulator; hence, the temperature should not have affected the set point. Inlet pressures for the regulator were within design limits.

Figure 18-27 shows the gas bearing differential pressure and platform ambient pressures on an expanded scale from liftoff to 780 sec, the period of greatest regulator set point drift. The differential pressure appears to shift almost in step intervals, with the largest shift at 145 seconds. This step at the time of S-IVB ignition can be expected at times, as some regulators show this characteristic under vibration. At present, there is no explanation for the continuing shift after 145 seconds. GN_2 temperature, vibration, decreasing reference pressure, and decreasing regulator inlet pressure may have some effect upon regulator set point shift.

The GN_2 heat exchanger performed satisfactorily. The exiting GN_2 was at the M/W temperature. The platform GN_2 temperature remained within the required 274.6°K to 310.4°K (35 to 100°F).

Figure 18-28 compares the GBS 0.056 m^3 (2 ft^3) GN_2 supply sphere pressure and predicted extreme pressures. The predicted pressures account for differences in GN_2 use rates and initial conditions, and extreme temperature changes of GN_2 in the spheres during flight. The measured sphere pressure was nominal for the data available.

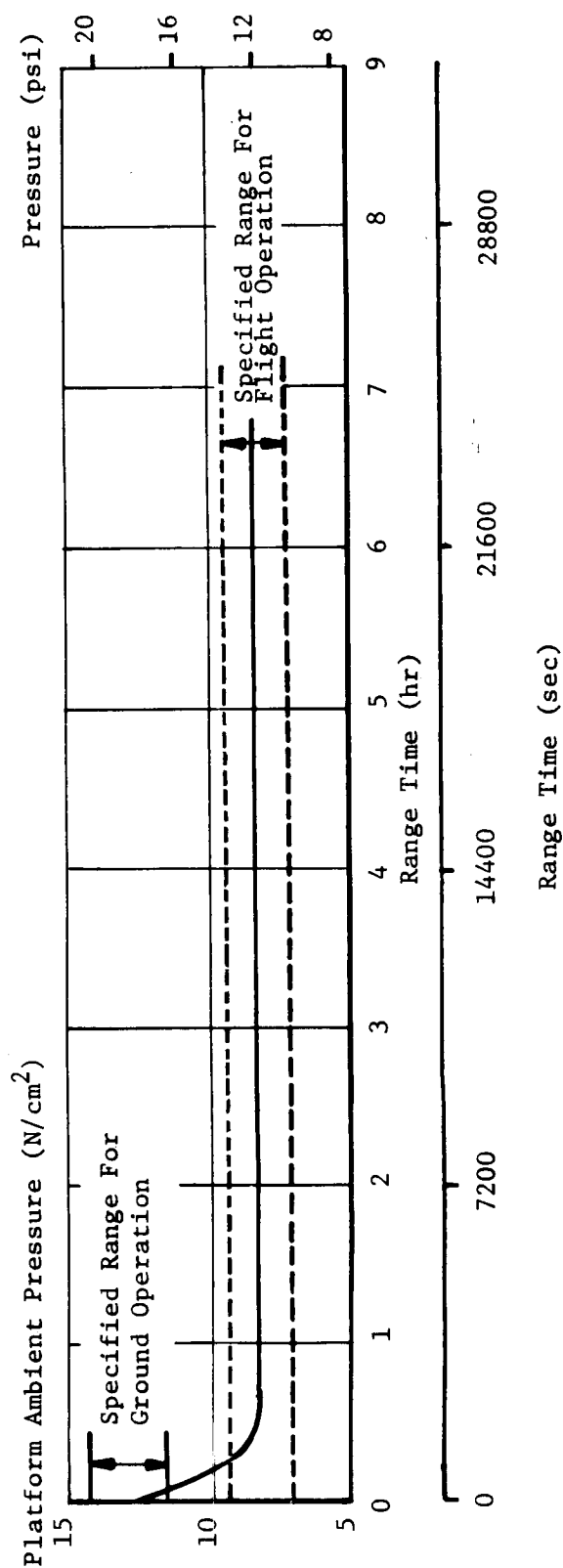
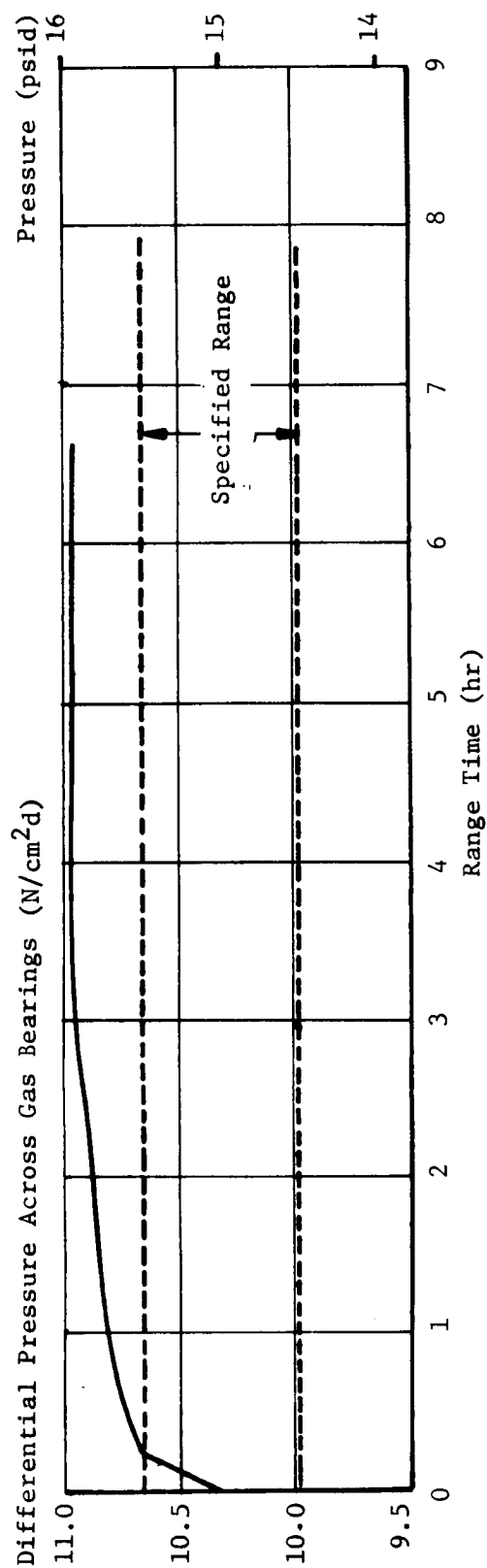


FIGURE 18-26 GAS BEARING SUPPLY SYSTEM PRESSURES

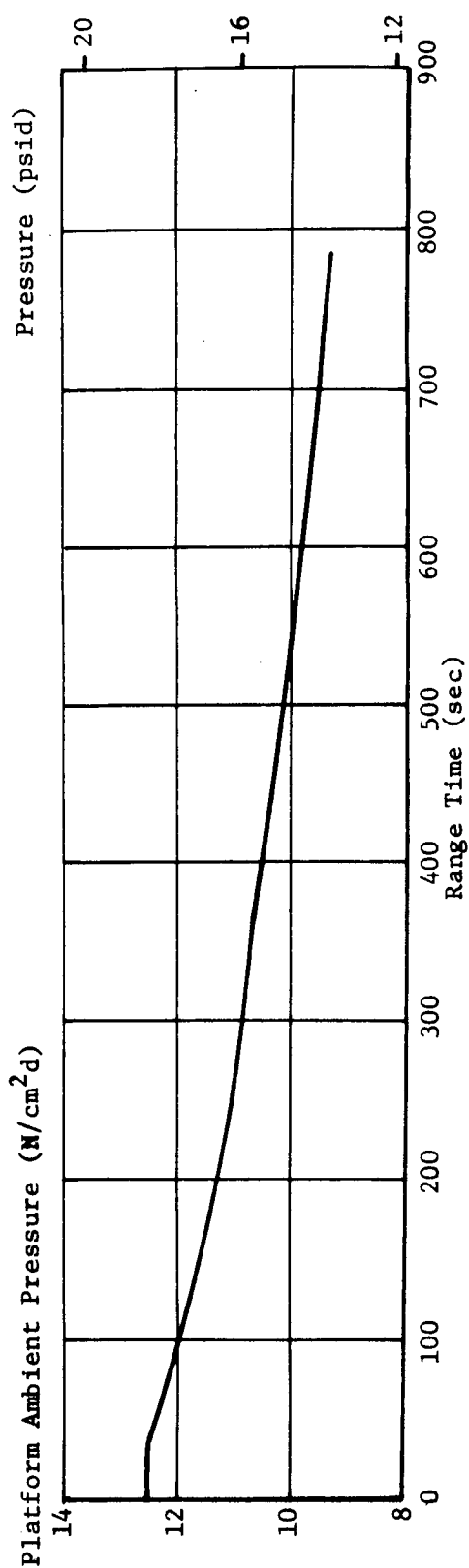
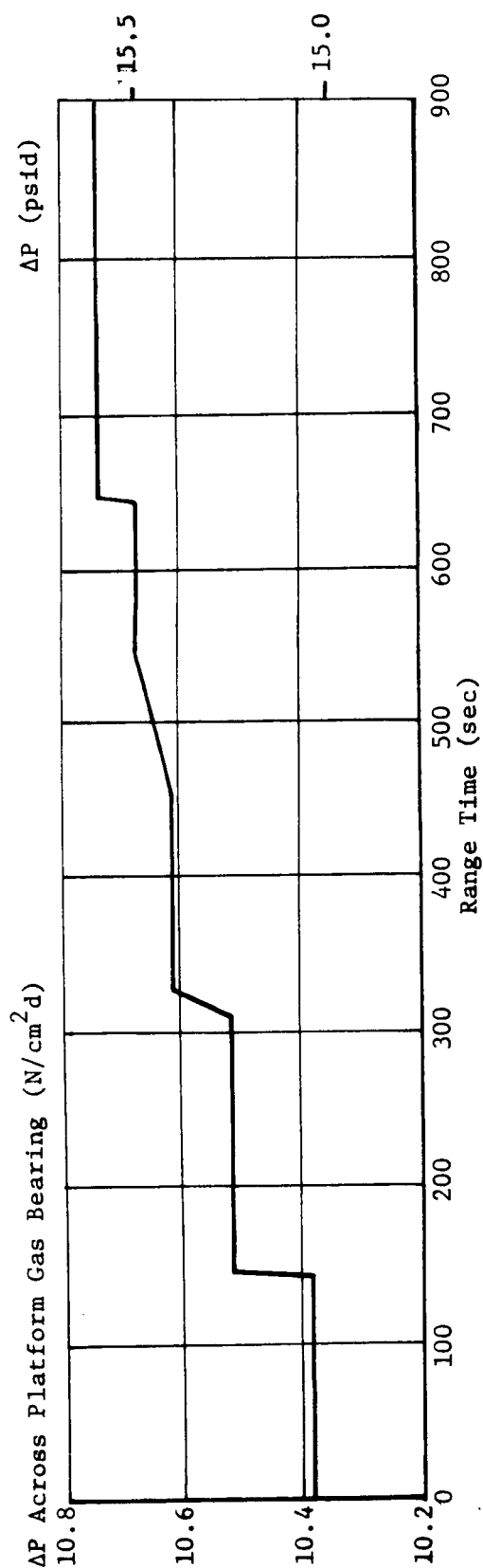


FIGURE 18-27 GAS BEARING SUPPLY PRESSURES DURING ASCENT

NOTES:

1. GN₂ use rate: 0.0085 to 0.0142 SCMM (0.3 to 0.5 SCFM)
2. Minimum pressure curve assumes sphere temp drops from initial 300°K (80.6°F) to 222°K (-59.8°F) in one hour.
3. Maximum pressure curve assumes sphere temp rises from initial 288°K (61°F) to 300°K (80.6°F) in one hour.

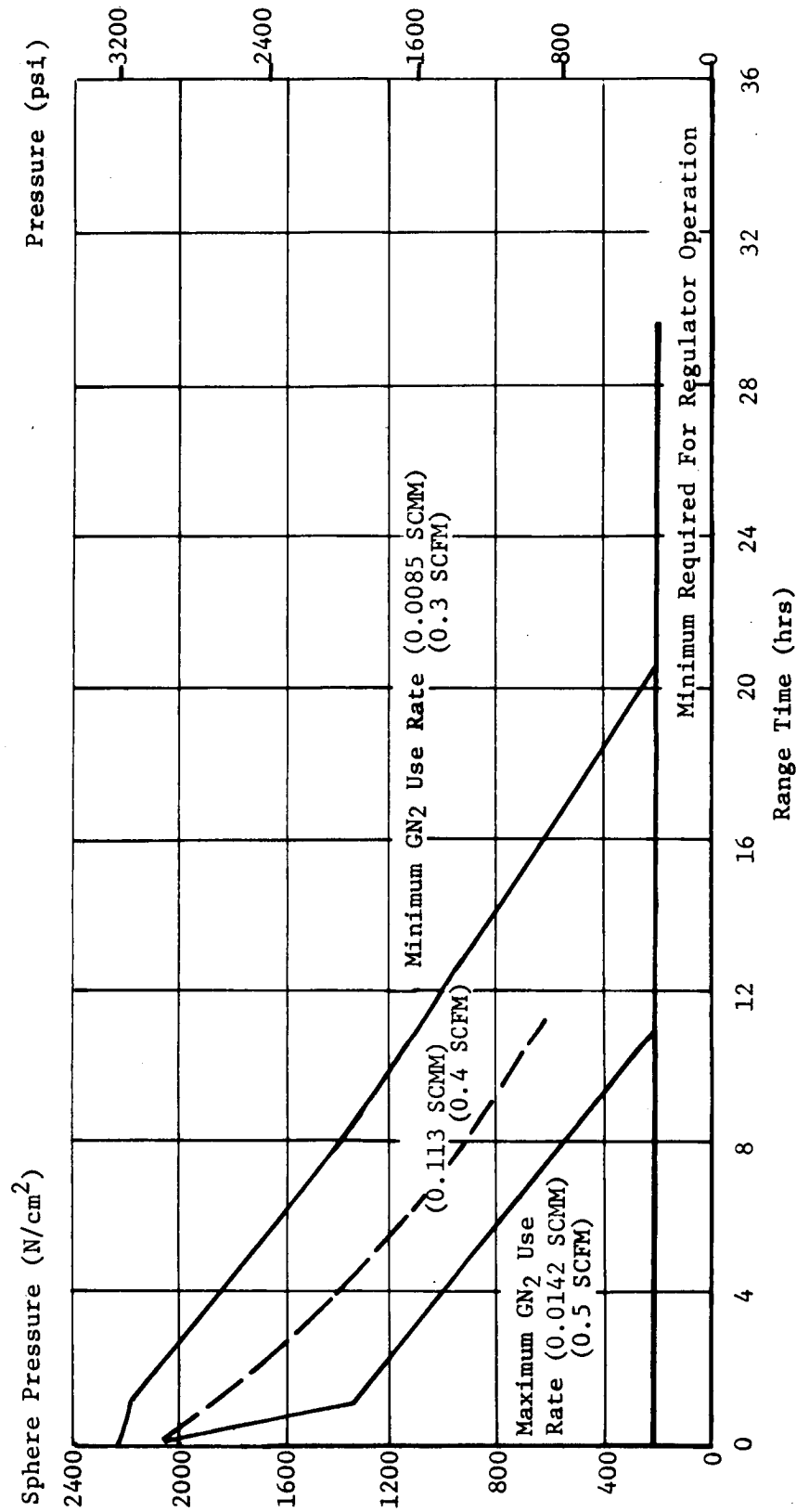


FIGURE 18-28 GBS SPHERE PRESSURE AND PREDICTED USAGE RATES

19.0 AERODYNAMICS

19.1 SUMMARY

Differential pressures measured across the fin exterior surfaces, and the corresponding wind tunnel data, were in good agreement. The base drag coefficients, determined from pressures measured in the base region, were generally lower than predicted throughout S-IB stage flight.

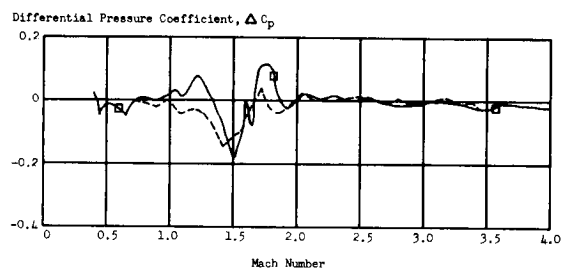
19.2 FIN SURFACE PRESSURES

Differential pressures, measured across the exterior surface of fins 5 and 7, are compared with wind tunnel data in Figure 19-1. Wind tunnel data shown on these plots correspond to the flight angle-of-attack. Since no Q-ball was used on AS-204, the angles-of-attack in pitch and yaw were taken from an elastic body planar simulation and from calculations using the FPS-16 winds (Figure 12-3). In general, the flight data were in good agreement with the wind tunnel data, except for two fin 5 measurements which were somewhat lower than the wind tunnel data.

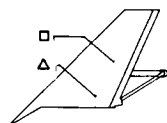
19.3 DRAG

The base drag coefficients, determined from measured base pressures, are compared with predicted values in the upper portion of Figure 19-2. Flight data generally indicated lower than predicted base drag throughout S-IB stage flight. After Mach 1.4, the base drag became negative; i.e., acted in the thrust direction. Base pressures were determined by four pressure measurements in the base region. Of the four measurements, three were on the heat shield and the other was located on the flame shield.

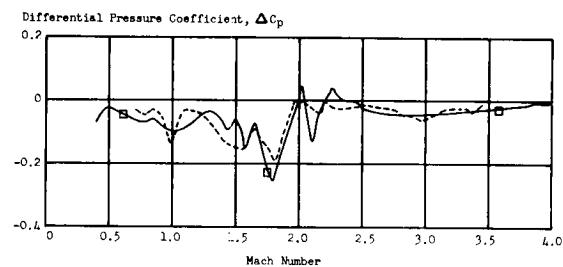
The axial force coefficients are shown in the lower portion of Figure 19-2. Included in this curve are the predicted bandwidth for the coefficient, the post-flight reconstructed coefficient derived from analysis of telemetered base pressures, and the coefficient obtained through flight simulation. The reconstructed and simulated coefficient curves exhibit good correlation throughout the flight, with the exception of the earliest portion of the flight. However, the telemetered base pressures during this region were extremely noisy and exhibited a wide deviation.



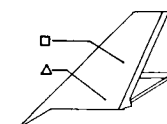
--- Wind Tunnel Data
— AS-204



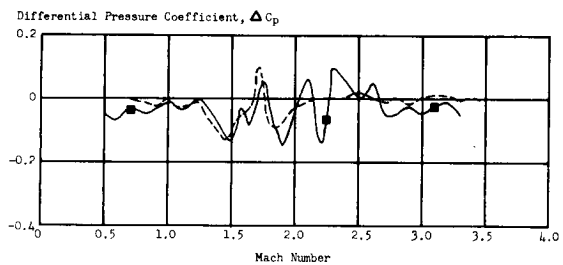
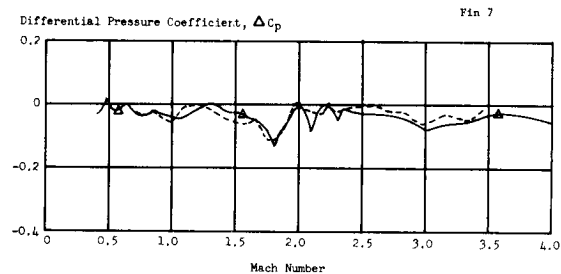
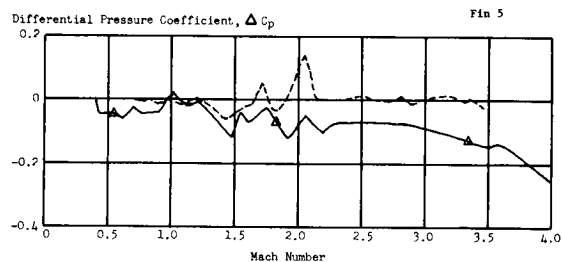
Fin 5



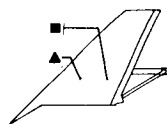
--- Wind Tunnel Data
— AS-204



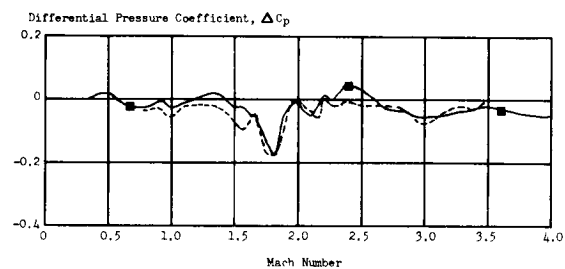
Fin 7



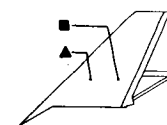
--- Wind Tunnel Data
— AS-204



Fin 5



--- Wind Tunnel Data
— AS-204



Fin 7

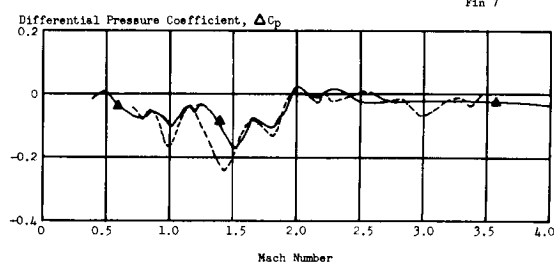
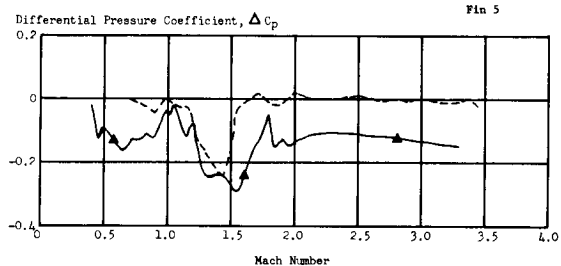


FIGURE 19-1 FIN DIFFERENTIAL PRESSURE COEFFICIENTS

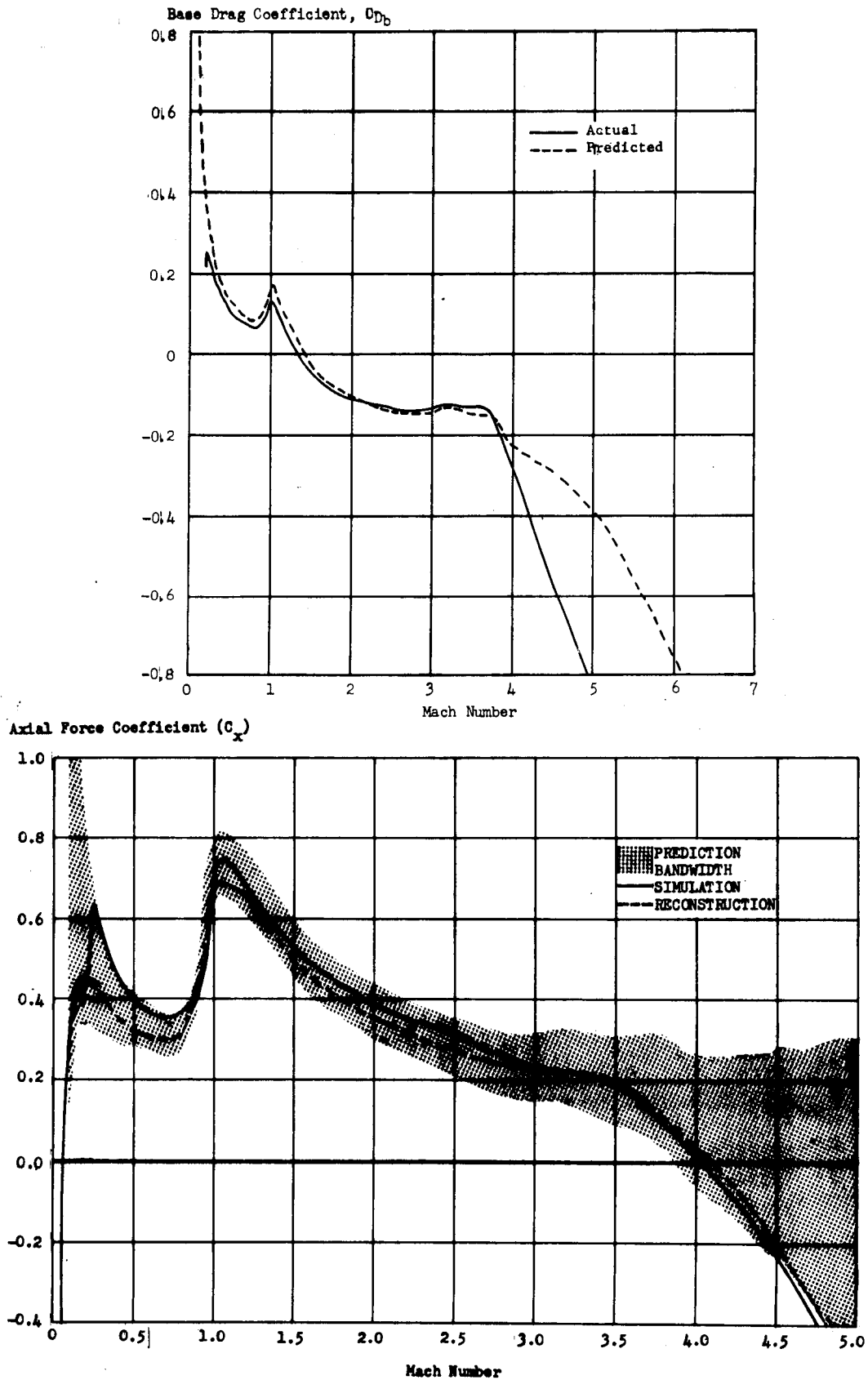


FIGURE 19-2 BASE DRAG AND AXIAL FORCE COEFFICIENTS

20.0 INSTRUMENTATION

20.1 SUMMARY

Performance of the AS-204 instrumentation was satisfactory throughout flight. The inflight measurement reliability from 1196 active measurements was 99.08% with only 11 failures. Only minor deviations occurred in the airborne telemetry and RF systems.

The airborne telemetry system, including calibrations and tape recorder, performed satisfactorily. The S-IVB CP-1 link experienced a low transmitter power output of 13.6 watts and 12.4 watts during the first and second revolutions, respectively. All stations, as expected, experienced signal reduction during flame attenuation and at separation.

Performance of the RF systems was satisfactory; however, PAFB tracked the LEM instead of the S-IB stage and therefore good data was not received. All other radars tracked as expected. The last S-IVB telemetry was received by Hawaii at 7 hrs: 32 min (27,150 sec). Ascension received the last telemetry signal from the IU at 10 hrs: 34 min (38,000 sec).

Camera coverage was excellent. The reliability from 96 engineering sequential cameras was 92.7%, with 7 malfunctioning.

20.2 VEHICLE MEASURING ANALYSIS

A total of 1226 measurements were programmed for the AS-204 flight. At liftoff there were 1196 active flight measurements. On the S-IB stage 2 were scrubbed, 8 were partially successful, and 3 were failures. The S-IVB stage assessment was: 10 scrubbed, 5 monitored by the S-IB stage, 11 used for checkout only, 1 not connected, 1 landline, 2 partially successful, and 8 failures. The IU had 2 partially successful and no failures or waivers. The above analysis results in an overall measuring system reliability of 99.08 percent. Data loss due to the 11 failures and the 9 partial successes had no adverse effect on the postflight evaluation. Table 20-I presents a summary of the measurement malfunctions per stage.

20.2.1 S-IB STAGE MEASURING ANALYSIS

There were 396 flight measurements scheduled on the S-IB stage. Of these, 2 measurements were waived prior to the automatic countdown sequence, 3 failed completely, and 8 were classified as partially successful. Based upon 3 failures out of 394 measurements expected to produce useful data, the assessed reliability was 99.24 percent.

TABLE 20-1 MEASUREMENT MALFUNCTIONS

STAGE	MEAS. NO.	MEASUREMENT TITLE	REMARKS
SCRUBBED PRIOR TO LAUNCH			
S-IB	XC179-F3 E535-01	Temperature Fuel Vib-Tank Fill and Drain Line	Intermittent prior to ignition. Transducer froze during LOX loading.
S-IVB	C0040-406 C0041-406 C0042-406 C0043-406 C0055-406 C0056-406 C0072-408 C0135-406 D0121-419 E0082-401	Temp-Oxidizer Tank Position 1 Temp-Oxidizer Tank Position 2 Temp-Oxidizer Tank Position 3 Temp-Oxidizer Tank Position 4 Temp-LOX Tank Ullage Gas 1% Temp-LOX Tank Ullage Gas 20% Temp-Fuel Tank Wall Internal-4 Temp-Oxidizer Tank Ullage Press-External-Aft Interstage 1 Vib-LOX Turbo Pump-Lateral	Off scale low (measurement gave valid data). Off scale low. Off scale low. Off scale low. Data intermittent Off scale low after LOX loaded (measurement gave valid data) Went off scale low during LH ₂ loading. Off scale high. 8% PP noise on data. Connector damaged during final preparation.
FAILURES			
S-IB	E276-4 E33-3 K2-12	Vib-Yaw Actuator Vib-Thrust Chamber Dome, Longt. First Motion	No usable data. Data not realistic. Prematurely triggered.
S-IVB	D0122-419 D0158-402 D0124-419 D0016-425 D0062-424] D0045-403 C079-409 C080-409	Press-External-Aft Interstage 2 Press-Interstage-Internal 2 Press-External, Aft Interstage 4 Press-Cold Helium Sphere Press-LH ₂ Circulation Return Line Tank Inlet Press-Engine Actuator Yaw, Diff. Temp-LH ₂ Tank, External 5 Temp-LH ₂ Tank, External 6	Uncorrectable shift in transducer output. Uncorrectable shift in transducer output. Temperature environment below 272°K (29.6°F). Erratic prior to liftoff Off scale low until 200 seconds. Data traces change but do not follow yaw position changes as expected. Off scale high at 3100 seconds. Off scale high at 3600 seconds.
PARTIALLY SUCCESSFUL			
S-IB	B501-4 C506-7 C605-8 D13-1 D13-5 E511-11 L20-F3 L49-04	Acoustic, Engine Shroud Temp-Heat Shield Radiation Calorimeter Temp-Aspirator Inlet Press-LOX Pump Inlet Press-LOX Pump Inlet Vib-Spider Beam, Longitudinal Fuel Level Discrete LOX Level, Continuous	Questionable data after 28 seconds. Data drop after approximately 120 seconds. Data shift at approximately 113 seconds. High output. High output. Invalid data between 60 and 110 seconds. Pulse 7 missing. Spurious data for approximately 128 sec, erratic data after 133 seconds.
S-IVB	B0012-427 E0084-401	Acoustic-Position II, External Vib-LH ₂ Turbopump, Lateral	Momentary decreases of amplitude; also occurred on AS-203 at approximately same times (-1, +1, +48, and +52 seconds). Gradual degradation of data from 298 sec on.
IU	F3-601 F7-601	Flow Rate Cold Plate Inlet Coolant Flow Rate IU Exit Coolant	Flow rate indication ceased between 1440 and 3121 seconds. Flow rate indication ceased between 3550 and 5427 seconds.

20.2.2 S-IVB STAGE MEASURING ANALYSIS

The performance of the S-IVB instrumentation system was satisfactory. Of 515 programmed measurements, 5 were monitored by the S-IB stage, 11 were used for checkout only, 1 was a landline, 1 was not connected because of stage configuration, and 10 malfunctioned prior to start of the automatic countdown sequence. The total number of measurements to be evaluated from automatic countdown sequence through the end of mission was 487. Of these measurements, 8 were failures, and 2 were partially successful. This yields an overall system reliability of 98.36 percent. Two of the 8 failed measurements occurred during orbital flight. The LOX vent valve closure indication following cold helium dump was not received and resulted in commands being sent to close the valve. (See Section 15.)

20.2.3 IU MEASURING ANALYSIS

There were 315 flight measurements flown on the IU. Of these measurements, there were 2 partial successes and no waivers or failures. The measuring performance reliability of the IU was 100 percent.

Confirmation of SLA panel deployment was not received in the proper sequence and resulted in backup mode commands being sent to deploy the panels. Analysis reveals that panel deployment occurred very near expected time. (See Section 15.)

20.3 AIRBORNE TELEMETRY SYSTEMS

The launch vehicle used 13 airborne telemetry links to transmit flight data to ground stations. Table 20-II lists the launch vehicle telemetry links and functions by stage.

Performance of the airborne telemetry system was generally satisfactory. The only problems indicated by the telemetry data were the low power output from the links CP-1, CF-3, and DP-1. These problems had no serious impact on the vehicle evaluation; however, special data processing was required.

20.3.1 S-IB STAGE

Four VHF airborne telemetry links (Table 20-II) transmit data from the S-IB stage inflight measurements to ground stations.

TABLE 20-II AS-204 LAUNCH VEHICLE TELEMETRY SYSTEM DESCRIPTION

Link No.	Frequency (MHz)	Modulation	Stage
GF-1	240.2	PAM/FM/FM	S-IB
GF-2	244.3	PAM/FM/FM	S-IB
GS-1	252.4	SS/FM	S-IB
GP-1	256.2	PCM/FM	S-IB
CF-1	258.5	PAM/FM/FM	S-IVB
CF-2	246.3	PAM/FM/FM	S-IVB
CF-3	253.8	PAM/FM/FM	S-IVB
CS-1	226.2	SS/FM	S-IVB
CP-1	232.9	PCM/FM	S-IVB
DF-1	250.7	FM/FM	IU
DF-2	245.3	PAM/FM/FM	IU
DS-1	259.7	SS/FM	IU
DP-1	255.1	PCM/FM	IU

Performance of the four telemetry systems was satisfactory and all calibrations and synchronization functioned as programmed.

20.3.2 S-IVB STAGE

Five airborne telemetry links (Table 20-II) transmitted data from the S-IVB stage inflight measurements to ground stations. Three separate modulation techniques were utilized.

All telemetry links provided acceptable data. Two minor problems were encountered with links CP-1 and CF-3. The CP-1 link was utilized as the prime data source for the Digital Data Acquisition System. Both CP-1 and CF-3 links experienced low transmitter power output (below 25 watts specification); however, the performance of these links was satisfactory. The PAM transmitter 3 (CF-3 link) power output was slightly low (24.9 watts) before launch but was rated as acceptable before liftoff. During flight, the measured output (N0017-411) decreased slightly to 24.8 watts. The PCM transmitter (CP-1 link) power output (N0018-411) indicated a sudden drop in power output at 1100 sec, dropping from 26.8 watts to 13.6 watts. At 1200 sec the transmitter recovered power to 19 watts and gradual degradation was indicated. The power output at 8925 sec was down to 12.4 watts. The most probable cause of the CP-1 link performance deviation was the transmitter or the RF power amplifier. Qualified data for the orbital portion of flight did not reveal degradation.

20.3.3 INSTRUMENT UNIT

The IU onboard telemetry systems were composed of four telemetry links (Table 20-II) and their associated components. All data reviewed indicated satisfactory performance of all telemetry systems. Usable data was provided through 10hrs:42min of flight.

Link DP-1 transmitter power output was below the minimum acceptable value of 15 watts from approximately 0 to 150 sec and during the orbital flight period. The minimum value reached was 13.8 watts.

20.4 AIRBORNE TAPE RECORDER

The airborne tape recorders recorded and stored real-time data during separation, insertion, and over-the-horizon periods of flight. On command from the various ground stations, recorded data was transmitted.

The performance of the S-IB stage tape recorder was satisfactory. The tape recorder start command occurred at 39.6 seconds. Playback of the recorded data began at 171.4 seconds. Examination of the data playback indicated excellent reproduction of the recorder input signals.

Tape recorder performance of the S-IVB stage was satisfactory throughout the mission. The tape recorder recorded all analog data on fast record, and played back on command. The Event-Ready to Record Indication was not active

prior to the fast-record command because the recording tape was advanced before liftoff in order to reduce the analog data recording time. This was necessary since the fast-record circuit configuration and the programming of the flight sequence would fast-record data in excess of the playback time and the significant S-IB/S-IVB separation data would be lost.

The IU tape recorder recorded the outputs of links DF-1 and DF-2 during retro-firing. The quality of the data was excellent. No problems were experienced with tape recorder operation. The "Record Period Start Command" occurred at 136.1 sec and "Record Period Stop" occurred at 161.2 seconds. Playback started at 597.4 sec and stopped at 625.5 seconds.

20.5 RF SYSTEMS ANALYSIS

The Launch Vehicle RF Systems performance during flight was satisfactory throughout the predicted life of the vehicle. The launch and powered flight portion of the mission was nominal. Coverage of the onboard RF systems, by ground tracking and instrumentation stations, was as expected. The simultaneous operation of two C-band radar transponders on the instrument unit did not appear to affect the tracking systems. Operators at Bermuda and Canary Island Stations did report double target returns but no tracking errors that could be caused by them. The signal levels at Bermuda were near marginal.

The S-IB stage telemetry signals were attenuated by approximately 35 db at maximum flame plume impingement on the look angles. The S-IVB and instrument unit telemetry signals were reduced by about 30 db in amplitude during this time. The stations affected by this signal attenuation were TEL 4 and CIF Telemetry. The GBI Telemetry Station was not affected by main engine flame plume. As was expected, all stations experienced a reduction in signal during the separation sequence. The RF system coverage is presented in Figure 20-1.

20.5.1 TELEMETRY

The telemetry signal levels from the S-IB stage were at saturation level for the first 90 sec of flight at the CIF and TEL 4 Stations, with a reduction of 6 db between 13 and 25 seconds due to multipath effects. Flame attenuation was severe at the Cape area stations, with up to 35 db of attenuation indicated at 105 seconds. The GBI Station began receiving data at 55 sec and tracked through 290 seconds.

The Cape area telemetry stations experienced similar flame attenuation of the S-IVB signals as on the S-IB stage. Cape area coverage was from liftoff through 555 seconds. The GBI Station began data reception at 55 sec and received good data through 370 seconds. The Bermuda Station began receiving S-IVB telemetry at 250 sec and received data through 777 seconds. Signal levels at Bermuda were near marginal during much of the launch phase, due to ground station problems, and resulted in noisy data. The noise was not of sufficient intensity to prevent data reduction and analysis. During the 5th revolution after the Hawaii dump at 7 hrs: 32 min (27,150 sec), the S-IVB

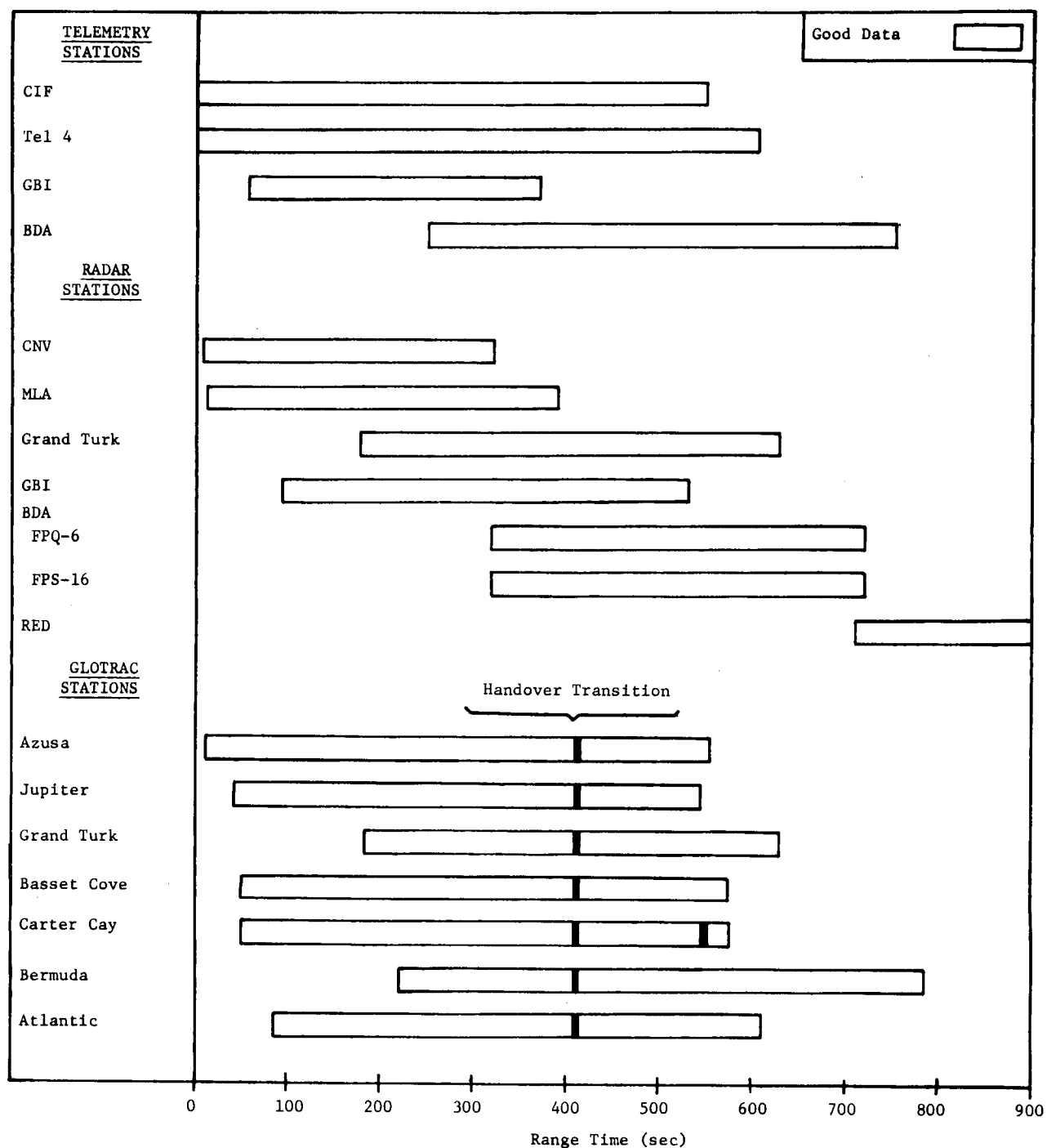


FIGURE 20-1 AS-204 RF SYSTEM COVERAGE

TM battery voltage dropped below the level required to operate the system.

The Cape area telemetry stations experienced a similar flame attenuation of the IU signals as on the above stages. Cape area telemetry coverage was from liftoff through 555 sec with minor drops at 26 and 29 sec and a dropout at separation sequence lasting approximately 3 seconds. The system performed satisfactorily in orbit. The last signal quality report received was from Hawaii, although the signal levels were weak, for the seventh revolution. This report indicated the IU was radiating good signals on links DF-1, DF-2, and DP-1. Ascension was the last station to receive telemetry signals at 10hrs:34min (38000 sec). Figure 20-2 shows the orbital telemetry system coverage.

20.5.2 TRACKING

During launch and powered flight, the radar systems operated satisfactorily, with only one reported deviation. The FPS-16 radar at PAFB tracked the LEM instead of the S-IB stage and therefore valid data was not received. All other radars tracked as expected. Orbital data show the FPS-16 at Bermuda experienced difficulty in interrogating the beacon during revolution 3. Data from GBI for the same period indicate no problem in maintaining track on the vehicle. The last radar tracking report received was from Hawaii FPS-16. This station tracked with valid data for 6 minutes during the seventh revolution of the vehicle. A later report from Ascension Island FPS-16 indicates no target found during the 10th revolution, using Houston IRV, Goddard Pointing data, and Hit Process techniques. Figure 20-3 shows the orbital radar coverage by the C-Band System.

The Mark II Azusa Station performed as assigned, with a lock on the target from 27 sec to 410 sec, as the prime station and from 410 to 564 sec in passive track with the Bermuda Glotrac Station as the interrogator. Handover transition to Bermuda was smooth, with a maximum reacquisition time of 6 sec taken by the Atlantic Station. The Grand Turk Station operator log reflects a noisier signal from the Bermuda Station than was transmitted by the Mark II Station. Continuous tracking was provided through 780 sec of the mission.

ODOP data was acquired but not evaluated, because no anomalies occurred on the AS-204 flight. The ground stations that were called up for ODOP tracking were: MARGO, PLUTO, METRO, MOLLY, CACTUS, MANDY, and SITE C.

There were no ODOP System malfunctions during the launch phase. ODOP signals were received and recorded from liftoff through 345 seconds. Periods of noise in the signal were experienced from 85 to 105 sec and from 240 to 268 seconds.

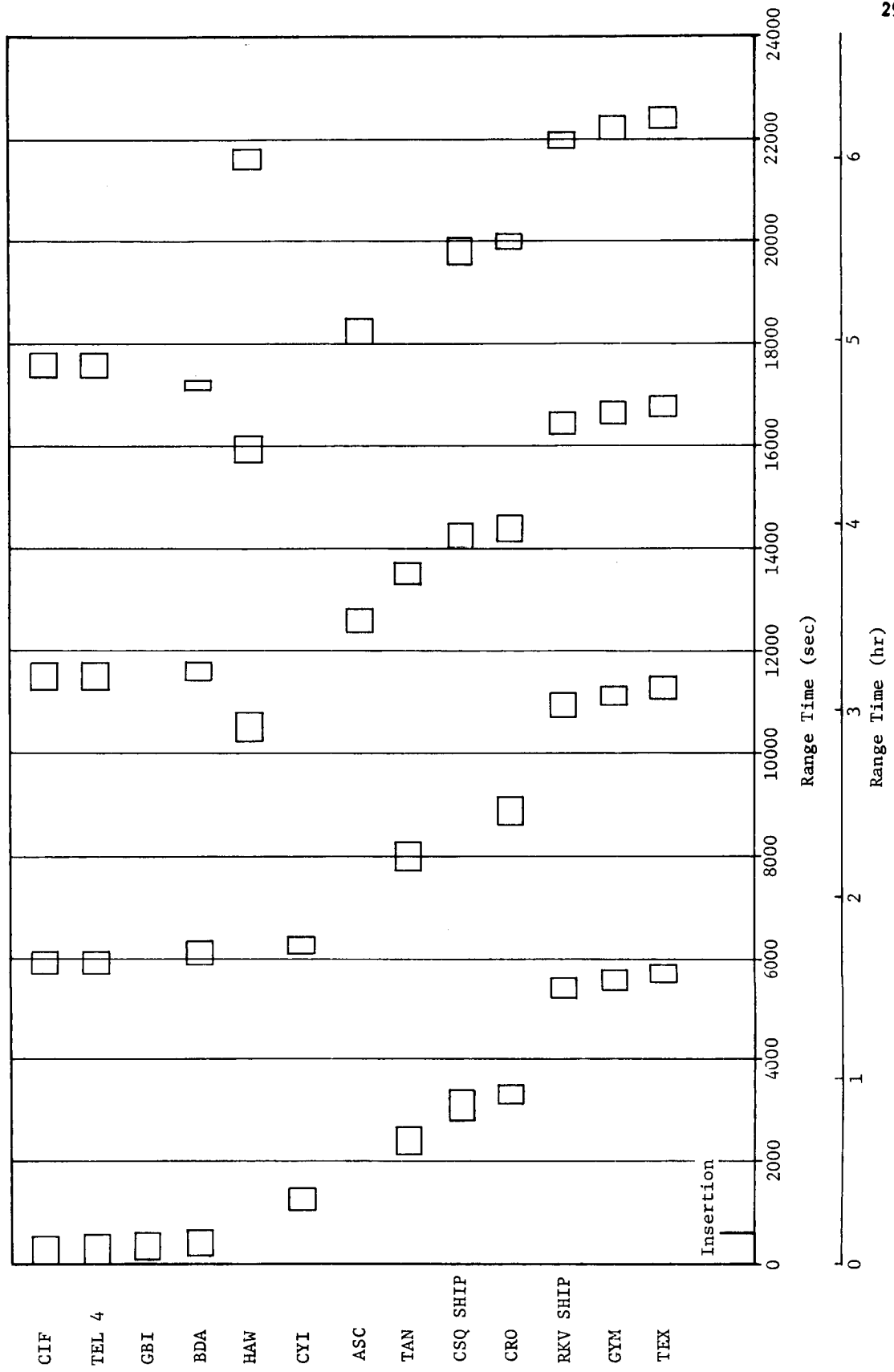


FIGURE 20-2 ORBITAL TELEMETRY COVERAGE

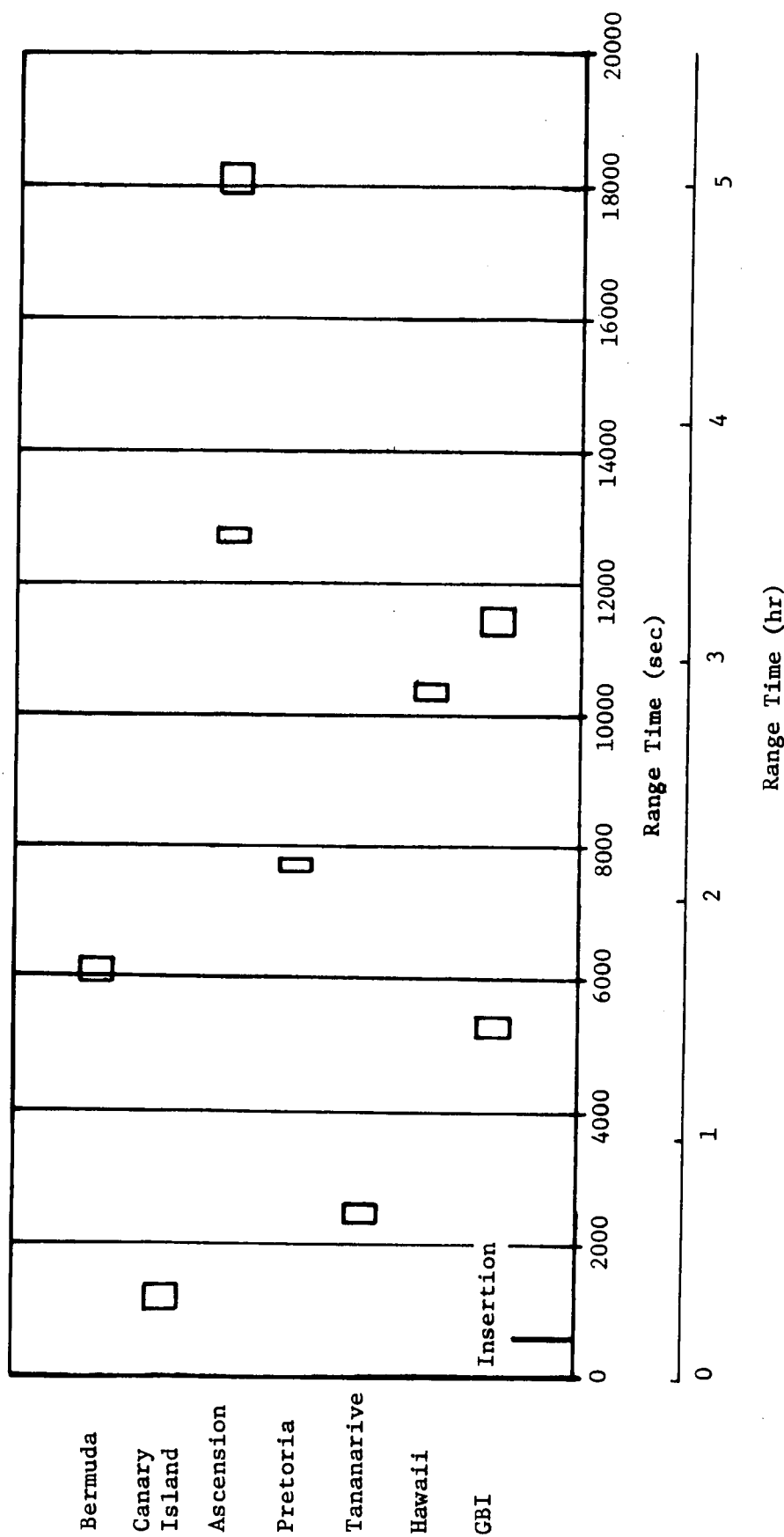


FIGURE 20-3 ORBITAL RADAR COVERAGE

20.6 OPTICAL INSTRUMENTATION

20.6.1 PHOTOGRAPHIC COVERAGE

The engineering photographic coverage of the launch was excellent. Photographic coverage was provided by 96 sequential cameras and is divided into three major categories: 83 fixed cameras to provide coverage during prelaunch operations and liftoff through three vehicle lengths of flight; 12 ground based tracking cameras, to track the vehicle from first acquisition to loss of view or film depletion; and 1 airborne tracking camera.

Of the 96 cameras programmed, 26 surveillance/malfunction films did not require processing, 2 cameras did not operate, 4 cameras were out of focus and data was not obtained, and 1 film produced no timing. The camera reliability was 92.7%.

20.6.2 FILM ANALYSIS

There was considerably more frost and ice observed on the vehicle than on previous launches. This icing was attributed to the 289.26°K (61°F) temperature, the 288.15°K (59°F) dew point, the low surface winds, the diffuse sky, and the low radiation level of the sun. On two of the holddown arms, part of the holddown shoe was observed to remain with the vehicle after release. It was also noted that two of the vehicle support struts moved laterally just prior to the release of the hold-down arms. The short cable mast II flame deflector cover failed to close until forced closed by the vehicle exhaust blast. The tank cover panel at swing arm 3 connect point was observed to strike the arm head after release, and the tank cover panel at swing arm 1 did not close completely.

21.0 SPACECRAFT

21.1 SUMMARY

The Apollo 5 mission, the first mission of a flight configuration lunar module spacecraft (LM-1), was successfully flown on January 22 and 23, 1968. The launch vehicle was the Saturn IB originally planned for use on the first manned Apollo mission. The primary objectives of the Apollo 5 mission were to flight-verify the ascent and descent propulsion systems and the abort staging function for manned flight. These objectives were met.

Liftoff occurred at 22:48:08 UT (17:48:08 EST). The S-IVB stage inserted the S-IVB/IU/LM-1 combination into an earth orbit after approximately 10 min: 3 sec (603 sec) of powered flight.

21.2 SPACECRAFT PERFORMANCE

The lunar module was separated from the S-IVB/IU at 53 min: 55.2 sec (3235.2 sec), using the lunar module reaction control engines. Low angular rates were observed during separation. The lunar module was maneuvered to a cold-soak attitude that was maintained until early in the third revolution.

Midway through the third revolution, the first descent engine firing was initiated. The planned duration of this firing was 38 sec; however, after only 4 sec, the guidance system shut down the engine because the thrust buildup did not satisfy the velocity/time criteria programmed in the guidance computer. As a result of the premature shutdown, an alternate mission was selected. This alternate mission had been previously planned to provide at least the minimum mission requirements. The major deletion was the long descent propulsion subsystem burn. Also the spacecraft was controlled by the program reader assembly rather than primary guidance during the propulsion burns.

The alternate mission was initiated at 6 hr: 10 min (22,200 sec) with a Descent Propulsion System burn program using the on-board secondary system of automatic guidance and control called the Program Reader Assembly Sequence III. This burn lasted 33 sec, followed by a 32 sec coast and another burn of 28 sec duration. The Ascent Propulsion System fire-in-the-hole abort staging was then successfully accomplished. The maneuver simulated a lunar mission situation in which, while descending to the lunar surface using the Descent Propulsion System, it is decided to abort the lunar landing and return to lunar orbit for eventual return to the earth. The maneuver was accomplished by near-simultaneous

shutdown of the Descent Propulsion System, separation of the Lunar Module ascent and descent stages, and ignition and burn of the Ascent Propulsion System. The first Ascent Propulsion System burn duration was 60 sec as planned in the selected alternate mission. The three burns and the abort staging were performed satisfactorily. The objective to demonstrate the ability to maintain cabin pressure to a minimum of 0.69 N/cm^2 (1 psi) through the staging event was successful.

The second firing of the ascent engine, initiated by mission programmer sequence V, began at 7 hrs: 44 min: 13 sec (27,853 sec) and continued until thrust decay at 7 hrs: 50 min: 3 sec (28,203 sec). During the initial portion of the firing, rate damping was maintained with propellants from the ascent propulsion system through interconnect valves to the control engines. However, the mission programmer automatically closed the interconnect valves, thus depleting control propellants; consequently, the vehicle began tumbling while the ascent engine was firing. All tracking was lost about 2 min after thrust decay, at approximately 7 hrs: 52 min (28,320 sec). The lunar module had been in a retrograde attitude during the controlled portion of the firing, and trajectory simulations show that the lunar module re-entered the earth's atmosphere over the Pacific Ocean. The predicted point of impact was approximately 644 km (400 miles) west of the coast of Central America.

Spacecraft systems performance was satisfactory, except for abrupt changes in spacecraft-received signal strength in the UHF command system. The problem, which was noted throughout the mission, was caused by an intermittent failure in the flight hardware.

Overall performance of the lunar module was good and met all the requirements for manned flight. General support from the NASA and Department of Defense network stations was excellent.

22.0 SUMMARY OF MALFUNCTIONS AND DEVIATIONS

22.1 SUMMARY

There were no malfunctions or deviations from nominal performance that produced a significant effect on the launch vehicle operation or the accomplishment of the assigned missions. However, certain minor modifications are planned for future vehicles to improve system operations.

22.2 SYSTEMS MALFUNCTIONS AND DEVIATIONS

The systems having significant deviations (actual operation deviated from expected operation), the probable nature of the deviation, and the recommended corrective action are summarized in Table 22-I. A more complete discussion of each problem area is included in the paragraphs of this report that are referenced in the table.

TABLE 22-1 SUMMARY OF MALFUNCTIONS AND DEVIATIONS

DEVIATIONS	VEHICLE SYSTEM	EFFECT ON MISSION	PROBABLE CAUSE	CORRECTIVE ACTION BEING TAKEN	EFFECT ON FUTURE MISSIONS
1. PCM/FM transmitter output power (N0018-411) dropped (from 26.8 watts to 13.6 watts) below the minimum 25 watts at 1100 seconds.	LV Telemetry System (S-IVB Stage)	None - See para. 20.3.2	Most probable cause was the transmitter or the RF power amplifier	Last mission for this model.	None
2. Three parameters indicate low water flow-rates during sublimator water startup, low sublimator water inlet pressure, and excessive GN ₂ consumption for these measured conditions.	IU TCS	None - See para. 18.4.1	Leak in high pressure line in the high side of the regulator.	Improved procedures for isolating leaks.	None
3. FM/FM transmitter 3 output power, as indicated by the telemetered measurement N0017-411, was 24.8 watts which was below the minimum requirement of 25 watts.	LV Telemetry System (S-IVB Stage)	None - See para. 20.3.2	Known to be slightly low (24.9 watts) before launch and documented on failure and rejection report (FRR) A259718.	Non indicated	None
4. A mass loss of 30 lbm of cold helium in the bottles is indicated between ECO and 3500 sec. It is not believed that mass losses occurred actually.	Cold Helium Supply System (S-IVB Stage)	None - See para. 9.6.4	Sphere instrumentation is thought to be responsible for this indication. Similar indicated mass losses occurred in AS-501 during orbital coast.	None	No known adverse effects.
5. The LOX vent valve "close" indication did not appear following cold helium dump until 1134 sec after the close command.	LOX Tank Pre-surization System (S-IVB Stage)	None - See para. 9.6.2	Solid O ₂ partially blocked the CH ₂ vent path.	None	None
6. The gas bearing differential pressure (D11-603) exceeded the maximum specification by 0.28 N/cm ² d (0.4 psid).	IU GBS	None - See para. 18.4.2	Inadequate testing procedure and fixtures.	Review procedures and test fixtures to insure adequacy and compatibility between the regulator and platform.	None
7. An undesirable 17 to 18 Hz oscillation appeared in the roll control rate gyro output during S-IVB powered flight, resulting in a maximum roll attitude error of 2.3 deg (1 deg nominal limit).	Roll Control Portion of APS (S-IVB Stage and IU)	None - See para. 12.3.4.2	Unknown	On AS-502 the roll attitude error limit was increased from +3.5 deg to +15.3 deg. The need for any action on vehicles subsequent to AS-502 is being investigated.	Dependent upon investigation now being conducted.

APPENDIX A

(U) VEHICLE DESCRIPTION

A.1 SUMMARY

The flight of AS-204 was the fourth to qualify and to flight test the Saturn IB vehicle. It was the first flight to demonstrate the Lunar Module (LM) and Saturn IB launch vehicle physical and flight compatibility. AS-204 measured approximately 55 m (181 ft) in length and consisted of the following four major units: S-IB Stage, S-IVB Stage, Instrument Unit, and Payload. A pictorial description of the vehicle is presented in Figure A-1.

A.2 S-IB STAGE

A.2.1 S-IB CONFIGURATION

The S-IB stage had nominal dimensions of 24.4 m (80.2 ft) in length and 6.5 m (21.4 ft) in diameter. A cluster of eight uprated H-1 engines powered the S-IB stage (Figure A-2) and produced a total sea level thrust of 7.12 million Newtons (1.6 million lbf). Each of the four outboard engines gimballed in a ± 8 deg square pattern to provide pitch, yaw, and roll control. Inboard and outboard engines were canted 3 deg and 6 deg outwards respectively from the vehicle longitudinal axis to minimize the disturbing moments that would be induced by an engine failure at critical dynamic pressure.

Propellants were supplied to the engines through suction lines from the clustered arrangement of nine propellant tanks. These tanks consisted of four 1.78 m (70 in) diameter RP-1 (fuel) tanks, four 1.78 m (70 in) diameter LOX (oxidizer) tanks, and a 2.67 m (105 in) diameter center LOX tank. Each outboard tank (LOX and RP-1) supplied propellants to one inboard and one outboard engine. The center LOX tank supplied the outboard tanks through the LOX interchange system. Thrust and longitudinal loads were carried by the pressurized LOX tanks, which were structurally retained at the forward end of the S-IB stage by the spider beam.

LOX and fuel tank pressurization modules regulated tank pressures during ground operation and S-IB flight. The control pressure system used GN_2 to actuate various valves for such purposes as vent relief, fill, and drain. The propellant utilization system consisted of LOX mass sensors, fuel mass sensors, and electronic assemblies. It was an open-loop system which initiated signals to cutoff the engines at appropriate times. Nominal stage propellant loading

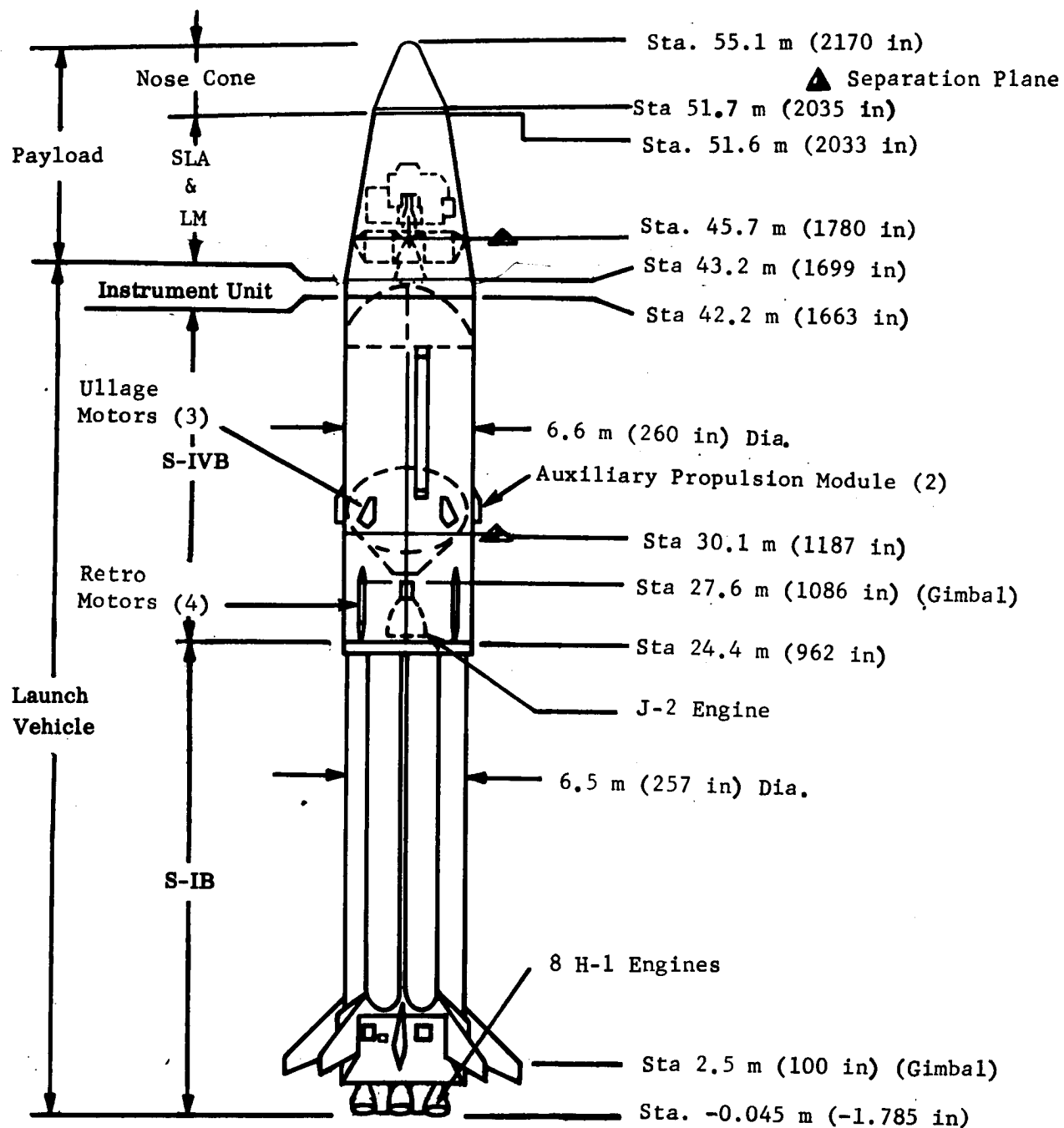


FIGURE A-1 AS-204 CONFIGURATION

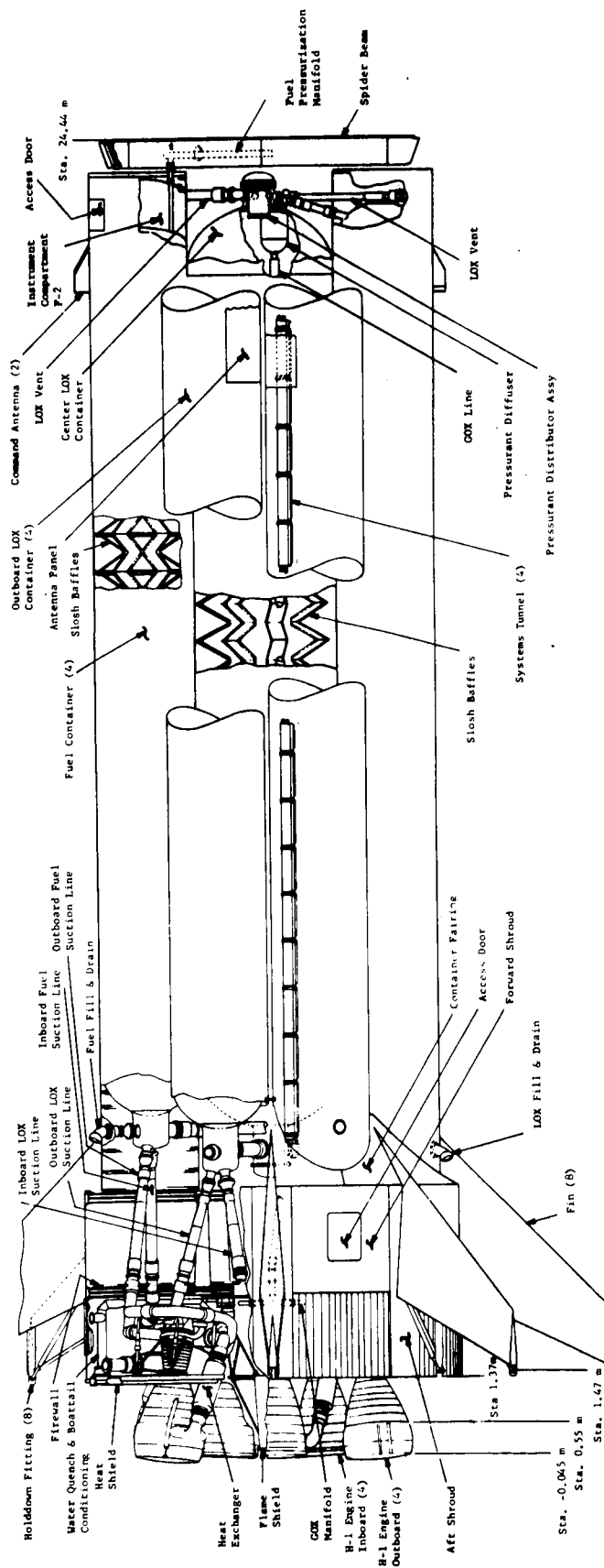


FIGURE A-2 S-IB STAGE

capacity was 400,976 kg (884,000 lbm).

Four 163,339 N (36,720 lbf) thrust solid propellant retro motors, mounted circumferentially on the S-IVB aft interstage (canted at 9.5 deg), decelerated the S-IB stage and S-IVB aft interstage to accomplish separation from the S-IVB stage. Eight fins were attached to the base of the S-IB stage to provide vehicle support and holddown points prior to launch and to provide inflight stability. Each fin projected an area of approximately 4.95 m² (53.3 ft²) and extended radially about 2.74 m (9 ft) from the outer surface of the thrust structure.

Additional systems on the S-IB stage included: (a) the flight control system; (b) the hydraulic system, which gimballed the outboard engines; (c) the electrical system, which distributed and controlled the stage electrical power; (d) the environmental control system, which thermally conditioned the aft compartment of instrument canisters F1 and F2; (e) the data acquisition system, which acquired and transmitted data for the evaluation of stage performance and environment; and (f) a secure range safety system. Guidance and control commands were received from the Instrument Unit.

A.2.2 S-IB-4 CONFIGURATION DIFFERENCES

The significant configuration differences between S-IB-4 and S-IB-2 existed in the structure, the control pressure system, the flight control system, the retrorocket system, the H-1 engine system, and the electrical system. The configuration differences listed below are the modifications to S-IB-2 that were incorporated on S-IB-4.

1. Structure

Tail Section - The metal thickness of sheet metal and machined elements in the tail section was reduced. The heat shield brazed honeycomb was redesigned and the turbine exhaust was rerouted. Rerouting the exhaust ducts along the thrust chamber instead of through the stub fins resulted in the following: (a) permitted removal of four turbine exhaust fairings (stub fins) from the exterior of the lower shroud, (b) dictated reorientation of the heat shield support structure, (c) entailed the redesign of the inboard honeycomb heat shield panels and inboard engine flame curtains, and (d) entailed redesign of the flame shield and its support structure. These changes were also incorporated on S-IB-3.

Drag-In Cable Door - The door was incorporated into the S-IB/S-IVB interstage to precluded routing the ground cabling through the access door. This eliminated a hazardous condition for personnel.

The door was located at station 28.2 m (1108 in), 27 deg from Position III towards Position IV.

2. Control Pressure System

One of the two fiberglass GN₂ spheres was removed, which decreased the system volume from 0.0566 m³ (2 ft³) to 0.0283 m³ (1 ft³). This was due to the reduction in instrumentation purge requirements resulting from the elimination of the mass spectrometer.

3. Flight Control System

Potentiometer - The printed circuit in the potentiometer of the servo actuator was replaced with standard insulated wire. This action minimized the likelihood of electrical opens in the solder joint and of cracking and corrosion in the printed circuit cable noted on earlier vehicles. The second change in the flight control system was the painting of the actuators to reduce the probability of a stress corrosion failure.

4. Retrorocket System

Retrorockets - The retrorockets were moved 16.5 cm (6.5 in) outboard to reduce the plume impingement on the interstage and to prevent possible collision of the J-2 engine bell and the aft interstage during separation in the event one retrorocket should fail to ignite. Relocation of the retrorockets resulted in redesign of the nose fairing, the aft fairing, and the forward and aft support fittings. A 16.5 cm (6 1/2 in) beam was designed to transmit the load from the support to the interstage. The expansion ratio of the rocket nozzles was increased from 4.26:1 to 7.03:1. This configuration was also incorporated on S-IB-3. Additional changes, not made on S-IB-3, included the following: To prevent case burn-through, insulation was added and inhibitor coating applied after final trim to the nozzle end. Sealant was used to fill the space between nozzle adapter and grain. Reliability of the retrorocket firing units was increased.

5. H-1 Engine System

Aspirator Shells - The shells were shortened by decreasing the extension past the chamber into the exhaust stream by 5.72 cm (2.25 in). This change eliminated an undesirable buckling condition in the lower portion of the aspirator.

LOX Seal - A redesigned turbopump LOX seal was incorporated. This change was also made on S-IB-3.

6. Electrical System

H-1 Electrical Harnesses - Premature ignition sensing and Conax position indicator electrical harnesses were incorporated into the engine system. This system permitted automatic engine shutdown in the event of a premature ignition of the Solid Propellant Gas Generator (SPGG) through the use of the gas generator igniter link break device. Also, if a Conax valve had fired prior to ignition command, the Conax position would have signaled launch abort. PR 905 potting and metal sleeves were incorporated in the connectors of the start and flight electrical harnesses. The potting-sleeve modification was also made on S-IB-3.

Measuring Racks - Eight measuring racks were deleted.

Camera System - The recoverable camera system and its associated circuitry were deleted.

Cutoff Circuits - The engine cutoff circuits were modified to require TOPS Switch deactivation prior to preclude closure command.

Vent Systems - The circuits for the LOX and fuel vent system were modified to accommodate the mechanical alterations to the vent systems.

Separation Systems - Redundant electrical circuits were added.

Switch Selector Power - Redundant electrical circuits were added.

Range Safety System - Provisions for the alternate range safety system (DRW-13) were deleted. Liftoff relay contacts were removed from the range safety engine cutoff circuitry to provide assurance that the range safety controller engine cutoff relay contacts were in an unenergized state prior to ignition.

A.3 S-IVB STAGE

A.3.1 S-IVB CONFIGURATION

The S-IVB stage (Figure A-3) had nominal dimensions of 18.0 m (59 ft) in length and 6.60 m (260 in) in diameter. A single gimbal-mounted J-2 engine powered the vehicle during the S-IVB stage portion of powered flight. The engine was mounted on the thrust structure and gimballed in a ± 7 deg square pattern. The engine provided 890,000 N (200,000 lbf) total thrust at vacuum conditions when the propellant mixture ratio (MR) was a nominal 5 to 1. At nominal MR, the PU valve was in the null position.

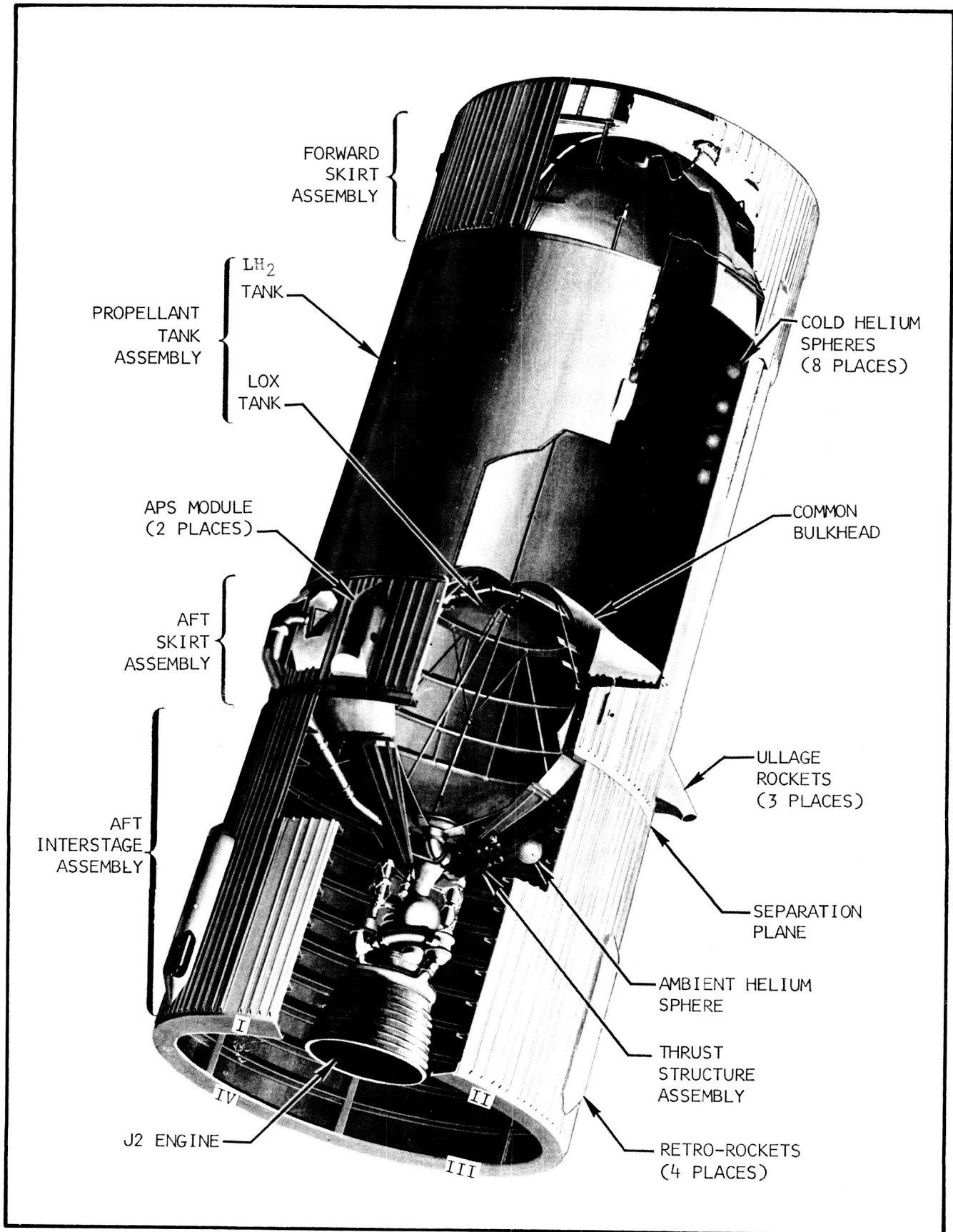


FIGURE A-3 S-IVB STAGE

The thrust structure provided engine thrust transfer to the LH₂ (fuel) and LOX (oxidizer) containers. The tanks, LH₂ forward and LOX aft, were separated by a common bulkhead. The LH₂ system consisted of a cylindrical container with a bulkhead at each end. The LOX system consisted of the common bulkhead connected to another bulkhead.

LOX and LH₂ tank pressurization modules regulated tank pressures during ground operations, S-IB boost phase, and S-IVB burn phase. The pneumatic control system used ambient helium to operate various valves for such purposes as vent relief, fill, and drain. The propellant utilization system consisted of a LOX mass sensor, a LH₂ mass sensor, electronics assembly, and a valve positioner. The system controlled the propellant mixture ratio into the J-2 engine to optimize consumption. Nominal propellant loading capacity was 103,646 kg (228,500 lbm).

A skirt assembly was attached to the aft end of the cylindrical portion of the propellant container. The S-IVB aft interstage and fairing was connected to the aft skirt assembly. Another skirt assembly was attached to the forward end of the cylindrical portion of the propellant container to support the Instrument Unit and Payload.

Three 15,124 N (3,400 lbf) thrust solid propellant ullage motors, mounted circumferentially on the S-IVB aft skirt (canted outwards at 35 deg), accelerated the S-IVB stage to provide proper positioning of the propellants prior to S-IVB stage ignition.

Roll control of the S-IVB stage was provided by two Auxiliary Propulsion System (APS) modules during S-IVB powered flight. The attitude was controlled to within ± 5 degrees. The APS provided attitude stabilization and reorientation after burnout, and attitude control during coast or maneuvering. The APS modules were mounted on opposite sides of the S-IVB aft skirt at Positions I and III. Each module was a self-contained unit composed of four basic systems: The oxidizer system, fuel system, helium pressurization system, and three 667N (150 lbf) thrust engines. Each APS module was a positive expulsion system with the hypergolic propellants contained in separate metal bellows, which, in turn, were contained in helium-pressurized ullage tanks. A high pressure helium sphere contained in the module supplied helium to the ullage tanks at regulated pressure. This pressure was exerted on the bellows to pressurize the propellants. Monomethyl-hydrazine (MMH) and nitrogen tetroxide (N₂O₄) were used as fuel and oxidizer, respectively. Each module contained two motors to provide roll control during S-IVB powered flight, and yaw and roll control after S-IVB engine cutoff. A third motor in each module was oriented perpendicularly to the S-IVB longitudinal axis to provide pitch control.

Additional systems on S-IVB stage included: (a) the flight control system, which included an auxiliary attitude control subsystem and a thrust vector control subsystem; (b) the hydraulic system which gimballed the J-2 engine; (c) the electrical system which distributed and controlled the stage electrical power; (d) the thermoconditioning system, which thermally conditioned the electrical/electronic modules in the forward skirt area; (e) the data acquisition and telemetry system, which acquired and transmitted data for the evaluation of stage performance and environment; and (f) a set of ordnance systems used for rocket ignition, stage separations, ullage rocket jettison, and range safety. Guidance and control commands were received from the Instrument Unit.

A.3.2 S-IVB-204 CONFIGURATION DIFFERENCES

The significant configuration differences between S-IVB-204 and S-IVB-202 existed in the structure, J-2 engine system, propellant system, tank vent/pressurization system, pneumatic control system, hydraulic system, APS, electrical system, EDS, and range safety system. The configuration differences listed below are the modifications to S-IVB-202 that were incorporated on S-IVB-204.

1. Structure

Insulation - External insulation of the same type used on S-IVB-203 was added to the stage for compatibility with the maximum aerodynamic heating associated with the AS-204/LM-1 trajectory.

Forward Skirt Vent - The vent area was reduced from 1290 to 645 cm² (200 to 150 in²) by decreasing each of the 8 vent areas equally. The same length-to-width ratio was maintained.

Auxiliary Tunnel Cover - Stiffeners and stringer formers were added to the tunnel cover, because of increased aerodynamic loads resulting from a change in the trajectory. This modification was also incorporated on S-IVB-203.

Aft Skirt - The stringers, tank-to-skirt joints, and skirt-to-interstage joints were redesigned to carry 20 percent increased loads.

LH₂ Tank - The skin thickness of the LH₂ tank was reduced because the LH₂ Tank ullage pressure limit was lowered from 28.9 to 26.8 N/cm² (42 to 39 psi).

2. J-2 Engine System

LOX Pump Seal Drain - An overboard drain line from the J-2

engine LOX pump seal cavity was added as a result of the S-IVB-501 flight. Venting into the closed interstage was thus precluded.

Start Tank - Tap-offs were added at the injector manifold and at the main fuel manifold to ensure repressurization of the start tank.

Oxidizer Turbine Valve (OTV) - A dual actuated OTV was added to give more positive valve opening.

Oxidizer Turbine Wheels - The first and second stage oxidizer turbine wheels were shot-peened for increased fatigue strength.

Engine Pneumatic Control System - A filter was added to preclude the entrance of helium accumulator contaminants into the control system.

Thrust Chamber Injector - A retaining lip was added to prevent O-ring unseating.

Engine strength - The thrust chamber struts were relocated and redesigned. Increased torsional rigidity was incorporated into the gimbal alignment plate. The gas generator control valve housing was stiffened to reduce deflections and vibrations. The 622,000 N (140,000 lbf) helium tank cover mounting bolts were replaced with 890,000 N (200,000 lbf) bolts to eliminate cover plate deflection at maximum relief valve pressure.

Purge Check Valves - The fuel jacket purge check valve and oxidizer dome purge check valve were hard anodized to prevent fretting.

Heat Exchanger Oxidizer Inlet Port - The inlet port adapter was redesigned to improve sealing.

ASI Fuel Line - The augmented spark igniter (ASI) fuel line was rerouted to eliminate interference with the restrainer.

3. Propellant System

PU System - The forward and feedback shaping networks were changed to optimize PU performance. The Reference Mixture Ratio was adjusted to 4.70:1.

LH₂ Feed Ducts - The aluminum burst discs were reworked with chromate primer to prevent corrosion. The bellows clearance was X-rayed. A locking device was added to the cover of the vacuum seal-off valve to prevent valve unseating during vibration.

LOX Chilledown Pump - The LOX auxiliary motor-driven chilledown pump was redesigned to improve the LOX shaft seal spring and to provide higher shaft nut torque.

Chilledown Valves - The LH₂ and LOX chilledown shutoff valves were redesigned to incorporate a new microswitch actuator spring for the open position indication switch. This enabled the bellows shaft to actuate the switch during critical component cycling. A silicone seal was used to preclude cryopumping of moisture into the switch housing.

LH₂ Chilledown Supply Duct - A bonded doubler was added to the chill system supply duct in the area of the seal-off valve in order to distribute the load over a larger area. The aluminum blowout discs were coated with zinc chromate primer to prevent galvanic corrosion.

Fuel Depletion Sensors - The point-level sensors were scheduled not to be activated unless a velocity cutoff did not occur, since it was determined that fuel depletion would not occur.

Fill and Drain Valves - The LH₂ and LOX fill and drain valves were redesigned. This modified the bearing, shaft, seals, and rack and pinion gear, which eliminated sluggish operation, piston binding, and leakage.

Fill and Drain Disconnects - The LH₂ and LOX disconnects were modified with new seals to correct the leakage problem reported on the first three flights.

4. Tank Vent/Pressurization System

LH₂ Vent System - An orbital vent initiation pressure switch was added to the LH₂ vent system in order to control orbital venting.

Tank Relief Valve - The LH₂ and LOX tank relief valves incorporated a redesign of the controller as follows: reduced clearance at the OD of the Belleville retainers, polished and lubricated retainer and bore of the controller to provide crack and reseal repeatability, adjustable controller bias spring for valve adjustment, partially helium back-filled controller aneroid, longer main poppet return spring, improved friction button material, and revised crack and reseal parameters. Other changes to the relief valve included replacement of aluminum spring spacers with beryllium-copper, replacement of aluminum adjusting nut with beryllium-copper and longer thread engagement, provision of closer assembly control, and addition of two more holes in the main valve chamber to improve pilot operation.

LH₂ Pressure Switch - The 19.3 to 21.4 N/cm² (28 to 31 psi)

pressure switch was removed and was replaced by the 21.4 to 23.4 N/cm² (31 to 34 psi) switch. The undercontrol or center orifice was resized to provide steady state or asymptotic ullage pressure of 21.4 N/cm² (31 psi).

Helium Fill Module - The redesigned module configuration deleted the relief valve, consequently increasing system reliability. The relief function was provided by the GSE supply.

Cold Helium Dump Module - The check valve in the top of the relief valve housing and the Belleville springs in the relief valve were redesigned. The main poppet seat material was changed from Mylar to Vespel.

LOX Tank Pressurization Control Module - Vespel poppet seats replaced the Mylar seats. A check valve was added in the regulator vent port to preclude the possible entrance of moisture, which in turn could affect the Belleville springs.

Cold Gas Check Valves - The two valves in the LOX pressurization systems featured an improved seal design to reduce internal and external leakage.

LOX Vent Angle - The angle was set at 31 degrees 33 minutes for AS-204. This angle optimized APS propellant usage during the propellant dump experiment.

5. Pneumatic Control System

Ambient Helium Sphere - The 0.127 m³ (4.5 ft³) sphere replaced the 0.0149 m³ (0.525 ft³) sphere to provide pressurization for propellant venting exercises in orbit. The weld integrity of the sphere was verified by Eddy current testing.

Power Control Module - The module was redesigned to provide dimensional control of regulator poppet and seat assembly lapped fit. Improved valve seat materials and O-rings were added. The vent valve solenoid was hermetically sealed. These changes corrected the low temperature leakage problem and provided new lubrication requirements.

Actuation Control Module - The module redesign provided vibration stops that prevented O-ring damage. A check valve was added to the vent port of the module to preclude the possibility of freezing the shutoff valve. Solenoid electromagnetic suppression was provided. Thermal isolation of the module was added to prevent a low temperature leakage problem.

6. Hydraulic System

Auxiliary Pump - This pump incorporated improved fluoro-silicone O-rings in the relief valve seat lock.

Actuators - The yaw actuator incorporated a strengthened tail stock forging, and the pitch actuator was checked with dye penetrant for cracks.

Main Pump - The pump compensator mounting bolts were changed to be compatible with the torque change from 5.4 to 7.9 N-m (48 to 70 lbf-in). The pump-discharge check-valve was redesigned to meet burst test strength requirements.

Accumulator-Reservoir - The MC-type ports were eliminated and improved low-pressure relief valves were installed. This configuration was also incorporated on S-IVB-203.

7. Auxiliary Propulsion System (APS)

Helium Pressure Regulator - The S-IVB-204 regulator (Apollo design) incorporated new Sealol bellows, positive plunger action, addition of a 0.119 cm (0.047 in) diameter orifice, and removal of the test port line. The crossover pressure switch was eliminated, resulting in a reduction of the electrical wiring harness requirements.

8. Electrical System

Childdown Inverter - A new configuration childdown inverter was used to eliminate possible improper engine-start conditions. A current limiting circuit and passive thermal conditioning have been added as a result of the qualification program.

Spare Depletion Sensor - Hardwire circuits were added to monitor the condition (wet or dry) of the spare LOX and LH₂ tank depletion sensors while the vehicle was on the pad. Considerable time savings would have resulted in the event that a sensor had failed that was intended to be active during flight. Sensors became interchangeable, merely by changing one connection.

Depletion Sensor Time Delay Modules - A time delay network was incorporated to delay the LOX depletion cutoff command and to utilize LOX residuals at burnout. The LH₂ depletion sensor time delay module was removed to prevent loss of fuel NPSP just prior to cutoff.

Automatic Passivation Electrical Kits - Kits were installed to passivate: the ambient helium sphere via the ambient helium dump

(helium dump valve rewired); the cold helium spheres and LOX tank via the LOX main engine valve (mainstage control solenoid rewired to permit independent LOX valve opening); the fuel tank via LH₂ main engine valve (ignition phase control solenoid rewired to permit independent LH₂ valve opening).

2 and 10 Amp Relays - The relays were modified as a result of failure during the low-temperature acceptance test.

Static Inverter Heat Sink - Mylar insulation was applied to the surface of the transistor relief holes in the heat-sink mounting plate, and insulation sleeves were installed with the transistors. This change eliminated the unpredictable heat-sink to mounting-plate shorting problem.

Sequencer and Aft Power Distribution Assemblies - Insulating washers were added to the mounting hardware of the diode modules located in these assemblies. Shorting of a diode to ground, as occurred on S-IVB-501, was thereby eliminated.

9. Emergency Detection System (EDS)

System Redundancy - The EDS was modified to ensure a completely redundant system, electrically and mechanically. The redundant circuits that were going through the same connectors and diode modules were changed to go through separate connectors and diode modules in the sequencer.

10. Range Safety System

Safe and Arming (S&A) Device - Vent ports with a debris shield were added to the S&A body. The ports prevented impingement of hot gasses on the propellant-dispersion-system explosive-fuse train in the event that an exploding bridgewire detonator was inadvertently initiated. The debris shield would have captured any fragments from the vent ports if the detonators had fired.

EBW Wiring Support - The exploding bridgewire (EBW) wiring support was reworked to eliminate that portion of the support that could possibly have caused chafing of the EBW cable.

A.4 INSTRUMENT UNIT

A.4.1 IU CONFIGURATION

The Instrument Unit (IU) was located just forward of the S-IVB stage. It was a three segment, cylindrical, unpressurized structure

having a diameter of 6.60 m (260 in) and a length of 0.91 m (36 in). The cylinder formed a part of the vehicle load-bearing structure and interfaced with the S-IVB stage and payload. Figure A-4 shows the Instrument Unit layout and antenna orientation. Figure A-5 shows the components located in each of the three segments.

The IU housed electrical and mechanical equipment that guided, controlled, and monitored vehicle performance from liftoff to atmospheric re-entry.

A.4.2 S-IU-204 CONFIGURATION DIFFERENCES

The significant configuration differences between S-IU-204 and S-IU-202 existed in the structure, the guidance system, the flight control system, the thermal conditioning system, and the gas bearing supply system. The configuration differences listed below are the modifications to S-IU-202 that were incorporated on S-IU-204.

1. Structure

ST-124M Mounting Frame - Several changes were made to the mounting frame to obtain additional clearance between the platform and the mounting frame. Thermal isolation pads were added to the mounting frame.

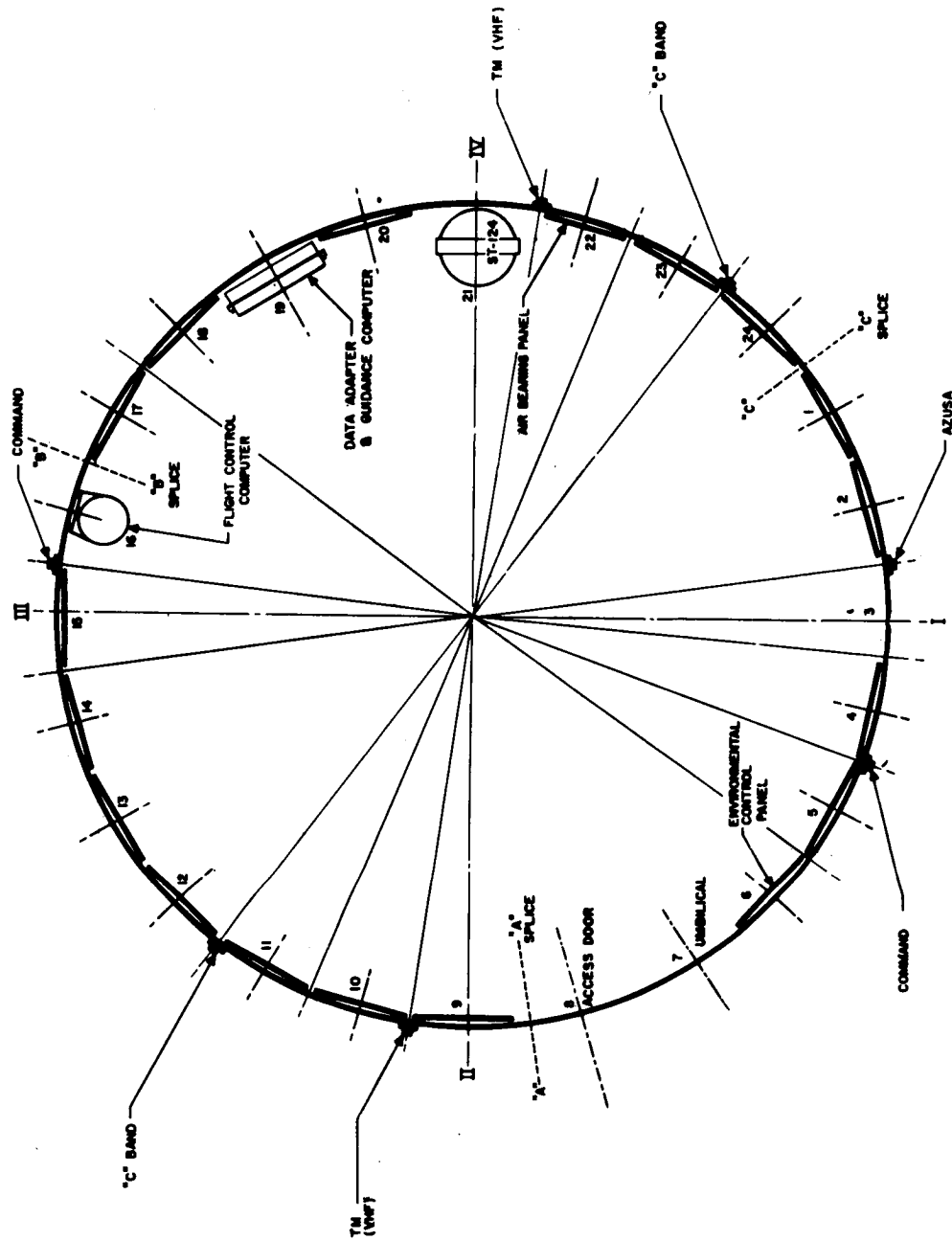
LVDC/LVDA Support System - Vibration-damping compound was added to the Launch Vehicle Digital Computer/Launch Vehicle Digital Adapter (LVDC/LVDA) Support System. This provided damping of localized resonances in the bracket assembly.

Segment Assembly - Shims under the hinge mechanism of the umbilical door were removed to facilitate closing the door. The core material density, under the flight control computer mounting pads, was changed to 131.2 kg/m^3 (8.1 lbm/ft^3).

2. Guidance System

LVDC - Two memory modules were added to the Launch Vehicle Digital Computer (LVDC), making a total of six. A functional change to the LVDC permitted checking the operation of the duplex memory redundancy while the equipment was installed in the IU. These changes were also incorporated on S-IU-203.

LVDA - Functional changes were made to the LVDA to increase the reliability of the discrete output circuits and the switch selector output signals. The teflon hose joining the logic sections was replaced with a stainless steel tube to prevent degradation of resistors in



AFT LOOKING FORWARD

FIGURE A-4 INSTRUMENT UNIT LAYOUT AND ANTENNA ORIENTATION

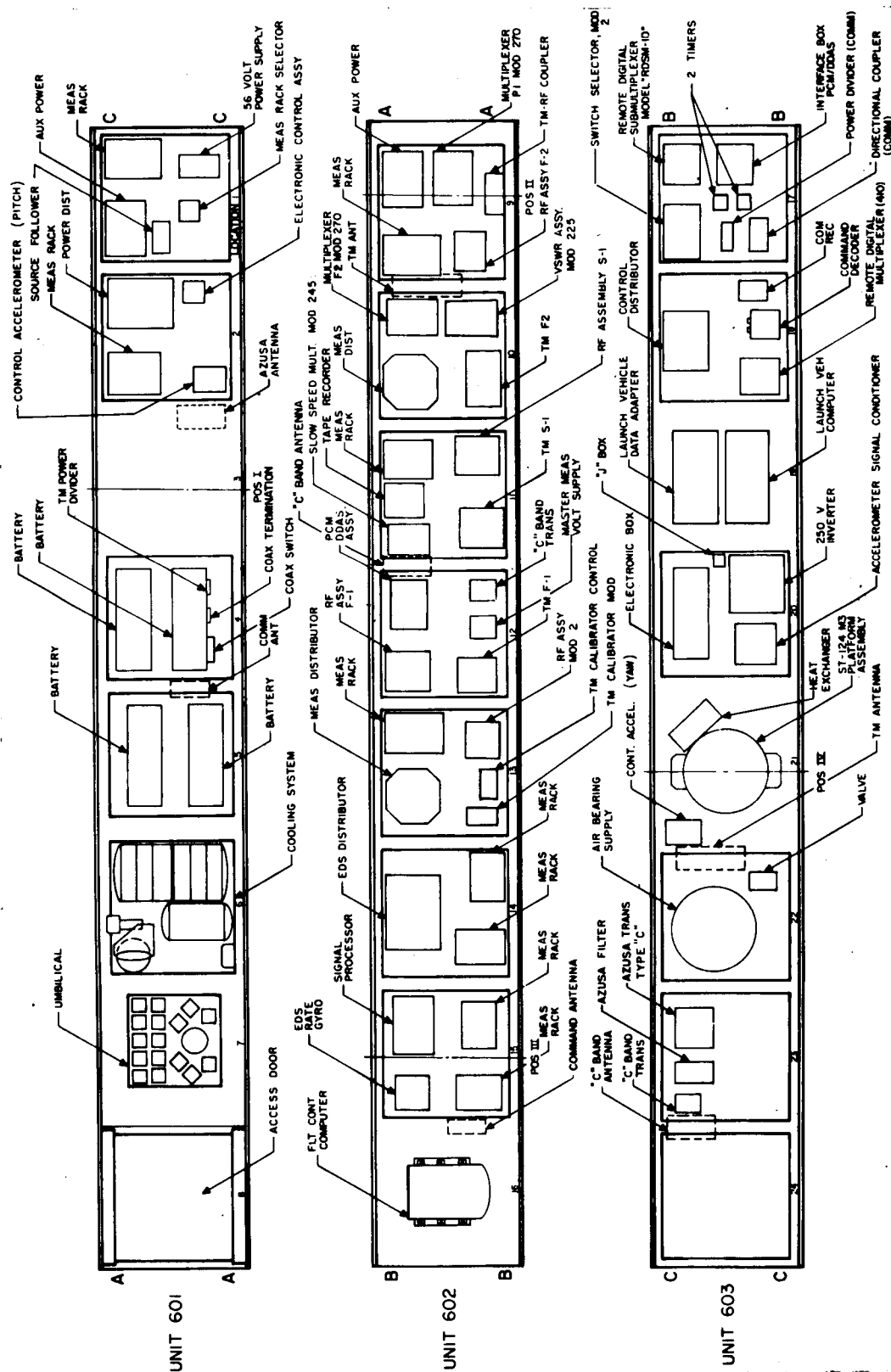


FIGURE A-5 INSTRUMENT UNIT COMPONENTS LAYOUT

some LVDA units. Only the functional changes to the LVDA were flown on S-IU-203.

ST-124M Stabilized Platform System

(a) Delay Module - The module was added to the Platform AC Power Supply (PACPS) to provide a voltage value ramp-up for the gyro and accelerometer spin motors. Control of the delay module was contained in the Platform Electronics Assembly (PEA). The PEA control circuitry was changed by the addition of a relay and time delay R-C network on the relay coil. This modification caused the voltage to start at 8 vac and rise linearly to 26.5v after three minutes. Previous operation applied 26.5 vac directly to the spin motors for their run-up to synchronous speed. This change minimized the thermal shock in the gyro and accelerometer motors during their run-up time by reducing the rate of change of the applied energy.

(b) Lock-Out Capability - Lock-out capability of the voltage ramp after switchover to battery power was provided. To avoid the possibility of a low voltage transient triggering the ramping operation of the PACPS in flight, the control power for the ramping function was isolated from battery power.

(c) Gyro Motors - Elkonite gyro motors were substituted for the Monel motors. The improved thermal characteristics of the Elkonite motor reduced the variation of unbalance and mass shift errors in the gyro assembly.

(d) Accelerometer Mirrors - A bead of adhesive was added around the mirrors in the optical encoder subassembly of the accelerometers because several mirrors had come loose from their mounts at the vendor's plant.

3. Flight Control System

Flight Control Computer (FCC)

(a) Redundant Inverters - Inverter redundancy was added to excite the first stage servo amplifiers. This improved the reliability of the FCC during first stage powered flight.

(b) Servo Amplifiers - Simulate windings in the 12 ma and 50 ma servo amplifiers were not utilized. These windings served no useful purpose and were creating an undesirable effect during assembled vehicle tests.

4. Thermal Conditioning System (TCS)

First Stage Regulator - The relief valve in this regulator was redesigned to ensure that overpressurization of the system would not occur because of the valve failing in the full-open position. The tolerance band of the relief valve was tightened to prevent a thin wall section which would be vulnerable to shear failure. In addition, the regulator body was modified to allow usage of a new mounting bracket design. This modification eliminated the vibration damping problem cited in the AS-203 Preflight Readiness Review.

Methanol/Water Accumulator - This accumulator was redesigned to incorporate a bladder with an O-ring, and an O-ring/groove in the flange to prevent bladder extrusion.

Preflight Heat Exchanger - The unit was redesigned to prevent crushing of the inlet and outlet fittings during installation. This modification was also made on S-IU-203.

Sublimator - The unit was modified to vent inside the IU, to eliminate any possible thrust contribution in orbit. This modification was also made on S-IU-203.

TCS Temperature Control (AS-204 Experiment) - The TCS was modified to provide orbital temperature control (programmed to initiate at 4322 sec) by controlling the supply of water to the sublimator.

Thermal Control Surfaces - These surfaces were covered with low emissivity tape due to excessive radiation heat losses experienced on S-IU-203.

Air/GN₂ Purge Duct - Modifications were made to the Air/GN₂ purge duct by adding eight 2.54 cm (1 in) holes to the "Y" segment of the purge duct, and one 5.08 cm (2 in) diameter orifice with a deflector to each end cap. This modification was made to increase the flow into the IU due to a GSE deficiency.

5. Gas Bearing Supply System

Low Pressure Switch - The low pressure switch incorporated provisions for a calip switch. The switch deactuated at a lower point and operated on a narrower actuate/deactuate band.

GN₂ Solenoid Valve - This valve was redesigned from a lubricated to a non-lubricated poppet actuation to ensure against contamination of the GN₂ supply.

Gas Bearing Regulator - A filter was added as an integral part of the unit, because of the unit's sensitivity to contamination.

Gas Bearing Heat Exchanger - The unit was relocated closer to the ST-124M in an attempt to provide the required temperature control throughout the entire mission. This change was made on S-IU-203.

A.5 PAYLOAD

The overall length of the Payload was 12.0 m (471 in). The maximum diameter was 6.6 m (260 in) at the IU/SLA interface. Figure A-6 shows the Lunar Module (LM), the Spacecraft LM Adapter (SLA), and the Nose Cone. The LM was the major component of the payload and was enclosed in the SLA. A Nose Cone was mounted on top of the SLA to provide an aerodynamic closure.

A.5.1 LUNAR MODULE (LM)

The LM was a two-stage vehicle having an overall height of 6.98 m (22.9 ft) from the top of the rendezvous radar antenna to the bottom of the landing gear, when extended. The overall diameter of the LM, from extended landing gear to extended landing gear, was 9.06 m (29.7 ft). However, landing gear was not included in the AS-204 LM (Figure A-6). The diameter at station 45.7 m (1780 in), where the LM is attached to the SLA, was 449 cm (232 in). The main body of the ascent stage was about 284 cm (111.5 in) high and 304 cm (120 in) wide (along one side). It housed the ascent engine, the reaction control engines, the cockpit for two astronauts, the docking tunnel, and a major portion of the electronics and communications equipment. The main body of the descent stage was about 267 cm (105 in) high and was 422 cm (166 in) wide (along one side). It housed the descent engine, descent control instrumentation, and scientific equipment not needed for the return trip from the moon.

The descent stage was powered by a 46,704 N (10,500 lbf), maximum thrust, gimbal-mounted rocket engine. The engine could be operated at 100% thrust or throttled between 10 and 92.5 percent to permit velocity control. The engine could be gimballed in a ± 6 deg square pattern to provide thrust vector trim control. The descent engine provided braking and hovering capability that would permit lateral movement to a suitable landing area on a lunar mission.

The ascent engine was designed to operate for powered ascent and insertion into an ascent transfer orbit. The engine position was fixed and developed a constant thrust of 15,568 N (3,500 lbf), and could be restarted as required. The ascent propellant supply section could also serve as a backup propellant source for the Reaction Control

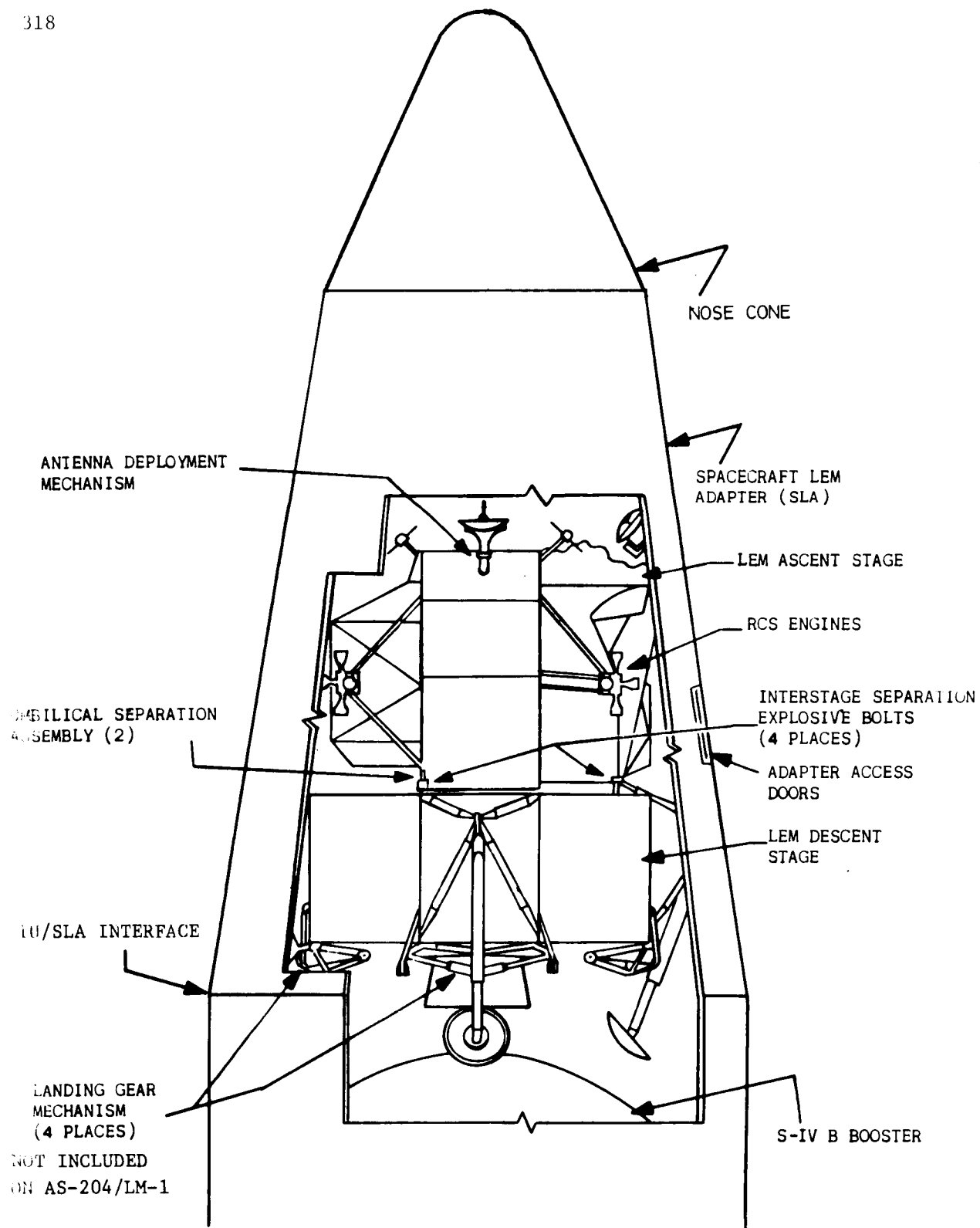


FIGURE A-6 AS-204 PAYLOAD

System (RCS), but would have provided forward acceleration only.

Control during ascent engine firing was made possible by the RCS system engines consisting of 4 clusters with 4 chambers per cluster. Each cluster was mounted 90 deg apart and each chamber developed 427 N (96 lbf) thrust. The RCS was composed of two independent and separate systems. Normally, both systems operate together but the thrust chamber arrangement is such that adequate control in all axes is possible with a failure of one system.

The two main LM engines used pressure-fed liquid propellants. The propellants consisted of unsymmetrical dimethyl hydrazine/hydrazine (UDMH/ N_2H_4) as the fuel and nitrogen tetroxide (N_2O_4) as the oxidizer. The mixture ratio in both engines was 1.6 to 1.0 by weight. Helium was used in both stages as the tank pressurant for the propellants.

The Apollo 5/AS-204/LM-1 mission required the LM to operate in earth orbit for system/subsystem developmental testing. The LM Mission Programmer (LMP) and the Developmental Flight Instrumentation (DFI) were added to accomplish crew switching functions and to obtain system/subsystem qualification data. The (LMP) was an onboard programmer with partial ground command capability and was used to provide control functions normally accomplished by the flight crew. The LMP consists of the Program Reader Assembly (PRA), Digital Command Assembly (DCA), Program Coupler Assembly (PCA), Power Distribution Assembly (PDA), and interfaced with the LM Guidance Computer (LGC) for sequential inputs.

The Development Flight Instrumentation (DFI) supplied the data to be used in conjunction with operational data for flight qualification of LM systems/subsystems. The DFI consisted of sensors, signal conditioning electronics, modulation packages, VHF transmitters, and C-Band beacons.

Five VHF telemetry transmitters, radiating through two similar antennas, were used to telemeter operational and DFI data to the MSFN. Three of these transmitters transmit PAM/FM/FM data, one FM/FM data, and one PCM/FM data. Two C-Band beacons, with associated antennas, were installed to permit ground tracking of earth orbital missions.

Systems in the LM, not discussed in detail, included the guidance and navigation system, stabilization and control system, radar system, environmental control system, electrical power system, communication system, instrumentation system, structural system, control-display panels, crew provisions, and scientific instrumentation.

A.5.2 SPACECRAFT LUNAR MODULE ADAPTER (SLA)

The SLA was a simple truncated cone 853 cm (336 in) long, having forward and aft diameters of 391 cm (154 in) and 660 cm (260 in), respectively. The adapter aerodynamic fairing provided the mating requirements for the Nose Cone and Instrument Unit. It also housed the LM/SLA Spacecraft Jettison Controller (SJC) and power supply.

The SLA is divided into two sets of four panels. The aft set is fixed and the forward set is deployable. The panels consisted of 4.3 cm (1.7 in) aluminum-alloy honeycomb, bonded to face sheets of aluminum.

The SLA panels were deployed by programmed command from the IU Switch Selector (or by backup mode) via the SJC logic. The SLA panels deployed 45 deg as a result of momentum from three elements: (1) the explosive devices that shear the panels from one another at the seam lines, (2) eight mechanical thrusters located at the corners of the panels, and (3) four cable spring-loaded exterior pulley assemblies (one pair per panel).

The momentum of the SLA panels was stopped by eight attenuator struts located between the aft panel and forward panels. These contain crushable aluminum honeycomb core to absorb energy. After the panels reach the deployed position, they are retained in that position by a clutch on each spring-loaded pulley assembly.

A.5.3 NOSE CONE

The Nose Cone consisted of a 25 deg semimonocoque cone-shaped structure that provided an aerodynamic closure for the top of the SLA. The overall length of the Nose Cone was 343 cm (135 in) and the base diameter was 391 cm (154 in). The Nose Cone was constructed with ring frames and skin stringers.

Separation of the nose cone was accomplished by utilizing 16 springs positioned symmetrical around the base of the nose cone and the forward SLA panels. The metallic interface between the nose cone and the SLA was sheared by a mild detonating fuse (MDF) which was ignited by two detonators 180 deg apart upon receipt of the programmed command from the IU switch selector or by backup ground command, via the SJC logic.

APPENDIX B

ATMOSPHERIC SUMMARY

B.1 INTRODUCTION

This appendix presents a summary of the atmospheric environment at time of the launch of AS-204. The format of the data is similar to that presented in launches of the Saturn I vehicles to allow comparisons to be made. Surface and upper air winds and thermodynamic data near the launch time are given.

B.2 GENERAL ATMOSPHERIC CONDITIONS AT LAUNCH TIME

There was a weak high pressure system over the southeastern United States. Surface wind flow over the Cape Kennedy area was from the north and of low magnitude. Above 5 km, the wind flow was from the west.

B.3 SURFACE OBSERVATIONS AT LAUNCH TIME

At launch time, there were high scattered clouds, heights unknown. Visibility was greater than 16 km (10 mi). Table B-I summarizes the surface observations at launch time.

Solar radiation data values measured by total horizontal and normal incident sensors were equal to the maximum design values expected in January. Likewise, the diffuse radiation values were low, indicating extremely clear air at the time of launch. These data are presented in Table B-II.

B.4 UPPER AIR MEASUREMENTS

Upper air wind data were measured with three of the four systems requested. Since the T + 6 hr Arcasonde rocket sounding gave data to a higher altitude than the T + 90 min Arcasonde, the additional data was used to extend the T + 90 min sounding. Data from the FPS/16 Jimsphere, rawinsonde, and both Arcasondes (T + 90 min and T + 6 hr) were used to compute the final meteorological tape. The triple theodolite data were not received. Table B-III summarizes the data used.

Wind Speed

There was an increase of wind speed with altitude from 2 m/s (3.9 knots) at the surface to a maximum of 35 m/s (68.0 knots) at 12 km

TABLE B-I SURFACE OBSERVATIONS AT AS-204 LAUNCH TIME

LOCATION	TIME AFTER T-O (MIN)	PRESSURE N/CM ² (PSIA)	TEMP- ERATURE °K (°F)	REL. HUM. (%)	VISI- BILITY KM (STA. MI)	SKY COVER			WIND	
						AMOUNT (TENTHS)	TYPE	HEIGHT OF BASE	SPEED M/S (KNOTS)	DIR. (DEG)
Kennedy Space Center	0	10.186 (14.77)	289.26 (61)	93	16 (10)	<3	-	-	1.0 (2.0)	070
Cape Kennedy Rawinsonde Measurements	10	10.180 (14.76)	288.71 (60)	90	-	-	-	-	1.0 (2.0)	070
Pad 39B Light Pole E (20.4 m)	0	-	-	-	-	-	-	-	4.2 (8.0)	045
Pad 39B Service Structure Top (112.5 m)									3.1 (6.0)	060

TABLE B-II SOLAR RADIATION (0.35 to 4.0 microns) AT AS-204 LAUNCH TIME

Hour Ending EST	Total Horizontal Surface gm cal/cm ² min	Normal Incident gm cal/cm ² min	Diffuse (Sky) gm cal/cm ² min
0800	0.06	0.26	0.05
0900	0.38	1.25	0.08
1000	0.91	1.61	0.19
1100	1.25	1.78	0.23
1200	1.50	1.83	0.29
1300	1.60	1.85	0.23
1400	1.54	1.86	0.21
1500	1.32	1.82	0.28
1600	0.99	1.64	0.25
1700	0.54	1.25	0.24
1800	0.12	0.44	0.10

The values shown are average intensity for the hour at Pad 37B, for January 22, 1968.

To obtain watt/m², multiply by 697.33

To obtain B.T.U./ft²hr, multiply by 221.20

TABLE B-III SYSTEMS USED TO MEASURE UPPER AIR WIND DATA, AS-204

TYPE OF DATA	RELEASE TIME JAN. 23, 1968		PORTION OF DATA USED			
	TIME (UT)	TIME AFTER T-0 (MIN)	START		END	
			ALTITUDE M (FT)	TIME AFTER T-0 (MIN)	ALTITUDE M (FT)	TIME AFTER T-0 (MIN)
FPS-16 Jimsphere	2303	15	Surface	15	16,750 (55,000)	72
Rawinsonde	2307	19	17,000 (55,800)	75	32,500 (106,600)	126
Arcasonde(T+90min)	0018 Jan 24	90	55,750 (183,000)	117	32,750 (107,400)	90
Arcasonde(T+6 hr)	0448 Jan 24	360	62,250 (204,000)	363	56,000 (184,000)	360

(39,400 ft). About 15 km (49,200 ft), the wind speed decreased with altitude to 20 km (65,600 ft) and again increased with altitude to 71 m/s (138.0 knots) at 62.25 km (204,000 ft). See Figure B-1.

Wind Direction

The surface wind was from the northeast. The direction shifted with altitude from the northeast at the surface to west at 5 km (16,400 ft) in a counter-clockwise direction. Above 5 km (16,400 ft), winds were generally west as shown in Figure B-2.

Pitch Wind Component

The pitch wind speed component was a tail wind at all altitudes above 3 km (9,800 ft). The maximum pitch wind in the high dynamic pressure region was 32.7 m/s (63.6 knots) at 15.25 km (50,000 ft) altitude. See Figure B-3.

Yaw Wind Component

The yaw wind speed component was from the left at most altitudes, reaching a maximum of 20.6 m/s (40.0 knots) at 12 km (39,400 ft). See Figure B-4.

Maximum Wind Speed Summary

Table B-IV summarizes the maximum wind speeds, scalar and components, in the high dynamic pressure regions for the Saturn IB vehicle, AS-201 through AS-204, and AS-501.

Component Wind Shears

Component wind shears ($\Delta h = 1000$ m) were of low magnitude at all altitudes, as shown in Figure B-5. A comparison of the extreme wind shear values in the high dynamic pressure region is given in Table B-V for the various Saturn vehicle launches.

B.5 THERMODYNAMIC DATA

Comparisons of the thermodynamic data taken at AS-204 launch time with the Patrick Reference Atmosphere (PRA) (1963) for temperature, density, pressure, and optical index of refraction are shown in Figures B-6 and B-7.

Temperature

Atmospheric temperatures at AS-204 launch time were generally lower

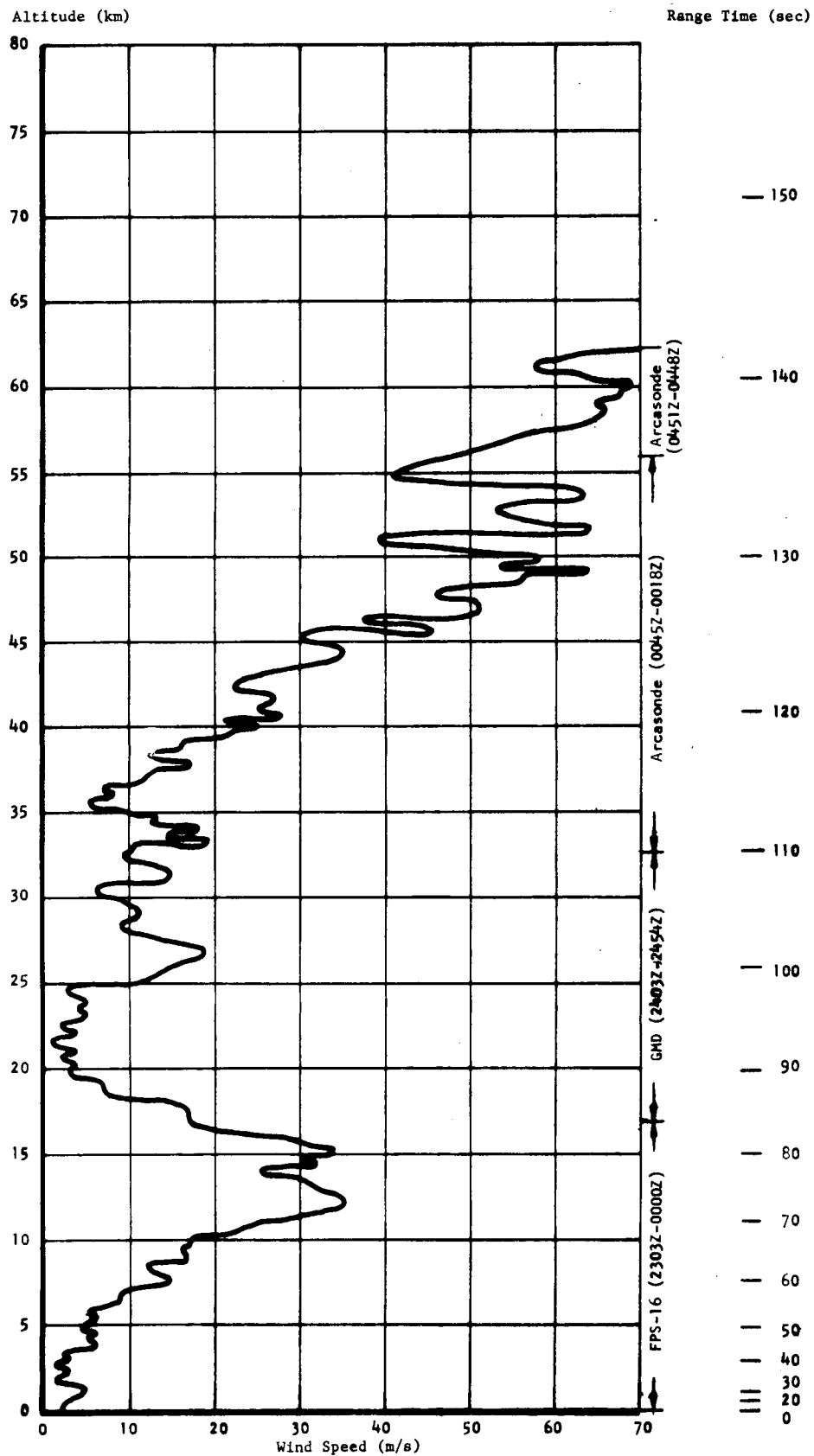
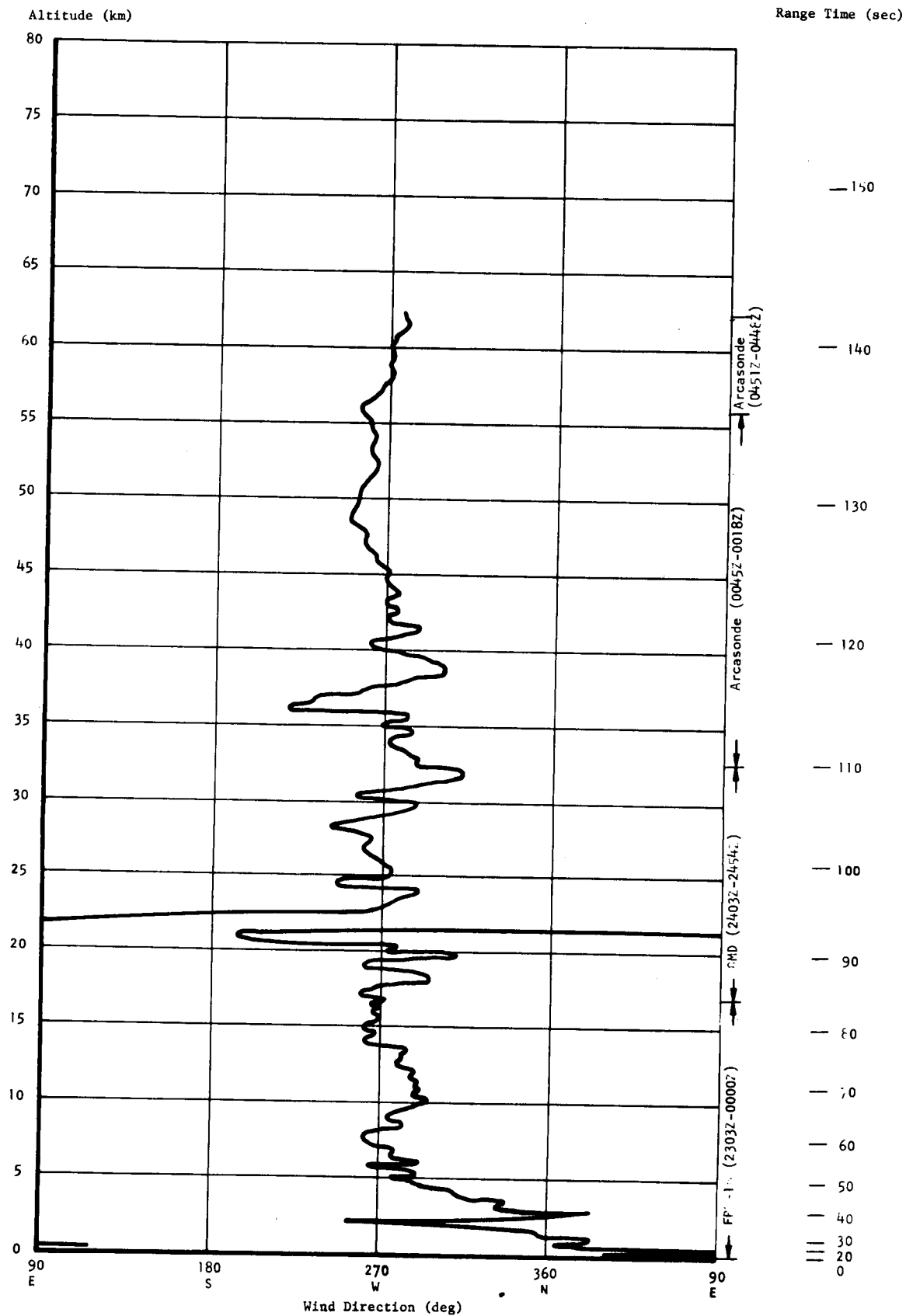
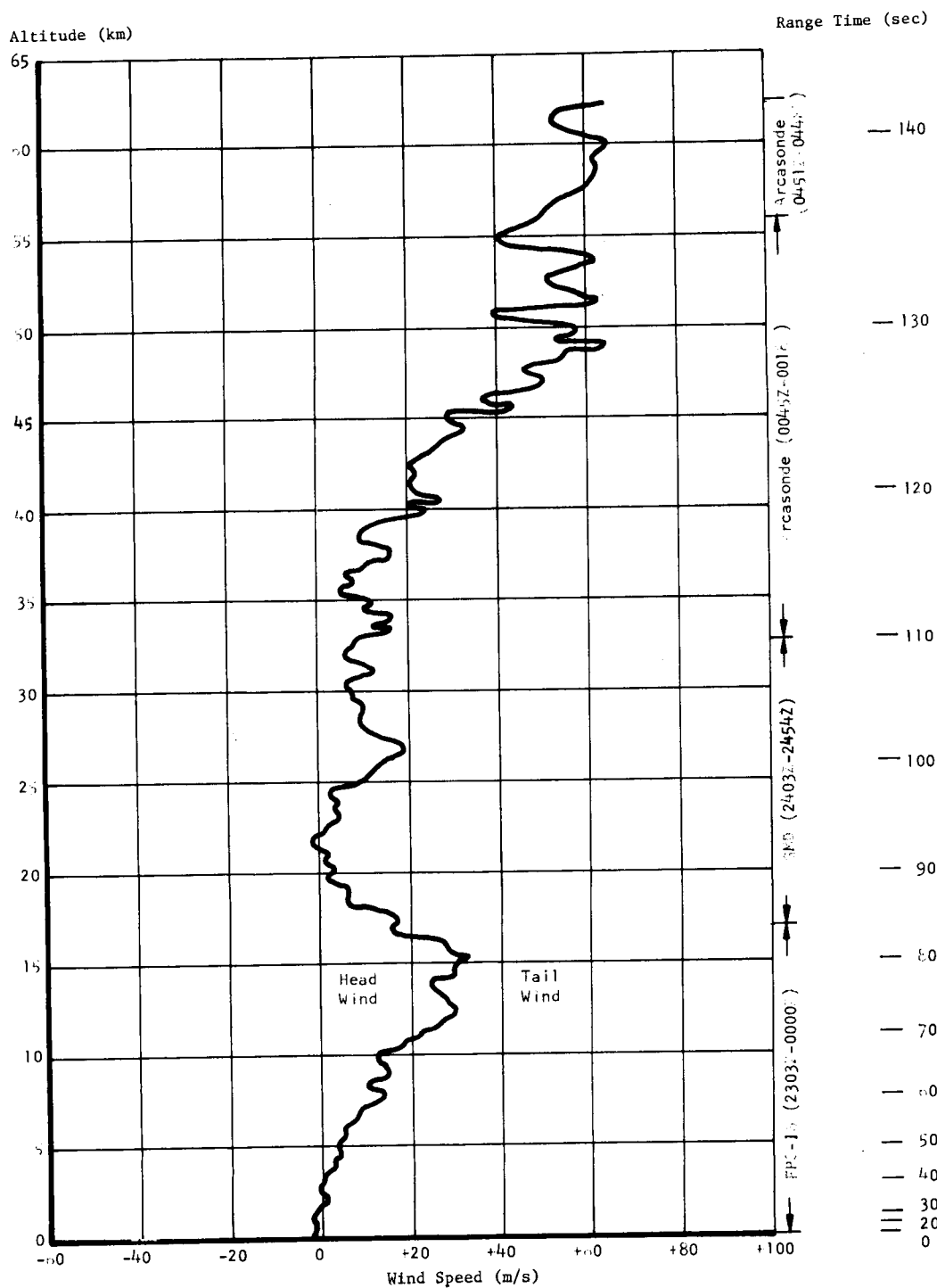


FIGURE B-1 AS-204 LAUNCH TIME SCALAR WIND SPEED



FIGURE B-3 AS-204 LAUNCH TIME PITCH WIND SPEED COMPONENT (W_x)

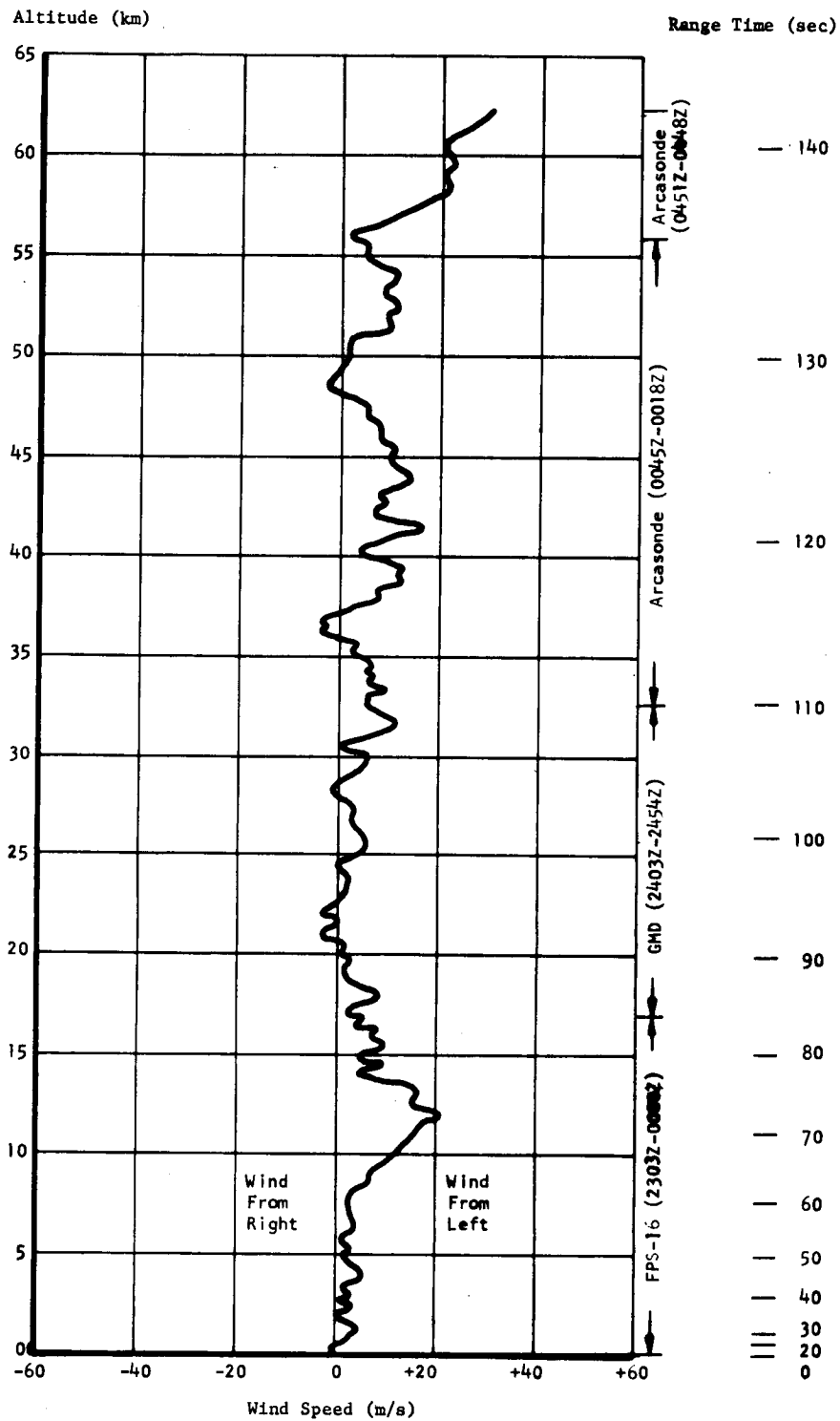
FIGURE B-4 AS-204 LAUNCH TIME YAW WIND SPEED COMPONENT (W_z)

TABLE B-IV MAXIMUM WIND SPEED IN HIGH DYNAMIC PRESSURE REGION

VEHICLE NUMBER	MAXIMUM WIND			MAXIMUM WIND COMPONENTS			
	SPEED M/S (KNOTS)	DIR (DEG)	ALT KM (FT)	PITCH (W_x) M/S (KNOTS)	ALT KM (FT)	YAW (W_z) M/S (KNOTS)	ALT KM (FT)
SA-1	47.0 (91.4)	242	12.25 (40,200)	36.8 (71.5)	13.00 (42,600)	-29.2 (-56.8)	12.25 (40,200)
SA-2	33.6 (65.3)	216	13.50 (44,300)	31.8 (61.8)	13.50 (44,300)	-13.3 (-25.9)	12.25 (40,200)
SA-3	31.3 (60.8)	269	13.75 (45,100)	30.7 (59.7)	13.75 (45,100)	11.2 (21.8)	12.00 (39,400)
SA-4	51.8 (100.7)	253	13.00 (42,600)	46.2 (89.8)	13.00 (42,600)	-23.4 (-45.5)	13.00 (42,600)
SA-5	42.1 (81.8)	268	10.75 (35,300)	41.1 (79.9)	10.75 (35,300)	-11.5 (-22.4)	11.25 (36,900)
SA-6	15.0 (29.2)	96	12.50 (41,000)	-14.8 (-28.8)	12.50 (41,000)	12.2 (23.7)	17.00 (55,800)
SA-7	17.3 (33.6)	47	11.75 (38,500)	-11.1 (-21.6)	12.75 (41,800)	14.8 (28.8)	12.00 (39,400)
SA-9	34.3 (66.7)	243	13.00 (42,600)	27.5 (53.5)	10.75 (35,300)	23.6 (45.9)	13.25 (43,500)
SA-8	16.0 (31.1)	351	15.25 (50,000)	12.0 (23.3)	11.00 (36,100)	14.6 (28.4)	15.25 (50,000)
SA-10	15.0 (29.2)	306	14.75 (48,400)	12.9 (25.1)	14.75 (48,400)	10.8 (21.0)	15.45 (50,700)
AS-201	70.0 (136.1)	250	13.75 (45,100)	57.3 (111.4)	13.75 (45,100)	-43.3 (-84.2)	13.25 (43,500)
AS-203	18.0 (35.0)	312	13.00 (42,600)	11.1 (21.6)	12.50 (41,000)	16.6 (32.3)	13.25 (43,500)
AS-202	16.0 (31.1)	231	12.00 (39,400)	10.7 (20.8)	12.50 (41,000)	-15.4 (-29.9)	10.25 (33,600)
AS-204	35.0 (68.0)	288	12.00 (39,400)	32.7 (63.6)	15.25 (50,000)	20.6 (40.0)	12.00 (39,400)
AS-501	26.0 (50.5)	273	11.50 (37,700)	24.3 (47.2)	11.50 (37,700)	12.9 (25.1)	9.00 (29,500)

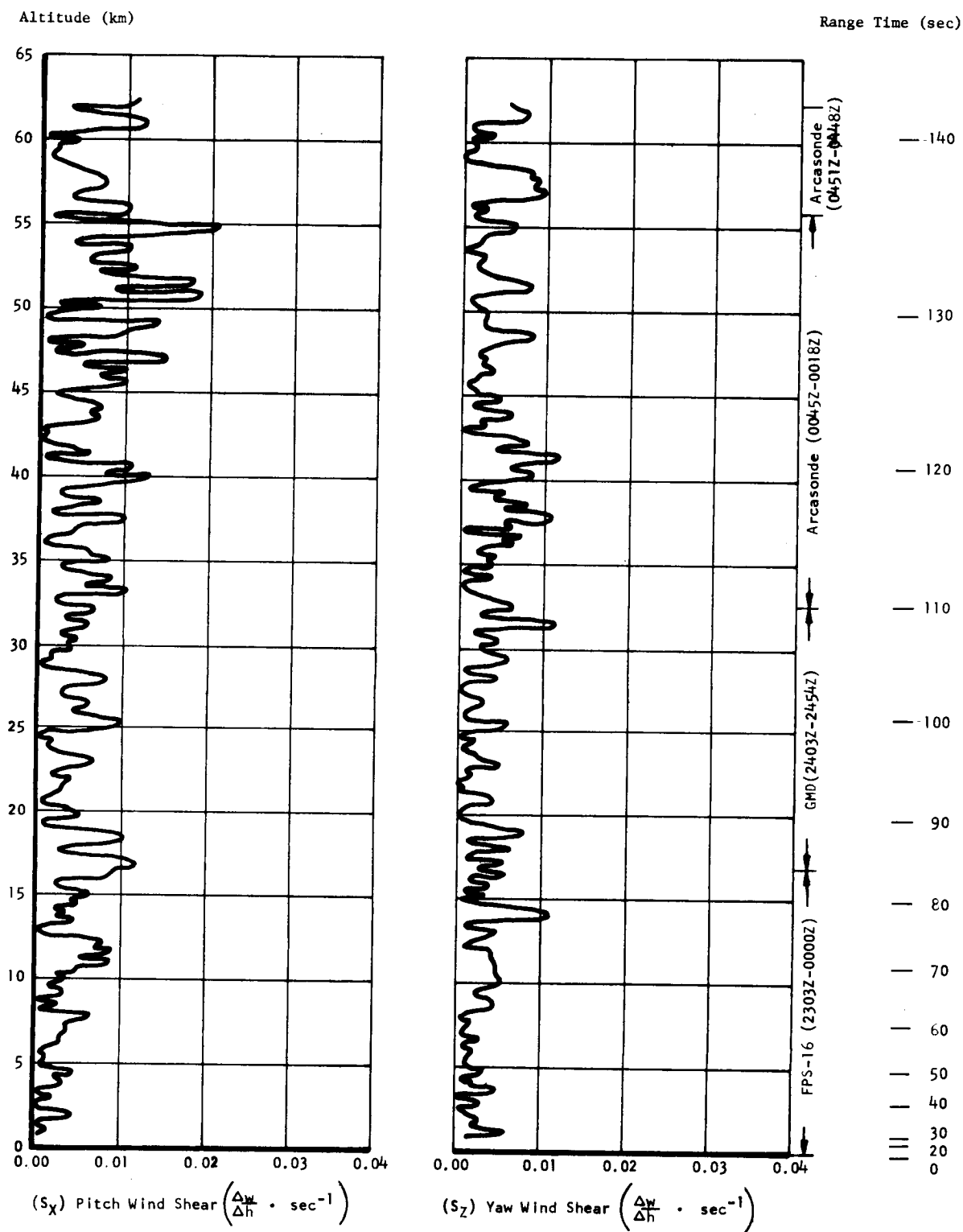
FIGURE B-5 AS-204 LAUNCH TIME PITCH (S_X) AND YAW (S_Z) COMPONENT WIND SHEARS

TABLE B-V EXTREME WIND SHEAR IN HIGH
DYNAMIC PRESSURE REGION

(Δh = 1000 M)				
VEHICLE NUMBER	PITCH PLANE		YAW PLANE	
	SHEAR (SEC ⁻¹)	ALTITUDE KM (FT)	SHEAR (SEC ⁻¹)	ALTITUDE KM (FT)
SA-1	0.0145	14.75 (48,400)	0.0168	16.00 (52,500)
SA-2	0.0144	15.00 (49,200)	0.0083	16.00 (52,500)
SA-3	0.0105	13.75 (45,100)	0.0157	13.25 (43,500)
SA-4	0.0155	13.00 (42,600)	0.0144	11.00 (36,100)
SA-5	0.0162	17.00 (55,800)	0.0086	10.00 (32,800)
SA-6	0.0121	12.25 (40,200)	0.0113	12.50 (41,000)
SA-7	0.0078	14.25 (46,800)	0.0068	11.25 (36,900)
SA-9	0.0096	10.50 (34,500)	0.0184	10.75 (35,300)
SA-8	0.0065	10.00 (32,800)	0.0073	17.00 (55,800)
SA-10	0.0130	14.75 (48,400)	0.0090	15.00 (49,200)
AS-201	0.0206	16.00 (52,500)	0.0205	12.00 (39,400)
AS-203	0.0104	14.75 (48,400)	0.0079	14.25 (46,800)
AS-202	0.0083	13.50 (44,300)	0.0054	13.25 (43,500)
AS-204	0.0118	16.75 (55,000)	0.0116	14.00 (45,900)
AS-501	0.0066	10.00 (32,800)	0.0067	10.00 (32,800)

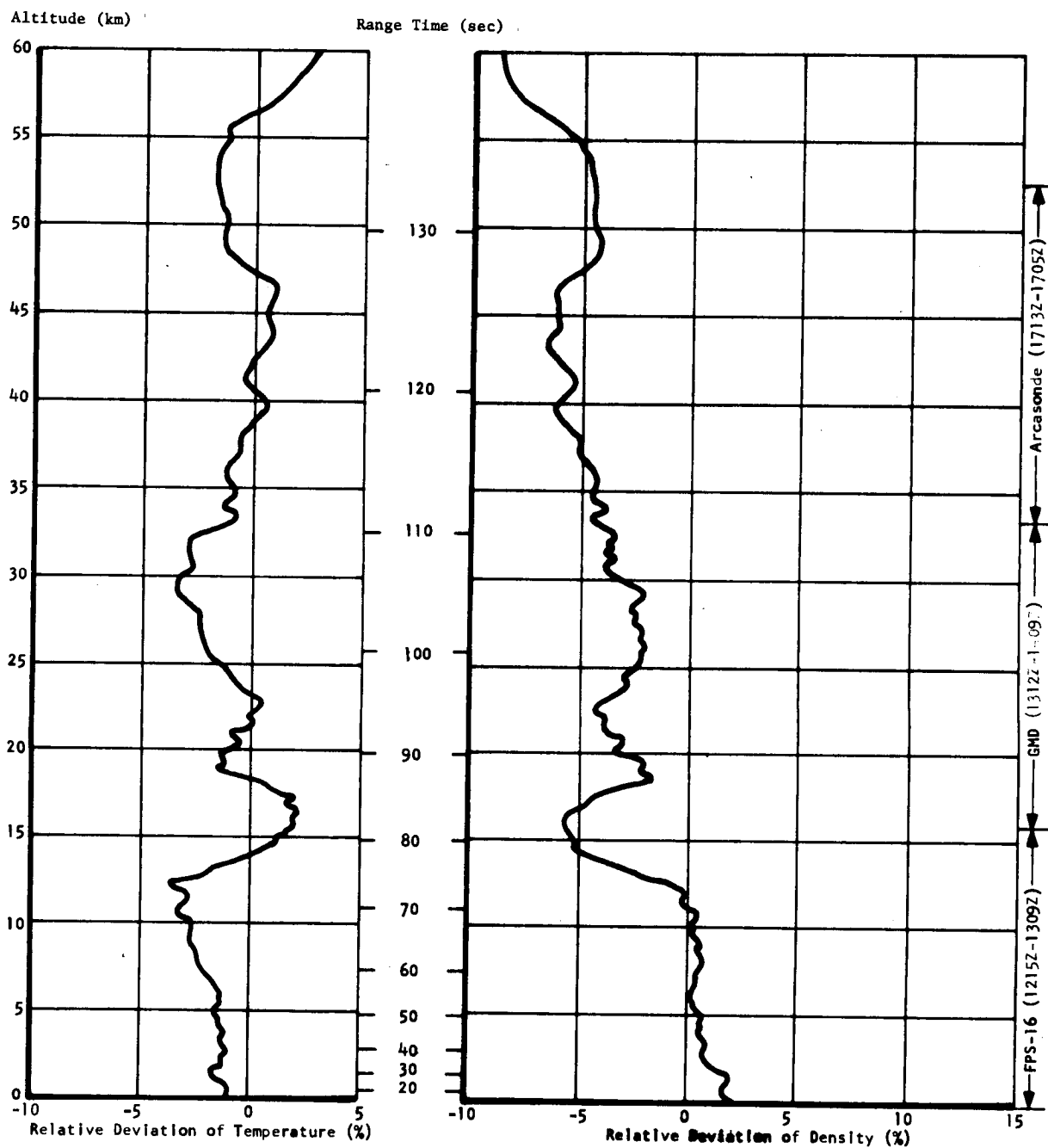
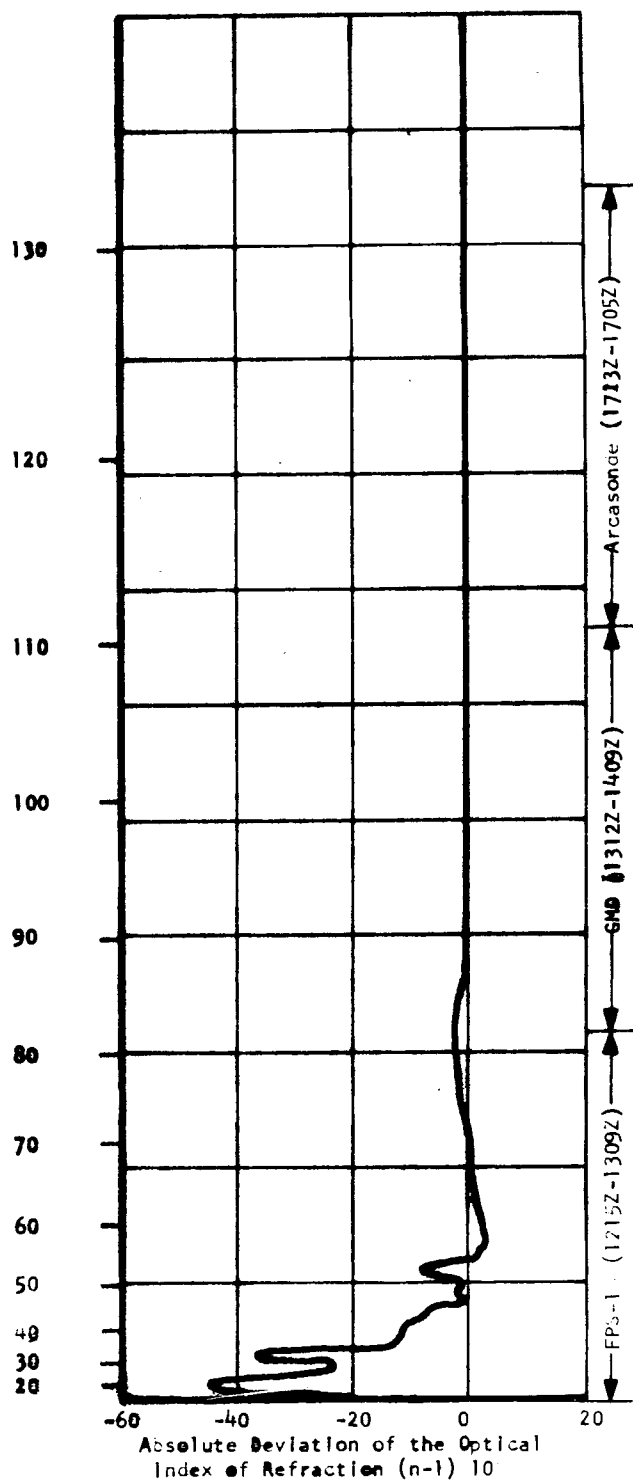
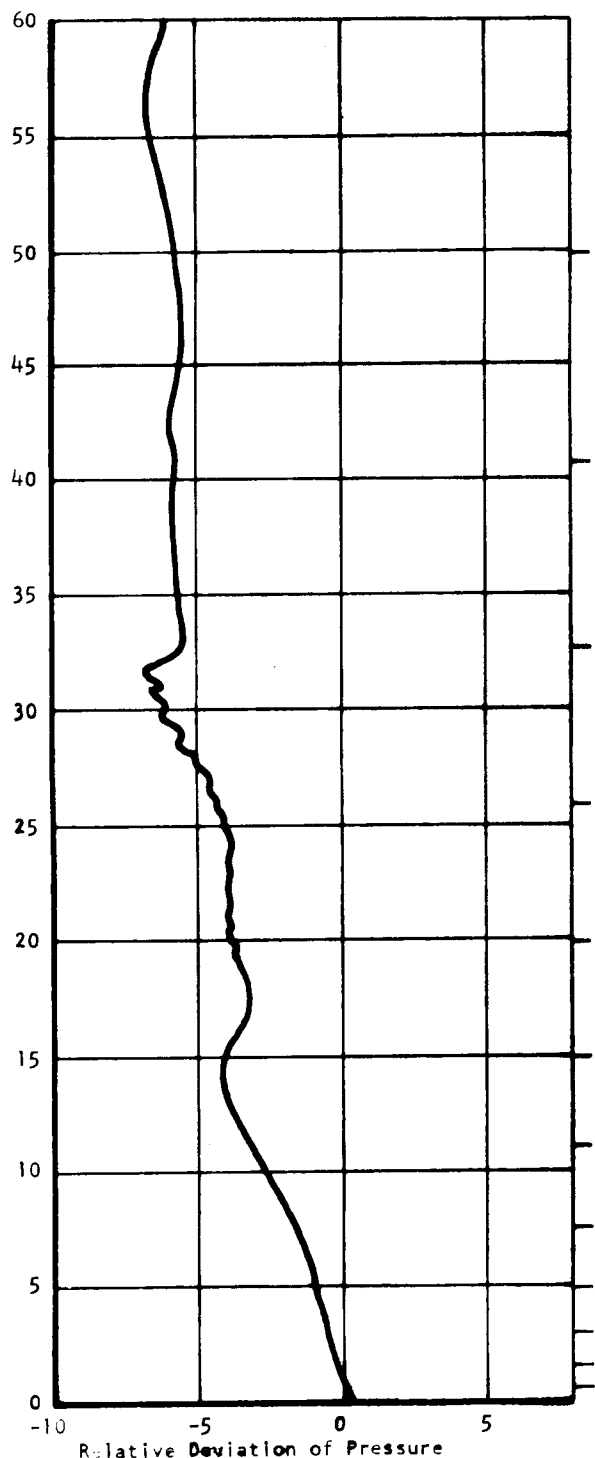


FIGURE B-6 RELATIVE DEVIATION OF AS-204 TEMPERATURE AND DENSITY FROM PAFB (63) REFERENCE ATMOSPHERE

Altitude (km)

Range Time (sec)



than the PRA temperature. The temperature reached a value of 3.5 percent below the PRA at 12.50 km (41,000 ft). Above 56.5 km (185,000 ft), the relative deviations are greater than the PRA, with a maximum of +5.4 percent greater than the PRA at 62.25 km (204,000 ft) as shown in Figure B-6.

Density

The surface air density at AS-204 launch time was +3.0 percent greater than the PRA density. The density deviation decreased with altitude, being zero at 11 km (36,000 ft). Above 11 km (36,000 ft), the density was lower than the PRA, reaching a maximum of -5.7 percent lower than the PRA density at 16 km (52,000 ft), -6.6 percent lower at 43.5 km (143,000 ft), and -9.8 percent lower at 62.25 km (204,000 ft).

Pressure

At AS-204 launch, the surface atmospheric pressure deviated less than 0.1 percent from the PRA. Above the surface, the pressure was less than the PRA, reaching maximum of -6.8 percent lower at 31.5 km (103,000 ft), and -7.0 percent lower at 56.25 km (184,000 ft).

Optical Index of Refraction

At the surface, the optical index of refraction was $-20.0 (n-1) \times 10^{-6}$ units lower than the corresponding value of the PRA. The deviation increased to $-46.9 (n-1) \times 10^{-6}$ units at 0.5 km (1600 ft), then decreased, reaching near zero at 20 km (65,600 ft) as shown in Figure B-7.

REFERENCES

1. R-P&VE-VAW-67-108, "AS-204 Final Predicted Mass Characteristics, Guidance Cutoff", dated August 1, 1967.
2. CCSD BB-3.1.3-10-M01 (TN-AP-67-255) Part IV, "AS-204/LM-1 Launch Vehicle Operational Flight Trajectory" (Revision 1), dated July 25, 1967.
3. SE 0008-001-1, "Project Apollo Coordinate System Standards", dated June, 1966.
4. TR-P&VE-67-58, "Final Flight Performance Predictions for Saturn AS-204 LM Propulsion System S-IB Stage", dated November 20, 1967.
5. TN-AP-68-89, "Final Saturn IB First Stage Flight Bending Modes, AS-206 Nose Cone Configuration".
6. MPR-SAT-FE-66-8 (Confidential), "Results of the First Saturn IB Launch Vehicle Test Flight AS-201", dated May 6, 1966.
7. MPR-SAT-FE-66-12 (Confidential), "Results of the Second Saturn IB Launch Vehicle Test Flight AS-203", dated September 22, 1966.
8. MPR-SAT-FE-66-13, "Results of the Third Saturn IB Launch Vehicle Test Flight AS-202", dated October 25, 1966.

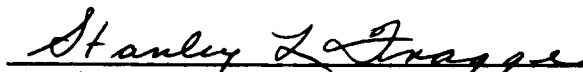
APPROVAL

MPR-SAT-FE-68-2

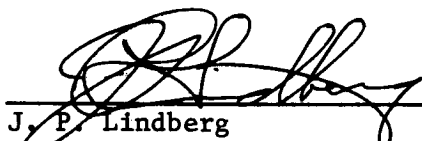
RESULTS OF THE THIRD SATURN IB LAUNCH VEHICLE TEST FLIGHT
AS-204


By Saturn Flight Evaluation Working Group


The information in this report has been reviewed for security classification. Review of any information concerning Department of Defense or Atomic Energy Commission programs has been made by the MSFC Security Classification Officer. The highest classification has been determined to be Unclassified.


Stanley L. Fragge
Security Classification Officer

This report has been reviewed and approved for technical accuracy.


J. P. Lindberg
Chairman, Saturn Flight Evaluation Working Group


Hermann K. Weidner
Director, Research and Development Operations


William Teir
Saturn I/IB Program Manager

DISTRIBUTION:

Dr. von Braun, DIR
 Dr. Rees, DEP-T
 Mr. Gorman, DEP-A

E-S

Mr. Maus, E-DIR
 Mr. Abbott, E-P
 Mr. Smith, E-S

I

Gen. O'Connor, I-DIR
 Dr. Mrazek, I-DIR
 Col. Teir, I-I/IB-MGR
 Mr. Huff, I-I/IB
 Mr. Johnson, I-I/IB-C
 Mr. Dunlap, I-I/IB-G
 Mr. Fikes, I-I/IB-T (2)
 Lt. Col. Kminek, I-I/IB-T
 Mr. Thompson, I-I/IB-S-I/IB
 Dr. Rudolph, I-V-MGR
 Mr. Wear, I-E-J
 Mr. Galey, I-V-IU
 Mr. Moody, I-V-Q
 Mr. McCulloch, I-I/IB-S-IVB
 Mr. Simmons, I-I/IB-U
 Mr. Ferrell, I-E-J
 Mr. T.P. Smith, I-E-H
 Dr. Speer, I-MO-MGR (4)
 Dr. Constan, I-MICH-MGR
 Mr. Riemer, I-MICH-QP
 Mr. Balch, I-MT-MGR
 Mr. Auter, I-MT-H

1 copy

R&D

Mr. Weidner, R-DIR
 Dr. Johnson, R-EO-DIR
 Mr. Williams, R-AS-DIR (2)
 Mr. Messer, R-OM-V
 Mr. Hamilton, MSC-RL
 Mr. Richard, R-SE-DIR

R-AERO

Dr. Geissler, R-AERO-DIR
 Mr. Jean, R-AERO-DIR
 Mr. Dahm, R-AERO-A (2)
 Mr. Holderer, R-AERO-A
 Mr. Wilson, R-AERO-AT
 Mr. Reed, R-AERO-AU
 Mr. Horn, R-AERO-D
 Mr. Deaton, R-AERO-DA
 Mr. Ryan, R-AERO-DD
 Dr. McDonough, R-AERO-D
 Mr. Lindberg, R-AERO-F (33)
 Mr. Baker, R-AERO-G
 Mr. McNair, R-AERO-P (3)
 Mr. Jackson, R-AERO-P
 Mr. Cummings, R-AERO-T
 Mr. Vaughan, R-AERO-Y
 Mr. O. E. Smith, R-AERO-Y
 Mr. Daniels, R-AERO-Y

1 copy

R-ASTR

Dr. Haeussermann, R-ASTR-DIR
 Mr. Hoberg, R-ASTR-DIR
 Mr. Digesu, R-ASTR-A
 Mr. Fichtner, R-ASTR-E

R-ASTR (Cont)

Mr. Stroud, R-ASTR-EA
 Mr. Robinson, R-ASTR-ESA
 Mr. Hosenstien, R-ASTR-F
 Mr. Blackstone, R-ASTR-F
 Mr. Mandel, R-ASTR-G
 Mr. Ferrell, R-ASTR-GSA
 Mr. Powell, R-ASTR-I
 Mr. Avery, R-ASTR-IM
 Mr. Kerr, R-ASTR-IR
 Mr. Threlkeid, R-ASTR-IT
 Mr. Boehm, R-ASTR-M
 Mr. Moore, R-ASTR-N
 Mr. Lominick, R-ASTR-NFS
 Mr. Nicaise, R-ASTR-NGI
 Mr. Taylor, R-ASTR-R
 Mr. Mack, R-ASTR-S
 Mr. Hammers, R-ASTR-S
 Mr. Wolfe, R-ASTR-S

R-COMP

Dr. Hoelzer, R-COMP-DIR
 Mr. Prince, R-COMP-DIR
 Mr. Fortenberry, R-COMP-A
 Mr. Cochran, R-COMP-RR

R-ME

Mr. Kuers, R-ME-DIR
 Mr. Wuencher, R-ME-DIR
 Mr. Orr, R-ME-M
 Mr. Franklin, R-ME-T

R-P&VE

Dr. Lucas, R-P&VE-DIR
 Mr. Hellebrand, R-P&VE-DIR
 Mr. Palaore, R-P&VE-DIR
 Mr. Goerner, R-P&VE-A
 Mr. Stein, R-P&VE-A
 Mr. Kingsbury, R-P&VE-M
 Mr. Thomson, R-P&VE-PA
 Mr. Fuhrmann, R-P&VE-PM
 Mr. McKay, R-P&VE-PP (2)
 Mr. Cobb, R-P&VE-PPE
 Mr. Nelson, R-P&VE-PPE
 Mr. Wood, R-P&VE-PT
 Mr. McAnelly, R-P&VE-PTD
 Mr. Hunt, R-P&VE-S
 Mr. Blumrich, R-P&VE-SA
 Mr. Key, R-P&VE-SSV
 Mr. Showers, R-P&VE-SL
 Mr. Frederick, R-P&VE-SS
 Mr. Furman, R-P&VE-SJ
 Mr. Green, R-P&VE-SVM
 Mr. Aberg, R-P&VE-V
 Mr. Hermann, R-P&VE-VAW
 Mr. Devenish, R-P&VE-VNP (2)
 Mr. Sells, R-P&VE-VOO
 Mr. Schulze, R-P&VE-V (2)
 Mr. Rothe, R-P&VE-XA
 Mr. Griner, R-P&VE-XSJ
 Mr. Boone, R-P&VE-XMK

R-QUAL (Cont)

Mr. Corder, R-QUAL-A
 Mr. Klaus, R-QUAL-J
 Mr. Brooks, R-QUAL-P
 Mr. Landers, R-QUAL-PC
 Mr. Peck, R-QUAL-QVS
 Mr. Brien, R-QUAL-R
 Mr. Smith, R-QUAL-R
 Mr. Wittmann, R-QUAL-T

R-RP

Dr. Stuhlinger, R-RP-DIR
 Mr. Heller, R-RP-T

1 copy

R-TEST

Mr. Heimburg, R-TEST-DIR
 Mr. Grafton, R-TEST-C
 Dr. Sieber, R-TEST-I
 Mr. Edwards, R-TEST-M
 Mr. Driscoll, R-TEST-S

MS

MS-H
 MS-I
 MS-IP
 MS-IL (8)
 MS-D

CC-P

Mr. Wofford, CC-P

KSC

Dr. Debus, CD
 Mr. Preston, DE
 Mr. Poppel, DE-MSD
 Mr. Sparks, NAA-ZK-2S
 Mr. Darby, DE-EEM-4
 Mr. Sandler, IN (4)
 Dr. Bruns, IN-DAT
 Mr. Collins, IN-QAL
 Mr. Jelen, IN-DAT-I
 Lt. Col. Petrone, LO (3)
 Mr. Mathews, AP-SAT
 Mr. Body, AP-RQA
 Dr. Knothe, EX-SCI
 Mr. Lee, I-K-I/IB
 Mr. Gossett, LB-2
 Mr. Williams, DE

LVO

Dr. Gruene, LV
 Mr. Rigell, LV-ENG
 Mr. Edwards, LV-INS
 Mr. Fannin, LV-MEL
 Mr. Pickett, LV-TOM
 Mr. O'Hara, LV-TOM

EXTERNAL

Headquarters, National Aeronautics & Space Administration
Washington, D. C. 20546

Mr. DiMaggio, MAR-R	Mr. Disher, MLD
Dr. Eggers, E	Mr. Bumgardner, MLT
Dr. Condon, KR	Dr. Adams, R
Dr. Mueller, M	Dr. Tischler, RP
Gen. Phillips, MA	Mr. Underwood, RVA
Capt. Holcomb, MAO	Dr. Naugle, S
Mr. White, MAR	Mr. Johnson, SE
Mr. Wagner, MAS (3 copies)	Mr. Mahon, SV (10 copies)
Mr. Ackerman, MAS	Dr. Leshner, U
Mr. Day MAT (8 copies)	Gen. Stevenson, MO
Mr. King, MAT	Mr. Schneider, MO-2
Capt. Freitag, MC	

Director, Ames Research Center: Dr. H. Julian Allen
National Aeronautics & Space Administration
Moffett Field, California 94035

Director, Flight Research Center: Mr. Paul F. Bikle
National Aeronautics & Space Administration
P. O. Box 273
Edwards, California 93523

Goddard Space Flight Center
National Aeronautics & Space Administration
Greenbelt, Maryland 20771
Attn: Herman LaGow, Code 300

John F. Kennedy Space Center
National Aeronautics & Space Administration
Kennedy Space Center, Florida 32899
Attn: Technical Library, Code RC-42
Mrs. L. B. Russell

Director, Langley Research Center: Dr. Floyd L. Thompson
National Aeronautics & Space Administration
Langley Station
Hampton, Virginia 23365

Lewis Research Center
National Aeronautics & Space Administration
21000 Brookpark Road
Cleveland, Ohio 44135
Attn: Director: Dr. Abe Silverstein
Robert Washko, Mail Stop 86-1
E. R. Jonash, Centaur Project Mgr.

Manned Spacecraft Center
National Aeronautics & Space Administration
Houston, Texas 77058
Attn: Director: Dr. Robert R. Gilruth
Robert E. McKann, Code PT-121 (3 copies)
John D. Lobb, PM4 (3 copies)
Charles M. Grant, Code BMI (2 copies)
M. J. Quinn, Code FS-2
George Low, Code PA
A. Mardel, Code PK

Director, Wallops Station: Mr. R. L. Krieger
National Aeronautics & Space Administration
Wallops Island, Virginia 23337

Director, Western Operations Office: Mr. Robert W. Kamm
National Aeronautics & Space Administration
150 Pico Blvd.
Santa Monica, California 90406

Scientific and Technical Information Facility
P. O. Box 5700
Bethesda, Maryland 20014
Attn: NASA Representative (S-AK/RDT) (25 copies)

Jet Propulsion Laboratory
4800 Oak Grove Drive
Pasadena, California 91103
Attn: Irl Newlan, Reports Group (Mail 111-122)
H. Levy CCMTA (Mail 179-203) (4 copies)

Office of the Asst. Sec. of Defense for Research
and Engineering
Room 3E1065
The Pentagon
Washington, D. C. 20301
Attn: Tech Library

Director of Guided Missiles
Office of the Secretary of Defense
Room 3E131
The Pentagon
Washington, D. C. 20301

Central Intelligence Agency
Washington, D. C. 20505
Attn: OCR/DD/Publications (5 copies)

Director, National Security Agency
Ft. George Mead, Maryland 20755
Attn: C3/TDL

U. S. Atomic Energy Commission, Sandia Corp.
University of California Radiation Lab.
Technical Information Division
P. O. Box 808
Livermore, California 94551
Attn: Clovis Craig

U. S. Atomic Energy Commission, Sandia Corp.
Livermore Br, P. O. Box 969
Livermore, California 94551
Attn: Tech Library

Commander, Armed Services Technical Inf. Agency
Arlington Hall Station
Arlington, Virginia 22212
Attn: TIPCR (Transmittal per Cognizant Act
Security Instruction) (5 copies)

Commanding General
White Sands Proving Ground
New Mexico 88002
Attn: ORD BS-OMTIO-TL (3 copies)

Chief of Staff, U. S. Air Force
The Pentagon
Washington, D. C. 20330
1 Cpy marked for DCS/D AFDRD
1 Cpy marked for DCS/D AFDRD-EX

Commander-in-Chief
Strategic Air Command
Offutt AFB, Nebraska 68113
Attn: Director of Operations, Missile Division

Commander
Arnold Engineering Development Center
Arnold Air Force Station, Tennessee 37389
Attn: Tech Library (2 copies)

Commander
Air Force Flight Test Center
Edwards AFB, California 93523
Attn: FTOTL

Commander
Air Force Missile Development Center
Holloman Air Force Base
New Mexico 88330
Attn: Tech Library (SRLT)

AFETR (ETLLG-1)
Patrick AFB, Florida 32925

Headquarters
6570th Aerospace Medical Division (AFSC)
U. S. Air Force
Wright Patterson Air Force Base, Ohio 45433
Attn: H. E. Vongierke

EXTERNAL (CONC)

Systems Engineering Group (RTD)
Attn: SEPIR
Wright-Patterson AFB, Ohio 45433

Director
U. S. Naval Research Laboratory
Washington, D. C. 20390
Attn: Code 2027

Chief of Naval Research
Department of Navy
Washington, D. C. 20390
Attn: Code 463

Chief, Bureau of Weapons
Department of Navy
Washington, D. C. 20390
1 Cpy to RESI, 1 Cpy to SP,
1 Cpy to AD3, 1 Cpy to REW3

Commander
U. S. Naval Air Missile Test Center
Point Mugu, California 93041

AMSMI-RBLD: RSIC (3 copies)
Bldg. 4484
Redstone Arsenal, Alabama 35809

Aerospace Corporation
2400 East El Segundo
El Segundo, California 90245
Attn: D. C. Bakeman

Aerospace Corporation
Reliability Dept.
P. O. Box 95085
Los Angeles California 90045
Attn: Don Herzstein

Bellcomm, Inc.
1100 Seventeenth St. N. W.
Washington, D. C. 20036
Attn: Miss Scott, Librarian

The Boeing Company
P. O. Box 1680
Huntsville, Alabama 35807
Attn: J. E. Scott, Mail Stop AF-67
K. H. Hagenau, Mail Stop AF-67

The Boeing Company
P. O. Box 29100
New Orleans, Louisiana 70129
Attn: R. H. Nelson, Mail Stop LA-42 (3 copies)
S. Johnson, Mail Stop LP-36
T. J. Kornell, Mail Stop LS-63

Chrysler Corporation Space Division
Missoud Operations
Dept. 2712, Bldg. 350
P. O. Box 29200
New Orleans, La. 70129
Attn: Mr. Leroy Smith (5 copies)

Chrysler Corporation Space Division
Huntsville Operations
1312 N. Meridian St.
Huntsville, Alabama 35807
Attn: H. D. Bader, Dept. 4800 (3 copies)
M. L. Bell, Dept. 4830 (2 copies)
G. Martin, Dept. 4820 (2 copies)

Douglas Aircraft Company
Missile & Space Systems Division/SSC
5301 Bolsa Avenue
Huntington Beach, Calif. 92647
Attn: R. J. Calkins (40 copies)

Douglas Aircraft Company, Inc.
George C. Marshall Space Flight Center
Bldg. 4481, Room 41
Marshall Space Flight Center, Ala. 35812
Attn: C. R. Schar (4 copies)

Grumman Aircraft Engineering Corp.
Bathpage, Long Island, N. Y. 11714
Attn: NASA Resident Office
John Johansen

International Business Machine
Flight Evaluation Dept., K-11
150 Sparkman Dr. NW
Huntsville, Alabama 35805
Attn: H. H. Weaver, F-03
D. Beazer, K-11

Martin Company
Space Systems Division
Baltimore, Maryland 21203
Attn: W. P. Sommers

North American Aviation
Space & Information Division Systems
12214 S. Lakewood Blvd.
Downey, California 90241
Attn: W. T. Schleich, BC-05 (2 copies)
W. F. Parker (1 copy)

Radio Corporation of America
Defense Electronic Products
Data Systems Division
8500 Balboa Blvd.
Van Nuys, California 91406

Rocketdyne
6633 Canoga Avenue
Canoga Park, California 91303
Attn: T. L. Johnson (5 copies)

Foreign Technology Division
FTD (TDBDP)
Wright Patterson Air Force Base, Ohio 45433